THE
PHYSICAL REVIEW

A journal of experimental and theoretical physics established by E. L. Nichols in 1893

SECOND SERIES, VOL. 79, NO. 5 SEPTEMBER 1, 1950

Neutron Cross Sections at 120 and 345 Ev

C. T. HIBDON
Argonne National Laboratory, Chicago, Illinois
(Received May 25, 1950)

Total neutron cross sections of 19 elements have been measured at 120 and 345 ev by employing the neutron resonance scattering properties of cobalt and manganese. Thin foils of cobalt and manganese were used as neutron detectors at 120 and 345 ev, respectively. A semilogarithmic plot of neutron counts *versus* thickness of sample was made for each element for each of the two energies. An initial curvature in the plot indicated that the detector resonance overlapped a resonance in the element under study. The cross section determined from either a straight-line plot or the asymptotic part of a transmission curve was identified as either the potential scattering cross section, the off-resonance scattering cross section, or as the minimum cross section in the neighborhood of a resonance.

I. INTRODUCTION

THE total neutron cross section at 120 and 345 ev for a series of elements were reported previously.[1] For these measurements, neutron energies were selected by using the property of neutron resonance scattering in cobalt and manganese. Thin foils of these elements were used as scattering detectors since cobalt and manganese scatter neutrons by resonance at 120 and 345 ev, respectively. A beam of cadmium filtered neutrons from the Argonne heavy water reactor were scattered into a BF_3 proportional annular counter by these resonance detectors (reference 1, Fig. 1). Semilogarithmic transmission plots of neutron counts *versus* absorber thickness were made for all the elements measured. These transmission curves were analyzed into two parts, yielding a resonance cross section and an asymptotic cross section. The first cross section represented the effect of a neutron resonance in the material studied overlapping the detector resonance. The second cross section was taken to be the potential scattering cross section, the off-resonance scattering cross section, or the minimum cross section in the neighborhood of a resonance. The latter values were called the asymptotic cross section, σ_{asym}.

II. THE DETECTORS

One-mil foils of cobalt and manganese were used as detectors.[1] As was indicated in reference 1, the resolving power (approximately the ratio of the resonance scattering to the potential or off-resonance scattering) of these particular foils was approximately 4 for cobalt and 9 for manganese. Early available data from neutron spectrometer studies gave a value of 115 and 300 ev for the location of the cobalt and manganese resonances, respectively.[2] More recent data[3] indicates the value of the cobalt resonance to be 120 ev.

From the overlapping effect of the resonance in manganese with sodium a resonance in sodium was indicated near the manganese resonance. Sodium was found by the Argonne neutron time-of-flight spectrometer to have[4] a resonance at 3000 ± 600 ev. The overlapping effect could then only be explained by the presence of a second resonance in manganese near the sodium resonance.

Neutron transmission of manganese as a function of energy was measured by Selove with the Argonne resonance-region time-of-flight neutron spectrometer. A second resonance in manganese located at about 2400 ev was observed.[5] The width of this resonance and the width of the sodium resonance are sufficient to explain the overlap effect observed. Also in Selove's data the low energy resonance of manganese was observed to be at 345 ± 25 ev, rather than at the previously indicated value[2] of 300 ev.

To determine the relative amounts of resonance scat-

[1] C. T. Hibdon and C. O. Muehlhause, Phys. Rev. **76**, 100 (1949).

[2] Goldsmith, Ibser, and Feld, Rev. Mod. Phys. **19**, 259 (1947).
[3] L. J. Rainwater, Phys. Rev. **76**, 161A (1949).
[4] Hibdon, Muehlhause, Selove, and Woolf, Phys. Rev. **77**, 730 (1950).
[5] W. Selove (private communication).

TABLE I. Epi-cadmium scattering cross sections for manganese with and without sodium filter in neutron beam and the fraction of neutrons scattered at each of the two resonances in manganese (cross sections in barns).

	Without Na filter (345 and 2400 ev)	With Na filter (345 ev)	Na difference (2400 ev)
σ_{epi-Cd}	35.8	30.5	
σ_p	3.4	3.4	
$\sigma_{epi-Cd}-\sigma_p$	32.4	27.1	5.3
Fraction of resonance scattering	1.00	0.84	0.16

TABLE II. Corrected values of σ_{asym}, σ_c, and Δ_p.

Element	Co σ_{asym} (barns)	Co Δ_p %	Mn σ_{asym} (barns)	Mn Δ_p %	σ_c (barns)	Chemical form measured
H	20.3	100	~19.7	100		Paraffin
D	3.34	100	3.32	100	3.11	D_2O
Li	2.24	100	1.65	100	2.95	LiF
C	4.72	100	4.72	100	4.60	Graphite
N	~9.9	100	~9.6	100	~8.5	TiN
Na	4.16	100	4.22	81	4.40	NaF
Si	2.21	100	2.30	100		Si and SiO_2
K	1.92	100	1.75	100	2.15	KF
Ti	4.69	100	~4.8	~100		Ti (corrected for small Mn impurity)
V	5.35	90	5.87	89	5.02	V
Fe	9.61	92	8.65	95	7.00	Puron (small impurity)
Sr	13.5	100	13.0	100		SrF_2
Nb	7.24	100	7.16	100		Nb_2O_5
Mo	6.78	79	5.55	93	6.40	Mo
Ru	6.51	100	6.70	87	7.05	Ru
Pd	5.95	95	5.78	84	5.71	Pd
Ba	5.76	100	6.05	100		BaF_2
La	5.86	100	4.94	100		La
Pt	12.6	91	11.9	92	13.2	Pt

tering of the two resonances in manganese, a thick sodium filter was used to remove neutrons from the beam in the region of 2400 ev. The average epi-cadmium neutron scattering cross section, σ_{epi-Cd}, of manganese was measured with and without the sodium filter by comparison with carbon (4.60 barns). From each of these cross sections the potential scattering cross section, σ_p(~3.4 barns)[6] was subtracted to obtain the component of resonance scattering. Results are tabulated in Table I.

The sodium difference represents the resonance scattering at 2400 ev and the fraction of resonance scattering at this energy is given by 5.3/32.4=0.16. Similarly the fraction of resonance scattering at 345 ev is given by 27.1/32.4=0.84.

[6] C. T. Hibdon and C. O. Muehlhause, Phys. Rev. (to be published). Results for manganese are in process of preparation for publication.

III. TRANSMISSION CURVES

The transmission curves were analyzed in the same manner as those in reference 1. From the straight-line plot or the asymptotic part of the curve the average value of either the potential scattering cross section, off-resonance scattering cross section, or minimum cross section was determined. An initial curvature in the plots represented the overlapping effect of the detector resonance with a resonance in the material under study. Carbon was used as a flat detector to determine σ_c, the asymptotic cross section of the carbon detected transmission curve. In some cases of resonance overlapping σ_{asym} from cobalt or manganese detection was less than σ_c. This lowest value of the cross section near a resonance was interpreted as the cross section resulting from interference of resonance and potential scattering. In these cases σ_c should be a better value of the potential or off-resonance scattering cross section.

Results for σ_{asym}, σ_c, and Δ_p, the percent asymptotic component of the transmission curve, are tabulated in Table II where Δ_p is written 100 percent for a straight-line plot.

IV. DISCUSSION AND EXTENSION OF TECHNIQUES

The cross section of carbon was re-determined using sufficient carbon to attenuate the neutron beam to a greater extent. By use of hafnium (7.7 ev) and vanadium (~2700 ev) detectors the cross section of carbon was determined at 7.7 and ~2700 ev. At each of these energies, the cross section is the same as those listed for carbon in Table II.

Resonance overlapping does not occur for "light" elements except in the one instance in which sodium overlaps manganese.

Values of the cross sections at 345 ev were perturbed owing to the presence of the second resonance in manganese at 2400 ev.

This technique of measuring neutron cross sections by resonance scattering detection has been extended to other energies. In resonance studies of chlorine and manganese detectors of hafnium (7.7 ev), samarium (10 ev), wolfram[186] (19.5 ev), and vanadium (~2700 ev) have been used.[6]

The author wishes to express his appreciation to Dr. C. O. Muehlhause who contributed valuable discussions.

Experiments on Cosmic-Ray Mesons and Protons at Several Altitudes and Latitudes*

MARCELLO CONVERSI†
Institute for Nuclear Studies, University of Chicago, Chicago, Illinois
(Received February 23, 1950)

Experiments to obtain further information about the meson component and the nucleonic component present in the atmosphere have been carried out near sea level, and in a B-29 aircraft flying at different altitudes and latitudes, using G-M counters simultaneously in delayed coincidence and in anticoincidence. A summary of the results obtained is given in Section V of this paper.

I. INTRODUCTION

EARLY investigations performed by means of counter telescopes showed, as is well known, that the ionizing particles of the cosmic radiation present near sea level may be empirically separated into two groups or components: a "soft" component, virtually absorbed by about 10 cm of lead, which has been recognized to be essentially of electronic nature, and a "hard" component made up of particles able to penetrate large thicknesses of material. As to the nature of the particles constituting the hard component, the investigations of the last decade have shown that near sea level these particles are mostly mesons. Since the discovery of the "heavy" or π-meson and of the $\pi-\mu$-decay process,[1] it has been generally believed that the mesons observed near sea level are the decay products of the π-mesons generated in the upper layers of the atmosphere by the interaction of the primary cosmic rays.

There is evidence, at present, that in addition to the generation of π-mesons the primary radiation is also responsible for the production of a large number of protons, of neutrons, and perhaps also of other elementary particles, which in their interaction with the nuclei of the atmosphere build up, possibly through a kind of "cascade process," the so-called nucleonic component. At high altitudes, therefore, the nucleonic component becomes presumably an essential part of the radiation observed, with a counter telescope, as the "hard" component.

Little information is available as yet about the structure of the hard component at high altitude, about the relative abundances and the energy distributions of the different particles of which it is composed. Investigations of this matter are mainly hindered by the difficulty of separating the different kind of particles.

Some information concerning the altitude dependence and the range distribution at high altitude of low energy mesons (less than 200 Mev) has been recently obtained by Rossi, Sands, and Sard,[2] and by Sands,[3] who, by means of delayed coincidences, separated ordinary mesons from other particles by taking advantage of the instability of the meson.

Information on the momentum distribution of the penetrating particles present at airplane altitudes, has also been obtained, with the cloud-chamber method, by Moore and Brode[4] and by Adams, Anderson, and Cowan.[5] Anderson and his co-workers have found evidence, moreover, of the presence of high energy protons at 30,000 feet.[6]

The research described in the present article was undertaken mainly with the aim of obtaining further information on the nature and the composition of the ionizing penetrating particles in the atmosphere, through an investigation of the altitude dependence and of the latitude dependence at airplane altitudes for mesons and for other ionizing particles ("X-particles") which are stopped after penetrating a certain thickness of lead. The method employed for distinguishing the meson component from the other ionizing particles consists essentially in the simultaneous observation of "delayed coincidences" and of "anticoincidences" associated with the stopping of the penetrating particles in a certain thickness of dense material (absorber). The exponential shape and the characteristic 2.2 μsec. decay constant of the curve representing the counting rate of the delayed coincidences *vs.* delay, yields, without ambiguity, the identification of ordinary mesons. By extrapolation, the number of stopped mesons is thus obtained. The anticoincidences, corrected for the contribution given by mesons, yield, on the other hand, the number of ionizing particles, different from mesons, stopping in the absorber. In comparing the two numbers it must be remembered, of course, that they may refer to particles of the same range but presumably not of the same energy.

The experimental method employed in the present research is suitable for measurements of absolute intensities. Indeed, using only delayed coincidences, in order

* Assisted by the joint program of the ONR and AEC. Owing to unavoidable circumstances the manuscipt of the present paper, which was ready in October 1949, reached the Editor with a delay of several months. The writer wishes to apologize for omitting references to works which have appeared in these last months.
† Now at the University of Rome, Rome, Italy.
[1] Lattes, Occhialini, and Powell, Nature **160**, 486 (1947).
[2] Rossi, Sands, and Sard, Phys. Rev. **72**, 120 (1947).
[3] M. Sands, Phys. Rev. **74**, 1237 (1948); M.I.T., Technical Report No. 28 (1949).
[4] D. C. Moore and R. B. Brode, Phys. Rev. **73**, 532 (1948).
[5] Adams, Anderson, and Cowan, Rev. Mod. Phys. **21**, 562 (1948).
[6] Adams, Anderson, Lloyd, Rau, and Saxena, Rev. Mod. Phys. **20**, 334 (1948).

to obtain from their observed counting rate the absolute number of mesons, it is necessary to know the average value of the probability, p, that a meson brought to rest in the absorber disintegrates into an electron which strikes the "delayed counters." This probability depends in particular on the range of the decay electrons in the stopping material. Owing to the distribution in energy of the decay products[7,8] and to the uncertainty of the range-energy relationship for electrons of such energies, a calculation of p appears to be rather unreliable. Instead, with the technique employed here, the average value of p can be deduced directly from the numbers of delayed coincidences and of anticoincidences obtained simultaneously under conditions in which practically all of the observed particles are ordinary mesons.

The same apparatus has also been used in order to obtain some information about the positive excess and the energy distribution of ordinary mesons.

Most of the measurements of the ratio between the numbers of positive and negative particles present in cosmic radiation have been performed so far using two different methods: (a) a cloud chamber in a magnetic field[6,9–13] and (b) magnetized iron bars.[14–20] In general, the positive excess so observed may be due in part to protons and in part to an actual excess of positive mesons. Furthermore, the investigation of the positive excess by these techniques cannot be extended easily to the low energy region of the meson spectrum, partly because of the large percentage of electrons which are present in the radiation observed without using shielding material.

The distinction made between ordinary mesons and other particles by the method of the delayed coincidences takes advantage of one of the properties typical of ordinary mesons. Another property which can also be considered as typical of these particles is their low interaction with nuclear matter. Because of this, negative mesons are captured only in elements of comparatively high atomic number, whereas in light materials they undergo spontaneous decay.[21] One can take advantage of this property to obtain the excess of positive mesons from the comparison of the numbers of delayed coincidences produced by the decay of mesons stopped in two "absorbers," one of *low* and one of *high* atomic number.

This method for separating positive from negative ordinary mesons was first used by Shamos, Levy, and Lower.[22] The same method, in association with a de-

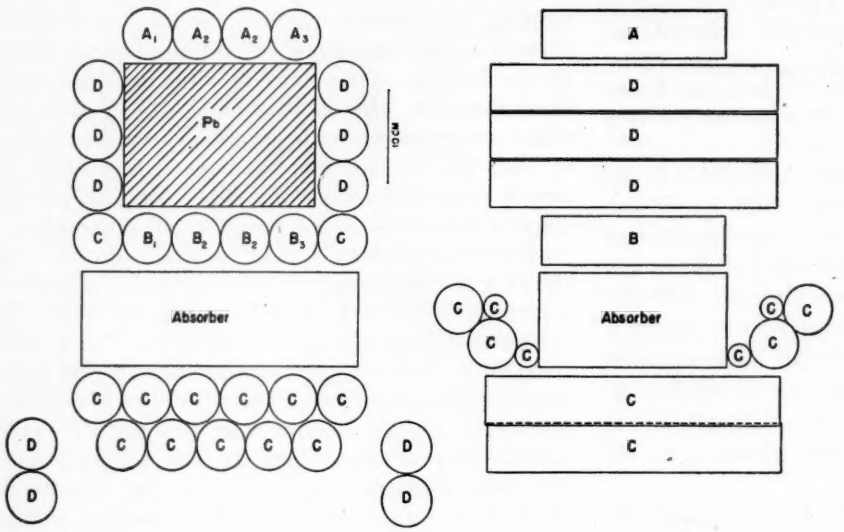

FIG. 1. Cross-sectional view of the counter tubes array.

[7] J. Steinberger, Phys. Rev. 74, 490 (1948).
[8] Leighton, Anderson, and Seriff, Phys. Rev. 75, 1432 (1949).
[9] P. M. S. Blackett, Proc. Roy. Soc. 159, 1 (1931).
[10] L. Leprince-Ringuet and J. Crussard, J. de phys. et rad. 8, 207 (1937).
[11] H. Jones, Rev. Mod. Phys. 11, 235 (1939).
[12] D. J. Hughes, Phys. Rev. 57, 592 (1940).
[13] M. Correll, Phys. Rev. 72, 1055 (1947).
[14] Bernardini, Conversi, Pancini, and Wick, Ricerca Scient. 12, 1227 (1941).
[15] M. Conversi and E. Scrocco, Nuovo Cimento 1, 372 (1943).
[16] Bernardini, Conversi, Pancini, Scrocco, and Wick, Phys. Rev. 68, 109 (1945).
[17] N. Nereson, Phys. Rev. 73, 565 (1948).
[18] Quercia, Rispoli, and Sciuti, Phys. Rev. 73, 532 (1948); 74, 1728 (1948).
[19] Ballario, Benini, and Calamai, Phys. Rev. 74, 1729 (1948).
[20] R. B. Brode, Phys. Rev. 76, 468 (1949).
[21] Conversi, Pancini, and Piccioni, Phys. Rev. 68, 232 (1945); 71, 209 (1947); T. Sigurgeirsson and K. A. Yumakawa, Phys. Rev. 71, 319 (1947).
[22] Shamos, Levy, and Lower, Phys. Rev. 74, 1237 (1948).

tector of penetrating showers, has been recently applied by Piccioni[23] to investigate the nature of the particle constituting penetrating showers locally produced in lead.

Some of the results of the experiment described in this paper have already been published in short reports.[24] Meanwhile a better determination of the constants of the instrument as well as a more refined evaluation of the corrections and of the experimental errors have been achieved. Some of the figures which appeared in the previous reports have undergone, accordingly, slight variations. Moreover, further measurements with graphite and sulfur absorbers have been taken near sea level, under different thicknesses of material, in order to obtain information as to the distribution of the positive excess in the low energy region of the meson spectrum.

II. APPARATUS AND EXPERIMENTAL METHOD

(A) Description of the Apparatus

Figure 1 represents, to scale, two cross-sectional views of the counters array. The effective length of counters A, B, of the two counters C (1 in. in diameter) adjacent to the absorber in Fig. 1B, and of the four lower[24a] counters D, was 20 cm. All other counters had an effective length of 32 cm. The thickness of the counter wall was 0.08 cm. The external diameter was 2 in. for all counters except for the four 1 in. diameter counters represented in Fig. 1B. All counters, filled with the usual alcohol-argon mixture, were of the all-metal type.

The two counters A_2 as well as the two counters B_2 were connected directly in parallel. Counters C as well as counters D were connected to a diode-mixer[25] so that their pulses were added at the output of the diode-mixer although each individual counter was uncoupled with respect to all of the others.

Counter A_1 was in coincidence with counters B_1 and B_2; counters A_2 were in coincidence with B_2; counter A_3 was in coincidence with counters B_2 and B_3. It can be seen from Fig. 1 that each one of the three solid angles defined by these double coincidences was completely covered by counters C and D.

The coincidence circuits (conventional diode-coincidence circuits[25] using crystal diodes) had a resolving time of about 2 μsec.

All of the indicated double coincidences, added by means of a diode-mixer, will be indicated in what follows as (AB).

The output pulse corresponding to any event (AB) started 0.7 μsec. after the time of occurrence of the *earliest* of the two counter pulses producing the coincidence, provided that both pulses occurred within 0.7 μsec. of each other. This was done, as suggested by Sands,[2,3] with the purpose of reducing the effect of the time lags of the G-M counters.

Most of the measurements have been performed with 6 in. of lead placed between counters A and counters B, as represented in Fig. 1. A 10-cm thick block of graphite (C) or sulfur (S), placed underneath counter B, was used as an "absorber" for the particles entering the solid angle defined by the coincidences (AB).[26] The pertinent dimensions of the absorber appear from Fig. 1. Mesons which were stopped in the C absorber after traversing in the vertical direction the 6 in. of lead interposed in the telescope, had energies in the range 224 to 255 Mev. With the S absorber the energy range was 224 to 257 Mev. The maximum permitted zenith angle for a meson entering the counter telescope and stopping in the absorber was about 35°.

Counters C were *at the same time* in delayed coincidences and in anticoincidence with respect to the coincidences (AB), while counters D were used only as additional "anticounters." An event was recorded as an anticoincidence $(AB-C)-$ or $(AB-(C+D))-$ if no counter $C-$ or $(C+D)-$ fired within 1.1 μsec. before or 7.8 μsec. after the time of occurrence of a double coincidence (AB).

The anticoincidences $(AB-C)$, registered in addition to the $(AB-(C+D))$, were used for introducing a correction in the number of the recorded delayed coincidences (see below).

The delayed coincidences were registered by four "channels," so that four points of the decay curve corresponding to the mesons stopped in the absorbers were obtained simultaneously.

The "time distance," θ, between each channel and the next one was 0.98 μsec. The "time width," $\Delta\theta$, of the channels was 2.8 μsec.

The "minimum delay," θ_m, for which a coincidence was recorded in the first channel was 1.15 μsec.

Some technical details concerning the electronic equipment are given in Appendix A.

(B) Corrections

A contribution to the delayed coincidences registered in each channel may be given by random events as well as by spurious delays associated with the discharge of the G-M counters. For an accurate determination of the decay curve of the stopped mesons a sufficiently exact knowledge of the spurious counting rate in each channel is required, especially if this counting rate is a considerable fraction (as it actually happens at high altitudes) of the total number of observed delayed coincidences.

For the interpretation of the experimental results, as

[23] O. Piccioni, Phys. Rev. **77**, 1 (1950).

[24] M. Conversi, Phys. Rev. **76**, 311, 444, 849, and 851 (1949).

[24a] During one series of measurements (Section III B) also these counters D had an effective length of 32 cm.

[25] Howland, Schroeder, and Shipman, Rev. Sci. Inst. **18**, 551 (1947).

[26] The S absorber was contained in a can made of copper sheet 0.08 cm thick. The author wishes to take this opportunity of thanking the Research Department of the Texas Sulfur Company for providing the block of sulfur.

well as for a computation of the counting rate, N_r, of the delayed coincidences produced in each channel by *random* events, it must be mentioned that the pulse-forming circuit triggered by the pulses of counters C (B.O.3 in Fig. 9, Appendix A) had a "recovery time" of 12.5 μsec. This time was larger than the maximum delay (6.89 μsec.) for which delayed coincidences were registered by the last channel. Random delayed coincidences could be caused, therefore, only by events in which a particle producing a coincidence (AB), but failing to discharge counters C (let $n_{(AB-C)}$ be the counting rate of these events) was followed after a short time by a single discharge of counters C. If n_c represents the background counting rate of counters C, we have then:

$$N_r = n_{(AB-C)} n_c \Delta\theta. \quad (1)$$

N_r, which is practically negligible near sea level under 10 or more cm of lead, becomes quite appreciable at high altitudes. However, all the quantities appearing on the right side of Eq. (1) can be measured with great accuracy.

The spurious delayed coincidences due to the time lags of counters C were strongly reduced by using a double layer of counters, since thus most of the particles traversing the counter telescope discharged two counters C and the counter which was discharged first triggered the corresponding pulse-forming circuit (B.O.3 in Fig. 9). Under these conditions, the percentage of delayed coincidences due to spurious delays larger than 1.15 μsec. was found to be completely negligible in the measurements taken near sea level (Sec. III). In the measurements performed at high altitudes, however, an appreciable fraction of the delayed coincidences registered by the first channel was recognized to be due to the effect of these spurious delays. On the basis of measurements performed without an absorber it is found that at 30,000 feet the coincidences registered in the first channel using the C absorber, previously corrected for the random events given by Eq. (1), must be multiplied by the factor 0.885 in order to represent only the contribution of the decay electrons. In the measurements with S absorber this factor is found to be 0.81. (See Appendix B for a detailed discussion of this point.)

The loss of delayed coincidences and of anticoincidences is negligible, for our apparatus, wherever measurements have been taken. It is shown also, in Appendix C, that the difference between the rates of anticoincidences recorded with and without an absorber represents, within a good approximation, the number of "true anticoincidences"; that is, events associated with the stopping of ionizing particles in the absorber.

(C) Relations among Measured Quantities

For the four points corresponding to the coincidence rates produced in each channel by the decay of the stopped mesons, the *most probable* disintegration curve corresponding to a given lifetime, τ, can be drawn. Let N_c be the coincidence rate obtained, using the C absorber, by extrapolation to the zero time of such a curve. Since the time width of the channels is $\Delta\theta$, N_c represents the number of mesons which are stopped per unit time in the C absorber after penetrating the counter telescope and which disintegrate between O and $\Delta\theta$ into electrons that discharge counters C. Therefore, if p represents the average value of the probability that a meson stopped in the C absorber decays into an electron discharging counters C, the number of mesons stopped in the C absorber after traversing the counter telescope is given by

$$M = N_c/p[1-\exp(-\Delta\theta/\tau)]. \quad (2)$$

As is shown by the results of our measurements (Discussion, Sec. IV) the contribution given to the delayed coincidences by positive π-mesons locally produced appears to be quite small, for our apparatus, at all altitudes at which measurements have been taken. Hence Eq. (2) refers essentially to *ordinary* mesons coming from the atmosphere above the apparatus.

Let I_a be the intensity of the "true anticoincidences," and let us remember that events are registered as anticoincidences when no "anticounter" fires within 7.8 μsec. after the time of occurrence of a coincidence (AB). Since the percentage (2.8 percent) of mesons decaying after 7.8 μsec. can be neglected, the contribution given by mesons to the intensity I_a is $(1-p)M$.

If particles *other than mesons* are stopped in the absorber, they will give an additional contribution, X, to the intensity I_a; so that we shall write, in general:

$$I_a = (1-p)M + X. \quad (3)$$

For the sake of brevity we shall call the particles responsible for this possible contribution "X-particles," without thereby implying that they are all particles of the same kind. The instrumental characteristics of the method employed impose some restrictions on the possible types of events appearing as X-particles. More precisely we can state as follows:

(a) X-particles must be ionizing particles[27] coming from the atmosphere and either stopping in the absorber after traversing counters A and B, or producing (in the lead between counters A and B) other ionizing particles, of which at least one traverses counters B, stopping in the absorber, and none of which strikes the "anticounters"; (b) after they or their secondary particles have been stopped in the absorber, no emission of secondary ionizing rays striking the anticounters has to take place within 7.8 μsec.

The absolute numbers (per unit range) of mesons and of X-particles can be derived from Eqs. (2) and (3) if the value of p is known. Actually this value can be deduced from measurements performed under experimental conditions in which the contribution X in Eq. (3) is negligible in comparison with $(1-p)M$. In these

[27] This is true for most of the measurements taken in the airplane, where a negligible amount of material was present above the apparatus.

TABLE I. Results of measurements of delayed coincidences performed in Chicago for the determination of p.

Series No.		1	2	3
Absorber (C)		on	on	off
Material above the absorber (g/cm²)		228 Pb +∼40 concrete	398 Pb +∼75 concrete	
Duration (minutes)		7595	16,785	16,725
Delayed coincidences registered in channel	1	533	1123	201
	2	337	694	137
	3	211	470	75
	4	145	309	50
Random delayed coincidences, N_r		2.7	6.1	4.1
Extrapolated[a] delayed coincidences per hour, N		6.90±0.27	6.73±0.18	1.15±0.075

[a] Correcting the number of counts registered in the four channels only for the random coincidences N_r (as given by Eq. (1)).

conditions, in fact, from Eqs. (2) and (3) it follows that:

$$1/p=1-[1-\exp(-\Delta\theta/\tau)](I_a/N_c). \quad (4)$$

For the determination of the excess of positive mesons, delayed coincidences were measured using alternately absorbers of graphite (C) and of sulfur (S).

According to Ticho, 72 percent of the negative mesons stopped in sulfur are captured while the remaining 28 percent decay with a lifetime of about 0.5 μsec.[28] Since in the first channel events which occur with delays between 1.15 μsec. and 3.95 μsec. are recorded (θ_m to $\theta_m+\Delta\theta$), one sees that the first channel detects 43 percent of the positive, and 2.7 percent of the negative, mesons. This means that if the excess of positive mesons is ∼20 percent, the counting rate of the coincidences registered in the first channel with S absorber must be multiplied by the factor 0.95 in order to represent the counting rate due *only* to positive mesons.[29] When this correction (which becomes completely negligible in the following channels) is applied in addition to the one due to the contribution of the spurious events, then by extrapolation of the decay curve so obtained one gets the number, N_s, of *positive* mesons which decay, between O and $\Delta\theta$, into electrons discharging counters C.

Let k be the ratio between the number of mesons stopped in the C absorber and the number of those stopped in the S absorber. Then let ρ represent the ratio between the probability for the decay electrons of mesons stopped in the C absorber to produce a delayed coincidence and the analogous probability relative to the S absorber. Setting $k\rho=1/a$ it is easily shown that the ratio of positive to negative mesons is given by

$$M_+/M_-=1/[a(N_c/N_s)-1] \quad (5)$$

with the assumption that *all* mesons decay in C.[30]

[28] H. K. Ticho, Phys. Rev. **74**, 1337 (1948).
[29] Neglecting the positive excess this factor would be 0.94.
[30] See footnote 40.

TABLE II. Results of measurements of anticoincidences performed in Chicago for the determination of p.

Series No.	1		2	
Absorber (C)	On	Off	On	Off
Material above the absorber (g/cm²)	228 g/cm² of Pb +∼40 of concrete		398 g/cm² of Pb +∼75 of concrete	
Duration of observation (min.)	3780	4020	8440	5700
Anticoincidences per hour, N_a	60.8±1.0	37.0±0.74	75.7±0.75	50.2±0.73
True anticoincidences per hour (I_a)	23.8±1.25		25.5±1.05	
I_a/N_c	3.45±0.22		3.79±0.19	
p	0.286±0.013		0.268±0.010	

III. RESULTS

(A) Experimental Conditions and Controls in the Measurements at High Altitudes

Measurements of delayed coincidences and of anticoincidences were performed in Chicago (about 600 feet above sea level), at China Lake, California (2100 feet), and in the rear pressurized cabin of a B-29 airplane at different altitudes and latitudes.

The measurements in the B-29 aircraft were carried out in two successive expeditions: the first from China Lake to Lima, Peru, and back; the second from China Lake to Fairbanks, Alaska, and back. The first expedition was undertaken entirely at a pressure altitude

TABLE III. Results of measurements of delayed coincidences at 30,000 feet, at different latitudes. Mesons observed belong to the energy range 224 to 255 Mev (momentum range 315 to 348 Mev/c). Absorber of graphite.

Expedition		1st	1st	1st	2nd	1st	2nd
Average geomagnetic latitude		9° N	28.5°	35.5°	40.0°	42.0°	59.0°
Duration (minutes)		350	298	220	290	142	220
Delayed coincidences registered in channel	1	203	208	204	271	[a]	249
	2	124	116	122	173	85	161
	3	83	86	[a]	120	56	106
	4	60	70	[a]	93	43	88
Anticoincidence ($AB-C$) per minute		35.1	46.7	51.6	53.8	56.2	64.3
Single counts (C) per 10^{-3} min.		38.5	43.1	45.7	50.6	48.4	59.3
Random delayed coincidence N_r		22.1	28.1	24.2	36.9	18.0	39.2
Corr.[b] extrapolated delayed coincidence N_e per hr.		46.5 ±3.3	53.3 ±3.9	72.0 ±5.8	76.9 ±4.8	73.2 ±8.4	87.1 ±5.4
Latitude ratio, $R(N_e)$		1.00 ±0.07	1.14 ±0.08	1.55 ±0.12	1.65 ±0.10	1.57 ±0.18	1.87 ±0.12

[a] Not recorded.
[b] Correcting all channels for the random coincidences N_r and the first channel also for the time lags of the counters (according to Eq. (9), Appendix B).

of 30,000 feet, while in the Northern flight observations were made at different altitudes. During both expeditions 6 in. of lead was placed between counters A and B. One flight was made over Lima with 4 in. of additional lead placed above counters A. The measurements were performed in both expeditions under the same experimental conditions with the following exceptions: (a) in the first expedition lateral blocks of lead (2 in. thick) were used in order to reduce the background counting rate of counters C; since their effect was not found to be considerable, they were removed at the end of the expedition; (b) only during the Northern expedition were the anticoincidences $(AB-C)$ recorded continuously; (c) only during the Northern flight was the background counting rate, n_c, of counters C measured directly by means of a 256-scaling unit. During the Southern expedition the value of n_c was obtained from the background counting rates of counters B as measured in flight (by means of a 64-scaler) assuming the same altitude dependence for the background counting rates of counters B and C; (d) during the Southern expedition measurements were taken alternately with and without a graphite absorber, while during the Northern one additional measurements with a sulfur absorber were performed alternately. It has to be mentioned, finally, that all counters were changed at the end of the first expedition. The consistency between the measurements performed in Chicago before and after the period of the expeditions shows, however, in a satisfactory manner, the stability of the performance of the apparatus.

During each flight the background counting rate of the different groups of counters was measured approximately every 20 minutes. Double coincidences (AB) were also measured in flight approximately every half-hour.

During the Northern expeditions, furthermore, the main points of the electronic apparatus were checked in flight by means of a syncroscope.

(B) Measurements for the Determination of p

The *hard* component of cosmic rays at sea level is known to be composed essentially of ordinary mesons.

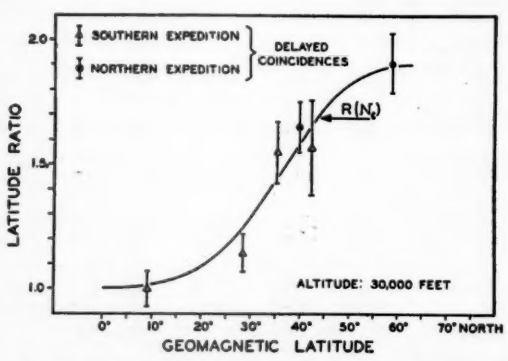

FIG. 2. Latitude dependence at 30,000 feet of mesons stopped in 10 cm of graphite after penetrating 6 in. of lead.

However, since no information is available on the energy distribution of the small percentage of protons which are believed to be present at sea level,[31,32] we cannot assume, without checking directly, that the contribution X in Eq. (3) is negligible at sea level under 20 or more cm of lead. For this reason, in order to obtain the value of the constant p defined in Sect. IIC two series of measurements, reported as No. 1 and No. 2 in Tables I and II.[33] have been carried out in Chicago under the amount of material specified in the third line of the tables. In both cases 6 in. of lead was placed between counters A and B, the remaining material being above the apparatus, in the solid angle of the counter telescope.

The "extrapolated delayed coincidences" [34] in the last line of Table I, have been obtained from the *corrected* delayed coincidences recorded in the four channels assuming a lifetime of 2.20 μsec. The percentage error in N has been assumed to be equal to the percentage error in the sum of corrected delayed coincidences registered in the first and last channels.[35]

The delayed coincidences recorded in each channel have been corrected only for the small contribution of random events, N_r, obtained through Eq. (1) and given in the sixth line of Table I. The correction for spurious delayed coincidences due to the time lags of the G-M counters is shown to be completely negligible by the results of measurements without an absorber reported in the same table as series No. 3. Indeed, within the experimental errors, the four points corresponding to the delayed coincidences recorded without absorber are on an exponential curve of 2.2 μsec. decay constant. Mesons slowed down in the counter walls and in the material (brass) of the frame are evidently responsible for the delayed coincidences so observed.

The anticoincidences reported in Table II have been measured simultaneously with the delayed coincidences reported in Table I. Table II contains, however, only those measurements which have been taken *alternately* with and without the graphite absorber. It will be observed that the ratio I_a/N_c between "true anticoincidences" and "extrapolated delayed coincidences" is the same, within statistical uncertainties, for both series of measurements. If particles other than mesons (X-particles) were present in appreciable amounts in the conditions of series No. 1, we should reasonably

[31] L. Janossy, *Cosmic Rays* (Oxford University Press, London, 1948).
[32] B. Rossi, Rev. Mod. Phys. **20**, 537 (1948).
[33] Errors indicated in these and in the following tables are statistical standard deviations.
[34] The quantities N_c, N_a, and N_0 (without absorber) will be indicated in general by the letter N.
[35] It can be proved easily that for a given value of the lifetime the percentage error of the most probable number of delayed coincidences extrapolated to the zero time from the numbers registered in two channels which are "independent" and "contiguous," is the same as for a single channel covering the same time interval as the two. Since in our case the first and fourth channels are "independent" but not exactly contiguous, the actual error of N is somewhat smaller than the one assumed.

TABLE IV. Results of measurements of anticoincidences with and without C absorber, taken at 30,000 feet, under 6 in. of lead, near the equator, at 32°, 40°, and above 55° N geomagnetic latitude. $R(N_a)$ and $R(I_a)$ represent the "latitude ratios" respectively of the anticoincidences with absorber and of the "true anticoincidences."

Geomagnetic latitude	5° N.		32°		40°		59°	
Absorber	on	off	on	off	on	off	on	off
Duration (minutes)	185	60	150	110	290	122	551	95
Anticoincidence per hour	1370±21	964±31	2117±29	1519±29	2579±23	1805±30	3276±19	2208±37
True anticoincidence per hour (I_a)	406±37.5		598±41		774±38		1068±42	
$R(N_a)$	1.02±0.016		1.58±0.022		1.92±0.017		2.44±0.015	
$R(I_a)$	1.02±0.094		1.50±0.102		1.94±0.095		2.68±0.105	

expect in passing from the first to the second series a decrease of the ratio I_a/N_e due to their absorption in the additional amount of material present in the conditions of series No. 2. Our results show, therefore, that X-particles are present in negligible amounts, if at all, in both cases. Then Eq. (4) holds and we obtain for p the values reported in the last line of Table II. By combining these two values we find

$$p=0.28\pm0.0085. \quad (6)$$

For $\Delta\theta=2.8\,\mu$sec. we obtain, then, from Eq. (2):

$$M\approx 5N_e.$$

Although I_a is the same, within statistical errors, for both series of measurements, there is a considerable difference between the rates of anticoincidences N_a reported in the fifth line of Table II. This is explained by the fact that in the first series (performed before the B-29 expeditions) the four lower counters D had an effective length of 32 cm, while later they were exchanged for counters 20 cm long.

(C) Measurements at 30,000 Feet at Several Latitudes

Table III contains the results of measurements of delayed coincidences taken with a graphite absorber at 30,000 feet, at different latitudes. During these measurements 6 in. of lead were interposed between counters A and B so that the observed mesons had energies in the range 224 to 255 Mev (for a vertical direction of incidence).

The data reported in each column of the table include two or more flights undertaken at approximately the same average latitude, with the exception of one flight at 35.5° and one at 42°. During these latter two flights, unfortunately, part of the delayed coincidences were not recorded. The internal consistency of the measurements performed in different flights at the same latitude was always satisfactory.

In the last line of Table III is reported the "latitude ratio" $R(N_e)$, namely the ratio between the counting rates of the extrapolated delayed coincidences, N_e, observed at each latitude and near the equator (9° N.). *The intensity of the observed mesons is found to increase by a factor of 1.87±0.14 between the geomagnetic equator and 59° N.*

Owing to the small number of points obtained and to their large statistical errors, little information is available about the shape of the latitude curve, $R(N_e)$, which has been represented in Fig. 2 in a rather arbitrary way.

Measurements without an absorber were usually taken for a short period, so that each individual anticoincidence measurement was affected in general by a rather large statistical error. Thus no large number of accurate points could be obtained for the latitude curve of the "true anticoincidences" from measurements performed while the plane was flying at a variable latitude. Flights at a constant latitude, in the experimental conditions previously specified, have been undertaken only at 32° and at 40° north geomagnetic latitude. Nevertheless, measurements performed around the geomagnetic equator and around 60° N. may be considered to be taken at a practically constant latitude, for in these regions the intensities of the several components so far observed do not undergo any appreciable change. The results of these flights are reported in Table IV. The latitude ratio, at 5° N., of the true anticoincidences, I_a (and also of the anticoincidences with absorber, N_a) has been assumed to be 1.02, as suggested by a first analysis of the results. The increase in the number of true anticoincidences between the equator and 59° N. is so found to be 2.68±0.27. The four points of the latitude curve of the true anticoincidences corresponding to the data contained in the last line of Table IV are represented by double circles in Fig. 3.

In order to obtain further information as to the shape of this curve, we will assume that for latitudes lower than 55° N. the latitude ratio, $R(I_a)$, of the true anticoincidences, can be expressed in terms of the latitude ratio $R(N_a)$ according to the relation

$$R(I_a)=(1+\alpha|\lambda|)R(N_a), \quad (7)$$

where α is a constant and λ represents the geomagnetic latitude in degrees. Since (as is shown by the data contained in the two last lines of Table IV) there is not much difference between the values of $R(I_a)$ and of $R(N_a)$, this assumption appears to be quite reasonable provided that the intrinsic efficiency of the apparatus did not change during the entire period of the flights. By comparing the values of $R(I_a)$ and of $R(N_a)$ given[36]

[36] In Table IV there have been included also values of N_a obtained with a sulfur absorber, during the Northern expedition. The ratio of anticoincidences with graphite and with sulfur

in Table IV at the four specified latitudes, we obtain for α four values which are consistent with one another within their statistical errors. By combining these four values we find $\alpha=8.3\cdot10^{-4}$. From Eq. (7) and from the values of N_a given in Table V we obtain thus the values of $R(I_a)$ reported in the same table and represented graphically in Fig. 3. As is indicated in Fig. 3, *the rate of anticoincidences seems to reach a "saturation" in the neighborhood of 55°.*

Using Eqs. (2) and (3) it is easily shown that the latitude ratio, $R(X)$, of the X-component is given by

$$R(X)=[R(I_a)-bR(N_c)]/(1-b), \qquad (8)$$

where $b=(1-p)(M/I_a)_{\lambda=0}$.

For the numerical values of $\Delta\theta$ and of p previously found, the ratio $(M/I_a)_{\lambda=0}$ between the numbers of stopped mesons and of true anticoincidences at the equator (which are given in Tables III and IV) is $\approx5(0.115\pm0.013)$. We find then $b=0.41\pm0.05$. From Eq. (8) and from the latitude curves $R(N_c)$ and $R(I_a)$ represented in Figs. 2 and 3, respectively, we obtain the latitude curve[37] $R(X)$ drawn in Fig. 4.

As to the accuracy of *the latitude effect of the X-component*, it may be observed that using the values of $R(N_c)$ and $R(I_a)$ near the equator and at 59° as given in Tables III and IV and introducing the error on b *we obtain for* $R(X)$ *at 59° the value* 3.21 ± 0.49.

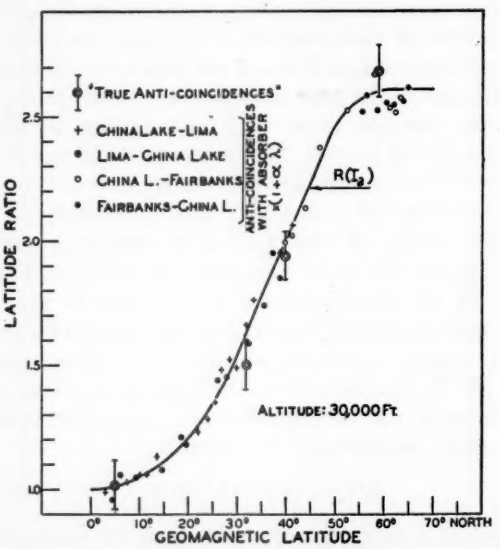

FIG. 3. Latitude dependence at 30,000 feet of the anticoincidences under 6 in. of lead. The "latitude ratio," $R(I_a)$, of the "true anticoincidences" is supposed to be $(1+\alpha|\lambda|)$ times the latitude ratio of the "anticoincidences with absorber," where λ is the geomagnetic latitudes and $\alpha=8.3\times10^{-4}$ (degree)$^{-1}$.

absorbers at 30,000 feet was found to be 0.99 ± 0.006, so that no correction needs to be applied in practice.

[37] In a previous report (reference 24) we used the value $p=0.29\pm0.015$, as obtained from measurements which were not so accurate as those reported in the present paper, and we assumed that $\alpha\lambda\ll1$ at all latitudes. This led to an underestimation of the latitude effect of the X-component.

TABLE V. Results of measurements at 30,000 feet of anticoincidences, N_a, with absorber, between 3° and 65° N. geomagnetic latitude. λ is the geomagnetic latitude in degrees; ϵ is the percentage error in the observed counting rate (N_a/hr.) of the anticoincidences N_a. The latitude ratio, $R(I_a)$, of the true anticoincidences is assumed to be $(1+8.5\cdot10^{-4}|\lambda|)$ times the latitude ratio of the anticoincidences N_a.

λ	Flight	N_a/hr.	$R(I_a)$	ϵ	λ	Flight	N_a/hr.	$R(I_a)$	ϵ
3.0	1	1328	0.99	3.2	33.5	1	2298	1.76	3.0
4.5	2	1288	0.96	4.8	35.5	2	2262	1.74	3.0
6.0	2	1422	1.06	4.6	37.5	2	2557	1.95	3.5
7.5	1	1380	1.03	3.3	39.0	2	2406	1.85	3.5
9.0	2	1392	1.04	3.2	39.5	1	2518	1.94	1.9
10.0	1	1416	1.06	4.6	40.0	3	2579	1.99	0.9
11.5	1	1422	1.07	4.6	41.0	3	2606	2.02	2.3
13.5	1	1502	1.13	3.8	41.5	1	2663	2.06	2.1
14.5	2	1429	1.08	3.3	44.0	3	2754	2.13	2.3
18.5	2	1596	1.21	5.0	47.0	3	3069	2.37	2.1
19.5	2	1554	1.18	3.6	52.5	3	3241	2.52	2.1
22.5	1	1626	1.23	4.3	55.5	4	3223	2.51	1.8
24.0	1	1692	1.28	4.3	56.5	4	3308	2.58	1.9
25.5	1	1776	1.35	4.1	58.0	3	3408	2.65	2.4
26.0	2	1888	1.44	3.3	58.5	4	3238	2.53	1.8
27.0	1	1947	1.48	3.9	60.5	4	3275	2.55	1.8
27.5	2	1910	1.45	3.3	61.0	3	3240	2.53	2.5
28.5	1	2001	1.52	3.9	62.0	4	3257	2.54	1.8
30.0	1	1950	1.49	3.9	62.0	3	3219	2.51	1.75
32.0	1	2172	1.66	2.1	62.5	3	3302	2.57	1.7
32.0	2	2080	1.59	1.8	63.0	4	3284	2.56	2.5
					65.0	4	3358	2.61	2.4

Flight No. 1, China Lake to Lima.
Flight No. 2, Lima to China Lake.
Flight No. 3, China Lake to Fairbanks.
Flight No. 4, Fairbanks to China Lake.

(D) Measurements at 30,000 Feet Taken at the Geomagnetic Equator under Ten Inches of Lead

During the Southern expedition one flight was undertaken over Lima (geomagnetic equator), at 30,000 feet, adding 4″ of lead (in the solid angle of the double coincidences) to the 6″ of lead placed between counters A and B. The results of these measurements are summarized in Table VI.

(E) Measurements at Different Altitudes

Measurements with 6 in. of lead between counters A and B and with graphite absorber have been performed at 600 feet (Chicago), 2100 feet (China Lake), 22,500 feet, 30,000 feet, and 36,000 feet. The results are reported in Tables VII and VIII. The data at 30,000 feet include only the measurements of the Northern Expedition.

In comparing the results obtained at different altitudes it must be taken into account that they do not all refer to the same latitude. For lack of information we are forced to assume that for the observed mesons, as well as for the X-particles: (a) there is no appreciable correction between 41° N. and 53° N. at altitudes lower than 2100 feet; (b) the latitude correction at 36,000 feet is approximately the same as at 30,000 feet, between 40° and 50° N.

Then, from the latitude curves at 30,000 feet given in Fig. 2 for the meson component and in Fig. 4 for the

X-component, we deduce the corresponding correction factors (reported also in the tables) to be used in order to refer all measurements to the same geomagnetic latitude of 50° N.

(F) Absolute Intensities

If Ω is the *effective* solid angle of the beam of particles which are stopped in the absorber after traversing the counter telescope, the absolute numbers of mesons and of X-particles per sec. steradian, and per gram of graphite, are obtained by multiplying respectively M and X by the factor $(3600\ \Omega s)^{-1}$, where s represents the *effective* thickness of the absorber in g/cm².

For the geometry of our counter arrangement (Fig. 1) some of the particles belonging to the solid angle defined by counters A, B, and C, do not traverse the absorber. More precisely, all those particles which traverse counters A, B, and one of the lateral counters C in Fig. 1B, do not traverse the *entire* thickness of the absorber. If we call $(ABC)_{lat}$ the counting rate of the threefold coincidences produced by these particles, then the difference $\Delta=(ABC)-(ABC)_{lat}$ represents the number of particles traversing the counter telescope and *the entire thickness of the absorber* per unit time.

Accurate measurements performed in the open air at Chicago with 6 in. of lead (271 g/cm²) placed between counters A and B, yield $\Delta=0.883$ particles per sec. On the other hand, from measurements of Greisen[38] the corrected number of particles traversing at Ithaca (850 feet above sea level) 167 g/cm² of lead in the vertical direction is found to be[32] $I_v=0.85\times10^{-2}$ per cm² per sec., per sterad. Under the conditions of our measurements this figure must be decreased by about 1 percent, so that $I_v=0.84\times10^{-2}$. Thus we find $\Delta/I_v\approx\Omega=105$ cm² sterad. Since the vertical thickness of the absorber is about 16.5 g/cm², we have $s\approx16.5$ g/cm² and, therefore, $(3600\Omega s)^{-1}\approx1.6\times10^{-7}$.

TABLE VI. Results of measurements at 30,000 feet taken over Lima, Peru (geomagnetic equator) under 10 in. of lead, using absorber of graphite. The observed mesons had energy in the range of 350 to 381 Mev (momentum range 445 to 478 Mev/c).

(a) Delayed coincidences results			(b) Anticoincidence results	
Duration (minutes)		174	Duration (minutes)	174 with C absorber 68 without absorber
Delayed coincidences registered in channel	1 2 3 4	101 57 43 31	Anticoincidence per hour	1182±23 with absorber 748±26 without absorber
Anticoincidences ($AB-C$) per minute		27.9	True anticoincidences per hour, I_a	434±35
Single counts (C) per 10^{-3} min.		33.9	X-particles per hour	263±39
Random delayed coincidences, N_r		7.6		
Corrected[a] extrapolated delayed coincidences, N_c, per hour		47.5 ±4.6		

[a] Correcting all channels for the random coincidences N_r and the first channel also for the time lags of the counters.

[38] K. I. Greisen, Phys. Rev. **61**, 212 (1942).

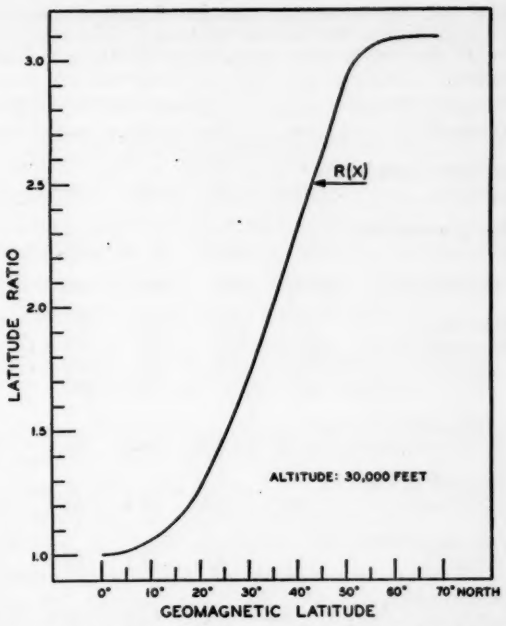

FIG. 4. Latitude dependence at 30,000 feet of the X-particles as deduced, through Eq. (8), from the curves $R(N_c)$ and $R(I_a)$ represented in Figs. 2 and 3.

By using this figure and introducing the corrections for the difference in latitude we obtain the absolute numbers of mesons (m) and of X-particles (x) reported in the last line of Tables VII and VIII and represented, as a function of the atmospheric depth, in Fig. 5.

Near sea level these absolute numbers refer to particles incident in the vertical direction if we assume the same zenith angle dependence for the particles stopped in the absorber and for those going through it. Although this assumption is certainly not true, the error related to it is very small on account of the comparatively narrow angular definition of our apparatus. It can also be observed that since Δ refers to particles traversing the *entire* thickness of the absorber, the previous absolute numbers have been somewhat overestimated by assuming $\Omega=\Delta/I_v$. On the other hand they have been somewhat underestimated by assuming the vertical thickness of the absorber to be nearly equal to its *effective* thickness. Both these errors are estimated to be only a few percent and the corresponding corrections have been therefore neglected.

(G) Positive Excess

Measurements of delayed coincidences with C and S absorbers have been performed in Chicago, under different thicknesses of material; at China Lake, without any lead in or above the counter telescope, and at 30,000 feet, during the Northern flight, with 6 in. of lead interposed in the counter telescope.

The results are reported in Table IX. This table also includes measurements with only C absorber, performed

TABLE VII. Results of measurements of delayed coincidences at different altitudes. Mesons observed belong to the energy range 224 to 255 Mev (momentum range 315 to 348 Mev/c). Absorber of graphite.

Altitude (ft.)		600	2100	22,500.	30,000	36,000
Atmospheric depth (g/cm²)		1010	957	427	306	231
Average geomagnetic lat.		51° N	42° N	50° N	49° N	40° N
Duration (minutes)		9470	6462	300	560	159
Delayed coincidences registered in channel	1	704	534	166	571	248
	2	467	338	107	378	169
	3	294	228	81	259	123
	4	195	150	51	202	93
Anticoincidence ($AB-C$) per minute		1.98	2.33	29.4	59.6	79.1
Single counts (C) per per 10^{-3} min.		5.12	4.93	31.8	55.4	73.4
Random delayed coincidences, N_r		4.4	3.5	13.1	86.3	43.1
Corr.* extrapolated delayed coincidence, N_c, per hr.		7.50 ±0.25	8.3 ±0.32	53.0 ±3.8	79.5 ±3.5	120 ±8
Mesons stopped per hr. ($M \approx 5N_c$)		37.5 ±1.3	41.5 ±1.6	265 ±19	398 ±18	600 ±40
Correcting factor for 50° geomagnetic latitude		1	1	1.00	1.01	1.1
$10^6 \times$no. of mesons per sec., g, steradian at 50° N		6.00 ±0.20	6.64 ±0.26	42.4 ±3.1	64.3 ±2.9	106 ±7.0

* Correcting all channels for the random coincidences N_r and the first channel, only in the measurements at 30,000 and 36,000 feet, also for the time lags of the counters.

in Chicago and at China Lake, under still different thicknesses of material, in order to obtain further points of the differential range spectrum of mesons (positive and negative) at the two stations.

The third column of Table IX contains the amount of material (in g/cm²) that a particle had to penetrate before reaching the absorber. Series No. 1 was carried out on the roof of the Ryerson Building in the University of Chicago, under a military tent of negligible thickness. Series No. 6 was performed at China Lake in a cabin covered with a thin roof roughly equivalent to 5 g/cm² of air. The 2.7 g/cm² of brass reported in Table IX for both series corresponds to the thickness of the counter walls.

A rather accurate determination of the ratio between the numbers of positive and negative particles near sea level has been carried out by Conversi and Nappo[39] using magnetic lenses and G-M counters in anticoincidence. More precisely these authors have measured in Rome (~50 m above sea level) the numbers of anticoincidences produced by positive and by negative particles stopped in 7 cm of lead after traversing 28 cm of iron (thickness of the magnetic lens). As is indicated by the results of the measurements reported in Section III B, under similar conditions the number of protons should be negligible in comparison with the corresponding number of mesons. Hence, the ratio, 1.24 ±0.05, between the numbers of positive and negative particles as found in Rome,[39] may be assumed to represent the ratio M_+/M_- for mesons having energies in the neighborhood of 400 Mev. Since the mesons observed in Chicago under 228 g/cm² of lead plus 40 g/cm² of concrete (fourth series), belong approximately to the energy range of 350 to 380 Mev, the measurements of this series can be compared to those performed in Rome. From this comparison we obtain from Eq. (5), $a=1.03$.[40] The values of the ratio M_+/M_- for the different series of measurements reported in Table IX have been obtained from Eq. (5) using this value of a. The errors relative to the ratios M_+/M_- do not include the error of a.[41] Indeed, we are more interested in the

TABLE VIII. Results of measurements of anticoincidences at different altitudes.

Altitude (feet)	2100		22,500		30,000		36,000	
Average geomagnetic latitude	42° N		50° N		49° N		40° N	
Absorber	on	off	on	off	on	off	on	off
Duration (minutes)	6462	1484	300	73	560	237	159	30
Anticoincidence per hour	90.8±0.9	54.0±1.45	1350±19	787±19	2835±18	1910±23	3986±40	2850±79
True anticoincidence per hour (I_a)	36.8±1.7		563±27		925±30		1136±89	
X-particles per hour ($I_a-(1-p)M$)	6.2±2.1		372±30.5		638±33		704±93	
Correcting factor for 50° geomagnetic latitude	1		1.00		1.02		1.3	
$10^6 \times$number of X-particles per sec., g, steradian at 50° N	0.99±0.34		59.5±4.9		104±5.4		146±19	

[39] M. Conversi and F. Nappo, unpublished results (University of Rome, 1947).

[40] This result is found with the assumption that all mesons disintegrate in C. If the fraction of negative mesons which actually decay in C is assumed to be 0.95 [M. H. Shamos and M. G. Levy, Phys. Rev. 73, 1396 (1948)] the value of a becomes 1.01 and, accordingly, $M_+/M_-=0.95/(1.01N_c/N_s-1)$. The values of M_+/M_- obtained from this formula do not differ appreciably from those deduced from Eq. (5), setting $a=1.03$.

[41] In the previous report (reference 24, p. 311) the error in a was included in the errors of the ratios M_+/M_-.

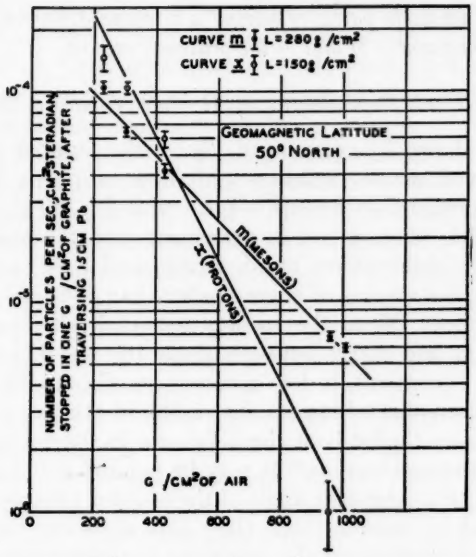

FIG. 5. Dependence upon altitude of the absolute numbers (sec.$^{-1}$, g^{-1}, sterad.$^{-1}$) of mesons (m) and of protons (x) stopped in 10 cm of graphite after traversing 6 in. of lead.

relative rather than the absolute values of the positive excess.

IV. DISCUSSION

Part 1: The Meson Component

(A) *Analysis of the Lifetime*

The results of the measurements of delayed coincidences at different altitudes, reported in Table VI, have been graphically represented in Fig. 6. It is seen from this figure that the decay curves obtained at all altitudes are consistent with a lifetime τ of approximately 2.2 μsec. The measurements of delayed coincidences corresponding to each flight have been also analyzed separately. When corrected for the random events given by Eq. (1) and for the spurious coincidences in the first channel due to the time lags of counters C (the second correction—see Appendix B—to be applied only in the measurements taken at 30,000 and at 36,000 feet), they have been found to be always in agreement, within experimental errors, with a 2.2 μsec. decay constant. Considering separately the results of the Southern and of the Northern flights the following values are obtained for the lifetime of the mesons observed at 30,000 feet under 6 in. of lead:

$\tau = 2.01 \pm 0.18$ μsec. from the Southern flight,
$\tau = 2.26 \pm 0.16$ μsec. from the Northern flight.

These two values of τ are equal within their errors. The difference between them, furthermore, is in the sense expected, because the correction for the time lags of the counters (which, as observed in Appendix B, is latitude dependent) has been applied, to the first channel, disregarding its latitude dependence. Of course, in computing the lifetime from the results of the Northern flight, where measurements have been taken using also S abosrber, allowance has been made for the small contribution given to the coincidences registered in the first channel by the decay of negative mesons in S (Section II).

By combining all of the measurements of the two expeditions (corresponding to the observation of approximately 1600 independent mesons) we find the value

$\tau = 2.14 \pm 0.12$ μsec. at 30,000 feet

to be compared with the value

$\tau = 2.18 \pm 0.05$ μsec. near sea level

obtained with the same apparatus through the observation, in Chicago and at China Lake, of about

TABLE IX. Results of measurements of delayed coincidences with absorbers of graphite (c) and sulfur (s).

1	2	3	4	5	6				7	8	9
Series	Place	g/cm² of material above the absorber	Absorber	Duration of observation (minutes)	Delayed coincidences registered in channel 1	2	3	4	Random delayed coincidences	Coincidence per hour from mesons decaying between 0 and $\Delta\theta$	M_+/M_-
1	Chicago	2.7 of brass	C	6015	433	270	184	133	24.4	6.8±0.28	$1.22^{+0.20}_{-0.15}$
			S	8997	420	267	175	114	37.5	3.85±0.18	
2	Chicago	~75 of concrete	C	9490	751	475	319	237	32.4	7.6±0.25	$1.27^{+0.18}_{-0.12}$
			S	12,150	631	385	269	177	42.6	4.4±0.17	
3	Chicago	172 Pb	C	9470	704	467	294	195	4.4	7.5±0.25	
4	Chicago	228 Pb +~40 concrete	C	7595	533	337	211	145	2.7	6.90±0.27	$1.24^{+0.18}_{-0.13}$
			S	10,988	427	276	179	120	4.2	3.93±0.17	
5	Chicago	398 Pb +~75 concrete	C	16,785	1123	694	470	309	6.1	6.73±0.18	$1.37^{+0.14}_{-0.12}$
			S	20,453	871	501	347	233	7.5	4.01±0.12	
6	China Lake	2.7 brass +~5 air[a]	C	7720	665	428	272	174	38.7	7.5±0.27	$0.99^{+0.16}_{-0.11}$
			S	5990	263	174	137	88	33.3	3.85±0.23	
7	China Lake	172 Pb	C	6462	534	338	228	150	3.5	8.5±0.33	
8	China Lake	398 Pb	C	7755	572	384	270	166	4.0	7.95±0.30	
9	30,000 feet	172 Pb	C	560	561	378	259	202	86.3	78.5±3.4	$1.54^{+0.28}_{-0.20}$
			S	770	593	331	262	220	115	49.0±2.3	

[a] Roughly corresponding to the roof of the cabin in which the measurements were taken.

10,000 independent mesons. Both values are in good agreement with previous accurate determinations of the lifetime of the ordinary meson.[42] *

For purposes of comparison the two decay curves corresponding to all of the measurements taken at 30,000 feet and near sea level have been represented together in Fig. 7. In this figure the origin of the time scale has been made arbitrarily coincident with the delay of the first channel and the counting rate of the first channel has been assumed arbitrarily to be equal to 100 in the upper curve (30,000 feet) and equal to 50 in the lower one. Both curves are drawn for $\theta/\tau=0.45$.

The 5.5 percent accuracy in the value of the lifetime at 30,000 feet given above may appear somewhat optimistic because the error does not include the uncertainties related to the corrections introduced. One has to remember, however, that the main correction, which is represented by the random events, can be determined with a very high statistical accuracy, while the uncertainty in the other small corrections (applied only to the coincidences registered in the first channel) does not have a great influence in the determination of τ. Our results, therefore, seem to *rule out the possibility of the presence in the atmosphere of any considerable number of unstable particles having a lifetime different from, but comparable to that of the ordinary meson.*

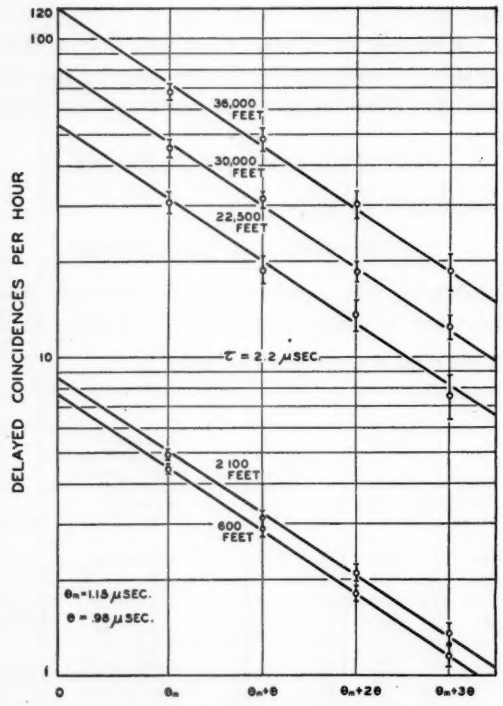

FIG. 6. Decay curves obtained at several altitudes for mesons stopped in 10 cm of graphite after penetrating 6 in. of lead. Each point of the decay curves is due to the contribution of mesons disintegrating between the instant t of the corresponding abscissa and $t+\Delta\theta$ ($\Delta\theta=2.8$ μsec.).

* *Note added in proof.*—Measurements of θ recently performed with a greater accuracy give an average value $\theta=0.96$ μsec. Accordingly the value $\tau=2.13\pm0.05$ μsec. is obtained from the sea level data.

[42] N. Nereson and B. Rossi, Phys. Rev. **64**, 199 (1943). M. Conversi and O. Piccioni, Nuovo Cimento **2**, 40 (1944).

(B) *Altitude Dependence and Absolute Number of Mesons*

As shown by curve m of Fig. 5, the number of the observed mesons decreases with the atmospheric depth, h, approximately as $\exp(-h/L)$, with $L=280$ g/cm² of air. This value is not in agreement with the one (240 g/cm²) obtained by Rossi, Sands, and Sard[2] and by Sands[3] for mesons of range smaller than 83 g/cm² of air equivalent. Since the mesons recorded with our apparatus had ranges between about 100 and 117 g/cm² of air equivalent, it does not seem possible to interpret the discrepancy between the results of the two experiments on the basis of the difference in the energies of the observed mesons.[43] It may be pointed out, instead, that due to the wide angle of the counter telescope employed by these authors, their data represent the altitude dependence of the *integrated intensity* rather than that of the *vertical intensity*,[32] whereas the opposite is true in the case of the present experiment. Although no information is available as yet concerning the dependence of the angular distribution of slow mesons on altitude, we shall expect a faster increase with altitude for the integrated intensity than for the vertical intensity. On the other hand, it should also be remembered

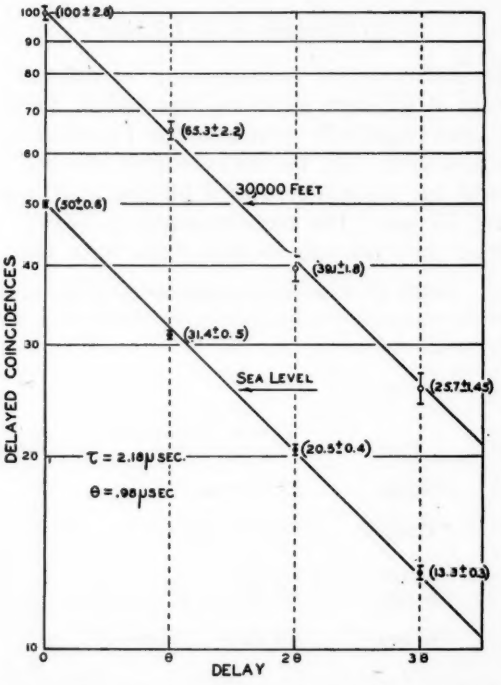

FIG. 7. Comparison between the decay curves obtained from measurements of delayed coincidences performed, with the same apparatus, at 30,000 feet (upper curve) and near sea level (lower curve). Ordinates are given in arbitrary units. The origin of the time scale is arbitrarily put in the first channel.

[43] Owing to the effect of the "time absorption" the rate of increase with altitude should become greater with decrease in the energy of the observed mesons.

that because of the rather large statistical errors, the measurements performed under different thicknesses of material by these authors give merely a rough indication that the rate of increase with altitude is the same for all mesons having range less than 83 g/cm².

The ordinates of Fig. 5 are given on an absolute scale based on the considerations reported in Section III F. By extrapolation of curve *m* in Fig. 5 *the absolute number of mesons at sea level traversing 6 in. of lead in the vertical direction* (approximately 100 g/cm² of air equivalent) and stopped by an additional g/cm² of graphite, is found to be about 5.2×10^{-6}/*sec.-g.-steradian*, in good agreement with the results obtained by other authors using different methods.[32,44]

Actually, curve *m* of Fig. 5 can be interpreted as giving at each altitude the absolute number of vertical ordinary mesons provided that the two following assumptions are correct: (a) mesons locally produced do not give any appreciable contribution to the registered delayed coincidences; (b) the possible change with altitude in the angular distribution of the observed mesons can be neglected for our apparatus. Due to the rather narrow angular definition of our counter telescope the latter of the two previous assumptions may be considered to be true with good approximation, if the former is true.

As to the first assumption we can argue as follows: if production of positive π-mesons by ionizing particles takes place in the 6 in. of lead between counters *A* and *B*, then some of the produced mesons could be stopped in the absorber and decay, in a time of the order of 10^{-8} sec.,[45] into ordinary mesons of very short range,[1] thus contributing to the observed rate of delayed coincidences. However, due to the recovery time (12.5 μsec.) of the pulse-forming circuit connected to the counters *C*, positive π-mesons stopped in the absorber can cause a delayed coincidence to occur only if they are not accompanied by other particles discharging counters *C*. The probability of a similar event appears to be quite small on the basis of an estimate of the average energy of the nucleons after the nuclear collision with meson production takes place. This seems to be true even allowing for the few cases in which nuclear events occur in the bottom of the lead and the nucleons are emitted under angles so as to miss the anticounters. Furthermore, penetrating showers which seem to be the typical events in which π-mesons of considerable energy are produced,[23] increase with altitude much faster than ordinary slow mesons.[46] Consequently, if local production of energetic π-mesons were responsible for part of the delayed coincidences registered by our apparatus, we would find in our case a faster increase with altitude than the one obtained without any lead by Rossi, Sands, and Sard.[2]

A contribution to the delayed coincidences could also be given by π-mesons produced in low energy nuclear events (star-like) taking place in the absorber or in the lowest centimeters of lead between counters *A* and *B*. Observations of photographic plates, however, show that only in a small percentage of the stars is there emission of π-mesons.[1] The number of stars, furthermore, is known to increase with altitude again much faster[47,48] than our delayed coincidences. It seems, therefore, that at least for altitudes of 30,000 feet or less[49] assumption (a) can be considered to be valid, with good approximation.

The determination of the altitude dependence of slow mesons may be used to obtain information about the production spectrum of mesons. This problem has been treated quantitatively by Sands,[3] with the assumption that mesons are created throughout the atmosphere by a primary component undergoing exponential absorption with an "absorption thickness" of 125 g/cm² of air. Qualitatively we can state here that our data indicate that the differential energy spectrum of mesons at production is even less abundant in low energy mesons than is indicated by the Sands results.

(C) *Positive Excess*

The rough indication of a disappearance of the positive excess at low energies previously reported[50] as given by the results of the sixth series in Table IX is not confirmed by the results of the first series, performed in Chicago after the end of the B-29 expeditions.

Although the percentage errors on the values of M_+/M_- are comparatively large in all series of measurements, the data of Table IX are consistent with the assumption that in the range of about 20 to 500 Mev, the excess of positive mesons is uniformly distributed in the differential spectrum near sea level.

For higher energies, instead, Brode[20] and Bassi, Clementel, Filosofo, and Puppi[51] have recently obtained an indication of an increase in the value of the positive excess. The experimental data mentioned above do not seem to agree with the theoretical prediction of Lewis, Oppenheimer, and Wouthuysen,[52] and of Heisenberg.[53] Indeed, according to these authors the positive excess should be inversely proportional to the square root of the meson energy at the point where mesons are created. If we assume that the mesons observed at sea level are the decay products of π-mesons produced essentially in the upper layers of the atmosphere, and if only

[44] W. L. Kraushaar, Phys. Rev. **76**, 1045 (1949). References to earlier literature will be found in this article.
[45] J. R. Richardson, Phys. Rev. **74**, 1720 (1948).
[46] J. Tinlot, Phys. Rev. **74**, 1137 (1948).
[47] Bernardini, Cortini, and Manfredini, Phys. Rev. **74**, 845 (1948); **74**, 1878 (1948).
[48] J. J. Lord and M. Schein, Phys. Rev. **75**, 1956 (1949).
[49] Our results indicate that between 30,000 and 36,000 feet the number of observed mesons increases faster than it does between sea level and 30,000 feet.
[50] See reference 24, p. 311.
[51] Bassi, Clementel, Filosofo, and Puppi, Phys. Rev. **76**, 854 (1949).
[52] Lewis, Oppenheimer, and Wouthuysen, Phys. Rev. **73**, 127 (1948).
[53] W. Heisenberg, Nature **164**, 65 (1949).

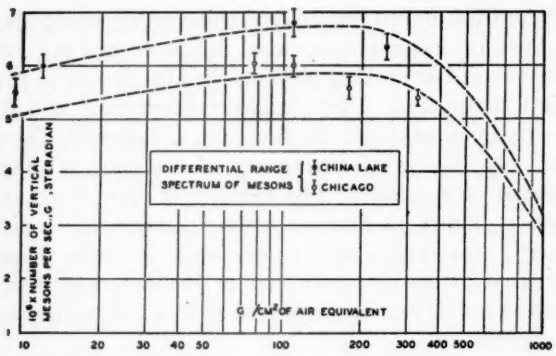
DIFFERENTIAL RANGE SPECTRUM OF MESONS
CHINA LAKE
CHICAGO
10⁴ × NUMBER OF VERTICAL MESONS PER SEC., G. /STERADIAN
G /CM² OF AIR EQUIVALENT
10 20 30 40 50 100 200 300 400 500 1000

FIG. 8. Differential range spectrum of mesons in Chicago and at China Lake.

energy-loss for ionization is taken into account, then the mesons observed by Brode[20] have an *initial* energy of about 3.7 Bev, whereas those observed in the experiment of Conversi and Nappo[39] have initial energy in the neighborhood of 2.4 Bev. According to the theory, the ratio M_+/M_- should be 0.96 smaller in the former than in the latter experiment. The experimental results yield instead, $(1.37\pm0.04)/(1.24\pm0.05)=1.10\pm0.055$ for the ratio of the two values of M_+/M_-.

It should be pointed out, however, that the various experimental data now available do not always appear to be quite consistent with one another. For instance, the dependence of the positive excess of the hard component at sea level upon the zenith angle, as obtained by Ballario, Benini, and Calamai[19] seems to be consistent with the theoretical predictions mentioned above,[54] while accurate cloud-chamber observations recently reported by J. G. Wilson at the Como Conference[55] do not appear to fit well with these predictions. On the other hand, the investigation of the energy dependence of the positive excess does not appear to be a very sensitive test for deciding whether "multiple" or "plural production" takes place in the upper layers of the atmosphere.[52–54, 56–61]

The results of the ninth series in Table IX give an indication of an increase in the value of the positive excess at 30,000 feet as compared to the sea level value. This result agrees with the findings of Quercia, Rispoli, and Sciuti,[18] although in their experiment the mesons were not separated from the other particles.

If local production of π-mesons gave some contribution to the delayed coincidences observed at 30,000 feet, this would cause the ratio given by Eq. (5) to increase, because negative π-mesons are presumably captured in both elements. It can be seen, indeed, from Eq. (5) and from the data at 30,000 feet reported in Table IX, that the positive excess of ordinary mesons at 30,000 feet would still be 20 percent, as near sea level, if 13 percent of the delayed coincidences registered with C absorber were due to positive π-mesons. However, as has already been pointed out, the local production of π-mesons should not give any serious contribution to our delayed coincidences. The result of the ninth series in Table IX gives therefore an *indication of an increase of the positive excess of low energy ordinary mesons with increasing altitude.*

(D) *Differential Range Spectrum*

From the data reported in the eight column of Table IX corresponding to measurements performed using a graphite absorber, we obtain five points of the differential range spectrum of mesons (positive and negative) in Chicago and three points at China Lake. These points are reported in a semilogarithmic plot in Fig. 8. The abscissa of each point represents approximately the *average* range of the observed mesons expressed in g/cm² of air equivalent. Conversion into g/cm² of air has been made using the calculations of Wick.[62] The ordinates of Fig. 8 are given in an absolute scale so that each point of the curve represents the number of vertical mesons per sec., cm², steradian, which are stopped by one g/cm² of air ($\approx$1 g/cm² of graphite) after traversing the thickness of air equivalent given by the abscissa.

The dotted curves in Fig. 8 reproduce (on an ordinate scale such as to obtain the best fit with our experimental points) the sea level differential range spectrum of mesons[63] as reported by Rossi[32] on the basis of most of the experimental data available. The results of Shamos and Levy[64] and those recently obtained by Kraushaar[44] are also in agreement with such a spectrum. At low energies, however, this spectrum gives a larger relative number of mesons than the Wilson spectrum.[65] The reason for the disagreement lies, perhaps, in the deversity of the two experimental methods; otherwise one should think that the range energy relationship for low energy mesons cannot be simply applied.

The absolute number of mesons at the end of their ranges, as given by the spectrum reported in Fig. 8, is about eight times as large as the number calculated by Rossi, Sands, and Sard on the basis of their measurements of delayed coincidences at sea level.[2] It is also partly than the number estimated on the basis of the observations of photographic plates made by Lattes, Occhialini, and Powell.[1] This latter discrepancy may

[54] G. Bernardini, Bristol Conference (1949).
[55] The author wishes to thank Drs. G. Bernardini and M. Schein for information on this matter.
[56] W. Heisenberg, Zeits. f. Physik **113**, 61 (1939).
[57] J. F. Carlson and M. Schein, Phys. Rev. **59**, 840 (1941).
[58] W. Heitler, Proc. Camb. Phil. Soc. **37**, 291 (1941). W. Heitler and H. W. Peng, Proc. Camb. Phil. Soc. **38**, 296 (1942). Hamilton, Heitler, and Peng, Phys. Rev. **64**, 78 (1943).
[59] L. Janossy, Phys. Rev. **64**, 345 (1943).
[60] W. Heitler, Proc. Roy. Irish Acad. **50**, 155 (1945). W. Heitler and P. Walsh, Rev. Mod. Phys. **17**, 252 (1945).
[61] W. Heitler and L. Janossy, Proc. Phys. Soc. **67**, 374 (1949).
[62] G. C. Wick, Nuovo Cimento **1**, 302 (1943).
[63] The elevation of China Lake is sufficiently low to justify the assumption that the shape of the meson spectrum is the same there as at sea level.
[64] M. H. Shamos and M. G. Levy, Phys. Rev. **73**, 1396 (1948).
[65] J. G. Wilson, Nature **158**, 415 (1946).

partly be accounted for in terms of the fading of the plates. The former discrepancy is due, at least in part, to the fact that the authors have overestimated the probability of detection of the decay electrons for their apparatus. If our finding is correct, therefore, the disagreement recently pointed out by Morpurgo,[66] between the expected and observed number of slow mesons at sea level, disappears. But the conclusion reached by him, namely, that no appreciable production of mesons occurs between sea level and 4000 meters, loses its validity. As a matter of fact, as was pointed out by Bernardini,[67] the assumption of an appreciable production of mesons in the lower layers of the atmosphere would yield a simple explanation of the discrepancy between direct measurements of the lifetime and the mass μ of the meson, and the determination of the ratio τ/μ by measurements of anomalous absorption.

The comparison between the results of Table III and those of Table VI concerned with the meson component shows that the number of delayed coincidences at 30,000 feet at the geomagnetic equator does not change appreciably by adding 4 in. of lead (above counters A) to the 6 in. of lead already present between counters A and B. This result agrees[68] with the momentum spectrum of negative mesons at 30,000 feet as reported by Adams, Anderson, and Cowan[5] if an analogous momentum distribution is assumed for the positive mesons and if we assume that the maximum of the spectrum does not shift considerably with latitude.

Part 2: The Nucleonic Component[69]

(E) *Identification of the X-particles*

We have previously defined the X-particles as those particles which are responsible for the anticoincidence rate corrected for the contribution of mesons. A few restrictions on the possible types of events appearing as X-particles have also been listed in Section IIIC. On the basis of the experimental results reported in Section III, we shall make an attempt now to identify the nature of the X-particles.

It must be pointed out first that no appreciable percentage of the observed anticoincidences can be due to electrons. In fact, it appears very unlikely that a large electronic shower, able to penetrate the 6 in. of lead interposed between counters A and B, could end in the absorber without striking any of the anticoincidence counters.

In addition, we may recall the discussion given above about the results concerned with the meson component. It has already been pointed out there that no serious contribution is given by locally produced π-mesons to the recorded delayed coincidences. For similar reasons we are led to exclude the possibility of a large contribution given to the anticoincidences by negative π-mesons locally produced and captured in the absorber.

If we assume that the X-component does not contain any appreciable amount either of electrons or of mesons, then the simplest interpretation as to its nature is that X-particles (which must be ionizing particles) are mainly protons coming from outer space. In fact, as appears from Fig. 5, the number of X-particles stopped in one gram of graphite at 30,000 feet is even larger than the corresponding number of ordinary mesons, and we cannot easily explain such an abundance of X-particles in terms of ionizing particles different than protons (electrons and mesons being excluded). If, instead, one assumes that X-particles are single protons coming from outer space, then one sees that in order to penetrate the 6 in. of lead placed between counters A and B and in order to be stopped in the graphite absorber they must have momentum in the range of 0.984 to 1.043 Bev/c if they lose energy *only* for ionization. From the data of Table VIII one finds, on the other hand, that the absolute number of these protons per sec., per cm^2, per steradian, per Mev/c of momentum, would be about 3.10^{-5} at 30,000 feet. From the results of the Anderson group at 30,000 feet,[6] Rossi estimates[32] that the number of protons with momentum between 0.4 and 1 Bev/c is of the order of 10^{-2}. This figure corresponds to about 1.7×10^{-5} protons per sec., per cm^2, per steradian, per Mev/c. The results of the two experiments are different by a factor of 1.8. However, owing to the difference in the angular definitions of the apparatus employed in the two experiments and considering also the uncertainty in the deduction of absolute intensities from cloud-chamber measurements, the two figures may be considered to be essentially in agreement.

The energy of the protons contributing to our anticoincidences cannot be less than 421 Mev if this figure correctly represents the energy lost by ionization in traversing 6 in. of lead. It could be higher, however, if we think that part of the anticoincidences may be produced by protons which, traversing the lead, give rise to nuclear events. We may recall, nevertheless, the conclusion reached in the discussion of the meson component and state that no large number of anticoincidences should occur when energetic nuclear events take place (in which mesons of considerable energy are produced). The energy involved in star-like nuclear events, which in general does not exceed a few tenths of a Bev, presumably represents, therefore, the uncertainty of the energy of the protons contributing to the observed anticoincidences.

The interpretation of the nature of the X-component in terms of protons is strengthened by the following arguments. (a) As shown by Fig. 4, at 30,000 feet the

[66] Morpurgo, Nuovo Cimento **5**, 285 (1948).
[67] G. Bernardini, Cracovie Conference (1947).
[68] Local production by neutral rays in the added 4 in. of lead should not affect appreciably the number of recorded delayed coincidences, for reasons similar to those discussed in Section IV B.
[69] The author wishes to thank Dr. G. Bernardini for valuable discussions on this topic.

intensity of the X-particles at 60° North geomagnetic latitude is about 3.2 times as large as the intensity at the equator. Such a large latitude effect as well as the shape of the latitude curve, are comparable to the results obtained, at the same altitude, on the neutron component[70] and on "bursts." [71] (b) As is shown by the curve x of Fig. 5, the dependence of the number of X-particles upon the atmospheric depth h may be approximately represented as $\exp(-h/L)$ with $L\approx 150$ g/cm². This result can be compared with those obtained for bursts[72–74] and for star-producing radiation.[47,48] Both of these arguments show that the bulk of the X-component is of nucleonic nature.

Primary protons (which are believed to represent the largest part of the primary component[75]) cannot contribute to the X-component observed at high altitudes because the energy of a proton stopped in the absorber after penetrating the atmosphere above, and the 6 in. of lead, is less than the energy corresponding to the magnetic cut-off at 50° (which is more than 2.5 Mev for the vertical direction), even allowing for a few tenths of a Bev corresponding to low energy nuclear events which may possibly take place in traversing the lead. It appears, therefore, reasonable to conclude that at least *most of the X-particles are secondary protons arising from energetic nuclear events which take place in the upper atmosphere.*

Additional points would be necessary for a more exact determination of the shape of curve x, which has been represented in Fig. 5 as an exponential. The number of protons at sea level obtained by extrapolation of such an exponential is likely to be in excess. It will be observed, indeed, that the experimental points reported in Fig. 5 for the X-component seem to indicate a greater rate of decrease with increasing atmospheric depth. As a matter of fact, the increase between 2100 and 22,500 feet corresponds to an "absorption thickness" $L\approx 130$ g/cm² of air, while between 22,500 and 36,000 feet $L\approx 220$ g/cm², assuming an exponential dependence in both intervals.

The lower rate of increase with increasing altitude suggests that the equilibrium between primary and secondary protons is not yet reached at an altitude as low as 30,000 feet. If this is the case, then by adding 10 cm of lead above the counter telescope the number of X-particles at 30,000 feet should not decrease by more than about 20 percent, even if the possible contribution due to nuclear events produced by neutral rays in the added lead is entirely neglected. Although performed at the geomagnetic equator (whereas curve x in Fig. 5 refers to 50° North), the measurements reported in Table VI yield some support to the previous view. Indeed, the comparison between these measurements and those taken near the equator and given in the Tables III and IV shows that within statistical errors no change in the number of X-particles is observed after adding 4 in. of lead above counters A.

(F) *Remarks on the Mechanism of Production of Mesons*

The comparison between the latitude effect of the X-component and that of the meson component clearly shows that X-particles are originated by primary cosmic rays considerably more sensitive to the magnetic field of the earth than those responsible for the production of the observed mesons.

We shall discuss this result briefly in an attempt to obtain some information as to the mechanism of production of mesons.

In a recent work by the Rome group[76] it has been shown that the behavior of the nucleonic component (as observed experimentally) can be satisfactorily described by assuming that the nucleons can be separated into three categories: (a) nucleons of very high energy (kinetic energy $E\gg Mc^2\approx 1$ Bev) which are absorbed essentially through radiative processes (high energy nuclear events involving meson production and correlated emission of secondary nucleons); (b) nucleons with E between 0.2 and 1 Bev, for which the absorption is assumed to be mainly due to nuclear evaporations (stars production) and roughly independent of E; (c) nucleons with $E<0.2$ Bev which lose their energy in one or two nuclear collisions and, if protons, by ionization. According to this scheme the total cross section of the nucleons is presumed first to decrease with decreasing energy E, afterwards to reach a broad minimum in the neighborhood of $\frac{1}{2}$ Bev, and then to increase. Thus, high energy nucleons quickly lose their energies and are brought into the energy region corresponding to category (b), where they are slowly absorbed because of the comparatively small value of the total cross section.

Since the protons observed with our apparatus as *X-particles* belong essentially to category (b), *a considerable part of them are presumably originated by primary nucleons of very high energy* ($E>10$ Bev) which have lost their energy in radiative collisions traversing the above atmosphere.

In the scheme of meson production as recently reported by Heitler and Janossy,[61] the total cross section for meson production at high energies E is independent of the energy E of the primary nucleon, while the average energy loss is proportional to E.[60,61] Consequently at high energies the average number of mesons produced by a primary nucleon traversing a certain thickness of air is independent of E while the average energy of the produced mesons increases with increasing E.

[70] J. A. Simpson, Jr., Phys. Rev. **73**, 1389 (1948).
[71] J. A. Simpson and R. B. Uretz, Phys. Rev. **76**, 569 (1949).
[72] H. Bridge and B. Rossi, Phys. Rev. **71**, 379 (1947).
[73] Bridge, Rossi, and Williams, Phys. Rev. **72**, 257 (1947).
[74] H. E. Tatel and J. A. Van Allen, Phys. Rev. **73**, 87 (1948).
[75] Schein, Jesse, and Wollan, Phys. Rev. **59**, 615 (1941). Schein, Iona, and Tabin, Phys. Rev. **64**, 253 (1943).
[76] B. Ferretti, Nuovo Cimento **6** (September, 1949); Bernardini, Cortini, Ferretti, and Manfredini (to be published).

Since the energy of a meson produced at the top of the atmosphere and stopped in our absorber[77] is about 0.8 Bev, *no considerable part of the observed delayed coincidences should be due to mesons produced by primary nucleons of very high energy* ($E>10$ Bev).[78]

It follows that the latitude effect of the mesons observed with our apparatus should be larger than the latitude effect of the X-component, in contradiction to the experimental results. The discrepancy seems to disappear in the scheme of a "multiple meson production." In this case, indeed, the "multiplicity" of the created mesons is an increasing function of the energy of the primary nucleons, and this, at least qualitatively, could account for the smaller latitude effect of the meson component as compared to the one of the X-component.

Some further support to the view of a multiple production of mesons seems to be given by the comparison between the altitude dependence of the mesons observed in the present research and the altitude dependence of very slow mesons as obtained by Bernardini, Cortini, and Manfredini[47] and by Lord and Schein.[48] This comparison shows, in fact, that at high altitudes a large number of mesons are produced with very low energies. At the same time, the results obtained by these authors show that the ratio between the numbers of mesons and stars increases strongly with altitude. Hence it appears that no large contribution to the number of slow mesons thus observed is caused by nuclear evaporations. It seems, therefore, that with increasing altitude the meson spectrum undergoes a change due to the increasing contribution of very slow mesons which are largely produced by primary rays. As has been pointed out by Bernardini *et al.*,[47] such a change appears to be understandable in the scheme of the multiple production, but not easily understandable in the one of the plural production.

V. CONCLUSIONS

The results of the experiments reported in this paper can be summarized as follows:

(a) The differential range spectrum of mesons near sea level is nearly flat in the interval 10 to 200 g/cm² of air equivalent, in agreement with some recent findings of other authors.

(b) The assumption of a positive excess of sea level mesons *uniformly* distributed in the differential spectrum is consistent with our results for energies between about 20 and 500 Mev.

(c) The absolute number of vertical mesons at sea level having ranges in the neighborhood of 100 g/cm² of air is 5.2×10^{-6} per sec., per g, per sterad., in good agreement with other recent results.

(d) Within the statistical uncertainty of a few percent, the lifetime of the observed mesons is the same at 30,000 feet as at sea level, and is equal to about 2.15 μsec.

(e) Between 36,000 feet and sea level the number of ordinary mesons having ranges in the neighborhood of 100 g/cm² of air decreases with the atmospheric depth h, as $\exp(-h/L)$ with $L\approx280$ g/cm².

(f) Between the geomagnetic equator and 60° N. the number of ordinary mesons present at 30,000 feet with ranges in the neighborhood of 100 g/cm² increases to about 1.9 ± 0.14.

(g) The positive excess of ordinary mesons having ranges in the neighborhood of 100 g/cm² seems to increase by a factor of 2 between sea level and 30,000 feet.

(h) At high altitudes a considerable number of ionizing particles (X) different from mesons are found to stop after traversing 6 in. of lead. While at sea level these particles are present in negligible amounts (if at all), at 30,000 feet their absolute number is found to be nearly 10^{-4} per sec., per g, per sterad., namely, 1.6 times the corresponding absolute number of ordinary mesons.

(i) The rate of increase in the number of X-particles seems to decrease with increasing altitude. If an exponential absorption is assumed for the X-particles between 2100 and 36,000 feet one obtains an "average absorption thickness" of about 150 g/cm² of air.

(j) Between the geomagnetic equator and 60° N. the number of X-particles present at 30,000 feet increases to 3.2 ± 0.5.

(k) A comparison between the results of this research and the results of other authors leads to the conclusion that the X-particles are mainly secondary protons of energy in the neighborhood of 0.5 Bev rising from energetic nuclear events which take place in the upper atmosphere. Their altitude dependence indicates then that the equilibrium between primary and secondary protons is not yet reached at an altitude as low as 30,000 feet.

(l) The comparison between the latitude effects of the mesons and of the X-particles at 30,000 feet, as well as the comparison between the altitude dependences of the mesons detected in our experiment and of the very slow mesons observed on photographic plates, seem to give support to the view that "multiple" rather than "plural" production of mesons takes place in the upper layers of the atmosphere.

VI. ACKNOWLEDGMENTS

The author is indebted to Dr. Samuel K. Allison for granting him a post-Ph.D. fellowship at the Institute for Nuclear Studies and for the many facilities that made this research possible. He wishes also to express

[77] According to current ideas the meson produced is a π-meson which afterwards decays in flight into a μ-meson. For the following discussion we may as well neglect the distinction between the initial π-mesons and the secondary μ-mesons thus simplifying our language.

[78] According to the recent paper by Heitler and Janossy (reference 61) the average number of effective collisions after which a primary nucleon becomes ineffective for meson production is about two. Thus, the average energy of a primary proton producing at its second collision the meson observed by our apparatus should not be much larger than a few Bev.

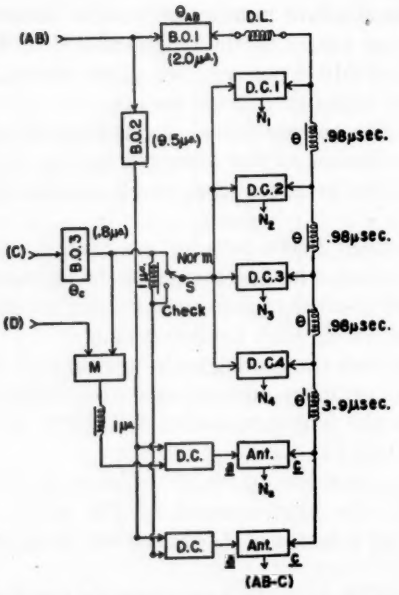

FIG. 9. Block diagram of the registering set. *Ant*: anticoincidence circuits; *BO*: pulse forming "blocking oscillator" circuits; *D.C.*: double coincidence circuits; *DL*, θ and θ': delay lines; *M*: crystal diode mixers; *S*: switch. Pulses are positive in all points except at the outputs of the anticoincidence circuits, where they are positive only when "anticoincidence events" take place. By setting short delay lines θ (0.1 or 0.2 μsec. instead of 0.98 μsec.) and for suitable values of *DL*, several points of the integral time distribution curve of the spurious delays of the counters can be quickly obtained. The flexion point of this curve yields the "zero" of the absolute time scale (reference 80). The points of the curve corresponding to the shortest delays are obtained with the switch *S* in "check position."

his warm thanks to Dr. Marcel Schein for the cordial hospitality in the Cosmic Ray Laboratory of the University of Chicago and for numerous discussions.

He is grateful to Mr. Clement S. Mokstad of the Institute for his invaluable help in handling the administrative problems.

The cooperation of Mr. Charles L. D'Ooge and the generous assistance of Mr. Bruce Jackson at the military base at China Lake are deeply appreciated.

The author wishes to express his gratitude to the men who flew the B-29, in particular to Major W. A. Gustafson, for their cooperation during the entire period of the flight and for their skillful handling of the plane.

It is also a pleasure to thank Mr. Ivar Kalberg for his assistance in assembling the apparatus and Mr. David M. Haskin for the preparation of the Geiger-Müller counters.

APPENDIX A

The Registering Set

The simultaneous registration of delayed coincidences and anticoincidences was obtained by means of an electronic apparatus of which the main parts were connected as is schematically represented in Fig. 9.

As stated in Section II, the output pulse corresponding to a coincidence (AB) starts 0.7 μsec. after the time of occurrence of the earliest of the two counter pulses producing the coincidence, provided that both pulses occur within 0.7 μsec. of one another. Therefore a particle entering the counter telescope and producing a coincidence (AB) causes both circuits B.O.1 and B.O.2 to be triggered 0.7 μsec. later.[79] The square pulse, θ_{AB}, from the output of B.O.1, is fed into a series of continuous delay lines terminating, at the c-inputs of the two anticoincidence circuits, on their characteristic impedances. Thus, if the switch S is in the "normal position" (Fig. 9) and θ_0 is the value of the proper delay of the interchangeable delay-line, D.L., plus 0.7 μsec., the pulse θ_{AB} will start at the inputs (on the right side of Fig. 9) of D.C.1, D.C.2, ···D.C.4, respectively, θ_0, θ_0 plus θ, ···θ_0 plus 3θ, after the arrival of a particle producing a coincidence (AB). The square pulse, θ_c, from the output of B.O.3 will give, therefore, a coincidence in D.C.1 (1st "channel") with the pulse θ_{AB} corresponding to a particle entering the telescope at the instant zero, only if counters C fire within the time interval $\theta_0-\theta_c$ to $\theta_0+\theta_{AB}$, or θ_m to $\theta_m+\Delta\theta$, where $\theta_m=\theta_0-\theta_c$ and $\Delta\theta=\theta_{AB}+\theta_c$. Similarly a coincidence will be registered by the second, . . . fourth channels, only if counters C fire within the time interval $(\theta_m+\theta)$ to $(\theta_m+\theta)+\Delta\theta$, ···$(\theta_m+3\theta)$ to $(\theta_m+3\theta)+\Delta\theta$, respectively. In this way four points of the decay curve corresponding to the mesons stopped in the absorber are obtained simultaneously.

Both pulse-forming circuits B.O.1 and B.O.2 are "blocking oscillators" controlled by delay lines. The time width $\Delta\theta=\theta_{AB}+\theta_C$ of the channels is therefore dependent only on the proper delay of these lines and no variation of its value can be expected to occur. Similarly no variation of the time distance, θ, between each channel and the next one can be expected.

The value θ_m of the minimum delay for which a coincidence is recorded in the first channel, has been determined by the method explained in a previous paper.[80]

APPENDIX B

Correction for the Spurious Delays Due to the Counter Discharge

The spurious delays associated with the counter discharge depend essentially on the position where the first ion pair is produced. More precisely, the rise time of the counter pulse (which is related to the propagation of the discharge along the wire after the first avalanche takes place) depends on the "axial coordinate" of the point where the first ion pair is produced;[81] the proper time lags, instead (which presumably represent the interval between the formation of the first ion pair and of the first avalanche) depend on the "radial coordinate." [82] Of these delays the former may be minimized by increasing the sensitivity of the input circuits; the latter by using counters of small radii;[83] both by operating the counter at the highest possible voltage.[84] In the present experiment, where events corresponding to delays shorter than 1.15 μsec. have not been recorded, the use of counters of 2 in. outer diameter, in a double layer, has still been possible. Nevertheless counters, previously selected, had to be operated at the upper limit of their plateau. Even in these conditions a contribution of spurious coincidences in the first channel is observed, but only in the measurements taken at high altitude. The appearance of this contribution at high altitude must be related to the increased background counting rate[85] of the counters C and can be qualitatively explained as follows.

---

[79] In the following, delays due to the counter tubes and proper delays of the circuits are neglected. Furthermore, pulses θ_{AB} and θ_c (the same symbols are also used for the time-widths of these pulses) are supposed to be literally "square pulses."

[80] M. Conversi and O. Piccioni, Phys. Rev. **70**, 874 (1946).

[81] Alder, Baldinger, Hubber, and Metzger, Helv. Phys. Acta **20**, 73 (1947).

[82] C. W. Sherwin, Rev. Sci. Inst. **19**, 111 (1948).

[83] Den Hartog, Muller, and Vester, Physica **13**, 251 (1947).

[84] D. R. Corson and R. R. Wilson, Rev. Sci. Inst. **19**, 207 (1948). This article also gives references to other literature.

[85] As a matter of fact, measurements taken in Chicago irradiating counters C so as to reproduce artificially the background

If a particle discharges a certain counter C_0 of the C tray at the zero time, the probability that another particle traverses the counter telescope and C_0 in the time interval (of some hundred μsec.) between the dead-time and the recovery-time of C_0, becomes quite appreciable (several percent) when the background counting rate of C_0 is as large as at high altitude (of the order of 100/sec. at 36,000 feet). If such an event takes place, then the size of the second pulse given by C_0 will be smaller than usual and a spurious delay may occasionally occur because of the finite value of the sensitivity of the input circuit triggered by C_0. By using a double layer of counters C the probability of such an event is considerably reduced. But of course even if the probability of a spurious delay larger than 1.15 μsec. (θ_m) is only a fraction of one percent, the percentage of spurious delays in the first channel can still be quite considerable, since the number of mesons contributing to the coincidences in the first channel is not much more than one percent of the number of particles producing prompt coincidences (ABC).

The correction for the spurious delays of the counters can be evaluated using the results of measurements performed without absorber. In 465 minutes of measurements taken without absorber at 30,000 feet (including both expeditions) the numbers of coincidences registered in the four channels were respectively 134, 80, 66, 53. By using Eq. (1) and the average counting rates $n_{(AB-C)}$, $n_{(c)}$ as measured in flight, it is found that the corresponding number of random coincidences in each channel was about 43. Correcting for this it can be observed, first, that the point corresponding to the first channel falls off from the 2.2 μsec. decay curve passing for the three points corresponding to the remaining channels. Furthermore, the counting rate of the first channel is $(N_1)_0=(11.7\pm1.23)$ per hour, while the corresponding average counting rate, $(N_1)_C$, with graphite absorber (as deduced from the data reported in Table III) is $(N_1)_C=(42\pm1.35)$ per hour. The ratio $(N_1)_0/(N_1)_c$ is so found[86] to be 0.28 ± 0.028 whereas the value 0.17 ± 0.011 is obtained for the same ratio near sea level from the data reported in Table I.[87] Since only positive mesons (disintegrating in the brass of the counters and of the frame) contribute to the delayed coincidences registered without absorber, and since the ratio of negative to positive mesons seems to decrease from 0.81 to 0.65 between sea level and 30,000 feet (see Table IX), we would expect for this ratio at 30,000 feet the value $(1.81/1.65)(0.17\pm0.011)=0.185\pm0.012$, which is still considerably less than 0.28 ± 0.028.

It is reasonable to assume that the excess of coincidences registered in the first channel at 30,000 feet is caused, through the mechanism previously sketched, by the spurious delays associated with the counter discharge. Then, by assuming equal numbers of spurious delays with and without absorber, one finds that the corrected number of delayed coincidences with graphite absorber, registered in the first channel, is given by

$$(N_1)_{corr}=\frac{1-0.28}{1-0.185}(N_1)_c=0.885(N_1)_c, \tag{9}$$

where $(N_1)_c$ represents the number of coincidences, corrected only for the random events, registered in the first channel with the absorber on.

Since the number of spurious delays due to the discharge of the G-M counters is proportional to the "prompt" coincidences (ABC), the percentage of these spurious coincidence is larger with S absorber where the number of "true" delayed coincidences is smaller than in C. Taking into account the difference between the values of the positive excess of mesons near sea level and at 30,000 feet, as suggested by a first analysis of the data reported in Table IX, one finds that in the case of S absorber, 0.81 must be substituted to 0.885 in the previous equation.

These corrections have been applied disregarding their statistical uncertainties. The fact has also been neglected that because of the different latitude dependence of the stopped mesons and of the total hard component (which is proportional to the number of spurious delays) the corrections themselves are latitude dependent.[88] Furthermore, the same correction has been applied to the results of the one flight undertaken at 36,000 feet.

APPENDIX C

Spurious Anticoincidences

Due to the geometry of the apparatus and to the small amount of material represented by the absorber, it appears very improbable that a lateral shower which in the absence of the absorber would strike some of the "anticounters" does produce an anticoincidence when the absorber is on. For the same reasons it seems also rather unlikely that a low energy particle, which otherwise would be stopped in the absorber, is scattered near the bottom of the lead, in such a way as to traverse counters B but none of the "anticounters," thus giving rise to an anticoincidence independently of the presence of the absorber. All other causes of spurious anticoincidences (such as inefficiency of the counters, random events, etc.) are not appreciably affected by the presence of the absorber.

On the basis of these considerations we have assumed that the counting rate of the anticoincidences registered without absorber yields the number of spurious events which must be subtracted from the anticoincidences registered with absorber in order to obtain the number of "true anticoincidences."

counting rate found at 30,000 feet have shown an appreciable increase in the spread of the time distribution curve of the spurious delays.

[86] Measurements with and without an absorber have been continuously alternated in flight. $(N_1)_0$ and $(N_1)_c$ refer, therefore, approximately to the same average geomagnetic latitude (about 35° N).

[87] Series No. 3 in Table I also includes measurements taken under amounts of material different from those of Series No. 1 and 2, but less than 300 g/cm² of air equivalent. Since the low range end of the differential meson spectrum at Chicago is nearly flat, the previous ratio may be assumed to be given by the ratio between the value of N_0 given by the last column of Table I and the average value $N_c=6.8\pm0.15$, deduced from the combined data of the two other series.

[88] If the ratio of the intensities between 60° N and the geomagnetic equator is 1.9 for the stopped mesons and 1.6 for the total hard component [see Biehl, Neher, and Roesch, Phys. Rev. 76, 914 (1949), as well as D. J. X. Montgomery, *Cosmic Ray Physics* (Princeton University Press, Princeton, 1949)] the corrections increase from 1 to about 1.2 in going from 60° N to the equator.

Cascades of Nuclear Disintegrations Induced by the Cosmic Radiation*

G. Cocconi, V. Cocconi Tongiorgi, and M. Widgoff
Laboratory of Nuclear Studies, Cornell University, Ithaca, New York

(Received April 3, 1950)

Energetic nuclear disintegrations induced by the N-component of the cosmic radiation have been studied by detection of the moderate energy neutrons released in the disintegrations themselves.

The pulses of the neutron counters appeared on the sweep of a cathode-ray tube. A hodoscope of neon bulbs connected to an arrangement of G-M counters was simultaneously used to study the relative number of neutral and charged primaries and the penetration of the ionizing particles produced in the disintegrations.

Lifetime, angular distribution, and average energy of the neutrons have been investigated. The multiplicities of the neutrons produced in absorbers of different thickness and material have been determined. Evidence has been derived of the existence of conspicuous cascades of nuclear disintegrations.

A tentative analysis of the nuclear cascade process is given.

I. INTRODUCTION

IT has recently become more and more evident that in energetic nuclear interactions particles can be produced which are capable of inducing further nuclear processes, hence of causing a cascade-like development of nuclear events. This has been borne out principally by the analysis of cloud-chamber pictures and of photographic plates in which successive correlated events were recorded.

The experiment we are going to describe is an attempt at obtaining quantitative information about the nuclear cascade process by using the neutrons released in the nuclear disintegrations as indicators of the disintegrations themselves. The justification of this method can be found in the following arguments.

The interpretation of stars of heavily ionizing particles as nuclear evaporations implies the assumption that neutrons of moderate energies[1] are emitted from the excited nuclei along with the ionizing particles observed in these low energy events.

The fact that moderate energy neutrons have been recorded in coincidence with penetrating showers,[2] as well as the fact that many cloud-chamber pictures of penetrating showers show heavily ionizing tracks either at the origin or in the development of the showers, indicates that neutrons of moderate energies are boiled off from the nuclei also when high energy events take place.

Since electron sensitive plates have been introduced to study nuclear events, practically all nuclear disintegrations showing showers of particles at minimum ionization have been found to be accompanied by heavily ionizing particles.[3]

The experimental evidence finds easy interpretation as high energy interactions are expected to leave the nucleus generally in an excited state. The neutrons of moderate energy and the charged particles capable of crossing the potential barrier are then the products of evaporation of the excited nucleus, hence the by-products of the main reaction among the fast particles.

These arguments lead one to infer that *all nuclear disintegrations induced by the cosmic radiation, whatever the energy involved in the process, release a number of neutrons of moderate energies, produced by nuclear evaporation. If a nuclear cascade occurs, neutrons of moderate energy are produced in each step of its development.*

The method has two main advantages.

(1) It can give information about the development of the nuclear processes *inside the detector* as the neutrons produced both in the primary and in secondary events have a large probability of emerging from the absorber. This is due to the fact that the absorbers commonly used, Pb, Al, and C, have very small cross sections for neutron capture.

(2) It allows the selection of nuclear events in a rather unbiased manner. In fact, the average energy and the angular distribution of the neutrons released in nuclear evaporations probably do not depend strongly on the energy and the nature of the process that excited the nucleus. The number of neutrons released will depend on these factors and a variation in neutron multiplicity will cause a variation in the probability of recording the events. However, this bias is removed by the possibility of determining the probability of recording all events as a function of the number of neutrons produced. This is not easily possible when detecting events by means of the charged products of the disintegrations.

The detection of nuclear disintegrations through the neutrons released in them has the disadvantage that the efficiency for neutron detection is necessarily small. However, this trouble is overcome in part, at least in absorbers of high atomic number, by the fact that the neutrons are produced with a rather high multiplicity.

II. EXPERIMENTAL

The experiment was performed at Echo Lake, Colorado (3260 m altitude, 708 g/cm^2 average pressure), during the summer of 1949.

The arrangement used is sketched in Fig. 1. Trays a, b, c, and d consisted of G-M counters, whereas trays A, B, C, and D consisted of BF_3 proportional counters.

The events studied were those occurring in the absorber Σ; the absorber S was used in part of the ex-

* The cost of instrumentation of this work was supported by the ONR.

[1] We shall call "neutrons of moderate energy" the particles with energies between about 0.5 and 50 Mev. Particles having energies above 50 Mev will be called "high energy," or "fast" neutrons.

[2] Cocconi, Tongiorgi, and Greisen, Phys. Rev. **74**, 1867 (1948).

[3] See, e.g., Kaplon, Peters, and Bradt, Phys. Rev. **76**, 1735 (1949).

periment to study the penetration of the ionizing particles produced in the nuclear disintegrations.

The large paraffin block (38×26×26 in.) in which the BF_3 counters were embedded served the purpose of slowing the neutrons of moderate energy down to thermal energies.

Trays *a*, *c*, and *d* consisted, respectively, of 23, 20, and 20 G-M counters, each of 1×16 in. effective surface. Tray *b* consisted of 24 G-M counters, each ½×10 in. The solid angle defined by trays *b* and *c* was mostly covered by the counters in tray *a*.

Three G-M counters, *s*, each 2×40 in., were located around the system at the vertices of a triangle of 3-m sides and were used as monitors for extensive showers. They facilitated the selection of the events associated with extensive showers of high local density, which were disregarded.

The BF_3 proportional counters in *A* and *D* had 1×20 in. effective area; those in *B* and *C* were somewhat shorter (1×18 in.). All of them were filled with BF_3 (96 percent B^{10}) at 1.5 atmos. They were constructed and operated as described in a previous paper.[4]

In the course of the experiment data were taken with the neutron counters connected in two ways: In one, which we shall call hereafter "up-down connection," the 10 counters *A* and *B* were connected in parallel and their pulses fed into an amplifier, N_1. A second amplifier, N_2, was connected to the counters *C* and *D* similarly connected in parallel. In the other case, which we shall call "close-far connection," the 10 counters *B* and *C* were connected in parallel and their pulses fed into the amplifier N_1, whereas the pulses of *A* and *D* were fed into N_2.

A master pulse, *MP*, was generated whenever a coincidence between trays *b* and *c* was accompanied by at least one pulse in any of the 20 BF_3 counters, occurring between 5 and 15 μsec. after the coincidence *bc* happened ($MP=bc, N$). This was realized by shaping the coincidences (b, c) in a 10-μsec. square pulse, delayed 5 μsec. The delay was introduced to remove the possibility of spurious *MP*'s due to pulses in the BF_3 counters caused by particles different from neutrons, released in the disintegration itself (slow protons, bursts of electrons, etc.).

The frequency of MP's due to chance coincidences has been evaluated as about 4 $hr.^{-1}$, while the frequencies of the recorded events ranged between 13 and 70 $hr.^{-1}$, depending on the thickness and nature of the absorber.

The requirement of the coincidence (bc, N) implies the presence of at least one ionizing particle emerging from the absorber, capable of crossing at least 22 g/cm^2 of paraffin (minimum energy for a proton ~170 Mev, for a meson ~75 Mev). This rules out a large number of events of low energy and makes our system sensitive to rather energetic nuclear interactions, with very little requirement about angular distribution and number of ionizing particles produced in these.

We think that no important fraction of the recorded events, chance coincidences subtracted, can be due to known processes other than the nuclear interactions which we intended to study. In fact, no contribution can arise from the capture in the absorber of negative μ-mesons, as no penetrating ionizing particles are emitted in such a process along with the neutrons. Spurious events could be produced by neutrons generated by photons through (γ, n) reactions, if associated ionizing particles capable of producing a coincidence (b, c) are also present. This may be the case, when a μ-meson gives rise to a burst in the absorber Σ. Levinger[5] has calculated that a photon of 10^{10} ev completely absorbed in lead can produce, on the average, about two neutrons. The rate of bursts of energies greater than 10^{10} ev produced in the thickest absorber Σ we used (4½-in. Pb, surface 1160 cm^2) can be expected to be around 0.2 $hr.^{-1}$, on the basis of results by Hudson.[6] As the rate of the events recorded with the same absorber is ~55 $hr.^{-1}$, the contribution due to meson bursts is negligible. Also small, in our opinion, is the background due to cascades produced by incident electrons and photons. In fact, only electrons and photons of very high energies have an appreciable probability of giving rise to an event capable of generating a *MP*. These are very rare, and they will probably fall on the apparatus accompanied by other electrons, in which case the events will be classified as due to "air showers," hence disregarded. It is, finally, important to point out that if an appreciable background is due to events of the kinds listed above, it must be confined essentially to the category of pictures showing a single neutron pulse, which have been disregarded in most of the discussions presented in this paper.

Whenever a *MP* occurred, a camera was triggered which took a picture of the following objects:

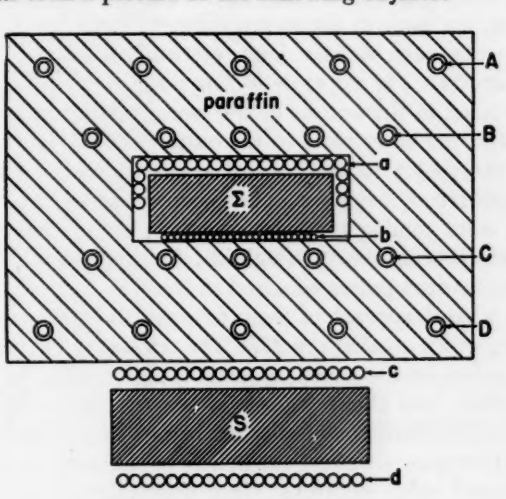

FIG. 1. Experimental arrangement.

[4] V. Cocconi Tongiorgi, Phys. Rev. **75**, 1532 (1949).

[5] J. Levinger, Nucleonics **6**, No. 5, 64 (1950).

[6] D. Hudson, thesis, Cornell University.

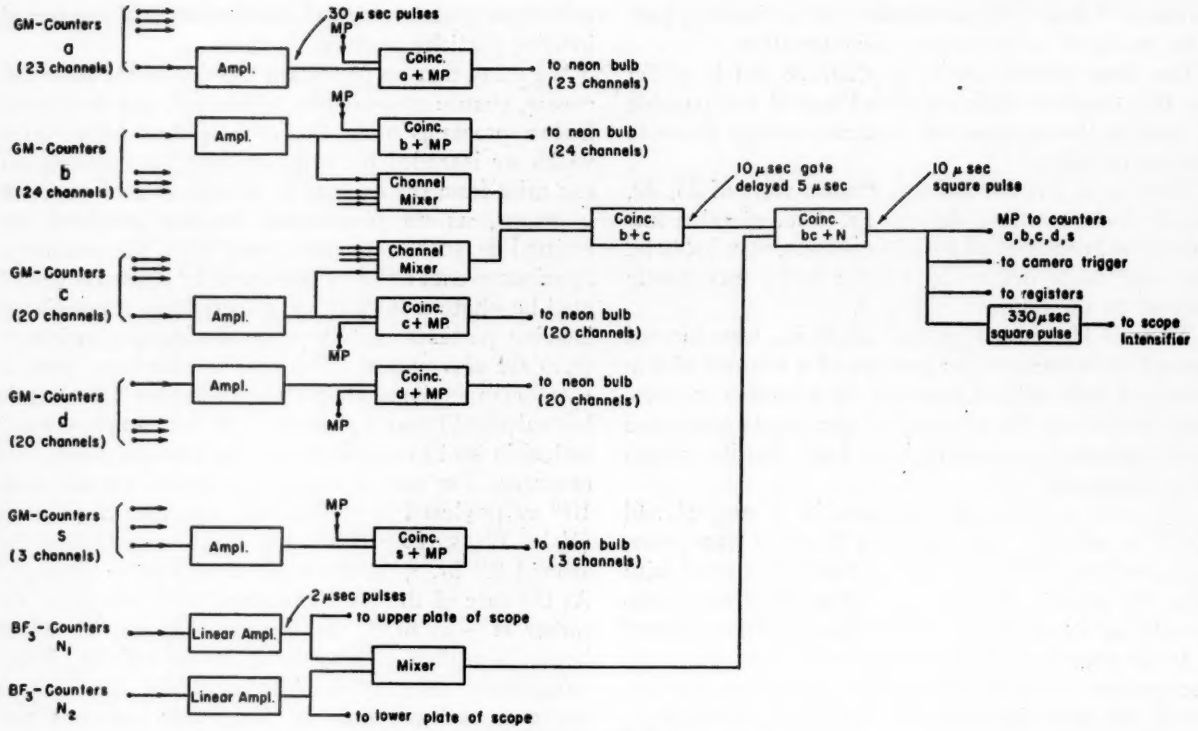

FIG. 2. Block diagram of the circuit.

(a) a mechanical register which numbered the pictures, and worked in parallel with another register located outside the camera box,

(b) a hodoscope of neon bulbs, each connected to one of the 90 G-M counters in trays *a*, *b*, *c*, *d*, and *s*, through a circuit that lighted the neon bulbs only when a pulse from the individual counter was followed within 30 μsec. by a *MP*;

(c) a five-in. cathode-ray tube (5*RP*-11, 5000 v accelerating potential), in which a linear sweep 330 μsec. long was started by the *MP*. To improve the time resolution, the path of the sweep followed eight horizontal saw teeth, each 40 μsec. long, vertically displaced from one another. The upper deflecting plate of the *CRT* was connected to the output of the neutron pulse amplifier N_1, and the lower plate to the output of N_2. Hence the neutron pulses (2 μsec. wide) appeared on the sweep as positive or negative pulses, depending on whether they were coming from amplifiers N_1 or N_2. We have therefore been able to establish, for each event, how many neutron pulses occurred in the BF_3 counters and with what delay each of them followed the first neutron pulse, which created the *MP*. The resolution in time of the pulses on the sweep, essentially determined by the amplifier, was about 1 μsec. It is worth pointing out that the occurrence of a pulse in one of the neutron counters does not affect the ability of the same counter to record other neutrons, since proportional counters have no deadtime, and the different pulses due to slowed-down neutrons are not likely to be simultaneous.

A block diagram of the circuit is given in Fig. 2.

Examples of the pictures obtained are presented in Figs. 3(a) and 4(a). These pictures are taken from the series of measurements made with $\Sigma=4\frac{1}{2}$-in. Pb and $S=0$. The BF_3 counters were in the up-down connection.

In the course of the experiment, approximately 30,000 pictures were taken, Each of these has been transferred to a card, as shown by the examples given in Figs. 3(b) and 4(b).

It is obvious that the neutrons observed are not all of the neutrons created in the interactions, but only those which our neutron detector, with its limited efficiency, could record. Our detector is sensitive to neutrons with energies between ~1 and ~15 Mev. In this energy range, its efficiency, E, for recording a neutron is given by:

$$E=\eta\cdot\alpha\cdot(\omega/4\pi)\cdot k,$$

where η is the probability that a thermal neutron entering a counter gives rise there to a pulse; α is the probability that a neutron is slowed down to thermal energies in the neighborhood of the counters and enters one of them; $\omega/4\pi$ is the probability that a neutron is produced in the useful solid angle (with the assumption of isotropic distribution of the neutrons emerging from Σ, see Section IV) and k is the probability that the pulse from the neutron counter occurs within the time interval determined by the circuit.

We have estimated $\eta\approx0.3$, $\omega/4\pi\approx0.8$, $\alpha\approx0.15$ for neutrons of energies between 1 and 15 Mev and our

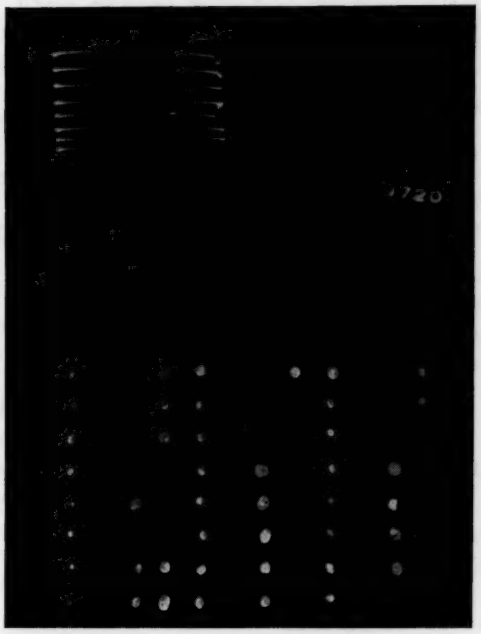

(a)

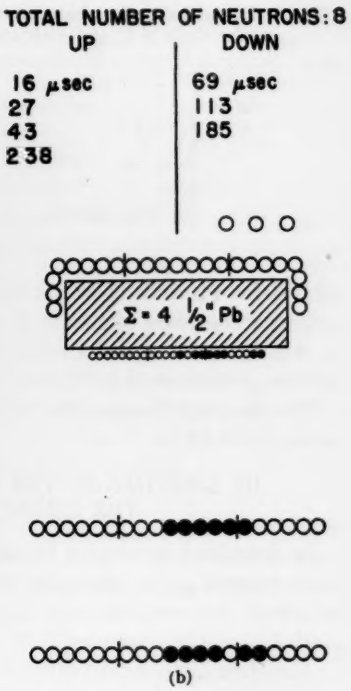

(b)

FIG. 3. Example of a picture (a) and a card (b) of a shower probably produced by a neutral primary. One neutron is required to trigger the sweep of the *CRT*, 7 neutron pulses are visible on the sweep. No neon bulbs are lit in columns 1, 2, and 3 of the hodoscope, which are connected to the counters in tray *a*. The bulbs in columns 4, 8, and 12 are always lit to provide fiducial marks. The bulbs in column 5, 6, and 7 are connected to tray *b*; 9, 10, and 11 to tray *c*; and 13, 14, and 15 to tray *d*.

20 BF_3 counters, hence in our apparatus we have $\eta\cdot\alpha\cdot\omega/4\pi\approx 0.04$. An experimental determination of this product has been made by measuring the counts produced in our BF_3 counter arrangement by a calibrated 1 mC (Ra+Be) neutron source. The result was 0.037. The fair agreement with our estimate must be taken with the reservation that the energy spectra of the neutrons released from the (Ra+Be) source and from the evaporation processes in the nuclei may be somewhat different.

Assuming a lifetime $\tau=155$ μsec. for the neutrons in our detector (see Section III), one has:

$$k=\int_5^{340} e^{-t/155}(dt/155)\approx 0.85.$$

Combining these results, we shall assume hereafter $E=0.03$. We attribute to this figure an uncertainty of ~30 percent.

The absorbers used in Σ were as follows: $\Sigma=0$, $\frac{1}{4}$-, 1-

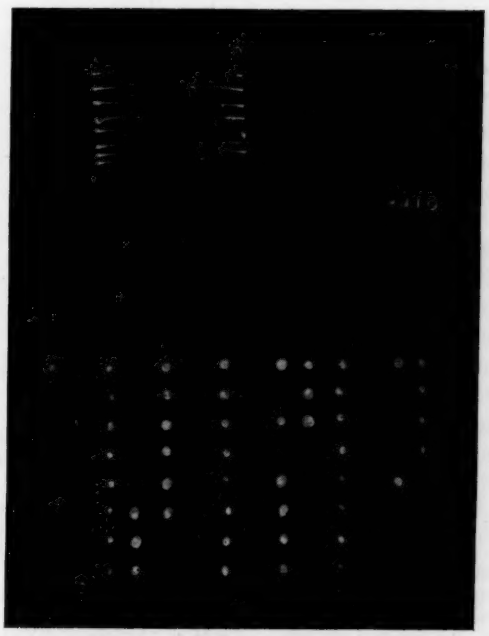

(a)

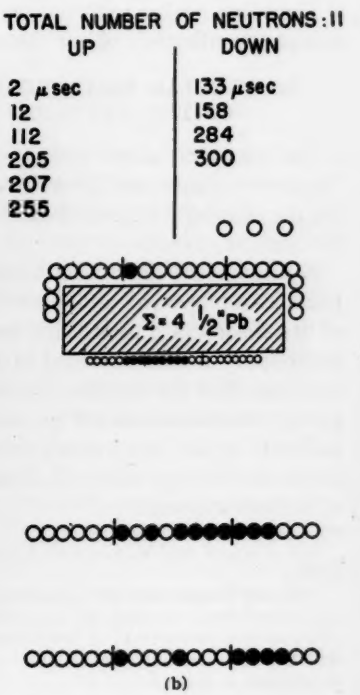

(b)

FIG. 4. Example of a picture (a) and a card (b) of a shower probably produced by an ionizing primary.

TABLE I. Ratio *close/far*, for neutrons observed with various absorbers in Σ, and with a (Ra+Be) source.

Σ	*C/F*
4½-in. Pb	4.1 ±0.3
1-in. Pb	3.8 ±0.3
¼-in. Pb	3.5 ±0.5
4¾-in. Al	3.4 ±0.6
(Ra+Be) source	4.35±0.2

and 4½-in. Pb and 4¾-in. Al. The ¼- and 1-in. Pb absorbers were made of sheets $\frac{1}{16}$ in. each, evenly spaced in the 4½ in. occupied by the thickest absorber. The surface of the absorbers Σ was always 15×12 in.

The absorber S was either $S=0$ or $S=6$-in. Pb, with surface 21×18 in.

III. LIFETIME OF THE NEUTRONS IN THE DETECTOR

As described in Section II, the time of occurrence of each neutron pulse, assuming as time zero the instant in which the neutron that started the *MP* was recorded, could be measured with an accuracy of ±3 μsec.

The time distribution of 3100 neutron pulses is given in Fig. 5. Only pulses with delays larger than 10 μsec. have been considered, to avoid the uncertainty of the location of the pulses at the very beginning of the sweep. The curve that fits the data is drawn in Fig. 5. It indicates a lifetime $\tau=155\pm5$ μsec.

The lifetime of thermal neutrons in an infinite medium of pure paraffin is about 190 μsec., due to capture by H nuclei. Taking into account the presence in our paraffin block of the B^{10} in the counters, the expected lifetime is ~160 μsec., close to the value experimentally found.

The value $\tau=155$ μsec. has been used in the computation of the efficiency of our apparatus.

IV. ANGULAR DISTRIBUTION AND ENERGY OF THE NEUTRONS RECORDED

The pictures taken with the BF_3 counters in the "up-down connection" give direct information concerning the angular distribution of the neutrons produced in the nuclear events.

No significant differences have been found in the frequencies of upward and downward neutrons for any of the absorbers Σ used. This result, in agreement with preliminary results obtained in a previous experiment,[7] indicates that the angular distribution of the moderate energy neutrons released in nuclear disintegrations is, at least in first approximation, isotropic, which supports the interpretation of these neutrons as products of nuclear evaporation.[8]

The pictures taken with the BF_3 counters in the "close-far connection" give information about the order of magnitude of the neutron energies. The ratios of pulses "close" to pulses "far," C/F, corrected for background and chance effects, are given in Table I for all absorbers Σ used. In the bottom row of the table is given the ratio obtained when a neutron source of 1 mC (Ra+Be) was put at the center of the space occupied by the absorbers Σ. It appears that the ratio obtained for the source is of the same order of magnitude as the ratios obtained for the neutrons recorded in our experiments.[9] The energy spectrum of the neutrons emitted by the source ends at about 11 Mev and has a maximum[10] at about 5 Mev.

A crude estimate of the neutron energies can be made as follows. Most of the pulses recorded in the "close" counters are due to neutrons slowed down to thermal energies in the neighborhood of those counters, i.e., to neutrons that crossed with moderate energies about 4 cm of paraffin. The neutrons which gave rise to pulses in the "far" counters, instead, crossed about 12 cm of paraffin. Their scattering mean free paths, are:

$$l_{\text{close}}=1/N\sigma\cong 4 \text{ cm},$$
$$l_{\text{far}}\cong 12 \text{ cm}.$$

With $N=7.8\times10^{22}$ cm^{-3} and the cross section $\sigma=9/E$ barns (E in Mev) one gets:

$$E_{\text{close}}\approx 3 \text{ Mev} \quad \text{and} \quad E_{\text{far}}\approx 9 \text{ Mev}.$$

V. RELATIVE NUMBER OF NEUTRAL AND CHARGED PRIMARIES OF NUCLEAR INTERACTIONS

The pictures obtained with Σ=4½-in. Pb and $S=0$ have been classified according to the number of counters struck in tray *a*, in order to obtain information on the relative number of neutral and charged primaries of nuclear disintegrations.

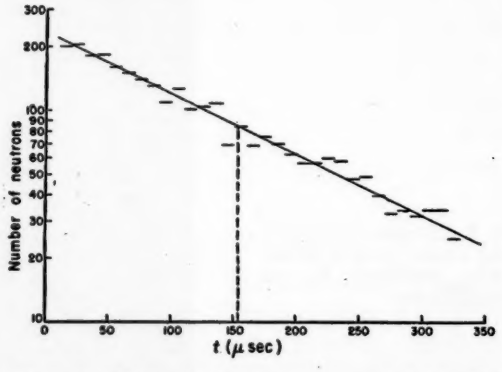

FIG. 5. Time distribution of the neutrons recorded. The lifetime of the neutrons in the detector is $\tau=155\pm5$ μsec.

[7] G. Cocconi and V. Cocconi Tongiorgi, Phys. Rev. **76**, 318 (1949).

[8] For the present and the remaining discussion in this section, only experiments in which the absorber S was removed have been used, as the presence of S introduces a distortion in favor of neutrons recorded by C and D, due to backscattering and neutron production in S itself.

[9] On the average, the energies of the neutrons emitted in nuclear evaporations seem to be slightly higher than the energies of the (Ra+Be) neutrons, although not different in order of magnitude. Therefore the use of a value for the efficiency of the apparatus based on a calibration with the (Ra+Be) source should not lead to a large error.

[10] H. L. Anderson, "Neutrons from α-emitters," National Research Council, Report No. 3, Chicago (1948).

TABLE II. Rates of non-ionizing (N), single (S), and multiple (T, M) ionizing particles in counters a, and ratio R=neutral particles/charged particles evaluated for the primaries that generate the showers in Σ.

	N (hr.$^{-1}$)	S (hr.$^{-1}$)	T (hr.$^{-1}$)	M (hr.$^{-1}$)	R Lower limit	R Upper limit
$n=2$	3.95±0.27	3.98±0.27	1.31±0.14	1.74±0.17	1.0 ±0.1	1.3±0.2
$n=3, 4$	3.83±0.27	4.50±0.28	2.22±0.22	2.61±0.22	0.86±0.09	1.3±0.2
$n\geqslant 5$	1.92±0.19	1.93±0.20	2.72±0.24	4.93±0.3	1.0 ±0.14	2.4±0.3

The interpretation of the results is complicated by three phenomena: the inefficiency of tray a, the back-scattering of particles produced in the absorber Σ, and the occurrence of events accompanied by showers produced in the air or in the paraffin above the absorber Σ. The efficiency ϵ of tray a has been experimentally evaluated as close to 0.90.

If N_0, S_0, T_0, M_0 are the observed frequencies of the events in which zero, one, two, and more than two counters, respectively, have been struck in tray a, the true frequencies of the same events, N, S, T, M, are in first approximation, such that:

$$N_0=N+S(1-\epsilon)+T(1-\epsilon)^2, \quad S_0=S\epsilon+2(1-\epsilon)T,$$
$$T_0=T\epsilon^2, \quad M_0=M.$$

The rates (hr.$^{-1}$) of the events N, S, T, M are given in Table II, subdivided according to the number n of neutrons recorded, namely for $n=2$, $n=3$ and 4, $n\geqslant 5$. The events in which a single neutron pulse was recorded ($n=1$) have been disregarded, as in such a category fall the chance coincidences, and practically all of the background due to spurious effects (see Section VIII). It is reasonable to assume that the number n of neutrons recorded is somewhat correlated with the energy involved in the event, hence that events with the same number n are generated by particles whose energies are of the same order of magnitude. Then, if one assumes that neutral and charged particles of the same energy have the same cross section for nuclear interactions as well as the same probability of producing particles in backward directions, the ratio $R=N/S$ for a given n, gives a lower limit of the ratio of neutral to charged particles for a given energy.

Actually, events produced by a neutral primary are classified as being produced by ionizing particles whenever ionizing particles produced in the interaction are projected backward and whenever ionizing particles accompany the neutral primary falling on tray a.[11]

An upper limit for the fraction of single particles scattered backward can be taken from the ratio T/S, hence an upper limit for R is approximately $N(1+T/S)/S$. The values of N/S and of $N(1+T/S)/S$ are given in Table II.

It can be seen that for all shower sizes (precisely, for all n's) the ratio R is close to unity. This indicates that all of the events observed are produced, in first approximation, by neutral and charged particles in equal number.

It is worth remembering that the same result has been obtained for the particles which generate penetrating showers, observed both in cloud chambers and with G-M counter arrangements.[12]

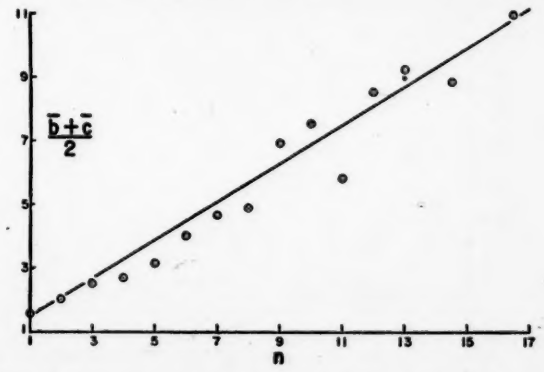

FIG. 6. Average number of counters struck per event in trays b and c (namely, $\frac{1}{2}(\bar{b}+\bar{c})$), *versus* number n of neutrons recorded. $\Sigma=4\frac{1}{2}$-in. Pb, $S=0$.

VI. CORRELATION BETWEEN NUMBER OF NEUTRONS AND NUMBER OF IONIZING PARTICLES PRODUCED IN NUCLEAR INTERACTIONS

In order to obtain information about the number of neutron pulses recorded and the sizes of the ionizing events associated with them, the pictures have been classified according to the number n of the recorded neutrons. For each absorber and for each value of n, the mean numbers $\bar{a}$, $\bar{b}$, $\bar{c}$, and $\bar{d}$ of G-M counters struck per event in trays a, b, c, and d, respectively, have been evaluated. In Fig. 6 the average of $\bar{b}$ and $\bar{c}$, $\frac{1}{2}(\bar{b}+\bar{c})$, is plotted as a function of the number n of neutrons observed, for $\Sigma=4\frac{1}{2}$-in. Pb and $S=0$. Similar behavior has been found for the other thicknesses of Σ. It is to be noted that the numbers given on the scales of the graph are the numbers of counters struck, not the true numbers of ionizing particles and of neutrons present. If n neutrons are recorded, the most probable number of neutrons present is approximately proportional to n. However, a G-M counter that records one ionizing particle is insensitive to further particles striking at the same time. Therefore, the most probable number of ionizing particles increases more rapidly than does the number of counters struck, this effect becoming strong when the probability is great for more than one particle to fall on a single counter. Consequently, if we were

[11] The pictures which could be recognized as arising from events accompanied by a shower (on the basis of counters s being struck and of the general appearance of the picture) have been disregarded. However, small showers can hardly be recognized as such.

[12] W. D. Walker, Phys. Rev. **77**, 686 (1950).

TABLE III. Ratios of average numbers of counters struck in trays c and d, with and without the absorber S=6-in. Pb.

		$n=3$	$n=4$	$n\geqslant 5$
Σ=4½-in. Pb, S=0	$\frac{\bar{c}}{\bar{d}}=\frac{\omega_c}{\omega_d}$	1.8	1.9	1.6
Σ=4½-in. Pb, S=6-in. Pb	$\bar{c}/\bar{d}$	4.9	4.2	4.3
	$\frac{\bar{c}}{\bar{d}}\cdot\frac{\omega_d}{\omega_c}$	2.7	2.2	2.7

TABLE IV. Frequency (hr.$^{-1}$) of events, *versus* number n of neutrons recorded, for S=0 and different absorbers in Σ.

n	Σ=0, S=0	Σ=4½-in. Pb, S=0	Σ=1-in. Pb, S=0	Σ=½-in. Pb, S=0	Σ=4½-in. Al, S=0
1	7.1±0.3	7.4 ±0.5	7.4 ±0.4	2.7 ±0.3	2.7 ±0.3
2	0.4±0.06	10.2 ±0.4	5.1 ±0.3	1.5 ±0.1	0.85±0.07
3	0.04	7.7 ±0.4	2.7 ±0.2	0.47±0.5	0.07±0.02
4		5.0 ±0.3	1.1 ±0.1	0.09±0.02	0.05
5		3.7 ±0.3	0.22 ±0.06	0.05±0.02	
6		2.5 ±0.2	0.13 ±0.04		
7		1.5 ±0.2	0.044±0.025		
8		1.1 ±0.2	0.015		
9		0.69±0.11			
10		0.58±0.10			
11		0.44±0.09			
12–13		0.19±0.08			
14–15		0.06±0.04			
⩾16		0.025			

able to plot the actual number of ionizing particles *versus* the actual number of neutrons, the graph in Fig. 6 would have a much greater slope at large values of $\frac{1}{2}(\bar{b}+\bar{c})$, and a not much greater slope at small values.

This indicates that the number of ionizing particles probably increases more rapidly with increasing shower size (or primary energy) than does the number of moderate energy neutrons.

In Fig. 7 are given examples of the distribution of the number of G-M counters struck in tray b, for a given number of neutrons observed, namely for $n=2$, $n=4$, $n=6$ (Σ=4½-in. Pb, S=0). The curves do not show a maximum, but exponential-like distributions, being the steeper the lower the value of n. Here again, if one could plot on the abscissae the average number of particles in trays b and c, instead of the average number of counters struck, it would strongly stretch the lengths of the tails of the curves. The results seem quite interesting as they show that a large number of neutrons of moderate energy can be released in events in which very few ionizing particles are present, and that, vice versa, a large number of ionizing particles does not necessarily imply the presence of a large number of neutrons.

VII. PENETRATING POWER OF THE IONIZING PARTICLES PRODUCED IN NUCLEAR INTERACTIONS

The average numbers, $\bar{c}$ and $\bar{d}$, of counters struck per event in trays c and d have been computed, as a function of the number n of neutrons recorded, for the following arrangements of absorbers: $\Sigma=0$, $S=0$; Σ=4½-in. Pb, $S=0$; $\Sigma=0$, S=6-in. Pb; Σ=4½-in. Pb, S=6-in. Pb.

The figures obtained for $\Sigma=0$, $S=0$, and $\Sigma=0$, S=6-in. Pb have been used to correct the results obtained for Σ=4½-in. Pb, $S=0$, and Σ=4½-in. Pb, S=6-in. Pb, respectively. When no absorber was present in $S(S=0)$ this background was smaller than five percent of the events recorded, for all events with $n\geqslant 2$. When the absorbers S was present (S=6-in. Pb), the background was smaller than 10 percent of the events recorded, for all events with $n\geqslant 3$. Therefore, for all events with $n\geqslant 3$, the uncertainties involved in the background correction applied are probably immaterial.

The ratios $\bar{c}/\bar{d}$ obtained for Σ=4½-in. Pb, $S=0$, and Σ=4½-in. Pb, S=6-in. Pb, corrected as indicated above, are given in Table III.

Assuming that the ratio $\bar{c}/\bar{d}$ obtained with $S=0$ equals the ratio ω_c/ω_d of the solid angles subtended at Σ by trays c and d, respectively, one gets the values given in the last row of Table III, which give the effect due to the presence of S. It appears that approximately 40 percent of the particles emerging from 4½-in. Pb are capable of crossing 6-in. Pb, and that the average penetration of the particles is the same for events in which different numbers of neutrons have been recorded.

To check this result, an attempt has been made to select from among all the pictures taken with Σ=4½-in. Pb, $S=0$ and Σ=4½-in. Pb, S=6-in. Pb only those showing events that could be recognized as originating in Σ. In this case no background correction was needed. The ratios c/d obtained in this way were found to be in agreement with the figures given in Table III.

VIII. FREQUENCY OF NUCLEAR DISINTEGRATIONS AS A FUNCTION OF THE NUMBER OF NEUTRONS RECORDED

The frequencies $f(n)$ per hour of the events recorded with $S=0$ and $\Sigma=0$, ¼-, 1-, 4½-in. Pb and 4¾-in. Al

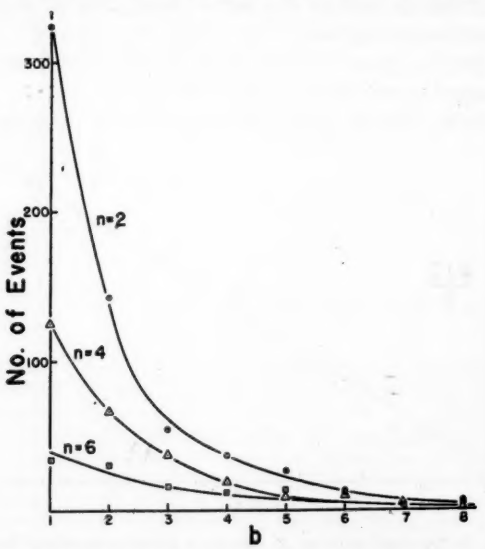

FIG. 7. Distribution of the number of counters struck per event in tray b for $n=2$, $n=4$, and $n=6$. Σ=4½-in. Pb, $S=0$.

have been determined, as a function of the number, n, of neutrons of moderate energy recorded.

The results are given in Table IV with their standard errors. All the figures referring to absorbers $\Sigma \neq 0$ have been corrected for the background effects recorded with $\Sigma = 0$.

The data for $\Sigma \neq 0$ are also plotted in Fig. 8. The curves given in the figure are not drawn according to the experimental points; they are the results of the calculations described in Section IX. Inspection of Table IV and of Fig. 8 leads one to the following qualitative deductions.

(a) With $\Sigma = 0$ no events have been recorded which show a high number of neutrons of moderate energy. Actually in 94 percent of these events only *one* neutron was recorded (i.e., the neutron *required* by the apparatus to create a MP). The reason for this is that about one-half (4 hr.$^{-1}$) of the events recorded with $\Sigma = 0$ are due to chance coincidences between a single neutron and a single ionizing particle capable of giving a coincidence (b, c). The remaining events are mostly due to nuclear disintegrations produced in the paraffin; in such events neutrons are produced with a rather low multiplicity, and furthermore the geometrical efficiency of our apparatus for detecting them is appreciably lower than it is for detection of neutrons produced in the absorbers Σ. This result is remarkably important for our experiment since, as a consequence, the background correction applied to the data taken with $\Sigma \neq 0$ is immaterial for all the events in which two or more than two neutrons ($n \geqslant 2$) have been recorded.[13]

(b) Higher neutron multiplicities have been recorded, on the average, in association with nuclear disintegrations taking place in Pb than in Al.

(c) The neutron multiplicities recorded in association with nuclear disintegrations occurring in lead are higher (on the average) the thicker the absorber.

(d) The frequencies of the events recorded with a given absorber decrease strongly with increasing n.

(e) The rate of decrease is different for different thicknesses of a given material, and for the different materials. It can be described by the following expressions:

for $\Sigma = 4\frac{1}{2}$-in. Pb, $f(n) \sim e^{-0.46n}$,
for $\Sigma = 1$-in. Pb, $f(n) \sim e^{-1.0n}$,
for $\Sigma = \frac{1}{4}$-in. Pb, $f(n) \sim e^{-1.36n}$,
for $\Sigma = 4\frac{3}{4}$-in. Al, $f(n) \sim e^{-1.8n}$.

Let us consider the data obtained with lead absorbers. The fact that the slope of the curves $f(n)$ is lower the thicker the absorber Σ can be explained with one of the following assumptions.

(1) The nuclear disintegrations occurring in the thicker absorbers, on the average, involve energies higher than those involved in events taking place in thin absorbers, and high energy events produce *in a single act* a much greater number of neutrons than do lower energy events.

(2) Each nuclear disintegration releases, on the average, a number of neutrons of moderate energy practically independent of the energy involved in the process, but there is a finite probability of release also of particles capable of giving rise to further reactions in which more neutrons are produced, the probability of such secondary reactions being larger in the thicker absorbers.

(3) A mixture of the two preceding assumptions is true; i.e., cascade-like processes take place in the absorbers, and furthermore, energetic processes release in each act more neutrons, on the average, than do low energy events.

If assumption (1) is correct, the frequencies of the events showing a given number of neutrons, recorded for absorbers of various thicknesses, cannot increase, with increasing thickness of the absorber, more than in proportion to the absorber thickness. Furthermore, the slopes of the curves obtained for large values of n (for which all events presumably have a probability close to unity of being recorded, for all thicknesses of the absorber) must be equal.

Neither of these conditions is fulfilled by our experimental points. The ratio of the frequencies recorded with $\Sigma = 4\frac{1}{2}$-in. Pb and with $\Sigma = \frac{1}{4}$-in. Pb (ratio of thickness = 18) is larger than 18 for all $n \gtrsim 3$. For $n = 6$ this ratio is already close to 200. Furthermore, up to 17 neutron pulses have been observed on our sweep, with $\Sigma = 4\frac{1}{2}$-in. Pb. This corresponds to an actual number of neutrons produced in Σ of the order of $17/E \cong 500$ ($E = 0.03$ is the efficiency of the apparatus). Such a huge number of neutrons is certainly not conceivable as the product of only one or even a few evaporations of Pb nuclei.

This indicates that assumption (1) is not consistent with the experimental results, and therefore either assumption (2) or (3) is true. Our data do not supply arguments for discrimination between these two possible cases.

Anyway, we can conclude that the existence of a cascade-like process of nuclear interactions is clearly proved by our data. The neutrons we record are produced both in the primary and in the secondary acts of the process, the contribution of the secondary acts being the more important the thicker the absorber used.

More precise conclusions will be obtained from the

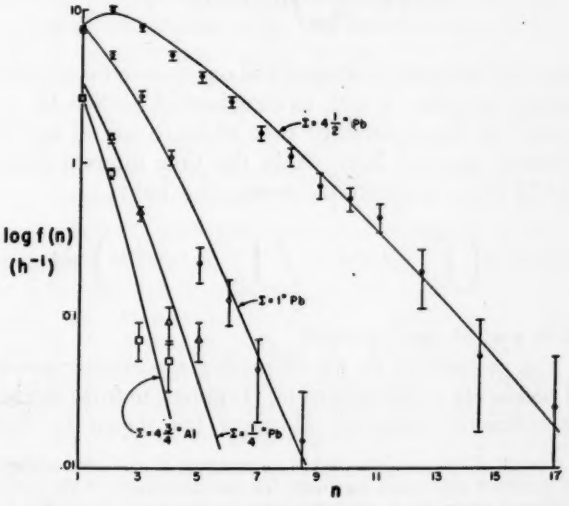

FIG. 8. Frequency (hr^{-1}) of the events in which n neutrons were recorded *versus* n, for $S = 0$ and $\Sigma = \frac{1}{4}$-in. Pb, 1-in. Pb, $4\frac{1}{2}$-in. Pb. $4\frac{3}{4}$-in. Al. The curves are the result of the analysis of Section IX,

[13] The results given in Table IV and plotted in Fig. 8 for $n = 1$ are somewhat uncertain as the correction for the background is certainly approximate. In fact, the presence of the absorber modifies slightly the rates of chance coincidences and affects to some extent the events occurring in the paraffin. No specific use of these data is made in the following discussion.

quantitative treatment of the problem given in the following section.

IX. MULTIPLICITY SPECTRA OF THE MODERATE ENERGY NEUTRONS RELEASED IN NUCLEAR INTERACTIONS

The functions $f(n)$ obtained in Section VIII from the experimental data represent the frequencies of the events occurring in Σ, in which n neutrons were recorded by our apparatus.

It is our purpose here to evaluate, from the functions $f(n)$, the functions $I(\nu)$, which give the frequencies of the events leading to the production of ν neutrons of moderate energies. We wish it to be clear that ν is the *true number* of moderate energy neutrons produced in the events, while $n \leqslant \nu$ is the number of neutrons *recorded* by our apparatus; $I(\nu)$ is the *true frequency* of the events with ν neutrons, while $f(n)$ is the frequency recorded by our apparatus for the events with n recorded neutrons. We shall call the functions $I(\nu)$, the "*multiplicity spectra*" of the moderate energy neutrons produced in nuclear disintegrations occurring in the absorbers Σ used.

It is quite plain that the functions $f(n)$ do not reproduce the functions $I(\nu)$, as the events occurring in Σ are weighted by our apparatus according to their probability of being detected; i.e., according to their probability of giving a master pulse.

As all of the events with $\nu \geqslant n$ have a finite probability of having n neutrons recorded, one must write

$$f(n)=\sum_{\nu=n}^{\infty} I(\nu)\cdot G(\nu, n)\cdot \Pi(n)\cdot P_{b,c}(\nu).$$

$G(\nu, n)$ is the probability that, out of ν-neutrons produced in an event, n are recorded in the time interval between 5 and 340 μsec., and is given by[14]

$$G(\nu, n)=\binom{\nu}{n}E^n(1-E)^{\nu-n},$$

where E, the over-all efficiency of our system for recording each neutron, is 0.03, as explained in Section II.

$\Pi(n)$ is the probability that at least one of the n neutrons recorded falls within the time interval from 5 to 15 μsec. to trigger the sweep. One has:

$$\Pi(n)=1-\left(\int_{15}^{340}(dt/\tau)e^{-t/\tau}\Big/\int_{5}^{340}(dt/\tau)e^{-t/\tau}\right)^n=1-r^n.$$

With $\tau=155$ μsec., $r=0.93$.

The probability $P_{b,c}(\nu)$ of getting a particle capable of producing a coincidence (b, c) cannot, unfortunately, be computed correctly. However (as shown by the curve in Fig. 6), the average numbers of particles recorded in trays b and c steadily increase when the number of neutrons recorded increases. For the sake of simplicity then we shall put

$$P_{b,c}(\nu)=1.$$

This assumption is probably near the truth for the events in which large number of neutrons are recorded, while it certainly is incorrect for small values of n. This approximation will not allow us to utilize the absolute values of the multiplicity spectra we shall obtain from this calculation. However, we feel that the main characteristics of the processes will not be strongly affected by it.

We can write finally:

$$f(n)=\sum_{\nu=n}^{\infty} I(\nu)\cdot\binom{\nu}{n}E^n\cdot(1-E)^{\nu-n}\cdot(1-r^n). \quad (1)$$

Equation (1) is to be satisfied by the introduction of an appropriate function for $I(\nu)$. The following working hypotheses have been tried: (a) All events have the same neutron multiplicity (in which case the sum in Eq. (1) is reduced to a single term); (b) $I(\nu)$ is a power spectrum: $I(\nu)\sim\nu^{-\gamma}$; (c) $I(\nu)$ is an exponential spectrum: $I(\nu)\sim e^{-a\nu}$. It has been found that assumptions (a) and (b) cannot satisfy the experimental data. Assumption (c), instead, can be worked out successfully. In this case, the solution of Eq. (1) is

$$f(n)=K(1-r^n)\cdot(E\cdot e^{-a})^n/[1-(1-E)\cdot e^{-a}]^{n+1}.$$

The functions $I(\nu)$ which satisfy the experimental points are as follows:

$$\begin{aligned}
&\text{for}\quad \Sigma=4\tfrac{1}{2}\text{-in. Pb}, \quad I(\nu)=10e^{-0.02\nu}\ \text{per hour},\\
&\text{for}\quad \Sigma=1\text{-in. Pb}, \quad I(\nu)=30e^{-0.06\nu},\\
&\text{for}\quad \Sigma=\tfrac{1}{4}\text{-in. Pb}, \quad I(\nu)=30e^{-0.1\nu},\\
&\text{for}\quad \Sigma=4\tfrac{3}{4}\text{-in. Al}, \quad I(\nu)=50e^{-0.17\nu}.
\end{aligned} \quad (2)$$

The functions given above are the differential multiplicity spectra of the moderate energy neutrons produced in the various absorbers Σ.

The functions $f(n)$ obtained by substitution of these spectra in Eq (1) are the curves drawn in Fig. 8.

X. AVERAGE NEUTRON MULTIPLICITIES

From the multiplicity spectra (2) given in the preceding section, one derives that the average multiplicities $\bar{\nu}=1/a$ of the moderate energy neutrons released by the nuclear disintegrations occurring in the absorbers used, are as follows:

$$\begin{aligned}
&\text{for}\quad \Sigma=4\tfrac{1}{2}\text{-in. Pb}, \quad \bar{\nu}=50,\\
&\text{for}\quad \Sigma=1\text{-in. Pb}, \quad \bar{\nu}=17,\\
&\text{for}\quad \Sigma=\tfrac{1}{4}\text{-in. Pb}, \quad \bar{\nu}=10,\\
&\text{for}\quad \Sigma=4\tfrac{3}{4}\text{-in. Al}, \quad \bar{\nu}=6.
\end{aligned}$$

The absolute values of the coefficients a in the exponents of the spectra, hence the $\bar{\nu}$'s, can be in error by a factor as large as 2, mainly because of the uncertainty in the

[14] In all of our previous papers on neutrons of moderate energy, an incorrect expression was used for the calculation of the probability of recording n neutrons, since we replaced $\exp(-En)$ by $(1-E)^n$. The two expressions differ only in the terms of order higher than the second, so that the numerical results remain unchanged.

estimate of efficiency E of the apparatus and of the extrapolation of the multiplicity spectra to low values of n. However, the relative values of $\bar{\nu}$ are believed to be correct within 20 percent.

The large increase with the thickness of the absorber of the average number of neutrons emerging from it confirms the strong secondary neutron production, as deduced in the qualitative discussion of the data.

Analogous variation of $\bar{\nu}$ with the thickness of the absorber was obtained in the preliminary experiment previously quoted.[7] There, however, the lack of information about the multiplicity spectra of the neutrons for the various absorbers left open the problem of whether the large number of neutrons emerging from thick absorbers were produced in a single act or in several successive acts.

In the light of the present experiment it clearly appears that when one concerns himself with the problem of the multiplicity of neutrons released in a given material, the most interesting and meaningful figure is the average number of neutrons released, in the material considered, *by a single nuclear interaction.* This figure can be derived experimentally only if the thickness of the absorber in which the processes take place is small enough to make the probability of secondary interactions practically negligible.

As a rule, we think that a reasonably good value for the multiplicity of neutron production in a single interaction can be obtained if the thickness of the absorber is smaller than, say, one-tenth to one-twentieth of the interaction mean free path (in the given material) of the radiation causing nuclear disintegrations (N-component). If one assumes mean free paths corresponding to the geometrical nuclear cross sections, the "thin target condition" stated above is fulfilled, in lead, if the thickness of the absorber is smaller than about 10 g/cm².

The figure $\bar{\nu}=10$ obtained with $\Sigma=\frac{1}{4}$-in. Pb (7 g/cm²), therefore, must be considered as our best approximation to the average multiplicity of the moderate energy neutrons released in Pb, in a single nuclear disintegration induced by the N-component. The value obtained for $\Sigma=1$-in. Pb (28 g/cm²) shows that secondary interactions already play a considerable role in that absorber.

For aluminum, the "thin target condition" is fulfilled only if the absorber is smaller than about 7 g/cm². The thickness of the Al absorber we used was about five times this value. The result we obtained with $\Sigma=4\frac{3}{4}$-in. Al, $\bar{\nu}=6$, indicates that the average multiplicity of a single nuclear interaction in Al is smaller than that, probably close to 2 or 3.

If the "thin target condition" is not satisfied, the average number of neutrons measured depends not only on the material used, but also on its thickness. This point is particularly important when comparisons of multiplicities of neutron production in different materials are made.

Of course, the thin target condition is the less important the lower the energies involved in the processes investigated. Nuclear events in which no relativistic particles are emitted, probably cannot induce many secondary interactions, and the multiplicities of the neutrons produced in these events are expected to be close to the multiplicities of neutrons released in a single act.

On this line of reasoning we now interpret the fact that the average multiplicity measured for neutrons released in nuclear disintegrations occurring in 2-in. Pb was found to be from 30 to 60 when association with a penetrating shower[2,7] or an extensive shower[4] was required; it was found to be only about 9 when such requirements were not made, since in the latter case neutrons mostly released in low energy stars were recorded.[15]

XI. COMPARISON OF MULTIPLICITY SPECTRA OF MODERATE ENERGY NEUTRONS AND OF HEAVILY IONIZING PRONGS OF STARS OBSERVED IN PHOTOGRAPHIC PLATES

It is interesting to compare the multiplicity spectra obtained for neutrons of moderate energy produced in nuclear disintegrations with the multiplicity spectra obtained for the stars of heavily ionizing particles observed in photographic plates.

The frequency $F(p)$ of stars with p heavily ionizing prongs, is given by

$$F(p)\cong e^{-\alpha p}$$

with $\alpha=0.3$ to 0.5.[16]

The neutron spectra given by Eqs. (2) also have an exponential form.

On the basis of the discussion given in Section X, we can assume that the neutrons produced in $\Sigma=\frac{1}{4}$-in. Pb collect only a very small contribution from secondary nuclear processes, hence we can compare the exponent $a=0.1$ with the values obtained for α. The fact that a is somewhat smaller than the figures obtained for α can be accounted for easily by the facts that no Coulomb barrier hinders the escape of neutrons from nuclei, that the average energy involved in the processes we observed is probably higher than that involved in the evaporations observed in photographic plates, and that the evaporations observed in the plates occur mostly in Ag and Br nuclei whose atomic numbers are lower than that of Pb.

Although the measurements are statistically quite poor, the results obtained with $\Sigma=4\frac{3}{4}$-in. Al give $a=0.17$, and this value must probably be increased by a factor of 2 or so to correct for secondary interactions. This can be taken as an indication that, as expected, the exponent a increases when the atomic number decreases.

---

[15] V. Cocconi Tongiorgi, Phys. Rev. **76**, 517 (1949).

[16] See, for example, B. Rossi, M.I.T. Report No. 26 (1944), and M. Addario and S. Tamburino, Phys. Rev. **76**, 983 (1949).

XII. TENTATIVE ANALYSIS OF THE CASCADE PROCESS FOR NUCLEAR INTERACTIONS

A discussion of the features of the cascade process for nuclear interactions requires the use of parameters which are up to now unknown: the mean free path of the N-component as a function of energy, the angular distribution, the energy and multiplicity spectra of secondary particles emitted, etc.

The information we can derive from our experiments is that the multiplicity spectrum of the neutrons of moderate energies emitted in nuclear disintegrations is $\sim\exp(-0.1\nu)$ when the phenomena occur in a Pb layer of $\frac{1}{4}$-in., where secondary processes have little probability of taking place, whereas the phenomena occurring in $4\frac{1}{2}$-in Pb, where the contribution of secondary processes is important, produce neutrons with a multiplicity spectrum proportional to $\exp(-0.02\nu)$.

Several models can be worked out to account for such a behavior. Although the results of the calculations depend strongly on the assumptions arbitrarily introduced, we thought it worth while to show how the experimental results can be described with some simple assumptions.

To describe the phenomena occurring in the absorber $\Sigma=4\frac{1}{2}$-in. Pb the following model is assumed. A particle belonging to the N-component, falling on the Pb absorber Σ, produces nuclear disintegrations with a mean free path $\lambda=1/N\sigma$ where σ is the geometrical cross section of the Pb nuclei ($\lambda=160$ g/cm^2).

A primary nuclear disintegration produces: (a) ν_1-neutrons of moderate energy, isotropically distributed, not capable of inducing further nuclear disintegrations. The probability of ν_1 such neutrons being produced is given by $H(\nu_1)=(1-e^{-a})\exp(-a\nu_1)$. On the basis of the experimental results obtained with $\Sigma=\frac{1}{4}$-in. Pb, we put $a=0.1$. (b) N_1 particles (fast neutrons, fast protons, π-mesons) emitted in the forward direction, capable of producing further disintegrations with the same mean free path λ as that of the primary radiation. In each of the secondary reactions induced by these particles, neutrons of moderate energies are produced, with the same angular distribution and the same probability as specified in (a).

The probability that N_1 of these fast particles are produced is assumed to be expressed by an exponential function, $F(N_1)=(1-e^{-b})\exp(-bN_1)$. The coefficient b is the unknown of the problem. Of course, $1/b=N_1$ will be the average number of such particles. For the sake of simplicity, the assumption is introduced that the energy degradation in the primary act and/or the energy of the primary particle are such as to make the importance of tertiary processes negligible in the absorber Σ considered (the thickness of Σ is $h=128$ g/cm$^2=\frac{4}{5}$ of a mean free path). For simplicity we consider here the vertical direction only.

The probability $P(\nu)$ of having ν-neutrons emerging from Σ can be written as the product of the probabilities of ν_1-neutrons being produced in the primary act, and of $\nu_2=(\nu-\nu_1)$ neutrons being produced in secondary reactions. Hence

$$P(\nu)=\sum_{\nu_1=0}^{\nu} H(\nu_1)\cdot J(\nu-\nu_1). \tag{3}$$

$J(\nu-\nu_1)$ is given by:

$$J(\nu-\nu_1)=\sum_{s=1}^{\infty} g(s)\cdot\Pi(s,\nu-\nu_1)$$

where $g(s)$ is the probability that s secondary disintegrations happen in the absorber, and $\Pi(s,\nu-\nu_1)$ is the probability that the s secondary disintegrations give rise to $(\nu-\nu_1)$ neutrons in total.

If h is the thickness of the absorber,

$$g(s)=\frac{1}{\lambda}\int_0^h \frac{e^{-x/\lambda}}{1-e^{-h/\lambda}}\cdot\sum_{N_1=0}^{\infty} F(N_1)\cdot\binom{N_1}{s}$$
$$\times[1-\exp(-(h-x)/\lambda)]^s[\exp(-(h-x)/\lambda)]^{N-s}dx$$

and

$$\Pi(s,\nu-\nu_1)=\frac{(s+\nu-\nu_1-1)!}{(s-1)!(\nu-\nu_1)!}(1-e^{-a})^s\exp[-a(\nu-\nu_1)].$$

After performing the sums and the integral in expression (3), one finds[17] that the probability $P(\nu)$ that ν-neutrons emerge from the absorber $\Sigma=4\frac{1}{2}$-in. Pb is given by:

$$P(\nu)=\frac{1-e^{-a}}{\lambda}\cdot\frac{e^{-a\nu}}{1-m}(1-\beta)\Big\}\lambda mB^{-(\nu+1)}\cdot C$$
$$\times\Big\{\frac{\exp[-\nu(\beta-D)U_1]}{U_1}-\frac{\exp[-\nu(\beta-D)U_2]}{U_2}$$
$$+[D-\nu(\beta-D)][E_i(-Y_2)-E_i(-Y_1)]\Big\}$$
$$-\{\lambda+m[\beta h-\lambda+\beta\lambda\ln(1-\beta m)/(1-\beta)]\}\Big\} \tag{4}$$

with:

$$\beta=e^{-b},\quad m=e^{-h/\lambda},\quad B=1-\beta(1-e^{-a}),$$
$$C=\exp\{-\nu/2(D-\beta)^2[(U_1+U_2)/2]^2\},$$
$$D=\beta e^{-a}/[1-\beta(1-e^{-a})],$$
$$U_1=m/(1-mD),\quad U_2=1/(1-D),$$
$$Y_1=U_1(\beta-D)\nu,\quad Y_2=U_2\nu(\beta-D).$$

Equation (4) has been solved for various values of $b=-\ln\beta$ and it has been found that the function $P(\nu)$ is very close to an exponential, $\sim\exp(-a'\nu)$, as required to satisfy the experimental result. It fits the data, i.e., it gives $a'\approx0.02$, for $b=0.1$. This would indicate that the fast particles released in nuclear disintegrations capable of inducing further nuclear processes, have a multiplicity spectrum analogous to that found for

[17] We are grateful to Professor R. P. Feynman for assistance in the solution of this equation.

moderate energy neutrons. In other words, with the assumptions introduced in our model, an average number $\bar{N}_1 \approx 10$ of fast particles are required to describe our experimental results.

The same model of the nuclear cascade process can be worked out more easily and can be extended to include tertiary, quaternary, etc. interactions, if one limits oneself to the consideration of the average numbers of particles emitted, rather than to their multiplicity spectra.

Let Π_0 be the number of primary particles falling on the absorber Σ, and $\Pi, S, T, \cdots$ the numbers of primary, secondary, tertiary, etc. fast particles at the depth x in the absorber. Let $\bar{N}_1, \bar{N}_2, \bar{N}_3, \cdots$ and $\bar{\nu}_1, \bar{\nu}_2, \bar{\nu}_3, \cdots$, respectively, be the average number of fast particles and of moderate energy neutrons produced in primary, secondary, tertiary, etc. acts.

One has:

$$\Pi = \Pi_0 \cdot e^{-x/\lambda}. \tag{5a}$$

For secondary particles, the following diffusion equation can be written:

$$dS/dx = (\bar{N}_1 \Pi - S)/\lambda,$$

which gives

$$S = \bar{N}_1 \Pi_0 \cdot x e^{-x/\lambda}/\lambda. \tag{5b}$$

Analogous differential equations can be written for the tertiary, quaternary, etc. particles and the solutions are:

$$T = \bar{N}_1 \bar{N}_2 \Pi_0 \cdot \tfrac{1}{2}!(x/\lambda)^2 e^{-x/\lambda} \tag{5c}$$

$$Q = \bar{N}_1 \bar{N}_2 \bar{N}_3 \Pi_0 \cdot \tfrac{1}{3}!(x/\lambda)^3 e^{-x/\lambda}. \tag{5d}$$

The total number $\bar{\nu}$ of moderate energy neutrons produced in the thickness h of the absorber Σ is then:

$$\bar{\nu} = \int_0^h \left(\bar{\nu}_1 \frac{\Pi}{\lambda} + \bar{\nu}_2 \frac{S}{\lambda} + \bar{\nu}_3 \frac{T}{\lambda} + \cdots \right) dx$$

where $\Pi, S, T, \cdots$ are given by the expressions (5). For comparison with the experiment, we consider

$$\bar{\nu}_h = \bar{\nu}/\Pi_0(1 - e^{-h/\lambda});$$

i.e., the average number of neutrons generated in a nuclear cascade process by a primary particle *interacting in the absorber* Σ. One has:

$$\bar{\nu}_h = \bar{\nu}_1 + \bar{\nu}_2 \bar{N}_1 \left(1 - \frac{h}{\lambda} \cdot \frac{e^{-h/\lambda}}{1 - e^{-h/\lambda}} \right)$$
$$+ \bar{\nu}_3 \bar{N}_1 \bar{N}_2 \left[1 - \frac{h}{\lambda} \frac{e^{-h/\lambda}}{(1 - e^{-h/\lambda})} \left(1 + \frac{1}{2!} \frac{h}{\lambda} \right) \right]$$
$$+ \bar{\nu}_4 \bar{N}_1 \bar{N}_2 \bar{N}_3 \left[1 - \frac{h}{\lambda} \frac{e^{-h/\lambda}}{(1 - e^{-h/\lambda})} \right.$$
$$\left. \times \left(1 + \frac{1}{2!} \frac{h}{\lambda} + \frac{1}{3!} \left(\frac{h}{\lambda} \right)^2 \right) \right] + \cdots.$$

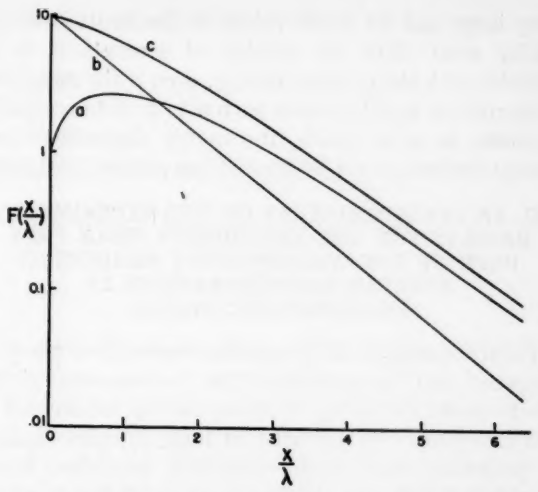

FIG. 9. Analysis of the absorption curve in lead of the radiation producing the nuclear disintegrations observed in non-electron sensitive photographic plates. Curve a: absorption of the radiation producing high energy events. Curve b: absorption of the radiation producing low energy events. Curve c: sum of curves a and b.

With $\lambda = 160$ g/cm² and $h = 128$ g/cm², one gets:

$$\bar{\nu}_h = \bar{\nu}_1 + 0.65\bar{\nu}_2\bar{N}_1 + 0.51\bar{\nu}_3\bar{N}_1\bar{N}_2 + 0.47\bar{\nu}_4\bar{N}_1\bar{N}_2\bar{N}_3 + \cdots. \tag{6}$$

If we introduce the same assumptions as those used in the first treatment of the problem, namely,

$$\bar{\nu}_1 = \bar{\nu}_2 = 10$$
$$\bar{N}_2 = \bar{N}_3 = \cdots = 0,$$

we deduce that in order to have $\bar{\nu}_h = 50$ as experimentally found, we must have $\bar{N}_1 = 6.2$.

The comparison of this figure with the result of the previous calculation, $\bar{N}_1 = 10$, gives an idea of the error introduced by considering the average numbers of particles rather than their multiplicity spectra.

It is worth noticing that with $h = 7$ g/cm² ($\Sigma = \frac{1}{4}$-in. Pb), introducing $\bar{N}_1 = 6.2$, one gets $\bar{\nu}_h = 11$, which is close enough to 10 to justify our statement that such an absorber is a "thin target;" i.e., makes the probability of secondary disintegrations practically negligible.

For $h = 28$ g/cm² ($\Sigma = 1$-in. Pb) one gets $\bar{\nu}_h = 16$, in good agreement with the experimental figure $\bar{\nu} = 17$.

If the cascade is not stopped at the second generation, and it develops down to tertiary, quaternary, etc. acts, it clearly appears from formula (6) that a smaller multiplicity of fast particles is required in each act.

In our opinion, however, only a small fraction of the nuclear cascades should be able to propagate that far, as most of the primary particles of the N-component have energies not very far above the minimum required to initiate the cascade process.

Nevertheless, the few particles of enough energy to allow tertiary, etc. processes to be probable, likely account for the few showers with very high neutron multiplicity.

Certainly a treatment which is to be valid both for

very large and for small values of the neutron multiplicity must allow the number of generations to be variable with the primary energy, even if the mean free path and the multiplicity in each act are not necessarily variable. In other words, the energy dependence and energy spectra cannot be ignored in a precise treatment.

XIII. AN INTERPRETATION OF THE EXPERIMENTAL RESULTS FOR THE ABSORPTION MEAN FREE PATH OF THE *N*-COMPONENT PRODUCING NUCLEAR DISINTEGRATIONS IN PHOTOGRAPHIC PLATES

From the analysis of the nuclear events given above it turns out that the particles of the N-component giving rise to moderate energy neutrons can be subdivided in two categories: (a) Particles of high energies capable of producing stars with relativistic particles, hence capable of inducing further nuclear disintegrations. Their total number under a thickness x of an absorber is (as shown in Section XII, Eqs. (5)):

$$\Pi+S+T+\cdots+\Pi_0 e^{-x/\lambda} \times\left[1+\bar{N}_1\frac{x}{\lambda}+\bar{N}_1\bar{N}_2\cdot\frac{1}{2!}\left(\frac{x}{\lambda}\right)^2+\cdots\right].$$

With the same assumptions as in Section XII, namely, $\bar{N}_1=6.2$, $\bar{N}_2=\bar{N}_3=\cdots=0$, and $\lambda=$constant, these particles are absorbed proportionally to $e^{-x/\lambda}[1+6(x/\lambda)]$ (curve a in Fig. 9). (b) Particles of not very high energies, capable of producing only stars without relativistic particles. These particles are absorbed in a thickness x of a given material with exponential law, i.e., proportionally to $e^{-x/\lambda}$ (curve b in Fig. 9), where λ is the interaction mean free path of such a radiation in the material considered.

Let us now consider the nuclear disintegrations produced in non-electron sensitive photographic plates, by the N-component. When an absorption curve of the radiation producing such disintegrations is made, one has to expect that the intensity of this radiation under a thickness x of material is described by an expression like the following, which is the sum of the two components (a) and (b):

$$F(x/\lambda)=Be^{-x/\lambda}+Ae^{-x/\lambda}[1+6(x/\lambda)],$$

where A and B are the intensities of the two components (a) and (b) falling on the absorber.

Curves a and b in Fig. 9 are plotted with the assumption[18] that $B/A=10$. Curve c represents the sum of curves a and b, hence the function $F(x/\lambda)$. It can be seen that for small values of x, $F(x/\lambda)$ approaches an exponential curve with an absorption mean free path $\lambda_{abs}\approx 2\lambda$.

The experimental results of several authors[19] agree in indicating that the absorption mean free path λ_{abs} in Pb of the radiation producing nuclear disintegrations, is close to 300 g/cm². On the basis of the interpretation given above, such a figure is consistent with the interaction mean free path ($\lambda=160$ g/cm²), deduced from the geometrical cross section for nuclear interactions in Pb and from the experimental cross section for the interactions in which penetrating showers are produced.[20]

We do not attribute much quantitative significance to the present argument, nor insist that the interaction mean free path of the radiation producing low energy events is as small as that given by the geometrical cross section, yet we strongly believe that the interpretation of the absorption curve of the N-component must be made following this line.

A more accurate treatment of the problem should take into account the contribution to the development of the nuclear cascade of tertiary, quarternary, etc. interactions. However, it is easy to see that the more generations are involved, the more closely the curve c approaches to pure exponential with $\lambda_{abs}>\lambda$.

We think that this is the reason why the absorption curve in air of the N-component looks like a pure exponential curve, with a mean free path about twice that deduced from the geometrical cross section.

Performance of this experiment was made possible by a grant from the Research Corporation.

The facilities of the Echo Lake Inter-University High Altitude Laboratory were of invaluable help.

We wish to thank Professor K. Greisen and Professor H. Bethe for discussions and suggestions.

---

[18] Bernardini, Cortini, and Manfredini, Phys. Rev. **76**, 1792 (1949).

[19] E. P. George, Nature **162**, 333 (1948). E. P. George and A. C. Jason, Proc. Phys. Soc. London **A62**, 243 (1949). See reference 18.

[20] G. Cocconi, Phys. Rev. **76**, 984 (1949). See reference 12. K. Sitte, Phys. Rev. **78**, 714 (1950).

Radioactive Isomers of Sn^{117} and Sn^{119}

J. W. MIHELICH* AND R. D. HILL
*Physics Department, University of Illinois,** Urbana, Illinois*
(Received May 22, 1950)

The 14-day Sn^{117m} activity has been found to consist of two transitions: 159 kev of multipole order 5, and 162 kev of multipole order 2.

An activity ~250-day half-life has been assigned to Sn^{119m} and a transition of 69 kev, multipole order 5, has been observed.

I. INTRODUCTION

BECAUSE of the large number of stable tin isotopes, and their low neutron capture cross sections, the activities from radioactive tin isotopes cannot be determined readily. Reference to the table of Seaborg and Perlman[1] shows only two tin activities of class *A* assignment, namely, 100-day $(K, e^-, \gamma)Sn^{113}$ and 28-hour $(\beta^-)Sn^{121}$. In a survey using separated isotopes, Lee and Pool[2] identified the following activities: 28-hour (β^-)-Sn^{121}, 40 min. $(\beta^-, \gamma)Sn^{123}$, 130-day $(\beta^-)Sn^{123}$, 10 min. $(\beta^-)Sn^{125}$, and 10 day $(\beta^-)Sn^{125}$. Duffield and Langer[3] who also used separated isotopes have investigated further the 40-min. $(\beta^-, \gamma)Sn^{123}$ and 10-min. $(\beta^-, \gamma)Sn^{125}$ activities. The present paper is concerned with the activities of Sn^{117m} and Sn^{119m} produced from Sn^{116} and Sn^{118} by neutron capture.

II. EXPERIMENTAL DATA

Four tin samples, enriched in Sn^{116}, Sn^{118}, Sn^{120}, and Sn^{122} were bombarded in the Oak Ridge pile for a period of one month. The compositions of the sources before bombardment are given in Table I. Following bombardment the activities were investigated principally by photographic and counter spectrometers.

Sn^{117m}

An isomeric activity of $14\pm\frac{1}{4}$ day has been assigned[4] to Sn^{117m}. This activity was previously[1] attributed to Sn^{119m}. Aluminum absorption showed the presence of a nearly monochromatic group of electrons of approximately 130 kev. An exposure in a spectrograph showed electron conversion lines corresponding to two γ-ray transitions of 159 ± 1 and 162 ± 1 kev. Table II shows the energies and relative intensities of these lines. Intensities of the lines were determined photometrically and over a period of one month it was found that all lines had the same decay rates to within about 10 percent.

The higher relative intensities of the 159 kev transition lines, together with their lower N_K/N_L ratio, indicate that this transition is of higher multipole order than the 162-kev transition, and is most likely associated with the 14-day decay of the Sn^{117m} isomer. An analysis of the experimental and theoretical values is given in Table III. The experimental N_K/N_L value for the 159 kev transition lies between the available theoretical values for 2^4 magnetic and 2^5 electric transitions.

Assuming that the 159-kev transition is followed only by the 162-kev transition, and also that the 159-kev transition is practically 100 percent internally converted, we can obtain immediately the *K*-conversion coefficient of the 162-kev transition. The experimental value of N_K/N_γ indicates that this transition is 2^1 magnetic.

Experiments by R. Stump, of this laboratory, have shown the existence of $e^- - \gamma$(~160 kev) and $X - \gamma$-(~160 kev) coincidences which confirm the double transition process assumed above. An upper limit of

TABLE I. Composition of tin sources.*

Stable isotope	"116" sample	"118" sample	"120" sample	"122" sample
112	<0.1%	0.2%	1.1%	<0.2%
114	<0.1	<0.1	0.2	<0.2
115	<0.1	<0.1	<0.1	<0.2
116	74.5	1.1	0.4	6.3
117	8.0	2.0	1.1	5.0
118	3.0	91.8	0.8	10.5
119	7.4	2.2	1.3	6.2
120	2.9	2.2	95.4	19.2
122	3.7	0.3	0.2	45.8
124	0.4	0.3	0.3	7.1

* The enriched isotopes used in this investigation were supplied by the Isotopes Division, Carbide and Carbon Chemical Corp., Y-12 Plant, Oak Ridge, Tennessee, and obtained on allocation from the U.S. Atomic Energy Commission.

TABLE II. Conversion electron lines of Sn^{117m}.

Energy (kev)	Relative Intensity	Assignment
130 ± 1	60	159—*K*
133 ± 1	10	162—*K*
155 ± 1	27	159—*L*
158 ± 1	4	162—*L* 159—*M*

* Now at Brookhaven National Laboratory, Long Island, New York.

** This work was assisted in part by the joint program of the ONR and AEC.

[1] G. T. Seaborg and I. Perlman, Rev. Mod. Phys. **20**, 585 (1948).

[2] J. C. Lee and M. L. Pool, Phys. Rev. **76**, 606 (1949).

[3] R. B. Duffield and L. M. Langer, Phys. Rev. **76**, 1272 (1949); **77**, 743 (1950).

[4] E. C. Mallary and M. L. Pool, Phys. Rev. **77**, 743 (1950); **77**, 75 (1950); J. W. Mihelich and R. D. Hill, Phys. Rev. **77**, 743 (1950).

TABLE III. Comparison of experimental and theoretical results.

Isomer	γ-energy (kev)	Lifetime Experiment (sec.)	Lifetime Theoretical[a] (sec.)	N_K/N_L Experiment	N_K/N_L Theoretical		N_K/N_γ Experiment	N_K/N_γ Theoretical	
Sn^{117m}	159±1	1.3×10^{6}	1×10^{4} ($l=4$)	2.2±0.4	4.1	2^4 mag.[b]		25.8	2^4 mag.[d]
			8×10^{6} ($l=5$)		0.7	2^5 elec.[c]		23.3	2^5 elec.[d]
	162±1		4×10^{-9} ($l=2$)		11.8	2^1 mag.[b]	0.10±0.03	0.13	2^1 mag.[d]
					6.5	2^2 elec.[c]		0.04	2^1 elec.[d]
								0.23	2^2 elec.[d]
Sn^{119m}	69±2	2.2×10^{7}	9.0×10^{8} 2^4 mag.	1.5±0.5	1.5	2^4 mag.[b]		2600	2^4 mag.[e]
			5.7×10^{7} 2^5 elec.		0.015	2^5 elec.[c]		1200	2^5 elec.[e]

[a] Theoretical lifetimes derived from the formula: $\tau_\gamma = 3(l!)^2/\rho^{2l}\cdot(137/W)^{2l+1}\cdot(\hbar/mc^2)$, for $\begin{cases}2^l \text{ elec.}\\ 2^{l-1} \text{ mag.}\end{cases}$, and the above tabulated values are equal to: $\tau_\gamma/(1+N_e/N_\gamma)$.
[b] Obtained from N. Tralli and I. S. Lowen, Phys. Rev. **76**, 1541 (1949). Curves apply to $Z=35$.
[c] Calculated from M. H. Hebb and E. Nelson, Phys. Rev. **58**, 486 (1940).
[d] Obtained from M. E. Rose and others, "Tables of *K*-Shell Conversion Coefficients," Phys. Rev. **76**, 1883 (1949).
[e] Calculated from S. D. Drell, Phys. Rev. **75**, 132 (1949) and M. H. Hebb and E. Nelson, reference c.

10^{-6} sec. was tentatively set for the lifetime of the intermediate state.

The proposed decay scheme for Sn^{117m} is shown in Fig. 1.

Sn^{119m}

A new activity of approximately 250-day half-life has been ascribed to Sn^{119m}. This activity has now been followed for more than 9 months and its decay curve thus far is shown in Fig. 2. The activity appears to be produced only weakly by neutron bombardment in the pile. The decomposition of the decay curve is complicated by the presence of other possible long-lived contaminants, such as: 104-day Sn^{113}, 130-day Sn^{123} and 2½-year Sb^{125}. However, by comparison of this decay curve with similar ones from samples "116," "120," and "122" tin, it is apparent that there is in the "118" sample a unique long-lived component ascribable to Sn^{119m}.

A long exposure in a spectrograph showed the presence of three very faint conversion lines which had energies corresponding to the *K*, *L*, and *M* conversions of a 69±2-kev transition. A search was then made in a counter spectrometer and the existence of these lines was confirmed, as is shown in Fig. 3.

Owing to the low energy and low intensity of the conversion lines, an accurate value of N_K/N_L for this

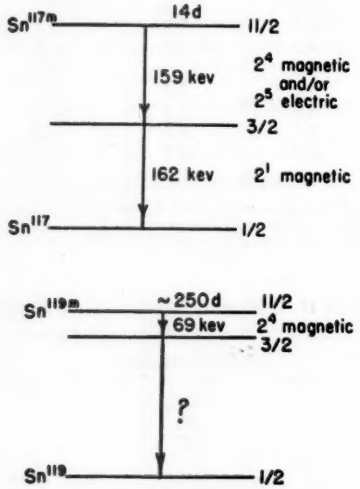

FIG. 1. Decay schemes for Sn^{117m} and Sn^{119m}.

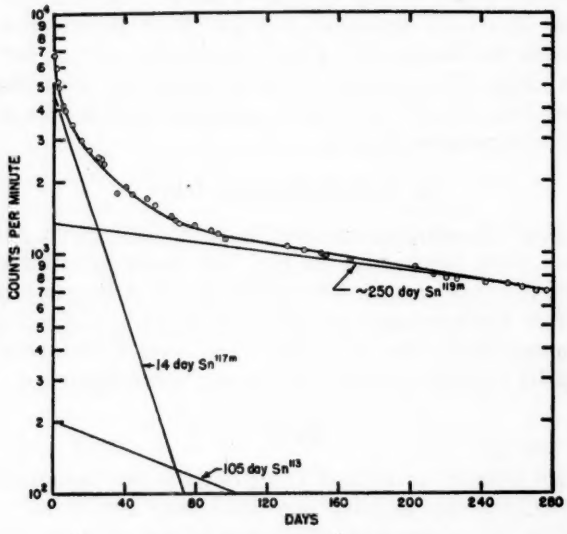

FIG. 2. Decay curves of Sn^{119m}.

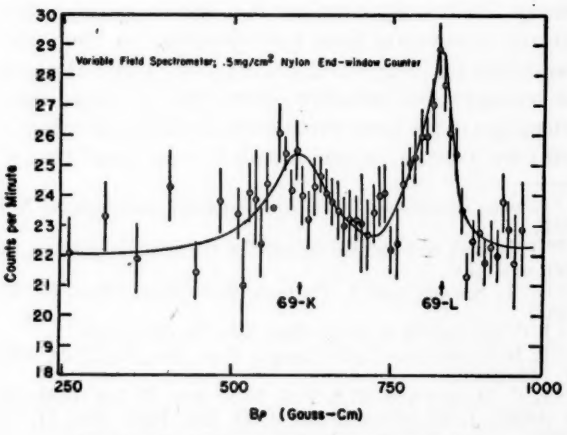

FIG. 3. Electron conversion lines from Sn^{119m}.

transition was difficult to obtain. After correcting for the ρ-values of the lines[5] and for absorption in the 0.5 mg/cm^2 Nylon window of the counter,[6] a value of $N_K/N_L=1.5\pm0.5$ was obtained. Comparison of this value with theoretical values is made in Table III. It would appear that the lifetime of the Sn^{119m} isomer is consistent only with a multipole order of 5 and the N_K/N_L ratio indicates predominantly magnetic 2^4-pole radiation.

The spin of the ground state of Sn^{119} has been measured[7] and observed to be $\frac{1}{2}$. If, as is indicated from current nuclear shell-structure theory, the angular momentum of the upper excited state of Sn^{119m} is 11/2, and if it is correct that the 69-kev transition is magnetic 2^4-pole, then the ground state of Sn^{119} can only be reached via a second transition, as in the case of Sn^{117m} decay. It is unlikely that the second transition would have been observed in our experiments because of its probable low internal conversion and the weakness of the source. The proposed decay scheme for Sn^{119m} is shown in Fig. 1.

[5] J. L. Lawson and A. W. Tyler, Rev. Sci. Inst. **11**, 17 (1940).
[6] D. Saxon, privately distributed absorption curves.
[7] W. G. Proctor, Phys. Rev. **76**, 684 (1949); H. Schüler and H. Westmeyer, Naturwiss. **21**, 660 (1933).

PHYSICAL REVIEW VOLUME 79, NUMBER 5 SEPTEMBER 1, 1950

Radioactive Isotopes of Gadolinium*

R. E. Hein** and A. F. Voigt
Institute for Atomic Research and Department of Chemistry, Iowa State College, Ames, Iowa
(Received April 24, 1950)

A 236-day neutron induced activity in gadolinium purified by ion exchange methods is assigned to Gd^{153}. The activity decays by K-electron capture emitting a 106-kev γ-ray giving rise to K- and L-electron groups. A 7.2±0.2 day and approximately 24-hour activity present in the neutron bombarded gadolinium were separated on an ion exchange column. The 7.2-day activity assigned to Tb^{161} decays by emission of 0.50-Mev β-particles. The 24-hour activity is tentatively assigned to Gd^{159}.

Half-life measurements on gadolinium produced by deuteron bombardment of europium extend over 600 days. The activity decaying with a half-life of 155 days initially is slowly lengthening into a longer half-life. A 265-kev γ-ray is detected in addition to the 106-kev γ-ray previously found in Gd^{153}. The 265-kev γ-ray is assigned to Gd^{151} which decays with a half-life of 150 days. This half-life is based on ratios of the 106-kev γ-ray to the 265-kev γ-ray observed over a 600-day period.

THE gadolinium activities produced by deuteron bombardment of europium and neutron bombardment of gadolinium are discussed in this paper.

The gadolinium oxide was loaned for this investigation by the rare earth group under Dr. F. H. Spedding. Spectrographic analysis indicated the presence of samarium (0.28 percent) and possibly terbium, but the amount of this contaminant could not be estimated. Samples of the gadolinium oxide were irradiated at two different times at the Argonne Laboratory. The first bombardment of 400 hours did not give a sufficiently intense sample of the long-lived gadolinium, so a second bombardment lasting 854 hours was obtained.

In order to eliminate possible europium and samarium activities produced by (n, p) and (n, α) reactions, the active sample was extracted several times with sodium amalgam. The small amount of activity extracted into the amalgam had the same energy characteristics as did the non-extracted portions. It appeared safe to say that no europium or samarium activities were present in the long-lived gadolinium.

Cation exchange experiments with Nalcite high capacity resin separated the rare earth contaminants that could not be separated by reduction methods. The irradiated gadolinium was adsorbed on a resin bed 1 cm I.D. and 20 cm long. The mesh size of the resin varied in different experiments. Generally the resin was put in the ammonium cycle and the activity eluted with 0.1 percent ammonium citrate solution. The separation of activities effected in such an experiment is indicated in Fig. 1. The counts/min./ml in the fractions of eluate were determined with a dipping counter tube and scaling circuit. The contaminants were identified by half-life and energy measurements with the Yb^{169} activity identification aided by electron coincidence measurements.

Half-life measurements on the neutron bombarded gadolinum now extend over 550 days. Measurements through 225 mg/cm^2 of aluminum give 236±3 days as the half-life value (see Fig. 2). No positrons could be detected by magnetic deflection experiments. The x-ray present was identified as the Eu K x-ray by critical

* Contribution No. 99. Work performed at the Ames Laboratory of the AEC.
** Abstracted from a dissertation submitted by Richard E. Hein to the graduate faculty of Iowa State College in partial fulfillment of requirement for the degree of Doctor of Philosophy, 1950. Present address: Chemistry Department, Kansas State College, Manhattan, Kansas.

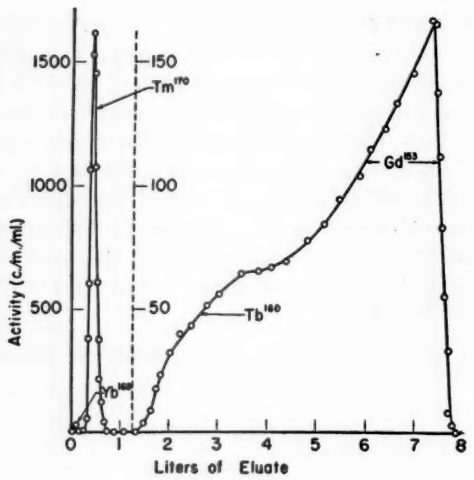

FIG. 1. Elution curve of neutron induced activities in Gd_2O_3. Eluting agent 0.1 percent ammonium citrate solution at a *p*H of 5.5.

absorption measurements. This identification will be discussed in more detail for the long-lived gadolinium produced in deuteron-bombarded europium. The isotope must then decay by *K*-electron capture and is assigned to Gd^{153}. Gd^{151} is the only other isotope that could decay to a stable europium. However the $(n, 2n)$ reaction necessary to produce this isotope is not observed with pile neutrons to an extent sufficient to explain the observed activity. The assignment of the 236-day activity is corroborated by mass spectrographic work. Inghram, Hayden, and Hess[1] showed that an isotope of half-life >72 days could be produced by neutron bombardment of gadolinium, the mass number of the active isotope being 153.

Copper absorption curves of the Gd^{153} indicate only one γ-ray with an energy of 106 kev (Fig. 3). It has been reported[2] that a long-lived neutron induced isotope of gadolinium decays to europium emitting gamma-radiation, highly converted, with an energy of 102 kev. The 106-kev γ-ray is undoubtedly the same as the 102-kev γ-ray.

The *K*-electrons from the conversion of the 106-kev γ-ray are too weak to be detected in an aluminum absorption curve under ordinary counting conditions. The *L* x-rays and *L*-conversion electrons are present as indicated by aluminum absorption curves.

A tentative decay scheme for Gd^{153} (see Fig. 4) is based on coincidence studies supplemented by aluminum and copper absorption curves. Only one group of electrons (*L*-conversion) are observed in the decay scheme as the ratio of $Ce\gamma/Ce$ is a constant. The conversion coefficient for the 106-kev γ-ray is greater than 0.9.

Two short-lived activities were present in the neutron bombarded gadolinium with half-lives of 24±3 hr. and 7.2±0.2 days (Fig. 5). Recently Butement[3] has reported similar values of 18±2 hr. and 6.75±0.1 days in addition to a 3.6-min. activity which was too short-lived to be observed here. Other investigators[4] reported approximately the same half-lives, 18 hr. and 5.5 days. The consensus appears to be that the 18-hr. activity should be assigned to Gd^{159}, the 7-day activity to Tb^{161} and the 3.6-min. activity to Gd^{161}. No long-lived activity was reported by any of these investigators. Recently it has come to our attention that other workers have also observed the long-lived neutron induced gadolinium activity, reporting 225 days for its half-life.[5]

The present investigation was not pointed toward the short-lived nuclides. However, it was possible to separate the 7.2-day activity from the gadolinium activities as is indicated in Fig. 6. This separation was effected by ion exchange resin columns in a manner similar to that described earlier in this paper.

As the separation was completed eight days after the sample was removed from the pile, the short-lived component had decayed to a low intensity. However this chemical separation would verify the assignment of the 7.2-day activity to an element other than gadolinium. Since the 7.2-day activity precedes the gadolinium activity from the ion exchange column, it is most probably a terbium isotope. Using the results of other investigators, the mass assignment is made to Tb^{161}. The short-lived gadolinium activity is not the parent of Tb^{161} as no 7.2-day activity grew into the separated gadolinium fraction. Presumably the 24±3-hour gadolinium would be assigned to Gd^{159}.

A β-ray of a half-thickness of 15 mg/cm² corresponding to 0.50 Mev is associated with the 7.2-day activity. A β-ray of half-thickness of 31 mg/cm² or energy of 0.80 Mev is associated with the decay of the 24-hour activity. The γ-ray energies connected with the short lived activities were not determined.

An experiment is planned to check the short half-lives produced in neutron-bombarded gadolinium. It is

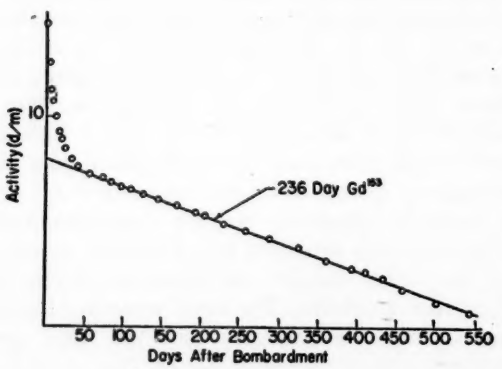

FIG. 2. Half-life curve for Gd^{153} from neutron-bombarded Gd_2O_3. Points taken through 225 mg/cm² of aluminum.

[1] Inghram, Hayden, and Hess, Phys. Rev. **71**, 643 (1947).
[2] Cork, Shreffler, and Fowler, Phys. Rev. **74**, 240 (1948).
[3] F. D. S. Butement, Phys. Rev. **75**, 1276 (1949).
[4] Krisberg, Pool, and Hibdon, Phys. Rev. **74**, 1249A (1948).
[5] B. H. Ketelle, unpublished results.

possible that the 24±3-hour activity is a mixture of the 18-hour half-life already reported for gadolinium and the 47-hour Sm^{153}, since samarium is a known impurity in the gadolinium.

The gadolinium produced by deuteron bombardment of europium was first given a half-life of 155 to 170 days and was shown to be chemically different from europium.[6] Recently published work has given a half-life of about 75 days to the activity produced by a deuteron bombardment of europium[7] but this material was not taken through a chemical separation and the 75-day half-life was observed as a minor component in the decay.

A sample of Eu_2O_3 loaned for this investigation by Dr. F. H. Spedding was given 870 microampere hours of bombardment with 20-Mev deuterons by the Berkeley 60-inch cyclotron. The gadolinium was purified with respect to europium (also any samarium or ytterbium present as impurities) by sodium amalgam extractions. Inactive europium carrier was added in later extractions to insure the removal of traces of active europium.

Decay measurements on the gadolinium now extend over 625 days. The half-life is lengthening from an original value of 155 days (see Fig. 7). The possibility of a long-lived europium contamination cannot be completely discounted but the probability seems slight in view of the extensive purification of the gadolinium.

Attempts have been made to establish the purity of the gadolinium fraction by ion exchange methods. The combination of a small ion exchange column, eluate counting cell and recording rate meter was used.[8] A sample of the active gadolinium was adsorbed on Dowex-50 resin and eluted with 5 percent ammonium citrate solution at a pH of 3.4. Only one sharp peak was observed on the rate meter circuit graph. Pre- and post-peak fractions gave identical aluminum absorption curves. To test the efficiency of the experimental set-up, a known mixture of Eu and Gd activities was adsorbed on the column and eluted as in the previous experiment. Only one broad peak was observed. However aluminum absorption curves on pre- and post-peak fractions indicated that a separation of the order of 20 percent was achieved. It was suspected that two peaks were not observed because the volume of the counting cell (0.5 ml) was too large with respect to the total volume of liquid in the column (0.9 ml) allowing mixing of the peaks at this point. A much smaller cell (0.01 ml) was prepared. However another sample of gadolinium activity on elution had only one sharp peak. Ion exchange experiments with large columns similar to those described in the purification of the neutron bombarded gadolinium also indicated that the gadolinium is a pure fraction.

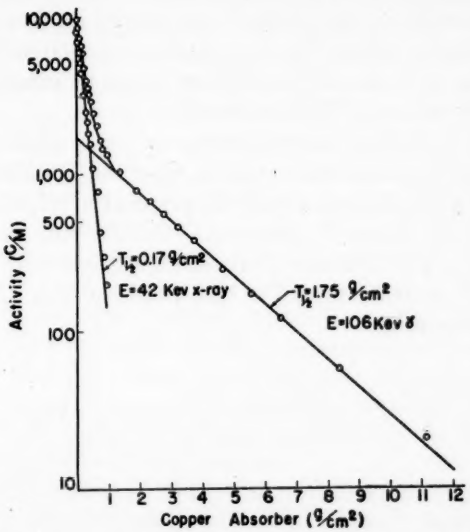

FIG. 3. Copper absorption curve of radiations of Gd^{153}.

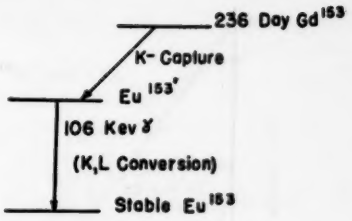

FIG. 4. Probable decay scheme of Gd^{153}.

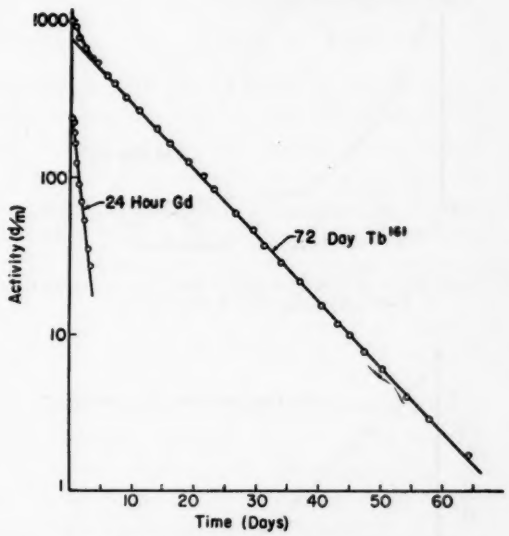

FIG. 5. Decay curve of short-lived components in neutron bombarded Gd_2O_3.

The γ-ray energies of 101 and 265 kev were determined by absorption in copper (see Fig. 8) and lead. The values from the copper curve are preferred because of the proximity of the 101-kev gamma and the K absorption edge (87.5 kev) in lead. The 101-kev γ-ray is probably identical with the 106-kev γ-ray in neutron bombarded gadolinium.

No positrons could be detected by means of magnetic deflection measurements. The x-ray present was identi-

[6] K. Fajans and A. F. Voigt, Phys. Rev. **60**, 533 (1941).
[7] Krisberg, Pool, and Hibdon, Phys. Rev. **74**, 44 (1948).
[8] Constructed by D. S. Martin and Darleane Christian of this Laboratory.

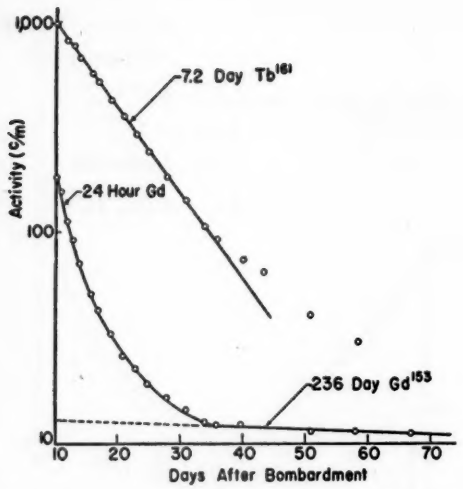

FIG. 6. Decay curve on fractions eluted from ion exchange column, Tb^{161} preceding Gd* from column.

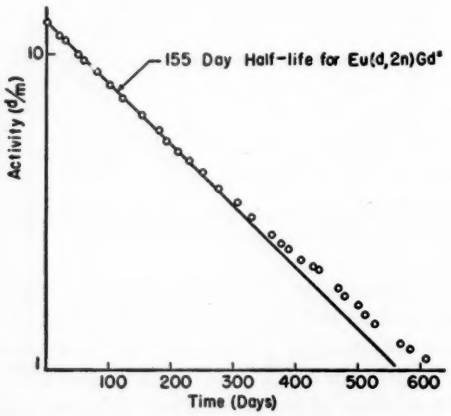

FIG. 7. Half-life curve for gadolinium activities from deuteron-bombarded Eu_2O_3.

fied as the Eu *K* x-ray by critical absorption measurements. The following absorbers of La, Ce, Pr and Nd oxides were weighed out in aluminum dishes: 180, 150, 120, 90, 60, 40 and 20 mg/cm². The same sample of active gadolinium was used with the same geometry for all the absorption curves. The experimental half-thicknesses are given as follows:

La	Ce	Pr	Nd
75 mg/cm²	72 mg/cm²	160 mg/cm²	156 mg/cm².

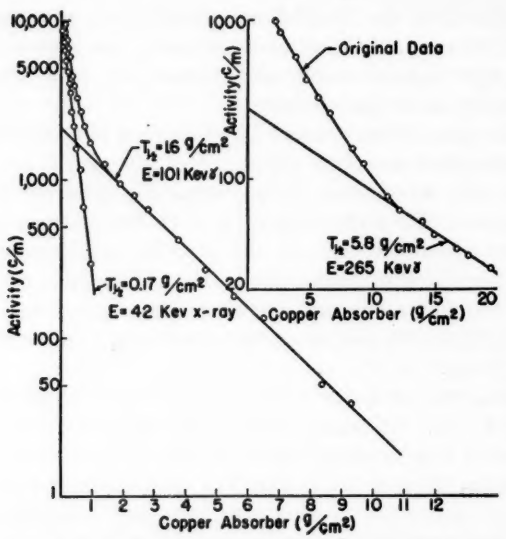

FIG. 8. Copper absorption curve for radiations of gadolinium activities produced in deuteron-bombarded Eu_2O_3. The 101-kev γ- and x-ray are subtractions from the original data in the inset.

From these data it appears quite conclusively that the x-ray energy is between the cerium and praseodymium absorption edges and is therefore due to europium.

Since the purity of the gadolinium activity produced by deuteron bombardment of europium has been established and since the γ-ray energy of the Eu(*d*, 2*n*)Gd* is different from that of $Gd^{152}(n, \gamma)Gd^{153}$, both Gd^{151} and Gd^{153} appear to be formed in deuteron bombarded europium. The 265-kev gamma-ray must be connected with the decay of Gd^{151}. Since this was the only γ-ray other than the 102-kev γ-ray of Gd^{153} the decay scheme of Gd^{151} is probably simple, like that of Gd^{153}. The ratio of intensities of the 102-kev γ-ray to the 265-kev γ-ray at different times, 590 days apart, was used with the 236-day half-life of the 102-kev γ-ray to calculate a half-life value of 150 days for Gd^{151}.

This calculated half-life agrees well with what would be expected from the over-all decay of the Eu(*d*, 2*n*)Gd* activity (Fig. 7). Apparently the process $Eu^{153}(d, 2n)Gd^{153}$ occurs to about 5 percent of the $Eu^{151}(d, 2n)Gd^{151}$ process. The 265-kev γ-ray is highly internally converted, as is evidenced by the presence of a 220-kev electron group.

The Neutrons from the Disintegration of C^{13} by Deuterons*

C. E. MANDEVILLE AND C. P. SWANN
Bartol Research Foundation of The Franklin Institute, Swarthmore, Pennsylvania
(Received May 19, 1950)

Nuclear energy levels in N^{14} are calculated from Q-values of neutron groups in the reaction $C^{13}(D,n)N^{14}$. Levels occur at 2.19±0.07, 3.47±0.07, 3.87±0.07, and 4.90±0.07 Mev. From a comparison with results of other measurements, it appears that several different nuclear reactions excite the same levels in N^{14}.

I. INTRODUCTION

THE neutrons from deuterons on carbon were investigated by Bonner and Brubaker[1] who irradiated the unseparated isotopes of carbon with deuterons of energy 0.9 Mev. The nuclear reactions are

$$C^{12}+D\rightarrow N^{13}+n^1+Q_1, \quad (1)$$

$$C^{13}+D\rightarrow N^{14}+n^1+Q_2 \rightarrow {}^*N^{14}+n^1+{}^*Q_2. \quad (2)$$

They measured the energies of the neutrons by noting the ranges of the recoil protons in a cloud chamber. These early measurements gave a value of -0.37 ± 0.05 Mev for Q_1, and 5.2 ± 0.4 Mev for Q_2. A group of neutrons was also noted at ${}^*Q_2=1.2$ Mev. Using the method of cloud-chamber recoils and a target of C^{13} having an isotopic concentration of 23 percent, an additional value of ${}^*Q_2$ was found at 0.40 Mev by the Rice group.[2]

Bennett and Richards[3] have shown that for bombarding energies of 2 Mev or less, the neutrons of reaction (1) are monochromatic. The Q-value for reaction (1) has recently been redetermined very accurately[4] at -0.281 ± 0.003 Mev. Since the neutrons of reaction (1) are endothermic in character, the exothermic neutrons of reaction (2) can be observed without ambiguity, regardless of the concentration of C^{12} in the target. Naturally occurring carbon is 99 percent C^{12}. In the present experiments, the isotopic concentration of C^{13} was 53 percent in $BaCO_3$ obtained from the Research Laboratory of the Eastman Kodak Company, Rochester, New York. Targets of $BaCO_3$, having a thickness of 100 kev at the bombarding energy employed, were obtained by preparing suspensions of $BaCO_3$ by mixing 100 mg of $BaCO_3$ with 1 cc of H_2O. A suspension of fine particles, obtained by allowing the original suspension to settle for 30 sec., was transferred with a pipette to a silver disk. The water was evaporated slowly under an infra-red heating lamp, leaving on the disk a smooth uniform film of $BaCO_3$. Occasional agitation of the evaporating suspension aided in producing a uniform deposition of the solid.

Recoil protons of the neutrons located in reactions (1) and (2) were detected in Ilford C_2 plates located at distances of 2 to 10 cm from the target and making angles of zero and 90 degrees with the bombarding beam in the laboratory system of coordinate axes. Recoils making angles within 12° of the forward direction were deemed acceptable, and the track lengths were measured in a microscope. The observed neutron energies were increased by two percent to allow for the use of the finite angle of acceptance. Suitable corrections were also made for variation with energy of the $n-p$ scattering cross section and acceptance probability.

II. THE NEUTRON SPECTRA

In the first exposure, photographic plates were located at zero degrees with the bombarding beam, the edges of the plates being a distance of 10 cm from the target. After an exposure of 7 μa-hr. at a mean bombarding energy of 1.43 Mev, the spectrum of Fig. 1 was obtained. Groups appear at neutron energies of 0.95, 1.65, 2.64, 3.04, and 6.42 Mev. The group at 0.95 Mev is assigned to $C^{12}(D,n)N^{13}$ whereas the one at 1.65 Mev arises from $C^{13}(D,n)N^{14}$ and was previously said[3] to have a Q-value of 0.40 Mev. The Q-value calculated from the present data is 0.27 ± 0.05 Mev.

In order to locate more precisely the groups of high energy, measurements were continued with the acceptance of only those tracks corresponding to energies

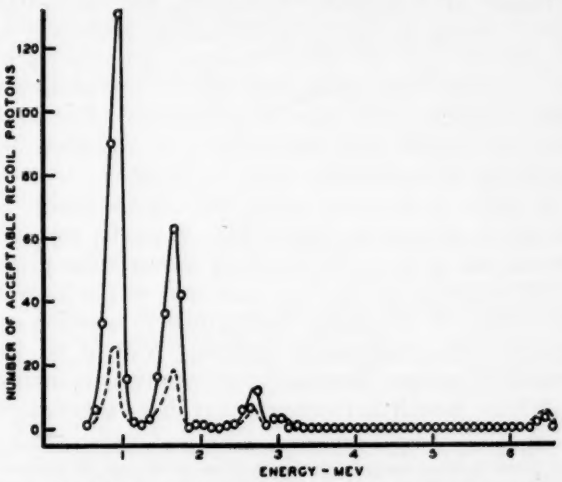

FIG. 1. Distribution in energy of the recoil protons knocked on by neutrons from $C^{13}(D,n)N^{14}$. Observations were made at an angle of zero degrees with the incident deuterons. Correction of the distribution for variation with energy of $n-p$ scattering cross section and acceptance probability is given by the broken line. The bombarding energy was 1.43 Mev.

* Assisted by the joint program of the ONR and AEC.

[1] T. W. Bonner and W. M. Brubaker, Phys. Rev. **50**, 308 (1936).

[2] Bennett, Bonner, Hudspeth, Richards, and Watt, Phys. Rev. **59**, 781 (1941).

[3] W. E. Bennett and H. T. Richards, Phys. Rev. **71**, 565 (1947).

[4] Bonner, Evans, and Hill, Phys. Rev. **75**, 1398 (1949).

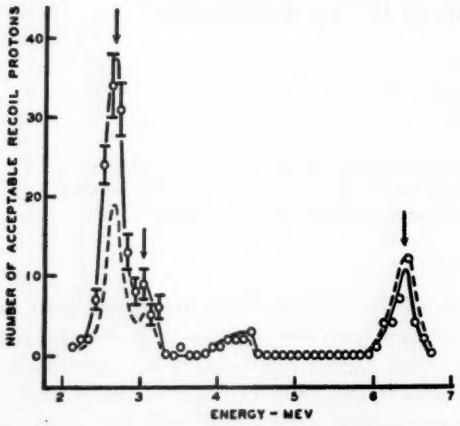

FIG. 2. High energy neutrons emitted in the forward direction from the disintegration of C^{13} by deuterons. The Q-values of the groups indicated by arrows are 1.30 ± 0.05, 1.70 ± 0.05, and 5.17 ± 0.05 Mev. A group of low intensity also is present, though poorly defined, between neutron energies of 4 and 5 Mev.

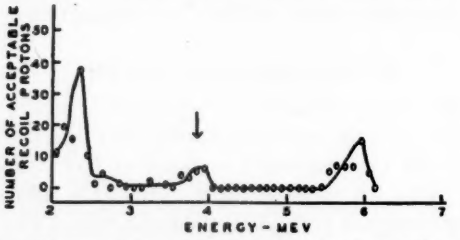

FIG. 3. Neutrons from $C^{13}(D,n)N^{14}$ emitted at 90° with the incident deuterons of energy 1.43 Mev. A neutron group at an observed energy of 3.85 Mev ($^*Q_2=2.98\pm0.05$ Mev) is clearly present.

greater than 2 Mev. When these newly observed tracks were combined with those of energy in excess of 2 Mev in Fig. 1, the energy distribution of Fig. 2 resulted. The observed energies of the neutron groups denoted by arrows are 2.68, 3.06, and 6.42 Mev, corresponding to Q-values[5] of 1.30 ± 0.05, 1.70 ± 0.05, and 5.17 ± 0.05 Mev. A poorly defined group of neutrons appears to be centered at about 4.3 Mev. However, only ten tracks are included in the group, although 2.5 cm² of surface area of photographic plate were surveyed. The weak group also appears near the energy where any deuteron-deuterium contamination might be found.

In order to determine more precisely the nature of the group of particles, near 4 Mev, a second exposure was carried out at 1.43 Mev with photographic plates at 90° with the bombarding beam and within 2 cm of the target. At this angle, the neutrons in question appeared with considerable intensity relative to the remaining groups. Their observed position in energy, 3.85 Mev, is such as to suggest that they cannot result from deuterium contamination of the target. The position of neutrons from the deuteron-deuterium reaction would have shifted from 4.66 Mev in the forward direction to 2.83 Mev at 90° with the incident deuterons. The deuteron-deuterium reaction has never been observed to contaminate any experiment at Bartol, but the low intensity of the group made it necessary to verify the assignment to $C^{13}(D,n)^*N^{14}$ by noting the change of energy with angle. The Q-value of this group of neutrons, calculated from its position in Fig. 3 is 2.98 ± 0.05 Mev.

[5] The group at $^*Q_2=1.70$ Mev appears as a satellite relative to the more intense one at $^*Q_3=1.30$ Mev. Although its presence might be difficult to justify on considering the statistical probable errors of the points, the breadth of the two groups at the base is too great to assign to a single group. This interpretation is strengthened by the fact that the satellite is located on the high energy side of the principal group. Had it appeared on the low energy side, it might easily have been explained by scattering of the more energetic particles.

III. DISCUSSION OF RESULTS

The groups of neutrons observed in these measurements establish energy levels in N^{14} at 2.19 ± 0.07, 3.47 ± 0.07, 3.87 ± 0.07, and 4.90 ± 0.07 Mev. Thomas and Lauritsen[6] have reported gamma-rays having energies of 6.1, 5.7, 5.1, 3.9, 3.4, 2.3, 1.6, and 0.73 resulting from deuterons on C^{13}. Many of these quanta can be accounted for by transitions between the levels of N^{14} reported in this paper. However, some of the gamma-rays may be related to the reactions

$$C^{13}+D\rightarrow C^{14}+H^1+Q_3 \rightarrow {}^*C^{14}+H^1+{}^*Q_3, \quad (3)$$

$$C^{13}+D\rightarrow B^{11}+He^4+Q_4. \quad (4)$$

For reaction (3), values of $Q_3=5.91\pm0.03$ Mev and $^*Q_3=0.32\pm0.03$ have been reported.[7] No excited states of B^{11} have as yet been observed in reaction (4). Sherr, Muether, and White[8] have reported gamma-rays of energy 2.3 ± 0.2 Mev emitted in de-excitation of N^{14}, formed in the radioactive decay of O^{14}. This level at 2.3 Mev compares favorably with the value 2.19 Mev obtained in these neutron measurements. Fowler, Lauritsen, and Lauritsen[9] report gamma-ray energies of 8.1, 5.8, and 2.3 Mev emitted in the reaction $C^{13}(p,\gamma)^*N^{14}$. Here again, the 2.3-Mev gamma-ray may result from de-excitation of the level observed in the present measurements.

Stuhlinger[10] has found energy levels in N^{14} at 4.0, 4.8, 5.4, 6.1, and 6.6 Mev in the reaction $B^{11}(d,N^1)N^{14}$. Alburger[11] has reported gamma-rays of energy 4.0 Mev and 2.3 Mev from the reaction $O^{16}(d,\alpha)N^{14}$.

Although uncertainties of several percent are associated with all of the quoted values, the frequent recurrence of at least some levels (e.g., the excited state at ~2.3 Mev), makes it seem reasonable to assume that the different methods of excitation do lead to the same excited levels of N^{14}.

The writers wish to express appreciation to Dr. Edward Shapiro for having prepared the thin targets of $BaCO_3$, and to acknowledge the continued interest of Dr. W. F. G. Swann, Director of Bartol.

[6] R. G. Thomas and T. Lauritsen, Phys. Rev. **78**, 88 (1950).
[7] C. D. Curling and J. O. Newton, Nature **165**, 609 (1950).
[8] Sherr, Muether, and White, Phys. Rev. **75**, 282 (1949).
[9] Fowler, Lauritsen, and Lauritsen, Rev. Mod. Phys. **20**, 236 (1948).
[10] E. Stuhlinger, Zeits. f. Physik **114**, 185 (1939).
[11] D. E. Alburger, Phys. Rev. **75**, 51 (1949).

A Mass Spectrometric Investigation of Branching in Cu^{64}, Br^{80}, Br^{82} and I^{128}

JOHN H. REYNOLDS*
*Department of Physics, University of Chicago, Chicago, Illinois***
(Received May 2, 1950)

An investigation of branching in certain neutron induced activities has been carried out by a mass spectrometric technique. Gram quantities of the elements in question were subjected to prolonged irradiation in a graphite moderated pile and were allowed to cool. The occurrence of negatron emission in the induced activities was identified with the presence in the irradiated sample of decay products of atomic number $Z+1$; positron emission and orbital electron capture, with the presence of decay products of atomic number $Z-1$. The amounts of these decay products were determined by adding to a solution of the irradiated sample, as tracers, weighed milligram amounts of the daughter elements in a form isotopically *different* from the radiogenic material. When isotopic mixing had occurred, the daughter elements were isolated for mass spectrometric analysis. In such a procedure, quantitative recovery is unnecessary: the branching ratio can be determined from the change in the isotopic constitution of the tracers. The following values of the branching ratio $\lambda_{\pm}$ (defined as the ratio of $Z\rightarrow Z-1$ transitions to $Z\rightarrow Z+1$ transitions) were determined:

Cu^{64} 1.62 ± 0.11; Br^{80} 0.090 ± 0.002; Br^{82} <0.00027; I^{128} 0.053 ± 0.002.

In addition, the following neutron absorption cross section ratios were evaluated. For moderated pile neutrons:

$$\frac{\sigma_a(Cu^{63})}{\sigma_a(Cu^{65})}=2.32\pm0.11; \quad \frac{\sigma_a(Br^{79})}{\sigma_a(Br^{81})}=3.86\pm0.05.$$

I. INTRODUCTION

AMONG the stable nuclear species now known, there are 62 even-even isobaric pairs which differ in atomic number by two and which are separated by an unstable odd-odd nucleus of intermediate atomic number. According to present theories of beta-decay, these intermediate nuclei are unstable with respect to both the isobaric transitions $Z\rightarrow Z-1$ and $Z\rightarrow Z+1$. Hence branching may be expected to take place in the decay schemes of these nuclei to an extent which may or may not be experimentally observable, depending chiefly on the energies available for the alternate modes of decay. Experimentally, branching has been reported as definitely occurring in only 12 of these 62 cases. This fact alone is good evidence that the decay schemes of such nuclei deserve more careful study.

The purpose of the work described in this paper was to examine the branching properties of a group of these nuclei which can be formed by the (n,γ) reaction. All such nuclei are known to emit negatrons so that the efforts of this investigation are necessarily focused on the question of whether or not the processes of positron emission or orbital electron capture are concurrent. The mass spectrometric method of investigation, first employed for artificial activities by Hayden, Reynolds, and Inghram[1] in a study of neutron irradiated europium, takes advantage of the fact that, whereas negatron emission leads to product nuclei of atomic number $Z+1$, positron emission or orbital electron capture lead to product nuclei of atomic number $(Z-1)$, Z being the atomic number of the irradiated element. The amount of a decay product in an irradiated sample, even though present only in parts per million, can be measured with precision by use of the mass spectrometer and an isotope dilution technique.

Results for four nuclei are presented in this paper: Cu^{64}, Br^{80}, Br^{82}, and I^{128}. Of these, Cu^{64} has long been known to decay by all three possible modes and the triple branching scheme has been studied with counting techniques by many investigators.[2-6] Br^{80}, Br^{82}, and I^{128} have been examined for positron emission by Barber[7] with a trochoidal apparatus. He was able to detect positrons only in the case of Br^{80}. No reliable evidence has existed heretofore on the question of orbital electron capture by these three nuclei.

II. EXPERIMENTAL METHOD

Gram quantities of reagent grade chemicals, checked spectroscopically for impurities, were used for the irradiations. Special attention was paid to impurities of atomic number $Z+1$ and $Z-1$ which would decrease the sensitivity of the technique. The elements for study were irradiated in a chemical form which met the following requirements:

(a) The form must be a convenient one from the standpoint of the chemical operations which are to be carried out after the irradiation,

(b) the form must be chemically stable with respect to physical conditions prevailing during the irradiation,

(c) the elements in chemical combination with the element of interest must not be strong neutron absorbers,

* National Research Council predoctoral fellow.
** Work done at Argonne National Laboratory.
[1] Hayden, Reynolds, and Inghram, Phys. Rev. **75**, 1500 (1949).
[2] Bradt, Gugelot, Huber, Medicus, Preiswerk, Scherrer, and Steffen, Helv. Phys. Acta **19**, 219 (1946).
[3] C. S. Cook and L. M. Langer, Phys. Rev. **73**, 601 (1948).
[4] C. S. Cook and L. M. Langer, Phys. Rev. **74**, 1241 (1948).
[5] R. Bouchez and G. Kayas, J. de phys. et rad. Ser 8, **10**, 110 (1949).
[6] Huber, Ruetschi, and Scherrer, Helv. Phys. Acta **22**, 375 (1949).
[7] W. C. Barber, Phys. Rev. **72**, 1157 (1947).

(d) the elements in chemical combination with the element of interest must not yield activities which will constitute a health hazard following the irradiation.

The samples were packed for irradiation in such a way that they could be unpacked by remote control. The samples in which rare gas decay products were sought were de-gassed before the irradiation and were packed in sealed quartz ampules to prevent any of the radiogenic gas from escaping.

After irradiation by moderated neutrons in a graphite moderated pile, the samples were allowed to cool for periods long in comparison with the half-lives in question. The samples were then unpacked by remote control and dissolved. The samples for rare gas analysis were outgassed in vacuum as will be described later. To the solutions there was added immediately a tracer solution containing weighed amounts of electromagnetically enriched isotopes of the elements $Z+1$ and $Z-1$. Electromagnetically enriched isotopes were used as tracers, rather than normal materials, so as to be able to correct for possible chemical contamination; $(Z+1)$ or $(Z-1)$-impurities in the original material or in chemical reagents used subsequently always have normal isotopic constitution, and could be observed during the final isotopic analyses at a mass number different from that of the electromagnetically enriched tracer and that of the isobaric transition under investigation. When possible, the two tracer elements were weighed into the same container and dissolved together. Thereafter the *ratio* of the amounts of the two tracer elements present in the tracer solution was fixed (was unaltered by spilling for example) and it is this quantity which enters, finally, into calculations of the branching ratio.

When isotopic mixing had taken place in the joint solution of irradiated material and tracers, quantitative chemistry was no longer required. It remained only to determine the isotopic constitution of the elements $Z+1$ and $Z-1$ as present in the solution. This was done by isolating the elements, converting them to a chemical form suitable for mass analysis, and carrying out the analysis with a single focusing, 6 in. radius, 60° magnetic sector type mass spectrometer of standard design.[8] Ion currents were measured with a 5×10^{10} ohm resistor and vibrating reed electrometer; they were automatically recorded on a moving chart. The method of magnetic scanning of ion peaks was used throughout.

Since only a fraction of a milligram of the element was available for analysis, these measurements had to be made with great care. The chief source of error in measurements of small samples is the possible contribution of impurities to the mass spectrum. Thus extraordinary care had to be taken to keep the apparatus clean. The entire spectro meterwas disassembled and re-built, prior to the series of measurements, with cleanliness as the prime object. New ion sources were installed thereafter only after parts had been vacuum and hydrogen fired at 1000°C. Frequent baking of the entire spectrometer tube, while under vacuum, was carried out in order to cut background to a minimum. As a further safeguard against impurity errors, for each element other than nickel, which was ionized thermally, the mass spectrum was observed in several different positions; e.g., singly charged metal ions, doubly charged metal ions, singly charged oxide ions, etc. Results were accepted as valid only when measurements at the several positions gave identical results.

After a satisfactory measurement of the "branching sample" was completed, the tracer for that element was subjected to mass analysis using the same technique. The tracer or "blank," of which milligram quantities were available, was always examined second in case there should be spectrometer "memory" of the first sample.

III. EXPERIMENTAL RESULTS

A. Copper

A quantity of neutron-irradiated copper metal was dissolved in nitric acid. To this solution there was added an aliquot of a tracer solution which had been prepared by dissolving weighed amounts of $Ni^{58}O$ and $Zn^{68}O$ in nitric acid. The combined solution was evaporated to eliminate excess nitric, diluted, and electrolyzed with platinum electrodes (rotating anode) until no trace of the blue cupric ion remained. The solution was made strongly acid with H_2SO_4 and treated with H_2S to precipitate final traces of copper. The nickel in the solution was then isolated by the standard dimethylglyoxime precipitation. The zinc was isolated by precipitating ZnS from a weakly acid solution.

In order to examine the isotopic constitution of the nickel isolated in this way, the organic precipitate was digested in nitric acid and a portion of the resulting solution was pipetted onto a wolfram ribbon which served, when heated in the mass spectrometer, as a source of Ni^+ ions. The ion peak at mass 64, negligible in the tracer nickel, was now prominent and could be compared with the principal peak at mass 58. The fact that the Ni^{60+} ions were no more abundant in this sample than in the tracer placed an upper limit of 0.2 percent on the amount of normal or contamination Ni^{64} present, and proved that the excess Ni^{64} was radiogenic in origin.

The zinc precipitate was converted to $ZnBr_2$ by the action of hydrobromic acid. A portion, in aqueous solution, was pipetted into a small quartz crucible which rested in a wolfram heater directly above the ion box of an electron impact ion source. By raising the heating current, the $ZnBr_2$ could be volatilized into the cross electron beam in a controlled way. Measurements were made on Zn^+, $ZnBr^+$, and $ZnBr_2^+$ ions. The amounts of Zn^{64} and Zn^{66} were greatly increased over those present in the tracer zinc; the constancy of Zn^{67}

[8] A. O. C. Nier, Rev. Sci. Inst. 11, 212 (1940).

placed an upper limit on the amount of normal zinc present and proved that the excess Zn^{64} and Zn^{66} was due to negatron decay from Cu^{64} and Cu^{66} respectively.

From the mass spectrometer measurements and from the weights recorded in the preparation of the tracer solution, the branching ratio $\lambda_{\pm}$, which can be defined as the ratio of $Z \rightarrow Z-1$ transitions to $Z \rightarrow Z+1$ transitions, was calculated. The result was

$$\lambda_{\pm}(Cu^{64}) = \text{radiogenic } Ni^{64}/\text{radiogenic } Zn^{64} = 1.62 \pm 0.11.$$

The quoted probable error of 6.8 percent is the result of an analysis of all possible sources of error. The largest uncertainty in this particular case arises from an uncertainty in the abundance of Zn^{67} in the "branching" sample of zinc; this introduces, in turn, an uncertainty in the amount of Zn^{64} present due to contamination. The cause of the uncertainty was the presence of small amounts of impurities which contributed a non-negligible ion background at mass 67.

It was also possible to calculate the ratio of the neutron absorption cross sections of Cu^{63} and Cu^{65}. For pile neutrons:

$$[\sigma_a(Cu^{63})]/[\sigma_a(Cu^{65})] = 2.32 \pm 0.11.$$

This is in poor agreement with Seren's[9] value of 1.5 ± 0.4 obtained by activation. The probable explanation for this discrepancy is that Seren's counting efficiency for the K captures in Cu^{64}, which constitute about 43 percent of the total disintegrations, was low.

In order to check on the over-all accuracy of the isotopic dilution method, a standard solution containing normal nickel and normal zinc in known proportions was prepared by weighing and dissolving gram quantities of these metals. A small fraction of this solution was then combined with a second aliquot of the Ni^{58}–Zn^{68} tracer solution used in the branching study. The nickel and zinc in the combined solution were isolated and subjected to mass analysis as before. The constants of the tracer solution and the mass spectrometer results were then used to calculate the ratio of Ni^{60} to Zn^{66} in the standard solution. The result checked the true value within 2.5 percent.

B. Bromine

For this investigation, a sample of neutron irradiated sodium bromide was processed in two weighed parts. The larger fraction was dissolved in water and combined with a weighed quantity of electromagnetically enriched Se^{78} in nitric acid. Excess nitric acid oxidized any metallic selenium present in the irradiated salt so that isotope mixing occurred on an atomic scale. The solution was then evaporated to dryness over the water bath in order to destroy nitric acid and was redissolved in 7.5 percent hydrochloric acid. Metallic selenium was precipitated by treating the solution with SO_2. The precipitate was filtered, washed, and dissolved in nitric acid. The selenium was reprecipitated from 18 percent HCl prior to mass analysis in order to increase the purity.

Mass analysis was carried out by depositing a nitric acid solution of the selenium in a small quartz crucible and following the same procedure that was used with zinc. Measurements were made on Se^+, SeO^+, and SeO_2^+ ions. A comparison of the mass spectrum of this sample with that of the Se^{78} tracer, analyzed immediately thereafter, showed a pronounced enrichment at mass 80 due to positron emission and/or orbital electron capture by Br^{80}. There was no enrichment at mass 82, showing that Br^{82} decays almost entirely by negatron emission. The abundance of Se^{76} was unchanged over that in the tracer, proving that less than 0.3 percent of the Se^{80} present was due to contamination by normal selenium.

The second smaller fraction of NaBr was processed in the apparatus shown in Fig. 1. This is a greaseless vacuum system designed specifically for the manipulation of rare gases and patterned after an arrangement used by Epstein and co-workers.[10] Symbols V1 through V5 indicate mercury valves which, normally open, may be closed by raising the level of the appropriate mercury column. C1 and C2 are activated charcoal traps for gas handling; C3 is an activated charcoal trap in which the final gas sample is isolated and sealed off. The special McLeod gauge at the right hand end of the system has been provided with an enlarged precision capillary so that amounts of gas up to 0.4 cm^3 can be measured accurately. With the apparatus arranged as in Fig. 1, the system was degassed by pumping while baking C1, C2, and C3 at 450°C. After raising V1, V3, and V5 so as to isolate the system from the pumps, a small amount of normal krypton, which served as the tracer, was introduced into the system from the gas pipette, after which the gas pipette was sealed off, completely isolating the system from stopcock grease and possible extraneous krypton. By cooling C2 with liquid air for several minutes, raising V4, and then heating C2 to 100°C, most of the tracer krypton was transferred to the bulb of the special McLeod gauge where it was isolated by compressing the gas in the bulb. The remainder of the system was then degassed by lowering V1, V3, and V5 to resume pumping and by baking C1, C2, and C3 at 450°C for 12 hours. The amount of tracer krypton stored in the McLeod gauge was measured to within 0.5 percent, meanwhile, by making repeated readings of the McLeod mercury levels.

The isotopic mixing was carried out by isolating the system from the pumps, transferring the tracer krypton to the left hand side of the system by cooling C1 and raising V4, breaking open the sealed ampule containing the irradiated salt, and allowing the gases to mix. To

[9] Seren, Friedlander, and Turkel, Phys. Rev. **72**, 888 (1947).

[10] S. Epstein, Proc. Conf. on Nuclear Chem., McMaster University, pp. 108–116 (May 1947).

make sure that all of the radiogenic gas mixed with the tracer gas, the temperature of the salt was raised until it distilled out of the ampule and refluxed vigorously down the walls of the outer quartz tube. The final gas mixture was purified by volatilizing calcium in the calcium furnace: calcium forms solid products with all but the rare gases. Purification was considered complete when the gas showed no reduction in volume, as measured in the McLeod, after successive treatments to calcium vapor. The final sample of purified krypton was isolated in the sample tube by cooling C3 and sealing off.

A mass analysis of the krypton so obtained was carried out by the standard technique of passing the gas through a small leak into the source region of the mass spectrometer. A greaseless spectrometer sample handling system was used so that there could be no possibility of contaminating the gas sample with other gases absorbed in the grease. The mass spectrum of the krypton showed heavy enrichment at masses 80 and 82 and measurements of the abundance of these isotopes were made by comparison with Kr^{83} and Kr^{84}.

With these data, the branching ratios for Br^{80} and Br^{82} were calculated:

$$\lambda_{\pm}(Br^{80}) = \text{radiogenic } Se^{80}/\text{radiogenic } Kr^{80} = 0.090 \pm 0.002;$$

$$\lambda_{\pm}(Br^{82}) = \text{radiogenic } Se^{82}/\text{radiogenic } Kr^{82} < 0.00027.$$

The data also yield the ratio of the neutron absorption cross sections of Br^{79} and Br^{81}. For pile neutrons:

$$[\sigma_a(Br^{79})]/[\sigma_a(Br^{81})] = 3.86 \pm 0.05.$$

This is in fair agreement with Seren's[9] value of 4.8 ± 1.4 obtained by activation.

C. Iodine

The procedure with irradiated NaI was very similar to that with NaBr. Again the sample was processed in two parts.

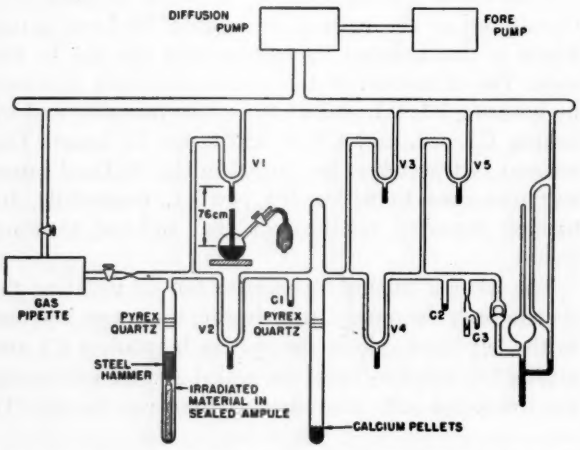

FIG. 1. Apparatus for the extraction and purification of radiogenic noble gases from neutron irradiated salts.

A tracer solution of Te^{130} in HCl was added to the solution of the irradiated salt, and, although tellurium appears to be reduced by the iodide ion, it remains in solution under these conditions so that isotope mixing takes place. Metallic tellurium was precipitated, after stirring, by neutralizing with NH_4OH and treating with SO_2. The mass analysis of the tellurium was carried out in the same way as with selenium. A reproduction of the mass spectrometer recorder tracings for both the "branching sample" and the tracer is shown in Fig. 2. The curves have been normalized at mass 130 for ease of comparison. As is evident on inspection, there has been considerable enrichment at mass 128. The constancy of the peak at mass 126 (not evident in Fig. 2) rules out the presence of normal tellurium and proves that the excess Te^{128} is radiogenic in origin.

The xenon procedure, utilizing the apparatus shown in Fig. 1, was identical with that for krypton. A small amount of normal xenon was used as a tracer. A mass spectrometer recorder tracing of the xenon obtained is shown in Fig. 3 along with the mass spectrum of normal xenon. The huge enrichment at mass 128 is evident upon inspection.

From the data the branching ratio of I^{128} was calculated:

$$\lambda_{\pm}(I^{128}) = \text{radiogenic } Te^{128}/\text{radiogenic } Xe^{128} = 0.053 \pm 0.002.$$

IV. DISCUSSION

The outstanding advantage of branching investigations of this type is the great sensitivity of the mass spectrometer method for detection of orbital electron capture. In a conventional study, using ion detectors, orbital electron capture is an elusive phenomenon, detectable only by secondary events such as nuclear γ rays, x-rays, or Auger electrons. In the present study, the sensitivity of detection for capture is equal to that for electron emission since the primary event—nuclear transformation—is the one observed.

Another advantage of the method is the precision obtainable. The branching ratios quoted here have an average probable error of 4.3 percent; the ultimate accuracy of the method is probably about 1.5 percent. Since relative measurements can be made precisely with ion detectors, it is probable that results obtained by the mass spectrometer method will be useful as standards. The mass spectrometric method is free of the common errors due to absorption and scattering of radiation, counter insensitivities and end effects, background, and the presence of impurities in the activities under investigation.

The obvious disadvantage of the method is its lack of discrimination between, (a) orbital electron capture and positron emission, and (b) isomeric activities with different decay periods (unless one is very long). Hence the studies must, for completeness, be supplemented by ion detector observations. The activities investigated

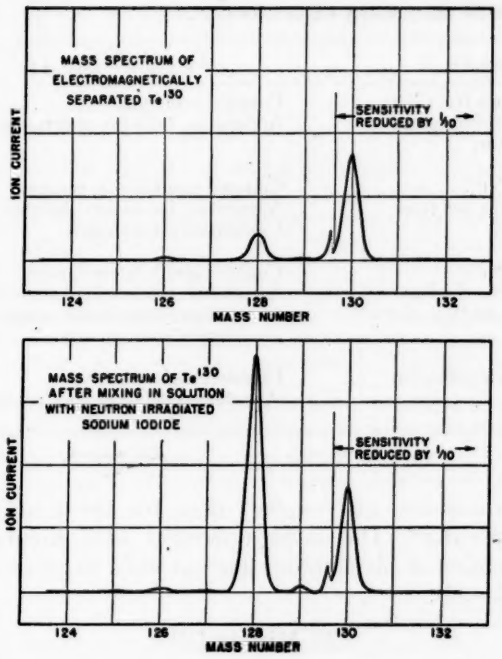

FIG. 2. Mass spectrum of electromagnetically enriched Te^{130} before and after mixing in solution with neutron irradiated NaI. The excess Te^{128} is due to branching in the decay of I^{128}. The peak at mass 129 is due to an impurity.

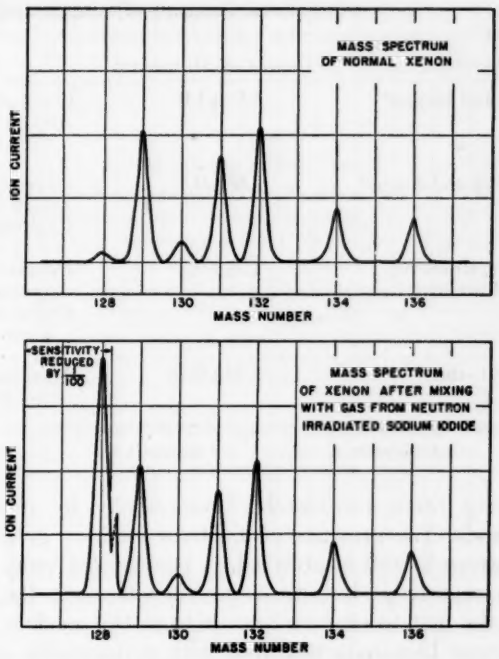

FIG. 3. Mass spectrum of normal xenon before and after mixing with the gas dissolved in neutron irradiated NaI. The excess Xe^{128} is due to beta-decay of I^{128}.

in this paper have all been studied before by conventional methods and there appears to be no ambiguity with regard to the periods with which the decays took place.

There follows a discussion of the results in light of the decay schemes of the particular nuclei investigated.

12.8 Hour Cu^{64}

This is an activity which has been much studied. It decays by negatron emission, by positron emission, and by orbital electron capture. The decay scheme was believed to be everywhere simple until a weak nuclear gamma-ray was detected by Bradt *et al.*[2] and confirmed by Deutsch[11] in a subsequent study. Deutsch placed the γ-energy at 1.35 Mev with a frequency of 1 γ-ray per 40 ± 5 positrons. This complicates the scheme only slightly and for most purposes this complexity may be overlooked. The negatrons and positrons have been studied with great care[8,12,13] and both serve as excellent examples of a simple spectrum with the allowed Fermi distribution.

Two investigators have determined the overall β^-/β^+ ratio by integration of the spectra. Cook and Langer[3] report a value of 2.0 negatrons per positron; Bradt *et al.*,[2] a value of 2.1. The value 2.05 ± 0.10 will be adopted for this quantity in the calculations to follow. This value, together with the ratio 1.62 ± 0.11 of $Z-1$ transitions to $Z+1$ transitions measured mass spectrometrically, determines the branching scheme: (a) by negatron emission, 38.2 ± 1.6 percent; (b) by positron emission, 18.6 ± 1.2 percent; (c) by orbital electron capture, 43.2 ± 2.0 percent (with 0.46 ± 0.06 percent decaying by electron capture to the 1.35-Mev state of Ni^{64} according to Deutsch[11]).

The K/β^+ ratio is of particular interest since it is independent of nuclear matrix elements and can be calculated from the Fermi theory. Huber, Ruetschi, and Scherrer[6] and Bouchez and Kayas[5] have each calculated this quantity using a formula due to Moeller[14] and the latest value of 0.657 Mev for E_{max} for Cu^{64} positrons. They find, respectively:

$$(K/\beta^+)^{Cu^{64}}_{Theor.}=2.08 \text{ and } 2.35.$$

The new experimental value is:

$$(K/\beta^+)^{Cu^{64}}_{Exp.}=2.32\pm0.28$$

and is in agreement with both the calculated values. This quantity has been measured before, but by very different methods and not with the present accuracy. Table I compares the past and present experimental values.

It should be mentioned that for the "allowed" Cu^{64} positrons, all variants of the Fermi theory predict about the same K/β^+ branching ratio.

18 Minute Br^{80}

Unlike the 4.4 hour metastable state of Br^{80}, which has been carefully investigated,[15] the 18-minute Br^{80}

[11] M. Deutsch, Phys. Rev. **72**, 729 (1947).
[12] L. Cranberg and J. Halpern, Phys. Rev. **73**, 259 (1948).
[13] C. S. Wu and R. D. Albert, Phys. Rev. **75**, 1107 (1949).
[14] C. Moeller, Physik Zeits. Sowjetunion **11**, 9 (1937).
[15] E. Segrè and A. C. Helmholz, Rev. Mod. Phys. **21**, 2 (1949).

TABLE I. Summary of experimental determinations of the quantity (K/β^+) for Cu^{64}.

Investigator	Value of (K/β^+) reported	K-capture evaluated by	β^+ emission evaluated by
Cook and Langer[a]	3.5 ±1.0	Counted Auger electrons from Ni^{64}. Apparatus: beta-ray spectrometer with 4-kev accelerator.	Counted positrons. Apparatus: beta-ray spectrometer.
Bouchez and Kayas[b]	2.65±0.4	Counted x-rays from Ni^{64}. Apparatus: thin window counter. Calibration: calculated.	Counted annihilation quanta. Apparatus: ionization chamber. Calibration: unspecified.
Huber, Ruetschi, and Scherrer[c]	1.75±0.2	Counted x-rays from Ni^{64}. Apparatus: thin window counter. Calibration: tandem counting with identical counters.	Counted annihilation quanta. Apparatus: thick-walled counter. Calibration: coincidence counting of annihilation quanta.
Present study	2.32±0.28	Mass spectrometric determination (by difference).	Counted positrons.[d,e] Apparatus: beta-ray spectrometers.

[a] Reference 4. [b] Reference 5. [c] Reference 6. [d] Reference 2. [e] Reference 3.

activity needs considerably more study by modern methods. The presence of a 2.0 to 2.2-Mev group of negatrons is well established. A penetrating γ-ray has been reported,[16] but its energy is unknown. Barber[7] was the first to observe branching in this nucleus. He observed 18-minute positrons with a trochoidal apparatus and gave the ratio of negatrons to positrons as about 35. By absorption measurements, he found E_{max} for the positrons to be 0.73±0.1 Mev. The positron activity has recently been confirmed in beta-ray spectrometer measurements by Dzhelepov, Anton'eva, and Shestopalova.[17] However, they report the ratio of negatrons to positrons as 98 with a maximum positron energy of one Mev.

The present study reveals a total branching of 0.090±0.002, or a ratio of negatrons to captures plus positrons of 11.1. It is evident that there is considerable orbital electron capture associated with this activity; i.e., the K/β^+ ratio is 2 or 8 depending upon whether one takes the result of Barber or of Dzhelepov *et al.* It is to be hoped that the positron-negatron ratio will be measured with greater precision. In order to compare the K/β^+ ratio with theory, it is also essential that a precise determination of the maximum positron energy be made, since the theoretical branching ratio is sensitive to this quantity.

34-Hour Br^{82}

Recent measurements on 34-hour Br^{82} by Siegbahn, Hedgran, and Deutsch[18] with beta-ray spectrometers of high resolution, indicate that the spectrum is complex: there are seven γ-rays present of different intensities. The mass spectrometric investigation shows that the number of $Z \rightarrow Z-1$ transitions per negatron is less than 1 in 3700 or 0.00027. Barber[7] has previously found the ratio of positrons to negatrons to be less than 0.004.

It appears that much less energy is available for the transition $_{35}Br^{82} \rightarrow {}_{34}Se^{82}$ than for the transition $_{35}Br^{82} \rightarrow {}_{36}Kr^{82}$. This is in agreement with Kohman's conception of the stability line[19] at mass 82 ($Z_A = 35.7$ for $A = 82$).

25 Minute I^{128}

The present study shows that the transition $I^{128} \rightarrow Te^{128}$ takes place in 5.0±0.2 percent of the disintegrations. This transition has not been reported heretofore. Barber[7] has found less than 0.002 positrons per negatron. It is probable that positron emission is energetically forbidden ($Z_A = 53.3$ for $A = 128$).

Siegbahn and Hole[20] have examined the beta-spectrum of I^{128}. They showed that there are prominent conversion lines in the spectrum due to a γ-ray of energy 0.429 Mev which is present to about seven percent. Accordingly they propose a decay scheme with two groups of negatrons separated in energy by 0.429 Mev, although the two groups are by no means clearly indicated by the Fermi plot.

It is possible that γ-rays may be associated with the 5.0 percent orbital electron capture. Certainly the decay scheme should be investigated more carefully with coincidence techniques and critical absorbers.

The electromagnetically enriched stable isotopes used as tracers in this investigation were produced by Carbide and Carbon Chemicals Corporation, Y-12 Plant, Oak Ridge, Tennessee and were obtained on allocation from the Isotopes Division of the Atomic Energy Commission.

The writer takes pleasure in acknowledging the invaluable assistance of Mr. Leon Markheim of the Argonne National Laboratory Remote Control Division. Mr. Albert Orstrom was responsible for construction of many critical components of the apparatus.

Finally, I wish to express my appreciation to Professor Mark Inghram, my sponsor in this research, who first suggested the problem and to whom I am indebted for wise counsel throughout its execution.

[16] J. H. Buck, Phys. Rev. **54**, 1025 (1938).
[17] Dzhelepov, Anton'eva, and Shestopalova, Dokl. Akad. Nauk, SSSR, **64** (No. 3), 309 (1949).
[18] Siegbahn, Hedgran, and Deutsch, Phys. Rev. **76**, 1263 (1949).
[19] T. P. Kohman, Phys. Rev. **73**, 16 (1948).
[20] K. Siegbahn and N. Hole, Phys. Rev. **70**, 133 (1946).

The Phenomenological Theory of Exchange Currents in Nuclei*

R. K. OSBORN AND L. L. FOLDY
Case Institute of Technology, Cleveland, Ohio
(Received May 1, 1950)

As was first pointed out by Siegert, the existence of exchange forces in nuclei implies the existence of accompanying exchange currents. Sachs has calculated an expression for these, by making the Hamiltonian containing exchange potentials gauge-invariant, and has applied it to the calculations of exchange magnetic moments in H^3 and He^3. The Hamiltonian obtained by Sachs is not the most general admissible one. More generally, the exchange current density is found to depend on a vector function whose irrotational part is completely determined by gauge-invariance but whose solenoidal part is arbitrary except for the requirements (following from conditions of translational invariance and symmetry in all nucleons on the Hamiltonian) that it be translationally invariant and antisymmetric under the exchange of the spin and space coordinates of each pair of nucleons. Making use of these conditions on the Hamiltonian, the explicit form of the dependence of the solenoidal part of the exchange current upon the spin and isotopic spin coordinates of the nucleons has been derived. In the resultant exchange moments, the irrotational part leads to the expression obtained by Sachs, while the solenoidal term contribution contains the spin operators of the nucleons in particular combinations, together with arbitrary functions of the nucleon separation. Villars' exchange moment expression, as obtained from meson theory, is included as a special case and hence the exchange contributions to the moments of H^3 and He^3 are explicable on a phenomenological basis, contrary to the results obtained in Sachs' special case. The generality and significance of the results are discussed in relation to the various meson theories.

I. INTRODUCTION

AS was first pointed out by Siegert,[1] the existence of charge exchange forces between nucleons together with the differential conservation law for electric charge require that electric currents must flow in the intervening space between interacting neutrons and protons. These so-called exchange currents will then interact with electromagnetic fields and modify the electromagnetic properties of nuclei in two important respects. First, they will give rise, in general, to a contribution to the magnetic moment of a nucleus above and beyond those arising from the intrinsic magnetic moments of the constituent nucleons and from their orbital motion. Second, they will lead to a modification of the cross sections for most photo-nuclear processes. Recently considerable interest has been aroused in the effects of these exchange currents as a consequence of recent highly accurate measurements[2] of the magnetic moments of H^3 and He^3 which appear to show definitely the existence of exchange contributions to these moments.

As Siegert also pointed out, the exchange current density required for conservation of charge is not completely determined by the exchange interaction itself. Only its irrotational (longitudinal) part is uniquely so determined while the solenoidal (transverse) part is arbitrary. Sachs[3] has recently determined a particular exchange current distribution which satisfies the condition of charge conservation in which the exchange currents are assumed to flow along straight line filaments connecting the interacting nucleons. He applied his results to the calculation of the exchange contributions to the magnetic moments of H^3 and He^3 and found that this current distribution could not account for the observed results. An examination of Sachs' results in the light of the present investigation shows that while his particular current distribution contains both an irrotational and a solenoidal part, only the irrotational part gives a contribution to the magnetic moment. One must therefore conclude that the major part of the exchange contribution to magnetic moments arises from the indeterminate solenoidal part of the exchange current distribution.

According to current views, the carriers of charge between nucleons are presumed to be the mesons responsible for nuclear forces. If these views are correct, the description of nuclear forces by any particular type of meson theory will lead to a unique expression for both the irrotational and solenoidal parts of the exchange current density and their contributions to the magnetic moments of nuclei. Villars[4] has performed a calculation along these lines employing the symmetrical pseudoscalar meson theory and has found that the experimental results on the moments of H^3 and He^3 can be explained on this model; however, similar calculations on the basis of other meson theories (vector and Møller-Rosenfeld mixture) have not been correspondingly successful.[5] The well-known deficiencies of all forms of meson theory at the present time promote interest, accordingly, in determining what features of exchange currents in nuclei can be formulated independently of specific assumptions concerning the field-theoretical nature of nuclear forces, that is, on a purely phenomenological basis. The investigation of this problem forms the subject matter of the present paper.

In view of these remarks, it is evident that such an investigation must largely be concerned with the deter-

* This work has been supported by the AEC.
[1] A. F. Siegert, Phys. Rev. **52**, 787 (1937).
[2] H. L. Anderson and A. Novick, Phys. Rev. **71**, 372 (1947); **73**, 919 (1948). Bloch, Graves, Packard, and Spence, Phys. Rev. **71**, 373, 551 (1947).
[3] R. G. Sachs, Phys. Rev. **74**, 433 (1948).
[4] F. Villars, Phys. Rev. **72**, 256 (1947); Helv. Phys. Acta **20**, 476 (1947). In this connection see also: S. T. Ma and F. C. Yu, Phys. Rev. **62**, 118 (1942); C. Møller and L. Rosenfeld, Kgl. Danske Vid. Math.-Fys. Medd. Sels. **20**, No. 12 (1943); W. Pauli and S. Kusaka, Phys. Rev. **63**, 400 (1943).
[5] A. Thellung and F. Villars, Phys. Rev. **73**, 924 (1948).

mination of restrictions on the possible form of the solenoidal part of the exchange current density. A number of restrictions are found below to arise from the usual conditions on the Hamiltonian for a system of nucleons of invariance under translation and (both proper and improper) rotations, and of symmetry with respect to all nucleons. The assumptions made in the present treatment are: (*a*) that only static two-body (but possibly spin-dependent, including tensor) interactions exist between nucleons; (*b*) that the exchange currents are proportional to the exchange interaction; and (*c*) that nucleons are spin $\frac{1}{2}$ particles whose states are characterized completely by a position, a spin, and an isotopic spin coordinate. Assumption (*a*) is probably too stringent in view of the probable existence of many-body[6] and velocity-dependent forces, but is retained in order to avoid undue complications. Assumption (*b*) can be somewhat relaxed without great complication and the effects of its relaxation are discussed below (proximity-induced currents). Assumption (*c*) is necessary in order to impose the condition that the Hamiltonian be symmetric under the exchange of coordinates of any pair of nucleons. To these assumptions should be added: (*d*) the charge density is assumed to vanish except at the positions of the nucleons. This assumption means that the nucleons are not to be regarded as carriers of a finite-sized charge distribution (as is the case in meson theories where a nucleon carries with it a cloud of charged virtual mesons) but as point charges. While for generality it would be desirable to drop this assumption, we have not done so initially in order to save additional complication of the derived expressions. The effects of dropping this assumption are briefly discussed in Section VIII.

II. GAUGE INVARIANCE FOR EXCHANGE POTENTIALS

As is well known, the differential conservation law for charge will be ensured if the Lagrangian function for the system is gauge-invariant. In the particular case of a system of nucleons interacting through exchange and possibly non-exchange) potentials this condition reduces to the condition that the exchange interaction between the nucleons be itself gauge-invariant since all other terms already automatically satisfy this condition or may be made to do so by standard methods. Employing isotopic spin notation, the exchange interaction terms can be written in the form:

$$H_x=\sum_{i,j} V_{ij}(\mathbf{r}_i-\mathbf{r}_j, \boldsymbol{\sigma}_i, \boldsymbol{\sigma}_j)(\tau_i^x\tau_j^x+\tau_i^y\tau_j^y), \quad (1)$$

where $\mathbf{r}_i$, $\boldsymbol{\sigma}_i$, and $\boldsymbol{\tau}_i$ are, respectively, the position, spin, and isotopic spin operators for the ith nucleon, and V_{ij} is the exchange part of the interaction potential between the ith and jth nucleons (apart from its explicitly indicated isotopic spin dependence) and is a function of the spin operators for the two nucleons and of their spatial separation. Since in the presence of electromagnetic fields this expression is not gauge-invariant, we are faced with the problem of modifying it properly so that it is gauge-invariant, with the condition that the modified expression reduce to (1) in the absence of electromagnetic fields.

Sachs[3] solved this problem by assuming Wheeler's representation[7] of the space-exchange operator as a differential operator and employing the usual method for making a differential operator gauge-invariant. The resultant expression is not unique, but an examination of the method of derivation allows one to write down the general result without difficulty. We shall here give the general result and then demonstrate that it is indeed gauge-invariant. The generalization of (1) which is gauge invariant in the presence of electromagnetic fields can be written

$$\begin{aligned} H_x=\sum_{i,j} V_{ij}\Big\{ & \tau_i^P\tau_j^N[F(u_{ij}^1, u_{ij}^2, \cdots) \\ & -iG(v_{ij}^1, v_{ij}^2, \cdots)]\exp\Big[-ie\int \boldsymbol{\xi}_{ij}\cdot\mathbf{A}d\mathbf{x}\Big] \\ & +\tau_i^N\tau_j^P[F(u_{ij}^1, u_{ij}^2, \cdots)+iG(v_{ij}^1, v_{ij}^2, \cdots)] \\ & \times\exp\Big[ie\int \boldsymbol{\xi}_{ij}\cdot\mathbf{A}d\mathbf{x}\Big]\Big\}(\tau_i^x\tau_j^x+\tau_i^y\tau_j^y). \end{aligned} \quad (2)$$

Here e is the charge on the proton, $\mathbf{A}=\mathbf{A}(\mathbf{x}, t)$ is the vector potential of the electromagnetic field, τ_i^P and τ_i^N are the operators

$$\tau_i^P=(1+\tau_i^Z)/2, \quad \tau_i^N=(1-\tau_i^Z)/2, \quad (3)$$

and F and G are arbitrary real scalar functions of their arguments satisfying only the conditions

$$F(0, 0, 0\cdots)=1, \quad G(0, 0, 0\cdots)=0. \quad (4)$$

The arguments u_{ij}^α and v_{ij}^α are defined as

$$u_{ij}^\alpha=e\int \mathbf{A}\cdot\mathbf{curl}_x\mathbf{n}_{ij}^\alpha d\mathbf{x}, \quad v_{ij}^\alpha=e\int \mathbf{A}\cdot\mathbf{curl}_x\boldsymbol{\zeta}_{ij}^\alpha d\mathbf{x}, \quad (5)$$

where

$$\begin{aligned} \mathbf{n}_{ij}^\alpha&=\mathbf{n}^\alpha(\mathbf{x}-\mathbf{r}_i, \mathbf{x}-\mathbf{r}_j, \boldsymbol{\sigma}_i, \boldsymbol{\sigma}_j), \\ \boldsymbol{\zeta}_{ij}^\alpha&=\boldsymbol{\zeta}_{ij}^\alpha(\mathbf{x}-\mathbf{r}_i, \mathbf{x}-\mathbf{r}_j, \boldsymbol{\sigma}_i, \boldsymbol{\sigma}_j), \end{aligned} \quad (6)$$

are arbitrary axial vector functions of $\mathbf{x}-\mathbf{r}_i$, $\mathbf{x}-\mathbf{r}_j$, and the spin operators of the ith and jth nucleons. The quantity

$$\boldsymbol{\xi}_{ij}=\boldsymbol{\xi}(\mathbf{x}-\mathbf{r}_i, \mathbf{x}-\mathbf{r}_j, \boldsymbol{\sigma}_i, \boldsymbol{\sigma}_j) \quad (7)$$

is an arbitrary polar vector function of its indicated arguments satisfying the equation

$$\mathrm{div}_x\boldsymbol{\xi}_{ij}=\delta(\mathbf{x}-\mathbf{r}_j)-\delta(\mathbf{x}-\mathbf{r}_i), \quad (8)$$

where the functions on the right are three-dimensional Dirac δ-functions.

[6] H. Primakoff and T. Holstein, Phys. Rev. **55**, 1218 (1939).

[7] J. A. Wheeler, Phys. Rev. **50**, 643 (1936).

Under the gauge transformation

$$\mathbf{A}\rightarrow\mathbf{A}+\mathbf{grad}\Lambda,\quad \Phi\rightarrow\Phi-\partial\Lambda/\partial t, \tag{9}$$

the wave function transforms as

$$\Psi\rightarrow\{\prod_i[\tau_i^P\exp[ie\Lambda(\mathbf{r}_i)]+\tau_i^N]\}\Psi, \tag{10}$$

and the expression (2) transforms to

$$\begin{aligned}&\{\prod_m(\tau_m^P\exp[-ie\Lambda(\mathbf{r}_m)]+\tau_m^N)\}\\&\times\sum_{i,j}\Big\{\tau_i^P\tau_j^N[F(u_{ij}^\alpha)-iG(v_{ij}^\alpha)]\\&\times\exp\Big[-ie\int\xi_{ij}\cdot(\mathbf{A}+\mathbf{grad}\Lambda)d\mathbf{x}\Big]\\&+\tau_i^N\tau_j^P[F(u_{ij}^\alpha)+iG(v_{ij}^\alpha)]\\&\times\exp\Big[ie\int\xi_{ij}\cdot(\mathbf{A}+\mathbf{grad}\Lambda)d\mathbf{x}\Big]\Big\}(\tau_i^x\tau_j^x+\tau_i^y\tau_j^y)\\&\times\{\prod_n[\tau_n^P\exp[ie\Lambda(\mathbf{r}_n)]+\tau_n^N)\},\end{aligned} \tag{11}$$

where use has been made of the fact that the u_{ij}^α and v_{ij}^α are invariant under the transformation. On commuting either the initial or final factors in braces through the remainder of the expression in (11), one finds easily that (11) resumes the form (2), that is, it is gauge-invariant, provided

$$\int\xi_{ij}\cdot\mathbf{grad}\Lambda d\mathbf{x}=\Lambda(\mathbf{r}_i)-\Lambda(\mathbf{r}_j). \tag{12}$$

But by an integration by parts and use of Eq. (8), one finds immediately that

$$\int\xi_{ij}\cdot\mathbf{grad}\Lambda d\mathbf{x}=-\int\Lambda\ \mathrm{div}_x\xi_{ij}d\mathbf{x}=\Lambda(\mathbf{r}_i)-\Lambda(\mathbf{r}_j), \tag{13}$$

establishing the gauge-invariance of (2). It is assumed in the above that $\mathbf{n}_{ij}^\alpha$, ζ_{ij}^α, and ξ_{ij} fall off sufficiently rapidly for large $\mathbf{x}$ that one may neglect surface integrals arising from integrations by parts.

However, it is not immediately obvious that (2) reduces to (1) in the absence of electromagnetic fields, since in this limit the expression in braces in (2) reduces to $(\tau_i^P\tau_j^N+\tau_i^N\tau_j^P)$. However, making use of the fact that the operators

$$\tau_i^P\tau_j^P(\tau_i^x\tau_j^x+\tau_i^y\tau_j^y),\quad \tau_i^N\tau_j^N(\tau_i^x\tau_j^x+\tau_i^y\tau_j^y), \tag{14}$$

are both identically zero, we may add the quantity $(\tau_i^P\tau_j^P+\tau_i^N\tau_j^N)$ inside the braces in (2) without changing its value, and then in the limit as A goes to zero, the expression in braces becomes

$$\begin{aligned}&\{\tau_i^P\tau_j^P+\tau_i^P\tau_j^N+\tau_i^N\tau_j^P+\tau_i^N\tau_j^N\}\\&\qquad=(\tau_i^P+\tau_i^N)(\tau_j^P+\tau_j^N)=1,\end{aligned} \tag{15}$$

demonstrating the equivalence of (2) and (1) in the absence of electromagnetic fields.

We note further that (2) is Hermitian and that it is invariant under translations and both proper and improper rotations of the coordinate system. However, it is not symmetric under the interchange of the coordinates of any pair of nucleons as it stands, but it becomes so if we add the additional requirement that under the simultaneous interchange of $\mathbf{r}_i$ with $\mathbf{r}_j$ and $\boldsymbol{\sigma}_i$ and $\boldsymbol{\sigma}_j$: (*a*) The function F is symmetric, (*b*) The function G is antisymmetric, and (*c*) The function ξ_{ij} is antisymmetric.

With these conditions (2) appears then to be the most general exchange interaction which is gauge-invariant and which satisfies the assumptions laid down in Section I.

If ξ_{ij} is written as the sum of its solenoidal and irrotational parts:

$$\xi_{ij}=\mathbf{grad}_x\varphi_{ij}+\mathbf{curl}_x\chi_{ij}, \tag{16}$$

we note that we can take χ_{ij} to be zero without loss in generality since any solenoidal part of ξ_{ij} can be combined into the function G.

III. THE EXCHANGE CURRENT DENSITY

If we limit our interest only to those exchange currents flowing in the absence of external electromagnetic fields (that is, neglect the exchange currents which are *induced* by external fields), then we can expand the exchange interaction (2) in a power series in the vector potential and retain only linear terms. The result of this expansion is

$$\begin{aligned}H_x=\sum_{i,j}V_{ij}\Big\{&(\tau_i^P\tau_j^N+\tau_i^N\tau_j^P)\\&\times\Big[1+e\int\mathbf{A}\cdot\mathbf{curln}_{ij}d\mathbf{x}\Big]-i(\tau_i^P\tau_j^N-\tau_i^N\tau_j^P)\\&\times\Big[e\int\mathbf{A}\cdot(\mathbf{curl}\zeta_{ij}+\mathbf{grad}\varphi_{ij})d\mathbf{x}\Big]\Big\}\\&\times(\tau_i^x\tau_j^x+\tau_i^y\tau_j^y),\end{aligned} \tag{17}$$

where

$$\mathbf{n}_{ij}=\sum_\alpha(\partial F/\partial u_{ij}^\alpha)_{A=0}\mathbf{n}_{ij}^\alpha,$$

$$\zeta_{ij}=\sum_\alpha(\partial G/\partial v_{ij}^\alpha)_{A=0}\zeta_{ij}^\alpha.$$

The desired operator for the exchange current density may then be obtained from (17) by taking its negative variational derivative with respect to the vector potential with the result:

$$\mathbf{j}_x=\mathbf{j}_t+\mathbf{j}_t', \tag{18}$$

$$\begin{aligned}\mathbf{j}_t&=ie\sum_{ij}V_{ij}(\tau_i^P\tau_j^N-\tau_i^N\tau_j^P)\,\mathbf{grad}\varphi_{ij}(\tau_i^x\tau_j^x+\tau_i^y\tau_j^y)\\&=e\sum_{i,j}V_{ij}(\tau_i^x\tau_j^y-\tau_i^y\tau_j^x)\,\mathbf{grad}\varphi_{ij},\end{aligned} \tag{19}$$

$$\mathbf{j}_t=e\sum_{i,j}V_{ij}(\tau_i^x\tau_j^y-\tau_i^y\tau_j^x)\,\mathbf{curl}\zeta_{ij}, \tag{20}$$

$$\mathbf{j}_t'=-c\sum_{i,j}V_{ij}(\tau_i^x\tau_j^x+\tau_i^y\tau_j^y)\,\mathbf{curln}_{ij}. \tag{21}$$

We shall now discuss these three contributions to the exchange current density separately.

The first of these, $\mathbf{j}_l$, obviously represents the irrotational (longitudinal) part of the exchange current density. By combining Eqs. (8) and (16) we obtain the equation

$$\nabla^2\varphi_{ij}=\delta(\mathbf{x}-\mathbf{r}_j)-\delta(\mathbf{x}-\mathbf{r}_i), \tag{22}$$

with the unique solution (which vanishes at infinity):

$$\varphi_{ij}=1/4\pi[(1/|\mathbf{x}-\mathbf{r}_i|)-(1/|\mathbf{x}-\mathbf{r}_j|)]. \tag{23}$$

Hence the irrotational part of the current density is completely determined by the condition of differential charge conservation, as would be expected. The contribution to this part of the current from each pair of interacting nucleons has the simple form of potential flow between a source and sink of charge of equal strength located at the positions of the nucleons. Conjugate pairs of nuclei are defined as those pairs having identical wave functions except for the interchange of neutrons and protons. Since the isotopic spin factor in the irrotational part of the exchange current density changes sign under an interchange of neutrons and protons in a nuclear wave function, we see that expectation values (diagonal matrix elements) of the irrotational exchange current density are equal but opposite in sign for two conjugate nuclei and therefore vanish for self-conjugate nuclei. It is important to note that this theorem is true only for the diagonal matrix elements; the fact that it is not true for the off-diagonal elements (existence of exchange current fluctuations) shows that an interaction of the irrotational currents with the electromagnetic field is still possible for self-conjugate nuclei (such as the deuteron) even though their average value is zero.

Turning now to the solenoidal (transverse) part of the exchange current density given by the two terms $\mathbf{j}_t$ and $\mathbf{j}_t'$, we see that the two terms are similar except for their different isotopic spin dependence. The isotopic spin dependence of the first is the same as that for the longitudinal part of the current and the same remarks as made above are therefore applicable to it. The second term, however, does not change sign under an interchange of protons and neutrons in a nucleus and hence gives equal expectation values for conjugate nuclei and a non-vanishing expectation value for self-conjugate nuclei. The significance of this fact will be discussed more fully below.

These solenoidal parts of the current distribution are not determined by the condition of charge conservation. The only conditions to which they are subject are those resulting as a consequence of the discussion near the end of the last section. These require that $\boldsymbol{\zeta}_{ij}$ be an axial vector function of $\mathbf{R}_i=\mathbf{x}-\mathbf{r}_i$, $\mathbf{R}_j=\mathbf{x}-\mathbf{r}_j$, $\boldsymbol{\sigma}_i$, and $\boldsymbol{\sigma}_j$, which is *antisymmetric* under the simultaneous interchange of $\mathbf{R}_i$ with $\mathbf{R}_j$ and $\boldsymbol{\sigma}_i$ with $\boldsymbol{\sigma}_j$; and that $\mathbf{n}_{ij}$ be an axial vector function of the same variables but *symmetric* under the interchange above. However, before discussing the exchange current density in more detail, we will first discuss the operators for the exchange contribution to the magnetic moment of a nucleus.

IV. EXCHANGE MAGNETIC MOMENTS

From the expression for the exchange current density, one can readily calculate the operator for the exchange magnetic moment of a nucleus. This also breaks naturally into three parts:

$$\mathbf{M}_x=\mathbf{M}_l+\mathbf{M}_t+\mathbf{M}_t', \tag{24}$$

$$\mathbf{M}_l=\tfrac{1}{2}e\sum_{i,j}V_{ij}(\tau_i^x\tau_j^y-\tau_i^y\tau_j^x)\int\mathbf{x}\times\mathbf{grad}\,\varphi_{ij}d\mathbf{x}$$

$$=-\tfrac{1}{2}e\sum_{i,j}V_{ij}(\tau_i^x\tau_j^y-\tau_i^y\tau_j^x)[\mathbf{r}_i\times\mathbf{r}_j], \tag{25}$$

$$\mathbf{M}_t=\tfrac{1}{2}e\sum_{i,j}V_{ij}(\tau_i^x\tau_j^y-\tau_i^y\tau_j^x)\int\mathbf{x}\times\mathbf{curl}\boldsymbol{\zeta}_{ij}d\mathbf{x}$$

$$=\tfrac{1}{2}e\sum_{i,j}V_{ij}(\tau_i^x\tau_j^y-\tau_i^y\tau_j^x)\mathbf{Z}_{ij}, \tag{26}$$

$$\mathbf{M}_t'=-\tfrac{1}{2}e\sum_{i,j}V_{ij}(\tau_i^x\tau_j^x+\tau_i^y\tau_j^y)\int\mathbf{x}\times\mathbf{curl}\mathbf{n}_{ij}d\mathbf{x}$$

$$=-\tfrac{1}{2}e\sum_{i,j}V_{ij}(\tau_i^x\tau_j^x+\tau_i^y\tau_j^y)\mathbf{H}_{ij}, \tag{27}$$

$$\mathbf{Z}_{ij}=\mathbf{Z}(\mathbf{r}_i-\mathbf{r}_j,\boldsymbol{\sigma}_i,\boldsymbol{\sigma}_j)=\int\mathbf{x}\times\mathbf{curl}\boldsymbol{\zeta}_{ij}d\mathbf{x}=\int\boldsymbol{\zeta}_{ij}d\mathbf{x}, \tag{28}$$

$$\mathbf{H}_{ij}=\mathbf{H}(\mathbf{r}_i-\mathbf{r}_j,\boldsymbol{\sigma}_i,\boldsymbol{\sigma}_j)=\int\mathbf{x}\times\mathbf{curl}\mathbf{n}_{ij}d\mathbf{x}=\int\mathbf{n}_{ij}d\mathbf{x}. \tag{29}$$

The first part, arising from the irrotational part of the current, is the same as that calculated by Sachs[3] who also evaluated its expectation value for H^3 and He^3 and found it to be of insufficient magnitude to explain the experimental results for these nuclei. The magnitudes of the remaining two parts depend, of course, on the form of the arbitrary functions occurring in them, but a considerable amount of information can nevertheless be obtained concerning them as a result of the remaining conditions on the arbitrary functions.

Consider first the quantity $V_{ij}\mathbf{Z}_{ij}$. The conditions of translational and rotational invariance, and symmetry of the Hamiltonian in all nucleons, requires that it be an axial vector function only of the vector separation of the ith and jth nucleons, $\mathbf{r}_{ij}=\mathbf{r}_i-\mathbf{r}_j$, and of the spin operators for the two nucleons, and that it be *antisymmetric* under the exchange of the coordinates of the two nucleons. Now, apart from a multiplying scalar function of the distance between the two nucleons, the only axial vectors which can be constructed from the polar vector $\mathbf{r}_{ij}$ and the two axial vectors $\boldsymbol{\sigma}_i$ and $\boldsymbol{\sigma}_j$ and which are *antisymmetric* under the interchange of coordinates of the two nucleons are the four quantities (see Appendix):

$$\begin{aligned}&\text{(a)}\quad \boldsymbol{\sigma}_i-\boldsymbol{\sigma}_j,\\ &\text{(b)}\quad [\mathbf{r}_{ij}\cdot(\boldsymbol{\sigma}_i-\boldsymbol{\sigma}_j)]\mathbf{r}_{ij},\\ &\text{(c)}\quad \boldsymbol{\sigma}_i\times\boldsymbol{\sigma}_j,\\ &\text{(d)}\quad (\mathbf{r}_{ij}\cdot\boldsymbol{\sigma}_i\times\boldsymbol{\sigma}_j)\mathbf{r}_{ij}.\end{aligned} \tag{30}$$

The most general form which $V_{ij}\mathbf{Z}_{ij}$ can take is therefore a linear-combination of these four quantities multiplied by arbitrary functions of the distance between the two nucleons.

On the other hand, the conditions on $V_{ij}\mathbf{H}_{ij}$ are the same as those on $V_{ij}\mathbf{Z}_{ij}$ except for the fact that this quantity must be *symmetric* under the interchange of space and spin coordinates of the pair of nucleons. There are only three such axial vectors (apart from an arbitrary multiplying scalar function of the distance between the nucleons):

$$\text{(e)} \qquad \boldsymbol{\sigma}_i+\boldsymbol{\sigma}_j,$$

$$\text{(f)} \qquad |\mathbf{r}_{ij}\cdot(\boldsymbol{\sigma}_i+\boldsymbol{\sigma}_j)]\mathbf{r}_{ij}, \qquad (31)$$

$$\text{(g)} \qquad (\mathbf{r}_{ij}\cdot\boldsymbol{\sigma}_i)[\mathbf{r}_{ij}\times\boldsymbol{\sigma}_j]+(\mathbf{r}_{ij}\cdot\boldsymbol{\sigma}_j)[\mathbf{r}_{ij}\times\boldsymbol{\sigma}_i].$$

The most general form of spin dependence of the magnetic moment operator is therefore determined by group-theoretical principles combined with the plausible symmetry conditions which we have imposed on the Hamiltonian. It is of interest to note that the existence of contributions to the magnetic moments arising from solenoidal exchange currents is consequent on the nucleons having spin. For spinless nucleons the exchange moment is completely determined by the irrotational exchange currents which in turn are completely specified by the requirement of gauge invariance.

The forms (a), (b), (e) and (f) which are linear in the nucleon spins, can be given a very simple physical interpretation. In the Hamiltonian, the forms (a) and (e) lead to terms having the form of the interaction of the magnetic moment of a nucleon with the magnetic field but for which the magnitude of the magnetic moment is a function of the spatial separation of this nucleon from the other nucleons present. Hence these terms correspond to a modification of the intrinsic magnetic moment of a nucleon by the presence of other nucleons in its neighborhood, that is, to a proximity effect on the intrinsic magnetic moments of nucleons. The forms (b) and (f) are similar except that they involve a modification of that component of the intrinsic magnetic moment of a nucleon parallel to the line joining the nucleon and its disturbing neighbor. Terms of this character if actually present will lead to non-additivity of the neutron and proton magnetic moments in the deuteron.

V. COMPARISON WITH MESON THEORY

It is interesting to compare the results obtained in the preceding section with those obtained by field-theoretical calculations on the basis of the exchange of mesons as the origin of exchange currents.[4] In such calculations as so far carried out, the exchange moment is found to be a combination of the longitudinal contribution (25) together with contributions of the form (30-c, d). The absence in meson theory of the other possible forms which we have found in the phenomenological theory is easily explained when one remembers that magnetic moment calculations in meson theory have been carried out only to the lowest non-vanishing order in e and in the meson coupling constant g (that is, to order g^2e). To this approximation there is a symmetry between positive and negative mesons and neutrons and protons such that the interchange of a neutron and proton causes a reversal in sign of the exchange currents and therefore of the magnetic moments. Hence, one cannot expect to obtain terms of the form (31-e, f, g) in a meson theory calculation which does not go beyond the order g^2e. Furthermore, meson theory calculations, to this order, while allowing one to obtain the meson contribution to the intrinsic magnetic moment of an isolated nucleon, still cannot account for any modification of this intrinsic moment by the proximity of another nucleon which is an essentially higher order effect. This rules out obtaining terms of the form (30-a, b) in a second order meson theory calculation.

It might be assumed that our phenomenological theory is of sufficient generality to contain all results (except for the form of the arbitrary functions which occur in our expressions) which could be obtained from any meson theory. This is not quite the case, for the following reason. We have assumed in our theory (assumption (*d*)) that while currents may flow in the intervening space between nucleons, the electric charge density vanishes everywhere except at the positions of the nucleons. This is not actually the case in meson theory. As a result of the emission and re-absorption of virtual mesons by a nucleon, there is a finite charge density in the region surrounding a nucleon of radius equal to the Compton wave-length of the meson in order of magnitude. It is this fact, for example, which is presumably responsible for the observed scattering of slow neutrons by electrons.[8] The existence of this charge density over a finite region does not influence the results obtained for the exchange magnetic moment in second-order meson theory, but will be of importance in higher orders. The effect in our phenomenological theory of having a finite distribution of charge about nucleons is discussed briefly in a later section.

VI. SPIN DEPENDENCE OF THE EXCHANGE CURRENT DENSITY

Returning again to the consideration of the operator for the exchange current density we note that by the application of the same methods as employed above for the magnetic moment operator we may find the possible forms of spin dependence of the solenoidal part of the exchange current. The two arbitrary functions ζ_{ij} and $\mathbf{n}_{ij}$ in Eqs. (20) and (21) must be axial vector functions formed from the four vectors $\mathbf{R}_i=\mathbf{x}-\mathbf{r}_i$,

[8] Havens, Rabi, and Rainwater, Phys. Rev. **72**, 634 (1947); Fermi and Marshall, Phys. Rev. **72**, 1139 (1947); Rainwater, Rabi and Havens, Phys. Rev. **75**, 1295 (1948); Slotnick and Heitler, Phys. Rev. **75**, 1645 (1949); K. M. Case, Phys. Rev. **76**, 1 (1949); Dancoff and Drell, Phys. Rev. **76**, 205 (1949).

$\mathbf{R}_j=\mathbf{x}-\mathbf{r}_j$, $\boldsymbol{\sigma}_i$ and $\boldsymbol{\sigma}_j$, and must be antisymmetric and symmetric, respectively, under the simultaneous interchange of $\mathbf{R}_i$ with $\mathbf{R}_j$ and $\boldsymbol{\sigma}_i$ with $\boldsymbol{\sigma}_j$. One finds without difficulty (see Appendix) that apart from multiplying scalar functions formed from $\mathbf{R}_i$ and $\mathbf{R}_j$, there are only 27 linearly independent axial vectors which may be formed from the four vectors listed above. There are:

$$
\begin{aligned}
&\text{(a)} && \mathbf{R}_1\times\mathbf{R}_2,\\
&\text{(b)} && \boldsymbol{\sigma}_1\pm\boldsymbol{\sigma}_2,\\
&\text{(c)} && (\mathbf{R}_1\cdot\boldsymbol{\sigma}_1)\mathbf{R}_1\pm(\mathbf{R}_2\cdot\boldsymbol{\sigma}_2)\mathbf{R}_2,\\
&\text{(d)} && (\mathbf{R}_1\cdot\boldsymbol{\sigma}_2)\mathbf{R}_1\pm(\mathbf{R}_2\cdot\boldsymbol{\sigma}_1)\mathbf{R}_2,\\
&\text{(e)} && (\mathbf{R}_1\cdot\boldsymbol{\sigma}_1)\mathbf{R}_2\pm(\mathbf{R}_2\cdot\boldsymbol{\sigma}_2)\mathbf{R}_1,\\
&\text{(f)} && (\mathbf{R}_1\cdot\boldsymbol{\sigma}_2)\mathbf{R}_2\pm(\mathbf{R}_2\cdot\boldsymbol{\sigma}_1)\mathbf{R}_1,\\
&\text{(g)} && \boldsymbol{\sigma}_1\times\boldsymbol{\sigma}_2,\\
&\text{(h)} && (\boldsymbol{\sigma}_1\cdot\boldsymbol{\sigma}_2)[\mathbf{R}_1\times\mathbf{R}_2],\\
&\text{(i)} && (\mathbf{R}_1\cdot\boldsymbol{\sigma}_1\times\boldsymbol{\sigma}_2)\mathbf{R}_1\pm(\mathbf{R}_2\cdot\boldsymbol{\sigma}_1\times\boldsymbol{\sigma}_2)\mathbf{R}_2, \qquad (32)\\
&\text{(j)} && (\mathbf{R}_1\cdot\boldsymbol{\sigma}_1\times\boldsymbol{\sigma}_2)\mathbf{R}_2\pm(\mathbf{R}_2\cdot\boldsymbol{\sigma}_1\times\boldsymbol{\sigma}_2)\mathbf{R}_1,\\
&\text{(k)} && (\boldsymbol{\sigma}_1\cdot\mathbf{R}_1\times\mathbf{R}_2)\boldsymbol{\sigma}_2+(\boldsymbol{\sigma}_2\cdot\mathbf{R}_1\times\mathbf{R}_2)\boldsymbol{\sigma}_1,\\
&\text{(l)} && \{(\mathbf{R}_1\cdot\boldsymbol{\sigma}_2)[\mathbf{R}_1\times\boldsymbol{\sigma}_1]+(\mathbf{R}_1\cdot\boldsymbol{\sigma}_1)[\mathbf{R}_1\times\boldsymbol{\sigma}_2]\}\\
&&& \pm\{(\mathbf{R}_2\cdot\boldsymbol{\sigma}_1)[\mathbf{R}_2\times\boldsymbol{\sigma}_2]+(\mathbf{R}_2\cdot\boldsymbol{\sigma}_2)[\mathbf{R}_2\times\boldsymbol{\sigma}_1]\},\\
&\text{(m)} && (\mathbf{R}_1\cdot\boldsymbol{\sigma}_2)[\mathbf{R}_1\times\boldsymbol{\sigma}_1]+(\mathbf{R}_2\cdot\boldsymbol{\sigma}_1)[\mathbf{R}_1\times\boldsymbol{\sigma}_2]\\
&&& +(\mathbf{R}_1\cdot\boldsymbol{\sigma}_2)[\mathbf{R}_2\times\boldsymbol{\sigma}_1]+(\mathbf{R}_1\cdot\boldsymbol{\sigma}_1)[\mathbf{R}_2\times\boldsymbol{\sigma}_2],\\
&\text{(n)} && (\mathbf{R}_2\cdot\boldsymbol{\sigma}_2)(\mathbf{R}_1\cdot\boldsymbol{\sigma}_1)[\mathbf{R}_1\times\mathbf{R}_2],\\
&\text{(o)} && (\mathbf{R}_2\cdot\boldsymbol{\sigma}_1)(\mathbf{R}_1\cdot\boldsymbol{\sigma}_2)[\mathbf{R}_1\times\mathbf{R}_2],\\
&\text{(p)} && (\boldsymbol{\sigma}_1\cdot\mathbf{R}_1\times\mathbf{R}_2)[\mathbf{R}_1\times\mathbf{R}_2]\pm(\boldsymbol{\sigma}_2\cdot\mathbf{R}_1\times\mathbf{R}_2)[\mathbf{R}_1\times\mathbf{R}_2],\\
&\text{(q)} && \{(\mathbf{R}_1\cdot\boldsymbol{\sigma}_1)(\mathbf{R}_1\cdot\boldsymbol{\sigma}_2)\pm(\mathbf{R}_2\cdot\boldsymbol{\sigma}_1)(\mathbf{R}_2\cdot\boldsymbol{\sigma}_2)\}[\mathbf{R}_1\times\mathbf{R}_2].
\end{aligned}
$$

All of these are either symmetrical or antisymmetrical under the interchanges mentioned above; hence by multiplying each of these by an arbitrary symmetrical or antisymmetrical scalar function formed from the vectors $\mathbf{R}_i$ and $\mathbf{R}_j$, taking appropriate linear combinations of the results for $\boldsymbol{\zeta}_{ij}$ and $\mathbf{n}_{ij}$, and substituting in Eqs. (20) and (21), we obtain the most general form for the solenoidal part of the exchange currents. The total number of terms will be reduced somewhat when the curl operations in (20) and (21) are explicitly carried out,[9] but since there are no immediate applications for these results, we have not carried the reduction any further.

It will be noted that if one had spinless nucleons then only one solenoidal term (32-a) would survive. This term corresponds to a current distribution which is rotationally symmetric about the line joining the two nucleons and for which the direction of flow of the current at any point lies always in the plane containing the point and the two nucleons. Such a current distribution obviously gives rise to no resultant magnetic moment.

Again comparing our results with those to be expected from a lowest order meson theory calculation, we note that for the same reasons as given above in regard to the magnetic moment operator we would not expect any terms symmetric under the interchange of the pair of interacting nucleons so that no contribution of the form (21) would appear, and we would not expect any terms linear in the spin of the nucleons in (20).

VII. PROXIMITY-INDUCED CURRENTS

It is apparent from what has been said above that the exchange of charge between two nucleons interacting under the influence of an exchange force is actually effected only by the irrotational part of the exchange current density. The solenoidal part of the latter simply describes the flow of currents in closed loops induced by some mechanism when two nucleons are in proximity. The term "exchange currents" applied to the solenoidal part of the current density is therefore somewhat of a misnomer and "proximity-induced currents" would be perhaps a more appropriate designation. We mention this fact because on a purely phenomenological basis there is no *a priori* reason for assuming (assumption (*b*)) that such proximity-induced solenoidal currents do not flow even about nucleons interacting under an ordinary force. In fact such currents would be expected to flow about two neutrons or two protons is conventional meson theory in higher order where pairs of oppositely charged mesons are exchanged. The possible forms which the current density and magnetic moment operators may take in such cases may be calculated by methods essentially identical with those used above.

VIII. EFFECT OF FINITE NUCLEONIC CHARGE DISTRIBUTION

We shall in this section describe briefly the effect on our theory of the existence of finite charge distributions about nucleons such as those connected with the occurrence of a cloud of virtual charged mesons about a nucleon. In our non-relativistic approximation one can regard such a finite charge distribution as being rigidly bound to a nucleon. The specific form of this charge cloud will depend on whether the nucleon is a proton or neutron and hence will involve τ^z. The direct interaction of the nucleon with the electromagnetic field will then not depend only on the value of the field quantities at the position of the nucleon but will involve integrals of the field over the charge distribution. This means that under the gauge transformation (9), the wave function will not transform according to (10) but

[9] That the number of terms is reduced follows from the fact that (20) and (21) represent polar vectors constructed from $\mathbf{R}_i$, $\mathbf{R}_j$, $\boldsymbol{\sigma}_i$ and $\boldsymbol{\sigma}_j$. One finds that apart from scalar multiplying factors there are at most 24 polar vectors which may be constructed from those above. However, since these must be solenoidal vectors, one must add the condition that the divergence of these expressions vanishes identically which may further cut down the number of independent terms.

will involve instead in each term of the parenthesis in (10), an exponential of an integral of the gauge function Λ over the charge distribution for proton or neutron. The condition for the gauge invariance of the exchange interaction term will then require that the function ξ_{ij} satisfy not Eq. (8) but another equation in which the δ-functions are replaced by finite source functions, viz.:

$$\begin{aligned}\operatorname{div}\xi_{ij}=&[\rho_P(\mathbf{x}-\mathbf{r}_j)-\rho_N(\mathbf{x}-\mathbf{r}_j)]\\&-[\rho_P(\mathbf{x}-\mathbf{r}_i)-\rho_N(\mathbf{x}-\mathbf{r}_i)],\\\int\rho_P(\mathbf{x})d\mathbf{x}=1,\quad&\int\rho_N(\mathbf{x})d\mathbf{x}=0,\end{aligned}\tag{33}$$

where ρ_P is the charge distribution function for the proton and ρ_N is the charge distribution function for the neutron. The net result is to leave our expression for the solenoidal exchange current the same but to modify the irrotational exchange current density and its contribution to the magnetic moment in accordance with the change (33).

IX. SUMMARY AND CONCLUSIONS

We have shown above that one can describe in a phenomenological theory the effects of electric currents induced by the interaction of two nucleons in the nonrelativistic approximation (including neglect of velocity-dependent interactions) with two-body forces. In such a theory it is possible to account for: (1) "true" (irrotational) exchange currents, (2) proximity-induced (solenoidal) currents, (3) proximity-induced changes in the intrinsic magnetic moments of nucleons (non-additivity of moments). The effects of a finite charge distribution in nucleons can be included in the theory.

A generalization to include many-body forces can probably be carried through by the same methods as used above, but with a considerable increase in complication. To include velocity-dependent forces and relativistic effects would, however, probably require major changes in methodology.

The shortcomings of a phenomenological approach to exchange currents lies in the fact that there is still considerable arbitrariness in the theory, only the irrotational exchange current density being fixed by the theory. The calculations[4] made on the basis of particular models for the exchange of charge (meson theories) have demonstrated that the results obtained do depend rather critically on the particular model assumed. Under these circumstances any further developments in the phenomenological theory must be based on experimental results.

APPENDIX

In the exposition above, we are faced with the problems (1) of finding the most general axial vector which can be formed from two spin vectors (say $\boldsymbol{\Sigma}$ and $\boldsymbol{\sigma}$) and a (polar) position vector (say $\mathbf{R}$), and (2) of finding the most general axial vector which may be constructed from two spin vectors ($\boldsymbol{\Sigma}$, $\boldsymbol{\sigma}$) and two (polar) position vectors (say $\mathbf{R}$ and $\mathbf{r}$). Each of these may obviously be written as a linear combination of all possible linearly independent axial vectors which may be constructed from the vectors enumerated above. Furthermore, each of these linearly independent axial vectors can be factored into an arbitrary scalar function of the position vector or vectors and a purely angle-dependent factor which has the required transformation properties. For the purposes of finding the latter we may consider the position vectors $\mathbf{R}$ and $\mathbf{r}$ as being of unit magnitude.

Since the spin vectors transform under both proper and improper rotations as antisymmetric tensors of the second rank, it is useful to represent them as two index quantities, viz:

$$\boldsymbol{\sigma}\rightarrow\sigma_{\mu\nu}=-\sigma_{\nu\mu},\quad\boldsymbol{\Sigma}\rightarrow\Sigma_{\mu\nu}=-\Sigma_{\nu\mu},$$

where we shall use the arrow to designate the process of changing the representation from tensor representation to vector representation, or vice versa. Since the spin vector components satisfy the algebra:

$$\begin{aligned}&\sigma_x^2=\sigma_y^2=\sigma_z^2=1,\quad&&\Sigma_x^2=\Sigma_y^2=\Sigma_z^2=1,\\&\sigma_x\sigma_y=i\sigma_z,&&\Sigma_x\Sigma_y=i\Sigma_z,\\&\sigma_z\sigma_x=i\sigma_y,&&\Sigma_z\Sigma_x=i\Sigma_y,\\&\sigma_y\sigma_z=i\sigma_x,&&\Sigma_y\Sigma_z=i\Sigma_z,\end{aligned}$$

any expression of higher than first degree in the components of either spin vector can always be reduced to one of first degree. Thus the only tensors which can be formed from the spin vectors (including the scalar, *unity*) are:

1	Scalar with 1 component.
$\left.\begin{matrix}\sigma_{\mu\nu}\\ \Sigma_{\mu\nu}\end{matrix}\right\}$	Antisymmetric second rank tensors with 3 linearly independent components each.
$\sigma_{\mu\alpha}\Sigma_{\alpha\nu}$	Second rank tensor with 9 linearly independent components.

These 16 quantities may be rearranged to form the more convenient tensors:

$\left.\begin{matrix}1\\ \sigma_{\alpha\beta}\Sigma_{\beta\alpha}\rightarrow(\boldsymbol{\sigma}\cdot\boldsymbol{\Sigma})\\ \sigma_{\mu\nu}\end{matrix}\right\}$	Two scalars each with 1 component.
$\left.\begin{matrix}\Sigma_{\mu\nu}\\ \sigma_{\mu\alpha}\Sigma_{\alpha\nu}-\sigma_{\nu\alpha}\Sigma_{\alpha\mu}\rightarrow\boldsymbol{\sigma}\times\boldsymbol{\Sigma}\end{matrix}\right\}$	Antisymmetric second rank tensors with 3 linearly independent components each.
$\frac{1}{2}\{\sigma_{\mu\alpha}\Sigma_{\alpha\nu}+\sigma_{\nu\alpha}\Sigma_{\alpha\mu}\}-\delta_{\mu\nu}\{\sigma_{\alpha\beta}\Sigma_{\beta\alpha}\}$	Second rank symmetric traceless tensor with 5 linearly independent components.

From the one vector $\mathbf{R}\rightarrow R_\alpha$ we can form the series of tensors:

$$1,\ R_\alpha,\ R_\alpha R_\beta,\ \cdots,\ R_\alpha R_\beta\cdots R_\gamma\cdots,\ \cdots.$$

If $\mathbf{R}$ is considered of unit magnitude, then any contraction on indices leads only to another tensor appearing earlier in the list.

Now antisymmetrical second rank tensors can be formed from the vector $\mathbf{R}$ and the two spin vectors in the following ways:

I. By multiplying the scalars 1, $(\boldsymbol{\sigma}\cdot\boldsymbol{\Sigma})$ with an antisymmetric second rank tensor formed from the R's. No such exist.

II. By multiplying the antisymmetric second rank tensors $\sigma_{\mu\nu}$, $\Sigma_{\mu\nu}$, $\sigma_{\mu\beta}\Sigma_{\beta\nu}-\sigma_{\nu\beta}\Sigma_{\beta\mu}$ by (A) the scalar 1, yielding:

A. 1. $\sigma_{\mu\nu}\rightarrow\boldsymbol{\sigma}$,
2. $\Sigma_{\mu\nu}\rightarrow\boldsymbol{\Sigma}$
3. $\sigma_{\mu\beta}\Sigma_{\beta\nu}-\sigma_{\nu\beta}\Sigma_{\beta\mu}\rightarrow\boldsymbol{\sigma}\times\boldsymbol{\Sigma}$,

or (B) by the second rank tensor $R_\alpha R_\nu$, contracting on one index and antisymmetrizing on the remaining index, yielding:

B. 1. $\sigma_{\mu\alpha}R_\alpha R_\nu-\sigma_{\nu\alpha}R_\alpha R_\mu\rightarrow(\boldsymbol{\sigma}\cdot\mathbf{R})\mathbf{R}$.
2. $\Sigma_{\mu\alpha}R_\alpha R_\nu-\Sigma_{\nu\alpha}R_\alpha R_\mu\rightarrow(\boldsymbol{\Sigma}\cdot\mathbf{R})\mathbf{R}$.
3. $[\sigma_{\mu\beta}\Sigma_{\beta\alpha}-\sigma_{\alpha\beta}\Sigma_{\beta\mu}]R_\alpha R_\nu-[\sigma_{\nu\beta}\Sigma_{\beta\alpha}-\sigma_{\alpha\beta}\Sigma_{\beta\mu}]R_\alpha R_\mu\rightarrow(\mathbf{R}\cdot\boldsymbol{\sigma}\times\boldsymbol{\Sigma})\mathbf{R}$.

III. By multiplying the symmetric traceless tensor,

$$\tfrac{1}{2}[\sigma_{\mu\beta}\Sigma_{\beta\alpha}+\sigma_{\alpha\beta}\Sigma_{\beta\mu}]-\delta_{\mu\alpha}(\sigma_{\beta\gamma}\Sigma_{\gamma\beta})$$

by the second rank tensor $R_\alpha R_\nu$, contracting on one index, and antisymmetrizing on the remaining indices:

$$\{\tfrac{3}{2}[\sigma_{\mu\beta}\Sigma_{\beta\alpha}+\sigma_{\alpha\beta}\Sigma_{\beta\mu}]-\delta_{\mu\alpha}(\sigma_{\beta\gamma}\Sigma_{\gamma\beta})\}R_\alpha R_\nu - \{\tfrac{3}{2}[\sigma_{\nu\beta}\Sigma_{\beta\alpha}+\sigma_{\alpha\beta}\Sigma_{\beta\nu}]-\delta_{\nu\alpha}(\sigma_{\beta\gamma}\Sigma_{\gamma\beta})\}R_\alpha R_\mu \rightarrow \tfrac{3}{2}\{(\mathbf{R}\cdot\boldsymbol{\sigma})[\mathbf{R}\times\boldsymbol{\Sigma}]+(\mathbf{R}\cdot\boldsymbol{\Sigma})[\mathbf{R}\times\boldsymbol{\sigma}]\}.$$

We thus obtain at most 7 linearly independent axial vectors formed from two spin vectors and a unit polar vector.

The process for finding the totality of linearly independent axial vectors from two spin vectors and two unit polar vectors is practically identical. One can now form more tensors from the polar vectors, viz.:

$$1,\ R_\alpha,\ r_\alpha,\ R_\alpha R_\beta,\ R_\alpha r_\beta,\ r_\alpha r_\beta,\ \text{etc.}$$

By multiplication and contraction with the tensors formed from the spin vectors one then finds the 27 linearly independent axial vectors given in the text.

PHYSICAL REVIEW VOLUME 79, NUMBER 5 SEPTEMBER 1, 1950

Diffusion in the Ionosphere

M. H. JOHNSON AND E. O. HULBURT
Naval Research Laboratory, Washington, D. C.
(Received April 12, 1950)

Diffusion is treated by showing that the action of a medium on a diffusing gas is that of a dissipative force. When the theory is applied to an electrically neutral ionic gas in a gravitational field it is found that the mixture of positive and negative ions diffuses as a single gas because of the electrical polarization charges within the ionic cloud. In the presence of a magnetic field, the diffusion cannot be expressed in terms of the ionic density until the electrodynamical equations governing the flow of electrical current have been explicitly solved. Solutions are obtained for special cases which show that a strong magnetic field completely inhibits the diffusion due to concentration gradients in the transverse plane and has little effect on the diffusion due to the gravitational force.

I. INTRODUCTION

THE role played by diffusion in the formation of ion banks in the upper ionosphere (F-region) is not settled in our opinion because no one has given an adequate treatment of the diffusion processes. Too little attention has been paid to the electrical polarization developed by the diffusion current and to the reaction of the resulting electric field on the diffusion, although the existence of these effects has been recognized.[1,2]

Transport phenomena are usually treated by the kinetic molecular theory which yields a distribution function for the different kinds of molecules. No one has yet explicitly formulated the diffusion equations for a three component mixture (positive ions, negative ions or electrons, neutral molecules), because of the inherent mathematical complexity of the kinetic molecular theory.

In the present paper this difficulty is avoided by introducing the concept of a dissipative force (Section II). The definition of the diffusion coefficient and the ideal gas law lead directly to a force equation which shows that the pressure gradient in a diffusing gas is balanced by a force proportional to the diffusion velocity. This force acts whenever a diffusion current flows. The diffusion current can then be obtained in any field of force from the balance of all the forces acting on the diffusing gas. In this way the kinetic molecular theory enters into the determination of the mass motion only through the diffusion coefficient and the ideal gas law.

A comparatively simple treatment of the migration of equal numbers of positive and negative ions through a neutral gas in a gravitational field is possible with the concept of dissipative force (Section III). It is shown that the mixture diffuses as a single gas whose diffusion coefficient, in case the negative ions are electrons, is equal to twice the diffusion coefficient of the positive ions and whose scale height is given by the average molecular weight of the ions. An electrical field exists throughout the ionic cloud which is derived from internal polarization charges. It is this electric field which binds the motion of the positive and negative ions together, thereby making it possible to describe the mixture as a single gas.

The treatment is extended to include the effect of a magnetic field (Section IV). The diffusion now depends on the force exerted by the magnetic field on any electrical currents which may be present. An exact solution is obtained for a constant diffusion coefficient and constant magnetic field which shows that a circulation of electrical current in the plane perpendicular to the magnetic field must take place in such a way that the diffusion due to pressure gradients becomes negligible for conditions in the ionosphere. The diffusion current due to gravity is unchanged and is accompanied by an electric field, derived from polarization charges, which is perpendicular to the magnetic and gravitational fields. In case the diffusion coefficient is not constant, additional electrical currents flow in such a way that the gravitational diffusion current of most of the ionic cloud is characterized by the diffusion coefficient at a certain median altitude. Thus the magnetic

[1] E. O. Hulburt, Phys. Rev. 34, 1167 (1929).
[2] T. G. Cowling, M.N.R.A.S. 93, 90 (1932).

field has a comparatively small effect on diffusion in the ionosphere even though the ratio of mean free path to radius of gyration is very large.

II. THE DISSIPATIVE FORCE

Let D be the diffusion coefficient of a gas whose molecular density is n. Then

$$n\mathbf{v} = -D\nabla n, \tag{1}$$

where $\mathbf{v}$ is the mean molecular velocity of the diffusing molecules. We assume that the gas exerts its own partial pressure p according to the ideal gas law

$$p = nkT, \tag{2}$$

where k is the Boltzmann constant and T the absolute temperature. Expressing ∇n in terms of ∇p, Eq. (1) becomes

$$-\nabla p = (kT/D)n\mathbf{v}. \tag{3}$$

The pressure gradient is the force per unit volume which the diffusing gas exerts upon itself because of its own density variations. The right-hand member of Eq. (3) can be interpreted as a dissipative force that is in equilibrium with the pressure gradient. The adjective "dissipative" implies that the force is in the opposite direction to, and is proportional to, the diffusion velocity. It may be considered a retarding force exerted by the medium on the diffusing gas. Equation (3) which has been derived for an ideal gas at a uniform temperature is a generally valid expression for the dissipative force and we shall take it as our starting point.

As an example, consider a gas of molecular weight m diffusing along the z axis under the influence of a gravitational force, mg. After adding the gravitational force per unit volume to the left side, Eq. (3) gives, for the diffusion current,

$$nv = (-D/kT)(nmg + dp/dz). \tag{4}$$

For a static density distribution, the divergence of nv is zero so that nv must be zero everywhere if it is zero at any point. In that case

$$nmg = -dp/dz = kTnd[\ln(nT)]/dz. \tag{5}$$

Integrating Eq. (5), we find

$$nT = n_0T_0 \exp\left[-(mg/k)\int_0^z T^{-1}dz\right], \tag{6}$$

where n_0 and T_0 are the density and temperature at $z=0$. It may be noted that the static density distribution given by Eq. (6) includes effects of thermal diffusion. In case the gas is at a uniform temperature Eq. (6) reduces to the usual barometric height formula in which mg/kT is the reciprocal of the scale height. Since the distribution is independent of the diffusion coefficient, it is valid whatever may be the medium in which the diffusion takes place.

III. NEUTRAL IONIC GAS IN A GRAVITATIONAL FIELD

Let y_1 be the density of ions carrying a charge $+e$ and y_2 be the density of ions carrying a charge $-e$, where e is the absolute value of the electronic charge. By a neutral ionic gas we mean that $y_1 - y_2$ can be neglected in comparison with y_1. We shall see that this condition is accurately satisfied in the ionosphere. Let $\mathbf{f}_1$ and $\mathbf{f}_2$ be the gravitational force on a positive ion and a negative ion, respectively, and let $\mathbf{E}$ be the electric field within the ionic cloud. The sources of $\mathbf{E}$ are the polarization charges which may be developed by the diffusion currents.

The equilibrium condition for the force per unit volume must now be applied to both positive and negative ions. Thus,

$$e\mathbf{E}y + \mathbf{f}_1y - \nabla p = (kT/D_1)y\mathbf{v}_1, \tag{7a}$$

$$-e\mathbf{E}y + \mathbf{f}_2y - \nabla p = (kT/D_2)y\mathbf{v}_2, \tag{7b}$$

where the subscripts 1 and 2 refer to positive and negative ions, respectively. Strictly speaking, the subscripts 1 and 2 should also appear on y in Eqs. (7a) and (7b), respectively. However, the condition of electrical neutrality allows us to put $y_1 = y_2 = y$ in both equations. Similarly we may put $p_1 = p_2 = p$ where

$$p = ykT, \tag{8}$$

provided temperature equilibrium has been established so that both positive and negative ions in a given region are at the same temperature as the medium.

The electrical current density, $\mathbf{u}$, is directly related to the diffusion currents,

$$\mathbf{u} = ey(\mathbf{v}_1 - \mathbf{v}_2). \tag{9}$$

The connection between $\mathbf{E}$ and the electrical current follows from Eq. (7), and is

$$\mathbf{E} = \frac{kT}{e^2y(D_1+D_2)}\mathbf{u} + \frac{D_1-D_2}{ey(D_1+D_2)}\nabla p + \frac{D_2\mathbf{f}_2 - D_1\mathbf{f}_1}{e(D_1+D_2)}, \tag{10}$$

a relation which must hold at every instant of time.

We shall first examine the conditions under which the electrical current can be zero. Since the sources of $\mathbf{E}$ are charges, the necessary condition that must be satisfied is that $\nabla \times \mathbf{E}$ be zero. The diffusion coefficients are, in general, functions of position because they depend on the molecular density of the atmosphere at the point under consideration. However, if the atmosphere has a uniform composition the ratio, $\kappa = D_1/D_2$, does not depend on position because both coefficients then vary with the molecular density in the same way. Since the ratio of the kinetic theory cross sections for the positive and negative ions is different for different constituents of the atmosphere, a variation in composition might well induce a variation in κ. We shall assume that variations in κ can be neglected so that D_1 and D_2 can be treated as constants in calculating

TABLE I. Values of the diffusion coefficient b.

T°K	b
300	0.685×10^{19}
400	0.864
500	1.04
700	1.32
1000	1.65
1500	2.00
2000	2.13

$\nabla\times\mathbf{E}$ from the last two terms in Eq. (10). As $\mathbf{f}_1$ and $\mathbf{f}_2$ are conservative forces, $\nabla\times\mathbf{f}_1=\nabla\times\mathbf{f}_2=0$ and therefore the curl of the last term in Eq. (10) is zero. The curl of the second term is zero only if

$$\nabla y\times\nabla p=0. \tag{11}$$

When there are no thermal gradients in the atmosphere, Eq. (11) is automatically satisfied in virtue of Eq. (8). If there are thermal gradients, they cannot in general be everywhere parallel to ∇y and there will be regions in which the curl of the second term of Eq. (10) is not zero. In such regions there must be a circulation of the electric current in such a way that $\nabla\times\mathbf{E}=0$. A similar remark applies to regions in which κ is not constant. To summarize, the electrical current can be zero everywhere only if the atmosphere has a uniform composition and is everywhere at the same temperature.

Let $\mathbf{E}_0$ be the electric field when $\mathbf{u}=0$. We next inquire what happens if at a certain instant, say $t=0$, $\mathbf{E}$ is not equal to $\mathbf{E}_0$. Then a current must flow in accordance with Eq. (10)

$$\mathbf{u}=e^2y(D_1+D_2)(kT)^{-1}(\mathbf{E}-\mathbf{E}_0). \tag{12}$$

This current produces a change in the charge density ρ,

$$\partial\rho/\partial t=-\nabla\cdot\mathbf{u}=\partial(\rho-\rho_0)/\partial t, \tag{13}$$

which in turn induces a change in the electric field according to

$$\nabla\cdot(\mathbf{E}-\mathbf{E}_0)=4\pi(\rho-\rho_0). \tag{14}$$

Hence

$$\nabla\cdot[(\partial/\partial t)(\mathbf{E}-\mathbf{E}_0)+4\pi e^2y(D_1+D_2)(kT)^{-1}(\mathbf{E}-\mathbf{E}_0)]=0. \tag{15}$$

If $y(D_1+D_2)$ is treated as a constant, the curl of the quantity in the brackets is also zero and the quantity must be a constant. The constant is zero because $\mathbf{E}$ ultimately must become equal to $\mathbf{E}_0$.

$$(\partial/\partial t)(\mathbf{E}-\mathbf{E}_0)+4\pi e^2y(D_1+D_2)(kT)^{-1}(\mathbf{E}-\mathbf{E}_0)=0. \tag{16}$$

It follows that $\mathbf{E}-\mathbf{E}_0$ decreases with time as $\exp(-t/\tau)$ where

$$\tau=kT/[4\pi e^2y(D_1+D_2)]. \tag{17}$$

Since y has been treated as a constant in the integration of Eq. (16), we have assumed that τ is very short in comparison with any time in which an appreciable variation in the ionic density can occur. For a typical numerical example take $T=300$°K, $D_2=10^9$, which is roughly the diffusion coefficient of an electron at a molecular density of 10^{12}, and $y=1$. Then $\tau=10^{-5}$ sec. Thus τ is indeed very small in comparison with any time intervals in which we are interested even for so low an ion density as $1/\text{cm}^3$. It follows that under any realizable conditions in the ionosphere, polarization charges are developed almost instantaneously. To a high degree of accuracy, $\mathbf{u}=0$ and the electrical field is given by the instantaneous value of $\mathbf{E}_0$.

We can now see how well the condition of electrical neutrality is satisfied. From Eqs. (14), (10) and (8)

$$y_1-y_2=\rho/e=(4\pi e)^{-1}\nabla\cdot\mathbf{E}=\frac{1-\kappa}{4\pi e(1+\kappa)}\nabla\cdot\left(\frac{\nabla p}{ey}\right)\sim-\frac{kT}{4\pi}e^2\nabla^2\ln y. \tag{18}$$

If l is a distance in which the ion density changes by a factor 2,

$$y_1-y_2\sim\pm kT/4\pi e^2l^2\cong10^5l^{-2}. \tag{19}$$

In the ionosphere l is of the order of tens of kilometers so y_1-y_2 is of the order 10^{-7} ion/cm^3. Hence y_1-y_2 is 10^{-10} times the smallest ion density of interest (1000 ions/cm^3) and the condition of electrical neutrality is very well satisfied.

A differential equation for y can be set up by equating the loss of ions per unit volume by diffusion to the gain of ions per unit volume from all other causes. The latter are functions of y and position only so that a determining equation for y is obtained if the loss of ions by diffusion, $(\nabla\cdot y\mathbf{v}_1)$, can also be expressed as functions of y and position only. By adding Eqs. (7a) and (7b)

$$y\mathbf{v}_1+\kappa^{-1}y\mathbf{v}_2=(D_1/kT)[(\mathbf{f}_1+\mathbf{f}_2)y-2\nabla p]. \tag{20}$$

Taking the divergence of Eq. (20) and using the condition of electrical neutrality to set $\nabla\cdot y\mathbf{v}_1=\nabla\cdot y\mathbf{v}_2$,

$$\nabla\cdot y\mathbf{v}_1=-\nabla\cdot[2\kappa D_1/kT(1+\kappa)][\nabla p-\tfrac{1}{2}(\mathbf{f}_1+\mathbf{f}_2)y]. \tag{21}$$

The assumption of a uniform atmospheric composition has again been used in treating κ as a constant with respect to the differentiation in Eq. (21). But from Eq. (14) the loss of ions by diffusion for a single component gas is

$$\nabla\cdot y\mathbf{v}=-\nabla\cdot D[\nabla p-\mathbf{f}y]/kT. \tag{22}$$

Hence a neutral ionic gas diffuses as a single component gas with

$$D=2\kappa(1+\kappa)^{-1}D_1, \tag{23a}$$

$$\mathbf{f}=\tfrac{1}{2}(\mathbf{f}_1+\mathbf{f}_2). \tag{23b}$$

In case the negative ions are electrons, $\kappa\cong100$ so that $D=2D_1$ and $\mathbf{f}=\mathbf{f}_1/2$. The fact that the diffusion coefficient is greater and the scale height smaller than that of the positive ions alone is easy to understand. The more mobile and lighter electrons impart these qualities, by means of the internal electric field, to the mixture.

The diffusion coefficient can be written as

$$D=b/n, \tag{24}$$

where n is the molecular density of the atmosphere. Values of b for the ionosphere at various temperatures are given in Table I which is taken from a paper by Ferraro.[3]

IV. NEUTRAL IONIC GAS IN A GRAVITATIONAL AND A MAGNETIC FIELD

When a magnetic field, $\mathbf{H}$, is also present, the ampere force on the diffusion currents must be included in the equilibrium of forces. Equation (7) becomes

$$ey(\mathbf{E}+\mathbf{v}_1\times\mathbf{H}/c)+\mathbf{f}_1y-\nabla p=(kT/D_1)\mathbf{v}_1, \tag{25a}$$

$$-ey(\mathbf{E}+\mathbf{v}_2\times\mathbf{H}/c)+\mathbf{f}_2y-\nabla p=(kT/D_2)\mathbf{v}_2. \tag{25b}$$

The condition of electrical neutrality has been used in exactly the same way as in Section III.

The connection between $\mathbf{u}$ and $\mathbf{E}$ is obtained by solving[4] Eqs. (25a) and (25b) for $\mathbf{v}_1$ and $\mathbf{v}_2$, respectively, and constructing $\mathbf{u}$ according to Eq. (9).

$$\begin{aligned}\mathbf{u}/e=(\mathbf{n}/kT)&[(D_2-D_1)(\mathbf{n}\cdot\nabla p)+y(D_1\mathbf{f}_1-D_2\mathbf{f}_2)\cdot\mathbf{n}\\&+ey(D_1+D_2)\mathbf{n}\cdot\mathbf{E}]\\&+(kT)^{-1}\left[\left(\frac{-D_1}{1+\lambda_1^2}+\frac{D_2}{1+\lambda_2^2}\right)\nabla_t p\right.\\&+y\left(\frac{D_1\mathbf{f}_{1t}}{1+\lambda_1^2}-\frac{D_2\mathbf{f}_{2t}}{1+\lambda_2^2}\right)\\&\left.+ey\left(\frac{D_1}{1+\lambda_1^2}+\frac{D_2}{1+\lambda_2^2}\right)\mathbf{E}_t\right]\\&+(kT)^{-1}\left[-\left(\frac{D_1\lambda_1}{1+\lambda_1^2}+\frac{D_2\lambda_2}{1+\lambda_2^2}\right)\nabla p\right.\\&+y\left(\frac{D_1\lambda_1\mathbf{f}_1}{1+\lambda_1^2}+\frac{D_2\lambda_2\mathbf{f}_2}{1+\lambda_2^2}\right)\\&\left.+ey\left(\frac{D_1\lambda_1}{1+\lambda_1^2}-\frac{D_2\lambda_2}{1+\lambda_2^2}\right)\mathbf{E}\right]\times\mathbf{n},\end{aligned} \tag{26}$$

where $\mathbf{n}$ is a unit vector in the direction of $\mathbf{H}$ and

$$\lambda_1=eHD_1(ckT)^{-1},\quad \lambda_2=\kappa\lambda_1,\quad \mathbf{A}_t=\mathbf{A}-\mathbf{n}(\mathbf{n}\cdot\mathbf{A}). \tag{27}$$

If the kinetic theory value of D is used in Eq. (27), λ becomes the ratio of the mean free path to the radius of gyration in the magnetic field. The first bracket on the right-hand side of Eq. (26) shows that the components of $\mathbf{u}$, ∇p, $\mathbf{f}_1$, $\mathbf{f}_2$, and $\mathbf{E}$ along the direction of the magnetic field are connected by the same relation that holds for these vectors in the absence of a magnetic field [compare Eq. (10)]. The rest of Eq. (26) refers to components transverse to $\mathbf{H}$ which are now differently related. The coefficients of the terms containing $\mathbf{E}$ are the components of the conductivity tensor which, in case $\lambda_2\gg\lambda_1$, reduce to formulas similar to those given by Cowling[2] for a completely ionized gas.

Equation (25) can also be solved for $\mathbf{E}$ in terms of $\mathbf{u}$. We find

$$\begin{aligned}\mathbf{E}=&\frac{kT(1+\lambda_1\lambda_2)}{e^2y(D_1+D_2)}+\frac{1-\kappa}{ey(1+\kappa)}\nabla p+\frac{\kappa\mathbf{f}_2-\mathbf{f}_1}{e(1+\kappa)}\\&+\frac{\kappa-1}{ecy(1+\kappa)}\mathbf{u}\times\mathbf{H}-\frac{\lambda_2(\mathbf{u}\cdot\mathbf{H})}{ecy(1+\kappa)}\mathbf{n}\\&+\frac{2\lambda_2}{ey(1+\kappa)}\nabla p\times\mathbf{n}-\frac{\lambda_2}{e(1+\kappa)}(\mathbf{f}_1+\mathbf{f}_2)\times\mathbf{n}.\end{aligned} \tag{28}$$

To simplify the subsequent discussion we will make two assumptions, $1\ll\kappa$ and $1\ll\lambda_1\lambda_2$, both of which are valid in the ionosphere when the negative ions are electrons. Equation (28) can then be written

$$\begin{aligned}\mathbf{E}=&-(ey)^{-1}\nabla p-(e\kappa)^{-1}\mathbf{f}_1+(ecy)^{-1}\mathbf{u}\times\mathbf{H}\\&+\lambda_1[(ecy)^{-1}H\mathbf{u}_t+2(ey)^{-1}\nabla p\times\mathbf{n}-e^{-1}f_1\times\mathbf{n}].\end{aligned} \tag{29}$$

This relation, just as Eq. (10), must hold at every instant of time. We shall further restrict the discussion to motions at right angles to a constant magnetic field.

Even in the case λ_1 does not depend on position, a case we shall consider first, it is at once apparent that $\mathbf{u}$ cannot be zero in Eq. (29) because the curl of $2(ey)^{-1}\nabla p\times\mathbf{n}$ cannot be zero. The curl of this term must be compensated by a circulation of $\mathbf{u}$. Let

$$\mathbf{u}_0=-(2c/H)\nabla p\times\mathbf{n}, \tag{30}$$

$$\mathbf{u}=\mathbf{u}_1+\mathbf{u}_0. \tag{31}$$

As the divergence of $\mathbf{u}_0$ is zero, $\mathbf{u}_0$ does not produce polarization charges and can therefore flow as a permanent current. Then Eq. (29) can be written as

$$\begin{aligned}\mathbf{E}=&(ey)^{-1}\nabla p-(e\kappa)^{-1}\mathbf{f}_1+(ecy)^{-1}\mathbf{u}_1\times\mathbf{H}\\&+\lambda_1[(ecy)^{-1}H\mathbf{u}_1-e^{-1}\mathbf{f}_1\times\mathbf{n}].\end{aligned} \tag{32}$$

If $\mathbf{u}_1=0$, the curl of $\mathbf{E}$ is

$$\nabla\times\mathbf{E}=-(ey^2)^{-1}\nabla y\times\nabla p-e^{-1}\nabla\lambda_1\times(\mathbf{f}_1\times\mathbf{n}). \tag{33}$$

Now when λ_1 is constant, i.e., D_1 is not a function of position, $\nabla\times\mathbf{E}$ is zero only if there are no thermal gradients in the atmosphere. Hence, if D_1 is constant and there are no thermal gradients, a possible electric field in the ionic cloud is given by Eq. (32) with $\mathbf{u}_1=0$. The electrical current at all points is then given by $\mathbf{u}_0$ of Eq. (30). We shall refer to this solution as Case A.

[3] V. C. A. Ferraro, J. Terr. Mag. **50**, 215 (1945). Apparently Ferraro has incorrectly taken the diffusion coefficient of the of the neutral ionic gas as $(\frac{2}{3})^{\frac{1}{2}}$ that of the positive ions. Hence the values shown in Table I are $2(\frac{2}{3})^{\frac{1}{2}}$ larger than the corresponding values given by Ferraro. Hulburt used $b=10^{19}$ in his first paper, Phys. Rev. **31**, 1018 (1928).

[4] If a vector $\mathbf{A}$ is determined by the equation $\mathbf{A}+\alpha(\mathbf{A}\times\mathbf{B})=\mathbf{C}$ where $\mathbf{B}$ and $\mathbf{C}$ are given vectors, then

$$\mathbf{A}=(1+\alpha^2B^2)^{-1}[\alpha^2(\mathbf{B}\cdot\mathbf{C})\mathbf{B}+\mathbf{C}+\alpha\mathbf{B}\times\mathbf{C}].$$

Suppose now that λ_1 is a function of position. A possible electric field can be obtained by making the bracket in Eq. (32) vanish. Thus

$$\mathbf{u}_1=(cy/H)\mathbf{f}_1\times\mathbf{n}. \tag{34}$$

Then

$$\mathbf{E}=(ey)^{-1}\nabla p-\mathbf{f}_1/e \tag{35}$$

and $\nabla\times\mathbf{E}$ is zero if there are no thermal gradients. The divergence of $\mathbf{u}_1$ is

$$\nabla\cdot\mathbf{u}_1=(c/H)\nabla y\cdot(\mathbf{f}_1\times\mathbf{n}) \tag{36}$$

and is not in general zero. However, if the ionic cloud is infinite in extent and the concentration gradient is at right angles to $\mathbf{f}_1\times\mathbf{n}$, the divergence of $\mathbf{u}_1$ is zero. Therefore a possible electric field is given by Eq. (35), accompanied by the current density of Eqs. (30), (31), and (34) provided that the cloud is infinite in extent, there are no thermal gradients and the concentration gradient is perpendicular to $\mathbf{f}_1\times\mathbf{n}$. We shall call this solution Case B. It may be noted that the solution remains valid if thermal gradients are present which are parallel to the concentration gradient. Case B might be approximated, for example, at the earth's magnetic equator if ionization were produced uniformly around the circumference of the earth and the concentration gradients were all vertical.

Another possible solution can be found for an ionic cloud whose lateral extension is large compared to its vertical extension. Let λ_{10} be the value of λ_1 at a median position in the cloud which we shall determine later. The surface $\lambda_1=\lambda_{10}$ then divides the cloud into an upper and lower part. Equation (32) can be written as

$$\mathbf{E}=(ey)^{-1}\nabla p-(e\kappa)^{-1}\mathbf{f}_1-(\lambda_{10}/e)\mathbf{f}_1\times\mathbf{n}+(ecy)^{-1}\mathbf{u}_1\times\mathbf{H}+(\lambda_1H/ecy)\mathbf{u}_1-e^{-1}(\lambda_1-\lambda_{10})\mathbf{f}_1\times\mathbf{n}. \tag{37}$$

Now suppose

$$\mathbf{u}_1=(cy/H)(1-\lambda_{10}/\lambda_1)\mathbf{f}_1\times\mathbf{n}. \tag{38}$$

Since the diffusion coefficient will generally be a function of altitude alone, the gradient of λ_1 is perpendicular to $\mathbf{f}_1\times\mathbf{n}$. Hence the divergence of $\mathbf{u}_1$ comes entirely from the gradient of y. But if the cloud has a large lateral extension, the gradient of y will also be vertical in the central part of the cloud and therefore the divergence of $\mathbf{u}_1$ differs from zero only in the peripheral parts of the cloud. A current given by Eq. (38) will thus produce polarization charges on the periphery of the cloud which can only modify the current flow in the neighborhood of the periphery. Thus the current flow given by Eq. (28), which is oppositely directed in the upper and lower parts of the cloud because of the change in sign of $(1-\lambda_{10}/\lambda_1)$, will be maintained in the central portions of the cloud and will be modified at the periphery in such a way as to close the current circulation. The value λ_{10} must be so chosen that the total current flow through a vertical section of the upper part of the cloud is equal and opposite to the total flow through the same vertical section of the lower part, that is,

$$\int_0^\infty y(1-\lambda_{10}/\lambda_1)dz=0. \tag{39}$$

The electric field is then given by

$$\mathbf{E}=(ey)^{-1}\nabla p-(\lambda_{10}/e)\mathbf{f}_1\times\mathbf{n}-(cy/H)(1-\lambda_{10}/\lambda_1)\mathbf{f}_1. \tag{40}$$

Therefore, a possible electric field in the interior of an ionic cloud of large lateral extension is given by Eq. (40) accompanied by the currents of Eqs. (30), (31), and (38) provided that there are no thermal gradients in the atmosphere and a median value of the diffusion coefficient is determined by Eq. (39). We shall call this solution Case C.

Suppose that an electric field and current have been found which satisfy Eq. (29) and are such that $\nabla\times\mathbf{E}$ and the divergence of $\mathbf{u}$ are zero. Let us find out what happens if different values of $\mathbf{E}$ and $\mathbf{u}$, say $\mathbf{E}'$ and $\mathbf{u}'$, exist at the time $t=0$. Since Eq. (29) must hold at every instant

$$\mathbf{E}'-\mathbf{E}=(ecy)(\mathbf{u}'-\mathbf{u})\times\mathbf{H}+(ecy)^{-1}\lambda_1H(\mathbf{u}'-\mathbf{u}). \tag{41}$$

Then by the same steps that led to Eq. (16)

$$\mathbf{u}'-\mathbf{u}=-(4\pi)^{-1}\frac{\partial}{\partial t}(\mathbf{E}'-\mathbf{E})$$

$$=-\frac{H}{4\pi ecy}\frac{\partial}{\partial t}[(\mathbf{u}'-\mathbf{u})\times\mathbf{H}+\lambda_1(\mathbf{u}'-\mathbf{u})]. \tag{42}$$

Equation (42) is very similar to the precession equations for a spinning charge in a magnetic field and may be solved by familiar methods to show that $\mathbf{u}'-\mathbf{u}$ decreases with time as $\exp(-t/\tau)$ where

$$\tau=H(1+\lambda_1^2)/(4\pi ec\lambda_1)=H^2D_1/(4\pi c^2kTY). \tag{43}$$

For a numerical example take $H=1$, $D_1=10^{13}$ which is the diffusion coefficient for positive ions at a molecular density of 10^6, $T=500°$K and $y=10^3$. Then $\tau=10$ sec., which is a time that is still short compared to the time required for an appreciable change in the ionic density. Hence $\mathbf{E}$ and $\mathbf{u}$ may be taken as the instantaneous values of the electric field and current without appreciable error. For molecular densities smaller than 10^6 this may no longer be true.

The divergence of the diffusion current can be found from Eq. (25) by the same steps that led from Eq. (7) to Eq. (12).

$$\nabla\cdot y\mathbf{v}_1=-\nabla\cdot(2D_1/kT)[\nabla p-y\mathbf{f}_1/2-\mathbf{u}\times\mathbf{H}/2c]. \tag{44}$$

Now it is no longer possible to express the loss of ions by diffusion as a function of y and position only because of the term $\mathbf{u}\times\mathbf{H}$ in Eq. (44). The electrodynamical problem must be solved first before the expression for diffusion can be evaluated. Consequently, we can only express the diffusion in a form which gives a deter-

mining differential equation for y in the three cases of motions perpendicular to the magnetic field for which we have obtained solutions of the electrodynamical problem.

Case A

Inserting the current given by Eq. (30) into Eq. (44) gives

$$\nabla \cdot y\mathbf{v}_1 = \nabla \cdot (yD_1\mathbf{f}_1/kT). \tag{45}$$

The effect of the magnetic field is to inhibit completely the diffusion from pressure gradients. The diffusion from the gravitational force is entirely unaffected.

Case B

Inserting the current given by Eqs. (30), (31),and (35) into Eq. (44) gives

$$\nabla \cdot (y\mathbf{v}_1) = 0. \tag{46}$$

The effect of the magnetic field is to inhibit completely all diffusion.

Case C

Inserting the current given by Eqs. (30), (31), and (38) into Eq. (44) gives

$$\nabla \cdot (y\mathbf{v}_1) = \nabla \cdot (yD_{10}\mathbf{f}_1/kT). \tag{47}$$

The gravitational diffusion for the whole cloud is now characterized by the diffusion coefficient D_{10} where D_{10} is the value of D_1 at the median point determined by Eq. (39).

Since calculation shows that gravitational and pressure diffusion are roughly of the same order of magnitude, and since Case B cannot be realized in the ionosphere, the presence of a magnetic field cannot substantially alter the effects of diffusion. The reduction by the factor[5] $(1+\lambda_1\lambda_2)^{-1}$ completely disappears as far as the gravitational diffusion is concerned because of the electric field originating in the polarization of the ionic cloud which, in turn, is caused by the diffusion current. These results agree with those of an earlier discussion of the falling of ions under the combined action of gravity and magnetic field.[1] Numerical solutions of the foregoing diffusion equations in special cases and their comparison with ionospheric observations are reserved for a future paper.

---

[5] A calculation without making the approximations in the text shows that the term involving ∇p is not exactly zero but is reduced by the factor $(1+\lambda_1\lambda_2)^{-1}$. *Added in proof:* That the diffusion coefficient, D of Eq. (23a), is reduced by the factor $(1+\lambda_1\lambda_2)^{-1}$ in a magnetic field has also been found by Fundingsland and Austin, Phys. Rev. **79**, 232 (1950). We are indebted to these authors for showing us their results.

Further Investigation of the Radioactivity of Sb^{124}*

L. M. Langer, R. D. Moffat, and H. C. Price, Jr.
Indiana University, Bloomington, Indiana
(Received May 15, 1950)

The shape of the highest energy beta-ray group in Sb^{124} is found to have a forbidden shape that is characteristic of a once-forbidden transition involving a change of two units of angular momentum and a change of parity. As a consequence, the end points of the three highest energy groups are changed somewhat to 2.291 ± 0.005, 1.69 ± 0.01, and 0.95 ± 0.03 Mev. A high resolution measurement of photo-electrons confirms the existence of the 0.607-, 0.653-, and 0.730-Mev gamma-rays. The internal conversion of the 0.607-Mev gamma-ray was studied. The character of the radiation and relation of the parity assignments to possible predictions of the nuclear shell model are discussed. A search for possible positron or K-capture transitions to Sn^{124} gave no indication of the existence of such radiation.

I. INTRODUCTION

WITH the availability from Oak Ridge of sources having high specific activities, it seemed desirable to reinvestigate certain aspects of the Sb^{124} (60-day) disintegration.

In particular, it was suspected that the highest energy negatron group, with an end point previously reported[1] as 2.37 Mev might, if studied in greater detail, exhibit a forbidden spectrum shape. Such a shape might be expected from the high comparative half-life ($ft\sim10^{10}$) associated with the transition. Previous investigations[1,2] probably should not have been expected to distinguish a forbidden shape because of insufficient intensity in the region near the end point.

Since the general experimental techniques are now somewhat improved over those used earlier, an attempt was also made to check on the gamma-rays previously reported at 0.608, 0.654, and 0.732 Mev with better resolution and reliability.

Since Sb^{124} lies between stable Te^{124} and the relatively stable[3] Sn^{124}, there exists the possibility that the negatron emission might be in competition with positron emission or K-capture. A search was made, therefore, for positrons and for the Auger electrons which would be expected if any appreciable amount of the decay goes by K-capture.

The internal conversion of the 0.607-Mev gamma-ray was also studied.

II. EXPERIMENTAL METHOD

The measurements were carried out in the 40-cm radius of curvature, shaped magnetic field spectrometer.[4] Accurate magnetic field measurements were facilitated by a continuous comparison with a standard Helmholtz field by means of a rotating coil, balance arrangement.[5]

For the beta-spectra measurements, the resolution was 0.5 percent. For the gamma-ray determinations, this was increased to 0.85 percent (for a 0.6-Mev gamma-ray) because of the energy degeneration of the photo-electrons emerging from the finite thickness of the Pb radiator.

The beta-source was prepared by spreading, with the aid of insulin, $SbCl_3$ on a backing[6] of 0.02 mg/cm² LC600. The source was 0.6 cm wide, 2.5 cm high, and had an average thickness of 0.5 mg/cm². Very rapid drying of the deposit close under an infra-red lamp seemed to give the best uniformity. The source was maintained at ground potential by means of two small tabs of 0.18-mg/cm² aluminum, contiguous to the deposit.

For the gamma-ray measurements, the activity was deposited in a copper box with walls just sufficiently thick to stop all the primary beta-radiation. The photo-electrons were then ejected from a 5.6-mg/cm² Pb radiator which had been deposited on the 0.4×2.5-cm front face of the box, by thermal evaporation in vacuum.

III. RESULTS

The momentum distribution of the beta-rays of Sb^{124} is shown in Fig. 1. The open circles represent the data obtained in one run of the present investigation. The closed circles represent the data obtained earlier by Cook and Langer,[1] adjusted to the same intensity by a factor of 22.8. The inset shows the results of a study of the internal conversion of the 0.607-Mev gamma-ray obtained with a source which was 7.2 times as intense.

It is clear that the present investigation yields much more detailed information in the high energy region and, in general, joins quite well with the earlier data.

Figure 2 shows a conventional Fermi plot of the data in the high energy region. The values for the Coulomb factor, F, were taken from a set of curves prepared by relativistic calculation.[7] It is evident that the points do

* This work was assisted by a grant from the Frederick Gardner Cottrell Fund of the Research Corporation and by the joint program of the ONR and AEC.
[1] C. S. Cook and L. M. Langer, Phys. Rev. **73**, 1149 (1948).
[2] Kern, Zaffarano, and Mitchell, Phys. Rev. **73**, 1142 (1948). This paper contains a complete list of references to earlier work.
[3] Sn^{124} has recently been reported to decay by double beta emission with a half-life of 6×10^{15} years. E. L. Fireman, Phys. Rev. **75**, 323 (1949).
[4] L. M. Langer and C. S. Cook, Rev. Sci. Inst. **19**, 257 (1948).
[5] L. M. Langer and F. R. Scott, Rev. Sci. Inst. **21**, 522 (1950).
[6] L. M. Langer, Rev. Sci. Inst. **20**, 216 (1949).
[7] S. A. Moszkowski (private communication).

not lie on a straight line; the highest energy group does *not* have a spectrum shape of the form associated with an allowed transition. The maximum energy, obtained by extrapolation of the curve, is $W_0=5.485\ mc^2$ or $E_0=2.291\pm0.005$ Mev.

Figure 3 shows the results of two attempts to fit the data with forbidden Fermi plots based on the two unique factors for once- and twice-forbidden transitions.[8,9] The factor $a\propto[(W^2-1)+(W_0-W)^2]$ is characteristic of once-forbidden transitions involving a change of two units of angular momentum and a parity change. The factor

$$c\propto[3(W^2-1)^2+3(W_0-W)^4+10(W^2-1)(W_0-W)^2]$$

is unique for a twice-forbidden transition involving a spin change of three units and no change of parity. It is clear that the once-forbidden factor gives a very satisfactory fit at high energy. A correction factor based on a general $(W_0-W)^2$ dependence,[9] presumably applicable to most twice-forbidden transitions with spin change other than 3, was also tried and found not to fit the data.

Figure 4 shows the conventional and once-forbidden Fermi plots of the data. The broken lines indicate the results of the first two subtractions based on the assumption that the highest energy group is satisfied by the factor, a, and that the next inner group has the allowed shape.[10] It is easily seen how, in the absence of detailed information very close to the end point, the conventional plot ($C=1$) might be interpreted to be a straight line extrapolating, as shown, to the higher end point reported earlier.[1,2] The forbidden shape of the highest energy group not only lowers the value of its own end point but also affects somewhat the values of the maximum energies attributed to the next two inner groups. We now determine these as 1.69 ± 0.01 and 0.95 ± 0.03 Mev.

The present data, which are concentrated in the high

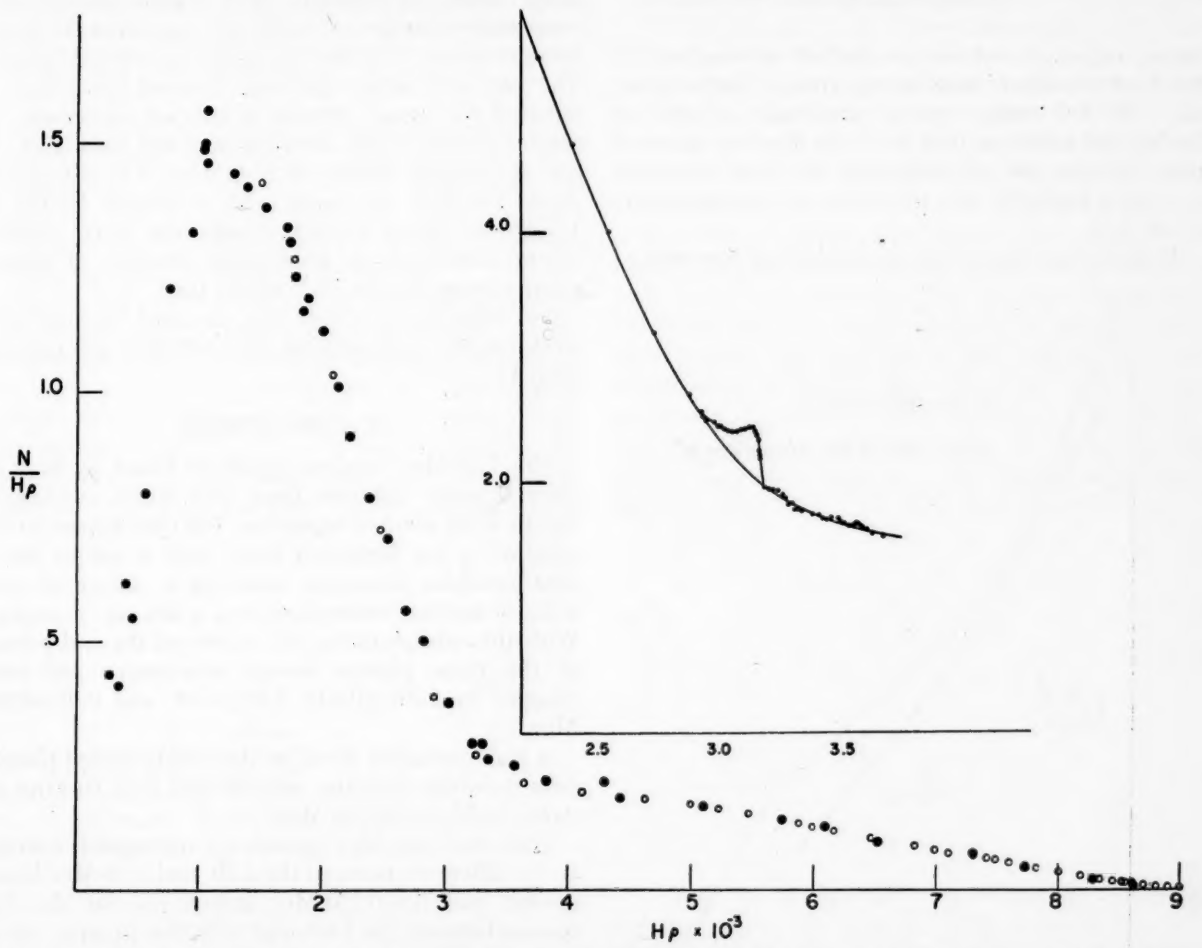

FIG. 1. Momentum distribution of the Sb^{124} negatrons. Closed circles represent the earlier data of Cook and Langer. The inset shows the internal conversion of the 0.607-Mev gamma-ray.

[8] L. M. Langer and H. C. Price, Jr., Phys. Rev. **76**, 641 (1949).
[9] E. J. Konopinski, Rev. Mod. Phys. **15**, 209 (1943).
[10] The *ft*-values for some of the inner groups are sufficiently high so that one might very well expect additional forbidden spectrum shapes. Unfortunately, inaccuracies introduced in making such subtractions would mask the possible existence of any forbidden shape.

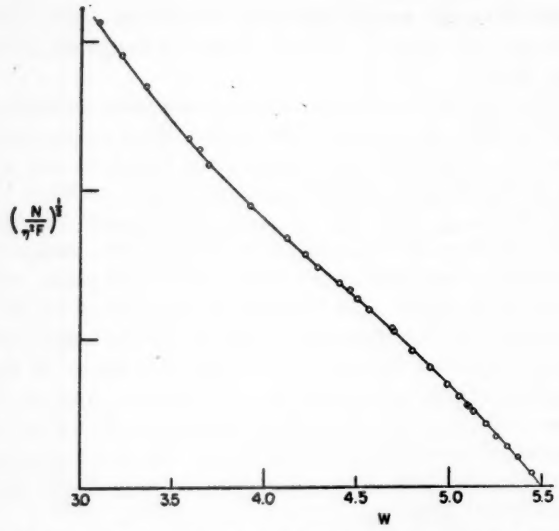

FIG. 2. Conventional Fermi plot of the Sb^{124} beta-distribution in the high energy region.

energy region, do not warrant further subtractions for the determination of lower energy groups. Furthermore, since the low energy spectra previously reported as having end points at 0.68 and 0.50 Mev are so much more intense, the determination of their maximum energies is negligibly affected by the new interpretation of the data.

Figure 5 is a plot of the photo-electron spectrum of the lower energy gamma-rays. The use of the thin radiator of only 5.6 mg/cm² of Pb yields much better resolution of these closely spaced lines than was obtained earlier. The photo lines corresponding to gamma-rays of 0.607, 0.653, and 0.730 Mev are now definitely resolved. As was suggested earlier, the *K*-line for the 0.730-Mev gamma-ray is superposed on the *L*-line of the 0.653-Mev gamma.

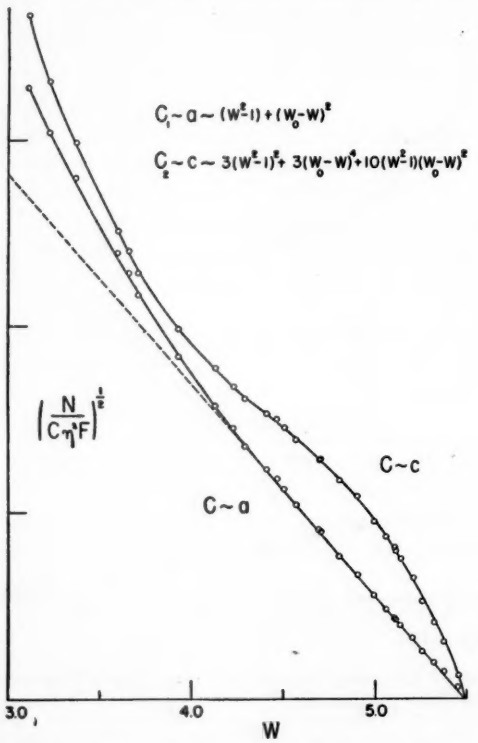

FIG. 3. Forbidden Fermi plots of the Sb^{124} beta-distribution at high energy. The once-forbidden factor $(W^2-1)+(W_0-W)^2$ gives a very good fit.

Inasmuch as the five beta-groups (2.29, 1.69, 0.95, 0.68, and 0.50 Mev) and the six gamma-rays (2.04, 1.71, 0.730, 0.653, 0.607, and 0.121 Mev) are difficult to fit into a unique energy level scheme, a search was made to determine whether any of the observed gammas might be associated with positron or *K*-capture transitions to Sn^{124}. A search was also made for the possible existence of a higher energy beta-transition directly to the ground state of Te^{124}. This is based on the assumption that the 2.29-Mev transition is to an excited state.[11] For these purposes, a beta-source was employed with seven times the intensity of a normal source. No measurable number of negatrons was observed with energies above 2.29 Mev. No positrons were detected. The very few Auger electrons observed could be attributed to a small amount of internal conversion of gamma-radiation and certainly was not indicative of any appreciable amount of *K*-capture. The search for Auger electrons was made with a counter having a 1.5-μg/cm² zapon window. Under the same experimental conditions, an appreciable intensity of Auger electrons was detected at 7 kev in Ga^{66}.

The same strong source was also used to study the weak internal conversion of the 0.607-Mev gamma-ray (Fig. 1).

IV. CONCLUSIONS

The 2.29-Mev beta-ray group is found to have a spectral shape different from that which is characteristic of an allowed transition. The data appear to be satisfied by the forbidden factor that is unique for a once-forbidden transition involving a change of two units of angular momentum and a change of parity. With this interpretation, the values of the end points of the three highest energy beta-groups are now changed to 2.291±0.005, 1.69±0.01, and 0.95±0.03 Mev.

A high resolution check on the closely spaced photo-lines definitely indicates gamma-rays with energies of 0.607, 0.653, and 0.730 Mev.

Since the 0.607-Mev gamma-ray corresponds exactly to the difference between the 2.29- and 1.69-Mev beta-groups, and the 0.730-Mev gamma-ray fits the difference between the 1.69- and 0.95-Mev groups, one is tempted to construct a level scheme on this basis. The high relative intensity of 0.607-Mev gamma-ray, how-

[11] Coincidence experiments are not capable of answering this question because of the extremely small relative number of electrons with energy higher than that of the 1.69-Mev group. See E. T. Jurney and A. C. G. Mitchell, Phys. Rev. **73**, 1152 (1948).

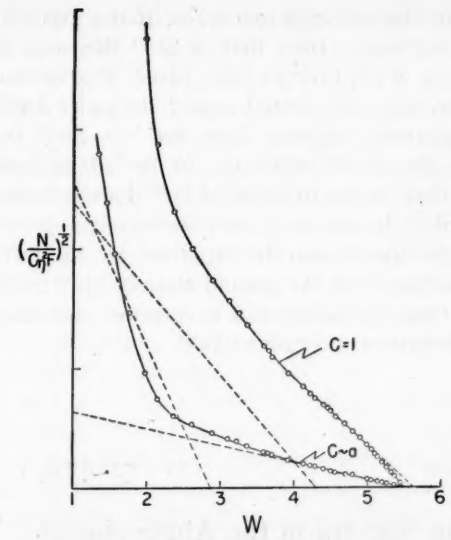

FIG. 4. Conventional and once-forbidden Fermi plots of the Sb^{124} data. The broken curves indicate the results of the first two subtractions. The extrapolation of the $C=1$ curve indicates how the incorrect maximum energy may be obtained in the absence of significant data near the end point.

ever, and the absence of any other gamma-ray of comparable intensity which could "feed" it, strongly suggests that the gamma-quanta of this energy must, for the most part, follow the 2.29-Mev beta-transition.[2] Unfortunately, the level scheme for the $Sb^{124}-Te^{124}$ disintegration remains somewhat ambiguous.

On the basis of the nuclear shell model[12] (extended to two odd nucleons), one might, at first glance, expect the ground state of Sb^{124} to arise from the combination of a $1g_{7/2}$ positron with a $1h_{11/2}$ neutron. Presumably, the resultant state should then have *odd* parity. Since the 2.29-Mev beta-transition is once forbidden, the product state in Te^{124} would then have *even* parity. Since the ground state of Te^{124} (which contains an even number of neutrons and protons) is expected to have *even* parity, the unobserved 2.9-Mev direct transition would be at least thrice forbidden. Under these conditions, the gamma-ray transition from the excited state in Te^{124} would involve no change of parity and could have a spin change as low as unity. This would be consistent with the classification of the radiation as magnetic dipole.

On the other hand, the amount of internal conversion is quite small. If one assumes that the 0.607-Mev gamma-transiton simply follows all beta-groups (neglecting the small amount associated with the 2.04-Mev gamma-ray) then the internal conversion coefficient (as determined by the ratio of the relative areas under the K-line and under the total beta-distribution) is 1.6×10^{-3}. This value is much too low for *magnetic* dipole radiation and is, in fact, in very good agreement with the theoretical value predicted for *electric* dipole radiation.[13]

If the 0.607-Mev gamma-ray is indeed *electric* dipole and does follow the 2.29-Mev beta-group, then the excited state in Te^{124} must have *odd* parity. Then, from the once-forbidden shape of the 2.29-Mev beta-group, one must conclude that the ground state of Sb^{124} has *even* parity and a spin of 3, contrary to the prediction based on the naive extension of the shell model to two odd nucleons.

It appears, however, that the beginning of the shell for the 51st proton is quite irregular.[14] The $2d_{5/2}$ and $1g_{7/2}$ states have approximately the same energy and either one might lie lower than the other and sometimes does. Furthermore, because of the preferential filling of the orbits by pairs, the $1h_{11/2}$ state, which has approximately the same energy as the $3S_{1/2}$, is suppressed, and one might therefore expect the 73rd neutron to be a $3S_{1/2}$. The combination of a $2d_{5/2}$ proton with a $3S_{1/2}$ neutron might be expected[15] to give a state with *even*

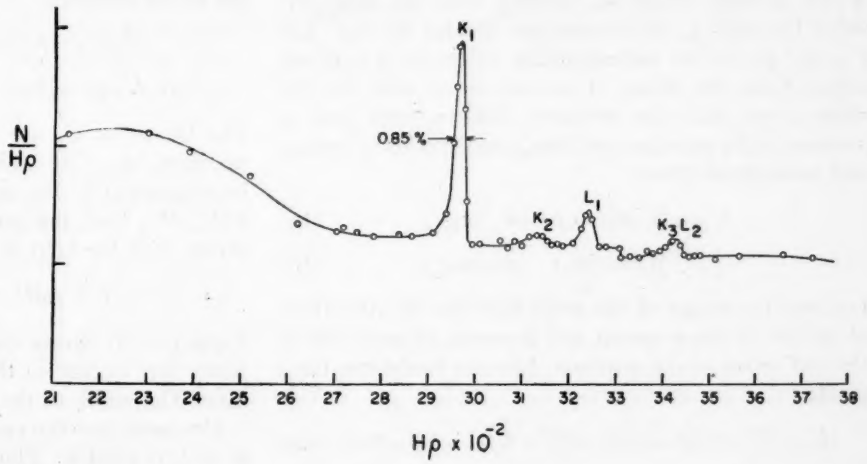

FIG. 5. Photo-electron distribution resulting from the 0.607, 0.653, and 0.730-Mev gamma-rays of Sb^{124}. A 5.6-mg/cm² Pb radiator was used.

[12] M. G. Mayer, Phys. Rev. **75**, 1969 (1949).
[13] M. E. Rose *et al.* (tables, privately distributed).
[14] M. G. Mayer, Phys. Rev. **78**, 16 (1950).
[15] L. W. Nordheim, Phys. Rev. **78**, 294 (1950).

parity with spin of 3. Such an *even* parity state with spin of 3 could undergo a once-forbidden transition to an excited state of Te^{124} having *odd* parity and spin 1. This is then consistent with an electric dipole transition to the *even*, spin zero, ground state of Te^{124}. The direct 2.9-Mev transition is not observed since it is then twice forbidden.†

The absence of positron emission or K-capture is interpreted in either of two ways. If the ground state of Sn^{124} lies higher than that of Sb^{124} then one should not expect K-capture to take place. Furthermore, if this is so, then one should expect the twice forbidden single negatron emission from Sn^{124} to Sb^{124} to out-compete the double beta-decay to Te^{124}. It is, however, possible that the ground state of Sn^{124} does lie lower than that of Sb^{124}. In this case, the absence of positron emission or K-capture may be explained by the fact that the transition from the ground state of Sb^{124} to that of Sn^{124} is twice forbidden and is therefore out-competed by the negatron emission to Te^{124}.

† *Note added in proof:* According to the empirical rules pointed out by Professor Nordheim, one would also obtain a state of even parity and spin 3 by combining a $g_{7/2}$ proton with the $S_{1/2}$ neutron. Since the measured spin of the nearby SB^{123} is 7/2, this is perhaps a better assignment.

PHYSICAL REVIEW VOLUME 79, NUMBER 5 SEPTEMBER 1, 1950

Relation between π- and μ-Meson Production Spectra in the Atmosphere*

GIULIO ASCOLI
Department of Physics and Laboratory of Nuclear Science and Engineering, Massachusetts Institute of Technology, Cambridge, Massachusetts

(Received May 25, 1950)

A method of obtaining the parent π-meson spectrum from the μ-meson spectrum is presented and the relation of the two spectra is discussed. It is concluded that the μ-meson spectrum must be rather smooth even if the parent spectrum is not.

I. ENERGY DISTRIBUTION OF μ-MESONS FROM THE DECAY IN FLIGHT OF π-MESONS

THE experimental information available suggests that all μ-mesons observed in cosmic rays arise from the decay of π-mesons. This note investigates the relationship between the production spectra of π- and μ-mesons.

Consider a π-meson (mass m_π) moving with velocity βc. Let U_π be its total energy divided by $m_\pi c^2$, p_π its momentum divided by $m_\pi c$. Let U_μ be the total energy of the μ-meson (mass m_μ) arising from its decay divided by $m_\mu c^2$, p_μ its momentum divided by $m_\mu c$. Let $U_{\mu 0}$ and $p_{\mu 0}$ be the corresponding values for a μ-meson arising from the decay of a π-meson at rest. On the assumption that the π-meson disintegrates into a μ-meson and a massless neutrino, conservation of energy and momentum gives:

$$U_{\mu 0}=\tfrac{1}{2}[(m_\pi/m_\mu)+(m_\mu/m_\pi)], \tag{1a}$$

$$p_{\mu 0}=\tfrac{1}{2}[(m_\pi/m_\mu)-(m_\mu/m_\pi)]. \tag{1b}$$

Let x be the cosine of the angle between the directions of motion of the π-meson and μ-meson as measured in the rest frame of the π-meson. Lorentz transformations yield:

$$U_\mu=(U_{\mu 0}+\beta p_{\mu 0}x)/(1-\beta^2)^{\frac{1}{2}}=U_{\mu 0}U_\pi+p_{\mu 0}p_\pi x, \tag{2a}$$

$$(p_\mu)_{||}=p_{\mu 0}U_\pi x+U_{\mu 0}p_\pi, \tag{2b}$$

where $(p_\mu)_{||}$ is the component of p_μ parallel to the motion of the π-meson. It is evident on physical grounds, and it follows from Eqs. (2), that $(p_\mu)_{||}>0$ (i.e., that the angle of emission of the μ-meson is less than 90°) provided that $U_\pi>U_{\mu 0}$. In what follows we shall always assume that $U_\pi>U_{\mu 0}$ and $U_\mu>U_{\mu 0}$. The limitation thus introduced is not serious; it excludes from consideration π-mesons of kinetic energy less than 5.5 Mev and μ-mesons of less than 4.17 Mev. Equations (2) then show that the energy and momentum of the μ-meson are in the intervals

$$U_{\mu 0}U_\pi-p_{\mu 0}p_\pi<U_\mu<U_{\mu 0}U_\pi+p_{\mu 0}p_\pi, \tag{3a}$$

$$U_{\mu 0}p_\pi-p_{\mu 0}U_\pi<p_\mu<U_{\mu 0}p_\pi+p_{\mu 0}U_\pi. \tag{3b}$$

The limits for U_μ are shown in Fig. 1 where we have taken $m_\pi/m_\mu=283/215$. All directions of emission must be equivalent in the rest frame. Hence the probability $F(U_\mu)dU_\mu$ that the μ-meson has energy U_μ in dU_μ is given, with the help of Eq. (2a), by:

$$F(U_\mu)dU_\mu=\tfrac{1}{2}dx=dU_\mu/2p_{\mu 0}p_\pi. \tag{4}$$

Equation (4) shows that $F(U_\mu)$ is independent of U_μ, hence any energy in the interval (3a) is equally probable. The width of the energy band is $2p_{\mu 0}p_\pi=0.56p_\pi$.

One sees that the energy spread of the decay mesons is not negligible. Thus, only if the parent π-meson spectrum is smooth, will the μ-meson production spectrum be closely similar to it. Irregularities in the parent spectrum are largely smoothed out in the decay process.

* Assisted by the joint program of the ONR and AEC.

II. THE μ-MESON PRODUCTION SPECTRUM EXPRESSED IN TERMS OF THE π-MESON PRODUCTION SPECTRUM

Let $P(U_\pi)$ be the differential spectrum of π-mesons at decay; i.e., let $P(U_\pi)dU_\pi$ represent the number of π-mesons of energy U_π in dU_π that undergo decay (per gram of air, per minute, and per unit solid angle). In the atmosphere, nuclear interactions and collision losses of mesons are negligible compared with decay except at rather high energies.[1] The distance traveled by a π-meson between birth and death may also be disregarded, so that P can also be interpreted as the local production spectrum of π-mesons.

Let $M(U_\mu)$ be the differential production spectrum of μ-mesons; i.e., let $M(U_\mu)dU_\mu$ be the number of μ-mesons produced in one gram of air per minute and per unit solid angle with energy U_μ in dU_μ. If the change in direction accompanying decay is neglected, Eq. (4) gives the following expression for $M(U_\mu)$

$$M(U_\mu)=\int_{U_{\pi l}}^{U_{\pi h}} F(U_\mu)P(U_\pi)dU_\pi$$

$$=\frac{1}{2p_{\mu 0}}\int_{U_{\pi l}}^{U_{\pi h}} P(U_\pi)\frac{dU_\pi}{p_\pi}. \quad (5)$$

In Eq. (5), $U_{\pi l}$ and $U_{\pi h}$ are the lower and upper energy limits of π-mesons that can give rise to a μ-meson of energy U_μ (see Fig. 1); $P_{\pi l}$ and $P_{\pi h}$ are the corresponding momenta. From Eqs. (2) one obtains:

$$U_{\pi l}=U_{\mu 0}U_\mu-p_{\mu 0}p_\mu, \quad U_{\pi h}=U_{\mu 0}U_\mu+p_{\mu 0}p_\mu, \quad (6a)$$

$$p_{\pi l}=U_{\mu 0}p_\mu-p_{\mu 0}U_\mu, \quad p_{\pi h}=p_{\mu 0}U_\mu+U_{\mu 0}p_\mu. \quad (6b)$$

Because of the finite angle between the directions of motion of the parent π-meson and of the μ-meson arising from its decay, the above results apply, strictly speaking, to the spectra P and M integrated over all directions rather than to the directional spectra. However, the angles of emission are small already at moderate energies[2] so that Eq. (5) applies approximately to the directional spectra.

III. THE π-MESON PRODUCTION SPECTRUM EXPRESSED IN TERMS OF THE μ-MESON PRODUCTION SPECTRUM

Equation (5) can be inverted to give the parent spectrum P in terms of the μ-meson production spectrum M. This is of some interest because more information is available on the latter than on the former at the present time.

Differentiation of Eq. (5) gives:

$$\frac{dM}{dU_\mu}=\frac{1}{2p_{\mu 0}}\left\{\frac{dU_{\pi h}}{dU_\mu}\frac{P(U_{\pi h})}{p_{\pi h}}-\frac{dU_{\pi l}}{dU_\mu}\frac{P(U_{\pi l})}{p_{\pi l}}\right\}.$$

With the help of Eqs. (6) one obtains:

$$dM/dU_\mu=[P(U_{\pi h})-P(U_{\pi l})]/2p_{\mu 0}p_\mu. \quad (7)$$

For convenience, define:

$$R(U_\mu)\equiv-2p_{\mu 0}p_\mu[dM(U_\mu)/dU_\mu]. \quad (8)$$

Equation (7) then reads:

$$R(U_\mu)=P(U_{\pi l})-P(U_{\pi h}). \quad (9)$$

Define a sequence:

$$U_{\pi 1}, U_{\mu 2}, U_{\pi 3}, U_{\mu 4}, \cdots \quad (10)$$

as follows: $U_{\mu 2}$ is the highest energy of a μ-meson born from a π-meson of energy $U_{\pi 1}$, $U_{\pi 3}$ is the highest energy of a π-meson capable of decaying into a μ-meson of energy $U_{\mu 2}$, and so on. Such a sequence is illustrated in Fig. 1.

For an arbitrarily chosen value of $U_{\pi 1}$, the sequence can be constructed with the help of Eqs. (3) and (6).

From Eq. (9) one obtains

$$P(U_{\pi 1})=R(U_{\mu 2})+P(U_{\pi 3}),$$
$$P(U_{\pi 3})=R(U_{\mu 4})+P(U_{\pi 5}), \quad \text{etc.}$$

Since $P(U_\pi)$ decreases rapidly with increasing $U_{\mu 1}$, the above equations give $P(U_{\mu 1})$ in the form of an infinite series

$$P(U_{\pi 1})=R(U_{\mu 2})+R(U_{\mu 4})\cdots. \quad (11)$$

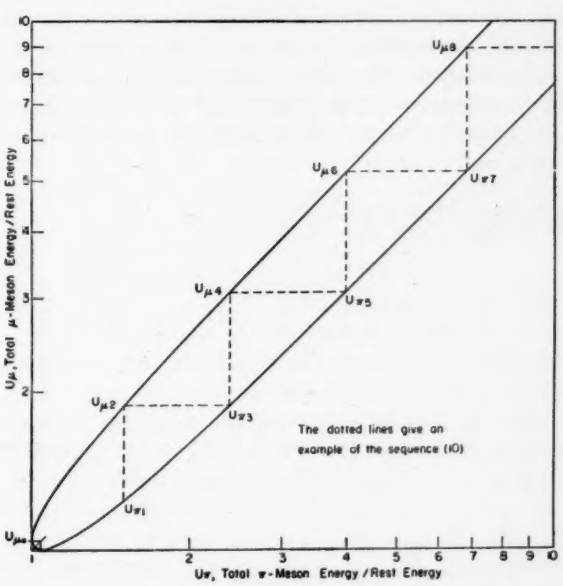

FIG. 1. Limits of μ-meson energy *vs.* π-meson energy.

[1] At sea level, assuming a mean life of 1.8×10^{-8} sec. and a cross section for nuclear interactions equal to the geometric cross section of the air nuclei, the probability of nuclear interactions equals the probability of decay at about 1.5×10^{10} ev.

[2] One can easily see that the maximum angle of emission, ϑ, is given approximately by $\vartheta\approx0.3/p_\pi$.

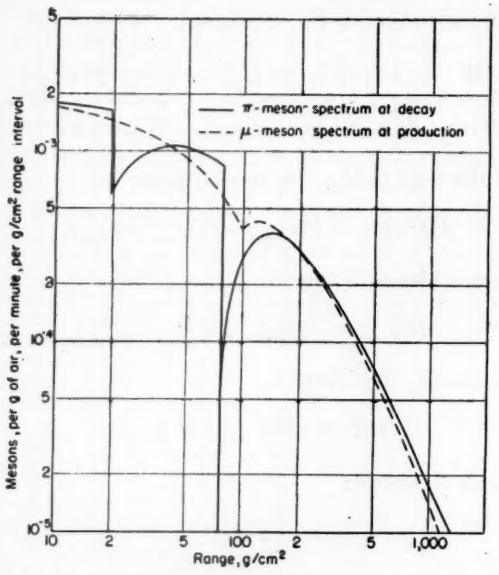
π-meson spectrum at decay
μ-meson spectrum at production
Mesons, per g of air, per minute, per g/cm² range interval
Range, g/cm²

FIG. 2. Differential range spectrum of π-mesons (normalized to the top of the atmosphere), from Sands' spectrum *XI*.

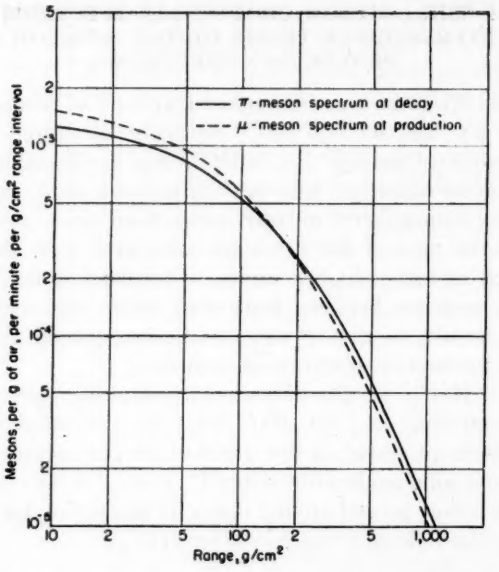
π-meson spectrum at decay
μ-meson spectrum at production
Mesons, per g of air, per minute, per g/cm² range interval
Range, g/cm²

FIG. 3. Differential range spectrum of π-mesons (normalized to the top of the atmosphere), from Sands' spectrum *X*.

IV. COMPUTATION OF THE π-MESON SPECTRUM IN THE ATMOSPHERE

The method outlined in the previous section has been applied to the μ-meson spectrum at production given by Sands.[3] In the calculation the masses of the π- and μ-mesons were taken as 283 and 215 electron masses. The range-energy relations given by Smith[4] were used except at high energies, where they had to be extended by integration. Sands' "best" spectrum (G_{XI}) and his smooth spectrum (G_X) have been thus transformed. The results are shown in Figs. 2 and 3, together with the μ-meson spectra on which they are based. They are presented as differential range spectra, at the top of the atmosphere, computed under the assumption of a mean production depth of 125 g/cm² and of an exponential dependence of the production rate on atmospheric depth. The parent spectrum of G_{XI} exhibits a dip to a negative value at about 5.5 g/cm² (not shown in the figure), a second one at 20 g/cm² and a third one at 76 g/cm².

[3] M. Sands, Phys. Rev. **77**, 180 (1950).
[4] J. H. Smith, Phys. Rev. **71**, 32 (1947).

V. DISCUSSION

The results show that any irregularities in the parent π-meson spectrum would be largely erased, and therefore one can say a priori that if all μ-mesons originate from decay of π-mesons the production spectrum of μ-mesons in the atmosphere must be fairly smooth. On the other hand, any irregularities in the latter must be taken as an indication of much more drastic irregularities in the parent spectrum. In order to evaluate any fine detail of the π-meson spectrum, however, a very accurate knowledge of the μ-meson spectrum is required. The results on Sands' spectrum G_{XI} illustrate this situation effectively. The suggested shape is seen to be physically impossible, since it would require the parent spectrum to be negative for some values of the energy. While some irregularities such as are indicated by Sands' spectrum cannot be ruled out entirely, they cannot have the exact form given and are probably less drastic.

This work was carried out at the Inter-University High Altitude Laboratory. The author is grateful to Professor Bruno Rossi for his interest in this work.

Radioactive Isotopes of the Rare Earths. III. Terbium and Holmium Isotopes

GEOFFREY WILKINSON* AND HARRY G. HICKS**
Radiation Laboratory and Department of Chemistry, University of California, Berkeley, California
(Received May 16, 1950)

A study has been made of neutron deficient radioactive isotopes of terbium and holmium produced respectively by α-particle bombardments of europium and terbium, and respectively by proton bombardments of gadolinium and dysprosium, using the 60-inch Crocker Laboratory cyclotron. Five new isotopes of each element have been characterized.

I. INTRODUCTION

THE experimental techniques of bombardments, chemical separations, and radioactivity measurements used in the study of radioactive rare earth isotopes have been previously described.[1] In the study of terbium and holmium activities, europium and terbium oxides were bombarded with α-particles of energy 38, 31, and 19 Mev, while gadolinium and dysprosium oxides were bombarded with 10-Mev protons. With the exception of two short-lived holmium activities, the chemical identity of the isotopes was proved by chemical separation using ion exchange resin columns. In europium bombardments, the target was dissolved and the bulk of the europium first removed by reduction of the boiling 6N hydrochloric acid solution with zinc amalgam and precipitation of europium III sulfate by addition of dilute sulfuric acid. A small amount of lanthanum was added to the solution before reduction to act as a holdback carrier for terbium activities. Rare earth activity in the supernatent solution was collected by coprecipitation with ferric hydroxide. The hydroxide was dissolved in dilute hydrochloric acid, the ferric chloride removed by ether extraction and, after adjustment of the acidity to 1N, the rare earths adsorbed on ion exchange resin for subsequent column separation.

In Table I the production and radiation properties of the terbium and holmium activities are summarized. All of the activities, with the exception of the 34-min. Ho^{164} activity decay with the emission of electromagnetic radiations of half-thickness 7 to 8.5 mg/cm^2 aluminum (6.3 to 6.8 kev), and 60 to 70 mg/cm^2 lead (46 to 48 kev), which correspond to the average energies of L and K x-radiation of gadolinium and dysprosium, respectively. The energies of the electromagnetic radiations were obtained from aluminum and lead absorption measurements; electron energies were obtained from both aluminum absorption measurements and from measurements on a simple beta-ray spectrometer. The latter allowed the decay of positive and negative electrons to be followed separately. In the resolution of aluminum absorption curves, the contribution of soft electromagnetic radiation was obtained by removal of electrons by beryllium absorbers; a correction for absorption of the L x-rays in beryllium was made before resolving the curves. The approximate ratios of the various components of the complex radiations found in the orbital electron capture isotopes studied were obtained from absorption and magnetic spectrometer data. For the standard argon-alcohol counter tubes used, counting efficiencies of 6.5 and 7.5 percent were taken for gadolinium and dysprosium L x-radiation, 0.5 percent for K x-radiation and one percent per Mev for harder gamma-radiation; fluorescence yields of 0.5 and 0.8 were assumed for L and K x-radiation, respectively. Corrections for absorption of soft radiations in counter windows, etc. were made, and backscattering of electrons was minimized by mounting carrier-free, column-separated samples on very thin backing.

II. TERBIUM ISOTOPES

In the bombardment of europium with α-particles, activities of half-lives 5.1 days, 17.2 hr., 190 days, and 5.0 hr. were observed; from the yields in bombardments using α-particles of energies 38, 31, and 19 Mev, allocation was made to masses 153, 154, 155, and 156, respectively. No evidence has been obtained for Tb^{152} which would be formed by α, $3n$ reaction on Eu^{151}, and an upper limit of about 5 min. can be set for the half-life. The 86-day Gd^{153} activity has been observed in the column separated gadolinium fractions from Eu+α bombardments, and the formation of this isotope from the 5.1-day terbium allocated to mass 153 has been confirmed. In the bombardment of gadolinium with 10-Mev protons, the 17.2-hr. activity was observed in very low yield agreeing with its allocation to Tb^{154}; the 5.0-hr. positron emitting activity Tb^{156} and the well-known beta-particle emitting 3.9-hr. and 73.5-day Tb^{160} activities were found in high yields, as would be expected from the abundances of the gadolinium isotopes. A new activity of half-life 4.7 days was found in this bombardment; since the present work was completed, Butement[2] reported a 5.9-day activity which appears to have radiation characteristics agreeing with those of the 4.7-day activity. Since the 4.7-day isotope was found neither in α-particle bombardments of europium nor in fast neutron bombardments of terbium, allocation

* Present address: Chemistry Department, Massachussetts Institute of Technology, Cambridge, Mass.

** Present address: Chemical Research Section, General Electric Company, Hanford Engineer Works, Richland, Washington.

[1] G. Wilkinson and H. G. Hicks, Phys. Rev. **75**, 1370 (1949).

[2] D. S. Butement, Phys. Rev. **75**, 1276 (1949).

TABLE I. Production and characteristics of terbium and holmium isotopes.

Isotope	Type of radiation	Half-life	Energy of radiation in Mev: Particles	γ-rays	Produced by
Tb^{153}	K, ϵ^-, γ	5.1±0.1 days	0.15, ~0.3	0.23, 1.2	Eu−α−2n
Tb^{154}	$K, \epsilon^-, \gamma, \beta^+(\sim 0.5\%)$	17.2±0.2 hr.	0.13, ~0.8(ϵ^-), 2.6(β^+)	1.3	Gd−p−n Eu−α, n, 3n
Tb^{155}	K, ϵ^-, γ	190 ±5 days	0.1	1.4	Eu−α−2n
Tb^{156}	$K, \beta^+(<25\%)$	5.0±0.1 hr.	~1.3		Eu−α−n Gd−p−n
Tb^{157}	K, ϵ^-, γ	4.7±0.1 days	0.09, 0.2	1.4	Gd−p−n
Ho^{160}	$K, \epsilon^-, \gamma, \beta^+(0.5\%)$	22.5±0.5 min.	0.17(ϵ^-), ~1.3(β^+)	~1.2	Tb−α−3n
Ho^{161}	K, ϵ^-, γ	4.6±0.1 hr.	0.1(ϵ^-)	1.1	Tb−α−2n Dy−p−n Dy−d−n
Ho^{162}	$K, \epsilon^-, \gamma, \beta^-(\sim 15\%)$	65.0±0.5 days	~0.1(ϵ^-), 0.8(β^-)	~1	Tb−α−n Dy−p−n Dy−d−2n
Ho^{163}	K, ϵ^-, γ	5.2±0.05 days	0.4	0.4 to 0.5 1.4	Dy−p−n Dy−d−n, 2n
Ho^{164}	β^-	34.0±0.5 min.	0.95		Dy−p−n

to mass 157 seems reasonable. The existence of further long-lived isotopes of terbium of masses 156, 7, or 8 is possible but the presence of long-lived Tb^{155} and Tb^{160} activities in proton-bombarded gadolinium makes recognition of a further activity by simple measurment a difficult task. No difference in the decays of the long-lived activities from the various Eu+α bombardments has been noted yet and all are decaying with the 190-day activity allocated to mass 155 on the basis of reaction yields.

5.1±0.1-Day Tb^{153}

The decay of this activity which was found in high yields in 38- and 31-Mev α-particle bombardments of europium was followed through ten half-lives. The radiations, which differ considerably from those of the 4.7-day activity described below consist of electrons ranges 32 mg/cm² (0.15 Mev), and ~90 mg/cm² (~0.3 Mev), and electromagnetic radiations of half-thicknesses 7 mg/cm² (6.3 kev) aluminum, 60 mg/cm² (46 kev), 570 mg/cm² (0.23 Mev), and 11.0 g/cm² lead (1.2 Mev). The approximate ratios of various radiations are 0.17 Mev ϵ^-:~0.3 Mev ϵ^-; L x-ray:K x-ray:0.23-Mev γ-ray:1.2-Mev γ-ray; 0.02:0.001:0.3:1:0.1:0.02. The aluminum and lead absorption curves are shown in Fig. 1.

17.2±0.2-Hr. Tb^{154}

In all bombardments of europium with α-particles, and in low yields in proton bombardments of gadolinium a 17.2-hr. positron emitting activity was observed. The decay of negative and positive electrons and γ-radiation was separated followed through ten half-lives. Using a simple beta-ray spectrometer, the positron of maximum energy 2.6 Mev as well as two groups of negative electrons corresponding to those measured in aluminum absorptions were studied, and the abundances measured by integrating the distribution curves. The positrons are in such low abundance that no annihilation radiation would be observed in absorption measurements. From the various measurements the following ratios were obtained: 0.13-Mev ϵ^-:~0.8-Mev ϵ^-:2.6-Mev β^+:L x-ray:K x-ray:1.3-Mev γ-ray=0.1:0.02:0.004:0.3:1:0.03. It seems reasonable to conclude that the isotope decays at least 98 percent by orbital electron capture to metastable or excited states of the daughter nucleus.

190±5-Day Tb^{155}

This activity was observed in all Eu+α bombardments after decay of the shorter-lived activities. The decay has been followed through three half-lives. The approximate ratios of the radiations were: 0.1-Mev ϵ^-:L x-ray:K x-ray:1.4-Mev γ-ray=0.4:0.3:1:0.3; in the calculation of yields it was assumed that ~0.5 of the K x-ray quanta represent one disintegration by orbital electron capture.

5.0±0.1-Hr. Tb^{156}

In bombardments of europium with 19-Mev α-particles, an activity of half-life 5.0±0.1 hr. measured through nine half-lives was observed in high yield. The aluminum absorption showed only a hard electron range 600 mg/cm² (~1.3 Mev), soft electromagnetic radiation 7 mg/cm² half-thickness (6.3 kev), and hard quantum radiation background. On a simple beta-ray

spectrograph, no negative electrons were observed, but only positrons of maximum energy ~1.4 Mev, which decayed with the 5.0-hr. half-life. Insufficient activity was obtained for measurement of a lead absorption curve of gamma-rays. Assuming 0.5 percent average counting efficiency for gamma-radiation, the ratios of the radiations obtained from aluminum absorptions gives: 1.3-Mev β^+: L x-ray: K x-ray and γ-ray radiation $=\sim 0.2:\sim 0.1:1$.

The isotope thus appears to decay mainly by orbital electron capture with less than 25 percent positron branching.

4.7±0.1-Day Tb^{157}

In the decay of the chemically separated terbium fraction from 10-Mev proton bombardments of gadolinium, an activity of half-life 4.7±0.1 days measured through seven half-lives has been observed. The radiation characteristics obtained by resolution of aluminum and lead absorption curves (Fig. 2) are quite different from those of the 5.1-day activity described above. The latter has been allocated to Tb^{153} on the basis of yields in the α-particle bombardment of europium, and hence would not be present in the terbium fraction from proton-bombarded gadolinium. The aluminum beryllium and lead absorption data show electrons total range ~11 mg/cm² (~0.09 Mev) and 40 mg/cm² (0.22 Mev), electromagnetic radiation half-thicknesses 7.5 mg/cm² aluminum (6.3 kev), ~60 mg/cm² lead (~46 kev), and ~12.7 g/cm² lead (1.4 Mev); the 46-kev ray was in very low abundance and may be a mixture of K x-radiation and unconverted gamma-radiation. The corrected ratios of the various radiations obtained were 0.09-Mev e^-:0.2-Mev e^-:L x-ray:K x-ray:1.4-Mev γ-ray=0.2:0.1:0.4:1:0.3.

A search for α-particle emission in radioactive isotopes of terbium from both Eu+α and Gd+d bombardments has been made using very active, ion exchange resin column separated samples. No α-particle emission was observed, and approximate upper limits for decay by α-particle branching can be set for the isotopes assuming that the measured K x-radiation represents decay by orbital electron capture; the upper limit for α-branching are: 5.1-day Tb^{153}, 5×10^{-8}; 17.2-hr. Tb^{154}, 10^{-9}; 190-day Tb^{155}, 2×10^{-7}; 5.0-hr. Tb^{156}, 5×10^{-6}; 4.7-day Tb^{157}, 2×10^{-8}; 73.5-day Tb^{160}, 10^{-7}.

III. HOLMIUM ISOTOPES

In the bombardment of terbium with α-particles of various energies, radioactive isotopes of half-lives 22.5 min., 4.6 hr., and 65 days were observed. Short bombardments of dysprosium with 10-Mev protons allowed characterization of a 34-min. beta-emitting isotope, together with the 4.6-hr. and longer-lived activities; in long bombardments of dysprosium with 10-Mev protons and 19-Mev deuterons, activities of 4.6-hr. and 65-day half-life, identical with those from Tb+α-bombard-

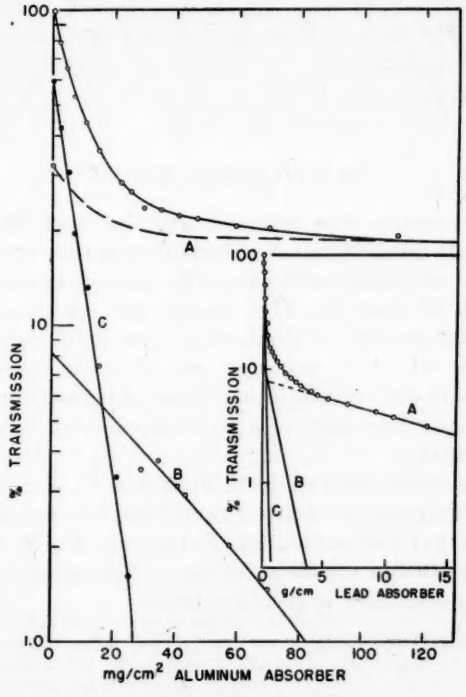

FIG. 1. Aluminum and lead absorptions of 5.1-day Tb^{153} activity from Eu+α-bombardment. Aluminum absorption A, B, and C are, respectively, the electromagnetic radiation contribution, ~0.3- and 0.15-Mev electrons. Lead absorption A, B, and C are, respectively, 1.2 Mev, 0.22-Mev gamma-rays, and K x-rays.

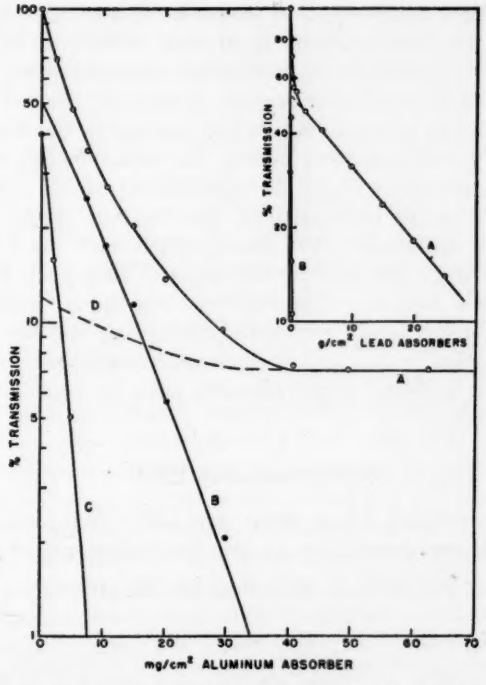

FIG. 2. Aluminum and lead absorptions of 4.7-day Tb activity from Gd+p bombardment. Aluminum absorption, K x-ray and γ-ray background (A), 0.2-Mev electron (B), 0.09-Mev electron (C), L x-rays (D). Lead absorption, 1.4-Mev γ-ray (A), K x-rays (B).

ments, were found together with an activity of 5.2-day half-life.

The allocation of the 22.5-min., 4.6-hr., and 65-day holmium activities to masses 160, 161, and 162, respectively, was made on the basis of yields in bombardments of terbium with 38-, 30-, and 19-Mev α-particles; the yields follow a pattern similar to that found for the production of thulium activities in α-particle bombardments of holmium.[1] The measured K x-radiation was taken as representing decay by orbital electron capture for the comparison of yields. The yields of the active isotopes formed in 10-Mev proton bombardments of dysprosium are approximately equal as would be expected from the similarity in abundance of the dysprosium isotopes of masses 161 to 164 inclusive. The 5.2-day activity is allocated to mass 163 since it was not observed in α-particle bombardments of terbium, or in fast neutron bombardments of holmium, but was formed in yields approximately the same as the other isotopes in proton bombardments of dysprosium.

34.0±0.5-Min. Ho^{164}

An activity of 47-min. half-life produced by fast neutron bombardment of holmium has been reported in an early paper.[2]

The 34-min. isotope here described was produced by short bombardments of pure dysprosium oxide with 10-Mev protons. Identification of the activity with holmium has not been proved by chemical separation but no activities due to known dysprosium isotopes have been observed, and longer-lived activities from the same bombardment have been shown to follow holmium chemistry. A half-life of 34.0±0.5 min. was obtained through eight periods, after subtraction of the longer-lived holmium activities, principally the 4.6-hr. activity, from the decay curves. The resolved aluminum absorption curve of the 34-min. activity shows this to have a simple beta-particle. The Feather range, 370 mg/cm² aluminum (0.95 Mev), agrees with the maximum energy obtained for the negative beta-particle on a simple beta-ray spectrometer. An upper limit of 0.05 γ-ray quanta per beta-particle can be set; no γ-radiation or conversion electrons attributable to the 34-min. activity were observed even in very active samples.

5.20±0.05-Day Ho^{163}

This activity whose decay was followed through six periods was found only in long bombardments of dysprosium with deuterons or protons. The ratio of the various radiations obtained from absorption measurements and corrected for counting efficiency, absorption in counter window, etc. are approximately, 0.4-Mev e^-; L x-ray,:K x-ray:~0.5-Mev γ-ray:1.4-Mev γ-ray, 0.04:0.6:1:~0.1:~0.25. The isotope thus appears to decay predominantly by orbital electron capture; the 0.04-Mev electron probably results from conversion of the weak 0.5-Mev γ-ray.

65±0.5-Day Ho^{162}

This activity, the decay of which has been followed for eight periods, is produced both in Tb+α and Dy+p bombardments and is identical in both cases. The Feather range of 300 mg/cm² (0.8 Mev) for the hard negative electron corresponds well with the maximum energy of 0.8 Mev obtained from the spectrometer. The ratios of the radiations are 0.1-Mev e^-:0.8-Mev β^-:L x-ray:K x-ray:1-Mev γ-ray=~0.1:~0.15:~1:1:<0.1. The isotope thus appears to decay predominantly by orbital electron capture with ~15 percent branching decay by negative beta-particle emission. The shape of the aluminum absorption curve of the 0.8-Mev particle and also its distribution on the magnetic spectrometer is that of a negative beta-particle.

4.6±0.1-Hr. Ho^{161}

This activity was observed with identical radiation characteristics in both Tb+α and Dy+p bombardments. The decay of both electron and electromagnetic was followed through seven half-lives. The approximate ratios of the various radiations obtained are: ~0.1-Mev e^-:L x-ray:K x-ray:1.1-Mev γ-ray≈~0.1:~1:1:~1.

22.5±0.5-Min. Ho^{160}

This activity was observed only in short 38-Mev α-particle bombardments of terbium together with the 4.6-hr. and 65-day activities. The decay was followed through six periods. The approximate ratios of the radiation are 0.17 e^-:β^+:L x-ray:γ-ray≈0.1:~0.005:~0.4:1:~1. Assuming that one K x-ray quantum represents one disintegration by orbital electron capture, branching decay by positron emission is about 0.5 percent.

The authors wish to thank Professors G. T. Seaborg and I. Perlman for their continued interest and advice and Dr. J. G. Hamilton, Mr. T. Putnam, Mr. B. Rossi, and the crew of the 60-inch Crocker Laboratory cyclotron for assistance in bombardments.

[3] M. L. Pool and L. L. Quill, Phys. Rev. **53**, 437 (1938).

The Radiofrequency Spectrum of $K^{39}F$ by the Electric Resonance Method*

LUDWIG GRABNER** AND VERNON HUGHES
Columbia University, New York, New York

(Received February 24, 1950)

The molecular beam electric resonance method has been used to investigate the rotational Stark spectrum of $K^{39}F$. In this method linear polar diatomic molecules in one, or at most two, rotational states and definite states of space quantization are selected by means of inhomogeneous electric fields. The molecular transitions are not of the ΔJ type (transition between different rotational states). Rather, the transitions are between states with the same value of J but different values of m_J, the electric quantum number characterizing the state of space quantization. Lines are observed as a change in intensity of the refocused beam when the frequency of an oscillating field, which is perpendicular to an homogeneous field, times Planck's constant is equal to the energy difference between different states of space quantization. The frequency of the rotational Stark line is determined by the value of the homogeneous static field. The Stark line was observed at low and high fields for $J=1$ and low fields for $J=2$. It is found to be split. The fine structure is due to an interaction of the nuclear electric quadrupole moment of the K^{39} nucleus with the rest of the charges of the molecule as well as a variation of $\mu^2 A$ with the vibrational state of the molecule. Here μ is the permanent electric dipole moment, and A is the moment of inertia. In addition, the quadrupole interaction constant is found to vary with the vibrational state. It is measured when the molecule is in the rotational state $J=1$ and the vibrational states $v=0$, 1, 2, 3 and 4; and $J=2$, $v=0$, 1 and 2.

The frequency dependence of the Stark line at strong fields permits the determination of μ and A; they were determined only for the zeroth vibrational state.

The results are: For $J=1$, $v=0$, $eqQ/h=(-7.938\pm0.040)$ Mc/sec. The absolute value of eqQ/h decreases about 1.3 percent when the vibrational quantum number increases by unity. Within experimental error the quadrupole interaction and its variation with vibrational state for $J=2$ is the same as for $J=1$. A complete tabulation of the results will be found in Table II. For the zeroth vibrational state $\mu=(7.33\pm0.24)$ Debye, $A=(138.4\pm6.9)\times10^{-40}$ g-cm^2. From A we find for the internuclear distance for the zeroth vibrational state $r=(2.55\pm0.06)$ angströms. From the variation in intensity with vibrational state for a single transition the vibrational constant $\omega_0=(390\pm39)$ cm^{-1}.

I. INTRODUCTION

THE electric resonance method[1-3] of molecular beams has one important feature which distinguishes it from the magnetic resonance method[4] in the investigation of the hyperfine structures of linear polar diatomic molecules. It is able to select for investigation a single rotational state of such a molecule. In the magnetic resonance method all of the rotational states are refocused, because a magnetic field is used. If the interactions causing the spectrum depend on the rotational state, the spectrum will be a superposition of those of all of the rotational states, and therefore will be of statistical character. The spectra observed in the electric resonance method are "pure," in the sense that they are caused by a single rotational state. Thus fine details are recorded in the simplest way and are not obscured by the presence of many rotational states. Therefore the interpretation is easier and the data more accurate.

The important disadvantage of the electric relative to the magnetic resonance method is that it is confined to molecular spectroscopy and even in that field can handle only polar molecules. Moreover, the method has thus far been worked out only for diatomic molecules. The magnetic resonance method is inherently free from these limitations. A nuclear g-value can, of course, only be measured by the magnetic resonance method; an electric dipole moment or a moment of inertia only by the electric resonance method. Quadrupole and $\mathbf{I}\cdot\mathbf{J}$ interactions[5,6] can be determined by both methods[2,7,8] if the molecule is a polar diatomic molecule.

II. EXPERIMENTAL

The apparatus used in this experiment is the one built by Hughes,[1] with the C-field modified by Trischka,[2] and has been described in detail by them. It is shown schematically in Fig. 1 of reference 1.

A refocused beam of molecules of a fixed rotational state J can be obtained in two distinct ways. This will be illustrated for the rotational state $J=1$. Figure 1 shows μ_e/μ as a function of $\lambda=\mu E/(\hbar^2/2A)$, a dimensionless parameter characterizing the value of the field, for various J, m_J states of a linear polar diatomic molecule. Here μ is the permanent, μ_e the effective electric dipole moment, A is the moment of inertia, E is the value of the electric field, m_J is the electric quantum number characterizing the state of space quantization. If the A and B fields are set at a λ value of $\lambda_A^{1,0}$ and $\lambda_B^{1,0}$, respectively (see Fig. 1), then, for the apparatus used in this experiment, a molecule in the 1, 0 state will suffer equal and opposite deflections in the A and B fields, assuming the directions of field and gradient of the field to be that shown in Fig. 1 of reference 1, and can be refocused on a suitably aligned detector. The values $\lambda_A^{1,0}$ and $\lambda_B^{1,0}$ shown in Fig. 1 were chosen be-

* This research has been supported in part by the ONR.

** Submitted by Ludwig Grabner in partial fulfillment of the requirements for the degree of Doctor of Philosophy in Physics at Columbia University.

[1] H. K. Hughes, Phys. Rev. **72**, 614 (1947).
[2] J. W. Trischka, Phys. Rev. **74**, 718 (1948).
[3] J. W. Trischka, Phys. Rev. **76**, 1365 (1949).
[4] Rabi, Millman, Kusch, and Zacharias, Phys. Rev. **55**, 526 (1939).
[5] H. M. Foley, Phys. Rev. **72**, 504 (1947).
[6] G. C. Wick, Phys. Rev. **73**, 51 (1948).
[7] W. A. Nierenberg and N. F. Ramsey, Phys. Rev. **72**, 1075 (1947).
[8] V. Hughes and L. Grabner, Phys. Rev. **79**, 314 (1950).

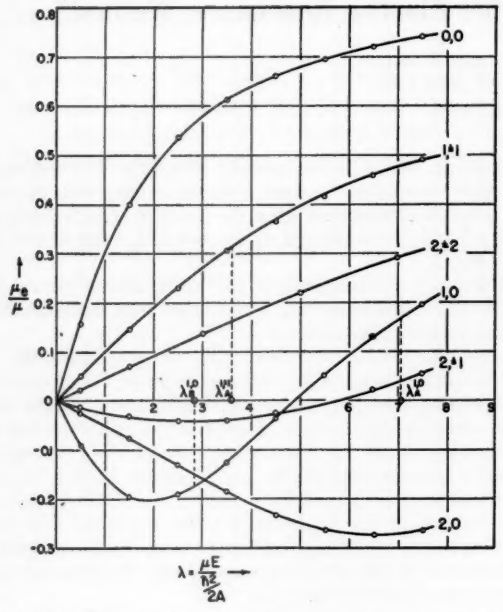

FIG. 1. Effective electric moments of a rotating polar diatomic molecule in an electric field.

cause they give a maximum deflection at the wire stop. A beam refocused in this way will be designated as a $(1, 0)_A - (1, 0)_B$ beam because the molecules that are refocused are in the state 1, 0 in both the A and B fields. There is, however, another way of refocusing molecules in the rotational state $J=1$. Since the magnitude and direction of the electric field change in the interfield regions, it is possible for a molecule to change its state of space quantization because of its passage through such a region. These non-adiabatic transitions can be used in the following way to refocus molecules in the rotational state $J=1$. If the B-field is left at its previous value $\lambda_B^{1,0}$ while the A-field is changed to $\lambda_A^{1,\pm1}$, shown in Fig. 1, a molecule in the 1, ±1 state will suffer the same deflection as a molecule in the 1, 0 state did when the A-field was $\lambda_A^{1,0}$. Non-adiabatic transitions from the 1, ±1 state to the 1, 0 state in the regions between the A and C fields and between the C and B fields will cause 1, 0 molecules of the proper deflection to enter the B-field. These are then refocused on the detector. A refocused beam obtained in this way will be designated as a $(1, \pm1)_A - (1, 0)_B$ beam because the molecules that are refocused are in the 1, ±1 state in the A-field and in the 1, 0 state in the B-field. Presumably most of the non-adiabatic transitions occur between the A and C fields since the collimator slit is placed there and causes larger variations of the field than there are between the C and B fields. Which type of refocused beam is chosen for experimentation is decided by which gives the greater intensity of transitions. Theoretically both are valid and give the same results.

A total beam of 500,000 cm measured on a galvanometer scale was used and stopped down by means of the wire stop to 20 cm. The refocusing conditions were such that the intensity of the refocused beam was 50 cm. For the moderately strong and strong field experiments the $(1, 0)_A - (1, 0)_B$ refocused beam was used. For the weak field experiments the $(1, \pm1)_A - (1, 0)_B$ refocused beam was used. The isotopes K^{39} and K^{41} are present in the refocused beam with percentages of 93.44 and

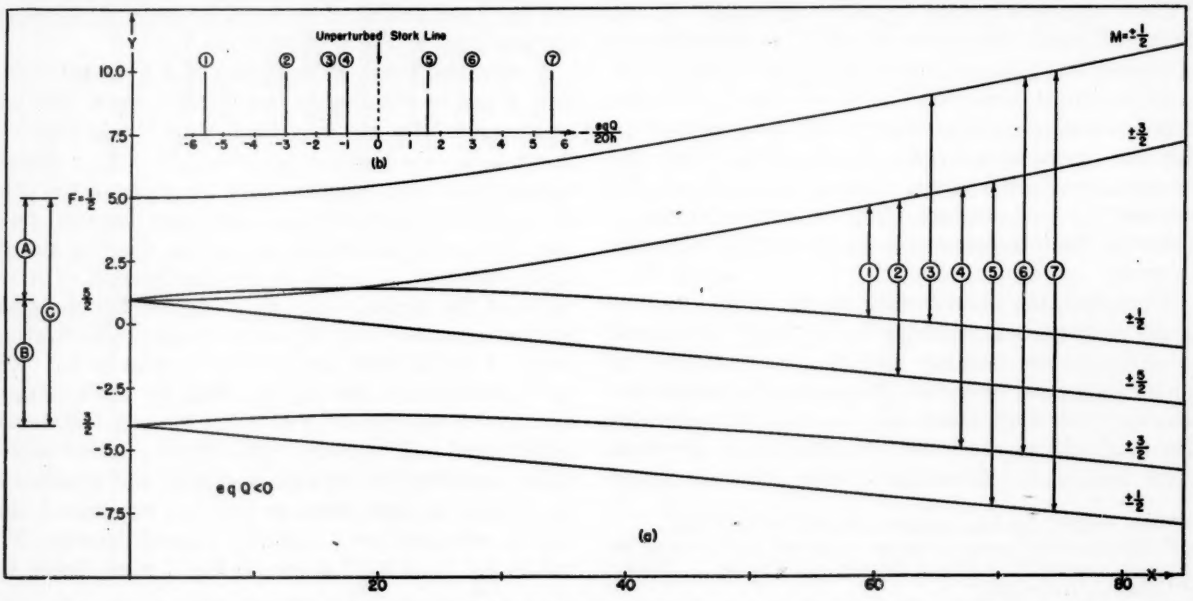

FIG. 2. (a) Plot of energy levels W *versus* the square of the electric field, E^2, for $J=1$, $I=\frac{3}{2}$ and $eqQ<0$; coordinates are in dimensionless units.

$$Y = -20\frac{W}{eqQ} \qquad X = -20\frac{(\mu E)^2}{eqQ(h^2/2A)}$$

(b) Strong field spectrum for $J=1$, $I=\frac{3}{2}$, $eqQ<0$.

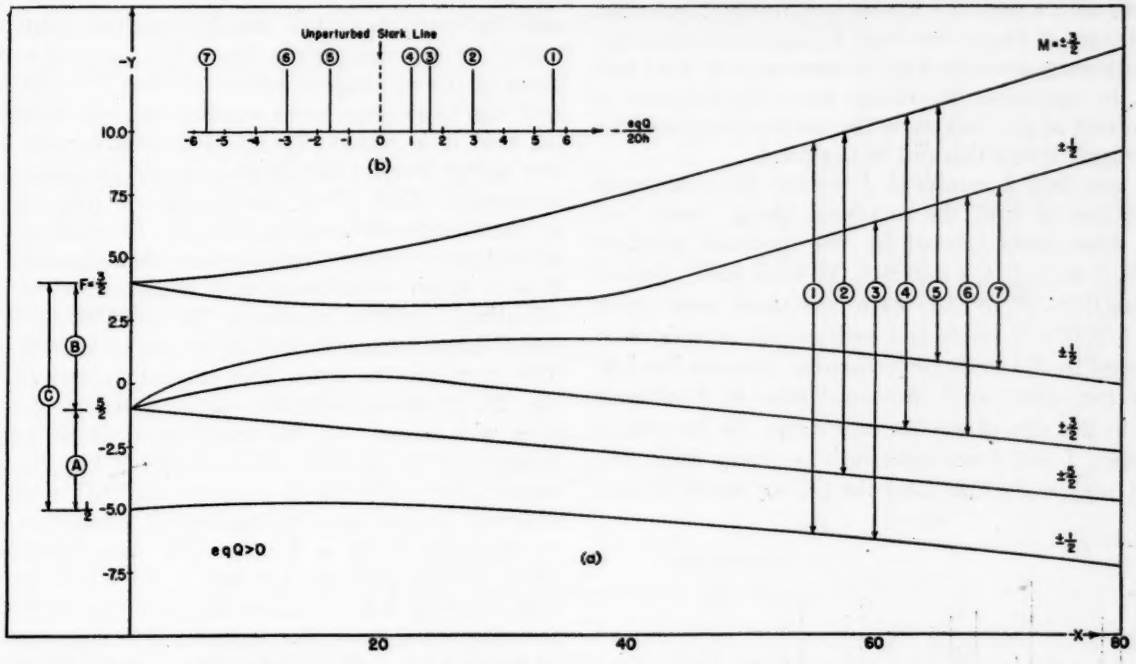

FIG. 3. (a) Plot of energy levels W *versus* the square of the electric field, E^2, for $J=1$, $I=\frac{3}{2}$ and $eqQ>0$; coordinates are in dimensionless units.

$$Y=-20\frac{W}{eqQ} \qquad X=-20\frac{(\mu E)^2}{eqQ(h^2/2A)}$$

(b) Strong field spectrum for $J=1$, $I=\frac{3}{2}$, $eqQ>0$.

6.55 percent, respectively. The r-f field induces transitions causing a maximum change of refocused beam intensity of 6 to 7 cm. Detector and beam stability were such that under best conditions a change of 5 mm in the refocused beam could be observed. Because of insufficient abundance the spectrum of $K^{41}F$ could not be observed.

III. THEORY

The results of the experiment can be interpreted by assuming the following Hamiltonian[9-11]

$$H=\frac{\hbar^2}{2A}\mathbf{J}^2-\boldsymbol{\mu}\cdot\mathbf{E}-eqQ\frac{\{3(\mathbf{I}\cdot\mathbf{J})^2+\frac{3}{2}(\mathbf{I}\cdot\mathbf{J})-\mathbf{I}^2\mathbf{J}^2\}}{2I(2I-1)(2J-1)(2J+3)}. \quad (1)$$

In the first term $\mathbf{J}$ is the angular momentum of rotation of the molecule and A is the moment of inertia. The second term represents the interaction of the field with the permanent dipole moment of the molecule. The third term represents the electric quadrupole interaction of the K^{39} nucleus with the rest of the charges of the molecule. e=the charge of the proton, Q=nuclear electric quadrupole moment, $q=\partial^2V/\partial z^2$ the second derivative of the electrostatic potential due to all the charges outside the nucleus, taken along the axis of the molecule at the position of the nucleus.[12] The quantity I is the spin of the K^{39} nucleus. The fluorine

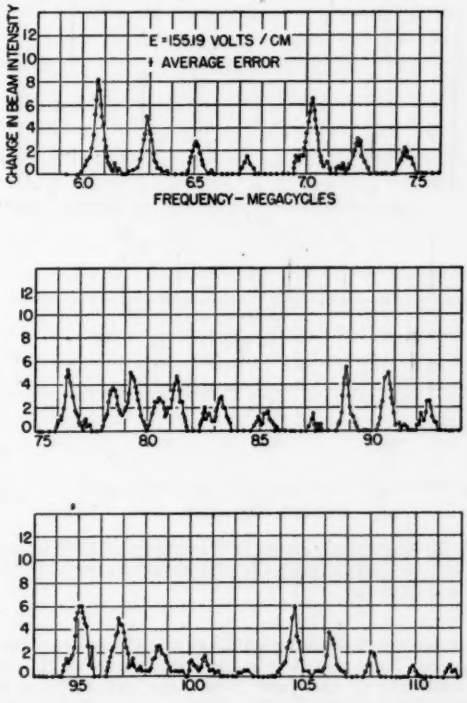

FIG. 4. Moderately strong field spectrum. This spectrum is drawn schematically in Fig. 5, where the lines are identified.

[9] U. Fano, J. Research Nat. Bur. Stand. **40** (1948) Research Paper 1866.
[10] Nierenberg, Rabi, and Slotnick, Phys. Rev. **73**, 1430 (1948).
[11] V. Hughes and L. Grabner (to be published).
[12] J. Bardeen and C. H. Townes, Phys. Rev. **73**, 97 (1948).

nucleus with a spin of $\frac{1}{2}$ has no quadrupole interaction. The theory of Fano[13] was used to calculate the energy level diagram shown in Fig. 2a when $eqQ<0$, $J=1$ and $I=\frac{3}{2}$. In calculating the energy levels the influence of the mixing of the J states on the matrix elements of the quadrupole interaction can be neglected.

At zero field $\mathbf{I}$ couples to $\mathbf{J}$ through the quadrupole interaction to split the rotational energy level $J=1$ into three levels labeled by the quantum numbers $F=I+J$ as 1/2, 3/2 and 5/2. At weak fields, defined by $|eqQ|\gg\mu^2E^2/(\hbar^2/2A)$ each zero field level splits into $1/2(2F+1)$ levels and each energy level is characterized by F and its projection m_F. Because the field is electric, states with the same value of F differing only in the sign of m_F are degenerate. As the field is increased $\mathbf{I}$ and $\mathbf{J}$ decouple until at strong fields (i.e., when $|eqQ|\ll\mu^2E^2/(\hbar^2/2A)$) the (J, m_J) states $(1, \pm1)$ and $(1, 0)$, which at low and intermediate fields are mixed by the quadrupole interaction, separate. Because of the quadrupole interaction the $(1, 0)$ level is split into two energy levels which increase in energy as the field is increased. The $(1, \pm1)$ level is split into four energy levels which decrease in energy as the field is increased. Each of the terms in Eq. (1) may depend on the vibrational state, so that Fig. 2a must be considered as the energy level diagram when the molecule is in a certain vibrational state characterized by the vibrational quantum number v. The selection rule[14] for transitions as strong fields is $\Delta(m_J+m_I)\equiv\Delta M=0, \pm1$. This gives rise to seven lines labeled numerically in Fig. 2a. At strong fields the relative positions of these lines with respect to the unperturbed Stark line is independent of the field, and is shown in Fig. 2b. The unperturbed Stark line is the single line that would be observed if there were no quadrupole interaction and no variation of the $\boldsymbol{\mu}\cdot\mathbf{E}$ interaction with vibrational state. In that case the 1, 0 and 1, ±1 levels are not split. If the $\boldsymbol{\mu}\cdot\mathbf{E}$ and quadrupole interaction vary with the vibrational state, the spectrum is a superposition of the spectra of all the vibrational states. The vibrational states are identified by the intensities of the lines. The intensities decrease as $\exp(-E_v/kT)$, E_v is the energy of the vibrational state v, k is the Boltzmann constant, and T is the absolute temperature of the oven. At weak fields the selection rules are $\Delta F=0, \pm1, \pm2$ and $\Delta m_F\equiv\Delta M=0, \pm1$. This gives rise to three lines which are identified by the letters A, B and C in Fig. 2a. At weak fields the $\boldsymbol{\mu}\cdot\mathbf{E}$ interaction is very small. Lines arising from transitions between different m_F levels into which each F level splits at weak fields were not resolved in the low field runs of this experiment. If the quadrupole interaction varies with the vibrational state, the spectrum again will be a superposition of those of all the vibrational states with an intensity distribution characterized by $\exp(-E_v/kT)$. Transitions within a rotational state are forbidden at zero field.

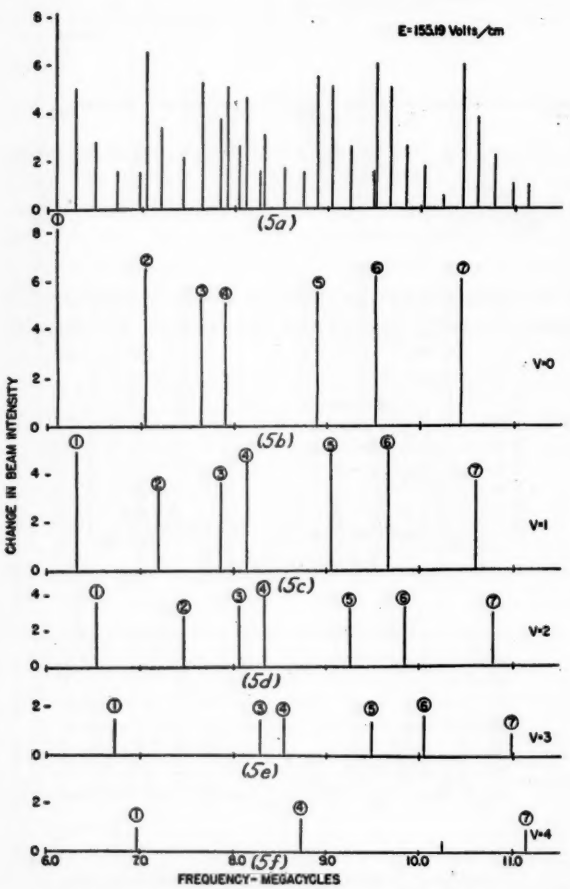

FIG. 5. (a) Moderately strong field spectrum of $K^{39}F$ (schematic). (b), (c), (d), (e), and (f) are the vibrational states $v=0, 1, 2, 3, 4$ as analyzed from (a).

The r-f field causing the transitions is arranged so that if it is decomposed into components parallel and perpendicular to the steady field, $E_{rf\perp}>E_{rf\parallel}$; $E_{rf\perp}$ gives rise to transitions for which $\Delta M=\pm1$, $E_{rf\parallel}$ to those for which $\Delta M=0$.

If $eqQ>0$ the energy level diagram is different and is sketched in Fig. 3a. The strong field spectrum is shown in Fig. 3b. The transitions in Fig. 3b are labeled in such a way that a transition between two levels has the same label as the corresponding transition has in Fig. 2a. The strong field spectrum shown in Fig. 3b is identical with that shown in Fig. 2b except for the position of

[13] See reference 9. Fano's definition of q differs from that used in this paper. Note also that in the initial report of this research in the abstracts of the June 1949 American Physical Society meeting at Cambridge, q' rather than q was used. Since our first report it has been agreed in this laboratory in the interest of uniformity to use q as defined by Bardeen and Townes. B. T. Feld and W. E. Lamb, Phys. Rev. 67, 15 (1948), use a definition of q which differs from Fano's q, q', and from the q of Bardeen and Townes. The relationship between these q's is:

$$q_{\text{Bardeen-Townes}}=2eq'=-eq_{\text{Fano}}=-2eq_{\text{Feld-Lamb}}(2J+3)/2J$$

e=proton charge, J=rotational quantum number. The advantage of $q_{\text{Bardeen-Townes}}$ is that it directly represents $\partial^2V/\partial z^2$ at the nucleus along the molecular axis and not a quantity which when multiplied by a suitable factor gives $\partial^2V/\partial z^2$.

[14] The selection rules are treated in detail in reference 11.

TABLE I. Comparison of observed and predicted lines. Lines are identified in Fig. 2. Lines 2, 3, 4, 5, 6; eqQ/h, μ^2A were calculated from lines 1 and 2.

Vibrational state ↓	Line→	(1)	(2)	(3)	(4)	(5)	(6)	(7)	$-(eqQ/h)$ Mc/sec.	$\mu^2A \times 10^{-16}$ e.s.u.
0	observed (Mc)	6.070	7.028	7.645	7.930	8.883	10.461	7.645	7.928	7419.3
	predicted		7.024	7.647	7.938	8.884	10.461			
1	observed	6.286	7.218	7.846	8.127	9.062	9.682	10.617	7.816	7598.1
	predicted		7.230	7.842	8.126	9.062	9.681			
2	observed	6.507	7.440	8.047	8.327	9.250	9.857	10.800	7.744	7789.4
	predicted		7.444	8.048	8.328	9.259	9.870			
3	observed	6.735		8.276	8.535	9.445	10.068	10.988	7.668	7986.4
	predicted		7.666	8.262	8.537	9.461	10.064			
4	observed	6.953			8.736		10.250	11.150	7.566	8166.6
	predicted		7.873	8.458	8.729	9.643	10.235			

line 4. If $eqQ>0$ line 4 lies to the right, if $eqQ<0$ to the left of the unperturbed Stark line. Thus a strong field spectrum not only determines the magnitude of the quadrupole interaction but the sign as well because of the asymmetry introduced by line 4.

It will now be shown that a weak field spectrum also allows the determination of the sign of eqQ even though the weak field spectrum is independent of the sign. This is possible because of the way in which a line is observed in a molecular beam experiment. Clearly a transition is observable only if it occurs between a state that is refocused and one that is not; i.e., it must be a transition between states that may be adiabatically transformed into levels that differ in the value of $|m_J|$. Regardless of whether the $(1, 0)_A-(1, 0)_B$ or the $(1, \pm1)_A-(1, 0)_B$ beam is refocused it is evident from Fig. 2a and 3a that lines B and C will be observed irrespective of the sign of the quadrupole interaction but that line A will be observed only if $eqQ<0$ because only in this case can the states between which transition A takes place be adiabatically transformed into states that differ in $|m_J|$. Therefore the appearance or absence of line A also decides the sign of the quadrupole interaction.

IV. THE SPECTRA

Figure 4 shows the spectrum obtained at a moderately strong field. The spectrum was observed by fixing the C-field at 155.19 volts/cm and varying the frequency. The lines are due to a quadrupole interaction with the K^{39} nucleus and a variation of the $\boldsymbol{\mu}\cdot\mathbf{E}$ interaction with vibrational state. In addition, it will be shown that the spectrum shows a variation of the quadrupole interaction with vibrational state. The value of the electric field is such that the splitting of the unperturbed Stark line due to the quadrupole interaction is not quite yet independent of the field; i.e., the spectrum is not a true strong field spectrum. Each transition occurs within all the vibrational states and its frequency relative to the unperturbed Stark line is determined, at this moderately strong field, principally by the quadrupole interaction. The unperturbed Stark line is determined by the $\boldsymbol{\mu}\cdot\mathbf{E}$ interaction. Since many more than the predicted seven lines are observed it is clear that the $\boldsymbol{\mu}\cdot\mathbf{E}$ interaction varies with vibrational state and that the magnitude of this effect is large enough to resolve the vibrational states of the molecule. In the center of the spectrum some of the transitions almost overlap. For clarity, therefore, the spectrum shown in Fig. 4 was plotted schematically in Fig. 5a. The positions and lengths of the lines in Fig. 5a are drawn at the frequency and equal to the intensity at which they were observed. The spectra of molecules in the vibrational states $v=0$, 1, 2, 3 and 4 were selected from Fig. 5a and redrawn separately in Fig. 5b, c, d, e and f, respectively. In the vibrational states $v=3$ and 4 not all the lines are resolved. The lines are labeled by numbers in Fig. 5 and the transition to which each

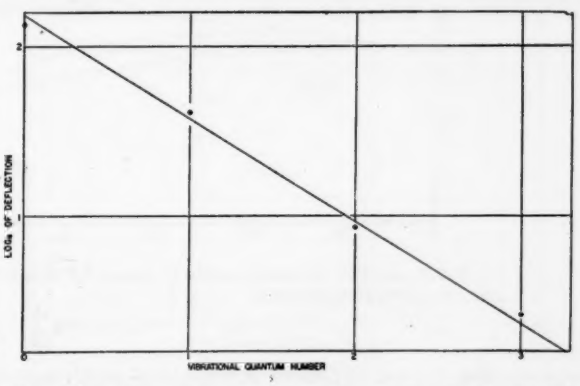

FIG. 6. Semi-log plot of the intensity of line 1, identified in Fig. 2, *versus* vibrational quantum number. Oven temperature 920°K. $\omega_0=(390\pm39)$ cm^{-1}.

corresponds is identified by the corresponding number in Fig. 2a. The spectrum was obtained from several different runs. Conditions determining the intensity of a line were not the same in the different runs. This is shown in the intensities of the different vibrational states which theoretically should be homologous. The identification of the vibrational state and, in fact, the principal reason for regarding these lines as transitions within several vibrational states is the variation of intensity of a single transition with vibrational state. The population of a vibrational state and therefore the intensity of its corresponding line goes as $\exp(-E_v/kT)$. If the natural logarithm of the intensity of a line is plotted as a function of the vibrational state a straight line should result. This is borne out particularly well by line 1, as is shown in Fig. 6. From the line intensities for the different vibrational states and the oven temperature[15] $\omega_0=(390\pm39)$ cm^{-1}. Inclusive of the $\Delta M=0$ transition, the theory predicts seven lines. All of these are observed. Several are missing for the

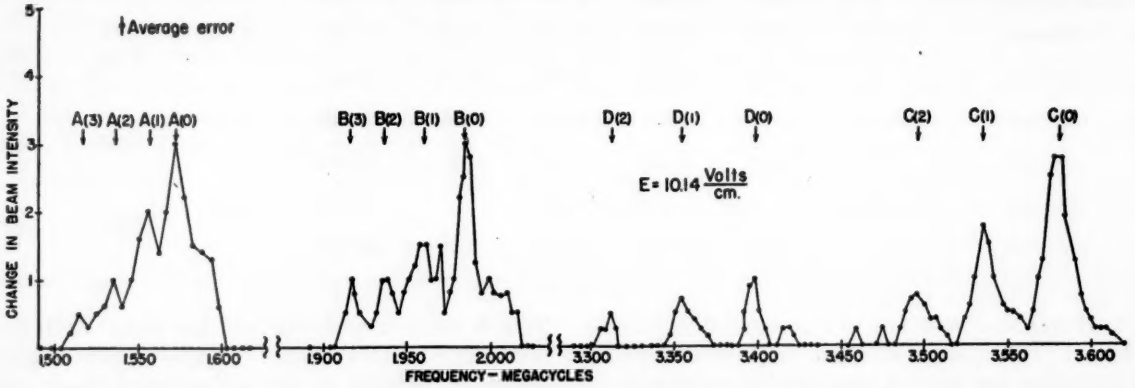
Average error
CHANGE IN BEAM INTENSITY
A(3) A(2) A(1) A(0)
B(3) B(2) B(1) B(0)
D(2) D(1) D(0)
C(2) C(1) C(0)
E = 10.14 Volts/cm.
1500 1550 1600 1900 1950 2000 3300 3350 3400 3450 3500 3550 3600
FREQUENCY - MEGACYCLES

FIG. 7. Weak field spectrum. Lines are identified in Fig. 2. Vibrational states are identified by vibrational quantum numbers attached to letters as subscripts.

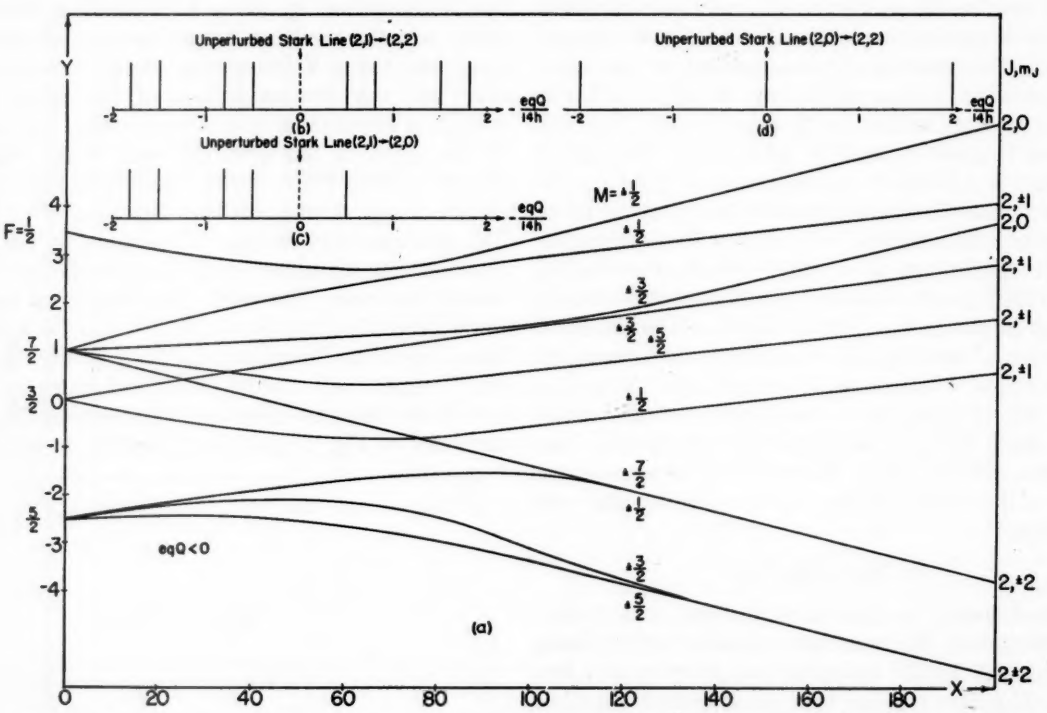

FIG. 8. (a) Plot of energy levels W *versus* the square of the electric field, E^2, for $J=2$, $I=\frac{3}{2}$, $eqQ<0$; coordinates are in dimensionless units.

$$Y=-14\frac{W}{eqQ} \quad X=-14\frac{(\mu E)^2}{eqQ(h^2/2A)}$$

(b), (c), and (d), strong field spectrum for $(J, m_J)\rightarrow(J, m_J')$ of $(2, 1)\rightarrow(2, 2)$; $(2, 0)\rightarrow(2, 1)$; and $(2, 0)\rightarrow(2, 2)$, respectively.

[15] G. Herzberg, *Molecular Spectra and Molecular Structure, I. Diatomic Molecules* (Prentice-Hall, Inc., New York, 1939), p. 101.

TABLE II. Quadrupole interaction constant eqQ/h for K^{39} in $K^{39}F$ for the vibrational states $v=0, 1, 2, 3, 4$ in rotational state $J=1$ and for vibrational states $v=0, 1, 2$ with rotational state $J=2$.

Rotational state J	Vibrational state V	"Strong" field $-(eqQ/h)$ Mc/sec.	Weak field $-(eqQ/h)$ Mc/sec. From line (A)	From line (B)	From line (C)	Average weak field data	Difference between "strong" and weak	Average of strong and weak field data $-(eqQ/h)$ Mc/sec.
	0	7.928	7.952	7.968	7.906	7.946	0.018	7.938±0.040
	1	7.816	7.856	7.842	7.828	7.842	0.026	7.828±0.040
1	2	7.744	7.766	7.742	7.724	7.744	0.000	7.744±0.040
	3	7.668	7.676	7.646	7.620	7.648	0.020	7.658±0.040
	4	7.566						
			From line (D)					
	0		7.928±0.040					
2	1		7.828±0.040					
	2		7.726±0.040					

vibrational state $v=3$ and 4 (see Fig. 5e and 5f) because they fell within the line width of lines in lower vibrational states and thus were not resolved. The resolution is determined by three factors.[16] (1) The inhomogeneity of the C-field sets a limit of 1 part in 1000 of the frequency, i.e., 18 kc/sec. (2) The uncertainty relation $\Delta\nu\Delta t\sim 1$ where $h\Delta\nu$ is the uncertainty in the energy, and Δt is the time the molecule spends in the oscillating field, results in a broadening of 16 kc/sec. for KF at an oven temperature of 650°C and for an effective length of the C-field of 4 cm. (3) The magnitude of the oscillating field. The theoretical width resulting from a combination of the first two estimates was not calculated. The half-width of the lines in Fig. 4 is 40 kc/sec. Subsequent experiments showed that the r-f voltage $=0.75$ r.m.s. volts was too large by a factor of about 10 and that a correct r-f field would have narrowed the lines to ~20 kc/sec.

The arithmetic mean of the frequencies of lines 1 and 7 give to a good approximation the frequency of the unperturbed Stark line, which is proportional to μ^2AE^2 at this moderately strong field.[17] Since the position of line 4 is to the left of the unperturbed Stark line $eqQ<0$ (see Figs. 2 and 3).

Taking into account the fact that Fig. 4 does not represent a strong field spectrum μ^2A and eqQ were calculated for each vibrational state. Any two lines in a given vibrational state determine μ^2A and eqQ for that vibrational state. From these two constants the consistency of the theory and the data can be checked by predicting the frequencies of the other lines and comparing these frequencies with those found in the experiment. Table I shows the results of such a calculation using lines 1 and 7 to calculate μ^2A, eqQ, and the positions of the other lines. Evidently the agreement between the predicted frequencies and those found experimentally is excellent. It is also significant that this moderately strong field experiment reveals a decrease in the magnitude of the quadrupole interaction as the vibrational quantum number increases, of approximately 1.3 percent when the vibrational quantum number increases by unity.

Structure at Weak Fields

At weak fields the $\boldsymbol{\mu}\cdot\mathbf{E}$ interaction is small compared with the quadrupole interaction. In particular, if the quadrupole interaction is not a function of the vibrational state, the lines that occur because $\boldsymbol{\mu}\cdot\mathbf{E}$ is a function of the vibrational state would not be resolved at the low fields used in this experiment. At weak fields the resolution is determined by the uncertainty relation, and is 16 kc/sec. Since the effect of the field on the spectrum is practically eliminated, it will exhibit primarily internal interactions. A variation of the quadrupole interaction is anticipated from the moderately strong field spectrum. A calculation of the effect of such a variation on a weak field spectrum shows that a single transition occurring in different vibrational states should be resolved. The effect of the field is to split the zero field energy levels as shown in Fig. 2a. The resultant splitting of the lines is of the same order of magnitude as the resolution, and is not expected to be resolved. Since $eqQ<0$, as determined from the moderately strong field experiment, the theory predicts three lines according to the selection rules $\Delta F=0, \pm1, \pm2$; $\Delta m_F=0, \pm1$. These transitions are labeled in the energy level diagram, Fig. 2a, as lines A, B and C. Figure 7 shows the data obtained at a

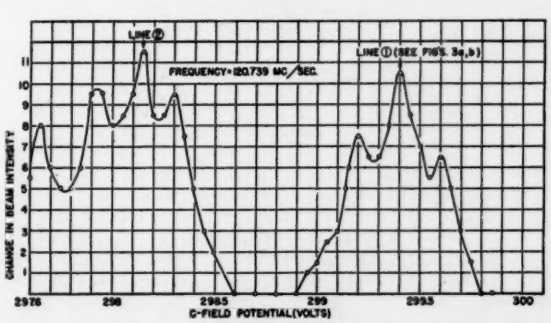

FIG. 9. Strong field spectrum showing the 0th vibrational state of lines 1 and 2 (see Fig. 2a,b) and the side peaks of lines 1 and 2 produced by the Millman effect. Peak at $V_c=297.65$ volts belongs to another line.

[16] See reference 2, p. 720.

[17] P. Debye, *Polar Molecules* (Dover Publications, New York, 1945).

C-field of 10.14 volts/cm. The lines are labeled by letters in Fig. 7 and the transition to which each corresponds is identified by the corresponding letter in Fig. 2a. The vibrational state within which the transition takes place is identified by the vibrational quantum number attached as a subscript. Since line A appears in the spectrum, $eqQ<0$, in agreement with the moderately strong field spectrum. The assignment of the lines is correct because their frequency ratios agree with the theory.

Line D (see Fig. 7) cannot be explained as arising from a transition in the energy level diagram of Fig. 2a. All possible transitions have already been exhausted by lines A, B, and C. Furthermore, it is impossible that it could be due to the effect of the field since any splitting of the lines caused by the field is far too small to account for it. An inspection of the energy level diagram corresponding to Fig. 2a for the rotational state $J=2$ shows that line D comes from a transition in which F changes from $5/2\rightarrow1/2$, the latter states arising from a perturbation of the rotational states $J=2$ by the quadrupole interaction. The energy level diagram for $J=2$, $I=3/2$, $eqQ<0$ is sketched in Fig. 8a. Two considerations support this conclusion. (1) The weak field data were obtained with the $(1,\pm1)_A-(1,0)_B$ refocused beam. The A and B fields required to refocus this beam will also refocus some of the $(2,\pm2)_A-(2,0)_B$ beam since not all of its molecules are eliminated by the wire stop. (2) If we assume that eqQ does not change with rotational state, the value of the quadrupole interaction calculated from the moderately strong field data or from the weak field lines A, B or C predicts a line exactly where line D occurs caused by the transition $F=1/2\rightarrow5/2$ within the energy levels of the rotational state $J=2$ perturbed by the quadrupole interaction (see Fig. 8a).

There are four other lines in the spectrum of $J=2$. They correspond to F changes of $7/2\rightarrow5/2$, $3/2\rightarrow1/2$, $7/2\rightarrow3/2$ and $5/2\rightarrow3/2$. Clearly, any one of these lines will be observed if the number of molecules in the "2, 0 state," which have resulted from non-adiabatic transitions from the "2, ±2 state," is either increased or decreased when an rf field of frequency equal to the frequency of the line is turned on. Whether an increase or decrease, or even a net "flop" of zero, results will depend on the quantitative aspects of the non-adiabatic interfield transitions about which nothing can be stated for a field as complicated as that which exists in the interfield regions of this apparatus. Line D is observed as an increase of the refocused beam; i.e., molecules in the "2, ±2 state" are "flopped into" the "2, 0 state" (lines A, B and C which come from $J=1$ are also observed as an increase of refocused beam). The frequencies of the lines corresponding to the $7/2\rightarrow5/2$ and the $3/2\rightarrow1/2$ transitions coincide with that of line A. An inspection of Fig. 8a shows that the $5/2\rightarrow3/2$ transition cannot be observed since molecules in the "2, ±1 state" are stopped by the wire-stop. The $7/2\rightarrow3/2$ transition could be observed (see Fig. 8a); however since it is not observed in the experiment it must be assumed that the quantitative aspects of the non-adiabatic transitions between the interfield regions are such as to make its intensity weak or even zero.

Table II summarizes the quadrupole interactions determined from the weak field data and compares them with those determined from the moderately strong field data. Within experimental error they agree very well. No difference is found between the quadrupole interaction for $J=1$ and $J=2$.

Finally, interactions of the type[2,5–8,10,11] $\mathbf{I}_1\cdot\mathbf{J}$ and $\mathbf{I}_2\cdot\mathbf{J}$ where $\mathbf{I}_1$ and $\mathbf{I}_2$ are the angular momenta of the K^{39} and the F nuclei, respectively, were not observed. The effect of $\mathbf{I}_1\cdot\mathbf{J}$ is to shift the lines, of $\mathbf{I}_2\cdot\mathbf{J}$ to split them. The $\mathbf{I}\cdot\mathbf{J}$ interactions are very weak compared to the quadrupole interactions. They are best observed at weak fields because at weak fields the resolution is best since the effect of the field on the broadening of the lines is eliminated.

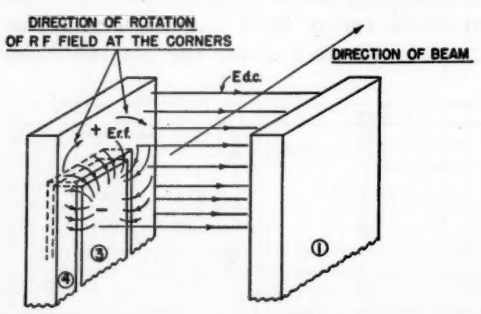

FIG. 10. Schematic perspective diagram of the C-field. 3 and 4 are at the same dc potential. The static homogeneous field, E_{dc}, is between 1 and 3, 4; the oscillating field, E_{rf}, is between 3 and 4. At the instant for which the diagram is drawn, 3 is charged negative, 4 is charged positive. With respect to a molecule moving in the direction of the beam, the oscillating field at the corners rotates in the direction shown. This direction is independent of the relative sign of 3 and 4.

Value of J

The spectrum shown in Fig. 4 was identified as coming from molecules in $J=1$ by the uniqueness of the hyperfine structure; i.e., the spectra obtained from $(J, m_J)\rightarrow(J, m_J')$ transitions of $(2,\pm1)\rightarrow(2,\pm2)$, $(2,\pm1)\rightarrow(2,0)$ or $(2,0)\rightarrow(2,\pm2)$ differ from the spectrum for a $(1,0)\rightarrow(1,\pm1)$ transition (compare Fig. 2b and 8b, c, d).

At weak fields lines A, B and C were assigned to the hyperfine structure resulting from the splitting of $J=1$ because the frequency ratios of these lines determine them uniquely as coming from that state. In addition, the values of the quadrupole interactions calculated from the weak field data for $J=1$ agree with those calculated from the moderately strong field data which has already been proved to come from the rotational state $J=1$.

V. THE DIPOLE MOMENT AND MOMENT OF INERTIA

When the $\boldsymbol{\mu}\cdot\mathbf{E}$ interaction is much larger than the quadrupole interaction, the splitting of the unperturbed Stark line is independent of the electric field, except for the mixing of the J states. However, when the electric field is large the energy of the molecule contributed by the $\boldsymbol{\mu}\cdot\mathbf{E}$ interaction is no longer proportional to E^2. W. E. Lamb, Jr., has calculated the exact solution of the Schrödinger equation for a linear diatomic molecule in an electric field. His solutions yield a three-term recursion formula. The energy eigenvalues are determined through the continued fraction method.[18] The analytical expression for the energy does not lend itself to the determination of μ and A. However, Hughes has fitted a polynomial[19] to Lamb's exact solution. He finds that for a $(1, 0)\rightarrow(1, \pm1)$ transition the dimensionless formula:

$$\Delta W_{(1,0\rightarrow1,\pm1)}=0.15\lambda^2-0.010768\lambda^4+0.00125\lambda^6 \quad (2)$$

fits Lamb's exact solution for λ in the range 0 to 1.0.

The transition frequency is

$$\Delta\nu_{(1,0\rightarrow1,\pm1)}=\alpha E^2-\beta E^4+\gamma E^6 \quad (3)$$

where

$$\alpha=\frac{0.15}{h}\times\frac{\mu^2}{(h^2/2A)},\quad \beta=\frac{0.010768}{h}\times\frac{\mu^4}{(h^2/2A)^3},$$

$$\gamma=\frac{0.00125}{h}\times\frac{\mu^6}{(h^2/2A)^5}.$$

The dipole moment and moment of inertia were determined by the following procedure. The frequency of line 1 defined in Fig. 2a was measured in the zeroth vibrational state at fields for which the λ^4 term of Eq. (2) is appreciable for three different fields corresponding to λ's of 0.38, 0.44, 0.49. From the theory of the hyperfine structure due to the quadrupole interaction, the frequency of the unperturbed Stark line was calculated. The effect of the mixing of J states on the frequency of line 1 is only 1 part in 15,000 of the frequency determined by the E^2 term of Eq. (3), and can be neglected in calculating the frequency of the unperturbed Stark line. Three simultaneous equations of the type of Eq. (3) yield α and β. From α and β

$$A=\frac{(0.15)^2}{0.0010768}\times\frac{h}{8\pi}\times\frac{\beta}{\alpha^2}(\text{g-cm}^2), \quad (4)$$

$$\mu^2=\frac{0.010768}{(0.15)^3}\times h^2\times\frac{\alpha^3}{\beta}(\text{e.s.u.})^2, \quad (5)$$

when E is expressed[20] in e.s.u. in Eq. (3).

[18] Reference 1, p. 620.
[19] H. K. Hughes, Phys. Rev. **76**, 1675 (1949).
[20] The field was measured in international volts/cm. E, however, is expressed in absolute units. The conversion factor is 1 international volt = 1.00034 absolute volts (Circular C 459, National Bureau of Standards, 1947). 1 e.s.u. = 299.796 absolute volts was also used.
[21] S. Millman, Phys. Rev. **55**, 628 (1939).

TABLE III. Quadrupole interaction constants eqQ/h of the alkali-fluorides.

Molecule	Method	$\frac{eqQ}{h}$ Mc/sec.	Remarks
CsF^a	Electric resonance	+ 1.240	vibrational states not resolved
$Rb^{85}F^b$	Electric resonance	−70.312	zeroth vibrational state
$Rb^{87}F^b$	Electric resonance	−34.000	zeroth vibrational state
$K^{39}F$	Electric resonance	− 7.938	zeroth vibrational state
NaF^c	Magnetic resonance	8.512	sign not determined
Li^7F^d	Magnetic resonance	0.408	sign not determined

[a] Reference 2.
[b] See reference 8.
[c] Private communication by D. Bolef and H. Zeiger.
[d] P. Kusch, Phys. Rev. **75**, 887 (1949).

Inserting the values of α and β in Eqs. (4) and (5), we obtain, for the zeroth vibrational state:

$$A=(138.4\pm6.9)\times10^{-40}\ \text{g-cm}^2,\ \mu=(7.33\pm0.24)\ \text{Debye}.$$

A Debye is 10^{-18} e.s.u. From the value of A the internuclear distance for $K^{39}F$ in the zeroth vibrational state is calculated to be (2.55 ± 0.06) angströms. The experimental errors are mainly due to the non-uniformity of the C-field. It was not possible to measure μ and A for the other vibrational states because their lines are not resolved at these high fields.

VI. THE MILLMAN EFFECT

Figure 9 shows the data taken for the determination of μ and A at $\lambda=0.38$. These lines are identified in Fig. 2. Each of the lines has two side peaks. It will now be shown that the side peaks are caused by the Millman[21] effect. The C-field is sketched in Fig. 10. The components are labeled to correspond to the labels of Fig. 2, reference 2, where the C-field is discussed in detail. The homogeneous static field is between plates 1 and plates 3, 4. Plates 3 and 4 are coplanar and at the same d.c. potential. The r-f field is superposed on the static field by connecting the output of a vacuum tube oscillator between 3 and 4. The lateral position of the beam is approximately midway between 1 and 3, 4. Its vertical position is such that its height (5 mm) is bisected by the horizontal boundary between 3 and 4. At the corners the direction of the field changes (see Fig. 10). With respect to a moving molecule the r-f field is linearly polarized only in the region between the corners. At the corners it is a superposition of oscillation and rotation. It is clear that the rotation takes place in the same direction during each half-period of the oscillation. The direction of rotation is indicated in Fig. 10 when 3 is negative and 4 is positive. If the linearly polarized oscillating field is resolved into two circularly polarized components, one rotating in the

same direction as the rotation at the corners, the other rotating in the opposite sense, we will have two frequencies at the corners, $\nu+\Delta\nu$ and $\nu-\Delta\nu$. Here ν is the applied oscillator frequency, and $\Delta\nu$ is the effective frequency of rotation of the linearly polarized field which the moving molecule sees at the corners. It is shown in the Appendix that the dipole matrix elements of both circularly polarized components are non-vanishing for a polar molecule in an electric field. Therefore if the oscillator frequency is fixed and the field is varied, which is the case for the data shown in Fig. 9, three lines will appear: two side peaks due to circularly polarized fields of frequency $\nu+\Delta\nu$ and $\nu-\Delta\nu$ at the corners, and a central peak due to each circularly polarized component of frequency at the central portion of 3 between the two corners. Only one side peak[21] is observed in the magnetic resonance data because only one circularly polarized component of the rf field gives a non-vanishing dipole matrix element.

The separation of a side peak from the central peak gives $\Delta\nu=160$ kc/sec. for $K^{39}F$. From the most probable molecular velocity in the beam the distance over which the rotation at a corner takes place is calculated to be 0.3 cm. Since plates 3 and 4 are separated by a distance of 0.04 cm, this seems a reasonable value. The total length of the C-field is 6 cm, the length of 3 (along the beam) is 4 cm.

VII. DISCUSSION

Table III gives the quadrupole interactions of all the alkali-fluorides measured to date. It is complete except for $K^{41}F$ and Li^6F. This table can tell little until the important problem of separating q and Q is solved. The value of q can be calculated if the molecular wave function is known.

It is probable that there is a variation of the quadrupole interaction with vibrational state in all the alkali fluorides of the same order of magnitude as that found[8] for $K^{39}F$, $Rb^{85}F$ and $Rb^{87}F$, namely, $\sim$1 percent when the vibrational quantum number increases by unity. The magnitude of this variation would be too small to be observed in CsF or Li^7F. Indeed, it was not observed in the electric resonance spectrum[2] of CsF.

If the sign of q is assumed to be identical for the alkali-fluorides, then the sign of the electric quadrupole moment of the K^{39}, Rb^{85} and Rb^{87} nuclei is opposite to that of the Cs nucleus.

The internuclear distance $r=2.55$A for $K^{39}F$ is of interest when viewed in the light of Trischka's experiment. For CsF, Trischka[3] found that the internuclear distance is 6 percent smaller than that of CsH^1. For $K^{39}F$ the internuclear distance in the zeroth vibrational state is 12 percent larger than that[22,23] of $K^{39}H^1$. Further, the internuclear distance of $K^{39}F$ is larger than that of CsF (2.34A); the internuclear distance of all the other potassium halides, however, is smaller than that of the corresponding cesium halide.[24]

We would like to express our gratitude to Professor I. I. Rabi for his continued interest and for many clarifying discussions. We would also like to thank Professor J. W. Trischka, who began this research with one of us, and S. Miller, who helped in the laboratory.

APPENDIX

The probability amplitudes of the energy eigenfunctions are related by the equation

$$i\hbar\dot{a}_k(t)=\Sigma_n a_n(t)[k|H'|n]\exp[-(i/\hbar)(E_n-E_k)t]. \quad (6)$$

H' is the interaction of the system with the oscillating field. Let $\omega_{kn}=E_k-E_n/\hbar$ and assume that at $t=0$, $a_j(0)=1$; then

$$i\hbar\dot{a}_k(t)=(k|H'|j)\exp(i\omega_{kj}t). \quad (7)$$

The linearly polarized oscillation:

$$E_x=4E_0^x\cos\omega t=2E_0^x[\exp(+i\omega t)-\exp(-i\omega t)] \quad (8)$$

can be replaced by the sum of the left-circularly polarized oscillation

$$E_L=\mathbf{i}E_0^x[\exp(+i\omega t)+\exp(-i\omega t) -\mathbf{j}iE_0^y[\exp(+i\omega t)-\exp(-i\omega t)] \quad (9)$$

and the right-circularly polarized oscillation

$$E_R=\mathbf{i}E_0^x[\exp(+i\omega t)+\exp(-i\omega t)] +\mathbf{j}iE_0^y[\exp(+i\omega t)-\exp(-i\omega t)]. \quad (10)$$

In (9) and (10) $E_0^x=E_0^y$. Since $H'=-\mathbf{p}\cdot\mathbf{E}=-(p_xE_x+p_yE_y)$, where $\mathbf{p}$ is the electric dipole moment of the system, (7) becomes

$$\begin{aligned}-i\hbar\dot{a}_k(t)=&E_0^x\{\exp[+i(\omega_{kj}+\omega)t+\exp[-i(\omega_{kj}-\omega)t]\}(k|p_x|j)\\ &-iE_0^y\{\exp[+i(\omega_{kj}+\omega)t-\exp[-i(\omega_{kj}-\omega)t]\}(k|p_y|j)\\ &+E_0^x\{\exp[+i(\omega_{kj}+\omega)t+\exp[-i(\omega_{kj}-\omega)t]\}(k|p_x|j)\\ &-iE_0^y\{\exp[+i(\omega_{kj}+\omega)t+\exp[-i(\omega_{kj}-\omega)t]\}(k|p_y|j). \quad (11)\end{aligned}$$

The sum of the first two terms on the right of (11) represent the matrix element of the left-circularly polarized component, the sum of the third and fourth terms that of the right-circularly polarized component. Now[25]

$$\pm i(m|p_x|m+1)=(m|p_y|m\pm1). \quad (12)$$

If the transition involves $m\rightarrow m+1$, Eqs. (11) and (12) show that only the left-circularly polarized component has a non-vanishing matrix element. Similarly, when $m\rightarrow m-1$, only the right-circularly polarized component has a non-vanishing matrix element. Since the energy of a diatomic molecule in an electric field is degenerate with respect to $+m$ and $-m$, both matrix elements are non-vanishing.

[22] T. Hori, Mem. Ryojun Coll. Eng. **6**, 1 (1933).
[23] M. Almy and C. D. House, Phys. Rev. **42**, 242 (1932).
[24] Maxwell, Hendricks, and Mosley, Phys. Rev. **52**, 968 (1937).
[25] E. U. Condon and G. H. Shortley, *Theory of Atomic Spectra* (Macmillan Company, Inc., New York, 1935), p. 63.

Energy Levels, Selection Rules, and Line Intensities for Molecular Beam Electric Resonance Experiments with Diatomic Molecules*

VERNON HUGHES AND LUDWIG GRABNER
Columbia University, New York, New York
(Received April 24, 1950)

In the molecular beam electric resonance method the energy levels in an electric field of a diatomic molecule which is in the ground electronic state, and a low vibrational and rotational state are studied. Transitions are produced between states with different space quantization of the molecule relative to the electric field and with different couplings of the angular momenta of the nuclei and of the molecular rotation. Thus the interaction of the molecule with the field and the internal molecular interactions (e.g., nuclear electrical quadrupole interactions and nuclear spin—molecular orbit interactions) are measured. In this paper we give the stationary state energy values and eigenfunctions for "very weak," "weak," and "strong" field conditions for a diatomic molecule in which one nucleus has a spin of $\frac{1}{2}$. Selection rules for the transitions are developed and some considerations on line intensities are discussed. Finally, there is presented the theory of double quantum transitions, which are predicted to occur at one-half the frequency given by the Bohr condition, $\Delta W = h\nu$, provided the radiofrequency field is sufficiently intense.

I. INTRODUCTION

RECENT experiments[1,2] by the molecular beam electric resonance method[3,4] of observing the energy levels of polar diatomic molecules have raised a number of questions related to selection rules and intensities for the spectra observed. In essence the method consists in selecting for study a single rotational (usually $J=1$ and occasionally $J=2$) and orientational state of a diatomic molecule in an electric field. This selection can be made because the force which an inhomogeneous electric field exerts on a molecule is dependent upon its rotational state and upon the orientation of its rotational angular momentum with respect to the field direction. The scheme employed is the familiar one of allowing the molecules to pass through two inhomogeneous electric fields, designated as the A and B-fields, which will produce equal and opposite deflections only for molecules in a single rotational and orientational state. Hence only these molecules will impinge upon the suitably placed detector.[5]

A study of the energy levels of these molecules in an electric field is made by inserting a homogeneous electric field, designated as the C-field, between the A and B-fields and impressing a radiofrequency field also in this region. At appropriate frequencies, ordinarily in the megacycle range, transitions are induced which bring the molecules to other energy states. In these different states the molecules will have different internal energies and (or) different interactions with the external field, but their rotational angular momentum and, of course, their nuclear spins will be unchanged. If the molecule which has been subjected to a transition in the C-field arrives in the B-field in a different state than it would have had if it had not suffered the transition, and, furthermore, if in this different state it is subjected to a different force in the B-field, then the transition will be observed as a change in the intensity of the molecular beam which strikes the detector.

The Hamiltonian for a polar diatomic molecule in an electric field should include a term for the interaction of the field with the electric dipole moment, terms for the electrical quadrupole interactions associated with the nuclei, terms for the spin-orbit coupling between each nuclear spin and the molecular rotational angular momentum, and, finally, the magnetic dipole-dipole interaction between the two nuclei. The energy levels are studied for field intensities ranging in value from those for which the field interaction term is negligibly small relative to the smallest internal interactions observed ($\sim$10 kc/sec.) to those for which the field interaction is large ($\sim$ several hundred megacycles) relative to the electrical quadrupole interactions. It will be convenient to distinguish several special cases characterized by the relative magnitude of the field interaction and the internal molecular interactions.

Thus far electric resonance experiments have been performed primarily with alkali fluoride molecules.[6] These molecules are especially simple because there is only an electrical quadrupole interaction associated with the alkali nucleus, since the spin of the fluorine nucleus is $\frac{1}{2}$. This paper will be restricted to the case in which the molecule has only one electrical quadrupole interaction. Still, it will be seen that many of the results can be rather simply extended to the case in which there are two electrical quadrupole interactions, but one of them is much smaller than the other. An extension to the more general case of two electrical quadrupole interactions of arbitrary magnitude can be made

* This research has been supported in part by the ONR.
[1] L. Grabner and V. Hughes, Phys. Rev. **79**, 819 (1950).
[2] V. Hughes and L. Grabner, Phys. Rev. **79**, 314 (1950).
[3] H. K. Hughes, Phys. Rev. **72**, 614 (1947).
[4] J. W. Trischka, Phys. Rev. **74**, 718 (1948).
[5] A majority of the molecules in the higher rotational states are deflected only a very small amount by the inhomogeneous fields and can most easily be prevented from reaching the detector by the use of a wire stop.
[6] Recently experiments have been performed with $TlCl^{35}$. See Lee, Carlson, Fabricand, and Rabi, Phys. Rev. **78**, 340A (1950).

with the help of the results of Bardeen and Townes, and of Racah.[7]

The second section of this paper will give the energy values and the eigenfunctions for several cases characterized by the magnitude of the field interaction. In the third section we shall present the selection rules which will apply for stimulated transitions in these various cases. Line intensities will be discussed in the fourth section. In this connection an important consideration is the correspondence that exists between states at low fields and states at high fields, assuming adiabatic change of the field parameter.

A condition is sometimes realized under very weak field conditions for which the intensity of the radiofrequency field is larger than that of the static field. Hence the field free state must be considered to be perturbed primarily by the radiofrequency field rather than by the static field. It turns out that in such a situation a two quantum transition is predicted. This matter is discussed in the final section of this paper.

II. STATIONARY STATE ENERGY VALUES AND EIGENFUNCTIONS

The most general Hamiltonian which it has been necessary to assume for the alkali fluoride molecule in an electric field is:

$$H=\frac{\hbar^2}{2A}\mathbf{J}^2-\boldsymbol{\mu}\cdot\mathbf{E}-eq_1Q_1\frac{\{3(\mathbf{I}_1\cdot\mathbf{J})^2+\frac{3}{2}(\mathbf{I}_1\cdot\mathbf{J})-\mathbf{I}_1^2\mathbf{J}^2\}}{2I_1(2I_1-1)(2J-1)(2J+3)}$$

$$+c_1(\mathbf{I}_1\cdot\mathbf{J})+c_2(\mathbf{I}_2\cdot\mathbf{J})+\frac{g_1g_2\mu_N^2}{r^3}$$

$$\times\frac{[3(\mathbf{I}_1\cdot\mathbf{J})(\mathbf{I}_2\cdot\mathbf{J})+3(\mathbf{I}_2\cdot\mathbf{J})(\mathbf{I}_1\cdot\mathbf{J})-2(\mathbf{I}_1\cdot\mathbf{I}_2)J(J+1)]}{(2J+3)(2J-1)}.$$

The first term in which $\mathbf{J}$ is the rotational angular momentum and A is the moment of inertia, is the rotational energy term. The second term gives the interaction of the external electric field $\mathbf{E}$ with the permanent electric dipole moment of the molecule. The third term is the electrical quadrupole interaction between the electrical quadrupole moment of the alkali nucleus, Q_1, and a second derivative of the electric potential at the position of the alkali nucleus, q_1, produced by the remaining charges in the molecule. q_1 and Q_1 are defined in reference 7a. Here e is the proton charge. (The subscript 1 refers to the alkali nucleus.) $\mathbf{I}_1$ is the spin of the alkali nucleus. There is no electrical quadrupole interaction with the F nucleus because its spin is $\frac{1}{2}$. This form of the electrical quadrupole interaction operator gives only the matrix elements diagonal[8] in J. The fourth and fifth terms are cosine couplings between the nuclear spins (F spin designated by $\mathbf{I}_2$) and the rotational angular momentum of the molecule. c_1 and c_2 are constants. The last term is the magnetic dipole-dipole interaction between the alkali and F nuclei, for which r is the internuclear distance, g_1 and g_2 are the gyromagnetic ratios for the alkali and F nuclei respectively, and μ_N is one nuclear magneton.[9]

In general it will be true that $\hbar^2/2A\gg eq_1Q_1\gg(c_2$ or c_1 or $g_1g_2\mu_N^2/r^3)$. We distinguish three cases which are of interest experimentally:

$$\mu^2E^2/(\hbar^2/2A)\ll c_2 \quad\text{or}\quad g_1g_2\mu_N^2/r^3 \qquad (\text{"very weak" field}) \quad (1)$$

$$(c_2 \text{ or } g_1g_2\mu_N^2/r^3)\ll\mu^2E^2/(\hbar^2/2A)\ll eq_1Q_1 \qquad (\text{"weak" field}) \quad (2)$$

$$eq_1Q_1\ll\mu^2E^2/(\hbar^2/2A)\ll\hbar^2/2A \quad (\text{"strong" field}) \quad (3)$$

(A) Very Weak Field Case

The energy eigenvalues and eigenfunctions for the very weak field case are given in the literature.[10,11] The energy values are:

$$W_{J,I_1,F_1,I_2,F=F_1\pm\frac{1}{2},M}=\frac{\hbar^2}{2A}J(J+1)-\frac{eq_1Q_1}{(2J-1)(2J+3)(2I_1)(2I_1-1)}\{\tfrac{3}{4}K_1(K_1+1)-I_1(I_1+1)J(J+1)\}$$

$$+\frac{c_1K_1}{2}\pm c_2\frac{F_1(F_1+1)+J(J+1)-I_1(I_1+1)}{4F_1(F_1+1)}(F_1+\tfrac{1}{2}\mp\tfrac{1}{2})+\frac{g_1g_2\mu_N^2}{r^3(2J+3)(2J-1)}\{3K_1g-2J(J+1)D'\}\frac{K}{2}$$

$$-\frac{\alpha^2\hbar^2}{2A}\frac{\left[3(M^2+\frac{1}{4})-F_1(F_1+1)\mp\dfrac{6M^2}{2F_1+1}\right][3D(D-1)-4F_1(F_1+1)J(J+1)]}{2J(J+1)(2J-1)(2J+3)2F_1(F_1+1)(2F_1-1)(2F_1+3)}$$

[7] [a] J. Bardeen and C. H. Townes, Phys. Rev. **73**, 97 (1948); [b] G. Racah, Phys. Rev. **62**, 438 (1942).
[8] H. B. G. Casimir, On the Interaction between Atomic Nuclei and Electrons (Teyler's Tweede Genootschap, 1936).
[9] J. M. B. Kellogg *et al.*, Phys. Rev. **57**, 677 (1940). It is shown that the spi-spin onperator can be written in this form.
[10] Nierenberg, Rabi, and Slotnick, Phys. Rev. **73**, 1430 (1948). Note that the term involving the field is different in this paper. Communication with W. Nierenberg established that a misprint was present in the reference.
[11] Reference given in reference 4. Note that the sign in front of the second term in the bracket differs from that of the reference.

in which

$$\mathbf{F}_1=\mathbf{I}_1+\mathbf{J};\quad \mathbf{F}=\mathbf{F}_1+\mathbf{I}_2;\quad K_1=F_1(F_1+1)-I_1(I_1+1)-J(J+1)$$

$$g=\frac{F_1(F_1+1)+J(J+1)-I_1(I_1+1)}{2F_1(F_1+1)};\quad D=F_1(F_1+1)+J(J+1)-I_1(I+1)$$

$$D'=\frac{F_1(F_1+1)+I_1(I_1+1)-J(J+1)}{2F_1(F_1+1)};\quad K=F(F+1)-F_1(F_1+1)-I_2(I_2+1)$$

$$\alpha=\mu E/(\hbar^2/2A).$$

The zeroth order eigenfunctions are characterized by the quantum numbers (J, I_1, F_1, I_2, F, M) and will be denoted $\phi(J, I_1, F_1, I_2, F, M)$. Terms 1, 3, and 4 of the Hamiltonian are diagonal in this representation. The contribution of terms 5 and 6 was computed by first-order perturbation theory which neglected off-diagonal elements connecting different F_1 states. The $-\boldsymbol{\mu}\cdot\mathbf{E}$ interaction has no diagonal matrix elements in this representation, and its contribution was computed by second order perturbation theory.

(B) Weak Field Case

For the weak field case the energy values are:[12]

(a) for $|m_{F_1}+m_2|\neq 0$

$$W_{J,I_1,F_1,m_{F_1}I_2,,m_2}=\frac{\hbar^2}{2A}J(J+1)-\frac{eq_1Q_1}{(2J-1)(2J+3)2I_1(2I_1-1)}\{\tfrac{3}{4}K_1(K_1+1)-I_1(I_1+1)J(J+1)\}+\frac{c_1K_1}{2}$$

$$-\frac{\alpha^2\hbar^2}{2A}\frac{[3m_{F_1}{}^2-F_1(F_1+1)][3D(D-1)-4F_1(F_1+1)J(J+1)]}{2J(J+1)(2J-1)(2J+3)2F_1(F_1+1)(2F_1-1)(2F_1+3)}+c_2m_2m_{F_1}g$$

$$+\frac{g_1g_2\mu_N{}^2}{r^3(2J+3)(2J-1)}\left[\frac{3}{2}\frac{m_2m_{F_1}D}{F_1(F_1+1)}-\frac{m_2m_{F_1}D'J(J+1)}{F_1(F_1+1)}\right]$$

(b) for $|m_{F_1}+m_2|=0$

$$W_{J,I_1,F_1,|\frac{1}{2}|,I_2,|\frac{1}{2}|}=\frac{\hbar^2}{2A}J(J+1)-\frac{eq_1Q_1}{(2J-1)(2J+3)2I_1(2I_1-1)}\{\tfrac{3}{4}K_1(K_1+1)-I_1(I_1+1)J(J+1)\}+\frac{c_1K_1}{2}$$

$$-\frac{\alpha^2\hbar^2}{2A}\frac{[3m_{F_1}{}^2-F_1(F_1+1)][3D(D-1)-4F_1(F_1+1)J(J+1)]}{2J(J+1)(2J-1)(2J+3)2F_1(F_1+1)(2F_1-1)(2F_1+3)}\pm\frac{c_2}{2}(F_1+\tfrac{1}{2}\mp\tfrac{1}{2})g$$

$$\pm\frac{g_1g_2\mu_N{}^2}{r^3(2J+3)(2J-1)}(F_1+\tfrac{1}{2}\mp\tfrac{1}{2})\left[\frac{3}{4}\frac{K_1D}{F_1(F_1+1)}-\frac{J(J+1)D'}{2F_1(F_1+1)}\right],$$

in which m_{F_1} is the projection of $\mathbf{F}_1$ on the field direction and m_2 is the projection of $\mathbf{I}_2$ on the field direction. The zeroth-order eigenfunctions are for case (a) characterized by the quantum numbers $(J, I_1, F_1, m_{F_1}, I_2, m_2)$ and will be denoted by $\phi(J, I_1, F_1, m_{F_1}, I_2, m_2)$. The eigenfunctions for case (b) have the quantum numbers $(J, I_1, F_1, |m_{F_1}|=\frac{1}{2}, I_2, |m_2|=\frac{1}{2})$ and are:

$$[\phi(J, I_1, F_1, \tfrac{1}{2}, I_2, -\tfrac{1}{2})+\phi(J, I_1, F_1, -\tfrac{1}{2}, I_2, +\tfrac{1}{2})]/\sqrt{2}$$

and

$$[\phi(J, I_1, F_1, \tfrac{1}{2}, I_2, -\tfrac{1}{2})-\phi(J, I_1, F_1, -\tfrac{1}{2}, I_2, +\tfrac{1}{2})]/\sqrt{2}.$$

(The first eigenfunction corresponds to the energy term with the upper signs.) With regard to the approximation involved in our result the same remarks apply for terms 1 to 4 as were made for the very weak field case. In the computation of the energy contribution of terms 5 and 6 first-order perturbation theory was employed and thus off-diagonal elements connecting different F_1 and m_{F_1} states were neglected.

(C) Strong Field Case[13]

The energy values are:

[12] This computation is readily made if we use the results of U. Fano, J. Research Nat. Bur. Stand. 40, 215 (1948) and the well-known matrix elements for angular momenta. (E. U. Condon and G. Shortley, *Theory of Atomic Spectra* (Cambridge University Press, London, 1935), Chapter III.)

[13] Reference cited in reference 10 contains solution to this case without the inclusion of the magnetic dipole-dipole interaction. Note that an omission appeared in formula (12) of the reference. The square sign (i.e., raise to power 2) is missing from the first set of inner brackets following the ± sign.

(a) For $|m_J| \neq 1$ or for $|m_J|=1$ and $|m_J+m_1|=I_1$ or I_1+1

$$W_{J,I_1,I_2,m_J,m_1,m_2}=\frac{\hbar^2}{2A}J(J+1)+\frac{\hbar^2}{2A}\alpha^2\left[\frac{J^2-m_J^2}{2J(2J-1)(2J+1)}-\frac{(J+1)^2-m_J^2}{2(J+1)(2J+1)(2J+3)}\right]$$
$$-eq_1Q_1\frac{[3m_J^2-J(J+1)]3m_1^2-I_1(I_1+1)]}{4I_1(2I_1-1)(2J-1)(2J+3)}+c_1m_1m_J+c_2m_2m_J+\frac{2g_1g_2\mu_N^2}{r^3(2J+3)(2J-1)}m_1m_J[3m_J^2-J(J+1)].$$

(b) For $|m_J|=1$ and $|m_J+m_1|<I_1$ there are two energy values:

$$W_{\pm}=\frac{\hbar^2}{2A}J(J+1)+\frac{\hbar^2}{2A}\alpha^2\left[\frac{J^2-1}{2J(2J-1)(2J+1)}-\frac{(J+1)^2-1}{2(J+1)(2J+1)(2J+3)}\right]$$
$$-eq_1Q_1\frac{[3-J(J+1)]\{[3m_1^2+6m_1+6]-I_1(I_1+1)\}}{4I_1(2I_1-1)(2J-1)(2J+3)}-c_1-\frac{2g_1g_2\mu_N^2[3-J(J+1)]}{r^3(2J+3)(2J-1)}$$
$$\pm\left\{\left[\frac{eq_1Q_1[3-J(J+1)]}{4I_1(2I_1-1)(2J-1)(2J+3)}(6m_1+6)+c_1(m_1+1)+c_2m_2+\frac{2g_1g_2\mu_N^2(m_1+1)}{r^3(2J-1)(2J+3)}[3-J(J+1)]\right]^2\right.$$
$$\left.+\left[\frac{3eq_1Q_1}{8I_1(2I_1-1)(2J-1)(2J+3)}\right]^2[(J+1)^2J^2(I_1-m_1)(I_1-m_1-1)(I_1+m_1+1)(I_1+m_1+2)]\right\}^{\frac{1}{2}}.$$

The zeroth order eigenfunctions for case (a) are characterized by the quantum numbers (J, I_1, I_2, m_J, m_1, m_2) and will be denoted $\phi(J, I_1, I_2, m_J, m_1, m_2)$. The two eigenfunctions for case (b) have the quantum numbers (J, I_1, I_2, $|m_J| \neq 1$, m_1, m_2) and will be linear combinations of the two states $\phi(J, I_1, I_2, 1, m_1, m_2)$ and $(J, I_1, I_2, -1, m_1+2, m_2)$. The correct linear combination can be chosen by the standard method of perturbation theory applied to two degenerate states.

The approximations involved in these results are (1) computation of the field energy to order α^2, (2) neglect of off-diagonal elements of the quadrupole operator which connect states with different field energy, (3) neglect of off-diagonal elements of all the other internal interactions which connect states with different field energies or different quadrupole energies.

III. SELECTION RULES

In the electric resonance experiments transitions are induced by an applied radiofrequency field between different stationary states of the molecules in a static electric field. We shall only be concerned with transitions which do not involve changes in the rotational energy, $\hbar^2J(J+1)/2A$.

Selection rules will be given by considering the matrix elements of the part of the Hamiltonian associated with the radiofrequency field between the initial and final states: $H'=-\boldsymbol{\mu}\cdot\mathbf{E}'e^{-i\omega t}$. In practice $\mathbf{E}'$ has its largest components in directions perpendicular to that of the static field $\mathbf{E}$ (z-direction), but there may also be an appreciable component in the z-direction as well.

We notice first that there can be no non-vanishing matrix elements between two states which are eigenstates of $\mathbf{J}^2$ with the same eigenvalue. This can be proved by expanding $\cos(\boldsymbol{\mu}, \mathbf{E}')$ with the aid of the addition theorem of spherical harmonics into terms involving either the factor $\cos\theta$ or $\sin\theta$ in which θ is the spherical coordinate angle between $\boldsymbol{\mu}$ and the z-axis. Such an expansion is possible provided the state is an eigenstate of $\mathbf{J}^2$. Since $\cos\theta$ and $\sin\theta$ have matrix elements[14] only when $\Delta J=\pm1$, the theorem is proved.

The transitions induced in the experiments occur because the static electric field perturbs a state which in the absence of the field would have a single J value, and thereby mixes in rotational states $J+1$ and $J-1$ in a first-order perturbation. There can be non-vanishing matrix elements of $-\boldsymbol{\mu}\cdot\mathbf{E}'$ between the perturbed part of a state whose zeroth order eigenfunction is characterized by a quantum number J and the zeroth order part of a final state which is also characterized by the value J. Another way of expressing this is to say that we have dipole radiation which occurs because of the dipole moment induced by the action of the static electric field on the molecule. We now consider in detail the selection rules which apply to the various field conditions treated in Section II.

(A) Very Weak Field

The zeroth order eigenfunctions are $\phi(J, I_1, F_1, I_2, F, M)$ and the $-\boldsymbol{\mu}\cdot\mathbf{E}$ interaction adds a perturbed first order state. But $-\boldsymbol{\mu}\cdot\mathbf{E}=-\mu_zE$ and μ_z is the z-component of a vector of the type $\mathbf{P}$ treated by Condon and Shortley.[15] This follows from the facts that $\mathbf{F}=\mathbf{F}_1+\mathbf{I}_2$, and $\boldsymbol{\mu}$ commutes with $\mathbf{I}_2$ and satisfies a certain commutation relation with respect to $\mathbf{F}$. Thus $-\boldsymbol{\mu}\cdot\mathbf{E}$ has

[14] E. U. Condon and G. Shortley, *Theory of Atomic Spectra* (Cambridge University Press, London, 1935), p. 53.

[15] Reference 14, p. 67. The proof that $\boldsymbol{\mu}$ is a $\mathbf{P}$ vector is given.

non-vanishing matrix elements only when $\Delta F=0, \pm1$, $\Delta M=0$, and $\Delta F_1=0, \pm1$. The discussion of the previous paragraph made clear that $\Delta J=\pm1$.

The components of the part of the Hamiltonian

$$H'=-\boldsymbol{\mu}\cdot\mathbf{E}'e^{-i\omega t}$$

are again those of a $\mathbf{P}$ vector. Hence non-vanishing matrix elements of H' exist only when $\Delta F=0, \pm1$, $\Delta F_1=0, \pm1$. Furthermore, for the term with μ_z, $\Delta M=0$ and for those with μ_x or μ_y, $\Delta M=\pm1$.

Thus from the results of the last two paragraphs we conclude that H' can induce a transition from a state with zeroth order eigenfunction $\phi(J, I_1, F_1, I_2, F, M)$ to another state with zeroth order eigenfunction $\phi(J, I_1, F_1', I_2, F', M')$ provided $\Delta F=0, \pm1, \pm2$ and $\Delta F_1=0, \pm1, \pm2$. For a radiofrequency field parallel to the static field $\Delta M=0$ and for a radiofrequency field perpendicular to the static field $\Delta M=\pm1$.

(B) Weak Field

The zeroth order eigenfunctions for the weak field case are:

$$\phi^0(J, I_1, F_1, m_{F_1}, I_2, m_2) \text{ for } M=m_{F_1}+m_2\neq0 \text{ (case (a))}$$

$$\begin{cases}[\phi^0(J, I_1, F_1, \frac{1}{2}, I_2, -\frac{1}{2})+\phi^0(J, I_1, F_1, -\frac{1}{2}, I_2, +\frac{1}{2})]/\sqrt{2} \\ \text{or} \qquad \text{for } M=0 \text{ (case (b))} \\ [\phi^0(J, I_1, F_1, \frac{1}{2}, I_2, -\frac{1}{2})-\phi^0(J, I_1, F_1, -\frac{1}{2}, I_2, +\frac{1}{2})]/\sqrt{2}.\end{cases}$$

Neither $-\boldsymbol{\mu}\cdot\mathbf{E}$ nor $-\boldsymbol{\mu}\cdot\mathbf{E}e^{-i\omega t}$ have matrix elements except for $\Delta m_2=0$. By an application of reasoning similar to that used for the "very weak" field case it follows that H' can induce a transition between two zeroth order eigenfunctions with the same J value provided $\Delta F_1=0, \pm1, \pm2$. For the z-component of $\mathbf{E}'$, $\Delta M=0$ and for case (a) states $\Delta m_{F_1}=0$, $\Delta m_2=0$, in addition. For the x or y components of $\mathbf{E}'$, $\Delta M=\pm1$, and a transition in which the initial and final states are case (a) states has, in addition, $\Delta m_{F_1}=\pm1$, $\Delta m_2=0$.

(C) Strong Field

The zeroth order eigenfunctions are:

$$\phi^0(J, m_J, I_1, m_1, I_2, m_2) \quad \text{for} \quad |m_J|\neq1 \quad \text{or} \quad |m_J|=1$$

and

$$|m_J+m_1|=I_1 \quad \text{or} \quad I_1+1 \quad \text{case (a)}$$

$$\begin{cases}a_1\phi^0(J, 1, I_1, m_1, I_2, m_2)+a_2\phi^0(J, -1, I_1, m_1+2, I_2, m_2) \\ \qquad =\psi_I \quad \text{for} \quad |m_J|=1, \quad |m_J+m_1|<I_1 \\ b_1\phi^0(J, 1, I_1, m_1, I_2, m_2)+b_2\phi^0(J, -1, I_1, m_1+2, I_2, m_2) \\ \qquad =\psi_{II} \quad \text{case (b)}.\end{cases}$$

The interaction with the static electric field will contribute a first-order perturbed eigenfunction:

$$\phi^{(1)}=\sum_{J'=J\pm1}\frac{[\phi^{(0)}(J', m_J, I_1, m_1, I_2, m_2)|-\boldsymbol{\mu}\cdot\mathbf{E}|\phi^{(0)}(J, m_J, I_1, m_1, I_2, m_2)]}{W_{J, m_J, I_1, m_1, I_2, m_2}-W_{J', m_J, I_1, m_1, I_2, m_2}}\phi^{(0)}(J', m_J, I_1, m_1, I_2, m_2) \text{ case (a)}.$$

There is a similar expression for the case (b) states. The added states for either unperturbed state are of the form of ψ_I and ψ_{II} but with $J\pm1$ substituted for J. This is seen to be true because $-\boldsymbol{\mu}\cdot\mathbf{E}$ has non-vanishing matrix elements only between wave functions with the same values of the quantum numbers $(m_J, I_1, m_1, I_2, m_2)$ and $J'=J\pm1$. Thus H' can induce transitions between states with the same value of J provided $\Delta m_2=0$. For the z-component of $\mathbf{E}'$, $\Delta(m_J+m_1)=0$. In addition, for case (a) states $\Delta m_J=\pm1$, $\Delta m_1=0$ and thus the initial and final states are identical. For the x and y components of $\mathbf{E}'$, $\Delta(m_J+m_1)=\pm1$, and, in addition, for case (a) states $\Delta m_J=\pm1$, $\Delta m_1=0$.

It should be remarked that the selection rules derived in this section apply only in the approximation to which the perturbation theory has been carried. A breakdown of these selection rules will appear if a higher order of perturbation theory is applied.

IV. LINE INTENSITIES

The problem of the line intensities in molecular beam electric resonance experiments is made difficult by certain features of the experimental arrangement. These features will be discussed later in this section.

(A) Observability Criterion

We now consider the so-called observability criterion, i.e., whether or not a transition which is allowed by the selection rules will actually be observed. In order to be observed a transition must be induced in the C-field which will result in a different deflection of the molecule in the B-field than would occur in the absence of the transition. If there is an adiabatic correspondence between the state of a molecule in the C-field and its state in the B-field, the transition in order that it shall be observed must be induced between two states in the B-field with different values of $|m_J|$, because the deflection of the molecule in the B-field depends on $|m_J|$.

We now develop rules to establish the adiabatic correspondence between states under C-field conditions and under B-field conditions. Usually in practice the static electric field intensity in the C-field region is much smaller than that in the B-field region and different sets of quantum numbers are required to specify states in the two cases. We consider a three vector system $(\mathbf{I}_1, \mathbf{I}_2, \mathbf{J})$ in the absence of an electric field. A stationary state is characterized by an eigenvalue of the total angular momentum $\mathbf{F}$ and of the

component, M, of the total angular momentum in an arbitrary direction. Consider now that an electric field of any magnitude is applied in an adiabatic fashion. The total angular momentum **F** need no longer be a good quantum number but the component, M, in the field direction is a constant of the motion. Two rules suffice to establish the correspondence between a state at zero field and at an arbitrary field: (1) The M value is the same. (2) In the adiabatic transition from the zero field states to the arbitrary field states two states with like M values never coincide in energy.

An outline of proofs of these two rules will now be given. That the component of the total angular momentum in the direction of the applied field remains constant under adiabatic change of the field value follows immediately from the fact that this quantity is a good quantum number independent of the field value.

That states with the same M value do not coincide in energy at any field value is a special case of the following general theorem.[16] Consider a Hermitian matrix (H_{jk}) whose n^2 complex quantities depend on certain real parameters $\lambda_1, \lambda_2 \cdots$. For a certain set of values of the parameters we assume that the matrix is general, i.e., no relationship exists between the H_{jk} which does not follow from the Hermitian character of the matrix. In particular, then, for this set of values of the parameters the eigenvalues of the matrix are distinct. The theorem states that three λ-values must be changed in order to achieve coincidence of two eigenvalues of (H_{jk}). If (H_{jk}) is a real Hermitian matrix then it is sufficient to change two λ-parameters in order to bring two eigenvalues into coincidence.

The matrix elements of the Hamiltonian (1) constitute a real Hermitian matrix whose elements we regard as functions of the field parameter, **E**. The component, M, of the total angular momentum in the direction of the applied electric field is a good quantum number; i.e., there are no matrix elements of the Hamiltonian connecting eigenstates with different M values. Hence, by the proper choice of representation, the matrix for the Hamiltonian can be split into submatrices which refer to different M values. If the eigenvalues of any one of these submatrices are distinct at zero field, the general theorem stated above assures that the eigenvalues will not coincide for any value of the electric field. In the special cases of interest to us we show that the eigenvalues referring to a given M value are indeed distinct at zero field.

A number of examples of the application of the observability criterion are to be found in the paper on[1] $K^{39}F$ and[2] RbF. It should be emphasized that the observability criterion that we have taken assumes that there are no non-adiabatic transitions induced as the molecule passes from the C-field to the B-field. The effective frequencies that a molecule sees as it passes from the C-field to the B-field are believed to be of the order of several hundred kc/sec. Such frequencies are small compared to the transition frequencies observed, so non-adiabatic transitions of the type of the transitions observed are not expected. It is possible, however, that lower frequency non-adiabatic transitions do occur. These involve essentially a reorientation of the molecular system with respect to the field direction.[17] The refocusing of a $(1, \pm 1)_A - (1, 0)_B$ beam[1] proves that non-adiabatic transitions occur somewhere in the region between the A- and B-fields. It is probable that these non-adiabatic transitions occur between the A- and C-fields because, owing to the presence of the collimator slit, the electric field conditions may be highly variable in this inter-field region. Non-adiabatic transitions between the A- and C-fields will influence the distribution of states present in the C-field and hence are important in determining what transitions will be seen.

(B) Relative Line Intensities

The line intensity problem in these experiments is complicated by the following features of the experimental arrangement.

(1) The distribution of the molecules of interest among the various states that they can have in the C-field region is not known. By molecules of interest is meant molecules which have passed through the A-field in a certain state of space quantization which depends on the refocusing conditions being employed. Only for such molecules can a transition induced in the C-field be observed. The distribution of these molecules among the states that they can have in the C-field region is not known because the exact character of the non-adiabatic transitions that occur in the interfield region between the A- and C-fields is not known. Relative line intensities will depend on the exact distribution of these molecules.

(2) The intensity of the radiofrequency field is adjusted to be high so that the maximum intensity of transition is observed. Hence the transition probability cannot be taken as simply proportional to the square of the product of a matrix element by the radiofrequency field intensity. It depends rather in the simple two state case upon a sin^2-function of these two quantities.[18] Relative line intensities will then depend upon the intensity of the radiofrequency field. But the exact value of the field is not known and cannot be determined easily.

V. HALF-FREQUENCY TRANSITIONS

Conditions are sometimes encountered experimentally in which the amplitude of the radiofrequency field is high compared with that of the static field. In this case we must consider the field free state as perturbed primarily by the radiofrequency field, and the transition, also induced by the radiofrequency field, is from the perturbed part of the initial state to the unperturbed

[16] J. Von Neumann and E. Wigner, Physik. Zeits. **30**, 467 (1929).

[17] E. Majorana, Nuovo Cimento **9**, (1932).

[18] H. C. Torrey, Phys. Rev. **59**, 293 (1941).

part of the final state. It will be shown that in this circumstance a transition between two states m and n can be induced at a frequency of $(E_m-E_n)/2h$. Such a half-frequency transition can be regarded as a transition in which two quanta supply the energy for the transition.

We consider the time dependent perturbation of a state $\phi(J, I_1, F_1, I_2, F, M)$ by the radiofrequency field $\mathbf{E}'e^{-i\omega t}$ in the absence of a static field. M is the component of $\mathbf{F}$ in the direction of the z-axis, which is the direction in which the static field is normally applied. We use formulas (240_1) and (240_2) of Pauli's *Handbuch* article.[19] The initial states (n) will be $\phi_n^{(0)}(J, I_1, F_1, I_2, F, M)$. The energy does not depend on M, since no static field is to be present, but such a function is a suitable zeroth order eigenfunction for the perturbation calculation. The final states (m) will be $\phi_m^{(0)}(J, I_1, F_1'', I_2, F'', M'')$ in which J is the same as for the initial state.

$$\Omega'_{kl}=[k|\mathfrak{y}\cdot\mathbf{E}'|l]e^{-i\omega t}\exp\left[\frac{i}{\hbar}(E_k^0-E_l^0)t\right]$$

is our perturbing matrix element

$$a_m^{(1)}(t)=-\frac{i}{\hbar}\sum_n a_{n(0)}{}^{(0)}\int_0^t\Omega'_{mn}(t)dt$$

in which the a's are state amplitudes and the superscripts refer to the order of perturbation.

This first-order perturbation yields a zero result since there are no matrix elements of Ω' between states with the same J. Second-order perturbation theory yields:

$$\begin{aligned}a_m^{(2)}(t)&=-\frac{1}{\hbar^2}\sum_n a_{n(0)}{}^{(0)}\sum_l\int_0^t\Omega'_{ml}(\tau)d\tau\int_0^\tau\Omega'_{l,n}(\tau')d\tau'\\&=-\frac{1}{\hbar^2}\sum_n a_{n(0)}{}^{(0)}\sum_l[m|\mathfrak{y}\cdot\mathbf{E}'|l][l|\mathfrak{y}\cdot\mathbf{E}'|n]\\&\quad\times\left\{\int_0^t e^{-i\omega\tau}\exp\left[\frac{i}{\hbar}(E_m^{(0)}-E_l^{(0)})\tau\right]d\tau\right.\\&\qquad\left.\times\int_0^\tau e^{-i\omega\tau'}\exp\left[\frac{i}{\hbar}(E_l^{(0)}-E_n^{(0)})\tau'\right]d\tau'\right\}.\end{aligned}$$

Evaluation of the bracketed expression yields:

$$\{\ \}=\frac{\exp\left[-i2\omega t+\frac{i}{\hbar}(E_m^{(0)}-E_n^{(0)})t\right]-1}{\left[-i\omega+\frac{i}{\hbar}(E_l^{(0)}-E_n^{(0)})\right]\left[-2\omega i+\frac{i}{\hbar}(E_m^{(0)}-E_n^{(0)})\right]}-\frac{\exp\left[-i\omega t+\frac{i}{\hbar}(E_m^{(0)}-E_l^{(0)})t\right]}{\left[-i\omega+\frac{i}{\hbar}(E_l^{(0)}-E_n^{(0)})\right]\left[-i\omega+\frac{i}{\hbar}(E_m^{(0)}-E_l^{(0)})\right]}.$$

[19] W. Pauli, *Handbuch der Physik* (J. Springer, Berlin, 1933), second edition, Vol. 24/1.

The l states are all intermediate states which differ in rotational energy from the m and n states (the latter two states differ in quadrupole energy). Hence

$$\omega\ll\frac{E_l^{(0)}-E_n^{(0)}}{\hbar}\quad\text{or}\quad\frac{E_n^{(0)}-E_l^{(0)}}{\hbar}.$$

There can be no resonance for the second term at the frequencies we employ so it can be neglected. However, resonance can occur for the first expression which becomes:

$$\frac{\exp[-i2\omega t+i/\hbar(E_m^{(0)}-E_n^{(0)})t]-1}{i/\hbar(E_l^{(0)}-E_n^{(0)})[-2\omega i+i/\hbar(E_m^{(0)}-E_n^{(0)})]}.$$

Our entire expression then becomes

$$a_m^{(2)}(t)=\frac{1}{\hbar^2}\sum a_{n(0)}{}^{(0)}\sum_l\frac{(m|\mathfrak{y}\cdot\mathbf{E}'|l)(l|\mathfrak{y}\cdot\mathbf{E}'|n)}{[(E_l^{(0)}-E_n^{(0)})/\hbar]}\times\frac{\exp[-i2\omega t+i/\hbar(E_m^{(0)}-E_n^{(0)})t]-1}{[-2\omega+(E_m^{(0)}-E_n^{(0)}/\hbar)]}.$$

Normally we have a well-defined initial state, so there is no sum over n, and we get

$$a_m^{(2)}=\frac{1}{\hbar^2}a_{n(0)}{}^{(0)}\sum_l\frac{(m|\mathfrak{y}\cdot\mathbf{E}'|l)(l|\mathfrak{y}\cdot\mathbf{E}'|n)}{[(E_l^{(0)}-E_n^{(0)})/\hbar]}\times\frac{\exp[-i2\omega t+i/\hbar(E_m^{(0)}-E_n^{(0)})t]-1}{[-2\omega+(E_m^{(0)}-E_n^{(0)})/\hbar]}.$$

Resonance occurs at: $\omega=(E_m^{(0)}-E_n^{(0)})/2\hbar$. The expression for $a_m^{(2)}$ is of the same form as the corresponding one for the normal transition with the principal exception that 2ω appears instead of ω. For the normal transition the matrix element $(l|\mathfrak{y}\cdot\mathbf{E}'|n)$ would be replaced by $(l|\mathfrak{y}\cdot\mathbf{E}|n)$ in which $\mathbf{E}$ is the static field intensity.

The selection rules for these half-frequency transitions are given by the following considerations. Non-vanishing matrix elements $(m|\mathfrak{y}\cdot\mathbf{E}'|l)$ and $(l|\mathfrak{y}\cdot\mathbf{E}'|n)$ exist when $\Delta J=\pm1$, $\Delta F_1=0$, ±1, and $\Delta F=0$, ±1. Furthermore, if $\mathbf{E}'$ is perpendicular to the z-axis $\Delta M=\pm1$ and if $\mathbf{E}'$ is parallel to the z-axis $\Delta M=0$ (see Section III). Thus over-all selection rules for transitions from a state n to a state m with the same eigenvalue of $\mathbf{J}^2$ are $\Delta F_1=0$, ±1, ±2, $\Delta F=0$, ±1, ±2. If $\mathbf{E}'$ is perpendicular to the z-axis $\Delta M=0$, ±2; if $\mathbf{E}'$ has a component parallel to the z-axis as well $\Delta M=0$, ±1, ±2. It will be noted that these selection rules are the same as for the normal case except for the selection rule involving M. Hence in so far as the M selection rule does not affect the situation all transitions are possible at the half-frequency which are possible at the normal frequency.

A study of the sums

$$\sum_l\frac{(m|\mathfrak{y}\cdot\mathbf{E}'|l)(l|\mathfrak{y}\cdot\mathbf{E}'|n)}{[(E_l^{(0)}-E_n^{(0)})/\hbar]}\quad\text{and}\quad\sum_l\frac{(m|\mathfrak{y}\cdot\mathbf{E}'|l)(l|\mathfrak{y}\cdot\mathbf{E}|n)}{[(E_l^{(0)}-E_n^{(0)})/\hbar]}$$

in which $\mathbf{E}$ is the static field intensity will give a measure of the transition probabilities for the half-frequency transitions ($\mathbf{E}=0$) and for the normal transitions ($\mathbf{E}\neq 0$, $\omega=(E_m-E_n)/\hbar$) respectively. It was found for the case of interest to us ($J=1$ in the initial and final states) that these sums are comparable provided $\mathbf{E}'$ and $\mathbf{E}$ are of the same magnitude. Hence, if a normal transition is observed when $\mathbf{E}'$ and $\mathbf{E}$ are equal, it is expected that a half-frequency transition will be observed with this same value of $\mathbf{E}'$ when $\mathbf{E}=0$.

The theory of half-frequency transitions in the presence of a static field is easily worked out. The representation $\phi(J, I_1, F_1, I_2, F, M)$ is applicable provided the static field is sufficiently weak. The expression $a_m^{(2)}$ for the case of zero field is modified to read:

$$a_m^{(2)}=-\frac{1}{\hbar^2}\sum_n a_n^{(0)}\sum_l (m|\mu\cdot\mathbf{E}'|l)(l|\mu\cdot\mathbf{E}'|n)\{\ \}$$

in which

$$\{\ \}=\frac{\exp\left[-i2\omega t+\frac{i}{\hbar}(E_m^{(0)}-E_n^{(0)})t\right]-1}{\left[-i2\omega+\frac{i}{\hbar}(E_m^{(0)}-E_n^{(0)})\right]\left[-i\omega+i\frac{E_l^{(0)}-E_n^{(0)}}{\hbar}\right]}$$

$$-\frac{\exp\left[-i\omega t+\frac{i}{\hbar}(E_m^{(0)}-E_l^{(0)})t\right]-1}{\left[-i\omega+\frac{i}{\hbar}(E_m^{(0)}-E_l^{(0)})\right]\left[-i\omega+i\frac{E_l^{(0)}-E_n^{(0)}}{\hbar}\right]}.$$

There is now a sum over a number of states n because our initial state is no longer a pure state $\phi(J, I_1, F_1, I_2, F, M)$, but involves a mixture of such states due to the perturbing effect of the static electric field. If the initial state were $\phi(J, I_1, F_1, I_2, F, M)$ in the absence of a static field, it will involve the states $\phi(J', I_1, F_1', I_2, F', M)$ in which $J'=J\pm 1$, $F_1'=F_1$, $F_1\pm 1$; $F'=F$, $F\pm 1$. Resonance occurs when $\omega=(E_m^{(0)}-E_n^{(0)})/2\hbar$ caused by the first factor within the brackets exactly as for the case of zero static field; at this resonance the second factor in the brackets is negligibly small. There is, of course, a first-order $a_m^{(1)}$ in this case which leads to the normal transitions between two states which at zero field have the same J value.

If the static field is sufficiently large so that the interaction of the field with the dipole moment is larger than the internal molecular interactions involving $\mathbf{I}_2$, then a weak field representation should be used. The resonance at the half-frequencies is predicted exactly as above. The transition probability is reduced somewhat, however, because the amplitude of that part of the initial state which is involved in the half-frequency transition $[\phi(J, I_1, F_1, I_2, F, M)]$ is reduced by the perturbation due to the static field.

If the static field is sufficiently large so that a strong field condition applies $[\mu^2E^2/(\hbar^2/2A)\gg eq_1Q_1]$ and if the radiofrequency field is perpendicular to the static field, then the M selection rule becomes $\Delta m_2=0$, $\Delta m_1=0$, $\Delta m_J=0, \pm 2$. Such a transition would not be observed for a $J=1$ state molecule because the deflection of a molecule in the A and B fields depends only upon $|m_J|$.

Professor I. I. Rabi first pointed out to us the possibility of half-frequency transitions. Also we wish to thank him for many stimulating discussions.

PHYSICAL REVIEW VOLUME 79, NUMBER 5 SEPTEMBER 1, 1950

Hyperfine Structure and Isotope Shift in Barium

O. H. ARROE
University of Wisconsin, Madison, Wisconsin*
(Received March 22, 1950)

Spectroscopic hyperfine structure studies with separated isotopes of barium have definitely confirmed a nuclear spin $\frac{3}{2}$ for the odd isotopes Ba^{135} and Ba^{137}. The lines of the even isotopes show no structure. The isotope shift is linear among masses of the same parity, but there is a relatively great odd-even shift: Note the order 138, 136, 134, 137, 135 in BaI, and 138, 136, 137, 134, 135 in BaII. The relative positions of the components (centroids, for odd masses) of the resonance lines, in $10^{-3}\pm 0.7.10^{-3}$ cm^{-1} are

	138	137	136	135	134
BaI $6s^2\,{}^1S_0-6s6p\,{}^1P_1$	0	+5.2	+2.2	+7.4	+4.4
BaII $6s\,{}^2S_{\frac{1}{2}}-6p\,{}^2P_{\frac{1}{2}}$	0	+6.0	+4.8	+11.1	+9.6
$6s\,{}^2S_{\frac{1}{2}}-6p\,{}^2P_{\frac{3}{2}}$	0	+6.4	+5.4	+12.6	+10.8

I. INTRODUCTION

SINCE hyperfine structure in the barium spectrum was reported by McLennan and Allen,[1] several investigators have tried to use the structure they found in several lines to determine the nuclear spin of the odd isotopes Ba^{135} and Ba^{137}. From the data of Ritschl and Sawyer,[2] Schuler and Jones[3] found the nuclear spin to

* Supported by Navy contract N7onr-285TO #1, NR 019 107.
[1] J. C. McLennan and E. J. Allen, Phil. Mag. **8**, 515 (1929).
[2] R. Ritschl and R. A. Sawyer, Zeits. f. Physik **72**, 36 (1931).
[3] H. Kallman and H. Schuler, Ergeb. d. exakt. Naturwiss. **11**, 134 (1932).

TABLE I. Ba isotope samples.

Conc. of in	130	132	134	135	136	137	138
"134"	0.032	0.079	51.39	20.94	7.06	4.42	16.08
"135"	0.019	0.032	1.475	67.32	12.35	5.63	13.17
"137"	0.02	0.02	0.07	0.29	1.67	38.98	58.97
"138"	0.101	0.097	2.42	6.59	7.81	11.32	71.66

"138" = natural barium

be $\frac{3}{2}$ for Ba^{137}, the more abundant of the odd isotopes. From intensity measurements Kruger, Gibbs, and Williams[4] found a most probable value of 5/2, while Murakawa[5] suggested $\frac{3}{2}$, after measurements of the same lines, which were mainly the BaII resonance lines $6s\,^2S_{\frac{1}{2}}-6p\,^2P_{\frac{1}{2},\frac{3}{2}}$. Benson and Sawyer[6] found the same result as did Murakawa from an investigation of more lines than had been considered before. Using a molecular beam resonance method and taking the value $\frac{3}{2}$ for the nuclear spin, Hay[7] found the magnetic dipole moments of Ba^{137} and Ba^{135} to be +0.9354 and +0.8363 nuclear magneton, respectively, with the ratio 1.1174±0.0010. Kopfermann and Wessel[8] tried to resolve the very small isotope shift in the BaI resonance line $6s^2\,^1S_0-6s6p\,^1P_1$ by atomic beam absorption. They found a shift of the lighter isotopes to higher frequency, dependent only upon the mass difference, with a distance of $12\cdot10^{-3}$ cm^{-1} between isotopes two mass units apart.

A serious difficulty in all investigations has been the great abundance of the even barium isotopes. In the present investigation of nuclear spin and isotope shift enriched samples[9] of the isotopes Ba^{134}, Ba^{135}, and Ba^{137} have been used. The isotopic constitution of the samples used is shown in Table I.

II. EXPERIMENTAL

The light source used was the specially constructed liquid-air-cooled hollow cathode described elsewhere,[10] in connection with a Hilger constant deviation spectrometer with a 60-mm aperture lens and prism system and focal lengths, respectively, 55 and 125 cm for the collimator and the camera. A Fabry-Perot interferometer with separators up to 40 cm and a corresponding resolving power of $3.5\cdot10^6$ was placed in the parallel beam between the collimator and the prism. The total half-intensity line width was about 0.018 cm^{-1}, corresponding to a temperature in the discharge about 20° above that of liquid air.

During the investigation of the very small isotope shift, exposures with the different isotopes were taken successively on the same photographic plate, which was moved in its own plane, perpendicular to the lines, making it possible to detect a shift of the order $1\cdot10^{-3}$ cm^{-1}. The exposure times ranged from less than one minute for the resonance lines to about one hour for the weakest of the lines.

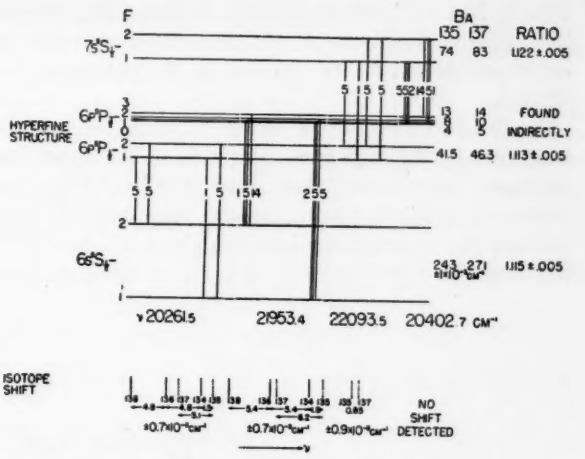

FIG. 1. Hyperfine structure in the lines $6s\,^2S_{\frac{1}{2}}-6p\,^2P_{\frac{1}{2},\frac{3}{2}}$ and $6p\,^2P_{\frac{1}{2},\frac{3}{2}}-7s\,^2S_{\frac{1}{2}}$ of Ba.

III. RESULTS

The hyperfine structure found in the lines $6s\,^2S_{\frac{1}{2}}-6p\,^2P_{\frac{1}{2},\frac{3}{2}}$ and $6p\,^2P_{\frac{1}{2},\frac{3}{2}}-7s\,^2S_{\frac{1}{2}}$ is shown in Fig. 1. This structure gives a verification of the nuclear spin $\frac{3}{2}$ for both odd isotopes, and the ratio found between corresponding intervals for the two isotopes agrees within the uncertainty with the ratio 1.1174 given by Hay.

The non-linear isotope shift found in the lines requires further explanation than a pure mass effect, such as possibly a difference between odd and even isotopes in nuclear polarizability[11] by electrons as well as a linear effect for mass numbers of the same parity. The same is the case qualitatively for the isotope shift in the BaI resonance line $6s^2\,^1S_0-6s6p\,^1P_1$, which is shown in

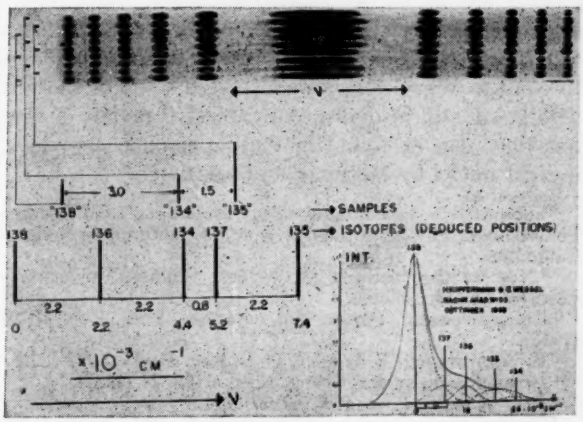

FIG. 2. Isotope shift in the BaI line $6s^2\,^1S_0-6s6p\,^1P_1$.

[4] Kruger, Gibbs, and Williams, Phys. Rev. **41**, 722 (1932).
[5] K. Murakawa, Sci. Pap. Inst. Phys. Chem. Research, Tokyo **18**, 304 (1932).
[6] A. N. Benson and R. A. Sawyer, Phys. Rev. **52**, 1117 (1937).
[7] R. H. Hay, Phys. Rev. **60**, 75 (1941).
[8] H. Kopfermann and G. Wessel, Nachr. d. Wissenschaften in Göttingen, Math.-Phys. 53 (1948).
[9] Produced by the Y-12 plant, Carbide and Carbon Chemicals Division, and obtained by allocation from the AEC.
[10] O. H. Arroe and J. E. Mack, J. Opt. Soc. Am. **40**, 387 (1950).
[11] Breit, Arfken, and Clendenin, Phys. Rev. **77**, 569 (1950); **78**, 390 (1950).

Fig. 2. Not only the magnitude of the shift, but also the relative positions of odd and even isotopes, are incompatible with the results of Kopfermann and Wessel.

In the BaI line $6s^2\,{}^1S_0-6s6p\,{}^1P_1$ both the odd isotopes are to the high frequency side of the three even isotopes, but in the BaII lines $6s\,{}^2S_{\frac{1}{2}}-6p\,{}^2P_{\frac{1}{2},\frac{3}{2}}$ the odd-even shift is approximately only half as great relative to the two-mass-unit shift, and 137 is situated between 136 and 134. In finding the deduced positions of the isotopes in the BaI line, it was necessary to assume that the even isotopes were evenly spaced, as was found to be the case in the BaII lines.

The investigations are being continued in an attempt to determine the shift in the transitions $6s^2\,{}^1S_0-6s6p\,{}^3P_1{}^0$ and $6s6p\,{}^3P_1{}^0-6p^2\,{}^3P_{0,1,2}$.

This work was carried out under the direction of Professor J. E. Mack, to whom the author wishes to express his gratitude for his encouragement and many valuable suggestions.

PHYSICAL REVIEW VOLUME 79, NUMBER 5 SEPTEMBER 1, 1950

Li^8 Splinters from Nuclear Bombardments*

S. COURTENAY WRIGHT**
Radiation Laboratory, Department of Physics, University of California, Berkeley, California
(Received April 28, 1950)

Li^8 has been produced by 340-Mev proton and 190-Mev deuteron bombardments of C, N, Ne, A, Kr, and Xe. The target element formed the gas of a proportional counter. The 0.88-second beta-decay of Li^8 produces Be^{8*} which disintegrates into two alpha-particles with a half-life of 10^{-21} seconds. Li^8 was detected by observation of these alpha-particles and identified by its half-life. Deuteron excitation functions for the production of Li^8 are given for C, N, Ne, and A. In the case of 190-Mev deuterons the cross section varies from about 13×10^{-28} cm² for C to 4×10^{-29} cm² for Xe. For 340-Mev protons the variation is from about 7×10^{-28} cm² for C to 3×10^{-29} cm² for Xe. A discussion of the process involved is given.

I. INTRODUCTION

SINCE the discovery of Li^8 by Crane *et al.*,[1] in 1935, its characteristics have been studied extensively. The ground state of Li^8 is probably $^3P_2$ according to Feenberg and Wigner.[2] It beta-decays with a 0.88 second half-life[3] to several excited states of Be^8. The maximum energy of the beta-particle is about 13 Mev. According to Wheeler[4] the principal Be^8 level involved is a $^1D_2$ state situated 3.3 Mev above the ground state and with a width of 1.8 Mev. The Be^8 nucleus breaks up promptly (10^{-21} seconds) into two alpha-particles. The total energy spectrum of the two alpha-particles gives a picture of the parent Be^8 level, apart from a small recoil energy from the original beta-decay. Recent experiments by Bonner *et al.*,[5] and Christy *et al.*,[6] tend to confirm Wheeler's views although some of the finer details are still in doubt. An extensive review of these questions can be found in the paper on energy levels in light nuclei by Hornyak and Lauritsen.[7]

Segrè and Wiegand[8] in an unsuccessful search for delayed proton emitters corresponding to the delayed neutron emitter N^{17} observed an alpha-particle activity of approximately 1 sec. half-life in 190-Mev deuteron bombardments of several elements. They ascribed this activity to Be^8 formed from Li^8. Their identification of this activity was based on the absence, apart from samarium, of other alpha-emitters in elements below lead and the similarity between the observed half-life and that of Li^8.

The purpose of this experiment was to study the systematics of Li^8 production in high energy bombardments of various elements. Li^8 has a convenient half-life and the alphas from its disintegration[8a] may be easily detected in the presence of other beta-activities. These factors make this isotope an amenable fragment to study in high energy nuclear disintegrations.

The average range of the alphas from Li^8 is about 1.3 mg/cm² of Al. This combined with the low cross section made the use of solid targets impractical. By the use of gaseous targets the yield in the counter was increased by a factor of 50 as will be described below. These gaseous targets also formed the counter gas. The absolute cross sections for Li^8 production in 340-Mev proton and 190-Mev deuteron bombardments of C, N, Ne, A, Kr, and Xe were determined. The deuteron excitation functions were obtained for all gases men-

* Submitted in partial requirement for the degree of Doctor of Philosophy in Physics at the University of California at Berkeley, California.

** Now at the Institute for Nuclear Studies, University of Chicago, Chicago, Illinois.

[1] Crane, Delsasso, Fowler, and Lauritsen, Phys. Rev. **47**, 971 (1935).

[2] E. Feenberg and E. Wigner, Phys. Rev. **51**, 95 (1937).

[3] Lewis, Burcham, and Chang, Nature **139**, 24 (1937).

[4] J. A. Wheeler, Phys. Rev. **59**, 27 (1941).

[5] Bonner, Evans, Malich, and Risser, Phys. Rev. **73**, 884 (1948).

[6] Christy, Cohen, Fowler, Lauritsen, and Lauritsen, Phys. Rev. **72**, 698 (1947).

[7] W. F. Hornyak and T. Lauritsen, Rev. Mod. Phys. **20**, 191 (1948).

[8] E. Segrè and C. Wiegand, private communication.

[8a] In the future for brevity the intermediate Be^8 state will be omitted in references to the decay of Li^8; i.e. Li^8 beta-decays to two alpha-particles.

tioned except Kr and Xe in which cases the yield was too small to make the measurement of a complete excitation function feasible.

Very recently Alvarez[9] has reported a 0.5 second activity which he ascribed tentatively to B^8 or C^9. Alpha-particles similar to those from Be^8 are involved in this decay and if the B^8 identification is correct it is likely that the alphas have the same origin as those from the decay of Li^8. In this case some of the alphas observed in the experiment reported here have probably been incorrectly assigned as originating from Li^8. Because of the increased barrier for the expulsion of B^8 over that for Li^8 the error involved should not be important for the heavier elements. For the light elements where it is believed that the Li^8 produced is the residue of a nucleus which has evaporated the necessary number of protons and neutrons, the error may become more important. However the half-life determinations show that in any event the effect of B^8 is small.

Lately the expulsion of heavy charged particles from nuclei has been receiving increasing attention. Experiments dealing with this phenomenon have been carried out in cosmic-ray studies using the recently developed electron-sensitive photographic emulsions. The identification of the charge of the fragments has been accomplished by an analysis of the delta-rays. Previous to these studies only Li^8 could be positively identified. Its trademark is a "hammer" track—the handle caused by the expelled Li^8, the head by the resultant alphas. An example of such an event is given by Freier *et al.*[10] The work of Hodgson and Perkins,[11] Bonetti and Dilworth,[12] Sorensen,[13] and Freier *et al.*,[10] indicates that most of the events involve several hundred Mev and their lack of isotropy points toward a knock-on process rather than to evaporation. It is hoped that the cross sections for Li^8 production found in this experiment will be of use in the clarification of these newly found reactions.

II. EXPERIMENTAL

Once Li^8 had been observed to be produced in deuteron bombardments the principal problem became one of intensity. The alphas used to detect Li^8 have a most probable energy of 1.5 Mev each. Thus with a thick carbon target in an ionization chamber, a 1 mbarn cross section, and a beam of 3×10^{-5} μamp., only about 3 Li^8 atoms will exist in the counting volume of the chamber under equilibrium conditions. This is too few atoms with which to deal effectively. However if the target is CH_4 at 1 atmos. in a proportional counter of effective counting length A cm and the counter axis is along the path of the beam, the number of Li^8 atoms existing under similar conditions will be 7A, an adequate number for this experiment. The gaseous target has the following advantages over the solid target: (1) a factor of four is gained in geometry over the thick target; (2) there is no self-absorption; (3) the thickness of the target is limited only by the length of the counter; and (4) possible targets, especially the rare gases, are available in a high state of purity. However, there are certain disadvantages, namely: (1) the number of target elements is limited since each must perform the role of a proportional counter gas; and (2) the characteristics of a proportional counter will vary with each gas used, which is deleterious in this case because the natural spread in energy of the Li^8 alphas will produce a flat bias curve below 1 Mev only under ideal conditions.

The essence of the experiment was the following. A proportional counter filled with the gas under investigation was traversed axially by the cyclotron beam. When Li^8 equilibrium was almost reached the beam was turned off and, after a short delay, the alphas were counted for nine half-lives of Li^8. This process was repeated periodically. The number of Li^8 atoms present at the end of a bombardment will be proportional to $\int I(t)e^{-\lambda t}dt$ where $I(t)$ is the current at the time t before the end of the bombardment and λ is the disintegration constant of Li^8. $\int I(t)e^{-\lambda t}dt$ will in future be called the effective charge. It is that charge which will, if delivered instantaneously at the end of the bombardment, produce the same quantity of Li^8 as the actual current used in the experiment. The measurement of the effective charge can be performed naturally or numerically as will be described below. The former method of integration was used in the measurement of relative yields, the latter in the determination of absolute cross sections. In practice all yields per unit effective charge were referred to that from carbon using the full energy beam. The absolute cross section was later measured for carbon itself. In this way all the cross sections were placed on an absolute scale.

The experimental arrangement employed was that schematically illustrated in Fig. 1. Proportional counter A had a $\frac{1}{2}$ inch i.d. and an effective counting length of

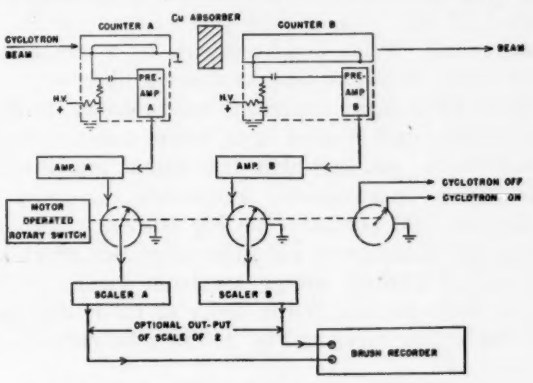

FIG. 1. Schematic diagram of the apparatus.

[9] L. Alvarez, unpublished work.
[10] Freier, Lofgren, Ney, Oppenheimer, Bradt, and Peters, Phys. Rev. 74, 213 (1948).
[11] P. E. Hodgson and D. H. Perkins, Nature 163, 439 (1949).
[12] A. Bonetti and C. Dilworth, Phil. Mag. 40, 585 (1949).
[13] S. O. C. Sorensen, Phil. Mag. 40, 947 (1949).

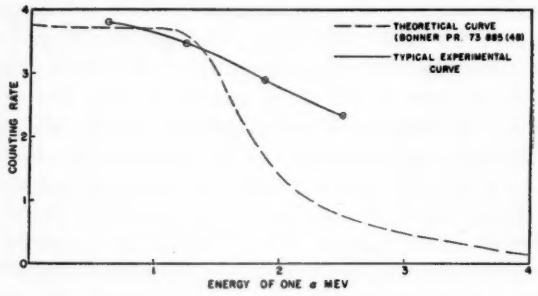

FIG. 2. Bias curve of a single Be^8 alpha-particle.

25 cm. Proportional counter *B* had a 3 inch i.d. and an effective counting length of 37 cm. The effective counting length was assumed to be the length of the central wire of the counter. Rossi and Staub[14] have shown that this assumption is accurate within a few millimeters. Thus, since the counters used in this experiment were very long, any errors introduced into the absolute cross-section measurements from this source were negligible. These two counters were employed for the following reason. While the beam of the cyclotron is relatively constant over successive periods exceeding several seconds, it varies within a factor of approximately two in successive periods of 0.2 sec., so that relative yields can only be compared if the effective charge integral is integrated over the period of the bombardment. This integration can be performed either numerically, if the current is measured on a recording ammeter during each bombardment, or naturally; i.e., since the effective charge is a common factor in the yields from both counters *A* and *B* in Fig. 1, counter *A* can be kept under constant conditions in all bombardments and form a relative measure of the effective charge, its purpose being merely to perform the integration. Counter *A*, which in the future will be called the monitor, was filled with CH_4 and, as may be seen in Fig. 1, was always traversed by the full energy beam.

During bombardments the cyclotron was first switched on for 10 sec., then switched off and 0.2 sec. later the counters were turned on. After 8 sec. the counters were switched off and following a short delay the cycle was repeated. One complete operation consumed 20 sec. This cycling process was carried out continuously during bombardments by a motor operated rotary switch as illustrated in the diagram.

Since Li^8 is easily ionized, it was probably drawn to the counter wall in most cases before counting began. Nevertheless, the fact that two alphas are produced traveling in approximately antiparallel directions will still allow 100 percent counting efficiency. Unfortunately the bias curves will suffer from this effect. The theoretical integral energy spectrum arising from a single alpha-particle in the decay of Li^8 is illustrated by the broken curve of Fig. 2. The solid curve in the figure represents a typical bias curve obtained in this experiment. If only one alpha from the decay of each Li^8 atom penetrates the counter gas, and all the ions produced along its path lie in the counting volume of the chamber, then the bias curves obtained should agree with the theoretical integral energy spectrum. The dissimilarity of the two curves can probably be accounted for by the following considerations. Firstly, an alpha-particle, if directed approximately parallel to the counter wall, will often spend the last part of its range in the chamber wall. Secondly, some alphas produced at the ends of the counter can lose part of their energy in the counting volume of the chamber and part outside of it. These forms of decay will affect the bias curve by tilting the low energy part away from the horizontal. Thirdly, the angle between the paths of the two alphas may differ from 180° by as much as 6° owing to the recoil from the Li^8 beta-decay so that in some cases both alphas may lose all or a fraction (as above) of their energy by gas ionization. And lastly, if Li^8 becomes a neutral atom during its travel toward the counter wall, it will stop in the gas, causing the ionization from both its alphas to be recorded. These latter types of disintegration will alter the high energy region of the bias curve and fill in the dip near 2 Mev.

All counters had small internal sources of polonium to calibrate the pulse heights in Mev except in the cases of krypton and xenon in which the yields were so low that any background at all would have been detrimental to the experiments. The pulse heights for these two elements were calibrated against an external 10 mg Ra-Be source placed one meter from the center of the counter in a direction perpendicular to the axis. The pulse heights to be expected from the Ra-Be source were found by placing the source in the position described with respect to a counter calibrated by polonium alphas.

In order to check the half-life of the alphas from each element investigated the monitor was filled with one atmosphere of CH_4 (the most copious Li^8 producer found) and counter *B* with the gas being studied. One pen of a Brush recorder was connected to the scale of two output of counter *A* scaler and the other pen to that of counter *B*, and the bombardment cycle started. The Brush recorder is a two-channel recording oscilloscope with a frequency response from d.c. to 100 cycles. Each input signal to the recorder is passed through an amplifier before it activates the magnetically operated pen unit. Both of the pens record on the same moving tape, the speed of which may be adjusted to 0.5, 2.5, or 12.5 cm per sec. The medium speed was used in this experiment. Since the two pens are in symmetric positions and the abundant supply of Li^8 from the monitor always produced pulses on the tape in the first 0.1 sec. of counting, the monitor pen provided a zero of time on the tape for the half-life measurement of the element in question.

In the measurement of excitation functions, mechan-

[14] B. Rossi and H. Staub, *Ionization Chambers and Counters* (McGraw-Hill Book Company, Inc., New York, 1949).

ical counters were linked to the scale of 256 output from each scaler. Copper absorbers placed between the monitor and counter *B* reduced the energy of the beam the amount required before it entered counter *B*. Relative excitation functions were obtained by comparison of the Li^8 counts in counter *B* with those from counter *A*, the latter being produced by the full energy deuteron beam. In the 184-inch Berkeley cyclotron the beam, after deflection from the tank is passed through a steering magnet which acts as a fine energy spectrometer. It is then collimated and emerges from a vacuum port ready for use. The energy of the deuterons has been measured repeatedly by observing their mean range in some absorber with the aid of a faraday cup. It turns out to be 18.85 ± 0.1 g/cm² of Al. This corresponds to 192.7 ± 0.4 Mev. This is the value which has been used in these experiments. The energy of the deuterons after passing through a given thickness of copper absorber was computed with the aid of tables prepared by Aron, Hoffman, and Williams of the theoretical group at the Radiation Laboratory based on the standard range energy formulas.[15]

The original collimation of the beam is reduced by multiple scattering when several grams of absorber are used. In order to avoid as much as possible errors in the excitation functions from this effect, counter *B* was built with an i.d. of 3 inches. In all of the experiments the original beam was confined in a circle 1 inch in diameter by the initial collimating system. After the deuteron beam has been reduced in energy to a few Mev, its energy will be inhomogeneous by approximately 5 Mev. This inhomogeneity is caused by straggling and in the case of 340-Mev protons may amount to as much as 40 Mev. Straggling in terms of range as defined by Bethe[15] is the difference between the mean and the extrapolated ranges. It is approximately equal to the standard deviation of the range. In deuteron excitation functions the effects of straggling and multiple scattering are not too important, although they should be considered in dealing with the low energy range of the excitation functions. However, the inaccuracies caused by these two effects will make it quite impracticable to determine proton excitation functions by this method.

In the reduction of the deuteron energy by absorbers the production of neutrons and protons by stripping[16] must be considered. At the energies involved neutrons should be about as efficient in the production of Li^8 as protons. With enough copper to absorb all of the charged particles in the beam, no Li^8 atoms were detected in counter *B*. This demonstrated that the neutrons from stripping had a negligible effect in this experiment. Since protons formed by stripping will quickly lose their energy in the absorber, it was assumed that they would be even less effective than neutrons.

[15] M. S. Livingston and H. A. Bethe, Rev. Mod. Phys. **9**, 245 (1937).
[16] R. Serber, Phys. Rev. **72**, 1007 (1947).

TABLE I. Absolute cross sections for Li^8 production from 340-Mev proton and 190-Mev deuteron bombardments of various elements (units of 10^{-29} cm²).

	C	N	Ne	A	Kr	Xe
(p, Li^8)	70±20	55±16	20±6	22±7	5.5±2	2.6±0.8
(d, Li^8)	135±40	68±20	25±7	22±7	4.1±1.3	3.6±1.0

The absolute cross section for carbon was measured in the following manner. A thin-walled ionization chamber of approximately 1-inch thickness, filled with air at atmospheric pressure, was placed before a single proportional counter containing CH_4 in the path of the beam. The chamber output was fed to one input of the Brush recorder and, after amplification, appeared on the recording tape. The input time constant was made to be 0.1 sec. by placing a 0.01 μf condenser in parallel with the 10 megohm input resistance of the recorder amplifier. This allowed the beam current to be amplified satisfactorily with the low frequency response amplifier of the Brush recorder, although the pulsed beam from the synchro-cyclotron appears at the deflection port for an interval considerably less than 1 μsec. 60 times per sec. The scale of two output on the scaler connected to the lone proportional counter in parallel with the ionization chamber was fed to the remaining pen of the Brush recorder. During bombardment cycles the recorder tape was run continuously. The beam current appeared on one pen of the recorder, the Li^8 counts appeared on the other. The instant the cyclotron beam was turned off was taken as zero on the time scale. A decay curve of the Li^8 counts was extrapolated back to this zero time in order to determine the number of Li^8

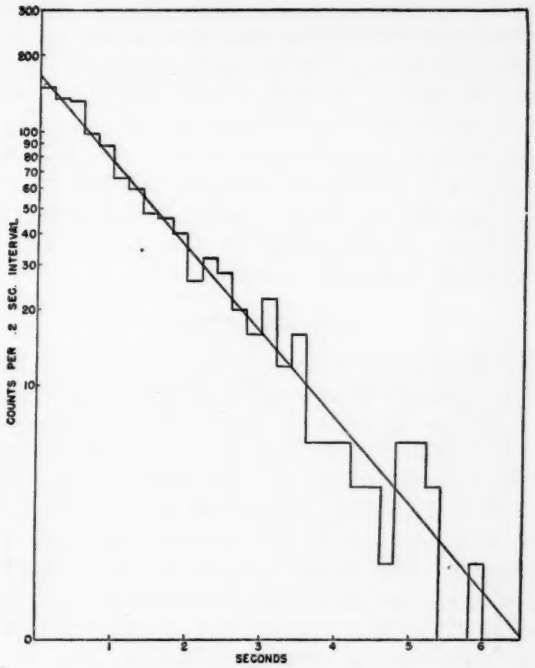

FIG. 3. Decay curve of Li^8 from 340-Mev protons on methane (CH_4).

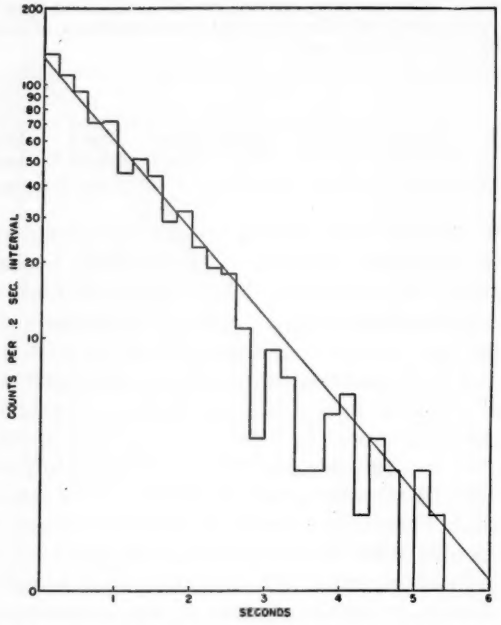

FIG. 4. Decay curve of Li^8 from 190-Mev deuterons on nitrogen.

atoms existing at the end of the bombardment and to account for the delay between stopping the cyclotron and turning on the counters. The effective charge integral $\int I(t)e^{-\lambda t}dt$ integrated over the bombardment period was calculated numerically from the recorder tape. This calculation required knowledge of the amplification factor of the ionization chamber and also that of the recorder amplifier. The former was measured directly with a faraday cup. The latter was ascertained with a potentiometer and a knowledge of the input resistance of the recorder. The cross section can then be determined from the Li^8 atoms available at zero time, the gas pressure and effective counting length of the proportional counter, and the effective charge integral. This cross section was found for bombardments of carbon with 190-Mev deuterons and 340-Mev protons. It is recorded in Table I under carbon. The cross sections for the other elements were then found from these values as mentioned before.

III. RESULTS

No effect was found from helium outside of the background statistics from a small polonium source within the chamber. In terms of cross sections, the result was $(0.5\pm1.0)\times10^{-29}$ cm². This was true with bombardments of 340-Mev protons and 190-Mev deuterons. This showed that any production of Li^8 from the central wire and windows (2 mil stainless steel) could be disregarded. Also no effect was found after the deuteron beam energy had been reduced considerably by copper absorbers placed in front of the chamber. The latter experiment showed that contributions due to the multiply scattered beam hitting the walls of the chamber could be neglected.

The decay curves of the alphas from C, N, Ne, A, Kr, and Xe are given in Fig. 3 to Fig. 8. They are plotted as histograms, the ordinate being the number of counts in a 0.2 sec. interval. This was the time interval used in reading the Brush recorder tapes. Since there is no apparent change in half-life in deuteron or proton bombardments, a single decay curve of each element is given. The straight lines on the graphs correspond to the ideal decay curve with a half-life of 0.88 sec. and the same total number of counts as in the experimental curve. It is seen that the agreement is excellent in all

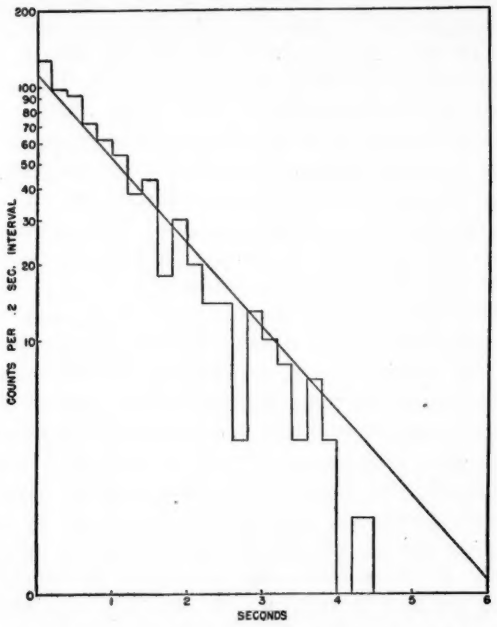

FIG. 5. Decay curve of Li^8 from 340-Mev protons on neon.

cases save that of neon, where some improvement is to be desired. However, even in this latter case the agreement with the Li^8 half-life is within statistical error. To give an idea of the counting rates in this experiment it may be remarked that the yield with Xe was so low that it required the counts from 150 equilibrium bombardments to produce the decay curve shown in Fig. 8.

The absolute cross sections for C, N, Ne, A, Kr, and Xe with 340-Mev protons and 190-Mev deuterons are collected in Table I. The difficulties mentioned in Section II in producing a flat bias curve and the change in counter characteristics with each new gas probably make these values accurate to no more than 30 percent. The values listed are those found with the scalers set to discriminate against alphas of less than 0.7 Mev. Much less discrimination would risk the acceptance of pulses originating from beta-disintegrations, since the counters were very long (45 cm). The theoretical integral energy spectrum of Fig. 2 makes it seem preferable, in view of the gaseous nature of the target and consequent lack of self-absorption, to determine the yield at a fixed low discrimination rather than to extrapolate the curves to zero bias. The cross sections found for Ne, A, Kr, and

Xe cannot be due to impurities of gases with a lower mass number. The argon used was 99.7 percent pure. Spectroscopic Ne, Kr, and Xe were used in which the only important impurity was N_2, present in quantities less than 0.05 percent of the total. Ne, Kr, and Xe, obtained in liter flasks at atmospheric pressure, were transferred to the counters by the use of a Toepler pump after the counters had been evacuated to a few microns pressure with a diffusion pump.

The deuteron excitation functions of C, N, Ne, and A are shown in Fig. 9 to Fig. 12. Statistical counting errors only are marked on the graphs. In the lower energy region some of the deuterons, multiply scattered by the copper absorber may be lost in the counter wall before traversing the whole counter. This would make the cross section at these low energies appear to be lower than it actually is.

IV. DISCUSSION

It is interesting to speculate on what process is involved in the production of Li^8 as described here. The graph of the cross section for Li^8 production with 190-Mev deuterons plotted against A, the mass number of the target element, in Fig. 13, provides some clues. It is seen that there is a sharp discontinuity in slope between the light nuclei (carbon, nitrogen, and neon) and the heavy nuclei (argon, krypton, and xenon). The curve drawn in the figure has no significance other than to emphasize this discontinuity. This indicates that different mechanisms are at work in the two regions. A plausible assumption is that the process for the light group is one in which the compound nucleus boils off the necessary number of neutrons and protons to leave a residue consisting of Li^8. This type of mechanism is obviously not applicable to the heavy group. There is not enough energy available to boil off thirty or more particles. Here it is more likely that Li^8 is expelled from the compound nucleus in a manner similar to evaporation.

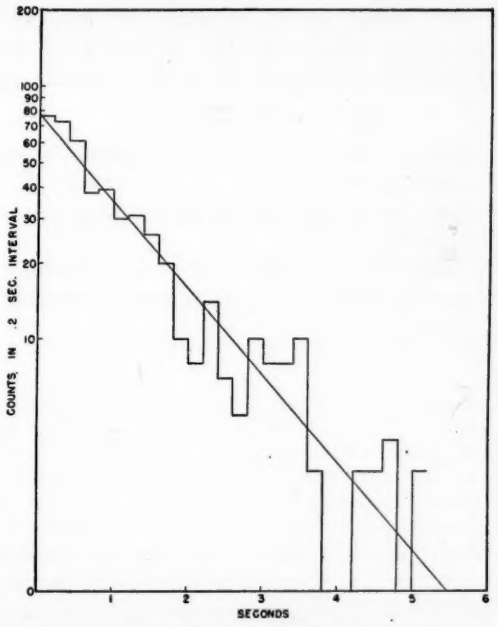

FIG. 6. Decay curve of Li^8 from 190-Mev deuterons on argon.

In the previous paragraph the formation of the compound nucleus was implicitly assumed. In other words, all of the energy of the incident particle was assumed to be distributed among the nucleons of the struck nucleus before any evaporation occurred. It has been pointed out by Serber[17] that this not always the case when the mean free path of the incident particle in nuclear matter is of the order of the nuclear dimensions. When such "transparency" conditions are met, as in this experiment, a whole range of excitation energies can be expected of the struck nucleus. If a collision involves only one or two nucleons which promptly remove themselves from the neighborhood of the nucleus, a small excitation energy will result. Other types of collisions, less "local" in character, will provide higher excitation energies. Sometimes the incident particle will be completely absorbed by the nucleus and a maximum excitation will occur. The treatment of the evaporation process which follows is so qualitative that the range of excitation energies of the struck nucleus will be neglected, and a compound nucleus with the maximum excitation will always be assumed.

Evaporation is a very difficult problem to treat theoretically in the case of light nuclei. It simplifies considerably if a temperature can be defined for the compound nucleus. Such is the case in heavy nuclei. By employing the principle of detailed balancing, Weisskopf[18] has derived a general formula for the evaporation of particles from a compound nucleus in terms of the cross section for the inverse process of capture. Let $W_n(E_A, \epsilon)d\epsilon$ be the probability per second of a nucleus A, excited to E_A Mev above the ground state, emitting a particle n of energy between ϵ and

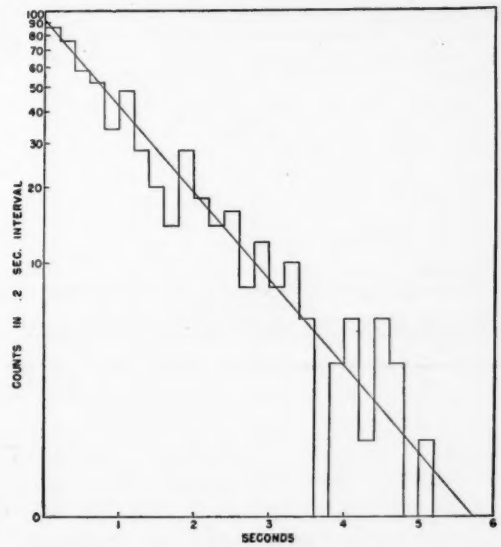

FIG. 7. Decay curve of Li^8 from 190-Mev deuterons on krypton.

[17] R. Serber, Phys. Rev. 72, 1114 (1947).
[18] V. Weisskopf, Phys. Rev. 52, 296 (1937).

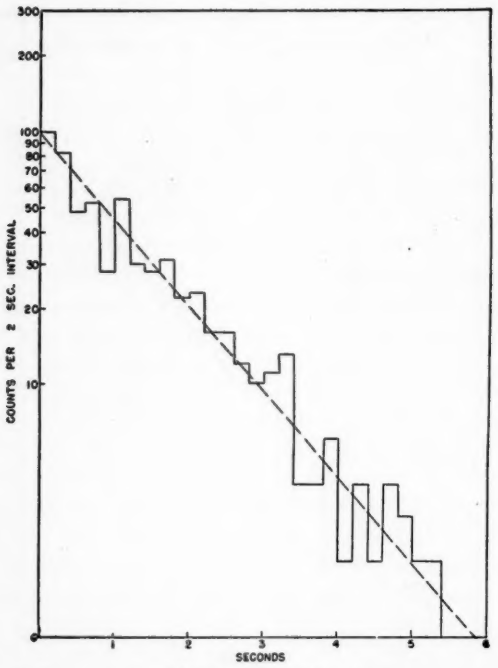

FIG. 8. Decay curve of Li^8 from 190-Mev deuterons on xenon.

$\epsilon+d\epsilon$ and leaving a residual nucleus B. For the inverse process, the capture of the particle with energy ϵ Mev by the nucleus B to form the nucleus A with excitation E_A, the probability per second is equal to $v\sigma(E_A, \epsilon)/\Omega$, where $\sigma(E_A, \epsilon)$ is the capture cross section under the stated conditions, v is the velocity of the particle, and Ω is the volume in which the whole system is enclosed. The principle of detailed balancing leads to the following relation among these quantities:

$$W_n(E_A, \epsilon)=\sigma(E_A, \epsilon)(gm\epsilon/\pi^2\hbar^3) \times\exp[S_B(E_A-E_0-\epsilon)-S_A(E_A)]. \quad (1)$$

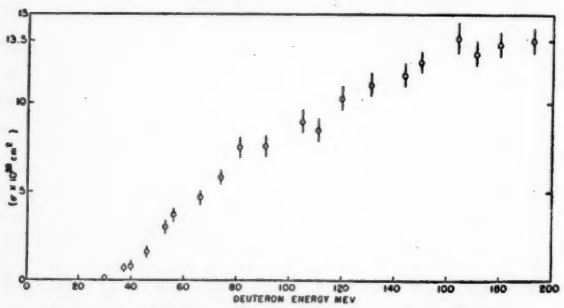

FIG. 9. Excitation function of the reaction C(d, Li^8).

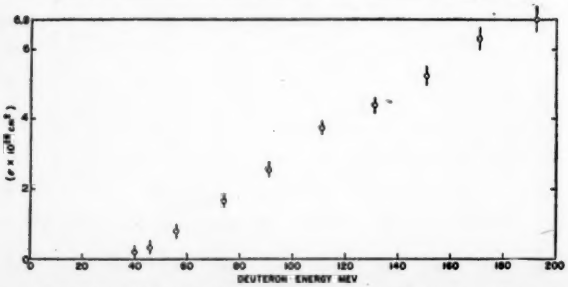

FIG. 10. Excitation function of the reaction N(d, Li^8).

This is Weisskopf's general evaporation formula. Here g is the statistical weight, m the mass of the particle, and E_0 is the binding energy of the particle to nucleus A. The entropy $S_A(X)$ of a nucleus of mass number A with excitation X in Mev is defined as the logarithm of the density of states of that nucleus with excitation X.

If the expression (1) is integrated over all possible values of ϵ for a given E_A, the result is the total probability per unit time for emission of the particle; i.e., the width Γ divided by $\hbar$. If the entropy

$$S_A(X)=(A\cdot X/2.2)^{\frac{1}{2}}$$

derived from the free particle model of the nucleus[19] is used in the calculation of the widths for proton, neutron, and Li^8 emission from argon, the following result is obtained:

$$(\Gamma_n+\Gamma_p)/\Gamma_{Li^8}\approx(10^4/5)_{200\text{ Mev }d},$$
$$\approx(10^4/2.2)_{80\text{ Mev }d}$$
$$\sigma_{\text{geom}}=0.8\times10^{-24}\text{ cm}^2.$$

This ratio should be near that of the cross sections for proton or neutron emission (about the geometrical) to the cross section for Li^8 emission. It is evident that the Li^8 cross section turns out to be about a factor of 2 higher than found, for E_A equal to 190 Mev and its reduction at E_A equal to 80 Mev is half of the experimental decrease. In the calculation, the classical formula

$$\sigma(E_A, \epsilon)=\sigma_{\text{geom}}(1-V/\epsilon)$$

for the cross section was used. V is the potential barrier of the particle with respect to the nucleus B. The influence of the barrier on the evaporation process is described in this term.

It is surprising that the order of magnitude of the results can be predicted on such a crude model. The

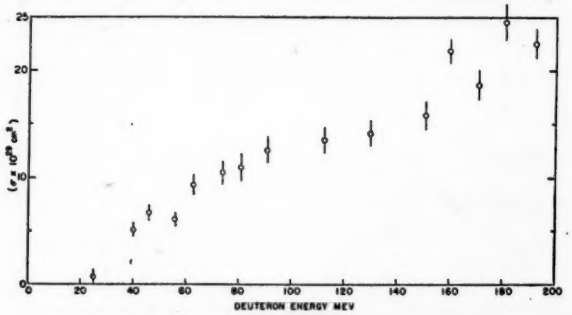

FIG. 11. Excitation function of the reaction Ne(d, Li^8).

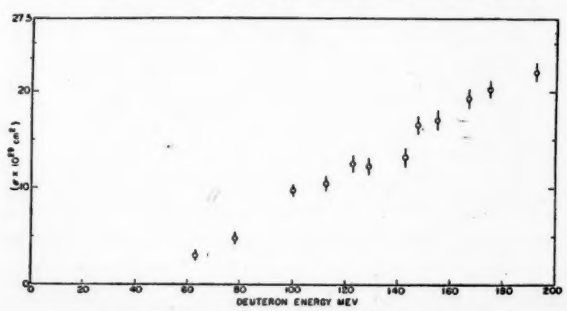

FIG. 12. Excitation function of the reaction A(d, Li^8).

[19] H. A. Bethe, Phys. Rev. **50**, 322 (1936).

important quantity in these calculations is, of course, the entropy. There is practically no experimental knowledge of its variation at the high energies here involved and the free particle model was used rather arbitrarily in the calculations.

Further experiments will be needed to fully justify the Li^8 production processes here advanced. For example, additional Li^8 cross sections for elements in the neighborhood of neon could verify the transition between the "residue" and evaporation reactions. Also more accurate and detailed excitation functions with light elements near the threshold should exhibit irregular features due to the fact that Li^8 can be reached from the compound nucleus by several alternate routes. These various routes will compete as they become energetically possible. For example, energetically Li^8 can be reached from C^{12} plus a proton most cheaply by emission of He^3 and two protons, more expensively by emission of a deuteron and three protons, and most expensively by emission of four protons and one neutron.

The production of Li^8 in nitrogen, a good cloud-chamber gas, may make it possible to test the conservation of momentum in the beta-decay of Li^8 more successfully than hitherto if the background difficulties can be circumvented.

The author wishes to thank Mr. C. Wiegand for a number of helpful suggestions during the course of the experiment and Mr. T. Thompson for help during the cyclotron bombardments. He is indebted to Professors R. Serber and G. Wick for discussions on the applicability of the evaporation formula to this case. It is a pleasure to acknowledge the stimulating guidance throughout the whole course of the investigation of Professor E. Segrè, who originally suggested this problem.

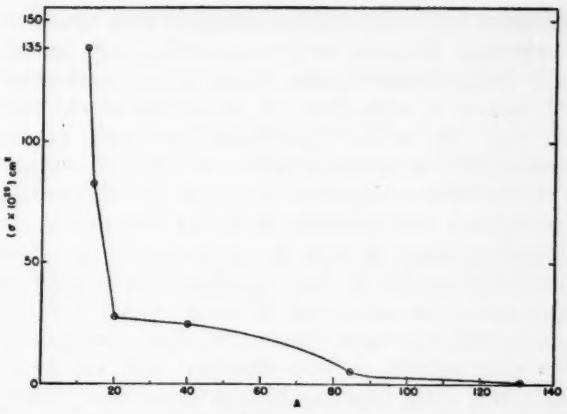

FIG. 13. Variation of the Li^8 cross section for 190-Mev deuterons as a function of A.

PHYSICAL REVIEW VOLUME 79, NUMBER 5 SEPTEMBER 1, 1950

Theory of the Superconducting State. I. The Ground State at the Absolute Zero of Temperature

H. FRÖHLICH*
Department of Theoretical Physics, University of Liverpool, Liverpool, England
(Received May 16, 1950)

In Bloch's theory of electronic conductivity the scattering of electrons by lattice vibrations is connected with the absorption or emission of vibrational quanta. As in field theories this gives rise to a self-energy which can be calculated by application of perturbation theory. The most interesting term as a result of the Pauli principle has the form of an interaction between electrons in momentum (k) space. The interaction between two electrons whose energy difference is small compared with their energy has a most interesting angular dependence. Roughly speaking, it is repulsive for equal energies but different directions of $\mathbf{k}$, and attractive otherwise. If strong enough it leads in the ground state to a distribution in momentum space which is different from the normal (Fermi) distribution. If this is the case then excited states exist in which some (ΔZ) electrons in view of their interaction in momentum space are concentrated in a narrow region in $\mathbf{k}$-space. These states are stable in the sense that it requires energy to remove one of the electrons. Their energies are higher than the ground state by a term proportional to $(\Delta Z)^2$.

The condition that the above-mentioned ground state (identified with the superconducting state) is realized requires that the interaction between electrons and lattice vibrations exceeds a certain value. With the help of the theory of high temperature conductivity, this condition can be expressed in terms of the resistivity ρ at 0°C. It is found that $\rho n \nu^{5/3}$ ($1/n$ = atomic volume; ν = number of free electrons per atom) must exceed a value depending on universal constants only. If $\nu=1$ is assumed, all monovalent metals except lithium do not satisfy the required condition, but most superconductors do. The energy difference between the normal and the superconducting state at absolute zero is about ms^2 (s = velocity of sound) per electron. It has thus the correct magnitude corresponding to a temperature of a fraction of a degree absolute. No application to higher temperatures or to the influence of external fields has been made yet.

I. INTRODUCTION

IN the theory of the electric conductivity of metals first developed by Bloch[1] electrons are considered to move freely through the lattice except for occasional scattering by the lattice vibrations. This scattering is connected with the absorption or emission of a vibrational quantum. Anyone who is familiar with modern field theories will conclude at once that an electron will have a self-energy in this vibrational field since it

* On leave at Department of Physics, Purdue University, Lafayette, Indiana.
[1] F. Bloch, Zeits. f. Physik **52**, 555 (1928).

produces a lattice deformation which in turn reacts on the electron. In polar lattices this self-energy has recently been calculated with the use of the methods of field theory;[2] it arises from the interaction of the electron with the lattice polarization produced by the electron itself. In metals it will be necessary to consider all of the electrons together. It will be shown presently that through the influence of the Pauli principle the interaction energy between the electrons and the vibrational field depends on their distribution in momentum space, and if the interaction is strong enough it will be seen to lead to a new distribution which—subject to later confirmation—will be identified with the superconducting state. One should then expect the velocity of sound to play an important role, and it is not accidental that the energy of an electron moving with the velocity of sound is of a similar order as the energy per electron involved in the transition between the normal and the superconducting state. Nor is it accidental that very good conductors do not become superconductors, for the required relatively strong interaction between electrons and lattice vibrations gives rise to large normal resistivity.

In the following the properties at the absolute zero of temperature only will be considered; the extension to higher temperatures and to the presence of external fields will be made later.

II. INTERACTION BETWEEN ELECTRONS AND THE VIBRATIONAL FIELD

In the absence of interaction with the vibrational field the electrons will be considered as free. A one-electron wave function is then a plane wave whose wave vector will be denoted by $\mathbf{k}$ (or sometimes by $\mathbf{q}$). The corresponding energy is $\epsilon_k=\hbar^2k^2/2m$ (m=electronic mass, $2\pi\hbar$=Planck constant). In the lowest state these electrons fill a sphere in $\mathbf{k}$-space of radius k_0 where

$$2(4\pi k_0^3/3(2\pi)^3)=4k_0^3/3(2\pi)^2=n_{el}. \tag{2.1}$$

Here n_{el} is the number of electrons per unit volume. Use has been made of the condition that the number of one-electron states is $1/(2\pi)^3$ times the volume in $\mathbf{k}$-space, and that each state can be occupied by two electrons (spin). It is well known that the Fermi energy

$$\zeta=\hbar^2k_0^2/2m \tag{2.2}$$

has the magnitude 10 ev.

The vibrational field will also be described in terms of plane waves whose wave number be $\mathbf{w}$. The corresponding energy is $\hbar ws$ where the velocity of sound, s, is considered to be independent of w. We shall be interested in longitudinal waves only, since transverse waves do not interact with the electrons. In Debye's approximation the maximum value of w, denoted by w_0 satisfies the relation

$$2w_0^3/3(2\pi)^2=n, \tag{2.3}$$

where n is the number of atoms per unit volume. The temperature θ_l given by

$$K\theta_l=\hbar w_0 s \tag{2.4}$$

(K=Boltzmann constant) is the Debye temperature if the velocity of sound of longitudinal and transverse waves is assumed to be equal.

A number of quantities derived from combinations of electronic and of vibrational terms will be of importance. They are the number of electrons per atom,

$$\nu=n_{el}/n, \tag{2.5}$$

the wave number of an electron moving with the velocity of sound,

$$\sigma_0=ms/\hbar, \tag{2.6}$$

and the ratio

$$\sigma_0^2/k_0^2=ms^2/2\zeta=(2^{\frac{1}{3}}\nu^{\frac{1}{3}}/8)(K\theta_l/\zeta)^2, \tag{2.7}$$

of which the order of magnitude is 10^{-5}.

The interaction between the electrons and the vibrational field is completely determined by the matrix elements M_w for the absorption or emission of a vibrational quantum by an electron. They have been calculated by Bloch[1] in terms of an interaction constant C. In Bethe's notation[3]

$$|M_w|^2=\left(\frac{4C^2\hbar w}{9nVMs}\right)\binom{n_w}{1+n_w}. \tag{2.8}$$

Here n_w is the number of quanta with wave number $\mathbf{w}$. At absolute zero, $n_w=0$; V is the volume and M is the atomic mass. The two possibilities refer to absorption ($\propto n_w$) and emission of a quantum respectively. Conserving momentum the electron makes then a transition into the state $\mathbf{k}+\mathbf{w}$ or $\mathbf{k}-\mathbf{w}$.

The interaction constant C has the dimension of an energy and is of the order of 10 ev, similar to ζ. Its magnitude is of fundamental importance for the following. As it appears only in the ratio C^2/M, it is convenient to define a dimensionless constant of the order of magnitude of unity,

$$F=C^2/(3\zeta Ms^2). \tag{2.9}$$

It will be found later that the exact value of this constant decides whether a metal becomes superconducting.

If the interaction is now treated as a small quantity, perturbation theory leads in second order to a change E in energy. From a formal point of view this energy can be attributed to the virtual emission and re-absorption of vibrational quanta, just as in radiation theory. Thus an electron in a state $\mathbf{k}$ absorbs a quantum $\hbar ws$ and is transferred into an intermediate state with wave vector

$$\mathbf{q}=\mathbf{k}-\mathbf{w} \tag{2.10}$$

from which it is re-absorbed into the original state. To satisfy the Pauli principle the transition must be pro-

[2] Fröhlich, Pelzer, and Zienau, Phil. Mag. **41**, 221 (1950).

[3] A. Sommerfeld and H. Bethe, *Handbuch der Physik* **24/2**, 517 (1933).

portional to the probability $f_{\mathbf{k}}(\leq 1)$ that the state $\mathbf{k}$ is occupied, as well as to the probability $(1-f_{\mathbf{q}})$ that state $\mathbf{q}$ is empty. Thus by a well-known formula

$$E=-2\sum_{\mathbf{k}}\sum_{\mathbf{w}}\frac{|M_w|^2 f_{\mathbf{k}}(1-f_{\mathbf{q}})}{\epsilon_q-\epsilon_k+\hbar s w}, \tag{2.11}$$

or using (2.8), (2.9), and (2.6)

$$E=-\frac{16F\zeta\sigma_0}{3nV}\sum_{\mathbf{k}}\sum_{\mathbf{w}}\frac{w f_{\mathbf{k}}(1-f_{\mathbf{q}})}{q^2-k^2+\sigma_0 w}. \tag{2.12}$$

The sums go over all values of $\mathbf{k}$ and $\mathbf{w}$ and are practically integrals. The factor 2 in (2.11) accounts for the two spin systems which can be treated independently.

The energy can be written as the sum of two terms,

$$E_1=-\frac{16F\zeta\sigma_0}{3nV}\sum_{\mathbf{k}}\sum_{\mathbf{w}}\frac{w f_{\mathbf{k}}}{q^2-k^2+\sigma_0 w}, \tag{2.13}$$

and

$$E_2=+\frac{16F\zeta\sigma_0}{3nV}\sum_{\mathbf{k}}\sum_{\mathbf{w}}\frac{w f_{\mathbf{k}} f_{\mathbf{q}}}{q^2-k^2+\sigma_0 w}. \tag{2.14}$$

Calculation of the energy E_1 is simple and will be published on another occasion. This energy term is uninteresting from our point of view as it can be considered as simply giving rise to a small shift of the electronic energy levels. Its magnitude is of the order $\zeta\sigma_0/k_0\simeq 10^{-3}\zeta$ per electron.

The second energy term, however, E_2, has very interesting features. It will be noticed that $\mathbf{q}=\mathbf{k}-\mathbf{w}$ may be introduced as summation index instead of $\mathbf{w}$ so that there is complete symmetry in $\mathbf{k}$ and $\mathbf{q}$, since $w=|\mathbf{q}-\mathbf{k}|$. Then since

$$\sum_{\mathbf{k}}\sum_{\mathbf{q}}\frac{f_{\mathbf{k}} f_{\mathbf{q}} w}{q^2-k^2+\sigma_0 w}=\sum_{\mathbf{k}}\sum_{\mathbf{q}}\frac{f_{\mathbf{k}} f_{\mathbf{q}} w}{k^2-q^2+\sigma_0 w},$$

we find

$$E_2=\frac{8F\zeta\sigma_0}{3nV}\sum_{\mathbf{k}}\sum_{\mathbf{q}}\left\{\frac{w}{q^2-k^2+\sigma_0 w}-\frac{w}{q^2-k^2-\sigma_0 w}\right\}f_{\mathbf{k}} f_{\mathbf{q}}$$

$$=-\frac{16F\zeta\sigma_0^2}{3nV}\sum_{\mathbf{k}}\sum_{\mathbf{q}}\frac{f_{\mathbf{k}} f_{\mathbf{q}} w^2}{(q^2-k^2)^2-\sigma_0^2 w^2}. \tag{2.15}$$

From a formal point of view each term in this sum can be considered as representing an interaction between two points $\mathbf{k}$ and $\mathbf{q}$ in $\mathbf{k}$-space, occupied with densities $f_{\mathbf{k}}$ and $f_{\mathbf{q}}$, respectively. This interaction energy is positive when $(q^2-k^2)^2$ is small but it is negative when this quantity is large. It tends to make $q-k$ of the order σ_0.

The purpose of the following section will be to find a distribution $f_{\mathbf{k}}$ such that the total energy of our system has its smallest value. This will be done by starting with the distribution function f_0 which minimizes the total energy in zero order (sphere of radius k_0) and then introduce small alterations.

Clearly such alterations will take place near the surface of the distribution only. Therefore instead of $\mathbf{k}$ and $\mathbf{q}$ we shall frequently use the coordinates

$$x=k-k_0, \quad y=q-k_0 \tag{2.16}$$

together with the polar angles θ_k, θ_q and the azimuths φ_k, φ_q. Then

$$f_0(x)=1 \text{ if } -k_0\leq x\leq 0, \tag{2.17}$$

and $f_0(x)=0$ otherwise. Also an alteration $f(x)$ in the distribution will be defined by

$$f_{\mathbf{k}}=f_0(x)+f(x,\theta_k,\varphi_k); \quad f(x)\geq 0 \text{ if } x\geq 0; \quad f(x)\leq 0 \text{ if } x\leq 0, \tag{2.18}$$

where

$$\sum_{\mathbf{k}} f(x)=0. \tag{2.19}$$

For simplicity we shall often write $f(x)$ for $f(x,\theta_k,\varphi_k)$ but by this do not wish to imply necessarily independence of θ_k and φ_k. The range of x within which $f(x)$ is different from zero must be very small compared with k_0. The quantity x/k_0 will therefore be treated as small of the order $\sigma_0/k_0\simeq 10^{-3}$. Then in good approximation using (2.16) and (2.10),

$$q^2-k^2=2k_0(y-x), \quad w^2=4k_0^2\sin^2\theta/2, \tag{2.20}$$

where θ is the angle between $\mathbf{q}$ and $\mathbf{k}$. Furthermore, in calculating the change of E_2 energy caused by rearrangement in $\mathbf{k}$-space we have to replace $f_{\mathbf{k}} f_{\mathbf{q}}$ in (2.15) by (use (2.18))

$$f_{\mathbf{k}} f_{\mathbf{q}}-f_0(k)f_0(q)=f_0(x)f(y)+f_0(y)f(x)+f(x)f(y). \tag{2.21}$$

The change S per unit volume of the total energy due to a rearrangement of the lowest zero order configuration in $\mathbf{k}$-space (Fermi distribution) is then the sum of three terms

$$S=S_1+S_2+S_3 \tag{2.22}$$

where

$$S_1=-\frac{16F\zeta}{3nV^2}\sum_{\mathbf{k}}\sum_{\mathbf{q}} f_0(x)f(y)\psi(x,y) \tag{2.23}$$

and

$$S_2=-\frac{16F\zeta}{3nV^2}\sum_{\mathbf{k}}\sum_{\mathbf{q}}\tfrac{1}{2}f(x)f(y)\psi(x,y) \tag{2.24}$$

represent the change of E_2 per unit volume. There

$$\psi(x,y)=\frac{2\sigma_0^2\sin^2\theta/2}{(y-x)^2-\sigma_0^2\sin^2\theta/2}. \tag{2.25}$$

Use has been made of (2.15), (2.20), (2.21) and of the symmetry in x and y. S_3 represents the change per unit volume in zero order energy. Treating again x/k_0 as small and applying Eqs. (2.16), (2.18), (2.19) and (2.2) we have (factor 2 for spin)

$$S_3=(2/V)(\hbar^2/2m)\textstyle\sum_{\mathbf{k}} k^2 f(x)=(4\zeta/Vk_0)\sum_{\mathbf{k}} x f(x). \tag{2.26}$$

The function $[-\psi(x,y)]$ plays the role of an interaction between two electrons in $\mathbf{k}$-space. It has a remarkable angular dependence: It is positive (repulsive in $\mathbf{k}$-space) if $\sin^2\theta/2>(y-x)^2/\sigma_0^2$ and negative (at-

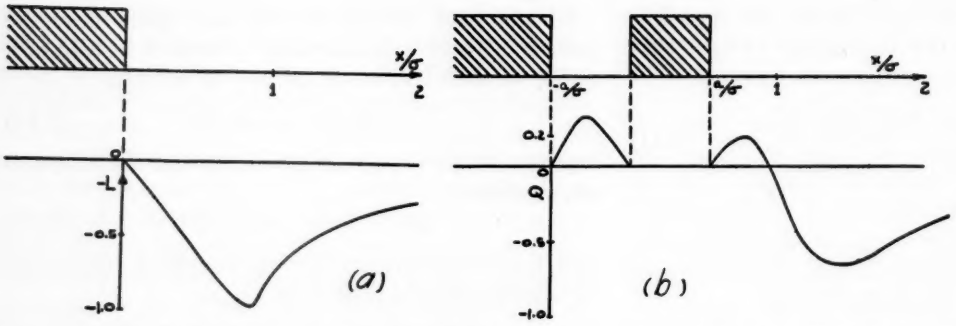

FIG. 1. (a) The energy required to remove an electron from the surface of a normal f_0 distribution ($\propto -L$). (b) The same for the f_1 distribution ($\propto Q$). Occupied x-values are indicated by shading.

tractive) otherwise. This tends to concentrate electrons into similar direction of motion provided $(y-x)^2<\sigma_0^2$.

Before evaluating the above expressions a word should be said about the use of perturbation theory. The denominator in the sums in equation (2.12) will vanish for certain values of $\mathbf{q}$ and $\mathbf{k}$. Integration can, however, always be carried out if principal values are used, and the final expressions converge. A vanishing denominator means that in zero order of approximation a transition into a different $f_\mathbf{k}$ distribution would be possible from an energetic point of view. Taking the energy in second order, however, these transitions are excluded energetically for the distribution with the lowest energy. For this case perturbation theory should be expected to yield reasonably good results. The same should be expected of metastable $f_\mathbf{k}$ distributions where no energy can be gained by shifting a few electrons only into different k-values.

III. INTEGRATIONS

In the present section the integrations required for the calculation of the energy will be carried out, but all essential discussions of the consequences are left to the next section. Since all important contributions to expressions (2.23) and (2.24) come from very small x- and y-values we can use the approximation $k^2dk=k_0^2dk$. Hence the transformation from sum to integral is

$$\sum_\mathbf{k}\{\cdots\}=[Vk_0^2/(2\pi)^3]\int dxd\cos\theta_k d\varphi_k\{\cdots\}. \quad (3.1)$$

In expression (2.23) for S_1, where $f_0(x)$ is independent of θ_k and φ_k one can use $\mathbf{q}$ as axis if the $\mathbf{k}$-integration is carried out first. Then with

$$u=\sigma_0\sin\theta/2, \quad (3.2)$$

one finds (see (2.25))

$$\sum_k \psi f_0(x)=[4k_0^2V/(2\pi)^2\sigma_0^2]\int_{-k_0}^{0}dx\int_0^\sigma \psi u du. \quad (3.3)$$

Since θ is the angle between $\mathbf{k}$ and $\mathbf{q}=\mathbf{k}-\mathbf{w}$ the upper limit σ is σ_0 if $w_0>2k_0$. Usually, however, $2k_0>w_0$ and the range of θ has then to be restricted so that $\sigma=\sigma_0 w_0/2k_0$, or using (2.1), (2.3) and (2.5)

$$\sigma_0^3/\sigma^3=4n_{el}/n=4\nu, \text{ if } (4\nu>1);$$
$$\sigma_0^3/\sigma^3=1 \text{ otherwise.} \quad (3.4)$$

Normally this would influence the limits in the radial integrations, but in our case of a very small range the effect of this is negligible. Then with the use of[4] (2.25)

$$-\int_\alpha^\beta dx\int_0^\sigma \psi u du=-\int_\alpha^\beta dx\int_0^\sigma \frac{2u^3du}{(y-x)^2-u^2}$$
$$=\int_\alpha^\beta\left[\sigma^2+(y-x)^2\ln\left(1-\frac{\sigma^2}{(y-x)^2}\right)\right]dx$$
$$=\frac{1}{3}\Big[\sigma^2x+(x-y)^3\ln\left(1-\frac{\sigma^2}{(y-x)^2}\right)$$
$$-\sigma^3\ln\frac{k-y-\sigma}{x-y+\sigma}\Big]_{x=\alpha}^{\beta}, \quad (3.5)$$

if $\beta=0$ and $\alpha=-k_0(\to-\infty)$ are used. Thus

$$-\sum_\mathbf{q} f(y)\sum_\mathbf{k} f_0(x)\psi=-\frac{4k_0^2V\sigma^3}{(2\pi)^2\sigma_0^2}\sum_\eta L(y)f(y), \quad (3.6)$$

where

$$L(y)=\frac{1}{3}\left\{\frac{y}{\sigma}+\frac{y^3}{\sigma^3}\ln\left(1-\frac{\sigma^2}{y^2}\right)+\ln\left(\frac{y+\sigma}{y-\sigma}\right)\right\}. \quad (3.7)$$

It follows from (2.23) that $-L(y)$ gives the y-dependence of the interaction energy when removing an electron a distance y from the k_0 surface. From Fig. 1a it is seen to be negative, thus tending to expel electrons from the surface. We shall therefore now calculate the change S of energy when all electrons in the shell between $x=-a$ and $x=0$ are moved outward into the shell between $x=0$ and $x=a$, as shown in Fig. 2a. Thus

$$f(x)=-1 \text{ if } -a\le x\le 0; \quad f(x)=1 \text{ if } 0\le x\le a. \quad (3.8)$$

It will be noticed then that

$$\int_{-a}^{a}\psi f(x)dx=\left(-\int_{-a}^{0}+\int_0^a\right)\psi dx$$
$$=\left(\int_0^a+\int_0^{-a}\right)\psi dx \quad (3.9)$$

[4] Absolute values of the arguments of the logarithmic function are always to be used.

holds. Since the angular integration can be carried out as for S, we require again the integral (3.5) but with the limits α and β as indicated by (3.9). Thus from (2.24), similar to (3.6), we require

$$-\frac{1}{2}\sum_{\mathbf{q}} f(y)\sum_{\mathbf{k}} f(x)\psi=+\frac{4k_0^2V}{(2\pi)^2}\frac{\sigma^3}{\sigma_0^2}\sum_{\mathbf{q}} J(y)f(y) \quad (3.10)$$

where

$$J(y)=\frac{1}{3}\left\{-\frac{1}{2}\frac{(y-a)^3}{\sigma^3}\ln\left(1-\frac{\sigma^2}{(y-a)^2}\right)\right.$$
$$-\frac{1}{2}\frac{(y+a)^3}{\sigma^3}\ln\left(1-\frac{\sigma^2}{(y+a)^2}\right)-\frac{1}{2}\ln\frac{(y+\sigma)^2-a^2}{(y-\sigma)^2-a^2}$$
$$\left.+y^3\ln\left(1-\frac{\sigma^2}{y^2}\right)+\ln\left(\frac{y+\sigma}{y-\sigma}\right)\right\}. \quad (3.11)$$

Angular integration in the now remaining $\mathbf{q}$-integration yields 4π, as there are no angular dependent terms left. Then with the help of (3.1) and with (3.8) and (3.6),

$$-\sum_{\mathbf{q}}\sum_{\mathbf{k}} f(y)(f_0(x)+\tfrac{1}{2}f(x))\psi$$
$$=-2[2k_0^2V/(2\pi)^2]^2(\sigma^4/\sigma_0^2)\int[L(y)-J(y)]dy/\sigma \quad (3.12)$$

with the same integration limits as in (3.9). The value of this integral is

$$P(\xi)=\tfrac{1}{3}\left\{\tfrac{1}{2}\xi+\tfrac{3}{4}\ln(1-4\xi)-\tfrac{3}{2}\ln(1-\xi)\right.$$
$$+4\xi^2\ln\left(1-\frac{1}{4\xi}\right)-\frac{1}{2}\xi^2\ln\left(1-\frac{1}{\xi}\right)$$
$$\left.+2\sqrt{\xi}\ln\frac{1+2\sqrt{\xi}}{1-2\sqrt{\xi}}\frac{1-\sqrt{\xi}}{1+\sqrt{\xi}}\right\}, \quad (3.13)$$

where

$$\xi=a^2/\sigma^2. \quad (3.14)$$

Hence by inserting (3.12) into (2.23) and (2.24)

$$S_1+S_2=-\frac{16F\zeta}{3n}2\left(\frac{2k_0^2}{(2\pi)^2}\right)^2\frac{\sigma^4}{\sigma_0^2}P(\xi). \quad (3.15)$$

Integration of expression (2.26) for S_3 is straightforward using (3.8). It yields

$$S_3=(4\zeta/k_0)(2k_0^2/(2\pi)^2)\sigma^2\xi. \quad (3.16)$$

By making use of Eqs. (2.1), (3.4), and (2.7) we obtain the total energy S from (2.22), (3.15) and (3.16), (per unit volume)

$$S=S(\xi)=-\frac{3}{2}\frac{ms^2n_{el}}{\nu^{\frac{1}{2}}2^{\frac{1}{2}}}[-F(4\nu)^{\frac{1}{2}}P(\xi)+\xi]$$
$$[=3ms^2n_{el}(-4\nu FP(\xi)+\xi), \text{ if } 4\nu<1]. \quad (3.17)$$

From Fig. 3 it will be seen that $S_1+S_2\propto -P(\xi)$ has a minimum at $\xi=\xi_0$, with

$$\xi_0=0.3, \quad \text{or} \quad \frac{a_0}{\sigma}=\sqrt{0.3}\simeq 0.55. \quad (3.18)$$

Also since $P(\xi)=\xi$ if $\xi\ll 0.3$, the total energy has a minimum only if

$$(4\nu)^{\frac{1}{2}}F>1; \quad [4\nu F>1, \text{ if } 4\nu<1]. \quad (3.19)$$

If this important condition is fulfilled then the distribution (Fig. 2a)

$$f_1(x)=f_0(x)+f(x) \quad (3.20)$$

has a lower energy than the $f_0(x)$ distribution.

We shall now calculate the energy required to remove an electron from the $f_1(x)$ distribution. This implies replacement of $f_0(x)$ in (2.23) by $f_1(x)$. The same integration as that leading to (3.6) has to be carried out but with x-limits $-k_0\leq x\leq -a$ and $0\leq x\leq a$. Inserting these limits into (3.5) we find

$$-\sum_{\mathbf{k}} f_1(x)\psi=+(4k_0^2V\sigma^3/(2\pi)^2\sigma_0^2)Q(y), \quad (3.21)$$

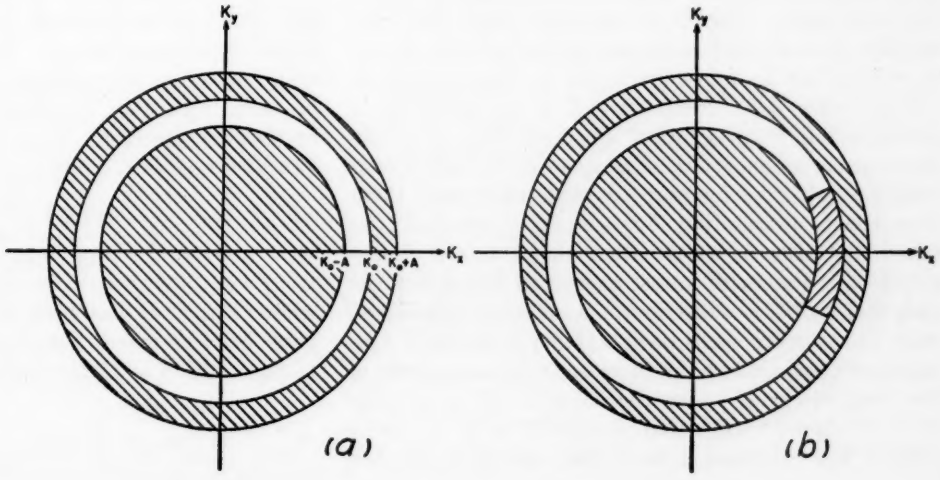

FIG. 2. (a) Distribution of electrons of a superconductor in $\mathbf{k}$-space, ground state. (b) Distribution in a nonsymmetrical excited state.

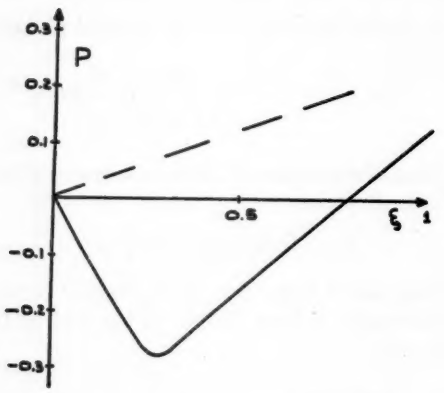

FIG. 3. Energy of an f_1 distribution as a function of gap width.

where

$$Q(y)=\frac{1}{3}\Big\{-\frac{y}{\sigma}+\frac{y^3}{\sigma^3}\ln\Big(1-\frac{\sigma^2}{y^2}\Big)-\frac{(y+a)^3}{\sigma^3}\ln\Big(1-\frac{\sigma^2}{(y+a)^2}\Big)-\frac{(y-a)^3}{\sigma^3}\ln\Big(1-\frac{\sigma^2}{(y-a)^2}\Big)-\ln\frac{(y+a)^2-\sigma^2}{(y-a)^2-\sigma^2}\Big\}. \quad (3.22)$$

Since

$$\frac{dP}{d\xi}=-\frac{1}{3}\Big\{1+8\xi\ln\Big(1-\frac{1}{4\xi}\Big)-\xi\ln\Big(1-\frac{1}{\xi}\Big)+\frac{1}{\sqrt{\xi}}\ln\frac{1+2\sqrt{\xi}}{1-2\sqrt{\xi}}\frac{1-\sqrt{\xi}}{1+\sqrt{\xi}}\Big\} \quad (3.23)$$

it will be seen that $Q(0)=Q(a)=Q(-a)=0$ if $\xi=\xi_0$. Also, in contrast to the $f_0(x)$ distribution, energy must now be spent to remove an electron from either of the surfaces as is shown in Fig. 1b. Beyond a certain distance outward from the outer surface the function $Q(y)$ decreases again, reaches a minimum and then approaches zero. In this latter part it thus behaves similar to $-L(y)$, but its minimum is not so deep as that of $-L(y)$ (ratio 2:3). Also, since it is separated by a potential hill from occupied levels so that relatively more zero order energy must be spent to move electrons from the f_1 distribution than was required to move them from the f_0 distribution. For simplicity we shall consider only cases in which either the f_0 or the f_1 distribution is that with lowest energy. If this is not the case then f_2, f_3, $\cdots$ distributions must be constructed with 2, 3 or more shells until stability is reached. This would of course lead to an increase in the magnitude of the total energy $|S|$ over the value (3.17) by a factor $G\gtrsim 1$. I should expect that at most G is of the order $(4\nu)^{\frac{1}{2}}F$. The existence of more than one shell does not alter condition (3.19), however, because this is the condition that f_1 has a lower energy than f_0.

Excited States

If the f_1 distribution leads to the lowest energy state, then distributions with a different sized single shell exist which are stable in the sense that energy must be expended to remove single electrons. In these distributions the gap and the shell are no longer of equal width and they have a higher energy than the distribution with equal width. They can be obtained from the original f_1 distribution by adding to (or removing from) the surfaces thin (compared with a) spherically symmetrical layers. The interaction $A(y-x)$ of such a layer at x with a single electron at y is proportional to expression (3.5) with $|\beta-\alpha|\ll a$, so that except for a numerical factor of order unity,

$$A(y-x)=\frac{16F\zeta}{3n}\Big[1+\frac{(y-x)^2}{\sigma^2}\ln\Big(1-\frac{\sigma^2}{(y-x)^2}\Big)\Big]t, \quad (3.24)$$

where t is the number of electrons contained in the layer. $A(y-x)$ is an even function of $(y-x)$, and is positive nearly up to $y-x\simeq\sigma$. The existence of these excited states can easily be proved. Let A_0t, A_1t and A_2t be the values of $A(y-x)$ at distance $y-x=0$, $\pm a$, $\pm 2a$, respectively. Also let the number of electrons in the three layers deposited on the three surfaces $(x=-a, 0, a)$ be z_1, z_2, z_3, respectively. We then require that the total change of interaction B with a single electron is the same near each of the three surfaces. This requires that

$$(A'+A_0)z_1+A_1z_2+A_2z_3=B \quad (3.25a)$$

for the surface $x=-a$, and similarly

$$A_1z_1+(A'+A_0)z_2+A_1z_3=B \quad (3.25b)$$

and

$$A_2z_1+A_1z_2+(A'+A_0)z_3=B, \quad (3.25c)$$

where A' is the change of interaction energy of an electron with the rest of the electrons (S_1-type). This quantity is determined by the slope of the function $Q(y)$ (3.22) which through (3.21) and (2.23) gives the required change of energy. This function behaves near each surface y_0 approximately as $2(y-y_0)/3a$ as can be seen from Fig. 1b. Also according to (3.1) the number of electrons in a shell of width $y-y_0$ is $8\pi k_0^2(y-y_0)/(2\pi)^3$. Thus

$$A'\simeq\frac{16F\zeta}{3n}\frac{1}{2}\frac{\sigma^3}{a\sigma_2}t\simeq\frac{16F\zeta}{3n}\frac{t}{2}, \quad (3.26)$$

where Eq. (3.4) has been used and $\nu=1$, $a^2/\sigma^2=0.3$ have been assumed. Inserting this value for a^2/σ^2 in (3.24) solution of (3.25) yields

$$z_1=z_3,\quad z_2/z_1=1+\frac{A_2-A_1}{A_0+A'-A_1}\simeq -9z_1. \quad (3.27)$$

Clearly if we start in the ground state these

$$\Delta z = z_1 + z_2 + z_3 = -7z_1 \tag{3.28}$$

electrons must be removed from the surfaces and placed in a different way. One possibility which will be of importance when dealing with higher temperatures is to put them out of the range of forces near the surfaces. The other case leaving them near the surfaces leads to cluster formation as will be shown presently. In both cases the total change in energy is composed of the contribution R_0 connected with removal from the surfaces, and R the contribution due to replacing the electrons. The value of R_0 is independent of the way of replacing the electrons because with (3.25) to (3.27)

$$R_0 = \tfrac{1}{2}(A_0 + A' - 9A_1 + A_2) z_1 \Delta z \simeq \frac{16F\zeta}{3n}(\Delta z)^2. \tag{3.29}$$

Non Symmetrical States*

In contrast to $S(\xi)$, the following calculations [as (3.29)] are intended to be accurate only up to a numerical factor of order one. Assume now the Δz electrons to be equally distributed over the whole (or a fraction) of the width of the gap, but let $\Delta z < z$ where (see (2.1))

$$z = 4k_0^2 a/(2\pi)^2 = 3n_{el}(a/k_0) \tag{3.30}$$

is the number of places available in the gap. Assume first that the distribution is spherically symmetrical. Then in contrast to all previously discussed distributions the average occupation number per level is neither zero nor unity, but $\Delta z/z < 1$. We shall now show that the angular dependence of the ψ interaction tends to concentrate the electrons into as small a volume as is compatible with the Pauli principle. The energy contribution R of such a distribution $g(x)$ is obtained from S (see (2.23), (2.24) and (2.26)) by replacing the distributions $f_0(x)$ and $f(x)$ by $f_1(x)$ and $g(x)$. The only term depending on the angular distribution is obtained from S_2 and will now be denoted as

$$R_2 = -(16F\zeta/3n)\tfrac{1}{2} \sum_{\mathbf{q}} g(y) \sum_{\mathbf{k}} g(x)\psi. \tag{3.31}$$

For simplicity assume $g(x)$ to be independent of x. We then require

$$-\frac{1}{2}\sum_{\mathbf{q}}\sum_{\mathbf{k}} g(y)g(x)\psi = \frac{1}{2}\left(\frac{z}{4a}\frac{1}{2\pi}\right)^2 \int d\cos\theta_k d\cos\theta_q d\varphi_k d\varphi_q \times \int_0^a dxdy \frac{(-2)u^2}{(y-x)^2-u^2}. \tag{3.32}$$

* Not required for the discussion of the ground state.

The x, y integration yields

$$-\int_0^a \frac{2u}{(y-x)^2-u^2} dxdy = 2u^2 \ln\left(1-\frac{a^2}{u^2}\right) - 2au \ln\left(\frac{u-a}{u+a}\right) \simeq 2\times 1.6ua \text{ if } u < 0.9a. \tag{3.33}$$

By inspection it is found that the exact expression approximately rises as $2\times 1.6ua$ up to $u \simeq 0.9a$ then decreases and approaches $2a^2$ as $u > a$. There is thus a tendency to concentrate electrons into as narrow an angular range as permissible by the Pauli principle. This can be verified by calculating the energy for such a distribution $g(x)$ as a function of its angular spread γ. Let thus $g(x)$ be constant in the range $0 \leq \theta \leq \theta_1$ and define

$$\gamma = \frac{1}{2}\int_{\cos\theta_1}^{1} d\cos\theta = \frac{1}{2}(1-\cos\theta_1) < 1. \tag{3.34}$$

Since according to (3.2), $u = \sigma_0 \sin\theta/2$ we shall require

$$\int_{1-2\gamma}^{1} d\cos\theta_k d\cos\theta_q \int_0^{2\pi} d\varphi_k d\varphi_q [1 - \cos\theta_k \cos\theta_q - \sin\theta_k \sin\theta_q \cos(\varphi_k - \varphi_q)]^{\frac{1}{2}} = (2\pi)^2(8/3)\gamma^3 \text{ if } \gamma < 1. \tag{3.35}$$

Then using the approximation $1.6ua$ in (3.33) which holds if $\gamma < a/\sigma$, we find with (3.31) to (3.35), and with $\Delta z = \gamma z$,

$$R_2 = (\Delta z)^2 \frac{\sigma_0}{a} 1.6 \times \frac{8}{3}\gamma \frac{16F\zeta}{3n} \simeq \frac{16F\zeta}{3n} 4(\Delta z)^2\gamma, \quad \text{if } \gamma < a/\sigma. \tag{3.36}$$

For constant particle number Δz, this expression thus decreases as the angular spread is reduced.

If we had assumed the distribution to extend only over a width $b \ll a$ instead of over the full gap width we would have found

$$\Delta z/z = b\gamma/a, \quad b \ll a. \tag{3.37}$$

In Eq. (3.33), a must then be replaced by b. With the use of (3.37), Eq. (3.36) is seen to obtain a factor a/b so that with a further use of (3.37)

$$R_2 = (16F\zeta/3n)4(\Delta z)^2\gamma a/b = (16F\zeta/3n)4z\Delta z\gamma^2. \tag{3.38}$$

The R_1 contribution corresponding to S_1 can be found in a similar way as A', (3.26). With the help of (2.23), (3.21) and (3.30) (using again $\nu = 1$, i.e. $\sigma^2/\sigma_0^2 \simeq 0.4$ and $a^2/\sigma^2 = 0.3$),

$$R_1 = (16F\zeta/3n)(\sigma^3/\sigma_0^2 a) z\Delta z\bar{Q} \simeq (16F\zeta/3n) z\Delta z\bar{Q}, \tag{3.39}$$

where $\bar{Q}$ is the average of $Q(y)$ (see (3.22) or Fig. 1b) over the occupied range. From Fig. 1b we see that

approximately (use (3.37))

$$\bar{Q}\simeq 0.2 \text{ if } b=a, \quad \bar{Q}\simeq b/2a=\Delta z/2z\gamma \text{ if } b\ll\tfrac{1}{2}a. \tag{3.40}$$

Finally the R_3 contributions, corresponding to S_3 are of the same type as R_1. They lead to a factor $(1\pm 1/(4\nu)^{\frac{1}{2}}F)$ if $b<a$ (+ near the lower, − near the upper surface) and thus vanish on an average. For $b=a$, R_1 vanishes exactly. Thus with (3.29), (3.36), (3.38) and (3.39) the total energy required to form the cluster of Δz electrons is

$$R=R_0+R_1+R_2\simeq(16F\zeta/3n)(\Delta z)^2\chi, \tag{3.41}$$

where χ is a factor depending on the shape. In particular (see 3.40)

$$\chi=1+(4\gamma^2 z/\Delta z)+(1/2\gamma) \text{ if } b\ll a \tag{3.42}$$

and

$$\chi=1+4\gamma+z/\Delta z=1+(4\Delta z/z)+z/\Delta z \text{ if } b=a. \tag{3.43}$$

It will be noticed that if $b\ll a$, R has a minimum for given Δz when $16\gamma^3=\Delta z/z$ or using (3.37) when $16\gamma^2=b/a$. But if b becomes larger, then the value of γ leading to the smallest value for R is $\gamma=\Delta z/z$.

Establishment of a cluster in the gap leads to a change of the energy of an electron near the outer surface by approximately (see (2.25))

$$-\frac{16F\zeta}{3n}\Delta z\frac{\sigma_0^2\sin^2\bar{\theta}/2}{(3a/2)^2-\sigma_0^2\sin^2\bar{\theta}/2} \tag{3.44}$$

if $\bar{\theta}$ is its average angle with the position of the cluster, and $3a/2$ its average distance. This quantity is negative (attractive) if

$$\sin\bar{\theta}/2<3a/2\sigma_0\simeq\tfrac{1}{2}. \tag{3.45}$$

Some energy can be gained therefore by removing a fraction of the Δz electrons to the outer surface within an angle $\bar{\theta}$. This will not change appreciably the energy R; in the form (3.41) for R it only leads to a slightly different definition of the form factor χ.

It might be expected that if $\Delta z/z\ll 1$ the form factor χ should be independent of Δz for the shape at which R has its minimum, so that $R\propto(\Delta z)^2$. That this is not true for the two cases (3.42) and (3.43) shows that we have not found the best shape. In fact one should hardly expect that this shape has sharp edges as have our models. Improvements will decrease the energy R_1+R_2; but since R_0 is independent of shape, always $\chi>1$. Equation (3.41) therefore represents the correct order of the energy R.

IV. DISCUSSION OF THE ENERGY

The results of the calculations of the previous section are based on the interaction energy $-\psi$ in k-space [Eq. (2.25)]. This quantity exhibits two tendencies as can also be seen from Fig. 4: for small energy difference $[(x-y)^2<\sigma^2]$ it tends to concentrate electrons into a narrow angular range in k-space. If this is impossible because all states are filled then the second tendency comes into play. It attempts to place electrons at distances of the order $x-y=\sigma$. In fact by averaging $-\psi$ over the angles we obtain, as in (3.5),

$$-\bar{\psi}=1+((y-x)^2/\sigma^2)\ln[1-\sigma^2/(y-x)^2]. \tag{4.1}$$

As can be seen from Fig. 5 this function is positive nearly up to σ, has a (negative) minimum just beyond it and then approaches zero.

For a first orientation on the influence of interaction on the distribution function it is useful to see that according to Eqs. (3.6) and (3.7), or to Fig. 1a, interaction energy can be gained by removing an electron from the surface of a normal (Fermi) distribution f_0. This suggests calculation of the change $S_1(\xi)+S_2(\xi)$ of interaction energy when a shell of width a is shifted outward from the surface leaving a gap of width a as shown in Fig. 2a. The change of interaction energy due to the establishment of this distribution depends on the interaction parameter $\xi=a^2/\sigma^2$ (see Eq. (3.13) and (3.14)) as illustrated in Fig. 3. It has a minimum at $\xi=\xi_0\simeq 0.3$. Zero order energy $S_3(\xi)$ on the other hand increases linearly with ξ as indicated by the dotted line. It follows that the total change in energy $S(\xi)$, [Eq. (3.17)] has a minimum only if condition (3.19) is fulfilled. Otherwise no minimum exists and the f_0 distribution remains stable. Again as before we can now investigate the change in interaction energy when a single electron is removed from one of the surfaces. Figure 1b drawn according to Eq. (3.22) shows the result if $\xi=\xi_0=0.3$. In contrast to the f_0 distribution the energy of interaction now increases near the surfaces. At a larger distance from the outer surface, however, a similar decrease to that found near the f_0 surface is repeated; again interaction energy can be gained when removing an electron from the surface to the minimum. But now the depth of the minimum is only about $\frac{2}{3}$ of what it was in the f_0 case, and the distance from the surface is larger by a factor two, approximately. Therefore the increase in zero order energy when removing an electron from the surface is larger than in the f_0 case. If the interaction parameter F (see (2.9)) is very large, removal of a second shell (f_2 distribution) from the surface may lead to a further decrease in total energy. We shall assume here that this is not the case. Its main effect would be to increase the magnitude of the total energy $S(\xi)$ by a factor smaller than two.

If condition (3.19) is not fulfilled little doubt can exist that in the approximation used here the f_0 distribution (normal state) has the lowest energy. If however (3.19) is fulfilled, then on the assumptions made it seems likely that the f_1 distribution leads to the lowest energy. A general proof has not been attempted, however, and would probably be very difficult.

In metals for which the f_0 distribution forms the lowest state excited states must exist in which electrons from near the surface are moved to higher energies similar to the case in which the interaction is neglected completely. It should be expected then that when the

thermal energy of the electrons is larger than S, ($\xi \simeq \xi_0$), these metals behave as in zero order, but that below this temperature deviations of a quantitative but not qualitative nature occur.

In case the f_1 distribution forms the lowest state there will also be excited states in which single electrons have been removed from the surfaces. This alters the energy and gap width of the remaining f_1 distribution as discussed in connection with Eq. (3.25). One should again expect that at temperatures sufficiently high, the metal behaves as in zero order. Below this temperature, however, changes of a qualitative nature occur because of the qualitative difference between the f_1 and f_0 distributions.

It was not intended in the present paper to deal quantitatively with excited states required for questions of temperature dependence. Another type of excited states may be of importance, however, even at the absolute zero of temperature. In these states denoted in Sec. III as non-symmetrical states electrons are clustered in the gap of the f_1 distribution as shown in Fig. 2b (or possibly near the outer surface). The energy of such a cluster was found in Sec. III by minimizing the energy, and it can be seen then that it is stable in the sense that energy must be expended to divide it into smaller parts or to remove single electrons. To return to the ground state would require, therefore, that the cluster be first dissolved. This would be impossible by processes acting on single electrons like scattering on lattice imperfections. In view of this stability the number Δz of electrons contained in the cluster which according to Eq. (3.41) determines its energy can be used as a parameter of the system. Then from (3.41) and (3.17) the total energy per unit volume is given by

$$S(\xi)+R(\Delta z)=S(\xi)+(16F\zeta/3n)\chi(\Delta z)^2. \qquad (4.2)$$

The formation of stable clusters can be understood in a qualitative way immediately from the interaction $-\psi$ [Eq. (2.25) and Figs. 4 and 5]. This interaction tends to concentrate electrons within the gap as far as is permissible by the Pauli principle. The opposite tendency, dispersal over all angles, would manifest itself only at sufficiently high energy differences requiring $(x-y)^2>\sigma_0^2$, and would thus require energy. The most important energy term (R_2) leading to cluster formation is derived from S_2 in Eq. (2.24) by replacing there the distribution $f(x)$ by the distribution function $g(x)$ of the cluster, according to (3.31). This term which might be denoted as the self-energy of the cluster is proportional to $(\Delta z)^2$, and to the average value $-\langle\psi\rangle_{Av}$ obtained by averaging the interaction $-\psi$ between two electrons in $\mathbf{k}$-space for both electrons over the cluster. Then consider two limiting cases on the assumption that Δz is very small: (i) a spherically symmetrical distribution in which the electrons fill a very thin shell. Then from (4.1), $-\langle\psi\rangle_{Av}=1$ if Δz is so small that the width of the shell is small compared with σ_0. On the other hand for a thin needle in radial direction $\langle\sin^2\theta/2\rangle_{Av}\to 0$ and $\langle(x-y)^2\rangle_{Av}\to\infty$ so that $-\langle\psi\rangle_{Av}\to 0$, showing that the needle shaped cluster has the lower self-energy. Other energy terms, however, behave in the opposite way and the result is a more regularly shaped cluster.

Finally it should be mentioned that the establishment of a stable configuration can also be understood in terms of the spontaneous transitions of electrons connected with the emission of lattice quanta. Whenever such transitions are possible, occupation of the final states by electrons leads to a decrease in ψ-interaction energy. On the other hand, it can be seen from Fig. 4 that once a cluster has been formed in the gap, transitions into other directions within the gap would require energy. Thus changes due to transitions will not spread the cluster over the gap.

It should also be pointed out here that the change from a f_0 to a f_1 distribution leads to an alteration of the distance correlation of two electrons in ordinary space. Its main effect is to increase the probability of finding two electrons at a distance smaller than $1/a$. The decrease in interaction is understandable in an elementary way because one electron can benefit from the lattice deformation produced by another one if it remains sufficiently close (in ordinary space) to it.

V. REMARK ON THE ELECTRODYNAMIC PROPERTIES

In Secs. III and IV it has been shown that in metals in which the f_1 distribution is realized in the ground state stable non-symmetrical states exist which lead to cluster formation in $\mathbf{k}$-space. In these clusters a number Δz of electrons move in a similar direction giving thus rise to an electric current in the absence of an electric field. We shall therefore identify the f_1 distribution with the superconducting state. It should be remembered that according to Eq. (4.2) the energy of these current carrying states is higher than the ground level by a term proportional to $(\Delta z)^2$.

The existence of such stable currents has often been postulated as an alternative phenomenological hypothesis to postulation of the London equations[5] and had first thought that the two are closely related. For if we assume clusters of a very small size so that all electrons move practically in the same direction with velocity $\hbar k_0/m$ the density of the electric current is

$$j=(e\hbar k_0/m)\Delta z. \qquad (5.1)$$

Inserting from here into Eq. (4.2) with the use of (2.2), the energy per unit volume is found as

$$S(\xi)+\tfrac{1}{2}\lambda j^2, \qquad (5.2)$$

where

$$\lambda=(16F\chi/3)(m/e^2n). \qquad (5.3)$$

From our discussion at the end of Sec. III it seemed likely that for small Δz the form factor χ is independent

[5] F. and H. London, Proc. Roy. Soc. A149, 71 (1935); also M. von Laue, Theorie der Supraleitung (Springer, 1947).

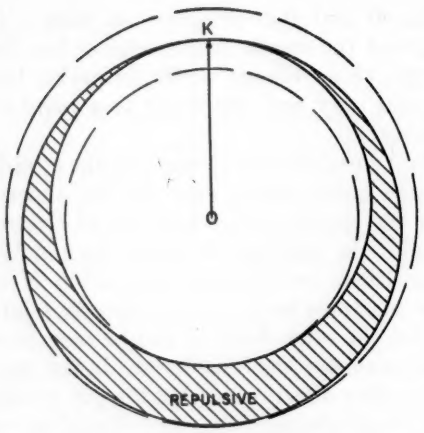

FIG. 4. The $-\psi$ interaction in **k**-space. It is repulsive between an electron in the shaded region and the electron **k**. Otherwise it is attractive. At the boundary it is singular.

of Δz and hence of j. Also $\chi \gtrsim 1$ and hence since condition (3.19) must be fulfilled,

$$16F\chi/3>4. \tag{5.4}$$

It must now be remembered that we have not yet taken account of the magnetic interaction energy between electrons connected with the current. Tentatively this might be done macroscopically by adding a term $H^2/8\pi$ representing the energy of the magnetic field H, where

$$\text{curl}\mathbf{H}=4\pi\mathbf{j}/c, \quad \text{div}\mathbf{H}=0. \tag{5.5}$$

Thus with (5.2) the total energy per unit volume is

$$U=U_0+S(\xi)+\frac{1}{2}\lambda j^2+\frac{H^2}{8\pi} \tag{5.6}$$

The existence of an energy term proportional to j^2, in addition to the H^2 term is characteristic of the London equations. The term U_0 represents the energy of the normal state, and $S(\xi)$ it will be remembered is the energy difference between the superconducting and the normal state in the absence of a current.

The above outlined procedure holds only for very thin layers, however, where the magnetic interaction is very small. Otherwise (5.1) becomes invalid. It will then be necessary to introduce the magnetic field at an earlier stage. (See *Notes added in proof*.)

VI. COMPARISON WITH EXPERIMENTS

The calculations of the previous sections were based on a free electron model. According to the electron theory of metals, permitted energy levels have a band structure. When such an energy band is not too highly filled the free electron model is sound. On the other hand, when a band is nearly filled a similar model applies if holes (empty levels) instead of electrons are considered. It can easily be seen that in this case all our previous results hold. For by introducing a hole distribution function $h_k=1-f_k$ we find that in our basic expression (2.11) we replace $f_k(1-f_q)$ by $h_q(1-h_k)$ thus interchanging k and q. In going to Eq. (2.12) the same interchange has to be carried out in the denominator, thus leaving the whole expression unaltered. From the experience gained in the theory of metals it appears that our calculations should apply reasonably well to most metals except for the transition metals and metals of the Bi group.

The Condition for Superconductivity

It has been assumed in the previous sections that in superconductors the distribution in the ground state is of the f_1 type shown in Fig. 2a. This condition is realized if the interaction between the electrons and the vibrational field is sufficiently strong to fulfill condition (3.19). Using (2.9),

$$(4\nu)^{\frac{1}{2}}F=(4\nu)^{\frac{1}{2}}C^2/3\zeta Ms^2>1, \quad (\text{if } 4\nu<1) \tag{6.1}$$

is thus the condition which must be fulfilled by a metal to make it a superconductor. Since the required strong interaction also leads to high normal resistivity ρ at high temperatures T where $\rho \propto T$ one should expect that condition (6.1) can be written in terms of ρ. In fact it is found that[6]

$$KT/\rho=(4\nu M/\pi^3 m)(\zeta/C)^2(K\theta_l)^2/k_0\hbar a_0, \tag{6.2}$$

where a_0 is the Bohr radius. By using the identities expressed by Eqs. (2.4), (2.3), (2.2), and (2.1), together with the definition of the number ν of free electrons per atom we obtained

$$KT/\rho=(12\nu^{4/3}/2^{\frac{1}{2}}\pi)(\hbar^3/m^2a_0)(Ms^2\zeta/C^2)n. \tag{6.3}$$

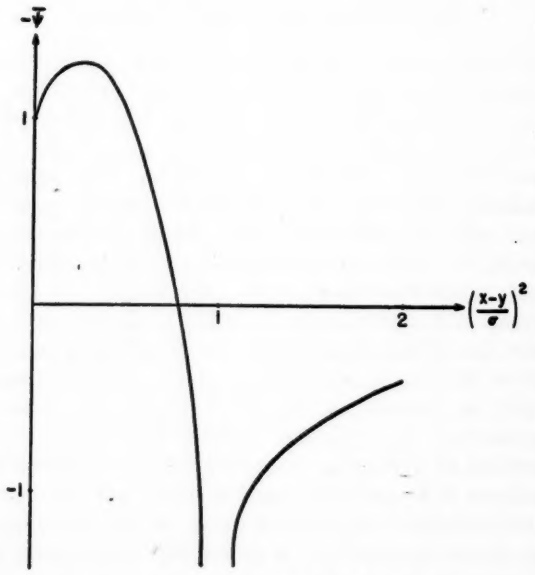

FIG. 5. Angular average $-\bar{\psi}$ of the $-\psi$ interaction.

[6] See Eq. (36.12) of reference 3. Replace there $(K_0 dE/dK_0)^2$ by $4\zeta^2$, n_0 by ν, θ by θ_l and k by **K**.

TABLE I. Data for normal metals.

Normal	Li	Na	K	Rb	Cs	Cu	Ag	Au	Be	Mg	Ca	Sr	Ba
$n\times10^{22}$ (cm^{-3})	4.63	2.56	1.33	1.08	0.87	8.50	5.90	5.93	12.5	4.34	2.33	1.80	1.59
ρ^{-1}(Ω^{-1} cm^{-1}, 273°)	12	24	16	8.6	5.6	65	67	49	18	25	24	3.3	1.7
$4^{\frac{1}{2}}F$	2.2	0.60	0.47	0.71	0.88	0.74	0.50	0.68	4.0	1.0	0.55	3.1	5.3

TABLE II. Data for superconducting metals.

Superconducting	Zn	Cd	Hg	Al	Ga	In	Tl	Sn	Pb
n	6.60	4.66	4.40	6.06	5.13	3.86	3.52	3.74	3.32
ρ^{-1}	18	15	4.4	34	1.9	12	7.1	10	5.2
$4^{\frac{1}{2}}F$	2.1	1.8	5.6	1.0	15	1.7	2.8	2.1	3.6

Consequently condition (6.1) becomes

$$(4\nu)^{\frac{1}{2}}F=(\rho n\nu^{5/3}/KT)D, \tag{6.4}$$

where

$$D=(2^{\frac{1}{2}}\times4/\pi)(\hbar^3/m^2a_0) \tag{6.5}$$

is a universal constant. The simplest way to find F for various metals is to take one metal, say silver, as a standard. Here according to Bethe[3] (p. 524), $(C/\zeta)_{Ag}=1.2$. Furthermore, from (2.2) and (2.1), $\zeta_{Ag}=5.5$ ev is obtained with $\nu=1$ (which follows from optical and Hall effect measurements). With the value $s=2.7\times10^5$ cm/sec. for the velocity of sound, and $\nu=1$ we find according to (6.1),

$$4^{\frac{1}{2}}F_{Ag}=(4^{\frac{1}{2}}/3)(C^2/\zeta Ms^2)_{Ag}=0.50<1, \tag{6.6}$$

which shows that silver does not fulfill the condition for superconductivity. With this value we can now express the condition (6.4) for superconductivity in the form

$$(4\nu)^{\frac{1}{2}}F=4^{\frac{1}{2}}F_{Ag}(\rho n\nu^{5/3}/\rho_{Ag}n_{Ag})$$
$$=0.50(\rho n/\rho_{Ag}n_{Ag})\nu^{5/3}>1. \tag{6.7}$$

In this condition the only quantity that brings some uncertainty is the number ν of free electrons per atom. This number is for most metals (not only for monovalent ones) of the order $\nu=1$ although accurate values are difficult to obtain. Tables I and II show the striking result that for none of the superconductors is $4^{\frac{1}{2}}F$ smaller than unity, and only for four (Li, Be, Sr, Ba) of thirteen normal metals is it larger than unity. It is of interest to see that this quantity is small for alkali metals because of their small value for n, but for noble metals because of their low resistivity. It should not be forgotten, however, that the uncertainty of the number ν of free electrons per atom reflects on the above results. Furthermore, the resistivity at 273° abs. used in the tables need not in all cases be in the high temperature range where $\rho\propto T$. It may also happen that electrons fill two energy bands, only one of which goes into the superconductive state. In this case (6.7) would be invalid. Finally, it should be of interest to see how the superconductivity condition (6.1) varies with the number of free electrons when other parameters are not altered. According to (2.1) and (2.2), $\zeta\propto n_{el}^{\frac{1}{3}}$. Thus if ζ_0 is defined as the value of ζ if $n_{el}=n$ ($\nu=1$) then (6.1) becomes

$$(1/\nu^{\frac{1}{3}})(4^{\frac{1}{2}}C^2/3\zeta_0Ms^2)>1;\quad(4\nu>1). \tag{6.8}$$

This shows that to make a normal metal superconducting the number of free electrons per atom, ν, should be reduced, providing this can be done without reducing C^2/Ms^2. It seems likely that an effect of this type occurs when alloys of normal metals become superconductive. It suggests the formation of an alloy between a monovalent metal and a transition metal in such a way that most electrons of the monovalent metal are used to fill up the incomplete shell of the transition metal. This occurs, for example, in Pd-Au with up to 40 percent Pd, as has been shown by Mott;[7] but the variation of the other parameters should be taken into account before making definite predictions.

TABLE III. Critical magnetic fields for superconductors.

	s (cm/sec.)	H_c (theory) ($\nu=1$)	H_c (exp. extrapolated to $T=0$), (gauss)
Zn	3.7	4100	
Sn	2.6	2800	300
Pb	1.3	1700	800

Critical Magnetic Field

On application of a magnetic field larger than a critical field, H_c, a superconductor is transferred into the normal state. It is shown in the phenomenological theory[8] that this is a thermodynamic consequence of the magnetic properties, and that $H_c^2/8\pi$ is the difference between the free energies of the metal in the normal and in the superconducting state. This energy difference has been calculated in Sec. III, Eq. (3.17)

[7] N. F. Mott, Proc. Phys. Soc. London **47**, 571 (1935).
[8] C. J. Gorter and H. Casimir, Physica **1**, 306 (1934).

and is denoted by $-S(\xi)$. Thus at $T=0$, using $\nu=n_{el}/n$, and (2.9)

$$\frac{H_c^2}{8\pi}=\frac{3\times 4^{\frac{1}{3}}F}{2\times 2^{\frac{1}{3}}}ms^2n\nu^{\frac{1}{3}}\left[P(\xi)-\frac{\xi}{F(4\nu)^{\frac{1}{3}}}\right]$$

$$=\frac{C^2}{\zeta}\frac{m}{M}n_{el}\left[P(\xi)-\frac{\xi}{(4\nu)^{\frac{1}{3}}F}\right]. \quad (6.9)$$

The expression in the bracket refers to the value of ξ at which it has its minimum. Its value is always less than 0.3 as can be seen from Fig. 3. It is close to 0.15 for values of $(4^{\frac{1}{3}}F)=2$, but 0.2 if $(4^{\frac{1}{3}}F)=3.6$ (Pb). To find H_c requires only the root which for both values will be equated to 0.4 which involves an error of only 10 percent. Thus from (6.9)

$$H_c=2.2\times(4^{\frac{1}{3}}F)^{\frac{1}{2}}(nms^2)^{\frac{1}{2}}\nu^{\frac{1}{3}}. \quad (6.10)$$

Values of $4^{\frac{1}{3}}F$ and of n are given in Table II. With $\nu=1$, Table III shows values of the order of 1000 gauss in agreement with the magnitude obtained experimentally, though somewhat larger. It follows that the energy difference calculated in Sec. III has the correct absolute magnitude. Finer details would no doubt be very sensitive to deviations from the free electron model.

Notes added in proof: (1) The isotope effect [see Reynolds *et al.*, Phys. Rev. **78**, 487 (1950); Maxwell, Phys. Rev. **78**, 477 (1950)] which has recently come to my notice follows quantitatively from the proportionality of $|S|$ with the inverse isotopic mass $1/M$ [see e.g. Eq. (6.9) where F depends on Ms^2 only and is hence independent of the isotopic mass] as was stated in a recent note [Frölich, Proc. Phys. Soc. **A63**, 778 (1950)]. This agreement provides a direct check for the fundamental assumptions of the theory.

(2) Dr. Kun Huang has checked the integrations without making the approximations $(q-k)^2\ll k_0^2$. He confirmed the values for S_1 and S_2; but the repulsive energy S_3 has to be reduced by a factor two. We have also found that the change of Coulomb exchange energy provides a further repulsive term; together with S_3 it leads approximately to a total increase in repulsive terms by a factor three. This reduces all F values of the table by about a factor 3 and thus does not essentially alter the conclusions. It reduces H_c for lead to about 1200 gauss thus improving the agreement with experiment.

(3) I have now been able to show that the assumption of a homogeneous magnetic field H, however weak, in a sufficiently extended metal would lead to a reduction of the magnitude of the S-interaction by a value independent of H. Such a field can therefore not exist in a superconductor as required by the Meissner effect. The calculations are not yet sufficiently advanced to decide whether the presence of a field always leads to the normal state or whether an intermediate state may occur.

Fluorescence of Solutions Bombarded with High Energy Radiation (Energy Transport in Liquids)*

HARTMUT KALLMANN AND MILTON FURST
Physics Department, New York University, Washington Square, New York, New York
(Received May 11, 1950)

It is experimentally shown that solutions bombarded with high energy radiation exhibit strong fluorescence when only small amounts of "fluorescent molecules" are added to the solvent. The same amount of fluorescent substance alone would give only about 0.01 of the observed light emission. The large emission in the solution is explained by a transport of excitation energy from the solvent to the fluorescent molecules. An analysis of the mechanism energy transport in the liquid is also given.

A. INTRODUCTION

IT is well known from different experiments, especially from those with fluorescent substances, that a transport of energy through solids can take place over distances which are of the order of 100 atomic distances and more. Such a transport of energy can be carried out by free electrons moving in the crystal or by migration of excitation energy from one molecule to the other. Such processes of migration of excitation energy have been discussed by different authors, especially by Frank and Teller[1] and by Frenkel.[2] The experimental demonstration for such a migration of energy can perhaps best be seen in experiments of Bowen[3] who has shown that for naphthalene excited by ultraviolet light, the light emission can be increased by adding to the naphthalene small amounts of anthracene of the order of 10^{-4} to 10^{-3} molecule of anthracene per naphthalene molecule. Such small amounts are already sufficient to shift the emission spectrum from the wave-lengths characteristic of naphthalene to those of anthracene and at the same time are sufficient to increase the total light output considerably. Similar results are obtained with other organic crystals as long as the wave-length emitted by the contaminant is longer than that of the bulk material.

If such crystals with small amounts of contaminating material are excited by gamma-radiation or alpha-particles instead of light, not only are the electrons of the contaminant excited, but also the electrons of the bulk material almost as strongly. The energy primarily absorbed by the contaminant is approximately proportional to the mass of the contaminant present; for instance, anthracene present in a mole concentration of 10^{-3} absorbs only 10^{-3} of the whole energy. In these cases also a shift in the emission spectrum to approximately that of the contaminant is observed if the spectrum of the contaminant is located at longer wavelengths than that of the bulk material. For example, the emission spectrum of anthracene which is not highly purified is shifted to the green, most likely because of the migration of energy to the small amounts of naphthacene present as an impurity. Similar shifts were also observed in naphthalene and phenanthrene contaminated with anthracene toward the spectrum of anthracene; anthracene has a longer fluorescent wave-length than these materials.

This idea of migration of energy and the considerable shift of the spectrum in fluorescent crystals, has suggested to us the carrying out of experiments with fluorescent liquid solutions in the hope of also finding an energy transfer from the bulk material to the dissolved molecules. In liquids the situation is, however, different from that in a solid. A pure liquid exhibits only an extremely small emission of its own fluorescent light when excited by such radiations. If a naphthalene crystal is molten, for example, its fluorescent intensity disappears almost completely. Earlier experiments seemed to indicate, however, that such a large intensity drop occurs only with pure substances and not to the same degree with substances containing a small amount of other molecules. The small light emission usually observed in pure liquids results because of the interaction between similar molecules. The molecules in a liquid have a considerable freedom of motion, and thus at times an excited molecule may come into much closer contact with another similar but unexcited molecule than would be the case for a solid.

Therefore, in a pure liquid excited by fast particles the excitation energy is mainly quenched. But if this liquid contains foreign molecules which can trap the excitation energy (for a more complete description of this process see Section E), it may be that the excitation energy is transported to the dissolved molecules before it is quenched.

To establish this idea the fluorescence of a large number of solutions when excited by gamma- and alpha-radiations was examined. Up to the present such solutions have been investigated only under excitation by light, and the light was not absorbed by the solvent but only by the dissolved molecule. One paper we found dealing with a fluorescent solution under gamma-irradiation, is that of Ageno, Chiozzotto, and Querzoli.[4]

* This work was supported by the Signal Corps Engineering Laboratories, Fort Monmouth, New Jersey.

[1] J. Franck and E. Teller, J. Chem. Phys. **6**, 861 (1938).

[2] J. Frenkel, Physik. Zeits. Sowjetunion **9**, 158 (1936).

[3] Bowen, Mikiewiez, and Smith, Proc. Phys. Soc. London **A62**, 26 (1949).

[4] Ageno, Chiozzotto, and Querzoli, Acc. dei Lincei **6**, 626 (1949). See also G. T. Reynolds, reference 5, and H. Kallmann, Phys. Rev. **78**, 621 (1950).

TABLE I. Light intensities of pure solvent when excited by gamma-radiation.

Solvent	Intensity relative to anthracene crystal of the same mass
Aniline	0.007
Benzene	0.009–0.012
Benzyl Alcohol	0.005
Benzyl Ether	0.005
Carbon Tetrachloride	0.006–0.007
Alpha-Chloronaphthalene	0.032
Cyclohexene	0.006
1,4 Dioxane	0.005
Ether	0.006–0.008
Ethyl Alcohol	0.009
n-Heptane	0.007
Hexane	0.008
Mesitylene	0.005
Naphthalene Monobromide	0.005
Paraffin Oil (mineral oil)	0.014
Pyridine	0.005
Quinoline (synthetic)	0.003
Styrene	0.006
Toluene	0.010–0.012
Xylene (commercial)	0.012–0.015
m-Xylene	0.012
o-Xylene	0.009
p-Xylene	0.008
Water, singly distilled	0.014
Water, doubly distilled	0.009

These authors seem to obtain some results similar to ours but since they have published results with naphthalene in xylene, it is difficult to compare our results with theirs.

B. EXPERIMENTAL ARRANGEMENT

Our experimental arrangement was quite simple. A commercial photometer with an RCA type 1P28 multiplier tube was used as the recording instrument. With this tube the spectrum from the ultraviolet up to 5000A can be adequately covered. To the housing of the multiplier tube a photographic shutter was attached, and a metal beaker was screwed to the shutter as shown in Fig. 1. This metal beaker contained a 1-millicurie gamma-source placed below a porcelain beaker into which the different solutions under investigation could be placed. The photographic shutter was introduced in order to distinguish between the light coming from the fluorescent substance and the effect of the radiation from the gamma-source on the photo-multiplier tube. With the gamma-source present and the shutter closed the instrument was adjusted to zero. With the shutter kept closed and the gamma-source absent a small deflection of the recording instrument was still observed. This indicated an effect of the gamma-source on the multiplier tube. To compensate for these spurious recordings the gamma-source was always kept in the same position, and the instrument was adjusted to zero before each reading. With the shutter opened the instrument thus recorded only the effect of the fluorescent light on the multiplier, since the shutter was so thin that it did not appreciably absorb the gamma-radiation. The arrangement was tested by taking readings without any fluorescent material; a reading of several divisions was still observed. This reading was found to come from the fluorescence of the glass beaker being used. When the glass beaker was replaced by a porcelain beaker, this effect vanished. The porcelain beaker has another important advantage in that it reflects the light emitted by the substance within the beaker into the multiplier.

To test the sensitivity of the arrangement, a fairly clear anthracene crystal of 5.5 gram mass was placed within the beaker. This crystal was wrapped in aluminum foil, except for the side facing the multiplier, to increase the back reflection of the light. With this crystal the multiplier gave a reading corresponding to approximately 2500 divisions with the gamma-source of one millicurie. All the intensities given below are referred to this reading since the solutions investigated were used in the same geometrical arrangement and with approximately the same volume of material in order to provide always the same amount of absorption of gamma-radiation.

This simple arrangement was quite sensitive and made possible the rapid testing of many solutions. The sensitivity of the arrangement can be judged from the fact that it was possible to detect the 1-millicurie gamma-source at a distance of 50 cm from the 5.5-gram anthracene crystal and also the neutron radiation of a 10-millicurie polonium berylium neutron source when it was placed just outside of the metal beaker. With this arrangement it was difficult to find any transparent substances which gave no fluorescence under gamma-radiation.

Two other arrangements were used for testing larger amounts of solutions. One of these arrangements also

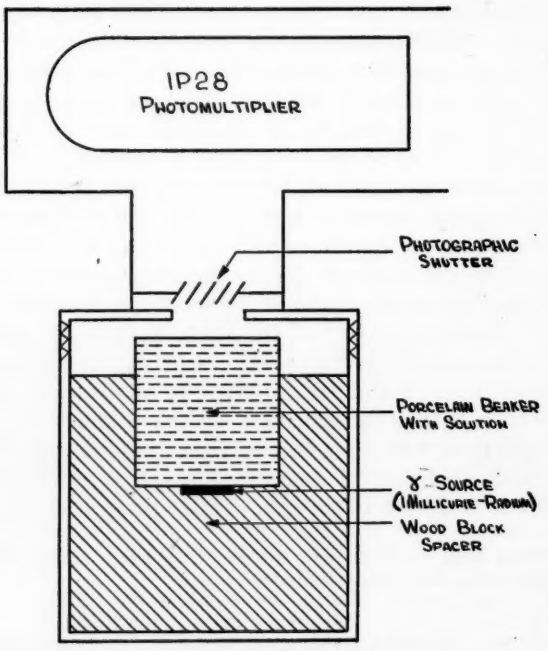

FIG. 1. Experimental arrangement.

was an integrating intensity device, but instead of the commercial photometer a photo-multiplier tube, type 5819, was used with a special electrical circuit. The multiplier tube had a large bottomless porcelain container cemented on the upper edge of the multiplier tube. It was much more sensitive than the previously described arrangement. With the 5.5-gram anthracene crystal placed on the top of the multiplier, this arrangement gave appreciable readings with the 1-millicurie gamma-source several meters away from the crystal. This arrangement has a different spectral response from the commercial one; it is more sensitive in the range above 4000A than is the 1P28 type tube.

The third arrangement was a counting device in which the pulses occuring at the anode of the multiplier type 5819 were fed to an oscillograph where their peak heights could be compared with those from the anthracene crystal.

It will be seen later that the peak heights produced by the solution are relatively higher compared to anthracene than the ratio of the readings of the integrating intensity meter using the commercial arrangement. One of the main reasons for this effect comes from the fact that in the counting arrangement the liquid makes close contact with the window of the multiplier and thus reduces the reflection losses of the glass surface to a minimum. The anthracene crystal, however, was placed directly on the window of the multiplier without being cemented to its surface. The intensity of its light flashes was, therefore, diminished by additional reflection at the thin air layer between the crystal and glass surfaces. For this reason the peak intensities of the solution expressed in anthracene values when observed on our oscilloscope are approximately 2 times higher than the ratio of the readings obtained with the commercial integrating intensity meter, even in cases where the emission spectrum was nearer the region of higher sensitivity of the 1P28.

C. EXPERIMENTAL RESULTS

The experimental results obtained with the first arrangement are reproduced in Figs. 2 to 5 and Tables I–VIII. Table I gives the readings for different pure solvents. The solvents used were obtained commercially and were classed as of highest purity. Our measurements, however, seem to indicate that the intensities recorded are not those of the pure solvent. It is well known from optical experiments that the fluorescent emission spectra of most of these solvents lie in the ultraviolet region. A rough filter analysis of the light emitted showed that the amount of ultraviolet light was very small and most of the emitted light in the neighborhood of 4000A. That the light emitted was not the characteristic spectrum of the solvent was shown by another experiment. A filter analysis was carried through with liquid and frozen benzene. The frozen benzene was found to emit a large amount of ultraviolet, but only a small amount was present in the liquid. We conclude from these measurements, and from the measurements described below, that the intensities

TABLE II. Substances increasing pure solvent intensity by at least a factor of 1.5.

Substance	Solvent	Approximate maximum concentration g/l	Relative intensity
Aniline	Xylene	2	0.036
Anthracene	Benzene	1	0.066
Anthracene	Benzyl alchol	4	0.039
Anthracene	Benzyl ether	5	0.029
Anthracene	Hexane	1	0.016
Anthracene	Mesitylene	1.2	0.026
Anthracene	Paraffin oil	1.5	0.029
Anthracene	Toluene	1.5	0.074
Anthracene	Xylene (commercial	1.4	0.090
Anthracene	m-Xylene	1.5	0.072
Anthracene	p-Xylene	1.5	0.057
Carbazole[a]	Benzene	1.5	0.074
Carbazole[a]	1,4-Dioxane	10	0.066
Carbazole[a]	Paraffin oil	0.5	0.034
Carbazole[a]	Xylene	1.4	0.12
Diphenyl	Benzene	2	0.017
Diphenyl	Xylene	3	0.027
m-Diphenylbenzene	Xylene	35	0.20
Diphenylbenzidine[a]	Xylene	0.25	0.10
Diphenylbutadiene	Xylene	1.5	0.14
Diphenylhexatriene	Xylene	1.5	0.20
Diphenyloctatetraene	Xylene	1	0.024
Fluoranthene[a]	Xylene	3	0.13
Fluorene[a]	Benzene	1	0.049
Fluorene[a]	Xylene	2	0.058
Naphthalene	Benzene	3	0.021
Naphthalene	Xylene	12	0.025
alpha-Naphthol[a]	Xylene	1	0.060
beta-Naphthol	Xylene	1.5	0.098
alpha-Naphthylamine[a]	Aniline	6	0.074
alpha-Naphthylamine[a]	1,4-Dioxane	10	0.14
alpha-Naphthylamine[a]	Hexane	1.5	0.016
alpha-Naphthylamine[a]	Xylene	2	0.22
beta-Naphthylamine[a]	Xylene	2.5	0.18
Phenanthrene[a]	Benzene	10	0.053
Phenanthrene[a]	Toluene	8	0.066
Phenanthrene[a]	Xylene	7.5	0.070
Phenol	Benzene	5	0.021
trans-Stilbene	Xylene	3	0.037
Terphenyl	Benzene	4.5	0.28
(p-diphenylbenzene)	Benzyl alcohol	1.8	0.056
(p-diphenylbenzene)	Benzyl ether	8	0.051
(p-diphenylbenzene)	Cyclohexane	2	0.028
(p-diphenylbenzene)	1,4-Dioxane	10	0.23
(p-diphenylbenzene)	n-Heptane	1.5	0.058
(p-diphenylbenzene)	Hexane	0.8	0.049
(p-diphenylbenzene)	Mesitylene	5	0.037
(p-diphenylbenzene)	Paraffin oil	0.5	0.045
(p-diphenylbenzene)	Toluene	5	0.39
(p-diphenylbenzene)	Xylene	5	0.46
(p-diphenylbenzene)	m-Xylene	5.5	0.44
(p-diphenylbenzene)	o-Xylene	6	0.26
(p-diphenylbenzene)	p-Xylene	5	0.16
Triphenylamine	Xylene	3	0.032
Xylene	Paraffin oil	120	0.030

[a] Substances have been additionally purified.

reproduced in Table I are mostly due to very small amounts of fluorescent material present in the pure solvent as contamination.

There is another experiment which shows that one must be very careful in accounting for these relatively small intensities. Pure aniline, for instance, gives an intensity about half that of toluene or xylene. With this solvent the addition of small amounts of anthracene even cuts down the intensity of the "pure" solvent. Also a substance like dihydrocollidine even in small concentrations is found to decrease the intensity of many solvents considerably though the crystal itself is highly fluorescent. Accordingly, one must also consider the possibility that the measured values representing the intensity of the pure solvent may also be quenched and thus in reality be higher than recorded. Mostly, however, the numbers shown in Table I are felt to represent the light intensities of the solvents contaminated perhaps by very small amounts of fluorescent material of the order of less than about 0.1 g/l.

The change in intensity caused by an addition of small amounts of fluorescent material to these solvents is shown in Figs. 2 to 5 and by Table II. The concenttrations shown are accurate to within about 15 percen and the intensities to 10 percent. The curves represent the change in light intensity with increasing concentration of the fluorescent material. Since the quantity of substance added was always very small, the amount of absorbed gamma-radiation is substantially the same for all solutions tested. All the curves show a rather steep increase at low concentration, then they go through a rather broad maximum and finally decrease slowly with higher concentration, except in such cases as commercial carbazole where a rapid decrease occurs on account of a quenching impurity (see Fig. 2).

In this paper we denote the fluorescent molecule added to the solvent as "fluorescent molecule." It should be remembered that the molecules of many of the solvents are also fluorescent, but their fluorescence is suppressed in the solvent. The intensities given in Tables II to V are the intensities of these added molecules not of the solvents as was roughly checked by filter analysis. All these measurements were made at room temperature.

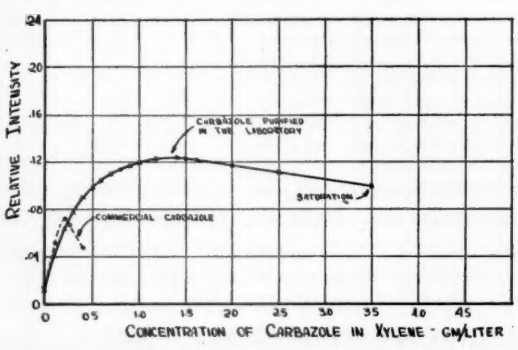

FIG. 2. Carbazole in xylene.

A substantially similar type of variation of relative intensity with concentration was found for all of the substances and solvents. Only the height of the maximum and its corresponding concentration vary from substance to substance. These maximum intensities and the concentration associated with them (maximum concentration) are collected in Table II.* Many substances have a maximum concentration lying between 1 and 5 grams per liter. Some, such as m-diphenylbenzene have a maximum concentration as high as 35 g/l. The low concentrations correspond approximately to one fluorescent molecule in 1000 solvent molecules. This means that only a tenth of one percent of the total energy absorbed from gamma-radiation is absorbed in the fluorescent molecule itself The intensities given in Table II, however, show that the increase in light output caused by these small amounts of substances represents a considerable amount of the total energy absorbed in the whole solution. The fact that these large intensities cannot be accounted for by the small amount of primary absorption in the fluorescent molecules can be seen from Table III.

The figures of Table III are determined in the following way: The emission of the 5.5-gram anthracene crystal is assumed to have an intensity of unity. In most solutions under investigation a total amount of about 0.01 to 0.05 gram of these substances was necessary for the maximum intensity. Assuming that the absorption of gamma-radiation and, therefore, the emission is proportional to the mass of the substance

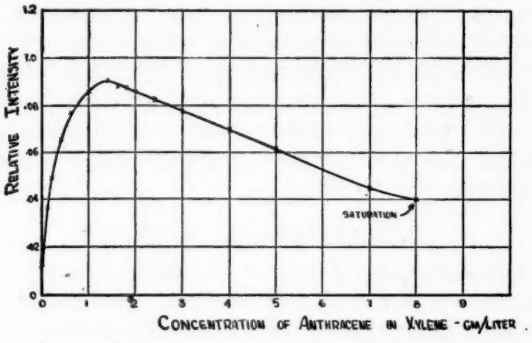

FIG. 3. Anthracene in xylene.

present, and taking into account the efficiency of fluorescence of the crystals compared to anthracene, the values in Table III are obtained. The values shown in Table III give the amount of fluorescent light (compared with that of 5.5 gram of anthracene) in three typical cases which should be obtained if the added substance alone would absorb energy and were entirely responsible for the fluorescence.

These values and those of Table II clearly indicate that the additional light emitted by the different mole-

* *Note added in proof:* Many other substances have been found since submission of the paper which give considerable fluorescence in solution under the same conditions.

cules in a solution cannot originate in the primary excitation of these fluorescent molecules. Instead, the excitation must be transferred from the excited molecules of the solvent to the dissolved molecule. This seems to be especially true for solvents such as benzene, toluene, xylene, mesitylene, heptane, p-dioxane and, paraffin oil. In paraffin oil, for example, only 0.5 g/l of terphenyl (a total of 0.003 g and equivalent to a reading of 0.0005 in Table III) exhibits an intensity which is only one-fifth that of 5 g/l of the same material when dissolved in xylene (Table II). These intensities are certainly far above the values which would be emitted by the same mass of the pure substance. With the other solvents under investigation it has not yet been established whether or not a considerable amount of energy is transferred from the solvent to the dissolved molecule. It may be noted that the intensity of alpha-naphthylamine and diphenyl hexatriene given in this table are not in their correct ratio with respect to most of the other substances, since these substances have a light emission also in the green where the response of the 1P28 is comparatively low. A measurement using the 5819 tube showed that these substances are almost as good as terphenyl.[5]

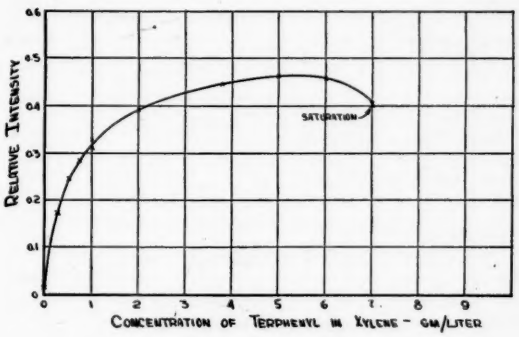

Fig. 4. Terphenyl in xylene.

Table IV gives the light emission of a number of solutions in which the added molecule does not increase, but instead considerably decreases, the light emission of the solvent. In this respect it is interesting to see that molecules which exhibit a high light intensity in some solvents act as quenchers in others. For instance, anthracene, carbazole, and terphenyl, all good fluorescent materials in xylene, diminish the light emission of pure aniline and alpha-chloronaphthalene. Even in solvents such as xylene, benzene, and dioxane similar quenching effects occur with substances which are usually known as fluorescent in the solid phase, for instance dihydrocollidine (which exhibits as a crystal a very bright blue fluorescence under ultraviolet radiation), diphenyl acetylene, and dibenzyl. The results of this table clearly indicate that for the complete understanding of this phenomenon, internal quenching effects

[5] Terphenyl was first proposed by Reynolds, Harrison, and Salvani, Phys. Rev. 78, 488 (1950).

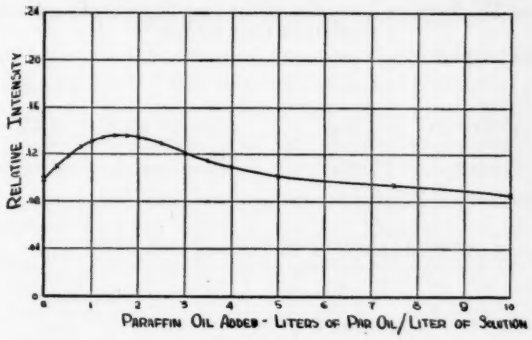

Fig. 5. Effect of adding paraffin oil to saturated solution of carbazole in xylene.

of the fluorescent molecules have to be taken into account. This will be done in Sections D and E.

In Table V the results of our measurements with mixed solutions are noted. The general results of these measurements can be described as follows. In some special cases the addition of another fluorescent material increases the light emission slightly above the maximum of either constituent in solution. In no case does the maximum light emission of the mixture of two substances equal the sum of the maximum light emissions of the substances alone. The greatest increase was obtained by adding fluorene to a solution of anthracene in xylene; in other solutions, however, such as, carbazole in xylene the addition of fluorene diminishes the light emission. Thus the same substance can act as a quencher in one solution and as a stimulator in another. Some cases such as naphthacene in a solution of anthracene in xylene are quite different and do not fit in with the results obtained with other substances. In such a solution naphthacene quenches in a concentration of as low as 10^{-3} g/l which means less than 10^{-3} mole percent. This quite special behavior of naphthacene comes from the fact that naphthacene has a strong absorption band just in the region of the anthracene emission spectrum. This effect will be explained below.

In connection with the results indicated in Tables IV and V it may be noted that all the results are influenced by rather small amounts of contamination, even in those solvents sold commercially as being of highest purity. Some solvents give results differing by 10 percent if samples from different bottles are used. Especially sensitive to impurities found in commercial products are substances like carbazole, phenanthrene, and diphenylbenzidine. The intensities of these substances were raised by a factor of two after they were additionally purified in our laboratory. Some others, like anthracene and alpha-naphthylamine, however, appear to be comparatively insensitive to commercially present impurities.

In Table VI some results with paraffin oil are presented, others are found in Table II. These figures show that the addition of carbazole, anthracene, and terphenyl to pure paraffin oil raises its intensity by a factor

TABLE III. Relative intensities of the pure fluorescence substance contained in the solutions.

Substance			Intensity
Anthracene	0.01 g	approximately	0.002
Carbazole	0.01 g	approximately	0.001
Terphenyl	0.03 g	approximately	0.005

TABLE IV. Quenching effects in pure solvents.

Solutions	Intensity relative to anthracene crystal
Aniline	0.007
Aniline+Anthracene (1.5 g/l)	0.002
Aniline+Carbazole (0.2 g/l)	0.005
Aniline+Terphenyl (0.5 g/l)	0.005
Benzene	0.012
Benzene+Dihydrocollidine (0.2 g/l)	0.003
Carbon Tetrachloride	0.006
Carbon Tetrachloride+Anthracene (1.5 g/l)	0.005
Carbon Tetrachloride+Carbazole (0.25 g/l)	0.003
Carbon Tetrachloride+Naphthalene (3 g/l)	0.003
Alpha-Chloronaphthalene	0.032
Alpha-Chloronaphthalene+Carbazole (1 g/l)	0.028
Alpha-Chloronaphthalene+Terphenyl (0.8 g/l)	0.030
Ether	0.006
Ether+Anthracene	0.004
Ethyl Alcohol	0.009
Ethyl Alcohol+Anthracene (0.2 g/l)	0.004
Ethyl Alcohol+Carbazole (0.5 g/l)	0.007
Ethyl Alcohol+Naphthalene (3 g/l)	0.005
Pyridine	0.005
Pyridine+Anthracene (0.2 g/l)	0.002
Pyridine+Dihydrocollidine (1 g/l)	0.002
Xylene	0.013
Xylene+Carotene (0.1 g/l)	0.001
Xylene+Dibenzyl (1 g/l)	0.011
Xylene+Dihydrocollidine (0.2 g/l)	0.004
Xylene+Diphenyl Acetylene (1 g/l)	0.007
Xylene+Fluorenone (0.5 g/l)	0.004
Xylene+Melaniline (1 g/l)	0.006
Water doubly distilled	0.009
Water+Uranyl Acetate	0.004
Water+Uranyl Nitrate	0.005

as high as four. The same is true when xylene is added to paraffin oil (in this case the maximum concentration is as high as 120 g/l). Quite a special effect, however, occurs if xylene plus carbazole or anthracene are added to paraffin oil as shown in Table VI. In the case of carbazole the maximum light output rises above the maximum value attained in a solution of carbazole in xylene without paraffin oil. The maximum light output occurs when 1 liter of xylene solution is dissolved in 1.5 or 2.5 liters respectively of paraffin oil. It can be seen from Fig. 5 that the intensities diminish only slightly with increasing amounts of paraffin oil. With 10 liters of paraffin oil to 1 liter of solution the intensity is almost as high as the intensity of the original xylene solution. It should be noted that in this case only one-tenth of the original amount of xylene plus carbazole is present,

TABLE V. Intensities in mixed solutions.

Solutions	Intensity relative to anthracene crystal
Xylene+Anthracene (1.5 g/l)	0.072
Xylene+Anthracene (1.5 g/l)+Fluorene (2 g/l)	0.086
Xylene+Anthracene (1.5 g/l)+Naphthacene (0.001 g/l)	0.062
Xylene+Anthracene (1.5 g/l)+Naphthacene (0.01 g/l)	0.041
Xylene+Anthracene (1.5 g/l)+Xanthone (3 g/l)	0.023
Xylene+Anthracene (0.5 g/l)	0.066
Xylene+Anthracene (0.5 g/l)+Naphthalene (1–10 g/l)	0.066
Toluene+Anthracene (1.5 g/l)	0.072
Toluene+Anthracene (1.5 g/l)+Fluorene (2 g/l)	0.079
Toluene+Anthracene (1.5 g/l)+Dihydrocollidine (0.2 g/l)	0.058
Xylene+Fluorene (2.5 g/l)	0.049
Xylene+Fluorene (2.5 g/l)+Naphthalene (1 g/l)	0.029
Benzene+Anthracene (1.5 g/l)+Fluorene (2 g/l)	0.066
Benzene+Anthracene (1.5 g/l)+Fluorene (2 g/l) +Benzyl Alcohol (0.25 l/l)	0.037
Xylene+Carbazole (0.35 g/l)	0.084
Xylene+Carbazole (0.35 g/l)+Fluorene (1 g/l)	0.064
Xylene+Terphenyl (5 g/l)	0.45
Xylene+Terphenyl (5 g/l)+m-Diphenylbenzene (12 g/l)	0.28
Xylene+Terphenyl (5 g/l)+Fluoranthene (1.5 g/l)	0.13
Xylene+Terphenyl (5 g/l)+Alpha-Naphthylamine (1.5 g/l)	0.17
Xylene+Terphenyl (5 g/l)+Anthracene (0.1 g/l)	0.10

Table VI. Measurements with paraffin oil.

Substances	Intensity relative to anthracene
Paraffin Oil	0.014
Paraffin Oil+Carbazole (0.5 g/l)	0.032
Paraffin Oil+Anthracene (1.5 g/l)	0.029
Paraffin Oil+Xylene (120 g/l)	0.028
Xylene	0.014
Xylene+Carbazole (saturated approx. 3.5 g/l)	0.098
Xylene+Anthracene (saturated approx. 8 g/l)	0.041
Xylene+Carbazole (saturated approx. 3.5 g/l) +Paraffin Oil (1.5 liters/liter)	0.13
Xylene+Anthracene (saturated approx. 8 g/l) +Paraffin Oil (2.5 liters/liter)	0.091

which means that the energy primarily absorbed in xylene is only one-tenth of that in the case of xylene without the paraffin oil and, nevertheless, such a high intensity is obtained. These results demonstrate a special effect of paraffin oil on these solutions which will be explained in the next section.

With some solutions, in which substantial increases were found by using the commercial intensity integration apparatus, experiments were also performed with the peak measuring arrangement and with the more sensitive circuit for large amounts of solution. The peak measurements showed that the maximum peak heights attained with these solutions were substantially proportional to the intensities in Table II (with the

exception of substances like naphthylamine and diphenyl hexatriene as explained previously). According to the peak measuring method, terphenyl, alpha-naphthylamine, and diphenyl hexatriene turn out to be practically equally effective. The ratio between the maximum peak height of the solution and that of our standard anthracene crystal turned out to be larger, by a factor between two and three, than the values in column four of Table II. This originates, as already mentioned, in the smaller reflection losses between the solution and the surface of the multiplier tube than between the crystal and the multiplier. It was further found that the solutions were sensitive to contamination in the beaker cemented to the photo-multiplier tube; the cement caused some decrease in the light output of these solutions. This was substantiated by re-testing the solutions in the standard porcelain crucibles and finding the intensities to be somewhat lower than previously. Some measurements were also made with the large beaker on the photo-multiplier tube completely filled with solutions. The integrated intensity results on some of the solutions were found to be superior to the anthracene crystal because of the large amounts of the solutions which can be used in this arrangement.

Some experiments were also carried out with alpha-particles of 5.3 Mev as the exciting radiation. The alpha-particles impinged on the upper surface of the solution and the peak heights of the pulses were measured with arrangement 3. When the thickness of the solution was about 1 cm the maximum pulse height was smaller than the maximum pulse height induced with gamma-radiation from a radium source. Since each alpha-particle transfers 5.3 Mev to the solution, whereas with the gamma-radiation at most 1.5 Mev is transferred to the solution, this shows that the light output when using alpha-particles is considerably less than with gamma-radiation when computed for the same amount of absorbed energy. The efficiency for alpha-particle excitation is about one-fifth that for gamma-excitation. This is nearly the same ratio as was found for anthracene crystals. The same experiments were repeated with a solution four times as deep. The solid angle of the incident light directly hitting the photo-multiplier is in this case considerably smaller than in the case of 1 cm and a larger amount of light impinges on the photo-multiplier only after being reflected from the walls, which were covered with a white highly reflecting layer. The ratio of the peak heights was 2.2/1.5 for the two thicknesses, indicating a noticeable loss of intensity caused by the reflection at the walls. The alpha-particles came from a polonium source and were fairly homogenous in energy. Nevertheless, the height of the peaks were not as uniform as might be expected for pulses of such high intensity. The peak heights were, of course, more homogenous than with gamma-radiation, but still rather large fluctuations were noted.

D. GENERAL CONSIDERATIONS

A general description and explanation of the processes underlying these experiments will be given in this section; in the next a more detailed theory will be presented. The experiments described above show that most of the energy which is emitted by fluorescent substances in solutions comes originally from that absorbed by the pure solvent. The mechanism of transport of excitation energy from the solvent to the fluorescent molecule will be described in the next section. There is an additional process which must be taken into account if the results are to be understood. This is the quenching of the excitation energy in the pure solvent (transformation into heat instead of emission as light) even though most of the molecules in solvents such as xylene, toluene, or benzene are in themselves fluorescent as is well known from optical experiments with alcoholic or other solutions of these substances.[6] If now a small amount of another fluorescent substance is added to the solvent, a part of the excitation energy of the solvent will be transported to these fluorescent molecules and be trapped there. This process of transportation of energy must be fast enough to avoid the primary quenching of the excitation energy in the solvent itself. The "trapping" of the excitation energy by the added fluorescent molecule is necessary to avoid final quenching by the solvent. If the excitation energy were to return to the solvent or would only remain at the fluorescent molecule for a small period of time, it would be quenched in the solvent. If the excitation energy is trapped in the added fluorescent molecule, two additional conditions must be fulfilled if large light emission is to occur: (a) the excitation energy added to the fluorescent molecule must not be quenched too much by interaction with the solvent or by internal conversion (both together described as internal quenching) and, (b) the concentration of these fluorescent molecules must be low enough that self-quenching by interaction between the fluorescent molecules themselves does not occur. Such self-quenching is well known from optical experiments and starts at concentrations of about a millimole per liter, which means a concentration of several one-tenths of a g/l. The resulting light emission by these molecules must, therefore, be considered to be a competition of the light emitting process and the quenching process, the latter becoming still more pronounced with increasing concentration of fluorescent molecules. These processes added to those of the quenching of the excitation energy in the solvent and the transport of the excitation energy and its trapping by the fluorescent molecules which were mentioned above, are necessary to account for the complete behavior of fluorescent molecules in solvents. The probability of transporting to and trapping the excitation energy by the fluorescent molecule is proportional to the concentration of the fluorescent molecule.

[6] P. Pringsheim, *Fluorescence and Phosphorescence* (Interscience Publishers, Inc., New York, 1949), p. 406.

Using these general ideas the results of the preceding paragraph can be described as follows. If $1/\tau_q(s)$ denotes the reaction probability of quenching the excitation in the solvent (defined by the well-known equation $dn/dt=[1/\tau_q(s)]n$), and if $1/\tau_t$ is the reaction probability of trapping the excitation energy at the fluorescent molecules ($1/\tau_t$ is proportional to the concentration of the fluorescent molecules), the number n_f of excited fluorescent molecules produced per unit time by energy transform from the solvent is given by

$$n_f=\tau_q(s)[\tau_t+\tau_q(s)]^{-1}n_e, \quad (1)$$

where n_e is the number of excited molecules created per unit time within the solvent by the external radiation (this is proportional to the incident intensity). The intensity of total light emission is then given by (The radiation of the solvent is neglected.)

$$I=\tau_t\tau_s(\tau_e\tau_i+\tau_e\tau_s+\tau_i\tau_s)^{-1}n_f$$
$$=n_e[(\tau_t/\tau_q)+1]^{-1}[(\tau_e/\tau_s)+(\tau_e/\tau_i)+1]^{-1}. \quad (2)$$

In this equation $1/\tau_e$ denotes the reaction probability that an excited fluorescent molecule emits light in unit of time, $1/\tau_i$ the reaction probability for internal quenching and $1/\tau_s$ the radiation probability for self-quenching. In Eq. (2) only the terms with τ_s and τ_t depend on the concentration of the fluorescent molecules. Both are inversely proportional to the concentrations. So that writing $\tau_t/\tau_q=k/c$, $\tau_e/\tau_s=k'c$, and $(\tau_e/\tau_i)+1=k''$, we get for the light intensity

$$I=[c/(k+c)][1/(k'c+k'')]n_e. \quad (3)$$

These considerations describe the final light emission as the competition of the following five separate reactions which are all necessary for the understanding of our experimental results. There are the reactions of trapping the excitation energy of the solvent at the fluorescent molecule and of its quenching in the solvent; there is the light emission of the fluorescent molecule, the internal quenching of this molecule and the self-quenching reaction between similar molecules. This equation gives an increase of light intensity for small concentrations porportional to the concentration; for higher concentrations it approaches saturation resulting from the denominator of the second term in (3) as long as $k\gg c$. For still higher concentrations, the intensity goes through a maximum and then gradually decreases because the denominator of the second factor becomes more important. The transport of energy to the fluorescent molecules, which is proportional to $c/(k+c)$, then no longer increases proportionately with the concentration but does so more slowly since only a limited amount of energy can be drawn from the solvent.

The investigations of the various substances used thus far show the following general characteristics. A sharp rise in intensity at small concentration, then a slower increase or almost constant intensity over a larger range of concentrations, and finally a slow decrease in intensity. During the first part of the curve the transport of excitation energy to the fluorescent molecules is most effective and little self-quenching between these molecules occurs. In the middle part of the curve self-quenching competes with the increasing transport of energy and in the decreasing part of the curve both self-quenching of the fluorescent molecules and saturation in the transport of energy to these molecules are effective.

With these ideas in mind the results of Tables IV and V can also be interpreted. The self-quenching effect of fluorescent molecules stems from a resonance interaction between the excited molecule and an unexcited molecule of the same kind. Many of the different molecules used, such as anthracene and carbazole, have excited states not very different from each other. If such unlike though similar molecules come close to each other, a resonance may be built up, and quenching effects, similar to those between molecules of the same kind, will occur. If to a solution which contains fluorescent molecules at a maximum concentration, fluorescent molecules of another but similar kind are added, the intensity of light emission is found to increase only slightly (see the results with anthracene and fluorene in xylene) or decreases (see for instance carbazole and fluorene in xylene). This arises from the fact that the addition of fluorescent molecules to a solution of almost optimal concentration increases the quenching between the fluorescent molecules. Another explanation for such behavior lies in the saturation effect occuring in the transport of energy from the solvent to the fluorescent molecule. We have seen earlier [Eqs. (1) and (3)] that no more than a certain amount of energy can be obtained from the solution. The decrease in the curves shown in Figs. 4 and 5 at the higher concentrations indicates that this region of saturation is being approached in these cases.

The case of anthracene in toluene plus dihydrocollidine on the other hand can be interpreted by assuming that dihydrocollidine exhibits considerable internal quenching. If a small amount of this substance is added to a solution of optimal concentration of anthracene plus toluene part of the energy of the solvent goes to the dihydrocollidine where it is quenched and thus lost for transfer to the anthracene. The fairly large decrease in intensity may indicate, however, that some energy from the anthracene also goes directly to the dihydrocollidine (by absorption of anthracene radiation see Section E) where it is internally quenched and thus results in an additional loss in intensity.

The results of Tables II and VI show, furthermore, that solvents such as paraffin oil, heptane, and p-dioxane give a considerable transport of energy from the solvent to the dissolved molecule. These substances are of special interest since their chemical structure is quite different from that of xylene, toluene, etc. In solvents such as benzene, toluene, xylene, and mesitylene the molecule of the solvent consists of a basic benzene ring

type structure. These benzene ring solvents are known to be fluorescent (by virtue of their conjugated double bonds) though they differ from the "fluorescent molecules," dissolved in the solutions in the wave-lengths of the absorption and emission spectra. The emission spectrum of these solvents is close to their longest absorption band, though shifted in wave-length toward the red. The molecules of the other solvents, however, are of different structure in that they contain no double-bonds at all. In the case of heptane and paraffin oil the molecules are long chains, and in the case of dioxane there is a ring of four C and two O atoms connected by single bonds. The absorption spectra of these solvents are in the ultraviolet and no substantial fluorescence has been reported for nearly all of these substances. Nevertheless, in solutions a considerable portion of the excitation energy of the bulk material is transferred to the fluorescent molecules. This proves that energy transport is not limited to benzene-like substances but depends on a much more general property of the solvents.

E. THEORETICAL CONSIDERATIONS

In this section we shall consider the reaction probabilities in detail. We begin with the quenching effects of the fluorescent molecules. As was previously noted in Section D, there exist two different types of quenching, namely, internal quenching and self or resonance quenching. These two types are clearly revealed by the following experiment with light. Naphthacene is fluorescent when dissolved in solid anthracene; it exhibits in this case a rather high degree of fluorescence. On the other hand, when a small amount of naphthacene is dissolved in alcohol or xylene, it exhibits only poor fluorescence when excited by light. In the latter case the exciting light is absorbed in the naphthacene bands themselves and, nevertheless, only a small amount of the absorbed light is re-emitted. Since the emission probability $1/\tau_e$ is an inherent property of the molecule itself, these experiments show that a large portion of the excitation energy of the naphthacene molecules is transformed into heat even if the concentration of naphthacene molecules is too small for self-quenching to occur. The same effect can also be observed with many other fluorescent substances.[7] Quenching occurs here most likely because of the interaction with the molecules of the solvent. The effect of self-quenching is revealed by the well-known experiments of Vavilow and many other authors.[8] These indicate that the intensity of light emission decreases with the concentration of the fluorescent molecules for a constant amount of absorbed light energy.

With the assumption of internal quenching our results with naphthacene and dihydrocollidine can be explained. The considerable quenching of the anthracene radiation by very small amounts of naphthacene (Table V) stems from an absorption by the naphthacene molecules of the light emitted by the anthracene molecules. The absorption coefficient of naphthacene for the anthracene radiation is of the order 10^4 with 1 mole per liter and a thickness of 1 cm. Such an absorption would cause a noticeable drop in intensity even for the low concentrations listed in Table V. Thus the anthracene radiation is absorbed and then quenched in the naphthacene. Without internal quenching the absorption in naphthacene would, of course, effect no loss in intensity.

Other substances like dihydrocollidine, diphenyl acetylene which are highly fluorescent as crystals similarly decrease the radiation from the pure solvent considerably when very small amounts are added to the solvent (Table IV). These results can be explained by assuming that a similar light absorption effect occurs even at small concentrations of the order of 0.1 g/l and internal quenching takes place.

In a solution of anthracene in xylene, however, dihydrocollidine in the same concentration as above quenches by only 20 percent. Dihydrocollidine has a fluorescent spectrum similar to that of anthracene and an absorption spectrum lying in the ultraviolet. Therefore, dihydrocollidine can only very weakly absorb the anthracene radiation and thus only slightly quenches the anthracene radiation. Carbazole radiation, however, being more in the ultraviolet than the radiation of anthracene should be absorbed more by dihydrocollidine and thus quenched if dihydrocollidine is a quencher. The results with carbazole and dihydrocollidine shown in Table VII bear out this theory.* The strong quenching effect by the dihydrocollidine molecule in the pure solvent shows indirectly that the radiation of the pure solvent lies further in the ultraviolet than does the anthracene radiation. Another example for this effect is aniline. The aniline available had a weak absorption band in the blue, and this absorbs blue radiation of anthracene and terphenyl and presumably quenches the absorbed energy. Thus we find no increase in radiation if these molecules are added to however, alpha-naphthylamine is added, which is reported[6] to have an emission spectrum more to the green, a noticeable increase in light intensity is observed (Table II). It may be emphasized that this effect occurs mostly when the absorbing molecule is an "internal quencher" which very rapidly transforms its excitation energy into heat by interaction with the surroundings. If the absorption coefficient of such dihydrocollidine molecules is of the same order as that of naphthacene, a concentration as low as 10^{-5} mole per liter should give noticeable quenching effects. It will be seen later that the self-quenching effect can only occur at much higher concentrations.

This theory of internal quenching also fits in with the experimental evidence that some substances only show

[7] P. Pringsheim, reference 6, p. 316.
[8] S. I. Vavilow, Acta Phys. Polonica 5, 417 (1936).

* *Note added in proof:* This absorption theory has in the meanwhile been substantiated by absorption measurements and spectral analysis.

TABLE VII. Quenching of carbazole by dihydrocollidine.

Substance	Intensity
Xylene+carbazole (1.4 g/l)	29.0
Xylene+carbazole (1.4 g/l)+dihydrocollidine (0.2 g/l)	3.0
Xylene+carbazole (1.4 g/l)+dihydrocollidine (0.5 g/l)	2.5

fluorescence after an extreme purification. If a substance contains as contaminant only a small number of internal quenching molecules absorbing radiation of the fluorescent molecule, the light intensity emitted by these substances in a solution is not given by Eq. (3) but by the following equation:

$$I=n_e cf(e^{-\kappa c})(k+c)^{-1}(k'c+k'')^{-1}, \qquad (4)$$

where κ is the absorption coefficient of the internal quencher multiplied by its relative concentration in the fluorescent molecule. The other symbols have been explained previously. The factors in this equation are the same as those in Eq. (3) except for the function of the exponential in the numerator which gives the absorption caused by the contaminating molecules contained in the fluorescent substance. If some fluorescent substance contains such quenching molecules it is to be expected that for larger concentrations the intensity drops according to an exponential function. Some of the poor results obtained with impure substances may be explained in this way.

The question may be raised as to whether all the decrease in intensity observed at higher concentrations (Figs. 2 to 5) can perhaps be explained in this way without assuming self-quenching between fluorescent molecules. From these figures it can be seen that no appreciable absorption by some unidentified contaminant occurs since the slope of the curves is much smaller than would be expected from Eq. (4) except in the case of commercial carbazole in xylene. Thus we conclude that most of the effects beyond maximum concentration where the intensity of the radiation decreases only slowly, stems from self-quenching and saturation of the energy transport. However, some of the effects described in the literature on the fluorescence of solutions when excited by light may be explained by the presence of very small amounts of highly absorbing and internal quenching molecules of contaminants. Certainly some deviations from the self-quenching equation [Eq. (3)] can be explained in this way.

From these considerations it can be concluded that self-quenching effects also play a very important role in all these reactions. For this reason the quenching interaction between the same or similar molecules will be considered in more detail. This interaction is closely connected with resonance between such molecules. If an excited molecule approaches an unexcited molecule of the same kind, the excitation energy will oscillate between these two molecules and the energy state of these two molecules together splits up into two states. It is well known that in many cases the state with the higher energy has a higher probability of light emission than that of lower energy so that the double molecule in the lower state has a smaller probability for light emission than the isolated molecule. If an excited molecule collides with an unexcited one at first both energy states are present but the state with the higher energy will undergo a transition to the state of lower energy and the excess energy will be transformed into heat. In this state of lower energy the two molecules attract each other and it may be that these molecules come so close together that a transformation of the excitation energy into atomic vibration can occur.

There is another possibility. The two molecules may form an excited double molecule with a certain binding energy and this excited double molecule will live until the excitation energy is quenched by interaction with the surroundings or the molecule is dissociated by the impact with the surroundings. In the state of the double molecule no light emission occurs. The lifetime of the excitation energy is thus prolonged by decreasing the chance of light emission and thus the probability of transformation of the excitation energy into heat is increased.[9] This process of quenching was first proposed by Foerster.[10] A more thorough investigation of this type of quenching may explain some of the effects found concerning the dependence of quenching on concentration. For this purpose one must look into the mechanism of quenching in these double molecules and determine whether it occurs by means of the solvent molecule or by collision with other fluorescent molecules.

From these considerations it follows that self-quenching (quenching between two similar molecules) occurs only after the collision between two fluorescent molecules or formation of a double molecule has occurred. The lifetime of an excited fluorescent molecule, when only light emission is considered, is of the order of 10^{-8} sec. A collision between the excited molecules and another fluorescent molecule must occur within this interval if self-quenching shall be noticeable. It is found by calculation that in such a period of time, the number of collisions become appreciable only with concentrations of at least 10^{-3} mole per liter. This means that self-quenching only sets in at concentrations about 100 times higher than those necessary for the weakening of the radiation by absorption and internal quenching (see beginning of Section E). Perhaps a still more general way of viewing the self-quenching process is that of saying that it comes from a general decrease in emission probability instead of an increase of quenching. With increasing concentration the probability of

[9] It may be remarked that the question as to whether the state of lower energy is always the non-radiative state requires further investigation. If dipole radiation interaction is assumed, the orientation of the molecules with respect to the dipole moment is the deciding factor as to radiation of the state of lowest energy. In an orientation where the interaction energy is strongest, the state of lowest energy is non-radiative. This may justify the assumption that when an excited molecule approaches an unexcited one, the probability of light emission is reduced.

[10] Ch. Foerster, Naturwiss. 33, 166 (1946).

the states of lower energy increases by a factor proportional to $\exp(|\Delta E|/kT)$ because $|\Delta E|$, the energy difference between the two states, increases on the average with increasing concentration. If this states does not radiate, increasing concentration must suppress the probability for light emission quite generally (see reference 9).

We will now use quite analogous ideas to explain the transport of energy from the solvent to the fluorescent molecule. It is well known from the experiments with solids (see Section A) that migration of energy can occur in these solids. Quite a similar migration can occur in liquids. Immediately after the excitation of the molecules of the solvent by the incident radiation the molecules may be excited to highly excited electron levels and atomic vibrations. In a very short time these energies are transformed into heat and the molecules return to a state of lowest excitation energy. The excitation energy (purely electronic excitation) in these molecules is of the order of several volts and cannot as easily be transformed into heat as the additional energies of the higher excited states, since the difference between energy levels in the higher states are smaller than the energy jump from the state of low excitation energy to the ground state. Besides this, these higher states are more strongly coupled with the atomic vibrations and are, therefore, easily quenched to the first excited state. Thus a very short time after the excitation most of the excited molecules are to be found in the first excited state. Then the migration of this excitation energy occurs. There are several mechanisms for the migration of energy which will now be described.

A theory of energy transport from the solvent to the fluorescent molecule must satisfy the following conditions. The light emission of the radiation of the solvent molecule itself is very weak with respect to the best solution. Therefore, the mechanism which described the energy transport must explain the fact that this radiation is very weak but the lifetime of the excitation energy is still long enough to allow a large amount of the excitation energy to be transferred to the fluorescent molecules. Further, the process must result in a trapping of the excitation energy by the fluorescent molecule. If this were not the case the excitation energy could return to the solvent, where the quenching effects of the solvent would be still effective; the large intensity output by the fluorescent molecules could not be explained.

The trapping mechanism is pictured as follows. The excited molecule of the solvent has an excitation level (exclusive of excitation of atomic vibrations) which has a higher energy when the pure electronic level of the fluorescent molecules. When such an excited solvent molecule interacts with a fluorescent molecule, it will transfer its energy to the fluorescent molecule thereby raising the fluorescent molecule to a state in which atomic vibrations are also excited. These excited atomic vibrations will be almost immediately transferred to other molecules and to other atomic vibrations and will be decoupled from the electronic excitation in the fluorescent molecule. The remaining excitation of the fluorescent molecule is then purely electronic. This energy is not large enough to re-excite the molecule of the solvent and thus the excitation energy can be trapped by the fluorescent molecule. As a result, the large intensities due to transportation effects are found only in those cases where the electronic excitation energy of the fluorescent molecule is smaller than that of the bulk material. This trapping mechanism is a most essential part of the energy transport from the solvent to the fluorescent contaminant; it also occurs in solids. It gives an explanation for the well-known experimental fact that the addition of a very small amount of certain substances not only shifts the spectrum of the fluorescent light almost totally into the spectrum of the added molecules, but also considerably increases the light output in some cases. The latter effect occurs because the excitation energy is trapped in the added molecules and thus restrained from being quenched in the bulk material. The same is also true for the solutions. The trapping of the excitation energy in the fluorescent molecules prevents the excitation energy from being quenched in the solvent and increases the probability that the excitation energy is emitted as light by the fluorescent molecule.

We will next consider the mechanism of the energy transport itself, giving three different possible mechanisms: (1) The excitation energy jumps from one molecule to a neighboring molecule by the well-known mechanism of energy exchange. If the average energy associated with this energy exchange is described by V_{ex}, then the time, τ_d which the energy takes to jump from one molecule to the other is given by $\tau_d = h/V_{ex}$. If the mole concentration of the fluorescent molecule is given by N_f/N_s where N_f represents the number of fluorescent molecules per unit volume and N_s the number of the solvent molecules per unit volume, then the average time τ_e required for the excitation energy to hit the fluorescent molecule is given by

$$\tau_e = \tau_d(N_s/N_f). \tag{5}$$

If it is assumed that each collision between the excitation energy and the fluorescent molecule effects a trapping of the excitation energy, then τ_e is identical with τ_t of Eq. (1). If not every collision between excitation energy and fluorescent molecule leads to trapping $1/\tau_e$ must be multiplied by a factor α (smaller than unity) which gives the probability that the excitation energy is trapped at such a collision, and we get for τ_t the reaction probability of energy transport

$$\tau_t = \tau_d N_s/\alpha c, \tag{6}$$

where c is written for N_f, and τ_d is a constant inherent in the solvent. In this picture the transfer of the energy to the fluorescent molecule can be described as a diffusion process through the bulk material. Of course,

Eq. (6) omits all finer details of the energy transfer through the solvent and can, therefore, only be looked upon as a first approximation. It should be noted that a similar process may be responsible for the migration of energy in crystals.

(2) Another method of energy transfer from the solvent to the dissolved molecule may occur in liquids as well as in solid solutions. Between the purely electronic excited levels in the solvent molecules and the excitation levels of the dissolved molecules there exists a sort of resonance when the spectrum emitted from the solvent molecule can be absorbed by the dissolved molecule. Emission of light by the solvent molecule is rather small as shown by our results. But even without radiation an energy exchange can occur from these molecules to the dissolved molecules over large distances and with considerable probability, for a certain resonance exists between these molecules. But this energy exchange takes place in such a way that the dissolved molecule, since its energy level is lower than that of the solvent molecule is excited with some nuclear vibration as well as with its electronic vibrations. These nuclear vibrations are at once transferred to other vibrations and molecules and thus only the purely electronic excited states of the dissolved molecules remains. A similar process has been calculated by Foerster[11] for the interaction of certain dye-molecules. The calculation leads to the following equation

$$1/\tau_t = (3\alpha c^2 \Delta / 8\tau_0^2)(\lambda_0/2\pi n)^6 \qquad (7)$$

with

$$\Delta = \int \xi_f(\nu)\xi_s(2\nu_0 - \nu)d\nu \Big/ \int \xi_s(\nu)d\nu \int \xi_f(\nu)d\nu$$

and where n is the index of refraction, τ_0 is the lifetime for light emission alone, λ_0 is the wave-length, ξ_f and ξ_s are the absorption coefficients of the dissolved and solvent molecules respectively, and $h\nu_0$ represents the purely electronic energy of the solvent molecule. The chief difference between Eqs. (7) and (6) lies in the different dependences on the concentration of the dissolved molecule. This difference arises because the energy exchange between the two molecules depends on the exchange energy which in the most favorable case of dipole interaction decreases with distance as $1/R^6$. From this it follows that Eq. (7) gives a smaller probability of energy transfer in the region of low concentration and a higher one for large concentrations. From this equation it seems as though the concentration, at which energy transfer to the dissolved fluorescent molecules should become noticeable, is about 5 to 10 times larger than the experimental values. Equation (7) is derived under the assumption of dipole interaction between the excited solvent molecule and the unexcited fluorescent molecule. The absorption coefficients are introduced in order to calculate the dipole strength of the transition involved. That of the fluorescent molecule is derived from the absorption coefficient by the law of mirror symmetry. ν_0 is the symmetry frequency of the fluorescent molecule, and is practically identical with the frequency of the electric transition. It is essential for the derivation of Eq. (7) that the excitation energy is trapped in the fluorescent molecules. There is a stream of energy from the excited molecule to the unexcited one, but no energy streams back. For details see the paper of Foerster.[11]

(3) The third mechanism of energy transport assumes that the excited solvent molecule interacts with its neighboring molecules and thus forms two energy states in which the lower one does not radiate energy (see reference 9). Now such an excited molecule may form a double molecule with its neighbor in an excited state but without radiation as was pointed out before. If these excited solvent molecules are not strongly quenched by the solvent itself they may have a long enough lifetime to undergo a collision with a dissolved fluorescent molecule and transfer their energy to the fluorescent molecule in a way similar to that described for the first process. The excitation energy is again trapped in the fluorescent molecule. The average time before such a double molecule collides with a fluorescent molecule and is trapped there may be described by τ_c, which is certainly inversely proportional to the concentration of the dissolved molecules. For $1/\tau_t$ we obtain then

$$1/\tau_t = \alpha g v c, \qquad (8)$$

where g and v denote something like the cross section for the collision process and the average velocity of the molecules respectively. This equation gives the same dependence on concentration as does Eq. (6) but it has the great advantage over the latter that the probability for light emission by the solvent molecule is reduced at the moment the double molecule is formed which, in general, may require a time of the order of 10^{-12} sec. This, therefore, differs considerably from the first process in which the solvent molecule can emit light during its whole lifetime. For the first process the following difficulty exists. Since the lifetime for light emission τ_e is of the order of 10^{-8} sec., and since only a small amount of light seems to be emitted by these molecules, the quenching time τ_q must also be assumed to be extremely short, of the order of 10^{-11} sec., to account for the very small amount of ultraviolet light emitted. With such a small value for τ_q the transfer of excitation energy to the fluorescent molecule must also be very short, also of the order of at most 10^{-11} sec., if a considerable amount of excitation energy is to go over the fluorescent molecule [see Eq. (1)]. Now a minimum value for this transfer time is given by $\tau_d N_s/N_f = 10^{-11}$ sec., and since N_s/N_f is of the order of 1000 or less it follows that in the cases of strong light output the time τ_d must be extremely short, of the order of 10^{-14} sec. or less. This corresponds to interaction energies of about one volt. If the third process, however, is sup-

[11] Ch. Foerster, Ann. d. Physik. 2, 56 (1948).

posed to be valid much larger values for the quenching time can be assumed since the extremely small light emission of the solvent molecule stems in this case from the fact that the states of lower energy do not radiate and, it is, therefore, not necessary to assume low values for the quenching time.

It may be, however, that the first and third mechanisms are not as different from each other as may appear at first sight. In both mechanisms a strong interaction between the excited molecule and its neighbor exists. Such an interaction energy may reduce the probability of light emission even when no double molecules are formed. (See previous part of this section for a similar development for the interaction between like molecules.) This means that also in the first mechanism a longer quenching time can be assumed. With an average interaction energy of several hundredths of a volt, the time of energy transfer comes out to be between 10^{-10} and 10^{-9} sec. According to the double molecule theory as calculated from simple collision theory a noticeable transfer of energy from the solvent to the fluorescent molecules might occur, within 10^{-9} to 10^{-8} sec. The values given are calculated for maximum concentrations of the fluorescent molecules. From this and from the high light output found in some of the solutions which shows that the quenching time must be longer than these values, we conclude that the time for quenching the excitation energy is of at least the same order of magnitude.

It is impossible at this stage of the investigation to decide whether one of the three processes is the correct one. The very high light output found with some substances seems, however, to be in favor of the third possibility since this mechanism best accounts for the following two most characteristic effects, a very high light output, almost equal to that of solid crystals with concentrations of one to ten thousandths of a mole per liter (or referred to the mole number of the solvent, this means less than a tenth of a mole percent) and the small output of light of the solvent molecule itself.

Two further questions naturally suggest themselves: why is the light output from different fluorescent molecules so different and what is the reason for the final quenching of the excitation energy?

In regard to the first of these questions one notes that the difference in light output of various fluorescent molecules can be explained by the difference of three factors; the factor α in Eq. (6), which represents the capability of the fluorescent molecule for accepting the excitation energy, the factor $1/\tau_e$, and $1/\tau_q$ [see Eqs. (1) and (2)]. All of these factors may vary from substance to substance. The factor $1/\tau_e$ can be calculated approximately from the absorption coefficient with the help of the law of mirror symmetry (see end of description of the second mechanism of transport). It varies from substance to substance but not strongly enough to account for most of the observed variations of fluorescence. We cannot decide how strong the influence of changes in the factor α may be. We can show, however, that the extreme differences in light output of some substances certainly originate in a strong variation of the internal quenching factor. Thus it is known from optical experiments[7] that naphthacene has a much smaller light output when optically excited than does anthacene. Its value of $1/\tau_e$ calculated as above is certainly not smaller than that of anthracene. We conclude that the quenching factor $1/\tau_i$ of naphthacene is considerably larger than that of anthracene. This conclusion is also borne out by many of our experiments (Tables IV and V) we can show that anthracene also has a considerable quenching factor $1/\tau_i$. We have observed that 0.1 g/l of anthracene added to a terphenyl solution in xylene decreases the terphenyl radiation considerably. It seems likely that anthracene absorbs the terphenyl radiation, but this would lead to no loss in intensity if anthracene would not internally quench. From the strong decrease in light output we conclude, however, that anthracene has a considerable internal quenching factor. A smaller quenching factor of terphenyl would therefore explain the differences in light output between these two substances. We suppose that some of the differences in light output of the fluorescent molecules listed in Table II come from such differences in internal quenching. We shall present some more evidence below that the internal quenching of terphenyl is less than that of anthracene.

We have further found that the substances which are most effective in solvents of the xylene, toluene, and benzene group are also most effective in dioxane, paraffin oil and the other solvents listed in Table II. This indicates that the internal quenching effects are not too different in various solvents. But there are quantitative differences in the ratios of light output of different fluorescent molecules in different solvents. Thus in xylene the ratio between terphenyl and anthracene was about 5 to 1 and in paraffin oil only 2 to 1. Such differences may be due to differences in the quenching factor of the different solvents.

From these considerations it may also be possible to explain the special effects in solutions of xylene and carbazole or anthracene in paraffin oil. It was shown in Fig. 5 that a considerable dilution of such a solution by adding paraffin oil did not cause a very large decrease in the light output. From a comparison of the light output of these solutions with that of anthracene or carbazole in paraffin oil without xylene it can be concluded that most of the energy of the emitted light must come from the xylene. The dilution by paraffin oil diminishes the number of excited xylene molecules and, therefore, it should be expected that the energy transferred from xylene to the anthracene should be diminished to the same degree. That such a decrease in light output does not occur can be explained by the assumption that the addition of paraffin oil also decreases the internal quenching of the anthracene or carbazole molecules and that these two effects balance

TABLE VIII. Effect of paraffin oil on solution of terphenyl in m-xylene.

Solutions	Relative intensity
m-Xylene+Terphenyl (5.5 g/l)	0.44
m-Xylene+Terphenyl (5.5 g/l)+Paraffin Oil (0.25 l/l)	0.43
m-Xylene+Terphenyl (5.5 g/l)+Paraffin Oil (0.5 l/l)	0.41
m-Xylene+Terphenyl (5.5 g/l)+Paraffin Oil (1 l/l)	0.37
m-Xylene+Terphenyl (5.5 g/l)+Paraffin Oil (2 l/l)	0.31
m-Xylene+Terphenyl (5.5 g/l)+Paraffin Oil (3 l/l)	0.26
m-Xylene+Terphenyl (5.5 g/l)+Paraffin Oil (4 l/l)	0.23
m-Xylene+Terphenyl (5.5 g/l)+Paraffin Oil (5 l/l)	0.21
m-Xylene+Terphenyl (5.5 g/l)+Paraffin Oil (7.5 l/l)	0.17
m-Xylene+Terphenyl (5.5 g/l)+Paraffin Oil (10 l/l)	0.14
m-Xylene+Terphenyl (5.5 g/l)+Paraffin Oil (15 l/l)	0.11
m-Xylene+Terphenyl (5.5 g/l)+Paraffin Oil (20 l/l)	0.095

each other in such a way that the total light output remains comparatively constant. The observations collected in Table VIII seem to favor this assumption. In these measurements, a solution of terphenyl in xylene has been diluted by paraffin oil and in this case, with increasing amounts of paraffin oil, the light output decreases constantly. Terphenyl should have, as was pointed out earlier, a much smaller internal quenching effect than does anthracene and, therefore, the decrease of this internal quenching effect by the addition of paraffin oil cannot match the decrease in the number of excited xylene molecules caused by the dilution with paraffin oil.

From all these measurements it follows that the quenching of the excitation energy of the solvent as well as that of the fluorescent molecules plays a most important role in these processes. But we have not yet found indications of the exact nature of the internal quenching effect.

In all these measurements and considerations we have investigated the energy transport from the solvent to the fluorescent molecule; this energy transport was observed by the light emission of the fluorescent molecule. But it is obvious that such a transport of energy also will occur to other molecules where it can be trapped and utilized perhaps for chemical reactions. Therefore, it may be that these considerations have also some importance for biological reactions induced by high energy radiation. It is ordinarily assumed that such a biological reaction starts from the change in one molecule produced by the hitting of one fast particle. According to our consideration it may be possible to extend this picture of the biological reaction by taking into account that these biological important reacting molecules may receive their energy not only by primary excitation from the primary or secondary electrons but may also draw their energy from the surrounding substance. This may occur when the substance is a solid as well as a liquid.

F. SUMMARY

It has been shown experimentally that a number of solvents when excited by high energy radiation exhibit a very weak light output, but that this light output can be greatly increased by a factor of as much as 35 by the addition of small amounts of fluorescent molecules to the solution. The energy directly absorbed in these dissolved molecules themselves is much too small to be responsible for the high light output of the solutions. This increase in light output is explained by energy transfer from the solvent to the dissolved molecule, by the trapping of the excitation energy in the fluorescent molecule and then by emission of this excitation energy in form of light from the fluorescent molecule. These processes of energy transfer trapping the excitation energy, and of light emission compete with three other processes: (a) An internal quenching of the excitation energy of the solvent molecule in the solvent itself. This competes with the transfer of the excitation energy to the fluorescent molecule. (b) There is the internal quenching in the fluorescent molecule which is independent of the concentration of the fluorescent molecule. This internal quenching seems to be responsible for the different efficiencies of different fluorescent molecules. (c) There is also self-quenching among similar fluorescent molecules. This self-quenching process increases with the concentration of the fluorescent molecule and is responsible for the maximum which one observes in all observed light curves in which concentration is a factor. The last two processes compete with the process of light emission in the fluorescent molecules.

Condensation Phenomena in a Clustering Bose-Einstein Gas*

WILLIAM BAND
Department of Physics, State College of Washington, Pullman, Washington
(Received January 31, 1950)

It has been shown that Mayer's theory of imperfect gases can be handled approximately as a problem in association in which the actual gas is replaced by a mixture of ideal gases consisting of clusters of all sizes and between which dissociative equilibrium exists. Kahn and Uhlenbeck have shown how Mayer's theory can be generalized to apply to quantum degenerate gases. The purpose of the present paper is to examine the clustering approximation to such a theory of the quantum degenerate Bose-Einstein gas. The symmetrized wave functions for the clustering assembly are set up and the partition function evaluated for all ways of clustering. Equations of state are deduced that include condensation into the liquid phase as a clustering avalanche at the saturation pressure. It is found that clustering has the effect of lowering the lambda-temperature due to statistical degeneracy right down to the saturated vapor line, so that the lambda-transition is entirely inhibited from the gas phase.

I. INTRODUCTION

IT is well known that the second virial coefficient of a classical imperfect gas can be calculated approximately as a problem in association.[1] The actual imperfect gas is replaced by a mixture of perfect gases, one of which is monomolecular and the other is formed of pairs of molecules (or atoms) bound together by their mutual van der Waals forces, and between which two gases dissociative equilibrium exists. Mayer's theory[2] of a classical imperfect gas goes far beyond the second virial coefficient, yielding formal equations of state that are valid down to the saturated vapor, and even include condensation into the liquid phase. It has been shown[3] that Mayer's theory can also be handled approximately as a problem in association in which the actual gas is replaced by a mixture of ideal gases consisting of clusters of all sizes and between which dissociative equilibrium exists. Condensation into the liquid phase appears formally on the clustering approximation as a clustering avalanche, in which the largest clusters suddenly become the most probable. The results of the rigorous Mayer theory are unavoidably expressed in forms that are very difficult to interpret numerically,[4] whereas those of the clustering approximation are comparatively easy to reduce to quantitative form.

Kahn and Uhlenbeck[5] have shown how Mayer's theory can be generalized to apply to quantum degenerate gases, and the purpose of the present paper is to examine the clustering approximation to such a theory of the quantum degenerate Bose-Einstein gas. Schiff[6] has examined the full effect of statistical degeneracy on the second virial coefficient. The approximate effect had already been studied by several writers.[7] The generalized Mayer theory would presumably yield formal relations between the lambda-transition and the vapor-liquid phase change, but they would undoubtedly resist an ordinary attempt at numerical interpretation. This type of trouble is well illustrated in the theory of mixtures of quantum degenerate gases.[8] By thus pushing rigor to the limit one may believe for *a priori* reasons that our results are exact, but they do not permit actual demonstration by comparison with experimental data; the usable content of the theory has practically vanished. It appears that by working instead with the clustering approximation, the results gain so much in usable content that the sacrifice in rigor can easily be tolerated.

II. SYMMETRIZED WAVE FUNCTIONS FOR A CLUSTERING ASSEMBLY

The clustering assembly consists of N_s clusters of s atoms each, all integral values of s, the total number of atoms being

$$N=\sum_{s=1} sN_s. \tag{1}$$

Consider a sub-assembly consisting only of the N_s clusters of size s, one particular value of s. Let the mass center coordinates of the jth cluster be represented by the vector $\mathbf{r}_{sj}$, and its momentum by the vector $\mathbf{p}_{sj}$. Each cluster has internal degrees of freedom with coordinates and momenta which will be represented collectively by q_{sj}. The wave function of the sub-assembly will be supposed to be separable into factors; the first factor $\phi_s(\{\mathbf{p}_s\}, \{\mathbf{r}_s\})$ depends on the whole set of variables $\mathbf{r}_{sj}$ and $\mathbf{p}_{sj}$, all j-values; and the other factors $\phi(q_{sj})$ depend only on the internal variables, and there is one such factor for each individual cluster in the sub-assembly. The first factor must be symme-

* The work was supported by funds from the ONR.

[1] See, for example, R. H. Fowler and E. A. Guggenheim, *Statistical Thermodynamics* (Cambridge University Press, London, 1939), Section 705.

[2] J. E. Mayer, J. Chem. Phys. **5**, 67 (1937). J. E. Mayer and S. F. Harrison, J. Chem. Phys. **6**, 87 (1938).

[3] W. Band, J. Chem. Phys. **7**, 324, 927 (1939). Tseng, Feng, Ch'eng, and Band, J. Chem. Phys. **8**, 20 (1940); **9**, 123 (1941).

[4] E. W. Montroll and J. E. Mayer, J. Chem. Phys. **9**, 626 (1941).

[5] B. Kahn and G. E. Uhlenbeck, Physica's Grav. **V**, 399 (1938). M. Born and K. Fuchs, Proc. Roy. Soc. **A166**, 391 (1938).

[6] L. I. Schiff, Phys. Rev. **59**, 751 (1941).

[7] G. E. Uhlenbeck and E. Beth, Physica's Grav. **III**, 729 (1936); **IV**, 915 (1937). J. de Boer, thesis, Amsterdam (1940). L. Gropper, Phys. Rev. **50**, 963 (1936); **55**, 1095 (1939). L. Goldstein, J. Chem. Phys. **14**, 276 (1946); **9**, 273 (1941).

[8] W. Band, J. Chem. Phys. **16**, 343 (1948).

trized among all the sub-assembly clusters. Because the non-ideal character of the gas is to be replaced by the dissociative reactions among the clusters, each sub-assembly is to be treated as an ideal gas, and the whole assembly is therefore described by a wave function which is simply the product of the wave functions for the sub-assemblies. The first factor of the latter is:

$$\phi_s(\{\mathbf{p}_s\},\{\mathbf{r}_s\})=(1/N_s!)^{\frac{1}{2}}V^{-\frac{1}{2}N_s}\sum_P \times\exp\left[(2\pi i/h)\sum_{j=1}^{N_s}(\mathbf{p}_{sj}\cdot\mathbf{r}_{sPj})\right] \quad (2)$$

where P_j means another suffix obtained from j by a permutation P among the N_s suffixes, and $\sum_P$ means the sum over all terms obtained by permuting the cluster suffixes in the covered expression. M is the mass of one atom, sM that of one cluster.

The assembly of N atoms is characterized by the set $\{N_s\}_N$ of numbers N_s, all s-values, and the wave functions of the whole assembly are

$$\phi(\{N_s\}_N)=\prod_{s=1}^{N}\phi_s(\{\mathbf{p}_s\},\{\mathbf{r}_s\})\prod_{j=1}^{N_s}\phi(q_{sj}). \quad (3)$$

These are functions of the set of numbers $\{N_s\}_N$ as well as of the coordinates and momenta of all the clusters. They are the steady states of the assembly, and processes of association and dissociation are regarded as transitions between them, caused by small perturbations representing the interactions between the clusters that have otherwise been neglected.

III. THE PARTITION FUNCTION FOR THE CLUSTERING ASSEMBLY

Let the Hamiltonian for a given sub-assembly of N_s clusters be written as

$$H_s(\{\mathbf{p}_s\},\{\mathbf{q}_s\})=\sum_{s=1}\sum_{j=1}^{N_s}(1/2sM)\mathbf{p}_{sj}^2+\sum_{s=1}\sum_{j=1}^{N_s}U_s(q_{sj}), \quad (4)$$

which is independent of $\{\mathbf{r}_{sj}\}$. The Hamiltonian of an assembly specified by any given set of numbers $\{N_s\}_N$ is the sum of the sub-assembly Hamiltonians:

$$H(\{N_s\}_N)=\sum_{s=1}H_s(\{\mathbf{p}_s\},\{\mathbf{q}_s\}). \quad (5)$$

The contribution to the partition function from a given set of numbers $\{N_s\}_N$ is

$$Q(\{N_s\}_N)=(1/N!)h^{-3N}\times\int_{-\infty}^{\infty}\cdots\int\phi^*(\{N_s\}_N)\exp[-H(\{N_s\}_N)/kT]\times\phi(\{N_s\}_N)\prod_{s,j}d\mathbf{r}_{sj}d\mathbf{p}_{sj}dq_{sj} \quad (6)$$

where $d\mathbf{r}_{sj}$ and $d\mathbf{p}_{sj}$ are volume elements in coordinate- and momentum-space, respectively. Using Eqs. (3) to (5), Eq. (6) becomes

$$N!Q(\{N_s\}_N)=\prod_{s=1}^{N_s}h^{-3N_s}\int\cdots\int\phi_s^*(\{\mathbf{p}_s\},\{\mathbf{r}_s\})\times\exp\left[-\sum_s\sum_{j=1}^{N_s}\mathbf{p}_{sj}^2/2sMkT\right]\times\phi_s(\{\mathbf{p}_s\},\{\mathbf{r}_s\})\prod_{s,j}d\mathbf{p}_{sj}d\mathbf{r}_{sj}\prod_s(s!)^{N_s}\times\exp(-N_sW_s/kT)V^{N_s} \quad (7)$$

where W_s is defined as follows:

$$V^{N_s}\exp(-N_sW_s/kT)=(s!)^{-N_s}h^{-3(s-1)N_s}\times\prod_{j=1}^{N_s}\phi^*(q_{sj})\exp[-U_s(q_{sj})/kT]\phi(q_{sj})dq_{sj}. \quad (8)$$

In writing (8) into (7) it is implied that we are averaging out the internal energies of the clusters of each size, and taking this same average for every set of clustering numbers $\{N_s\}_N$. The processes of dissociation and association are in this way regarded as not changing the average internal energy of clusters of any given size.

The integrations over the momenta in (7) are of the following type:

$$\begin{aligned}&\int_{-\infty}^{\infty}\cdots\int\left\{\sum_P\exp\left[-2\pi i/h\sum_{j=1}^{N_s}(\mathbf{p}_{sj}\cdot\mathbf{r}_{sj})\right]\right\}\times\left\{\exp\left[-\sum_{j=1}^{N_s}\mathbf{p}_{sj}^2/2sMkT\right]\right\}\\&\times\left\{\sum_P\exp\left[2\pi i/h\sum_{j=1}^{N_s}(\mathbf{p}_{sj}\cdot\mathbf{r}_{sj})\right]\right\}\prod_j d\mathbf{p}_{sj}\\&=\sum_P\sum_{P'}\int\cdots\int\exp\left[2\pi i/h\sum_{j=1}^{N_s}\mathbf{p}_{sj}\cdot(\mathbf{r}_{sPj}-\mathbf{r}_{sP'j})-\sum_{j=1}^{N_s}\mathbf{p}_{sj}^2/2sMkT\right]\prod_j d\mathbf{p}_{sj}\\&=\sum_P\sum_{P'}\prod_{j=1}^{N_s}(2\pi sMkT)^{3/2}\times\exp[-2\pi^2sMkT/h^2(\mathbf{r}_{sPj}-\mathbf{r}_{sP'j})^2]\\&=N_s!(2\pi sMkT)^{3N_s/2}\sum_P\times\exp[-2\pi^2sMkT/h^2\textstyle\sum_j(\mathbf{r}_{sj}-\mathbf{r}_{sPj})^2]. \quad (9)\end{aligned}$$

The final result, using (2) and (9) in (7) is:

$$N!Q(\{N_s\}_N)=\prod_{s=1}^{N}(2\pi sMkT/h^2)^{3N_s/2}(s!)^{N_s}\times\exp(-N_sW_s/kT)\int\cdots\int\sum_P\times\exp\left\{-(2\pi^2sMkT/h^2)\sum_{j=1}^{N_s}(\mathbf{r}_{sj}-\mathbf{r}_{sPj})^2\right\}\prod_{s,j}d\mathbf{r}_{sj}. \quad (10)$$

In the last integral over configuration space the exponential sum

$$\sum_{j=1}^{N_s}(\mathbf{r}_{sj}-\mathbf{r}_{sPj})^2$$

breaks up into m_μ closed loops each linking just μ distinct suffixes j of the form

$$(\mathbf{r}_{s1}-\mathbf{r}_{s2})^2+(\mathbf{r}_{s2}-\mathbf{r}_{s3})^2+\cdots+(\mathbf{r}_{s\mu}-\mathbf{r}_{s1})^2.$$

For any particular permutation P the integral breaks up into a product of factors in the following fashion:

$$\int\cdots\int \exp-(2\pi^2 sMkT/h^2)\sum_{j=1}^{N_s}(\mathbf{r}_{sj}-\mathbf{r}_{sPj})^2\prod_j d\mathbf{r}_{sj} = V^{m_1}\prod_{\mu 2}(B_{s\mu})^{m\mu}, \quad (11)$$

where

$$B_{s\mu}=\int\cdots\int \exp\{-(2\pi^2 sMkT/h^2)[(\mathbf{r}_{s1}-\mathbf{r}_{s2})^2 +\cdots+(\mathbf{r}_{s\mu}-\mathbf{r}_{s1})^2]\}d\mathbf{r}_{s1}\cdots d\mathbf{r}_{s\mu} = V(2\pi sMkT/h^2)^{3(1-\mu)/2}\mu^{-3/2}. \quad (12)$$

Note that from (12) if we write $\mu=1$, then $B_{s1}=V$ so that the right-hand side of (11) could have been written $\prod_{\mu=1}(B_{s\mu})^{m\mu}$. Summing over all P's in evaluating the integral (10) is equivalent to summing over all possible sets of numbers $\{m_\mu\}$ of loops, each set of numbers occurring repeatedly, the set $\{m_\mu\}$ occurring

$$\prod_{\mu=1}^{N_s} N_s!/m_\mu!\mu^{m\mu}$$

times (see Kahn and Uhlenbeck[5]). Integration of (10) thus gives:

$$N!Q(\{N_s\}_N)=\prod_{s=1}^{N}(s!)^{N_s}\exp(-N_sW_s/kT)\sum_{\{m\mu\}N_s}N_s! \times\prod_{\mu=1}^{N_s}(1/m_\mu!)\{V(2\pi sMkT/h^2)^{3/2}\mu^{-5/2}\}^{m\mu} \quad (13)$$

where $\sum_{\{m\mu\}N_s}$ means the sum over all sets of numbers $\{m_\mu\}$ such that

$$\sum_{\mu=1}^{N_s}\mu m_\mu=N_s. \quad (14)$$

Because of (14) the first factor on the right of (13) can be written inside the last factor on the right of (13) in the form

$$(s!)^\mu\exp(-\mu W_s/kT).$$

To complete the partition function for the assembly of N atoms, the expression (13) has to be summed over all ways of clustering. The ways of clustering specified by the one set of numbers $\{N_s\}$ can occur with $N!/\prod_s N_s!(s!)^{N_s}$ significantly different arrangements of atoms. Therefore, summing over all significant ways of clustering yields

$$Q_N=\sum_{\{N_s\}_N}\{N!/\textstyle\prod_s N_s!(s!)^{N_s}\}Q(\{N_s\}_N) = \sum_{\{N_s\}_N}\prod_s\sum_{\{m\mu\}N_s}^{N_s}\prod_{\mu=1}^{N_s}(1/m_\mu!) \times\{V(2\pi sMkT/h^2)^{3/2}\mu^{-5/2}\exp(-\mu W_s/kT)\}^{m\mu}. \quad (15)$$

IV. EVALUATION OF THE PARTITION FUNCTION IN THE LIMIT OF INFINITE N

Inspection of (15) shows that Q_N is the coefficient of X^N in the following power series in X:

$$\exp[\textstyle\sum_s\sum_\mu V(2\pi sMkT/h^2)^{3/2}\mu^{-5/2} \times\exp(-\mu W_s/kT)X^{s\mu}]. \quad (16)$$

The two product signs in (15) become the sums in the exponent of (16), and the restricted summations in (15) are automatically taken care of in selecting those terms in (16) that contain X to the power N. Therefore, going over to the complex plane and writing $\mathbf{X}$ in place of X we have:

$$Q_N=(1/2\pi i)\oint\mathbf{X}^{-(N+1)}\exp[V\chi(\mathbf{X})]d\mathbf{X}, \quad (17)$$

where

$$\chi(\mathbf{X})=\textstyle\sum_s\sum_\mu(2\pi sMkT/h^2)^{3/2}\mu^{-5/2} \times\exp(-\mu W_s/kT)\mathbf{X}^{s\mu}. \quad (18)$$

To evaluate this in the limit of infinite N we write Q_N with all values of N as the coefficients in another power series:

$$F(\mathbf{Z})=\sum_{N=1}^{\infty}Q_N\mathbf{Z}^N \quad (19)$$

and note that the $\lim N\to\infty$ of Q_N is $(1/R)^N$, where R is the radius of convergence of the power series (19). The argument from this point is identical with that given by Kahn and Uhlenbeck.[5] Putting (18) into (19) and writing

$$v=V/N \quad (20)$$

we find

$$F(\mathbf{Z})=(1/2\pi i)\oint(d\mathbf{X}/\mathbf{X})\sum_{N=1}^{\infty}[\mathbf{Z}\mathbf{X}^{-1}\exp v\chi(\mathbf{X})]^N. \quad (21)$$

The use of (20) implies that in going to the limit of infinite N we keep the intensive properties of the assembly unchanged, $v=$constant. Provided now that

$$|\mathbf{Z}\mathbf{X}^{-1}\exp v\chi(\mathbf{X})|<1, \quad (22)$$

the series in (21) can be summed:

$$F(\mathbf{Z})=\frac{1}{2\pi i}\oint\frac{d\mathbf{X}}{\mathbf{X}}\frac{\mathbf{Z}\mathbf{X}^{-1}\exp v\chi(\mathbf{X})}{1-\mathbf{Z}\mathbf{X}^{-1}\exp v\chi(\mathbf{X})}. \quad (23)$$

Application of the Cauchy theorem to this yields

$$F(\mathbf{Z})=v\mathbf{X}_0\chi'(\mathbf{X}_0)/[1-v\mathbf{X}_0\chi'(\mathbf{X}_0)] \quad (24)$$

where the prime indicates differentiation with respect to $\mathbf{X}_0$ and $\mathbf{X}_0$ is the value of $\mathbf{X}$ that just violates (22), namely:

$$\mathbf{Z}\mathbf{X}_0^{-1}\exp v\chi(\mathbf{X}_0)-1=0. \tag{25}$$

Evidently the radius of convergence of $F(\mathbf{Z})$ is the modulus of that value of $\mathbf{Z}$ that reduces the denominator in (24) to zero, and this will be found by using (25) in the following equation:

$$1-v\mathbf{X}_0\chi'(\mathbf{X}_0)=0. \tag{26}$$

In other words,

$$1/R=|\mathbf{X}_0^{-1}\exp v\chi(\mathbf{X}_0)| \tag{27}$$

where $\mathbf{X}_0$ is found from (26). From the statement immediately following Eq. (19) we finally have

$$\lim_{N\to\infty}(Q_N)^{1/N}=|\mathbf{X}_0^{-1}\exp v\chi(\mathbf{X}_0)|. \tag{28}$$

The Helmholtz free energy per molecule is[9]

$$A=\lim_{N\to\infty}-kT\ln(Q_N)^{1/N} \tag{29}$$

and the pressure exerted by the gas is

$$p=-\partial A/\partial v. \tag{30}$$

Thus

$$A=-\ln X_0+v\chi(X_0)kT \tag{31}$$

and therefore

$$p=kT\chi(X_0) \tag{32}$$

where, of course, X_0 is the value of $\mathbf{X}_0$ obtained from (26). The validity of the derivation, and the fact that X_0 is real, depend on conditions satisfied by the series $\chi(\mathbf{X}_0)$ and enumerated in detail by Kahn and Uhlenbeck.[5]

V. CONDENSATION PHENOMENA

The physical results of the foregoing analysis are contained in Eqs. (32), (26), and (18). Writing λ in place of X_0, these equations may be expressed in the following form:

$$p/kT=\sum_s\sum_\mu(2\pi sMkT/h^2)^{3/2}\mu^{-5/2}\lambda^{s\mu}\times\exp(-\mu W_s/kT) \tag{33}$$

where λ is determined by

$$N/V=\sum_s\sum_\mu(2\pi sMkT/h^2)^{3/2}s\mu^{-3/2}\lambda^{s\mu}\times\exp(-\mu W_s/kT). \tag{34}$$

To study the clustering avalanche resulting in condensation into the liquid phase it is convenient to express these equations in the form

$$p=\sum_s p_s \quad\text{and}\quad N=\sum_s s\bar{N}_s, \tag{35}$$

where

$$\left.\begin{aligned}p_s/kT&=\textstyle\sum_\mu(2\pi sMkT/h^2)^{3/2}\mu^{-5/2}\lambda^{s\mu}\\&\quad\times\exp(-\mu W_s/kT)\\ \bar{N}_s/V&=\textstyle\sum_\mu(2\pi sMkT/h^2)^{3/2}\mu^{-3/2}\lambda^{s\mu}\\&\quad\times\exp(-\mu W_s/kT)\end{aligned}\right\}. \tag{36}$$

Evidently p_s can be regarded as the partial pressure due to the sub-assembly of clusters of size s, and $\bar{N}_s$ is the mean number of clusters of size s. The clustering avalanche will occur if the ratio of the series $\sum_{s\geqslant 2}\bar{N}_s/V$ to the quantity $\bar{N}_1/V$ has a finite sum at its radius of convergence λ_c. Then at the temperature at which λ equals λ_c there will be a definite proportion of the assembly in clusters, whereas at an infinitesimally small temperature below this, the number of unclustered atoms goes suddenly to zero.

From (36) the ratio of the total number of clusters of any size to the number of unclustered atoms is

$$\frac{\sum_{s\geqslant 2}\bar{N}_s/V}{\bar{N}_1/V}=\frac{\sum_{s\geqslant 2}\sum_\mu(s/\mu)^{3/2}\lambda^{s\mu}\exp(-\mu W_s/kT)}{\sum_\mu\mu^{-3/2}\lambda^\mu\exp(-\mu W_1/kT)}. \tag{37}$$

However, in the denominator the energy W_1 is identically zero, for it means the internal energy of a cluster of size 1. All energies W_s, $s\geqslant 2$ are necessarily negative, so the radius of convergence of the series in the numerator of (37) is less than that of the denominator. Moreover, as will be shown in detail in the next section, its sum at its radius of convergence, is finite, therefore a clustering avalanche occurs at that temperature at which $\lambda=\lambda_c$ and $\lambda_c<1$.

To study the lambda-transition due to statistical degeneracy we observe that through (34) this can be done for the assembly as a whole or through (36) for each sub-assembly of uniformly sized clusters separately. Comparison between the series (34) and the series in the numerator of (37) at once reveals the fact that, as the difference between the two series is simply the (finite) sum N_1/V, the radii of convergence of the two are identical. This means that the lambda-transition cannot occur before the clustering avalanche. Furthermore, comparing the radii of convergence of the series for the separate sub-assemblies in (36), it becomes clear that the sub-assemblies with the largest size clusters suffer the lambda-transition first: namely simultaneously with the clustering avalanche, while the smaller sized clusters cannot undergo the lambda-transition until later, and then they are no longer present! More mathematically expressed: the radius of convergence of the series (34) is equal to the limit of the radius of convergence of one sub-assembly as the size of the cluster increases, and the radius of convergence of the sub-assembly decreases monotonically as the cluster size increases.

We therefore arrive at the interesting theorem, that a Bose-Einstein gas in which the van der Waals forces

[9] J. E. Mayer and M. G. Mayer, *Statistical Mechanics* (John Wiley and Sons, Inc., New York, 1940), Chapter 10 and Appendix XI.

cause clustering cannot undergo the lambda-transition at all, it will always condense into the liquid phase first. As presumably any gas that does condense into a liquid phase, does so because of van der Waals clustering, we are led to believe that no real gas will ever show the lambda-transition in its gaseous phase. Whether the transition can occur in the liquid phase, and what it would mean in that case, are of course entirely different questions.

VI. SATURATED VAPOR PRESSURE CURVE

Further progress is possible only on the basis of reasonable assumptions about the dependence of the internal energy W_s of the clusters on the cluster size s, particularly as regards its asymptotic behavior at large s.

It will be assumed here that W_s is the sum of two parts, one negative proportional to the number s, representing the internal energy neglecting surface effects, and the other positive proportional to the number of atoms in the surface of the cluster, and so roughly proportional to $s^{2/3}$. We write

$$W_s=-sW+s^{2/3}S. \tag{38}$$

The term S is strictly a slowly changing function of s, because at $s=1$ it must equal W in order to reduce W_1 to zero, whereas at large s it must approach and remain equal to the surface tension of the liquid phase. In studying the convergence of the series (34) however only the constant asymptotic value of S is of importance.

The radius of convergence λ_c of the series (34) is now obtained by taking first a particular value of μ and writing down the ratio of the $s+1$th term to the sth term and finding the limit of this ratio as s approaches infinity:

$$\{(s+1)/s\}^{5/2}\lambda^{\mu}\exp-\mu(W_{s+1}-W_s)/kT \rightarrow\lambda^{\mu}\exp\mu(W+Ss^{-1/3})/kT\rightarrow\lambda^{\mu}\exp(\mu W/kT).$$

Thus the radius of convergence is independent of μ:

$$\lambda_c=\exp(-W/kT). \tag{39}$$

The radius of convergence of the μ-series (36) for the clusters of some given size s is similarly found by writing down the ratio of the $\mu+1$th term to the μth term and taking the limit as $\mu\rightarrow\infty$:

$$\{(\mu+1)/\mu\}^{-3/2}\lambda^{s}\exp-W_s/kT\rightarrow\lambda^{s}\exp-W_s/kT$$

so that the radius of convergence for the s-type clusters is

$$\lambda_{sc}=\exp W_s/kT =\exp[-W/kT+Ss^{-1/3}/kT]>\lambda_c.$$

Only as the size of the cluster s approaches infinity does the radius λ_{sc} reduce to the value λ_c.

The value λ_c at the temperature T_c produces in the numerator of (37) the onset of the clustering avalanche. Putting these values into (33) for the pressure gives the saturated vapor pressure as a function of temperature:

$$p_{sat}/kT=\sum_s\sum_\mu(2\pi sMkT/h^2)^{3/2}\mu^{-5/2}\times\exp-\mu Ss^{2/3}/kT. \tag{40}$$

The s-series converges rather slowly, but for large enough s it approaches an integral that can be transformed into a gamma function, so there is no trouble about numerical computation if S is given some definite value. It is proposed to apply this equation to the saturated vapor curve of helium.

VII. DISCUSSION

It is of some interest to compare the lambda-temperature given by (34) with that for an ideal non-clustering gas:

$$N/V=(2\pi MkT/h^2)^{3/2}\sum_\mu\mu^{-3/2}. \tag{41}$$

This expression is simply the first term of the s-series in (34) at its avalanche point. For the clustering gas, using (39) in (34) we have instead:

$$N/V=(2\pi MkT/h^2)^{3/2}\sum_s\sum_\mu(s/\mu)^{3/2}\times\exp-\mu s^{2/3}S/kT. \tag{42}$$

Whether, at a given T, this sum turns out to be greater than or less than the sum in (41) depends on the numerical magnitude of the surface tension S. Very approximately

$$\sum_s s^{3/2}\exp-\mu s^{2/3}S/kT=\int_0^\infty s^{3/2}\exp(-\mu s^{2/3}S/kT)ds$$

$$=(3/2)(kT/\mu S)^{15/4}\int_0^\infty z^{11/4}e^{-z}dz$$

$$=(3/2)(kT/\mu S)^{15/4}\Gamma(15/4).$$

Equation (42) thus becomes approximately

$$N/V=(2\pi MkT/h^2)^{3/2}(kT/S)^{15/4}\times(3/2)\Gamma(15/4)\zeta(21/4). \tag{43}$$

Write T_c for the transition temperature given by (43) for the clustering gas and T_1 for that given by (41) for the ideal gas, then we have

$$1=(T_c/T_1)^{3/2}(kT_c/S)^{15/4}(25.6\doteq 2.61). \tag{44}$$

It follows that, very approximately

$$T_c\gtrless T_1 \quad\text{as}\quad S\gtrless 1.84kT_c. \tag{45}$$

If surface tension is considerably less than thermal energy the assembly will be a gas at the temperature and density satisfying (41) so that one would, on the ideal gas approximation, expect to find a lambda-transition; however, the clustering inhibits the transition there.

The present theory of a clustering gas has neglected the finite size of the atoms and clusters. An ideal gas

of hard spheres may be expected to yield, to a first approximation, in place of (41):

$$N/(V-b)=(2\pi MkT/h^2)^{3/2}\sum_\mu \mu^{-3/2}, \qquad (46)$$

where b is the region of configuration space excluded by the spheres. This raises T_1. Roughly the same correction would apply to (42) for the clustering gas, so that the comparison between clustering and non-clustering gases is not essentially altered by the correction. On the other hand it may be remarked that long-range repulsive forces might be expected to lower the lambda-temperature because they would oppose the condensation, and attractive forces conversely may raise the temperature. These effects are very small, however, even compared with the volume effect[10] in (46). It is only insofar as the attractive forces are sufficient to cause clustering that they have any appreciable effect, and this is to lower the transition temperature right down to the saturated vapor line. The physical reason for this is simply that the degenerate Bose-Einstein gas prefers to go into the lowest energy states, and these are the clustered ones; it may even be asserted that the lambda-condensation itself forces the condensation into the liquid phase and can never occur without it.

[10] L. I. Schiff, Phys. Rev. 59, 758 (1941).

PHYSICAL REVIEW VOLUME 79, NUMBER 5 SEPTEMBER 1, 1950

Crystal Statistics of a Two-Dimensional Triangular Ising Lattice

G. F. NEWELL
University of Illinois, Urbana, Illinois
(Received May 4, 1950)

An example of a two-dimensional crystal in which each lattice point interacts with six neighbors is the so-called "triangular Ising lattice." The unit cell is a parallelogram with interactions along each of the sides and along the shorter diagonal. The thermodynamic properties of this lattice can be calculated for arbitrary interaction constants in the three independent directions by a simple extension of the procedure used previously by the author to solve the two-dimensional rectangular Ising lattice.

The triangular lattice generally has an order-disorder transition of a type very similar to that of the rectangular lattice, which is indeed but a limiting case of the triangular problem. The only lattice having no transition is that for which one or three of the three interactions are antiferromagnetic (negative) and the two interaction constants of smallest absolute magnitude have equal absolute value.

I. INTRODUCTION

A GENERAL technique for calculating the thermodynamic properties of certain two-dimensional crystal problems has been developed by Onsager[1] and Kaufman.[2] One makes use of the known relationships between the $2n$-dimensional orthogonal group and its 2^n-dimensional spinor representation. Wannier[3] has recently reported that the two-dimensional triangular Ising lattice can also be solved, at least in the case of equal interactions in all directions, by making use of the dual transformation[4] which relates the triangular problem to one essentially the same as the rectangular problem.

The triangular problem can also be solved for arbitrary interaction constants in the three directions using the procedure recently applied to the two-dimensional rectangular lattice[5] in which a matrix $\mathbf{M}$ is associated with each lattice point of the crystal instead of with an entire row.

Using the notation of reference 5, the triangular lattice is obtained from the rectangular one by adding an interaction

$$-J_2\mu_j\mu_{j+n-1}$$

between the jth point and the $(j+n-1)$th. The partition function is

$$Z=\sum_{\mu_j=\pm1}\exp[\sum_{j=1}^{nm}(H_0\mu_j\mu_{j+1}+H_1\mu_j\mu_{j+n}+H_2\mu_j\mu_{j+n-1})], \qquad (1)$$

$$H_0\equiv J_0/kT, \quad H_1\equiv J_1/kT, \quad H_2\equiv J_2/kT.$$

We introduce a matrix $\mathbf{M}$ defined by

$$M_{\mu_n'\cdots\mu_1',\,\mu_n\cdots\mu_1}\equiv\exp(H_1\mu_n'\mu_n)\exp(H_0\mu_n'\mu_1)\times\exp(H_2\mu_n\mu_1)\prod_{j=1}^{n-1}\delta(\mu_j'-\mu_{j+1}). \qquad (2)$$

Z can be written as

$$Z=\sum_{\mu_i=\pm1}\prod_{i=1}^{nm}M_{\mu_{n+i}\cdots\mu_{i+1},\,\mu_{n+i-1}\cdots\mu_i},$$

$$Z=\mathrm{trace}\mathbf{M}^{nm}=\sum_{i=1}^{2^n}\lambda_i{}^{nm}, \qquad (3)$$

where λ_i are the 2^n eigenvalues of the matrix $\mathbf{M}$.

[1] L. Onsager, Phys. Rev. 65, 117 (1944).
[2] B. Kaufman, Phys. Rev. 76, 1232 (1949).
[3] G. H. Wannier, Phys. Rev. 78, 341 (1950).
[4] G. H. Wannier, Rev. Mod. Phys. 17, 50 (1945).
[5] G. F. Newell, Phys. Rev. 78, 444 (1950).

$\mathbf{M}$, which may be considered either as an operator defined in a 2^n-dimensional vector space or as a 2^n-dimensional matrix, can be expressed in terms of the operators $\mathbf{C}_r$, $\mathbf{s}_r$, and $\mathbf{R}$ defined in reference 5.

$$\mathbf{M}=\exp(H_1\mathbf{s}_n\mathbf{s}_{n-1})(e^{H_0}+e^{-H_0}\mathbf{C}_n)\exp(H_2\mathbf{s}_n\mathbf{s}_{n-1})\mathbf{R}$$

or, with

$$H^*=\tanh^{-1}(e^{-2H_0}),$$

$$\mathbf{M}=(2\sinh 2H_0)^{\frac{1}{2}}\exp(H_1\mathbf{s}_n\mathbf{s}_{n-1})\times\exp(H^*\mathbf{C}_n)\exp(H_2\mathbf{s}_n\mathbf{s}_{n-1})\mathbf{R}. \quad (4)$$

II. SOLUTION OF THE EIGENVALUE PROBLEM

Equation (4) differs from Eq. (9) of reference 5 only by the factor containing H_2. Since $\exp(H_2\mathbf{s}_n\mathbf{s}_{n-1})$ is a representative of a rotation in a $2n$-dimensional space, the new problem is but slightly more complicated than the rectangular one. The reduction of the problem to a $2n$-dimensional eigenvalue problem follows in an obvious manner from reference 5, Sections 3 and 4. Equation (27) of reference 5 is replaced by

$$\mathbf{M}=(2\sinh 2H_0)^{\frac{1}{2}}[\tfrac{1}{2}(1+\mathbf{U})c_+\mathbf{M}_+ +\tfrac{1}{2}(1-\mathbf{U})c_-\mathbf{M}_-],$$

$$\mathbf{M}_+\equiv\exp(-iH_1\mathbf{P}_n\mathbf{Q}_{n-1})\exp(iH^*\mathbf{P}_n\mathbf{Q}_n)\times\exp(-iH_2\mathbf{P}_n\mathbf{Q}_{n-1})\mathbf{A}_+, \quad (5)$$

$$\mathbf{M}_-\equiv\exp(-iH_1\mathbf{P}_n\mathbf{Q}_{n-1})\exp(iH^*\mathbf{P}_n\mathbf{Q}_n)\times\exp(-H_2\mathbf{P}_n\mathbf{Q}_{n-1})\mathbf{A}_-,$$

where $\mathbf{P}_j$, $\mathbf{Q}_j$, $\mathbf{U}$, $c_\pm$ and $\mathbf{A}_\pm$ have the same meanings as in reference 5.

$\mathbf{M}_\pm$ are spin representatives of rotations $\mathfrak{M}_\pm$ in $2n$-dimensional space.

$$\mathfrak{M}_\pm=\begin{bmatrix}
0&0&1&0&0&\cdots&\cdots&\cdots&\cdots&\cdots&\cdots&\cdots&\cdots&\cdots\\
0&0&0&1&0&\cdots&\cdots&\cdots&\cdots&\cdots&\cdots&\cdots&\cdots&\cdots\\
0&0&0&0&1&\cdots&\cdots&\cdots&\cdots&\cdots&\cdots&\cdots&\cdots&\cdots\\
\cdots&\cdots&\cdots&\cdots&\cdots&\cdots&\cdots&\cdots&\cdots&\cdots&\cdots&\cdots&\cdots&\cdots\\
0&0&0&\cdots&\cdots&\cdots&\cdots&\cdots&\cdots&\cdots&\cdots&1&0&0\\
0&0&0&\cdots&\cdots&\cdots&\cdots&\cdots&\cdots&\cdots&\cdots&0&1&0\\
a&b&0&\cdots&\cdots&\cdots&\cdots&\cdots&\cdots&\cdots&\cdots&0&0&g\\
c&d&0&\cdots&\cdots&\cdots&\cdots&\cdots&\cdots&\cdots&\cdots&0&0&h\\
e&f&0&\cdots&\cdots&\cdots&\cdots&\cdots&\cdots&\cdots&\cdots&0&0&t
\end{bmatrix}, \quad (6)$$

$$\left.\begin{aligned}
&a=\mp i(c_1s_2+s_1c^*c_2), \quad e=\pm is^*c_2\\
&c=\mp(s_1s_2+c_1c^*c_2), \quad b=\pm s_1s^*\\
&g=c_1c_2+s_1c^*c_2, \quad d=\mp ic_1s^*\\
&h=-i(s_1c_2+c_1c^*s_2), \quad f=\mp c^*\\
&t=-s^*s_2, \quad s_r=\sinh 2H_r, \quad c_r=\cosh 2H_r\\
&s^*=\sinh 2H^*, \quad c^*=\cosh 2H^*
\end{aligned}\right\}. \quad (7)$$

The eigenvalues e^ε of $\mathfrak{M}_\pm$ can be found by solving the determinantal equation

$$\det(\mathfrak{M}_\pm-e^\varepsilon I)=0.$$

This leads to the equation

$$\cosh n\varepsilon=t\cosh(n-1)z+b\cosh z+c,$$

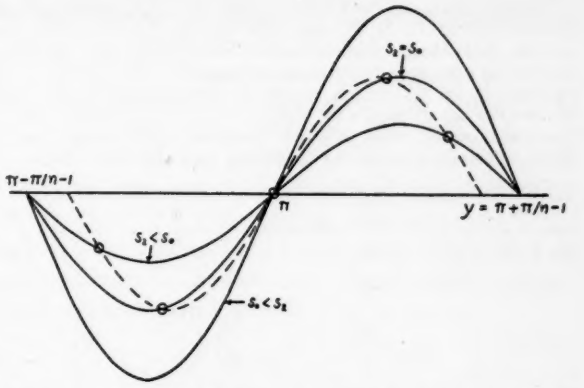

FIG. 1. The dashed line shows $s_0\sin ny$, the solid line $-s_2\sin(n-1)y$, s_2, $s_0>0$, for $s_2>s_0$, $s_2=s_0$, $s_2<s_0$. The circles occurring at the intersection of the two curves are the solutions of Eq. (9a). There are three such solutions in the interval shown if $s_2\leq s_0$; one if $s_2>s_0$.

or, substituting $z=x+iy$, one obtains the two real equations

$$s_0\cosh nx\cos ny+s_2\cosh(n-1)x\cos(n-1)y\mp s_1\cosh x\cos y=\mp\beta, \quad (8)$$

$$s_0\sinh nx\sin ny+s_2\sinh(n-1)x\sin(n-1)y\mp s_1\sinh x\sin y=0, \quad (9)$$

with

$$\beta=s_0s_1s_2+c_0c_1c_2=\sinh 2H_0\sinh 2H_1\sinh 2H_2+\cosh 2H_0\cosh 2H_1\cosh 2H_2.$$

Of particular interest is the solution of Eqs. (8) and (9) for $n\gg 1$. For simplicity, let us assume that as $n\to\infty$, $x\to 0$ (nx does not go to zero). In this limit (8) and (9) becomes

$$s_2\cosh nx\sin y/\sin ny\mp s_1\cos y=\mp\beta, \quad (8a)$$

$$s_0\sin ny=-s_2\sin(n-1)y. \quad (9a)$$

If one considers a plane triangle with sides s_0 and s_2, then he can take as the opposite angles $-(n-1)y$ and ny, respectively, in agreement with (9a). The law of sines for the third angle and side gives

$$s_2\sin y/\sin ny=(s_0^2+s_2^2+2s_0s_2\cos y)^{\frac{1}{2}} \quad (10)$$

from which

$$\cosh nx=\mp(\beta-s_1\cos y)(s_0^2+s_2^2+2s_0s_2\cos y)^{-\frac{1}{2}}. \quad (11)$$

With but few exceptions, there is a solution of (9a) for y in each interval $r\pi/n\leq y\leq(r+1)\pi/n$. This interval can be made arbitrarily small by choosing n sufficiently large. The solutions nx of (11) in turn can be found exactly in the limit $n\to\infty$, since it contains only $\cos y$ (not $\cos ny$). Equation (10) determines the sign of the square root appearing in (10) and (11). In general, $\sin y/\sin ny$ alternates in sign as r increases by integral steps. Equation (10) has a solution only if the right side is positive; thus half of the y-values go with $\mathfrak{M}_+$, the other half to $\mathfrak{M}_-$. The only exceptions to the above-

TABLE I. Data at $T=T_c$ where $x=0$. J_i, J_j, J_k stand for some permutation of J_0, J_1, J_2, such that $|J_i| \leqslant |J_j|$, $|J_k|$. The first column gives those constants which are positive, the remaining ones being negative. The second column gives the number of the equation in the text which locates the temperature T_c. The third column has the value of y for which $x=0$. The last column denotes the space (odd or even) to which the value $x=0$ belongs. Case A, B are so classified in the text following Eqs. (19) and (20).

$J_\alpha>0$	T_c	Value of y	Space
J_i, J_j, J_k	(19)	0	odd
J_j, J_k	(20)	0	odd
J_i, J_k	(20)	π if $J_j \equiv J_1$ π if $J_i \equiv J_1$ 0 if $J_k \equiv J_1$	case A case B even
J_i or J_k	(19)	π if $J_1<0$ 0 if $J_1>0$	case B even
none	(20)	π if $J_i \neq J_1$ 0 if $J_i \equiv J_1$	case A even

stated rules, for $0 \leq y < 2\pi$, are at $y=0$, $y=\pi$ and $y \sim 2\pi$. These are also the only points for which (11) could fail to justify the assumption that $x \to 0$ as $n \to \infty$. These solutions must be considered separately.

The number of discrete solutions of (9a) depends on the relative values of s_0 and s_2. Figure 1 shows a graph of $s_0 \sin ny$ and $-s_2 \sin(n-1)y$ for $s_0, s_2 > 0$; $\pi - \pi/(n-1) < y < \pi + \pi/(n-1)$. If $s_0 \geq s_2$ there are three solutions in the interval shown, but as s_2 is increased past s_0 these three points converge at $y=\pi$, giving only one solution for $s_0 < s_2$. For $s_2, s_0 > 0$ there is one solution $y=0$ in the interval $0 \leq y < \pi/n$ but none in the interval $2\pi - \pi/n \leq y < 2\pi$. There are all together $2n$ solutions if $s_0 \geq s_2$, but only $2n-2$ solutions if $s_2 > s_0$.

For s_0, s_2 not necessarily positive one finds $2n$ solutions if $|s_0| \geq |s_2|$, $2n-2$ solutions if $|s_2| > |s_0|$. If s_0, s_2 have the same sign, the "missing" solutions are at $y=\pi$, but if s_0, s_2 have opposite signs they are at $y=0$. To find the "missing" solutions in the former case, we consider Eq. (8) with $y=\pi$. This becomes

$$s_0 \cosh nx - s_2 \cosh(n-1)x = \mp(-1)^n(\beta + s_1 \cosh x). \quad (12)$$

For $s_0 \geq s_2 > 0$, the left side is positive for all x. If the right side is also positive, there is only one solution. This solution satisfies the condition $x \to 0$ as $n \to \infty$ and is correctly given by (11). If $s_2 > s_0 > 0$ and the right side is negative, there is a solution for which $x \to 0$ as $n \to \infty$; but irrespective of the sign of the right side, there is a solution of (12) for which x does not go to zero. As $n \to \infty$ this solution becomes

$$|s_0| e^{|x|} = |s_2|. \quad (13)$$

Solutions of the type (13) are obtained in all cases $|s_0| < |s_2|$, not only $s_2 > s_0 > 0$.

The complete set of solutions are as follows: If $|s_0| \geq |s_2|$, Eq. (10) gives $2n$ values of $|x|$, half of which go with $\mathfrak{M}_+$, half with $\mathfrak{M}_-$. If $|s_0| < |s_2|$, Eq. (10) gives, for each choice of sign, $n-1$ solutions for $|x|$. The remaining two solutions are of type (13). The values of y are in each case densely distributed in the interval $0 \leq y < 2\pi$.

The eigenvalues of $\mathbf{M}_+$ can be written in the form

$$(\pm) \exp(\tfrac{1}{2} \sum_{r=1}^{n} \epsilon_r z_r), \quad \epsilon_r = \pm 1 \quad (14)$$

those of $\mathbf{M}_-$ as

$$(\pm) \exp(\tfrac{1}{2} \sum_{r=1}^{n} \epsilon_r' z_r'), \quad \epsilon_r' = \pm 1 \quad (15)$$

where $z_r = x_r + iy_r$ are the n solutions of (8) and (9) with the upper sign and $z_r' = x_r' + iy_r'$ are the n solutions of (8) and (9) with the lower sign. The 2^n eigenvalues result from taking all possible sign combinations of ϵ_r, $\epsilon_r' = \pm 1$ and one of the signs in front.

III. SELECTION OF EIGENVALUES

To obtain the eigenvalues of $\mathbf{M}$, one must select those eigenvalues (14) and (15) belonging to the odd and even spaces respectively, in agreement with (5), and determine the sign in front of these expressions. The rule governing the selection of eigenvalues is that those eigenvalues of (14) and (15) with an even number of $\epsilon_r = -1$ belong to one of the two spaces (even or odd), those with an odd number of minus signs belong to the other space. Since (8) and (9) do not determine the sign of z_i, it is necessary to adopt some convention for this sign.

Any z_i whose real part x_i does not vanish for any value of T can be chosen positive. If x_i does vanish for some temperature T_c at which $dx_i/dT \neq 0$, then one must allow the sign of x_i to change at this point if x_i is to be an analytic function of T. In this case, we shall take x_i to be positive for $T > T_c$. The same convention applies to the z_i'. (This is the opposite convention to that used in reference 5 for x_0.)

According to a theorem by Frobenius and Oldenburger,[6,7] the largest eigenvalue of $\mathbf{M}$, $\max\lambda_+$, comes from $\mathbf{M}_+$; it is real and non-negative. If the z_i are so ordered that $x_j \leq x_k$ if $j<k$, then either $x_1 = x_2$ and z_2 is the complex conjugate of z_1 or x_1 is a unique smallest and $y_1 = 0$ or π. This is a consequence of the fact that if z is a solution of (8) and (9), then so is its complex conjugate, but no solution is multiple. $y=\pi$ and $y=-\pi$ are however the same solution.

From (14) we see that the largest eigenvalue of $\mathbf{M}_+$ for the even space has $\epsilon_r = +1$, $2 \leq r \leq n$ but ϵ_1 depends on whether the eigenvalues of the even space have an even or odd number of values $\epsilon_i = -1$. If $y_1 \neq 0, \pi$ then $\epsilon_1 = +1$, for if it were -1 the corresponding eigenvalue of $\mathbf{M}$ would be complex, contrary to Frobenius' theorem. If $y_1 = 0, \pi$ Frobenius' theorem is of no help.

The choice of the correct ϵ_1 if $y_1 = 0, \pi$ depends on the calculation of Z in the limit of large temperatures in which case all x_i are positive and Z is known to be 2^{nm}

[6] S. B. Frobenius, Preuss, Akad. Wiss., p. 514 (1909).
[7] R. Oldenburger, Duke Math. J. 6, 357 (1940).

as evaluated from (1). This results from (3) if $\max\lambda_+$ is non-degenerate and $\epsilon_1=+1$. If $\epsilon_1=-1$, Z is complicated because of near degeneracies of $\max\lambda_+$ with those eigenvalues having $\epsilon_1=+1$ and some $\epsilon_i=-1$, $i\neq 1$ and also with the largest eigenvalues of $\mathbf{M}_-$. In no case does $\epsilon_1=-1$ give the correct limit $Z=2^{nm}$. The eigenvalues of $\mathbf{M}_+$ belonging to the even space must therefore be those with an even number of $\epsilon_i=-1$.

$$\max\lambda_+=(2\sinh|2H_0|)^{\frac{1}{2}}\exp(\tfrac{1}{2}\sum_{i=1}^{n}x_i). \tag{16}$$

The determination of the number of allowed $\epsilon_i'=-1$ rests on the above-mentioned requirement that $\max\lambda_+$ be a unique largest eigenvalue of $\mathbf{M}$ for $T>T_c$. The eigenvalue (15), belonging to the odd space, with the largest absolute magnitude has $\epsilon_i'=+1$, $2\leq i\leq n$, if the z_i' are ordered as were the z_i.

For $T>T_c$, all x_i' are positive and if $\epsilon_1'=+1$, the largest odd eigenvalue, $\max\lambda_-$, of $\mathbf{M}$ is real. As $n\to\infty$, the x_i' form a dense sequence of values interspaced between the x_i. $\Sigma x_i'\to\Sigma x_i$ and the largest eigenvalue of $\mathbf{M}_-$ becomes degenerate with the largest eigenvalue of $\mathbf{M}_+$. To avoid a degeneracy of $\max\lambda_+$, one must assume that the eigenvalues of $\mathbf{M}_-$ belonging to the odd space have an odd number of $\epsilon_i'=-1$. In general $\max\lambda_-$ will not be real.

The eigenvalues of $\mathbf{M}$ are:

$$(\pm)(2\sinh 2H_0)^{\frac{1}{2}}c_+\exp(\tfrac{1}{2}\sum_{i=1}^{n}\epsilon_i z_i), \tag{17}$$

$$(\pm)(2\sinh 2H_0)^{\frac{1}{2}}c_-\exp(\tfrac{1}{2}\sum_{i=1}^{n}\epsilon_i' z_i'), \tag{18}$$

$$\begin{aligned} c_+&=-i, \quad c_-=1, \quad \text{for } n \text{ odd},\\ c_+&=1, \quad c_-=-i, \quad \text{for } n \text{ even}. \end{aligned}$$

The signs in front are chosen such that Z is positive for all T. The number of $\epsilon_i=-1$ is even; the number of $\epsilon_i'=-1$ is odd.

IV. DEGENERATE EIGENVALUES

As was true in the rectangular Ising lattice, the existence of values of x which pass through zero means that the largest eigenvalues become degenerate as $n\to\infty$ for temperatures below the point T_c where some z is zero. If all the interaction constants J_i are positive, one obtains a twofold degeneracy, as was true of the rectangular case, but if some of the J_i are negative, the degeneracy may be many-fold. The reason for this can be traced to the fact that for some J_i negative, in general one cannot obtain a state of as high degree of order as for $J_i>0$.

Though these deviations from "complete order" at low temperature are usually caused by the screw type periodic boundary conditions which were introduced merely to simplify the problem, and have no physical significance, the manner in which this anomalous behavior appears in the theory is of some interest from the mathematical point of view.

To investigate this, one must find those x_i, x_i' which pass through zero for some temperature. These can be found from (11) by minimizing the right side as a function of y and setting the left side equal to unity. The values of y which make the right side a minimum will be either 0 or π depending on which of the J_i are negative and which $|J_i|$ is the smallest. The results are given in Table I. The formulas, as indicated in Table I, for the temperature at which $x=0$ are

$$|s_i\ s_j|+|s_j\ s_k|+|s_i\ s_k|=1, \tag{19}$$

$$|s_i\ s_j|-|s_j\ s_k|+|s_i\ s_k|=-1. \tag{20}$$

In (20), $|s_i|<|s_j|$, $|s_k|$. Case A and B of Table I are classified as follows: For case A, $x=0$ belongs to the even space if $s_0>s_2$ and n is odd or if $s_0<s_2$ and n is even. It belongs to the odd space if $s_0>s_2$ and n is even or $s_0<s_2$ and n is odd. If $s_0=s_2$, there is no solution $x=0$. For case B, $x=0$ belongs to the even space if $s_0<0$ ($s_2>0$) and n is even or $s_2<0$ ($s_0>0$) and n is odd. Otherwise $x=0$ belongs to the odd space.

It is significant that for any fixed value of J_i, there is, at most, one solution $x=0$ of (11). This solution belongs to either the even space or the odd space, not both. That $|x_i|$ or $|x_i'|$ which is smallest of its respective set for one temperature, is the smallest for all temperatures. In view of the convention for ordering the x_i, x_i', that x_i or x_i' which is zero at $T=T_c$ is either x_1 or x_1'. *There is no solution $x=0$ if one or three of the J_i are negative and there is no unique smallest J_i.* This case will be called type I in the following.

If there is no degeneracy for large T and no x_i, x_i' changes sign, then there is no degeneracy for low temperatures. For a type I lattice, $\max\lambda_+$ is sufficient to determine Z for all temperatures, assuming $m\gg 1$.

A lattice for which $x_1'=0$ at $T=T_c$ will be called a type II lattice; that for which $x_1=0$ at $T=T_c$ a type III lattice. Type II is the type considered in the rectangular model with positive interactions. For $T<T_c$, $\max\lambda_-$, which is in this case real, contains the sum of positive numbers $|x_i'|$ by virtue of the negative x_1 counteracting the one minus sign $\epsilon_1'=-1$; $\max\lambda_+$, which has no $x_i=0$ retains its positive definite sum

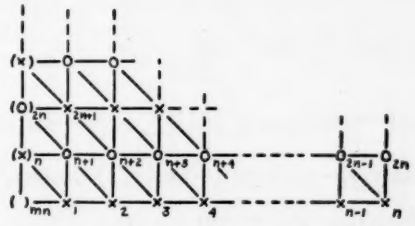

FIG. 2. State of highest order $H_1>0$, $H_0<0$, $|H_2|<|H_0|$, $|H_1|$. The crosses denote one sign of μ_i; the circles, the opposite sign. The screw-type boundary condition is indicated by repeating, in parenthesis, the nth column in its relation to the first. H_1 is the interaction constant in the row, H_0 in the column, and H_2 along the diagonal.

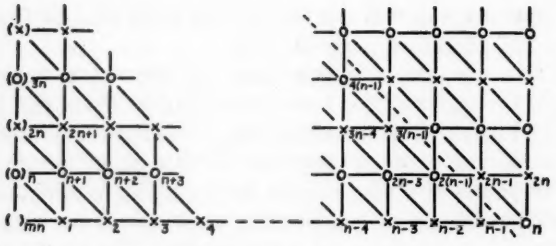

FIG. 3. State of highest order $H_1>0$, $H_2<0$, $|H_0|<|H_1|$, $|H_2|$. H_1 is the interaction constant in the row, H_0 in the column, and H_2 along the diagonal. The diagonal dashed line represents the position of the discontinuity in the pattern.

below T_c. The next largest eigenvalues contain two negative quantities in the exponent and therefore are not to be considered with the above. The degeneracy become twofold as $\max\lambda_- \to \max\lambda_+$ for $T<T_c$, $n\to\infty$.

For a type *III* lattice, $\max\lambda_+$ has one negative term in the sum over $\epsilon_i x_i$ if $T<T_c$ as does $\max\lambda_-$ for all T. They are $+x_1$ and $-x_1'$ respectively. As $n\to\infty$, the values of $|x_i|$ form a dense sequence with $|x_1|$ as a lower limit. By changing the sign of ϵ_1 and one other ϵ_i for which $x_i \to |x_1|$ as $n\to\infty$, one obtains another eigenvalue with a permissible number of $\epsilon_i=-1$. The same is also true for the x_i'. The absolute magnitude of these eigenvalues tend toward $\max\lambda_+$ as $n\to\infty$. $\mathrm{Max}\lambda_+$ is thus the upper limit of a dense sequence of $|\lambda_+|$ and $|\lambda_-|$. This sequence for $|H_0|<|H_2|$ contains $2n$ eigenvalues, n from λ_+ and n from λ_-, corresponding to the n ways of assigning one minus sign to the n x_i's If $|H_0|<|H_2|$, x_n and x_n' satisfy (13) and are not of a size comparable with the set of x_i, x_i' satisfying (11). In this case there are only $2n-2$ eigenvalues in the above sequence instead of $2n$.

Substituting the values λ_+, λ_- in Eq. (3), neglecting all but the largest eigenvalues, we obtain the following expressions for Z.

Type *I* lattice or type *II*, *III* with $T>T_c$

$$Z=(2|s_0|)^{\frac{1}{2}nm}\exp(\tfrac{1}{2}nm\sum_1^n x_i). \tag{21}$$

Type *II* lattice, $T<T_c$

$$Z=2(2|s_0|)^{\frac{1}{2}nm}\exp(\tfrac{1}{2}nm\sum_1^n x_i). \tag{22}$$

Type *III* lattice, $T<T_c$, $|H_0|\geq|H_2|$

$$Z=(2|s_0|)^{\frac{1}{2}nm}\exp(\tfrac{1}{2}nm\sum_1^n|x_i|)[\sum_{i=1}^n\exp(-nm|x_i|)\times\cos nm(y_i-y_1)\pm\exp(-nm|x_i'|)\cos nmy_i']. \tag{23}$$

Type *III* lattice, $T<T_c$, $|H_0|<|H_2|$

$$Z=(2|s_2|)^{\frac{1}{2}nm}\exp(\tfrac{1}{2}nm\sum_1^{n-1}|x_i|)[\sum_{i=1}^{n-1}\exp(-nm|x_i|)\times\cos nm(y_i-y_1)\pm\exp(-nm|x_i'|)\cos nmy_i']. \tag{24}$$

To obtain Eqs. (22) to (24), it has been assumed that m is of the same order as n, thus $0(m/n^2)\ll 1$. This is used for instance to justify replacing $\frac{1}{2}nm\sum x_i'$ by $\frac{1}{2}nm\sum x_i$. In (23) and (24) one makes use of the fact that the z_i, z_i' occur in complex conjugate pairs to remove the imaginary part of the λ's. The $\pm$ sign of (23) and (24) must be determined by some extra conditions such as the low temperature limit discussed in the next section.

V. LOW TEMPERATURE EFFECTS OF THE BOUNDARY

In this section, we shall be concerned primarily with the interpretation of the rather complicated form of Eqs. (23) and (24).

The quantity in the bracket of (23), we shall call B_1. Each term of its sum is, in absolute magnitude, less than $\exp(-nm|x_1|)$ for s_i finite.

$$|B_1|\leq 2n\exp(-nm|x_1|).$$

The equality can be true only in the limit $T\to 0$. For $|H_0|>|H_2|$ and $T\to 0$.

$$nx_r'\to nx_r\to|nx_1|\to\begin{cases}2|H_2+H_1| \text{ for } H_0>0\begin{cases}ny_r\to(2r+1)\pi\\ ny_r'\to 2r\pi\end{cases}\\ 2|H_2-H_1| \text{ for } H_0<0\begin{cases}ny_r\to 2r\pi\\ ny_r'\to(2r+1)\pi.\end{cases}\end{cases} \tag{25}$$

The simple form of (25) is based on the limit $s_2/s_0\to 0$. We thus obtain

$$B_1\to\exp(-nm|x_1|)\,[(n\pm n)+\text{terms of order } s_2/s_0 \text{ or smaller}]. \tag{26}$$

If the minus sign is correct we obtain for Z an expression of the form $\infty\cdot 0$ which cannot be evaluated in this order of approximation. If the plus sign is correct, we obtain for Z, the expressions

$$Z\to\begin{cases}2n\exp(nm|H_0|)\exp[m(n-2)|H_2+H_1|], & H_0>0,\\ 2n\exp(nm|H_0|)\exp[m(n-2)|H_2-H_1|], & H_0<0.\end{cases} \tag{27}$$

Many of the cases given in Table I are of the type to which (23) applies. We shall consider as an example $H_1>0$, $H_0<0$, $|H_2|<|H_0|$, $|H_1|$. The state of lowest energy is shown in Fig. 2. It is apparent from the figure that the interactions between the points jn and $jn+1$, $j=1, 2, \cdots$ is not the favorable one. This discontinuity in the pattern may with equal probability be located along any one of the n columns. An additional complication will arise if m is odd due to the periodic boundary conditions between the 1st row and the mth. The pattern is unchanged if all the μ_i are changed to $-\mu_i$. Assuming m even, there are thus $2n$ equivalent states of lowest energy. The energy contribution from the column interactions is nmJ_0, that from the row and diagonal interactions $-(n-2)m(J_1-J_2)$. This checks with the expression (27).

If m is odd, one chooses the minus sign in (26). An exact calculation is difficult because the first $n-1$ corrections to (26) will also vanish, until the expression for Z contains factors $m-2$ in the exponent instead of m. The degeneracy of the lowest state being of order nm^n.

We conclude that the complications of (23) are in this case due entirely to the forced boundary conditions which prevent the system from attaining a state of complete order. Further examples would show that this is true in all cases in which (23) applies.

The bracket of (24), which we denote by B_2, is even more cumbersome to analyze for $T\to 0$. nx_r, nx_r', y_r' now satisfy

$$\begin{aligned} &2|H_0+H_1| \text{ for } H_2>0\begin{cases}(n-1)y_r\to(2r-1)\pi\\(n-1)y_r'\to 2r\pi\end{cases}\\ &nx_r'\to nx_r\to|nx_1|\to\\ &2|H_0-H_1| \text{ for } H_2<0\begin{cases}(n-1)y_r\to 2r\pi\\(n-1)y_r'\to(2r-1)\pi\end{cases}\end{aligned} \tag{28}$$

to order s_0/s_2.

$$|B_2|\to\exp(-nm|x_1|)\times\left|\sum_{r=1}^{n-1}\left(\cos\frac{mn2r\pi}{n-1}\pm\cos\frac{mn(2r-1)\pi}{n-1}\right)\right|. \tag{29}$$

To this order of approximation, B_2 vanishes unless nm is an integer multiple of $n-1$, and vanishes even then for one of the choices of sign in (29). Higher order calculations will show that B is of order

$$n[m\exp(|2H_0|-|2H_2|)]^{\gamma},$$

$\gamma=nm \bmod(n-1)$ for one choice of sign and of order $n[m\exp(|2H_0|-|2H_2|)]^{-\gamma+n-1}$ for the other choice.

The source of the complication is again apparent if we consider an example. Suppose $|H_0|<|H_1|$, $|H_2|$; $H_2<0$, $H_1>0$. The lowest energy state is of the form shown in Fig. 3. The discontinuity in the pattern occurs along the diagonal line $j(n-1)$, $j=1, 2, \cdots$. This pattern will not satisfy the periodic boundary conditions between the mth row and the first unless nm is an integer multiple of $2(n-1)$.

If such be the case, the degeneracy of the state is $2(n-1)$. There are n positions in a row through which the discontinuity can pass but one of the resulting n patterns is the same as that obtained by changing all μ_i to $-\mu_i$.

By the proper choice of sign in (29), one can force B_2 to vanish in first order unless nm is an even multiple of $n-1$. In this case, $B_2\to 2(n-1)\exp(-nm|x_1|)$ which is in agreement with the above picture.

If the pattern of Fig. 3 fails to close on itself, then each additional unfavorable interaction caused by this failure to close may be placed in any one of the m rows adjacent to the discontinuity already present. The resulting degeneracy is of order nm^{α}, $\alpha=nm \bmod 2(n-1)$ or $\alpha=2(n-1)-nm \bmod 2(n-1)$, $\alpha\leq n-1$ which by a proper choice of sign in (29) leads to at least qualitative agreement even in these cases.

We are forced to conclude that the quantities in the brackets of both (23) and (24) are only an expression of the effects caused by the imposed boundary conditions. Their contribution to the thermodynamic properties of the system as a whole is negligible at all temperatures, except perhaps in the immediate vicinity of $T=0$. The entropy at $T=0$ for instance is appreciably changed by the boundary conditions, though it is essentially zero in either case. The smallness of these effects can be verified mathematically as well as by physical arguments..

The thermodynamic properties of the system will in all cases be calculated from (21) instead of the more complicated forms (23) and (24).

VI. THERMODYNAMIC PROPERTIES

In deriving the thermodynamic properties of the system, one replaces the sum of (21) by an integral.

$$\left.\begin{aligned}\frac{1}{nm}\log Z&=\tfrac{1}{2}\log 2|s_j|+\frac{1}{4\pi}\int_0^{2\pi}dy\,nx(y)\\ |s_j|&=\begin{cases}\sinh|2H_0| & \text{if } |H_0|\geq|H_2|\\ \sinh|2H_2| & \text{if } |H_2|\geq|H_0|\end{cases}\end{aligned}\right\}, \tag{30}$$

$nx(y)$ is given by (11).

Though Z cannot be expressed in closed form, the internal energy and specific heat can. By differentiation under the integral sign, one obtains integrals of the form

$$\int_{-1}^{+1}du[f(u)/Q^{\frac{1}{2}}]$$

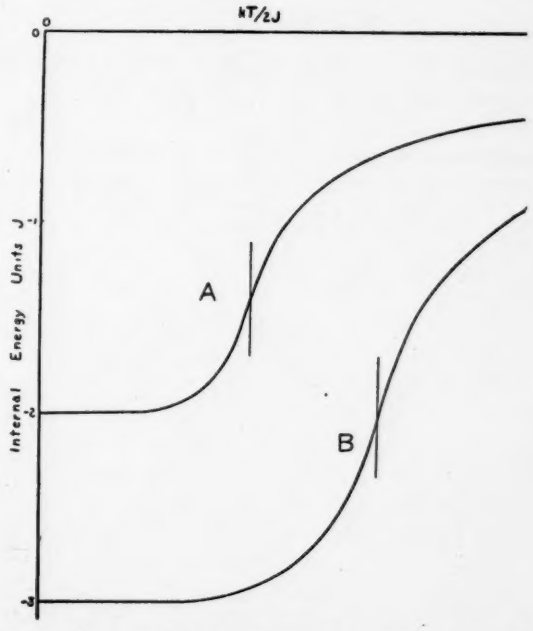

FIG. 4. Graph of the internal energy per lattice point vs. the temperature. Curve A is for the square lattice $J_0=J_2\equiv J$, $J_1=0$. Curve B is for the equilateral triangle lattice $J_0=J_1=J_2\equiv J$. The vertical line corresponds to the transition point.

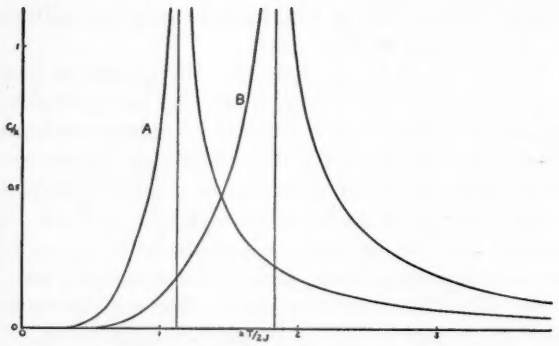

FIG. 5. Graph of the specific heat per lattice point *vs.* the temperature. Curve *A* is for the square lattice $J_0=J_2\equiv J$, $J_1=0$. Curve *B* is for the equilateral triangle lattice $J_0=J_1=J_2\equiv J$.

$u=\cos y$ and Q is a fourth-degree polynomial in u. The method for transforming such integrals to elliptic integrals is well known. The expression for the internal energy per lattice point, U, will in general involve both $K(k_1)$ and $\Pi_1(n, k_1)$, the complete elliptic integral (Legendre standard form) of the first and third kind respectively. The latter can be re-expressed in terms of incomplete elliptic integrals of the first and second kinds.

Finding the explicit form of U for arbitrary J_i is somewhat tedious. The resulting expression is not simple and will not be given here.

The important feature of the expression is the argument k_1 of the elliptic integrals.

$$k_1^2=4\delta/(\delta+1)^2\leq 1,\quad \delta=[\beta^2-(1+s_0^2+s_1^2+s_2^2)]^{\frac{1}{2}}. \tag{31}$$

It follows that $k_1=1$ if $\delta=1$,

$$\beta^2=2+s_0^2+s_1^2+s_2^2. \tag{32}$$

Equation (32) is equivalent to Eqs. (19) and (20), thus some $z=0$ implies that $k_1=1$ and vice versa.

As was true in the rectangular case, $K(k_1)$, which is logarithmically infinite at $k_1=1$, is multiplied in the expression for U by a factor that vanishes linearly at $T=T_c$. There is, therefore, no discontinuity in the internal energy but the specific heat has a logarithmic singularity at $T=T_c$.

If $J_0=J_2=J$, most of the thermodynamic expressions are simplified considerably by the substitution

$$\coth 2L\equiv\exp(2H_1)\cosh 2H. \tag{33}$$

The transition point occurs at

$$|\exp(2H_1)\sinh 2H|=1. \tag{34}$$

The internal energy is

$$U=-J_1\coth 2H_1-(2/\pi)\{k'\sin\theta(J_1+J\coth 2H)K(k_1)+(J_1\coth 2H_1-J\coth 2H)[K(k_1)F(k',\theta)-E_1(k_1)F(k',\theta)-K(k_1)E(k',\theta)]\}, \tag{35}$$

where

$$\sin\theta=\frac{\sinh 2H+\sinh 2L}{\cosh 2H\cosh 2L},\quad k'=\frac{\sinh 2H-\sinh 2L}{\sinh 2H+\sinh 2L},$$
$$k_1^2=1-k'^2.$$

$K(k_1)$, $E_1(k_1)$ are the complete elliptic integrals of the first and second kind, respectively; $F(k', \theta)$, $E(k', \theta)$ are the incomplete elliptic integrals.

If all three J_i are equal, this reduces to

$$U=-J\coth 2H[1+(2/\pi)k'\times\sin\theta(1+\tanh 2H)K(k_1)]. \tag{35a}$$

If one of the three J_i is zero, the triangular lattice reduces to the rectangular net which has been treated in some detail.[1]

In Figs. 4 and 5, the internal energy and specific heat are plotted as functions of the temperature, for the two simple cases $J_0=J_2\equiv J$, $J_1=0$ (square lattice) and $J_0=J_1=J_2\equiv J>0$ (equilateral triangle lattice).

This paper was written under the guidance of Professor A. Nordsieck and supported by a predoctoral fellowship by the AEC.

Letters to the Editor

PUBLICATION of brief reports of important discoveries in physics may be secured by addressing them to this department. The closing date for this department is five weeks prior to the date of issue. No proof will be sent to the authors. The Board of Editors does not hold itself responsible for the opinions expressed by the correspondents. Communications should not exceed 600 words in length.

Superconductivity in Tin-Germanium "Alloys"

RALPH P. HUDSON
Purdue University, Lafayette, Indiana
June 30, 1950

MEASUREMENTS of the variation with temperature of the resistivity in tin-germanium "alloys,"[1] and x-ray investigation,[2] have shown that the major portion of the tin taken up[3] remains free along grain boundaries, forming paths of relatively high electrical conductivity through the bulk germanium. A calculation[4] based on the assumption that veins of free tin were responsible for the observed conductivity gave results in good agreement with experiment.

The transition to the superconducting state has been measured for this material, which becomes effectively a mesh of superconducting filaments and might be expected to show a similar behavior to that observed in alloys. For the latter, the transitions are spread out over a relatively wide range of temperature, the lines of magnetic induction being pushed out of the specimen gradually as the temperature is lowered. The crowding of these lines in other parts of the specimen suppresses the transition there until a lower temperature is reached, where the critical field is correspondingly greater.[5]

The conventional magnetic method was employed, in which the specimen is made the core of a mutual inductance. The secondary coil is connected to a ballistic galvanometer and the throw on reversing the primary current is observed. The apparatus was enclosed in a bath of liquid helium, the specimen being in a small inner vessel also containing liquid helium. The temperature of the latter could be reduced by pumping off the helium vapor and was measured by means of the vapor pressure.

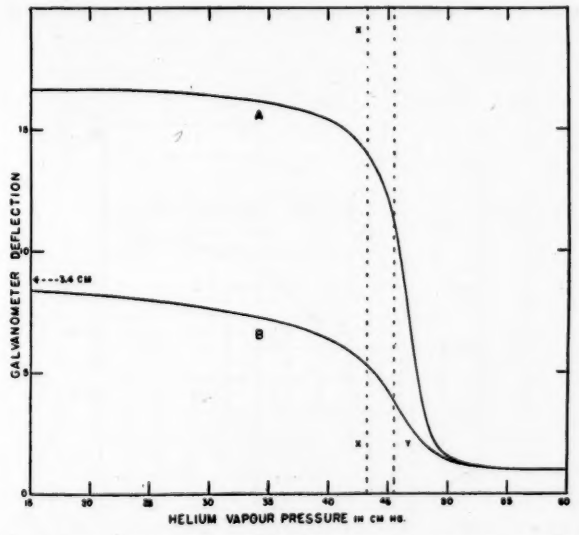

FIG. 1. Superconducting transition curves for tin-germanium "alloys." Measuring field approximately 4 oersted.

Measurements were made on two specimens of practically identical shape and volume, made by rounding off the edges of small rectangular blocks, the one (A) with 9.3 atomic percent of added tin and the other (B) with 2.3 percent. Each in turn was cooled (or allowed to warm up) very slowly through the transition range in the constant magnetic field of the primary coil, which was approximately 4 oersted. The cooling and heating curves coincided when the specimen was just covered by the liquid helium and when the rate of change of temperature was kept small.

Curves for specimens A and B are shown in Fig. 1. The transitions are very much extended and begin at the relatively high temperature of 3.90°, presumably due to strain. Whereas A is completed at 3.05°, curve B does not flatten off until 2.14°.

The total change in the galvanometer deflection indicates that in the case of B, with the smaller tin content, the "superconducting volume" is considerably smaller than the actual volume of the specimen; i.e., even when the transition is complete the magnetic flux is not wholly excluded from the specimen. It seems, therefore, that the "mesh" of tin is able to shield the bulk germanium in the case of A but only partially so in B. (By treating the specimens as ellipsoids of the respective length and diameter, allowance could be made for the demagnetizing effect and the calculations indicate, within the limits of this approximation, that specimen A shows a complete volume participation but B only 50 percent.)

The dotted lines, X, Y indicate, for comparison, the approximate limits of the transition for a sphere of pure, polycrystalline tin. The shift of the transition curves to lower temperatures on using stronger measuring fields was observed to be about the same as that for pure tin.

The investigation was carried out at the suggestion of Dr. K. Lark-Horovitz and was supported by the Signal Corps.

[1] W. W. Scanlon and K. Lark-Horovitz, Signal Corps Report, Purdue (December 1946), unpublished.
[2] L. Dowell and K. Lark-Horovitz, unpublished.
[3] This was found to be less than the amount of tin added, *viz.* from 25 to 50 percent in different specimens, the remainder presumably being lost by evaporation. The amount taken up into the lattice varied from 0.25 to 0.50 percent.
[4] V. A. Johnson, unpublished.
[5] K. Mendelssohn, Proc. Roy. Soc. **A152**, 34 (1935).

Radiofrequency Spectrum of H_2 in a Magnetic Field*

H. G. KOLSKY,† T. E. PHIPPS, JR.,‡ N. F. RAMSEY, AND H. B. SILSBEE
Lyman Laboratory of Physics, Harvard University, Cambridge, Massachusetts
June 29, 1950

THE radiofrequency spectrum of H_2 in a magnetic field has been studied with a new molecular beam apparatus of high resolution. This apparatus is similar to that used by Kellogg, Rabi, Ramsey, and Zacharias[1–3] in the original study of the r-f spectra of the hydrogen molecules. In order that much narrower resonances might be obtained, the effective length of the homogeneous field region was increased from the 13.5 cm of the original studies to 149 cm. As a result, the total length of the beam was increased from 77 cm to 269 cm. The separated oscillating field method suggested by Ramsey[4] was used to increase the sharpness of the resonances and to average out the inhomogeneities which are almost unavoidable with such a long iron magnet. The beam was detected with a Stern-Pirani detector of improved design.

Figure 1 shows graphically the difference in results between using a single r-f field along the *C*-magnet and using the two separated fields. Somewhat more than optimum r-f current was used in each case to gain greater total intensity. For the single field case this results in a broadening of the peaks, whereas in the separated oscillating field method, the peaks have approximately the same width for all r-f currents.

It was found that the end sections of the *C*-magnet, where the r-f is applied in the separated field method, did not have quite the same average value of magnetic field as did the center section.

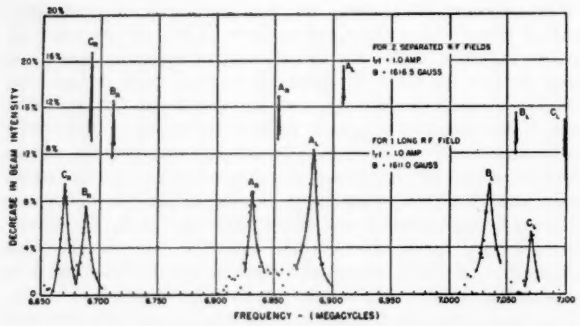

FIG. 1. Radiofrequency spectrum of ortho-H_2 for transitions with $\Delta m_J=\pm 1$ and $\Delta m_J=0$. Lower curve is with the conventional technique while the upper is with separated oscillating field method.

They were brought into agreement by passing appropriate small currents through two extra coils wrapped around the end sections of the C-magnet.

The r-f spectrum obtained with this apparatus for nuclear transitions of the first rotational state of ortho-H_2 in a magnetic field of about 1600 gauss is shown in Fig. 1. The half-widths of the sharp resonances are 0.7 kc, in contrast to the half-widths of 13 kc obtained in the previous studies of ortho-H_2. From these data the values for H′, the magnetic field at the position of the protons caused by the rotation of the molecule in its first rotational state, and H″, the field at one proton due to the magnetic moment of the other, are:

$$H'=26.74\pm 0.05 \text{ gauss},$$
$$H''=33.85\pm 0.09 \text{ gauss}.$$

This work is continuing and a more complete report will be made later.

* This work was assisted by the joint program of the ONR and AEC.
† AEC Fellow.
‡ NRC Fellow.
[1] Kellogg, Rabi, Ramsey, and Zacharias, Phys. Rev. **56**, 728 (1939).
[2] Kellogg, Rabi, Ramsey, and Zacharias, Phys. Rev. **57**, 677 (1940).
[3] N. F. Ramsey, Phys. Rev. **58**, 226 (1940).
[4] N. F. Ramsey, Phys. Rev. **76**, 996 (1949); Phys. Rev. **78**, 695 (1950).

The Zero-Point Energy of Helium

C. L. PEKERIS
Department of Applied Mathematics, Weizmann Institute, Rehovoth, Israel
June 30, 1950

THE basic problems in the behavior of helium at low temperatures are to explain (a) why of all substances helium alone remains liquid down to absolute zero, for pressures below 25 atmos.; (b) why its molar volume at 0°K of 27.6 cc is about three times greater than the volume which a classical crystal would assume under the known forces acting between helium atoms; (c) why it has an energy at 0°K of −14.2 gram calories per mole, as compared with a value of about −150 for the classical crystal. It was Simon[1] who first proposed that these are quantum-mechanical effects stemming from the large zero-point energy of helium, which compensates most of the negative potential energy, and also "blows" it up. *If* these are quantum-mechanical effects, then the first problem can be explained. It was pointed out by J. De Boer[2] that the quantum effects depend on the magnitude and range of inter-atomic forces through the parameter $\Lambda^*=h/(\sigma^2 m\epsilon)^{\frac{1}{2}}$, where m denotes the atomic mass and ϵ and σ are the parameters in the Lennard-Jones type expression for the potential $\varphi(r)$ between a pair of atoms:

$$\varphi(r)=4\epsilon[(\sigma/r)^{12}-(\sigma/r)^6]. \tag{1}$$

ϵ and σ have been determined from the second virial coefficient (and in some cases also theoretically), and De Boer finds that for He, H_2, D_2, Ne, Λ^* has the values 2.64, 1.73, 1.22 and 0.591, respectively. F. London[3] estimated the zero-point energy of helium by adopting as a model a gas of rigid spheres. Since the latter quantum-mechanical problem has been solved only for the limiting case of low densities, he had to make an extrapolation to high densities. By choosing the best-fitting value for the molecular diameter, he showed that under these approximations problems (b) and (c) can be explained. In this theory the zero-point energy is taken to be independent of the structure of the liquid.

We have determined the zero-point energy of liquid helium on the basis of the Lennard-Jones and Devonshire[4] theory of liquids. This theory is based on the assumption that in a liquid each atom is hemmed in by its immediate neighbors with whom it suffers multiple collisions, and that the migration of the atom from its cage is an infrequent event when compared with the average time it spends inside its cage. The potential of an atom within its cage is computed, in the first approximation, as a function $U(r)$ of the distance r from the center of the cage by assuming the neighbors to be situated in a crystalline lattice, and then averaging the potential over the sphere of radius r. If a denote the distance to the nearest neighbors, c the number of nearest neighbors (coordination number), then on using expression (1) for the potential between a pair of atoms, one finds that

$$U(x)=4\epsilon c[(\sigma/a)^{12}A(x)-(\sigma/a)^6 B(x)], \quad x=r/a, \tag{2}$$
$$A(x)=-1.011+(1.011+12x^3+25.2x^4+12x^6)/(1-x^2)^{10}, \tag{3}$$
$$B(x)=-1.200+(1.200+0.625x^2+0.185x^4+0.08x^6)(1-x^2)^4. \tag{4}$$

Here we have included a correction to the original expression of Lennard-Jones, introduced by De Boer and Lunbeck,[5] which takes account of the contribution from atoms which are not nearest neighbors. Lennard-Jones's theory yields values for the critical temperatures, boiling temperatures, and heats of evaporization of the heavy elements which are in good agreement with observations.

Using the experimentally determined values of $\epsilon=1.403\times 10^{-15}$ ergs, $\sigma=2.56\times 10^{-8}$ cm in (2), as quoted by De Boer[2] for helium, we have solved the Schrödinger equation for the atom in its cage and determined the proper value λ of the energy in the ground state. If N denotes Avogadro's number, then the energy E per mole at 0°K is given by

$$E=\{2N\epsilon c[1.011(\sigma/a)^{12}-1.200(\sigma/a)^6]\}+N\lambda, \tag{5}$$

where the expression in braces represents the energy of a classical crystal.

With the spherically symmetrical potential $\varphi(r)$ of (1), the atoms would crystallize into a face-centered cubic, for which $c=12$ and $a^3=\sqrt{2}\cdot V$. Figure 1 shows E, computed from (5), as a function

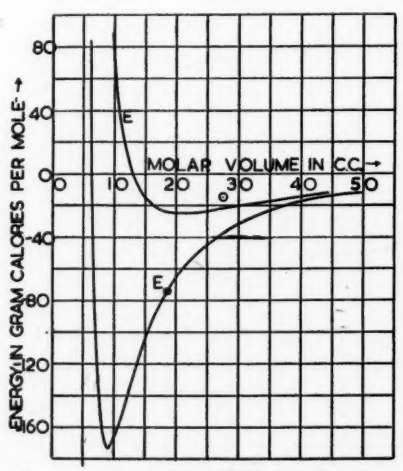

FIG. 1. Computed energy E of liquid helium as a function of the molar volume V. E_0 is the classical energy of a face centered cubic crystal (coordination number 12). ⊙ is the observed value for liquid helium.

of the molar volume V for a liquid based on this structure. The minimum E of -24.6 at $V=21$ cc, as compared with -174 and 9.2 cc respectively for the classical crystals, is in line with the effects (b) and (c), but the agreement with the observed values shown by the point ⊙ is poor. Better agreement can be secured by taking $c=10$, for which $a^3=1.39V$, as shown in Fig. 2. The shift from $c=12$ to $c=10$ was advocated by De Boer and Lunbeck,[5] who found that with such a change one can obtain better agreement with observations for the liquid molecular volumes of heavy atoms computed by the Lennard-Jones theory. Figure 3 gives the results for liquid helium based on a face-centered cubic which is only 50 percent populated. E has a minimum of about -1 calorie at about 80 cc, showing that a coordination number 6 is definitely too low. Although at the observed value of $V=27.6$, E_0 decreases with decreasing c, the quantum-mechanical effects bring about the opposite trend in the minimal values of E. Interpolating the minimal values obtained for the three coordination numbers, we find that the observed values of $E=-14.2$ and $V=27.6$ would be simultaneously achieved at about $c=9.5$.

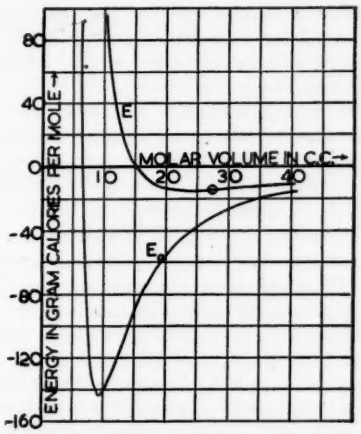

FIG. 2. Computed energy E of liquid helium as function of the molar volume V, for the case when the coordination number c is 10. E_0 is the classical energy of a crystal having a coordination number equal to 10. ⊙ is the observed value for liquid helium. At the minimum, $E=-14.7$, $V=24.0$, as against the observed values of -14.2 and 27.6.

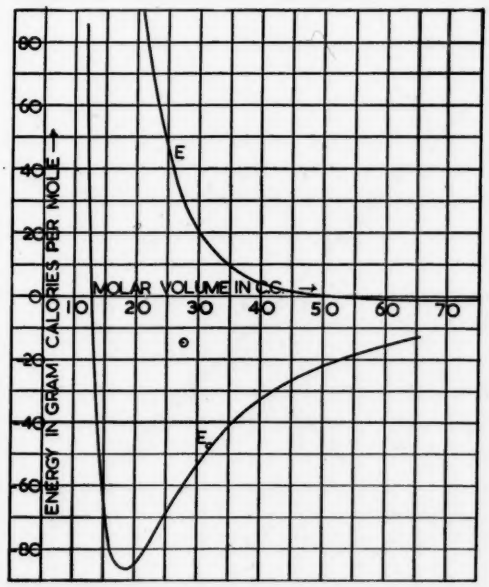

FIG. 3. Computed energy E of liquid helium as a function of the molar volume V, based on a model of a face-centered cubic which is only 50 percent populated and has a coordination number 6. E_0 is the classical energy. ⊙ is the observed value for liquid helium.

We have also computed the compressibility χ from the curvature of curve E in Fig. 2 at the minimum:

$$(1/\chi)=\rho(dp/d\rho)=V(d^2E/dV^2), \tag{6}$$

and obtained a value of 9×10^{-3} atmos.$^{-1}$. The observations go down only[6] to $T=1.25$°K, and an external mean pressure of 3 atmos., where $\chi=10\times10^{-3}$ atmos.$^{-1}$. However, extrapolation to zero external pressure indicates that χ may reach a value of 12×10^{-3} atmos.$^{-1}$. Even so, the agreement of this sensitive quantity is better than one of order of magnitude.

Further test of the theory will be afforded when the higher energy levels are determined and applied to the study of the thermodynamics (λ-point) and hydrodynamics of liquid helium. The results presented here suggest a point of attack on the now deadlocked problem of helium, namely to provide a quantum theoretical justification[7] of the scheme underlying the Lennard-Jones theory.

[1] F. Simon, Nature 133, 460, 529 (1934).
[2] J. De Boer, Physica 14, 144 (1948).
[3] F. London, Proc. Roy. Soc. A, 153, 576 (1936).
[4] J. E. Lennard-Jones and A. F. Devonshire, Proc. Roy. Soc. A, 163, 53 (1937).
[5] J. De Boer and R. J. Lunbeck, Physica 14, 522 (1948).
[6] W. H. Keesom, *Helium* (Elsevier Publishing Company, Amsterdam, 1942), p. 240.
[7] J. E. Mayer and M. G. Mayer, *Statistical Mechanics* (John Wiley and Sons, Inc., New York, 1940), p. 323.

A Ferromagnetic Curie Point in $KTaO_3$ at Very Low Temperatures

J. K. HULM, B. T. MATTHIAS,* AND E. A. LONG
Institute for the Study of Metals, University of Chicago, Chicago, Illinois
June 26, 1950

SINCE the ferroelectric Curie points discovered up to the present time all lie at temperatures above the boiling point of liquid nitrogen, and it is generally believed that at a transition point of this type there is a balance between the disordering thermal energy and the lattice dipole interaction energy, the existence of a ferroelectric Curie point at very low temperatures has hitherto seemed rather improbable. Recently, however, we have observed in potassium tantalate, $KTaO_3$, a Curie point at about 13.2°K characterized by a maximum in dielectric constant of the type shown in Fig. 1 and by the appearance of a ferroelectric hysteresis loop in the polarization-field curve as the temperature is lowered through the critical value.

The unusual dielectric properties of $KTaO_3$ at ordinary temperatures have already been reported.[1] The ferroelectric Curie point was then stated to lie in the neighborhood of room temperature, a result which was due to the presence of considerable amounts of sodium in the first crystals. In subsequent measurements (made by J. P. Remeika) on comparatively pure crystals at the Bell Telephone Laboratories, the dielectric constant at liquid nitrogen temperatures was found to follow a Curie-Weiss law with a Curie temperature between 10° and 20°K.

We therefore studied two $KTaO_3$ crystals at temperatures below 80°K; one to 12°K and the other to 1.3°K. The crystals were of about 1 mm thickness and 2 mm edge, mounted so that the electric field was applied normal to a 100 plane. Temperatures were measured with an accuracy of 0.1°K, using a helium gas thermometer and a copper-constantan thermocouple.

The dielectric constant, ϵ, of both crystals is plotted in Fig. 1. The difference in numerical values, too large to be accounted for by errors of measurement, is thought to be due to differences of internal strain. The temperature dependence of ϵ is, however, roughly the same for both crystals and is well represented between 85°K and 52°K by the Curie-Weiss law

$$\epsilon=C/(T-\theta) \tag{1}$$

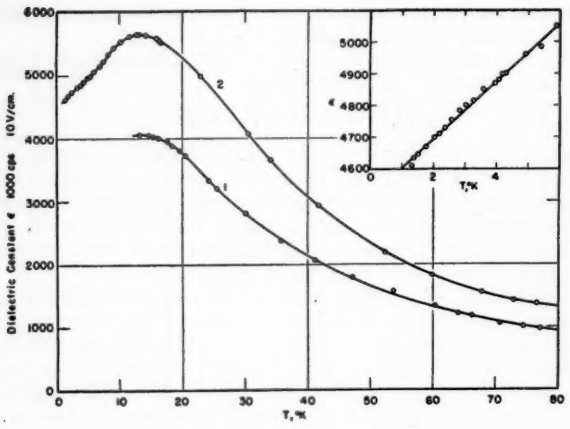

FIG. 1. Dielectric constant of $KTaO_3$ at low temperatures.

with $C=6.1\times10^4$, $\theta=14.0°K$, (No. 1), $C=8.3\times10^4$, $\theta=14.6°K$, (No. 2). Below 52°K, ϵ was smaller than is predicted by Eq. (1), and passed through a maximum at 13.2°K. At liquid helium temperature ϵ showed an almost linear decrease which continued down to 1.3°K, as shown in the inset of Fig. 1. Below 13°K the polarization-field curve exhibited a small reversible spontaneous polarization superimposed upon a high induced polarization; at the maximum field strength of the present experiment, 5000 volts/cm, the crystal was far from saturated, so that a reliable value of the spontaneous moment was not obtained.

The relatively good agreement between θ and the temperature of the maximum of ϵ demonstrates once again the validity of using the Curie-Weiss law to estimate the position of a ferroelectric Curie point. Smolenskii[2] has recently concluded from an application of this law to the dielectric constants above room temperature of calcium, strontium, and cadmium titanate that the last two substances have ferroelectric Curie points at 10° and 50°K, respectively. However, as yet unpublished measurements by Hulm ($SrTiO_3$) and Matthias ($CdTiO_3$) to 80°K gave negative values of θ, while further measurements by Hulm on $SrTiO_3$ showed that this substance is not ferroelectric above 1.3°K.

The absence of spontaneous polarization from the above mentioned titanates evidently indicates that the $Ti\text{-}O_6$ octahedra are much more sensitive to a change of lattice constant or structure than are other similar octahedra, such as $Nb\text{-}O_6$ and $Ta\text{-}O_6$, which give ferroelectric behavior in a number of different compounds and structures.[1,3]

* On leave of absence from Bell Telephone Laboratories, Murray Hill, New Jersey.

[1] B. T. Matthias, Phys. Rev. **75**, 1771 (1949).
[2] G. A. Smolenskii, Doklady Akad. Nauk S.S.S.R. **70**, 405 (1950).
[3] B. T. Matthias and J. P. Remeika, Phys. Rev. **76**, 1886 (1949).

A New Long-Lived Krypton Activity

JOHN H. REYNOLDS
Argonne National Laboratory, Chicago, Illinois
June 29, 1950

IN the course of a study of branching in the neutron induced activities of bromine,[1] I had cause to examine the isotopic constitution of the krypton distilled from a sample of sodium bromide which had been subjected to prolonged and intense neutron radiation. From this krypton all other elements except argon and xenon had been removed chemically and a slight amount of pure atmospheric krypton had been added for purposes of standardization. The gas was found to consist principally of the isotopes Kr^{80} and Kr^{82} from the reactions $Br^{79}+n\rightarrow Br^{80}\xrightarrow{\beta^-}Kr^{80}$ and $Br^{81}+n\rightarrow Br^{82}\xrightarrow{\beta^-}Kr^{82}$. In addition, a small ion peak was observed at mass 81 which, after the usual tests common to mass spectrometric technique, proved to be due to Kr^{81} and not due to an impurity element or to a rare krypton compound ion such as KrH^+. The formation of Kr^{81} is attributed to the second-order reaction $Kr^{80}+n\rightarrow Kr^{81}$. The value of the percentage abundance of Kr^{81} at the time of measurement was sufficient in itself to place a lower limit on the half-life of this nuclide of 30 days, using a value of 200 barns for the maximum neutron absorption cross section of Kr^{80}. 200 barns safely exceeds a preliminary value for this cross section due to Thode.[2]

An aliquot of this gas was introduced to the interior of an argon-ethanol filled Geiger tube. By manipulating a Toepler pump and reading a manometer, it was possible to study the counting rate as a function of the total gas pressure in the counter tube. This quantity, corrected for background, gave a linear plot which intersected the origin when extrapolated to zero pressure, showing clearly the presence of a radioactive gas in the counting system.

A larger sample of the gas was then used to fill a Pyrex cell, equipped with a 1.8 mg mica window, which could be installed within the shield of a conventional end window counting arrangement. An aluminum absorption curve of the radiations from the cell, taken with an argon-ethanol filled mica window counter, showed the presence of soft beta-particles. Although the beta-particle counting rate corrected for geometry amounted to only six percent of the total radiation as counted internally, the effect was large enough to mask the absorption characteristics of soft γ-rays in the insensitive end window arrangement.

It seemed probable that this beta-particle component was due to long-lived A^{39} formed by second-order neutron absorption on Cl^{37} impurity in the NaBr. In accordance with this hypothesis, the gas sample was treated by diluting it heavily with pure argon and pumping it briefly from a charcoal trap at dry ice temperature. Prior pumping tests with artificially prepared argon-krypton mixtures showed that under these conditions 99.8 percent of the argon is removed, while only 60 percent of the krypton (and negligible xenon) is lost. The Pyrex cell was refilled with the purified krypton and used to obtain the aluminum absorption curve shown in Fig. 1. A xenon-ethanol filled end window counter

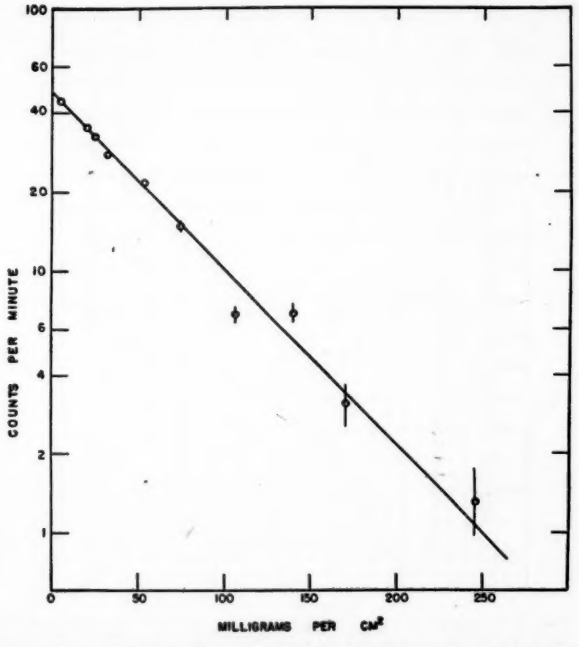

FIG. 1. Absorption in aluminum of radiations from purified krypton distilled from neutron-irradiated NaBr.

was used to increase the counting efficiency for the radiations. As may be seen from the curve, the soft beta-component is now non-detectable, confirming the assignment of this component to long-lived argon. The energy of the γ-radiation as determined from the absorption half-thickness in aluminum is 12.1 ± 0.4 kev. This is in good agreement with the accepted value of 11.9 kev for bromine K_α x-rays.

Finally, internal counting of the purified krypton showed that the radiations so counted had been reduced as a result of the purifying procedure by about 70 percent. This demonstrated that essentially all of the original *internal* counts were due to a krypton activity and not to an argon or xenon activity.

It is concluded that long-lived Kr^{81} decays by K-capture to Br^{81} with a half-life of $2.1\pm0.5\times10^5$ years. The neutron absorption cross section of Kr^{80} for the formation of the long-lived nuclide is 12.5 ± 1.5 barns.

I am grateful to Drs. Mark Inghram and Anthony Turkevich for several helpful discussions.

[1] J. H. Reynolds, Phys. Rev. **79**, 789 (1950).
[2] H. G. Thode (private communication).

Atomic Moments of Ferromagnetic Alloys

R. M. Bozorth
Bell Telephone Laboratories, Murray Hill, New Jersey
June 28, 1950

THE atomic moments of the ferromagnetic elements and their alloys with each other have been plotted against atomic number by Slater,[1] Pauling,[2] Shockley,[3] Seitz[4] and Goldman,[5] who have discussed the filling of the 3*d*-shell in relation to the magnetic moment of the atom.

Because of the rather frequent use of the curve so obtained, this note is written to show that the relation between atomic moment and atomic number is not nearly so simple as the published curves indicate, if the additional available data are used, especially the data relating to the alloys of Co and Ni with Mn, Cr and V. In Fig. 1 have been plotted all of the data which the writer has been able to find on the binary solid solutions of the elements V to Cu. The one point above the curve for Ni-Mn alloys is for well-ordered Ni_3Mn, obtained by annealing for three weeks at 470°C. All of the data were obtained by the French school.[6]

Although a rather smooth curve, corresponding to Pauling's[2] theory, is obtained for alloys between neighboring elements in the periodic table, drastic departures exist for the alloys which are two atomic numbers or more apart. Especially the Co-Mn alloys, but two numbers apart, show no indication that the moments go over a maximum at the electron concentration of 26.3 per atom as they do in the Fe-Co alloys.

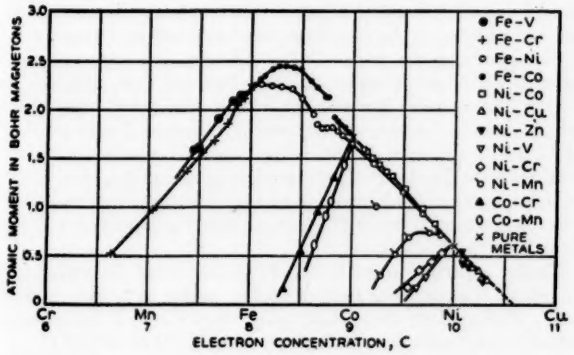

FIG. 1. Average atomic moments of binary alloys of the iron-group elements.

It is commonly believed that in manganese both $3d+$ and $3d-$ bands are partially filled to the same extent, leaving a net moment of zero, while in cobalt one band is filled. Apparently the tendency for the two partly filled bands to coexist is carried over from manganese to the Co-Mn alloys, for the additional vacancies caused by addition of manganese to cobalt would *increase* the atomic moment if only one 3*d* band remained unfilled, whereas a decrease is observed.

[1] J. C. Slater, J. App. Phys. **8**, 385 (1937).
[2] L. Pauling, Phys. Rev. **54**, 899 (1938).
[3] W. Shockley, Bell Sys. Tech. J. **18**, 645 (1939).
[4] F. Seitz, *The Physics of Metals* (McGraw-Hill Book Company, New York, 1943), p. 308.
[5] J. E. Goldman, J. App. Phys. **20**, 1131 (1949).
[6] M. Peschard, Comptes Rendus **180**, 1836 (1925); Weiss, Forrer, and Birch, Comptes Rendus **189**, 789 (1929); R. Forrer, J. de phys. et rad. **1**, 325 (1930); C. Sadron, Ann. de physique **17**, 37 (1932); M. Fallot, Ann. de physique **6**, 305 (1936); V. Marian, Ann. de physique **7**, 459 (1937); C. Guillaud, Comptes Rendus **219**, 614 (1944).

A New Determination of h/e*

C. L. Hemenway† and F. G. Dunnington
Rutgers University, New Brunswick, New Jersey
July 3, 1950

THIS letter is to present a tentative result of a determination of the ratio of Planck's constant to the charge of an electron through the measurement of an excitation potential of helium ($1s\,2p$) by a new method.

The basic part of the apparatus consists of an electron gun, a first slit system, an excitation chamber, a second slit system and a Faraday cage all located in a uniform magnetic field directed perpendicularly to the circular electron path through the slit systems. The electron gun and the first slit system are electrically insulated from the rest of the apparatus. A variable potential (ΔV potential) is applied between the first slit system and the second slit system (essentially across the small excitation chamber). Measurements of the excitation potential are made by first determining the ΔV potential (approximately zero) required to make the electrons which do not excite or otherwise interact with helium atoms traverse the second slit system and be detected, then determining the ΔV potential (approximately 21.2 volts) required to allow only those electrons which have excited the $1s\,2p$ level of helium to pass through the second slit system and be detected. The difference between these ΔV potentials constitutes a measurement of the excitation potential of helium.

The radius of the slit systems is 10 cm and measurements have been made at slit widths of 0.02 cm and at 0.03 cm. The volume of the excitation chamber in which detected excitations take place is approximately 0.02 cm³. Measurements have been made with electrons of 90, 135, and 180 volts energy.

It should be noted that the difference technique employed eliminates first-order errors due to surface charges, space charges and contact potentials. Second-order surface charge errors have been minimized by carefully cleaning the inner surfaces of the apparatus by positive ion bombardment and by evaporating a fresh coating of gold over all inner surfaces just before each series of measurements. The data taken thus far have revealed no dependence on electron energy, gas pressure, electron currents, initial ΔV potential, and time after gold plating.

Twenty successful runs have been made yielding 96 measurements. A measurement consists of about 15 to 20 observations of the ΔV voltages. The data fall into an approximate Gaussian distribution and lead to an excitation potential ($1s\,2p$) of helium of 21.2004 international volts with an observational uncertainty of ±0.0016 international volts. The value of the excitation potential was found not to depend significantly on the weighting of these data. The tentative total probable error assigned to the excitation potential is ±0.0053 international volts.

Combining the observed excitation potential with the velocity of light,[1] the ratio of the absolute volt to the international volt[2]

and the wave number[3] leads to a ratio of h/e of $(1.37902\pm0.00035)\times10^{-17}$ erg sec./e.s.u. This value of h/e, which is only a tentative value, agrees with the indirect determination of h/e, $(1.37926\pm0.00009)\times10^{-17}$ ergs sec./e.s.u., given by Dumond and Cohen.[4] The latter was obtained from a least squares solution using all determinations of atomic constants.

We shall submit for publication a full report and final value of h/e from this work after further data are taken and our standard cells have been calibrated.

* Assisted by a grant from the American Philosophical Society.
† Now at Union College, Schenectady, New York.
[1] $(2.99776\pm0.00004)\times10^{10}$ cm/sec. R. T. Birge, Reports on Progress in Physics, London VIII, 90 (1942).
[2] (1.00033 −0.00003) abs. volts/int. volts. Report of the National Research Council Committee on Physical Chemistry, Subcommittee on Fundamental Constants, July 1, 1949.
[3] 171129 ± 15 cm^{-1}, Atomic Energy Levels, Circular 467, National Bureau of Standards 1949.
[4] J. Dumond and R. Cohen, Rev. Mod. Phys. 21, 651 (1949).

Domain Structure of a Cobalt-Nickel Crystal

R. M. Bozorth and J. G. Walker
Bell Telephone Laboratories, Murray Hill, New Jersey
June 28, 1950

THE geometry of the magnetic powder patterns which have already been observed on materials of cubic symmetry, for example the iron-silicon crystals described by Williams and his colleagues,[1] is closely connected with the fact that their directions of easy magnetization are [100]. Heretofore no simple patterns have been reported on crystals, like nickel, in which the directions of easy magnetization are [111]. It seemed probable that the failure to observe patterns in such crystals was connected with the fact that their crystal anisotropy was too small (for nickel the anisotropy constant K is 60,000 as compared with 280,000 for iron containing several percent of silicon). Consequently a crystal of a cobalt-nickel alloy containing 60 percent cobalt and having an anisotropy constant of 200,000, according to Shih,[2] has been prepared by slow cooling of the melt as described by Walker, Williams, and Bozorth.[3] The surface of the crystal was cut parallel to a (011) plane so that four of the eight directions of easy magnetization were parallel to the surface, and was annealed in hydrogen and electrolytically polished. One of the patterns and its interpretation are shown in Fig. 1.

All of the theoretically expected angles between adjacent domains—180°, 109°, 71°—were observed. The geometry is shown by the diagram at the lower right-hand part of the figure. It is also noticed that the domain structure is smaller than that usually observed on iron-silicon crystals. This difference in size may be due to the more complicated pattern that may be expected in a structure having eight instead of six directions of easy magnetization and having no 90° boundaries. Also, the domain wall energy and the magnetostrictive energy are different in the Co-Ni and the Fe-Si alloys, and as a result the area of wall will be different. Since the anisotropy is less and the magnetostriction greater in the Co-Ni alloys, the state of minimum energy is to be expected when the total area of domain boundaries is greater.

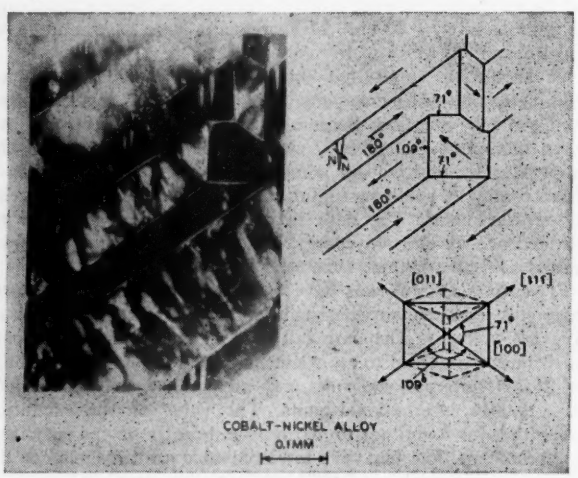

FIG. 1. Pattern on a (011) surface of a cobalt-nickel crystal, in which [111] is the direction of easy magnetization.

The effect of a magnetic field, applied parallel to the [110] direction, horizontal in the figure, is to move domain boundaries so that the vertical lines—109° boundaries—are increased in number at the expense of the 71° and 180° boundaries. The pattern is finally a series of vertical lines perpendicular to the direction of the applied field, the magnetization alternating in direction between the two [111] directions which are nearest to the applied field and which make the angle of 109° with each other.

Small "spikes" are visible in the pattern, and one is shown in the diagram at the right. These, like those observed in Fe-Si crystals on sloping surfaces and around holes and inclusions,[1] are associated with magnetic poles ("N" in the diagram) and permit magnetic flux to pass through localized areas from the material to the air.

[1] H. J. Williams, Phys. Rev. 70, 106 (1946) and subsequent brief reports; Williams, Bozorth, and Shockley, Phys. Rev. 75, 155 (1949); H. J. Williams and W. Shockley, Phys. Rev. 75, 178 (1949).
[2] J. W. Shih, Phys. Rev. 50, 376 (1936).
[3] Walker, Williams, and Bozorth, Rev. Sci. Inst. 20, 947 (1949).

The Spin of the Neutron

M. Hamermesh and E. Eisner
Argonne National Laboratory, Chicago, Illinois
June 29, 1950

THE spin value ½ for the neutron is based mainly on the ortho-para hydrogen scattering discussed by Schwinger.[1] This evidence (and other evidence from purely nuclear experiments) can be objected to on the ground that it involves nuclear theory and is not sufficiently direct. One would prefer a direct determination of the spin by means of a Stern-Gerlach experiment. However, even with the present pile intensities such an experiment would be extremely difficult. On the other hand, there is an experiment already completed and reported which does the equivalent of the Stern-Gerlach experiment for neutrons.

Hughes and Burgy[2] have studied the reflection of neutrons from magnetized iron mirrors. In such an experiment one obtains a different critical angle of total reflection for each value of the z component I_z of the neutron spin. Thus, the number of peaks in the reflection pattern is $2I+1$ (where I is the neutron spin), and the angular positions of the peaks are proportional to $(C+(e^2/mc^2)SgI_z)^{\frac{1}{2}}$ where C is the coherent scattering amplitude per iron atom, S is the uncompensated spin per iron atom, and g is the gyromagnetic ratio of the neutron. All three of these quantities are known experimentally. One can then compute the critical angles under the assumptions of spin ½ and spin ⅜. For spin ½, one obtains the curve shown in reference 2 with peaks at 14.2′, 30.7′. For spin ⅜, the $-\frac{3}{2}$ component would not exhibit total reflection, but one should see two peaks at the same angles as before, and a third peak (from the $+\frac{3}{2}$ component) at 41.3′. The rough observations of Hughes and Burgy are already sufficient to exclude the spin value ⅜.

Similar experiments with nickel mirrors would (*assuming* spin ⅜) exhibit the complete pattern of four peaks, at angles of 20.5′, 25.4′, 29.4′, 33.1′; for cobalt only the $+\frac{1}{2}$, $+\frac{3}{2}$ components undergo total reflection, giving two peaks at 23.6′ and 34.1′.

[1] J. Schwinger, Phys. Rev. 52, 1250 (1937).
[2] D. J. Hughes and M. T. Burgy, Phys. Rev. 76, 1413 (1949).

Energy Levels Associated with Se^{75}*

J. M. Cork, W. C. Rutledge, C. E. Branyan, A. E. Stoddard, and J. M. Le Blanc
University of Michigan, Ann Arbor, Michigan
June 26, 1950

THE nucleus Se^{75} was first produced and identified[1] by the bombardment of arsenic with deuterons. Since Se^{74} has a normal abundance of only 0.87 percent, neutron capture in the pile yields only a relatively weak long-lived radioactivity. A selenium specimen enriched in mass 74 to 12.1 percent was made available to us by the AEC and irradiated in the Oak Ridge pile. Spectrometric studies of this sample yield a great number of electron lines as shown in Fig. 1, whose $K-L-M$ differences are characteristic of arsenic, as expected, following positron emission or K-capture in selenium. Successive spectrograms in the figure show the energy resolution with different fixed magnetic fields.

Unpublished results by Deutsch and Osborne had evaluated five gamma-rays at 97, 122, 136, 267, and 403 kev. A subsequent study gave[2] the corresponding energies at 97, 122, 137, 265, and 400 kev. The energies of the many electron lines observed in the present investigation are shown collectively in Table I, together with their interpretations. A summary of the resultant eleven gamma-rays with arbitrarily assigned numbers in the order of increasing energy is presented in Table II.

TABLE I. Electron energies from radioactive selenium.

Electron energy	Interpretation	Energy sum	Electron energy	Interpretation	Energy sum
23.2 kev	L^1	24.7 kev	136.0 kev	M^6	136.2 kev
24.4	M^1	24.6	186.9	K^7	198.8
54.3	K^2	66.2	197.2	L^7	198.7
64.6	L^2	66.1	253.3	K^8	265.2
68.9	K^3	80.8	263.6	L^8	265.1
85.0	K^4	96.9	268.2	K^9	280.1
95.3	L^4	96.8	278.5	L^9	280.0
96.4	M^4	96.6	293.4	K^{10}	305.3
109.4	K^5	121.3	303.4	L^{10}	304.8
119.6	L^5	121.1	390.0	K^{11}	401.9
124.3	K^6	136.2	400.5	L^{11}	402.0
134.7	L^6	136.2			

TABLE II. Gamma-energies in As^{75}.

Arbitrary number	Gamma-energy	Arbitrary number	Gamma-energy
1	24.7 kev	7	198.8 kev
2	66.2	8	265.2
3	80.8	9	280.1
4	96.8	10	305.0
5	121.2	11	401.9
6	136.2		

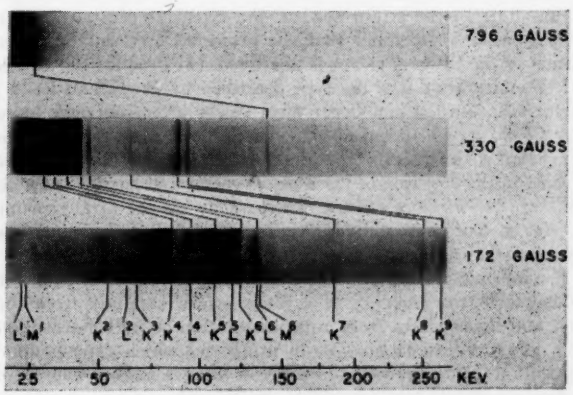

FIG. 1. Spectrograms showing the electron lines from Se^{75} with different magnetic fields.

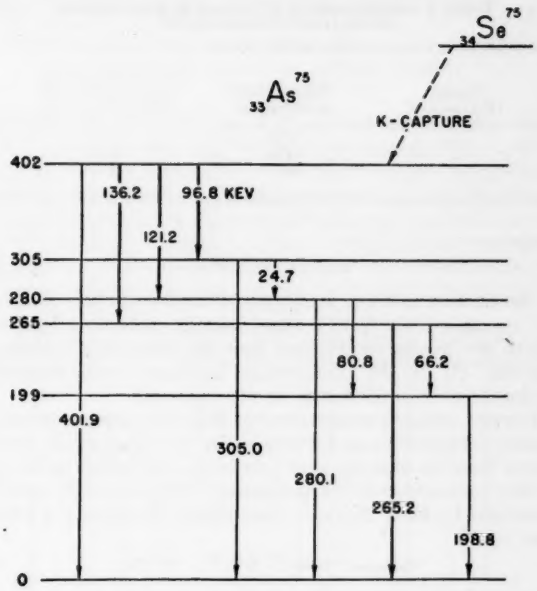

FIG. 2. Level scheme in As^{75}, following K-capture in Se^{75}.

It is now possible to construct a plan of six energy levels as shown in Fig. 2 so that all observed eleven gamma-rays arise in transitions with a remarkably satisfactory agreement.

The half-life of the present specimen appears to be 128 days. A careful search for the presence of positrons by a magnetic field and counter arrangement showed no evidence for their existence. The x-rays to be expected following K-capture in selenium were observed by noting their absorption in aluminum.

* This investigation was made possible by the joint support of the AEC and ONR.

[1] C. V. Kent and J. M. Cork, Phys. Rev. 61, 389 (1942).

[2] Jensen, Laslett, and Pratt, AECD 1836, April (1948), unpublished; see also Friedlander, Seren, and Turkel, Phys. Rev. 72, 23 (1947); and Cowart, Pool, McCown, and Woodward, Phys. Rev. 73, 1454 (1948).

Thermal Equilibrium in Neutron-Irradiated Semiconductors

J. H. Crawford, Jr. and K. Lark-Horovitz
Oak Ridge National Laboratories, Oak Ridge, Tennessee
June 29, 1950

THE conductivity *vs.* irradiation curves of Ge semiconductors exposed to fast and thermal neutron flux in the Oak Ridge pile were recently analyzed. The results indicate that the decrease in electron concentration in N-type Ge is of the order of 3 per incident fast neutron, but that the increase in hole concentration in P-type Ge is much smaller. Additional experiments show that, depending on temperature, 0.6 to 0.8 carrier is released initially per incident neutron. These results are tabulated in Table I.

Bombardment effects on N-type and P-type Ge differ, since, in the case of P-type Ge, only those bombardment-introduced acceptors which are thermally ionized can contribute to conductivity. This explanation holds whether these acceptors have identical or a wide distribution of activation energies.

In all experiments on N-type Ge carried out in the reactor and, therefore, subject to γ- and β-radiation, the maximum resistivity reached during bombardment is smaller than the predicted value, which should be even greater than that of intrinsic Ge due to the additional introduced scattering centers.

Using the mobility and equilibrium values previously reported,[1] it was concluded[2] from the expression for the minimum con-

TABLE I. Initial change in *P*-type carrier concentration during neutron bombardment.

Sample (*P*-type Ge)	Temperature of exposure	Increase in hole concentration per incident neutron
1	0°C	0.61
2	20°C	0.70
3	30°C	0.77

ductivity,

$$\sigma_{\min.}=2e\mu_e(\kappa/c)^{\frac{1}{2}} \quad (1)$$

(μ_e the electron mobility, c the ratio of electron to hole mobility, and $\kappa=n_e n_h=AT^3e^{-\epsilon/kT}$) that ionizing radiation does not disturb the thermal equilibrium, since the values of μ_e calculated from Eq. (1) at the conductivity minimum were somewhat smaller than the initial values, as was expected.

However, proper interpretation[3] of Hall effect measurements in impurity semiconductors leads to lattice mobilities which are far greater than the ones reported previously, and which agree with mobility values from drift experiments.[4] Using these new mobility values and 1.5 for c, the ratio of mobilities, the value of κ follows from

$$\sigma_{\text{intrinsic}}=n'e\mu_e'(1+1/c); \quad n'^2=\kappa \quad (2)$$

(n' is intrinsic concentration of electrons or holes and μ_e' the electronic lattice mobility.) κ is now 3.6×10^{26} at 300°K as compared with the earlier value of 3.7×10^{27}.

The revised value is considerably smaller than that formerly used, but its correctness can hardly be doubted because of the experimental data which are used for its derivation, and also, since by using these equilibrium values Johnson and Fan[5] have been able to predict correctly the temperature dependence of the energy gap in Ge. The new value is only about twice the theoretical value obtained by using the electronic rest mass $A=2^3(2\pi mk)^3/h^6$ whereas the earlier value was about 20 times larger.

The new value of κ in Eq. (1) leads in all cases to apparent mobilities at the conductivity minimum far greater than the one observed at the beginning of the experiment. Therefore, in high resistance material, measured in the pile, photo-effects due to ionizing radiations do play an important part. These increase the conductivity and must be considered in the theoretical interpretation of the "in pile" conductivity measurements on Ge.

[1] Purdue Progress Report to Signal Corps, May 1, 1948, p. 12 (unpublished).
[2] J. H. Crawford and K. Lark-Horovitz, Phys. Rev. **78**, 815 (1950).
[3] V. A. Johnson and K. Lark-Horovitz, Phys. Rev. **79**, 176, 409 (1950).
[4] Pearson, Haynes, and Shockley, Phys. Rev. **78**, 295 (1950); Purdue Progress Report to Signal Corps, March 1, 1949, p. 11.
[5] V. A. Johnson and H. Y. Fan (unpublished).

On the Formation of Dislocations from Vacancies

FREDERICK SEITZ
Physics Department, University of Illinois, Urbana, Illinois
June 30, 1950

CRYSTALS formed from the melt have the property that they contain a relatively high concentration of lattice defects when at the temperature of the melt. Existing measurements[1] indicate that NaCl and KCl have a mole fraction of about 10^{-4} of positive and negative-ion vacancies (Schottky defects). AgCl and AgBr contain[2] of the order of one percent of imperfections, which may be either interstitial silver ions and silver-ion vacancies (Frenkel defects) or Schottky defects. The latter seem to be most probable. A metal such as copper presumably possesses of the order of 10^{-3} atom percent of vacancies at the melting point, if the energy required to form a vacancy is close to the theoretical value of 1 ev calculated by Huntington.[3] The vacancies may disappear in three ways when crystals containing vacancies are cooled from the melting point: (a) By migration to the surface, an unlikely process; (b) by joining dislocations having Taylor-Orowan character; or (c) by condensing on particular lattice planes to form plates or disks, somewhat like precipitates in alloys. Once disks of this type have a sufficiently large radius, the portions of the crystal on either face of the disk will join to form a general dislocation ring. The Burgers vector associated with the dislocation ring will be determined by the vector distance through which the faces on opposite sides of the disk move in joining. When the crystal contains one atom or molecule per unit cell the dislocation ring automatically will be of the simple type in which the lattice is in registry everywhere except at the periphery of the ring if the plate of vacancies is one monolayer thick. In other cases the lattice may be in disregistry over the ring unless the disk of vacancies is several monolayers thick. The energetically most stable arrangement in the latter type of case would presumably be one in which the disk of vacancies is sufficiently thick to produce registry over most of the area, but tapers to a monolayer of vacancies near the edge, thereby forming a dislocation which is a generalization of the type Heidenreich and Shockley[4] have termed "extended." It is evident that the aggregates of vacancies will be more stable as general dislocation rings having a high degree of registry than as spheroidal or needle-like aggregates, once the aggregates become sufficiently large.

It is difficult to estimate the relative likelihood of vacancies vanishing during cooling by the possibilities (b) and (c) listed above. Probably the second possibility would be preferred if dislocations were present to the extent of 10^8 or 10^9 lines/cm^2, since they would be the best nuclei for condensation. On the other hand, it is quite possible that a carefully grown pure crystal contains very few dislocations near the melting point. Frank[5] has demonstrated very convincingly that dislocations having a component of screw character undoubtedly play an important part in crystal growth by furnishing steps at the surface for adding new layers. However, only a very small number of such dislocations (of the order of one per growing face) are required for this catalytic activity. Griffin's observations[6] on the prism faces of beryl, presumably grown from solution, also seem to show that only a relatively small density of dislocation lines is required to promote crystal growth under idealized conditions. The density appears to be as small as 10^6 lines/cm^2 in some areas of his specimens.

The writer would like to propose that the practical, realizable, lower limit to the number of dislocations found in crystals which are carefully grown from the melt is determined by the condensation of vacancies into plates to form general dislocation rings. A density of vacancies of 10^{18} per cc is sufficient to produce 4×10^8 dislocation lines/cm^2 by forming rings 2.10^{-5} cm in diameter, the density of rings being 10^{12} per cc. The general rings formed in this way appear to have all the characteristics required to explain properties of crystals which depend upon the existence of dislocations. More specifically, they can do the following things: (1) Produce all the strain needed[7] for extensive plastic flow by moving in such a manner that the projected area on the plane normal to the Burgers vector is unaltered. (2) Produce slip bands by the multiplication of the type described by Frank and Read.[8] Such multiplication can occur most easily after the rings have become elongated during normal plastic flow. (3) Promote prismatic slip[9] of the material contained within the cylinder generated by lines in the direction of the Burgers vector and passing through the ring. (4) Produce mosaic structure by proper arrangement. (5) Act as sources or sinks for vacancies in any of the numerous processes that require this property.

The foregoing proposal implies that there should be an inherent difference in the behavior of crystals grown carefully from the melt and those grown from aqueous solution or by condensation well below the melting point, in properties which depend upon dislocations. For example, it suggests that a higher degree of perfection should be attainable in crystals grown slowly at temperatures well below the melting point than in those grown from the melt. There is already considerable evidence to support

this point.[10] It also suggests that a crystal of NaCl grown carefully from aqueous solution may have mechanical properties that differ in a marked way from those of a crystal grown from the melt. In this connection it is worth noting that the silver halides, and presumably the thallous halides, have about 100 times as many imperfections as do the alkali halides at the melting point. It would be interesting to know whether crystals of the silver and thallous halides grown from the melt exhibit those properties associated with dislocations more markedly than does an alkali halide crystal prepared under almost identical conditions. It is possible that a high density of such vacancies in the thallous salts promotes the prismatic slip observed by Smakula and Klein.[9]

It is highly unlikely that vacancies are trapped in a non-equilibrium manner during slow growth from the melt. Kelting and Witt[1] have found that Ca, Sr and Ba achieve equilibrium between solid and melt when crystals are grown at the rate of 1.6×10^{-5} cm/sec. We should expect vacancies to achieve equilibrium with the melt at least as easily.

[1] C. Wagner and P. Hantelmann, J. Chem. Phys. **18**, 72 (1950); H. Kelting and H. Witt, Zeits. f. Physik **126**, 697 (1949); H. Etzel and R. J. Maurer (to be published).
[2] E. Koch and C. Wagner, Zeits. f. physik. Chemie **B38**, 295 (1938); F. Seitz, Phys. Rev. **56**, 1063 (1939); A. W. Lawson, Phys. Rev. **78**, 185 (1950); J. W. Mitchell, Phil. Mag. **40**, 249, 667 (1949).
[3] H. B. Huntington, Phys. Rev. **61**, 315 (1942).
[4] R. D. Heidenreich and W. Shockley, *Report of Bristol Conference on Strength of Solids* (Phys. Soc. London, 1947), p. 57.
[5] F. C. Frank, *Crystal Growth* (Discussions of Faraday Society, 1949), p. 48. See also paper by Frank in *Pittsburgh Symposium on Plastic Deformation of Crystalline Solids* (to be published by Naval Research Laboratory). Frank has pointed out that dislocations could be formed by precipitation of vacancies, but has not attempted to develop the idea as a practical topic. See, also, F. R. N. Nabarro, *Bristol Conference* (Phys. Soc. London, 1947), p. 75.
[6] L. J. Griffin, Phil. Mag. **41**, 196 (1950).
[7] See, for example, a paper by the writer in the *Pittsburgh Symposium* (footnote 5) and a paper by W. T. Read and W. Shockley *Imperfections in Almost Perfect Crystals* (to be published) in which these ideas are developed independently).
[8] F. C. Frank and W. T. Read, Phys. Rev. **79**, 722 (1950).
[9] A. Smakula and M. W. Klein, J. Opt. Soc. Am. **39**, 445 (1949); F. Seitz, Phys. Rev. **79**, 723 (1950).
[10] R. W. James, *Optical Principles of the Diffraction of X-rays* (Bell and Sons, Ltd., London, 1949), Chapter VI. It is to be noted that M. Renninger (Zeits. f. Krist. **89**, 344 (1934)) has observed regions that are very nearly perfect in sodium chloride grown from the melt; however, the specimens were imperfect as a whole.

The Fierz and Kopfermann-Brix Explanation of the Spectroscopic Odd-Even Isotope Shift Staggering

G. Breit
Yale University, New Haven, Connecticut*
July 3, 1950

THE writer has published a note on "The Schmidt Model and the Odd-Even Staggering of the Isotopic Shift."[1] It has since been pointed out to him that very similar and in some respects identical considerations have been published previously by Fierz[2] and independently by Kopfermann.[3] It is desired to record the fact that the credit of prior publication of the possibility of such a connection belongs to Fierz and Kopfermann. At the time of writing the note the writer was not aware of the existence of the statements by Fierz and by Brix and Kopfermann.

It may be remarked that the connection of odd-even staggering with the Schmidt model, which has been speculatively considered for some time, has become more concrete by 1950, both because of the indication of strong spin-orbit forces[4] and the existence of calculations[5] indicating that while the polarization of nuclei by electrons may be an appreciable contributor to the odd-even staggering there is nevertheless room for the existence of contributions from other causes.

* Assisted by the joint program of the ONR and AEC.
[1] G. Breit, Phys. Rev. **78**, 470 (1950).
[2] M. Fierz, Göttingen Nach. **3**, 1 (1947). This paper contains an account of a lecture to the Physical Society of Zürich, February 17, 1947.
[3] P. Brix and H. Kopfermann, Göttingen Nach., Heft **2**, 31 (1947).
[4] M. G. Mayer, Phys. Rev. **74**, 235 (1948), **75**, 1969 (1949).
[5] Breit, Arfken, and Clendenin, Phys. Rev. **78**, 390 (1950).

Disintegration of Ru^{103}

Evani Kondaiah
Nobel Institute of Physics, Stockholm, Sweden
June 30, 1950

THE 42-day activity in Ru has been assigned[1,2] to Ru^{103}. Absorption and coincidence measurements were made by Bohr *et al.*[3] and Mandeville *et al.*[4] Spectroscopic measurements were made by Hole.[5] In the present investigation metallic Ru was bombarded in the Harwell pile[6] and was chemically purified by W. Forsling. The pure and fine metallic powder was spread with a thickness of 4 mg/cm² over a 0.15 mg/cm² aluminum foil.

Three different samples have been followed for three half-lives each, giving the half-life of Ru^{103} as 39.8 ± 0.4 days.

Ru^{103} has been studied in two spectrographs[7,8] several times. One of these runs is produced in Fig. 1. The electron peaks at 17

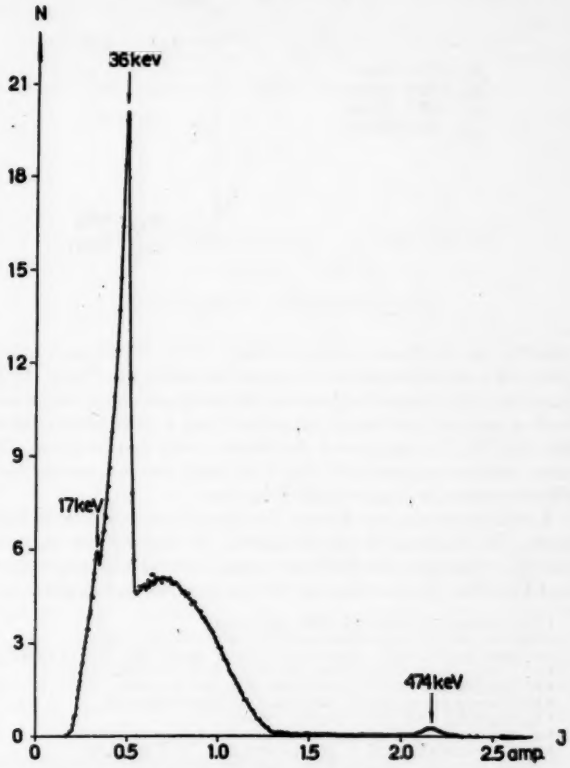

FIG. 1. Beta-ray spectrum of Ru^{103}.

and 36 kev are the K and L lines of 40-kev γ-ray and that at 474 kev is the K line of 497-kev γ-ray. The existence of the faint K line of 40-kev γ-ray emitted by the metastable level in Rh^{103}, which has not been observed before, now makes it certain that the strong β-line is an L-line and not a K-line, as has been suggested by some investigators.[9] The photo-spectrum has also been studied in the same spectrographs, which showed two photo-lines identified as the K and L lines of a 498-kev γ-ray. From the internal conversion lines and photo-lines, the energies of the two γ-rays emitted by Ru^{103} are fixed as 40.0 ± 0.5 kev and 498 ± 2 kev.

The Fermi plot of the β-spectrum shows that it is complex. The maximum energy of the hard component is found to be 698 ± 10 kev. The soft component has a maximum energy of 217 ± 4 kev. The Fermi plots of the two components seem to deviate from straight lines.

No γ-γ-coincidences could be found. The β-γ-coincidence rate as a function of the thickness of aluminum absorbers placed before the β-tube showed that the 498-kev γ-ray follows the soft β and not the harder one. β, e^- coincidences made in the spectrograph[8]

showed that the 36-kev conversion electrons, i.e. the 40-kev γ-ray, are not in coincidence with either of the two β-components. This shows that the 40-kev γ-ray is emitted by a metastable level.

From the β-spectrum, the K to $(L+M)$ conversion ratio for the 40-kev γ-ray is found to be 0.20 ± 0.04. Comparison of this value with theoretical values is postponed as the present formulas do not predict exact values for such a low energy γ-ray. In the case of the 498-kev γ-ray (N_e/N_β) is found to be about one percent. Comparing this rough value with Rose's tables[10] it is found that it is consistent with a 2^2 or perhaps 2^3 pole electric or magnetic transition.

A decay scheme, taking the observed facts into consideration, is suggested in Fig. 2. A discussion of the spin and parity assign-

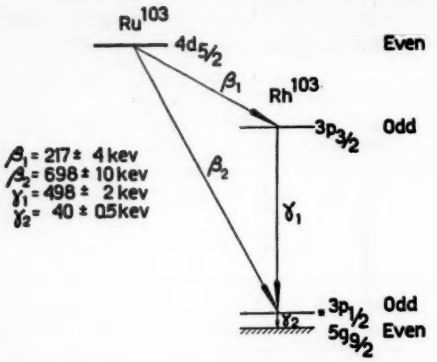

FIG. 2. Proposed decay scheme of Ru^{103}.

ments of the levels as well as the shape of the Fermi plots will be given in a detailed paper, to appear in Arkiv för Fysik. As an infinitely thin source can be obtained using an isotope separator, such a separation is being planned so that a more reliable value for (N_K/N_L) in the case of the 40-kev γ-ray can be given. The term scheme suggested in Fig. 2 is based on the nuclear shell theories given by Mayer[11] and Feenberg.[12]

I wish to convey my sincere thanks to Professor Manne Siegbahn, the director of this institute. My thanks are also due Dr. Kai Siegbahn, for constant encouragement and supervision, and Fil. Mag. W. Forsling for making the chemical purifications.

[1] J. J. Livingood, Phys. Rev. **50**, 425 (1936).
[2] Sullivan, Sleight, and Gladrow, Phys. Rev. **70**, 778 (1946).
[3] E. Bohr and N. Hole, Arkiv Mat. Astron. Fysik **32A**, No. 15 (1945).
[4] C. E. Mandeville and E. Shapiro, Phys. Rev. **77**, 439 (1950).
[5] N. Hole, Arkiv Mat. Astron. Fysik **36A**, No. 2 (1948).
[6] My thanks are due to Dr. Seligman for this irradiation.
[7] K. Siegbahn, Phil. Mag. **37**, 162 (1946).
[8] H. Slätis and K. Siegbahn, Arkiv f. Fysik **1**, No. 17 (1949).
[9] H. F. Gunlock and M. L. Pool, Phys. Rev. **74**, 1264 (1948).
[10] Rose, Goerzel, Spinard, Harr, and Strong, private communication; Phys. Rev. **76**, 184 (1949).
[11] M. G. Mayer, Phys. Rev. **78**, 16 (1950).
[12] E. Feenberg and K. C. Hammack, Phys. Rev. **75**, 1877 (1949).

Temperature Variation of the Compressibility of Molten Sodium

T. E. POCHAPSKY AND S. L. QUIMBY
Columbia University, New York, New York
June 29, 1950

A MODIFICATION of the standard pulse method for the measurement of sound velocity[1] permits the measurement of the temperature coefficient of this quantity for molten sodium with an accuracy better than one percent. Pulses of 12.2 Mc longitudinal waves of 1 μsec. duration are initiated by a quartz crystal at one end of a fused quartz bar 30 cm long. A coaxial fused quartz reflecting disk is attached by quartz rods 5 cm distant from the other end of the bar, and the two are immersed in sodium melted in a vacuum furnace. Pulses reflected from the end of the bar and from the reflector are observed on a Dumont type 256D oscilloscope. An electrical time delay between the initiation of the pulse and of the oscilloscope sweep eliminates the transit time in the quartz bar and permits the use of the expanded scale of the oscilloscope, thereby enhancing the accuracy of measurement of the sound velocity.

TABLE I. Adiabatic compressibility of molten sodium.

T°C	$\mu\times10^{12}$ cm²/dyne
97.6	16.69
100	16.71
120	16.95
140	17.19
160	17.43
180	17.68
200	17.93
220	18.19
240	18.45
260	18.71
272	18.87

The modification consists in the superposition, on the oscilloscope screen, of pulses received from the specimen upon others initiated simultaneously and transmitted in a carefully thermostated column of mercury the length of which is varied by means of a fine micrometer screw. Proper adjustment of this length annihilates the resultant pulse, and observation of the change in length required to maintain this condition affords the aforementioned accurate measure of the change in the sound velocity in the specimen.

Measurements made on singly and triply distilled sodium are indistinguishable. The velocity of sound at the melting point (97.6°C) is found to be $252{,}600\pm500$ cm/sec., and the temperature coefficient between this and 272°C, which is constant, to be -52.4 ± 0.3 cm/sec.-deg. Values of the adiabatic compressibility, μ, of the material computed with these data and those of Rinck[2] on the density of molten sodium are given in Table I.

A complete report of these experiments will be submitted for publication later.

[1] H. B. Huntington, Phys. Rev. **72**, 321 (1947).
[2] E. Rinck, Ann. Chim. Phys. **18**, 395 (1932).

Scattering of Positrons and Electrons by Nuclei*

H. J. LIPKIN AND M. G. WHITE
Palmer Physical Laboratory, Princeton University, Princeton, New Jersey
June 30, 1950

ACCORDING to relativistic quantum mechanics[1,2] there is a marked difference between the nuclear scattering of positrons and of electrons because of the manner in which spin-orbit coupling enters into the calculation. A comparison of the scattering of electrons and positrons by light and heavy nuclei is thus a check on relativistic quantum mechanics and on the spin of the positron. For small atomic number both classical and quantum-mechanical theories agree in predicting a scattering cross section which is practically independent of sign, but for $Z/137\approx1$ the calculations of various authors[2,3] show that at 57.6° a platinum foil should scatter electrons of 1.52 Mev kinetic energy nearly three times as strongly as positrons. Experimental work[4,5] thus far tends to confirm these predictions but suffers from rather large statistical errors.

An accurate experiment to check these calculations has been carried out using electrons from 300 mc of Ce^{144} and positrons from 30.0 mc of Ga^{66}. Scattering foils were 0.015 in. of polystyrene, 0.00068 in. of copper and 0.0001 in. of platinum. Source and scatterer were placed inside a solenoidal type β-spectrograph at the conjugate foci for 0.7–1.3-Mev particles. Particles scattered down the axis of the solenoid were analyzed by a second magnetic field before detection by a thin window G-M counter in order to select only the elastically scattered particles. These particles,

TABLE I. Ratio of e^-/e^+ scattering by platinum.

Kinetic energy (Mev)	e^-/e^+ exp (percent)	e^-/e^+ (unscreened theory) (percent)
0.7	3.15± 5	2.74
1.0	3.13± 4	2.90
1.3	3.60±10	2.98

having suffered a mean scattering of 57.6°, were predominantly single scattered particles. The equipment was best adapted to studying the ratio of electron to positron scattering as a function of Z and the energy. Therefore comparison with theory was made by assuming that the theoretical ratio,[6] e^-/e^+, for polystyrene of 1.08 was correct and then using this datum to normalize the apparatus. For heavy nuclei it is necessary to take into account the screening of the nucleus by the atomic electron shells. Calculations for the scattering of electrons by heavy atoms have been made by Mohr,[7] but we know of no similar calculations for positrons. For 1.0-Mev electrons on platinum one finds from Mohr's theory that the screened nucleus should scatter more strongly than the unscreened by a factor of 1.12. However, positrons will behave somewhat differently because of a tendency to remain farther from the nucleus. There may also be other differences between electrons and positrons in a screened field. Pending the working out of calculations for positrons in a screened field, we can only compare our ratio e^-/e^+ with theory using a Coulomb field. Table I shows that our results agree only approximately with unscreened calculations. Presumably the discrepancy is to be explained by neglect of screening. The experimental errors quoted are just the statistical errors caused by a limited number of counts; we assume that our equipment behaves the same for positrons and electrons.

It is a pleasure to acknowledge the help of the Oak Ridge National Laboratory in providing the Ce^{144}, and we are particularly indebted to Mr. Dean Cowie of the Department of Terrestrial Magnetism for kindly providing the Ga^{66}. We also appreciate the help of Dr. Fulbright and Dr. Goeckermann in preparing the sources. One of us (H.J.L.) is indebted to the DuPont Company and the Hercules Powder Company for fellowships early in the course of this work.

* This work was supported by the ONR and AEC.

[1] N. F. Mott, Proc. Roy. Soc. **A124**, 425 (1929).
[2] M. S. W. Massey, Proc. Roy. Soc. **A181**, 14 (1942).
[3] Bartlett and Watson, Proc. Am. Acad. **74**, 53 (1940).
[4] W. A. Fowler and J. Oppenheimer, Phys. Rev. **54**, 320 (1938).
[5] Lasich, Australian J. Sci. and Res. **A1**, 249 (1948).
[6] W. A. McKinley, Jr. and H. Feshbach, Phys. Rev. **74**, 1759 (1948).
[7] C. B. O. Mohr, Proc. Roy. Soc. **182A**, 189 (1942).

The Reaction $C^{14}(n,\gamma)C^{15}$

L. YAFFE AND W. H. STEVENS
Chemistry Branch, Atomic Energy Project, National Research Council of Canada, Chalk River, Ontario, Canada
June 26, 1950

HUDSPETH, Swann, and Heydenburg have recently reported[1] the production of C^{15} by the reaction $C^{14}(d,p)C^{15}$. They bombarded both "normal" $BaCO_3$ and $BaCO_3$ containing about 40 percent C^{14} and obtained a β-emitter from the latter with an energy of 8.8 Mev and a half-life of 2.4 seconds. This they assigned to C^{15}. Using this data they have calculated the mass of C^{15} to be at least 15.01434 a.m.u. If this transition does not go to the ground state of N^{15} the mass will then be correspondingly greater. The reaction $C^{14}(n,\gamma)C^{15}$ should accordingly take place with an energy release greater than 2 Mev.

We have attempted to prepare C^{15} by the above reaction. If there is to be no doubt as to the proper assignment of the activity, the active and inactive $BaCO_3$ must be shown to be chemically identical, since the short half-life precludes any chemical separation after the irradiation. To ensure chemical identity both the active (6 atom percent C^{14}) and inactive Na_2CO_3 were reduced to elemental carbon using the same technique and the same reagents.[2] This reduced the impurities present and guaranteed, if not purity, at least the presence of the same impurities. Both active and inactive samples of elemental carbon were bombarded with neutrons in the rapid action "rabbit" of the Chalk River NRX pile. We have been unable to detect any activity which could be ascribed to C^{15}.

Lithium was bombarded under identical conditions and the resulting Li^8 observed. This is a β-emitter with a half-life of 0.88 second and a maximum energy of 12.7 Mev. Using the value of 33 millibarns[3] for the reaction $Li^7(n,\gamma)Li^8$, we have set limits for the capture cross section of C^{14}. If the half-life of C^{15} is 2.4 seconds, then the cross section of C^{14} for thermal neutron capture must be less than 1 microbarn.

A full report of this work is being submitted to the Canadian Journal of Research.

[1] Hudspeth, Swann, and Heydenburg, Phys. Rev. **77**, 738 (1950).
[2] We are indebted to Professor W. F. Libby for a private communication of his method of reducing CO_2 to C.
[3] Hughes, Hall, Eggler, and Goldfarb, Phys. Rev. **72**, 646 (1947).

Low Energy Electrons at the End of μ-Meson Tracks

WILLIAM F. FRY
Department of Physics, Iowa State College, Ames, Iowa
July 3, 1950

ELECTRON sensitive nuclear track plates (Eastman NTB-3) were exposed to cosmic radiation in the stratosphere by means of meteorological balloons. A systematic search has been made for meson tracks which stopped in the emulsion. 158 mesons were found which fulfilled this requirement. Of these, 36 are σ-mesons, 14 are π-μ-decays, and 4 are π-μ-e-decays. The remaining 104 mesons show no associated tracks other than electron tracks. Low energy electrons (10 kev$<E<$60 kev) are observed to originate from the ends of 17 of these tracks. Figure 1 shows an example of such an event. The number of low energy electrons from mesons is in rough agreement with the results of Occhialini[1] and of Franzinetti.[2] In three cases, two low energy electrons are observed to originate from the end of the same meson track. No low energy electrons and high energy decay electrons have been observed from the end of the same track. The spectral energy histogram of 20 low energy electrons, originating from mesons, is shown in Fig. 2.

FIG. 1. Mosaic of a meson and two low energy electrons. The meson entered the emulsion from the left. The electron at the very end of the meson doubled back upon itself giving a false impression of the grain density. The electron to the right and below the meson has an energy of 45 kev.

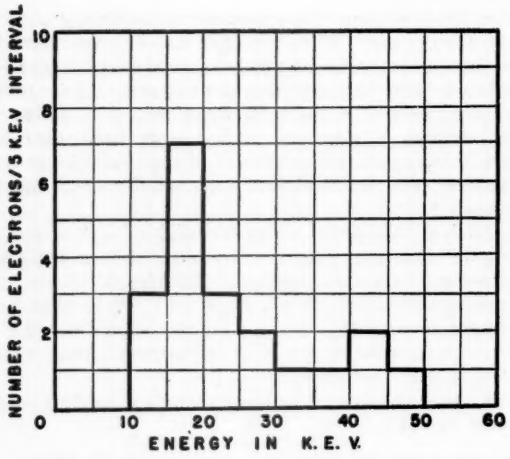

FIG. 2. Spectral energy histogram of 20 low energy electrons from mesons.

The density of random electron tracks in the emulsion has been measured. It is estimated that less than two percent of the mesons ending in the emulsion would appear to have associated electron tracks due to this background.

Assuming that the stopping power of the various constituents of the emulsion, for low energy mesons, is proportional to the atomic number, an estimate can be made of the relative number of mesons ending in gelatine and in silver bromide crystals. Assuming equal numbers of positive and negative μ-mesons,[2] 40 negative mesons are estimated to have stopped in silver bromide crystals, while 12 stopped in gelatine. If the observed electrons are due to the interaction of the meson with the orbital electrons, it seems improbable, from radiation considerations, that electrons of this energy originate from the lighter elements. The present data indicate that a negative meson, which has been captured in the field of a heavy atom, has a probability of 1/2 of having an associated electron in the 10 to 60 kev range; the probability that it have two such electrons is about 1/12.

[1] Cosynes, Dilworth, Occhialini, and Shoenberg, Proc. Phil. Soc. **62**, 801 (1949).
[2] C. Franzinetti, Phil. Mag. **41**, 86 (1950).

Restriction of Prismatic Punching to a Limited Class of Crystals

F. R. N. NABARRO
Department of Metallurgy, The University, Birmingham, England
June 30, 1950

SMAKULA and Klein[1] have observed that when a small single crystal of thallium bromoiodide is indented, mounds appear on the other surfaces at points lying in ⟨100⟩ directions from the indentation. Seitz[2] has attributed this prismatic punching to the formation of rectangular loops of dislocation, a typical loop lying in two (110) planes and two $(1\bar{1}0)$ planes, with the slip direction [001]. He has discussed the formation of such loops. Whether they arise from internal nuclei, as he suggests, or at the free surface where it meets the indenter, they can geometrically lead to the observed prismatic punching.

Why has this behavior so far been observed only in the thallium halides? It would be geometrically possible for prismatic punching to occur in aluminum, with a loop lying in two (111) planes and two $(\bar{1}11)$ planes, with the slip direction $[0\bar{1}1]$, but it has not been observed. The simplest explanation seems to be that the slip vectors ⟨100⟩ in thallium halides form an orthogonal set. It is not possible to resolve the $[001]a$ slip vector into two other permissible slip vectors, and slip must always be parallel to the axis of the prism. For aluminum the case is different. The slip vector $[0\bar{1}1]a/\sqrt{2}$ in the plane (111) may dissociate into the two permissible slip vectors $[\bar{1}01]a/\sqrt{2}$ and $[1\bar{1}0]a/\sqrt{2}$ in the same slip plane. A similar dissociation is commonly observed in the bubble model. Unless slip occurs equally in these two directions the resultant will not be parallel to the axis of the prism. A complicated system of internal strains is then set up, and propagation of glide down the prism ceases. In a homogeneously stressed single crystal, the tendency to dissociation of the slip vector is not very noticeable, because the crystal is already slipping on that glide system for which the resolved shear stress is greatest. In a polycrystal, branching of the slip bands is commonly observed near the grain boundaries. The condition for prismatic punching is that there should be no linear relation connecting the permissible slip vectors.

I am indebted to Professor Seitz for allowing me to see his letter before publication, and to Professor Cottrell for discussion.

[1] A. Smakula and M. W. Klein, J. Opt. Soc. Am. **39**, 445, 890 (1949).
[2] F. Seitz, Phys. Rev. **79**, 723 (1950).

Luminescence of Color Centers in Alkali Halides

CLIFFORD C. KLICK
Crystal Branch, Naval Research Laboratory, Washington, D. C.
June 23, 1950

WHEN alkali halides are x-rayed various color centers are formed. The one giving the strongest absorption is the F-center which is generally agreed to be an electron trapped at a vacant negative ion site. The next strongest absorption band is due to the M-center which Seitz[1] has suggested as being due to an electron trapped in a complex of two negative ion vacancies and a positive ion vacancy. Because these color centers are simple cases of impurities in solids there has been much investigation on their optical absorption and photo-conductive properties. The investigation reported here was to determine under what conditions these color centers luminesce and the effect of temperature on the luminescence emission. Gurney and Mott[2] have suggested

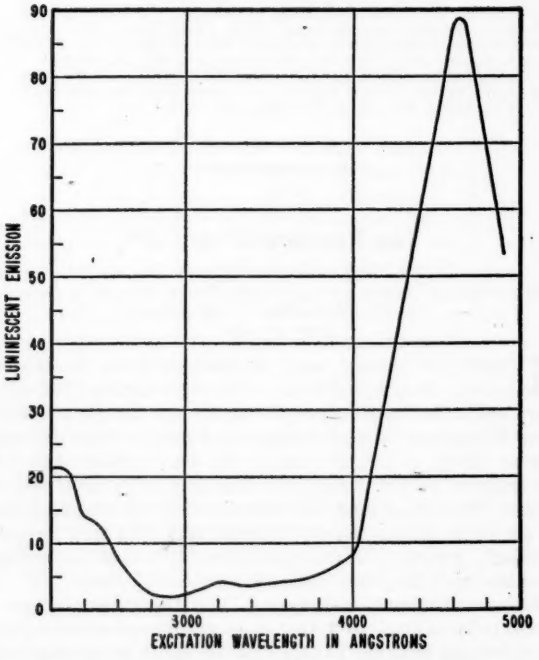

FIG. 1. Excitation spectrum of x-rayed lithium fluoride.

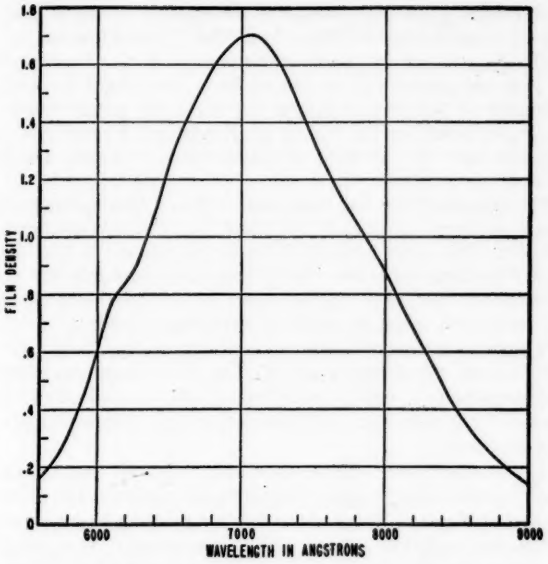

FIG. 2. Densitometer trace of luminescent emission of lithium fluoride due to excitation in the M-absorption band. Emission is at room temperature.

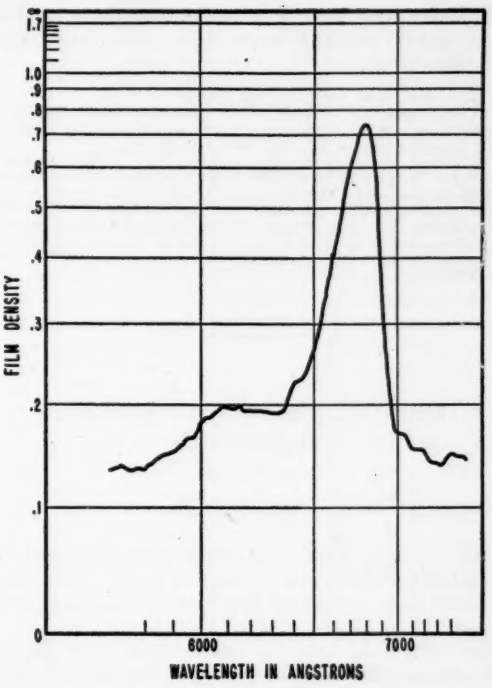

FIG. 3. Densitometer trace of luminescent emission of lithium fluoride caused by excitation in the M-absorption band. Emission is at 4°K.

that absorption in the F-band raises an electron from the ground state to an excited level and that at ordinary temperatures thermal motion raises this excited electron to the conduction band. At low temperatures the excited electron should be bound to the center and return to the ground state either with luminescent emission or by a dissipation process. Mott and Gurney[3] give arguments for believing that of these two processes luminescent emission is to be expected.

Both lithium fluoride and sodium chloride were investigated. For lithium fluoride the F-center absorption band is at 2500A and the M-band, which Molnar found to be luminescent at room temperature,[4] peaks at[5] 4600A. In order to avoid bleaching the F-band in sodium chloride, additively colored material[6] with a permanent F-band was used. The absorption peak of this band at low temperatures is at 4600A.

The luminescent output of x-rayed lithium fluoride at c.p. grade has been measured at room temperature as a function of the wave-length of the exciting light. The output, corrected to equal energy of excitation, is plotted in Fig. 1. There appear to be excitation peaks at 2200A, 2500A, 3100A, and 4600A. Only the 4600A peak gave an emission sufficiently intense so that its spectral distribution could be measured. However, information on the spectral emission of the other peaks was obtained by measuring the excitation spectrum with a variety of filters placed between the luminescent powder and the recording photo-tube. These measurements showed that the relative heights of the 2500A, 3100A, and 4600A peaks are reasonably constant, indicating that they all give the same emission. Excitation at 2200A gives an emission of shorter wave-length.

The large peak in excitation at 4600A coinciding with the M-band absorption indicates that this luminescence is due to M-centers. However, the excitation peak at 2500A is probably not due to F-centers since the excitation peak is quite small while the F-band absorption is always much larger than the M-band. Similarity of the emission due to excitation at 2500A and 4600A suggests that the 2500A excitation is due to some secondary effect such as the formation of M-centers by irradiation in the F-band. Molnar[4] has found this effect in other alkali halides, but if it occurs in lithium fluoride the effect is so small that absorption measurements did not detect it. Neither the 2200A excitation peak nor the 3100A peak correspond to absorption peaks found in our x-rayed material. The fact that in single crystals of lithium fluoride grown by Harshaw and Optovac excitation at 2200A produced an emission even before x-raying indicates that this band may be due to impurities.

At room temperature, then, apparently the only luminescent color center is the M-center. Its emission has been given by Molnar as a band centering at 6500A. Figure 2 gives a densitometer trace of this room temperature emission taken with I-L film upon excitation with the mercury 4358A line. The peak appears at 7050A because this film is sensitive further into the red than was that used by Molnar.

The low temperature emission of the M-centers was obtained by immersing the lithium fluoride in liquid nitrogen and liquid helium at atmospheric pressure. Figure 3 gives a densitometer trace of the M-center emission at liquid helium temperature. A second emission peak appears on the short wave-length side. The large apparent shift of the peak compared with Fig. 2 is caused by the use of film sensitive only to 7000A.

It is evident from Fig. 3 that the M-center emission does not become a line emission as absolute zero is approached. A similar inherent range of emission wave-lengths at liquid helium temperatures has been found for manganese activated zinc silicate, silver activated zinc sulfide, and for zinc tungstate. Further experiments are planned to decide between various possible explanations of this effect.

X-rayed lithium fluoride was also irradiated in its F-band (2500A) at liquid helium temperature. No luminescence was observed in the range of 4000A to 7000A. The ratio of emitted wave-lengths to exciting wave-length observable ranged from 2.8 to 1.6. To check the possibility that the F-center luminescence was close to the exciting wave-length, sodium chloride was irradiated in its F-band (4600A). No emission was detected at liquid helium temperatures with film sensitive out to 7000A. The ratio of emitted wave-length to exciting wave-length observable ranged from 1.5 to 1. Failure to find F-center luminescence in LiF at room temperature in a ratio of emitted wave-lengths to exciting wave-length ranging from 2.8 to 1 and the failure to find this luminescence at low temperatures either for LiF in the range of ratios from 2.8 to 1.6 or for NaCl in the range 1.5 to 1 forces one either to postulate that the luminescence occurred outside the

range of observation, possibly in the infra-red with a ratio of 3 or more, or that the excited F-center returns to its ground state by a radiationless transition.

[1] F. Seitz, Rev. Mod. Phys. 18, 384 (1946).
[2] R. W. Gurney and N. F. Mott, Proc. Phys. Soc. London **A49**, 32 (1937).
[3] N. F. Mott and R. W. Gurney, *Electronic Processes in Ionic Crystals* (Oxford University Press, London, 1940), p. 136, 222.
[4] J. P. Molnar, thesis, Physics Department, M.I.T. (1948), unpublished.
[5] Professor Pringsheim in a private communication has suggested that the 4600A band in lithium fluoride is not a true M-band in that it is formed at room temperatures by the rapid decay of a 6200A band produced by x-raying. Other differences are the difficulty in bleaching the 4600A band and the absence of an increase in the M-band on irradiation in the F-band.
[6] We wish to thank Mr. C. P. Glover of this laboratory for supplying this material.

Beta-Decay of Ag^{111} and Spin-Orbit Coupling in Cd^{111}

STIG JOHANSSON
Nobel Institute for Physics, Stockholm, Sweden
June 27, 1950

THE radiation of Ag^{111} has been studied by several investigators.[1] The maximum energy of the beta-rays has been determined to be 1.06±0.03 Mev.[2] No gamma-rays have been observed.

When Pd is irradiated with slow neutrons, Pd^{111} (26 min.) is formed among other isotopes. Pd^{111} gives rise to Ag^{111} (180 hr.). In this way it is possible to obtain Ag^{111} quite free from Ag^{106} (197 hr.). The half-life of a sample was followed during ~1000 hr. and was found to be 180±3 hr.

The gamma-radiation has been studied in a lens spectrometer and a 0.007-mm lead converter was used. The photo-electron spectrum is shown in Fig. 1. Two different gamma-lines can be distinguished. The first photo-line corresponds to the K photo-line of a gamma-ray of 243±2 kev. The L photo-line belonging to this gamma-ray is to some extent masked by the K photo-line of a second gamma-ray of 340±2 kev. Also, the L photo-line belonging to this second gamma-ray gives the energy 340 kev. Estimates based on the curves by Evans and Evans[3] give the intensity ratio 8:1 between the gamma-rays of energy 340 and 243 kev.

The beta-spectrum has been measured in a lens spectrometer. From the Fermi analysis it is evident that the beta-spectrum is complex. The upper limit of the main component is 1.04 Mev. As will be discussed below, the beta-spectrum probably has three components, but since the intensity of the third one is only ~1 percent it cannot be resolved in the Fermi analysis.

A gamma-gamma-coincidence measurement has been carried out. No real effect was observed. The beta-gamma-coincidence measurement gave coincidences, but to such a small extent that none of the gamma-rays could follow the main component of the beta-spectrum.

A distintegration scheme consistent with all experimental results is presented in Fig. 2. A search was made for the internal conversion line and the L photo-line corresponding to a possible gamma-ray of 340 to 243 kev with negative result. The intensity ratio between the components has been determined by means of calibrated beta- and gamma-ray counters. The calculation has been made under the assumption that the intensity ratio between the gamma-lines is 8:1.

It is known that Cd^{111m}, which can be produced for instance by a (n,n) reaction, decays to the ground level by the successive emission of two quanta of 148 and 247 kev, respectively.[4,5] The last gamma-ray is the same as the one observed[6] in the K-capture decay of In^{111}. Although there is a small discrepancy in energy, it seems probable that this excited level in the Cd^{111} nucleus is common for Ag^{111}, Cd^{111m}, and In^{111} disintegrations.

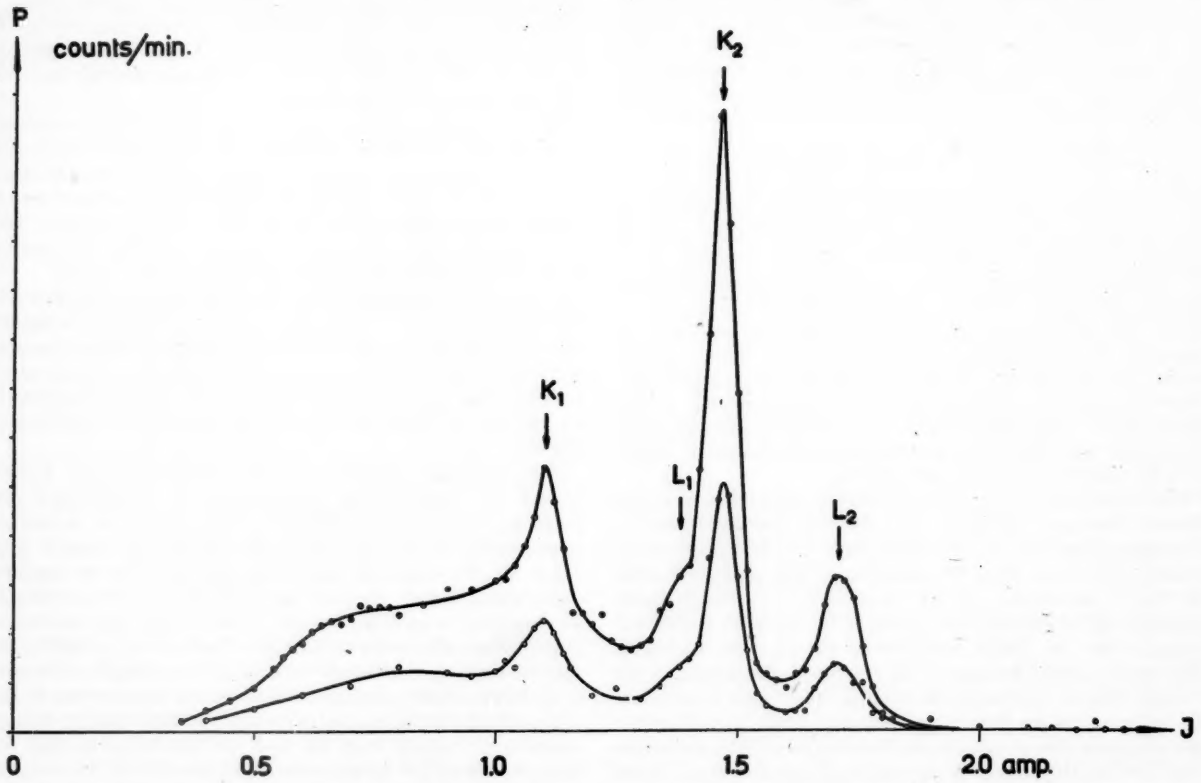

FIG. 1. Photo-electron spectrum of Ag^{111}. The lower curve taken 216 hr. later than the top curve. The half-lives for the three lines K_1, K_2, and L_2 are correct within statistical errors.

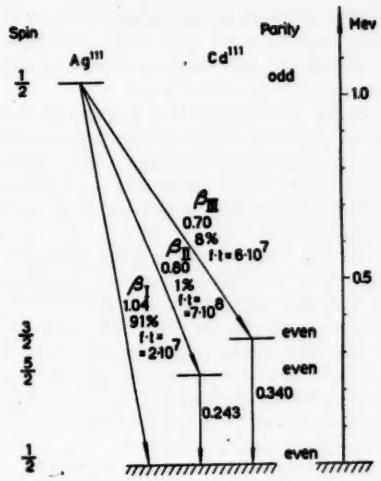

FIG. 2. Disintegration scheme of Ag^{111}.

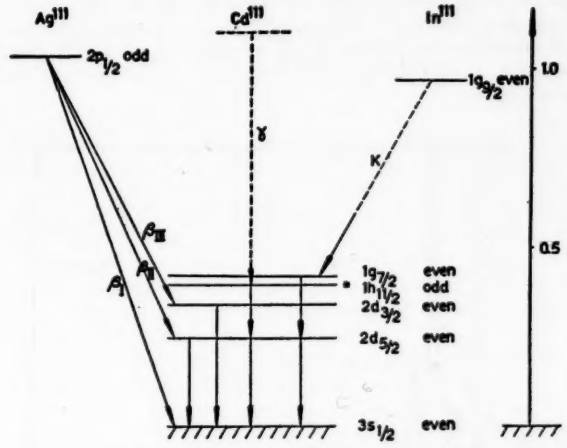

FIG. 3. Term scheme of Ag^{111}, Cd^{111m}, and In^{111}.

The spins given in Fig. 2 are based on the following arguments. The spin of Cd^{111} in the ground state is known to be 1/2. From the beta-spectrum the conversion coefficient of the 340-kev gamma-ray is determined to be ~0.015 and the conversion coefficient of the 243-kev gamma-ray is estimated to be <0.08. Using the calculated values[7] the transitions are found to be electric quadrupole or a mixture of electric quadrupole and magnetic dipole, i.e., the spins of the excited levels are 5/2 or 3/2.

The *ft*-values are given in Fig. 2. According to the rules given by Nordheim[8] the components β_I and β_{III} are first forbidden with $\Delta L=1$ and $\Delta I=0$ or 1, which would give a spin 1/2 or 3/2 for Ag^{111}. The high *ft*-value for β_{II} suggests that this can be a transition with $\Delta L=1$ and $\Delta I=2$. (In that case the beta-spectrum should differ from the allowed shape, but as the intensity is only ~1 percent it is impossible to see it from the Fermi plot.) If this is assumed, one gets the spins given in Fig. 2. From half-life measurements Deutsch and Stevenson[9] have found that the 247-kev (from In^{111}) gamma-transition ($\tau=(8\pm1)\cdot10^{-8}$ sec.) is probably electric quadrupole. This gives some support for spin 5/2 for the first excited level.

Spins and parities in the Ag^{111} disintegration scheme are in agreement with the spin-orbit coupling scheme of the nuclear shell model.[10,11] The quantum state of the ground level would then be $3s_{1/2}$, the first excited level $2d_{5/2}$ and the second $2d_{3/2}$. For Ag^{111} the spin-orbit scheme predicts spin 1/2 or 9/2 but from the *ft*-values 9/2 is impossible, leaving as the only alternative for Ag^{111} to be a $2p_{1/2}$ state, which gives $\Delta L=1$ for the beta-transitions.

In Fig. 3 a complete term scheme[5,6,12] is given for Ag^{111}, Cd^{111m}, and In^{111}. According to this scheme Cd^{111} possesses four excited levels one of which is metastable with the spin 11/2. It is interesting to note that the spin-orbit coupling scheme predicts all these low excited levels and no more for an odd neutron in the shell between the magic numbers 50 and 82.

The transition $1g_{7/2}-2d_{5/2}$ with an energy of 173 kev should be a mixture of electric quadrupole and magnetic dipole radiation. The internal conversion coefficient of this line has been measured before[2] and was found to be 0.18, which is consistent with the calculated values[7] $\alpha_2=0.17$ and $\beta_1=0.092$. The gamma-transition from the excited level should have $\Delta I=3$ and change in parity which gives electric 2^3 pole radiation. This however is not in agreement with the classification by Axel and Dancoff.[13]

Details of the investigation, also describing the chemical procedure, will be given in *Arkiv för Fysik*.

The author wishes to express his gratitude to Dr. Kai Siegbahn for many helpful discussions.

[1] For a complete list of references see G. T. Seaborg and I. Perlman, Rev. Mod. Phys. 20, 585 (1948); J. Mattauch and A. Flammersfeld, Zeits. f. Naturforschung, Isotopic Report (1949).
[2] Helmholtz, Hayward, and McGinnis, Phys. Rev. 75, 1469 (1949).
[3] R. D. Evans and R. O. Evans, Rev. Mod. Phys. 20, 305 (1948).
[4] A. C. Helmholz and C. L. McGinnis, private communication to Seaborg and Perlman (see reference 1).
[5] N. Hole, Arkiv f. Mat., Astr. o. Fys. 36A, No. 9 (1948).
[6] J. L. Lawson and J. M. Cork, Phys. Rev. 57, 982 (1940).
[7] Rose, Goertzel, Spinrad, Harr, and Strong, Phys. Rev. 76, 1883 (1949).
[8] L. W. Nordheim, Phys. Rev. 78, 294 (1950).
[9] M. Deutsch and D. T. Stevenson, Phys. Rev. 76, 184 (1949).
[10] Haxel, Jensen, and Suess, Phys. Rev. 75, 1766 (1949).
[11] M. G. Mayer, Phys. Rev. 75, 1969 (1949); 78, 16 (1950).
[12] Bradt, Gugelot, Huber, Medicus, Preiswerk, and Scherrer, Helv. Phys. Acta 19, 77 (1946).
[13] P. Axel and S. M. Dancoff, Phys. Rev. 76, 892 (1949).

The Radiations of Ce^{141} and Pa^{233}

M. S. FREEDMAN AND D. W. ENGELKEMEIR
Argonne National Laboratory, Chicago, Illinois
June 16, 1950

OUR studies of the radiations of Ce^{141} result in essential confirmation of the findings of Shepherd[1] and indicate the source of the disagreement with the results of Ter-Pogossian *et al.*[2] with respect to their reported 315 kev gamma-ray. The alleged 70 μsec. state[3] in Pr^{141} was sought in vain.

Cerium oxide samples irradiated in the Clinton and Argonne piles were purified (after the 33 hr. Ce^{143} had decayed) by fluoride and iodate precipitations, including specific separation of praseodymium activity. A Zr $(IO_3)_4$ scavenging was made to separate suspected zirconium and hafnium impurities. Uniformly spread spectrometer samples of <0.2 mg/cm² were prepared on LC-600 films (rendered conductive with Aquadag) by precipitating the fluoride in a drop of $CeCl_3$ solution on the film using hydrogen fluoride vapor.

The electron spectrum (Fig. 1) obtained in our automatic recording double lens spectrometer showed two allowed shape components (see Kurie plot, Fig. 2) with $E_0=0.581\pm0.003$ Mev and $E_0=0.442\pm0.003$ Mev although the *ft*-values (5.16×10^7 and 9.8×10^6, respectively) indicate empirically first-forbidden transitions. On the basis of both shapes being allowed the intensities are 33 percent and 67 percent, respectively.

Conversion lines at 102.9 kev and 138 kev which arise in the *K* and *L* conversion of a gamma of 145 kev were found. No conversion electrons corresponding[4] to a 137.1 gamma-ray appeared.

Photo-electron spectra with ~2 mg/cm² gold radiators revealed only *K* and *L* lines of the 145 kev gamma, whereas the photoelectron spectrum of unpurified CeO_2 showed, in addition to the 145 kev gamma, a strong 316 kev gamma and others of lower intensity. The 316 kev gamma-emitter followed zirconium during purification of the cerium. Measurement of the extraction coeffi-

TABLE I. 32 .5 day Ce^{141}; multipolarity of gamma-radiation.

Multipolarity l	Lifetime[a] (sec.)	K conv. coeff.[b] (N_ϵ/N_γ) Electric	Magnetic	K/L ratio Electric[c]	Magnetic[d]
1	1.26×10^{-16}	0.080	0.43	9.5	11.9
2	8.1×10^{-9}	0.42	2.80	4.6	8.6
3	2.34×10^{-4}	1.68		1.9	4.5
Experimental value	$<10^{-8}$	0.254[e]		5.5	

[a] P. Axel and S. M. Dancoff, Phys. Rev. 75, 892 (1949).
[b] Rose, Goertzel, Spinrad, Harr, and Strong, AECU-550 (October 18, 1949), (unpublished).
[c] M. Hebb and E. Nelson, Phys. Rev. 58, 486 (1940).
[d] I. S. Lowen and N. Tralli, Phys. Rev. 75, 529 (1949).
[e] Value from spectrometer data.

cient in di-isopropylketone indicated that it was probably Pa^{233} resulting from the neutron activation of the thorium impurity in the CeO_2, although spectroscopic analysis showed $<10^{-4}$ part of thorium. The half-life[2] of Pa^{233} is 27.4 days, quite close to our value[5] of 32.5±0.2 days, for a pure sample of Ce^{141} followed on an ionization chamber. No tailing off of the decay over seven lives is observed.

The electron spectrum of the impurity activity shows conversion lines at 288, 221, 192, 77.5, 61, and 50 kev, all but the last matching the observations of Haggstrom[6] on the Pa^{233} spectrum. The beta-continuum, however, extends beyond her reported maximum of 230 kev to ~530 kev in weak intensity, which corresponds to the total decay energy expected.[7] The identification of the impurity as Pa^{233} is thus confirmed, presumably also in the samples of Ter-Pogossian *et al.*[2]

Beta-gamma-coincidence measurement with scintillation detectors indicated an ~420 kev beta in coincidence[2,8] with ~150 kev gamma, and that the higher beta was followed by little if any gamma-ray energy. The decay scheme of Fig. 3 is thus indicated. The conversion coefficient deduced from coincidence measurements $[N(\epsilon)/N(\gamma)]$ is 0.7, in disagreement with the value from the spectrometer data of 0.254. The reason for this is not understood. With a resolving time $2T=5\times10^{-8}$ sec. using stilbene crystal detectors, delayed β-γ-coincidences were sought, and an upper limit on the gamma-emission lifetime of $<10^{-8}$ sec. was established, in agreement with the observations of Bunyan *et al.*[9]

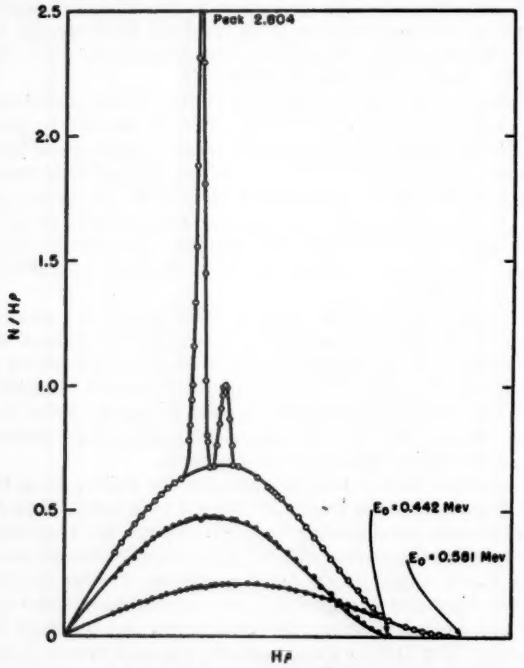

FIG. 1. Momentum spectrum of Ce^{141}.

Although there is observed an asymmetry of very low intensity in the resolving time curve for Ce^{141} it does not exhibit an exponential time dependence, and certainly cannot be ascribed to the 70 μsec. period reported by Hirzel *et al.*[3]

The data on the gamma-radiation is given in Table I. From the upper limit on the half-life of the gamma-transition one can eliminate any gamma-polarity higher than quadrupole. The spectrometer value for the K conversion coefficient is consistent with either EQ or MD radiation and the K/L conversion ratio restricts the choice to EQ.

According to the nuclear shell model proposed by Maria Mayer,[10] the predicted level assignments are as follows: For Pr^{141}, $d_{5/2}$ (the spin has been measured[11] as 5/2); for Ce^{141}, either $h_{9/2}$ or $f_{7/2}$, the former considered the more likely, and for the 145 kev level in Pr^{141}, $g_{7/2}$. The gamma-transition, if $g_{7/2}-d_{5/2}(|J-J'|=1, 2\cdots6$; no parity change), permitting electric quadrupole or magnetic dipole radiation,[12] is consistent with our observation. For the $f_{7/2}$ assignment in Ce^{141}, the low and high energy beta-transitions would be $\Delta J=0$, yes, and $\Delta J=-1$, yes, respectively, and for the $h_{9/2}$ assignment, $\Delta J=-1$, yes, and $\Delta J=-2$, yes, all leading to first-forbidden interactions[13] with either Fermi or Gamow-Teller selection rules, except the last, which requires the Gamow-Teller rules. In this case ($\Delta J=2$, yes) only, a non-linear Kurie plot is predicted, which suggests, on the basis of the short but quite linear portion of the Kurie curve of the higher energy beta (Fig. 2), that the $f_{7/2}$ assignment is correct or that G-T rules do not apply.

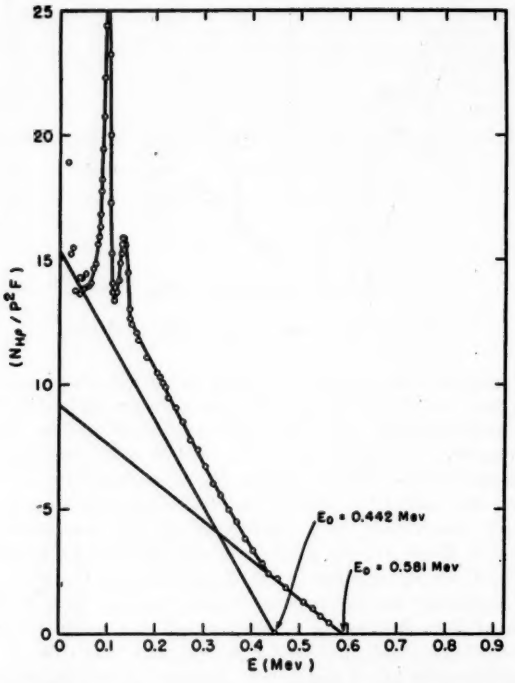

FIG. 2. Kurie plot of Ce^{141} spectrum. Relativistic Fermi function used.

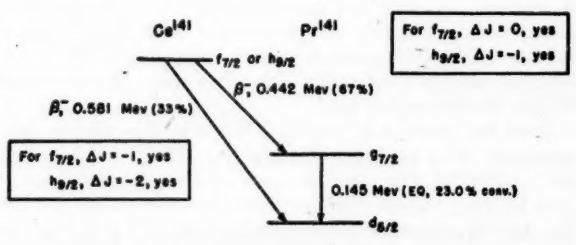

FIG. 3. Decay scheme of Ce^{141}.

We wish to thank Frank Wagner, Jr. for assistance in operating the spectrometer and Jack May for his aid in the computations. A more detailed report of this work will be submitted to this Journal.

[1] L. R. Shepherd, Research 1, 671 (1948).
[2] Ter-Pogossian, Cook, Goddard, and Robinson, Phys. Rev. 76, 909 (1949). See in particular note added in proof.
[3] Hirzel, Stolland- and Waffler, Helv. Phys. Acta 20, 241 (1947).
[4] Cork, Shreffler, and Fowler, Phys. Rev. 73, 1220 (1948).
[5] D. Walker, Proc. Phys. Soc. London 62A, 799 (1949) reports 33.11 ±0.23 days for the half-life of Ce^{141}.
[6] Edith Haggstrom, Phys. Rev. 62, 144 (1942). The line at 221 kev was not reported, but can be seen in her Fig. 5; we estimated it to be 220 kev. Also, P. W. Levy, Phys. Rev. 72, 352 (1947).
[7] A. H. Wapstra, Physica 16, 33 (1950).
[8] C. E. Mandeville and E. Shapiro, Phys. Rev. 75, 1834 (1949) report β-γ-coincidences to 90 mg/cm² of Al, about 0.33 Mev β-range.
[9] Bunyan, Lundby, and Walker, Proc. Phys. Soc. London 62A, 253 (1949).
[10] Maria G. Mayer, Phys. Rev. 78, 16 (1950) and private communication.
[11] J. E. Mack, Rev. Mod. Phys. 22, 64 (1950).
[12] S. M. Dancoff and P. Morrison, Phys. Rev. 55, 122 (1939).
[13] E. J. Konopinski, Rev. Mod. Phys. 15, 209 (1943).

Temperature Dependence of the Energy Gap in Germanium from Conductivity and Hall Data*

V. A. Johnson and H. Y. Fan
Purdue University, Lafayette, Indiana
July 5, 1950

Optical absorption experiments, measurements of the threshold of internal photoelectric effects, and consideration of crystal volume change with temperature all show that the energy gaps in silicon and germanium decrease with rising temperature.[1] The same result has been obtained by analysis of the high temperature resistivity and Hall data for silicon.[2] We describe here the calculation of the temperature dependence of the energy gap in germanium from high temperature (500°K to 850°K) conductivity and Hall data.

The free electron concentration, n_e, and hole concentration, n_h, in a semiconductor in thermal equilibrium[3] are related by

$$n_e n_h = A^2 T^3 \exp(-E_G/kT), \tag{1}$$

where E_G is the energy gap between the full and conduction bands, and

$$A^2 = 32\hbar^{-6}(m_e m_h)^{\frac{3}{2}}(\pi k)^3, \tag{2}$$

where k is the Boltzmann constant, h the Planck constant, and m_e and m_h the effective electron and hole masses. If $m_e \approx m_h \approx m_0$, the free electron mass, then $A = 4.84\times10^{15}$ cm^{-3} deg.$^{-\frac{3}{2}}$. If one writes

$$E_G = E_G^0 + (\partial E_G/\partial T)T, \tag{3}$$

then

$$(n_e n_h/T^3)^{\frac{1}{2}} = A' \exp\{-E_G^0/(2kT)\}, \tag{4}$$

where

$$A' = A \exp\{-(\partial E_G/\partial T)/(2k)\}. \tag{5}$$

The n_e and n_h values at various temperatures, high enough for impurity scattering to be negligible, were calculated from the measured conductivity (σ) and Hall coefficient (R) curves for several N-type germanium samples.[4] First, c, the ratio of electron to hole mobility, is calculated from

$$1-\frac{1}{c} = \frac{-3\pi eR(\sigma/eb_e)^2/8 - N}{(\sigma/eb_e) - N}, \tag{6}$$

where b_e is the electron mobility and N the electron density at exhaustion. In view of recent measurements[5] and calculations[6] pertaining to electron mobility in germanium, we used $b_e = 17\times10^6 T^{-\frac{3}{2}}$ cm²/volt-sec. Thus c is found to be approximately 1.5 for all samples. Then n_h is calculated from

$$n_h = \{(\sigma/eb_e) - N\}(1+1/c)^{-1}, \tag{7}$$

and n_e from $n_h + N$. When $\ln\{(n_e n_h)^{\frac{1}{2}}/T^{\frac{3}{2}}\}$ is plotted *vs.* $1/T$, a straight line is obtained for each sample (Fig. 1). The slope is essentially the same for each sample and its value determines E_G^0 as about 0.73 ev. The average of the intercepts gives $A' = 9.2\times10^{15}$ cm^{-3} deg.$^{-\frac{3}{2}}$. By use of Eq. (5), one obtains $\partial E_G/\partial T = (-1.1\pm0.1)\times10^{-4}$ ev/°K if $(m_e m_h/m_0^2)^{\frac{1}{2}} = 1$. This value compares well with the value calculated by Fan[1] by considering volume change and the thermal excitation of lattice vibrations, but is too low by a factor of 4 to agree with the optical measurements.[7] Two possibilities should be considered in connection with this discrepancy: (1) $\partial E_G/\partial T$ would have a larger negative value if $m_e m_h$ is less than m_0^2; and (2) the value of $\partial E_G/\partial T$ may be a function of temperature. However, since the R and σ data indicate that $\partial E_G/\partial T$ is constant between 500°K and 850°K, and the optical data indicate a constant value, four times larger, between 80°K and 300°K, it is not likely that one value changes to the other in the intervening temperature range; this point will be checked by extending the optical measurements to high temperatures.

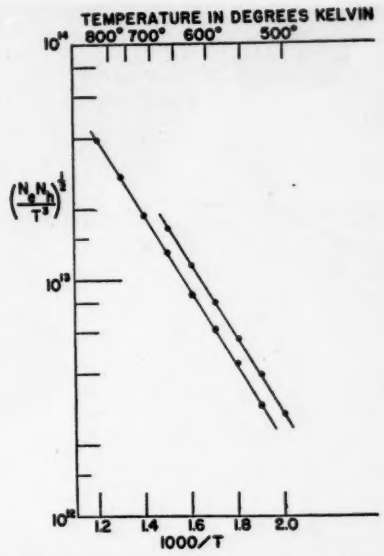

Fig. 1. Plot of $(n_e n_h/T^3)^{\frac{1}{2}}$ *vs.* $1/T$ for two of the germanium samples investigated. The n_e and n_h values are calculated from measured conductivities and Hall curves.

* Assisted by Signal Corps Contract.
[1] H. Y. Fan, Phys. Rev. 78, 808 (1950). Additional references given here.
[2] G. L. Pearson and J. Bardeen, Phys. Rev. 75, 865 (1949).
[3] A. H. Wilson, *The Theory of Metals* (Cambridge University Press, London, 1936), p. 67.
[4] Data from K. Lark-Horovitz, NDRC Report 14-585, pp. 27-33 (November 1945), unpublished.
[5] Pearson, Haynes, and Shockley, Phys. Rev. 78, 295 (1950).
[6] V. A. Johnson and K. Lark-Horovitz, Phys. Rev. 79, 409 (1950).
[7] M. Becker, private communication.

Emission of Neutral Radiation in Cosmic-Ray Stars

E. Pickup and L. Voyvodic
Division of Physics, National Research Council, Ottawa, Canada
July 12, 1950

In a search for electron pairs associated with meson showers in photographic emulsions we have so far obtained one fairly definite case of an identified electron pair associated with a 43-pronged star. We also find numerous electron pairs not obviously associated with stars,[1,2] with a fairly wide distribution in energy around several hundred Mev.

Figure 1 shows a photo-micrograph of the event, found in Ilford G5 emulsion (300μ) developed to make minimum ionization tracks particularly visible. The pair originates 120μ from the star center, inside a wide angle cone of about 15 shower particles. The electrons were identified by grain counting and multiple

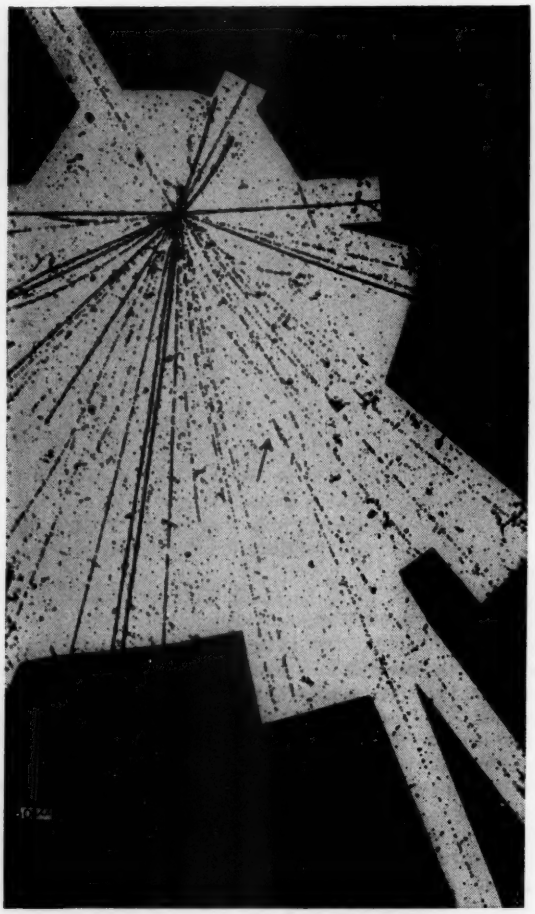

FIG. 1. Mosaic of photo-micrographs of 43-pronged star with wide angle shower. An electron pair probably associated with the star is indicated by the arrow.

scattering measurements, their energies being 65 ± 10 and 8 ± 2 Mev, giving 73 ± 12 Mev as the energy of the initiating γ-ray. The direction of the more energetic electron, when projected back, passed within one or two microns of the star center, both in the horizontal and vertical planes.

Recent Berkeley experiments[3-5] have indicated the probable emission in high energy events of a neutral meson, decaying into two photons with a very short lifetime. Kaplon *et al.*[6] have described a large cosmic star with multiple pair production inside a narrow shower cone, suggesting an explanation in terms of the emission of neutral mesons, the lifetime being $\lesssim10^{-13}$ sec.

While the present event does not in itself give direct evidence for a neutral meson, the pair is compatible with its being produced by a lower energy photon of a coincident photon pair from a neutral meson decaying somewhere in the shower cone, and within a few microns of the star center, i.e., within a time $\lesssim10^{-14}$ sec., if we assumed a fairly low energy neutral meson ($E\sim$a few times mc^2).

Assuming that approximately equal numbers of charged and neutral mesons are emitted in a shower,[6,7] that most of the charged shower particles are mesons, and that the neutral meson decays almost immediately into γ-rays with a radiation length in the emulsion, $\lambda=2.9$ cm, the probability of an electron pair starting within 120μ of the star in Fig. 1 is ~0.12. This is much greater than the chance of a random pair pointing to the star center. In a systematic search of 1.6 cm^2 of emulsion in the center of the stack of plates, 41 random electron pairs were found projected mostly into the lower hemisphere, giving a probability ~0.005 of a pair starting in any 120μ sphere. If this contained a star then the chance of a random pair pointing to the star center would, of course, be much less.

The above density of random pairs would indicate about 12.5 neutral mesons/cm^2, assuming equilibrium inside the emulsion stack (15 vertical$\times$7.5$\times$5 cm), mostly glass ($\lambda\sim12$ cm), and neglecting pair multiplication. The density of neutral mesons can also be estimated from the observed number of charged shower particles. A rough count of shower particles from stars[8] indicated about 6 charged mesons/cm^2 in the emulsion. The agreement between this value and that given above for neutral mesons would indicate that the numbers of neutral and charged mesons emitted in cosmic-ray stars are the same, at least in order of magnitude. Further data on random, and also on associated pairs should confirm this, and give more detailed information on the production of neutral mesons.

These emulsions were carried aloft through a collaborative program of cosmic-ray investigations by the Bartol Research Foundation, and the National Research Council of Canada, with the cooperation of the ONR project, "Skyhook."

[1] We find them in emulsions both at airplane and balloon altitudes.
[2] See mention of work of Bristol group in report on Edinburgh Conference, Nature **165**, 54 (1950).
[3] Bjorklund, Crandall, Moyer, and York, Phys. Rev. **77**, 213 (1950).
[4] Steinberger, Panofsky, and Steller, Phys. Rev. **78**, 802 (1950).
[5] Panofsky, Aamodt, and York, Phys. Rev. **78**, 825 (1950).
[6] Kaplon, Peters, and Bradt, Phys. Rev. **76**, 1735 (1949). Bradt, Kaplon, and Peters, Helv. Phys. Acta **23**, 24 (1950).
[7] Lewis, Oppenheimer, and Wouthuysen, Phys. Rev. **73**, 127 (1948) indicate approximately equal numbers of neutral and charged mesons for pseudoscalar theory.
[8] Star density ~6/cm^2 on these plates, flown in high altitude balloon flights. About one-sixth had showers.

Magnetic Analysis of the $B^{10}(p,\alpha)Be^7$ Reaction*

D. M. VAN PATTER, A. SPERDUTO, E. N. STRAIT, AND W. W. BUECHNER
Physics Department and Laboratory for Nuclear Science and Engineering, Massachusetts Institute of Technology, Cambridge, Massachusetts
June 19, 1950

AN excited level in Be^7 at 434 ± 5 kev was first reported by Brown *et al.*[1] from the $B^{10}(p,\alpha)Be^7$ reaction. This level was soon confirmed by other investigators,[2-6] of whom only Grosskreutz and Mather[3] reported additional levels at 205 ± 70 and 470 ± 70 kev using the $Li^7(p,n)Be^7$ reaction.

The purpose of the investigation reported here was to search for alpha-groups from the reaction $B^{10}(p,\alpha)Be^{7*}$ corresponding to the 205- and 745-kev levels reported by Grosskreutz and Mather. The alpha-particles emitted at 90° to the incident beam were analyzed by a high resolution magnetic spectrometer employing 180-degree focusing and detected by means of nuclear track emulsions. The target used for most of the work was a layer of 96 percent enriched B^{10} evaporated onto a thin film of Formvar.

In the range of energies investigated, both alpha-particles and elastically scattered protons are found, the latter being considerably more intense. While both types of particles are recorded simultaneously on the plates, they are plotted separately in Fig. 1. As shown in the top curve at 1.790-Mev bombarding energy, two alpha-groups were found, corresponding to the ground state of Be^7 and an excited state at 431 kev. The regions *A* and *B* indicate where alpha-groups would be expected if levels existed in Be^7 at 205 ± 70 and 745 ± 70 kev. In the region *B*, no alpha-group was found with an intensity greater than one percent of the ground-state alpha-group. At this bombarding energy, it was not possible to count alpha-particles in the region *A* because of the intense groups of protons elastically scattered from C^{12} and O^{16}. The spectrum of elastically scattered protons at 1.790-Mev bombarding energy is shown in the middle curve of Fig. 1, the scale of ordinates being reduced by a factor of 100 compared to the scale for the top curve. Proton groups scattered from B^{10}, C^{12}, O^{16}, and Si^{28}

were identified, in addition to a group X, scattered from an unknown contaminant of high atomic number which amounted to less than one percent of the target material.

In order to look for an alpha-group corresponding to a level in Be^7 at 205 kev, the bombarding energy was decreased to 1.600 Mev, and the results are shown in the lowest curve of Fig. 1. At region A, corresponding to a level at 205±70 kev, no alpha-group was detected with an intensity greater than 3 percent of the intensity of the ground-state alpha-group. The entire region B, corresponding to a 745-kev level in Be^7, was not surveyed because the target was destroyed before the completion of the results; however, in the region surveyed, no alpha-group was found of intensity greater than 2 percent of the ground-state alpha-group. The position of the elastically scattered proton groups is shown. No attempt was made at this lower bombarding voltage to detect the alpha-group corresponding to the 430-kev level because of the presence of protons elastically scattered from B^{10} and C^{12}.

Using fresh targets of B^{10} evaporated onto platinum, the Q-values of the two alpha-groups were determined to be 1.152±0.004 and 0.721±0.006 Mev, corresponding to the ground state of Be^7 and an excited state at 431±5 kev. After a correction of 18 kev for surface contamination was added to the Q-values measured from the B^{10} Formvar target, these values agreed with those from the fresh targets. This correction was made by a comparison of the energies of the proton groups elastically scattered from B^{10} and C^{12}. The errors given on the Q-values do not include any estimate of the effect of surface contamination; however, it is believed that this is less than the stated errors. The results are in agreement with the Q-values reported by Brown *et al.*[1] of 1.148±0.006 and 0.714±0.008 Mev. The position of the excited state of Be^7 agrees with the two most accurate published values of[1] 435±5 and[2] 429±5 kev.

The observation of the proton group elastically scattered from the B^{10} on Formvar at 1.790-Mev bombarding energy permits the estimation of the relative yields of the $B^{10}(p,\alpha)Be^7$, $B^{10}(p,\alpha)Be^{7*}$, and $B^{10}(p,p)B^{10}$ groups which were in the ratio 1.0:0.4:10. Since the $B^{10}(p,p)B^{10}$ and $B^{10}(p,\alpha)Be^{7*}$ groups occurred at the same field setting, the relative intensity of these groups is considered to be the most accurate, reliable to 30 percent. In addition, if Rutherford scattering is assumed at 90 degrees for the 1.790-Mev protons from B^{10}, it is possible to estimate the absolute differential cross sections for the $B^{10}(p,\alpha)Be^7$, $B^{10}(p,\alpha)Be^{7*}$ alpha-groups to be 4.1 and 1.8 millibarns/atom/steradian. The accuracy of the differential cross sections calculated by this method cannot be stated since the validity of assuming Rutherford scattering is not known. This assumption leads to an estimate of 4 percent of Si^{28} in the enriched B^{10} material instead of less than 2 percent, as given by the Oak Ridge analysis. This indicates that the scattering of 1.790-Mev protons at 90 degrees from boron may be at least a factor of 2 lower than predicted by Rutherford scattering.

From these results, it may be concluded that there is no indication that levels in Be^7 at 205 and 745 kev are excited by the $B^{10}(p,\alpha)Be^7$ reaction at the bombarding energies used.

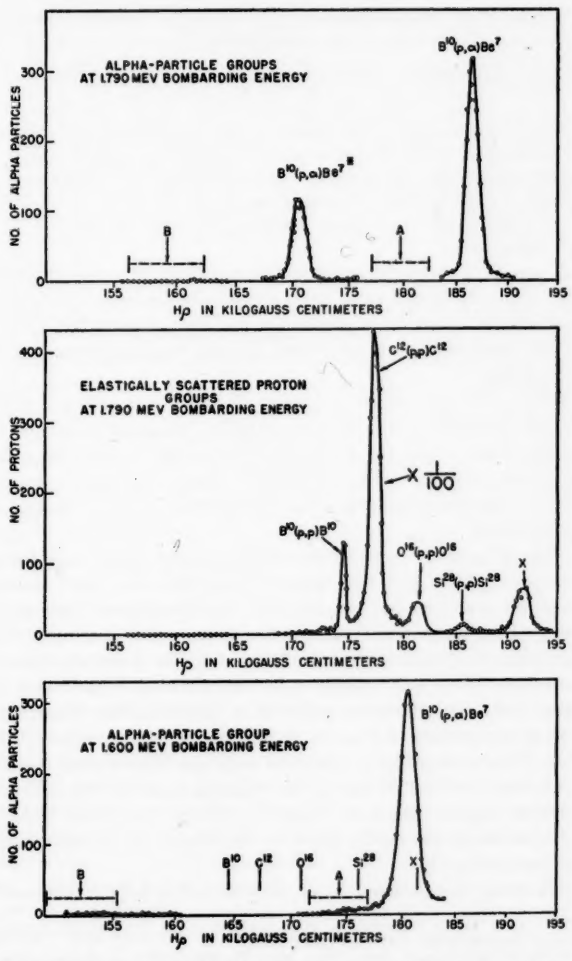

FIG. 1. Proton and alpha-particle groups from a thin target of enriched B^{10} on Formvar bombarded by protons.

* This work was assisted by the joint program of the ONR and AEC.
[1] Brown, Chao, Fowler, and Lauritsen, Phys. Rev. **78**, 88 (1950).
[2] T. Lauritsen and R. G. Thomas, Phys. Rev. **78**, 88 (1950).
[3] J. C. Grosskreutz and K. B. Mather, Phys. Rev. **77**, 580 (1950).
[4] Johnson, Laubenstein, and Richards, Phys. Rev. **77**, 413 (1950).
[5] B. Hamermesh and V. Hummel, Phys. Rev. **78**, 73 (1950).
[6] Freier, Rosen, and Stratton, Phys. Rev. **79**, 239 (1950).

Radiations of Krypton[85]

H. ZELDES, B. H. KETELLE, AND A. R. BROSI
*Chemistry Division, Oak Ridge National Laboratory, Oak Ridge, Tennessee**
July 12, 1950

A LONG-LIVED krypton activity was found among the products of uranium fission by Hoagland and Sugarman.[1] From aluminum absorption measurements they concluded that this krypton emitted beta-radiation with a maximum energy of 0.74 Mev and no gamma-radiation. Later Thode[2] using mass spectrometer measurements assigned this krypton to mass 85 and gave 9.4 yr. as the half-life.

In the course of work in which gaseous activities were separated by elution with helium from a charcoal column, gamma-radiation was found associated with the long-lived krypton activity after extensive purification. A more detailed study of the beta- and gamma-radiations of Kr^{85} was therefore made and is reported below.

In measurements of beta-spectra of gaseous activities a major problem is the source container which should have a low mass in order to reduce distortion of the spectra from absorbed and scattered radiation. In this work the gas was contained in a 6-mm diameter bulb with a thickness of 0.7 mg/cm² which was blown on the end of a quartz capillary tube 0.8 mm o.d. and 0.4 mm i.d. Experimental data obtained with gaseous activities contained in this bulb indicated that there was very little distortion of beta-spectra at energies above 150 kev.

The experimental beta-energy distribution of Kr^{85} obtained with a thin lens spectrometer is shown in Fig. 1 as a Kurie plot for an allowed transition. Because of the curvature shown in Fig. 1, the data have been replotted in Fig. 2 on the assumption that the transition is first forbidden with a spin change of two and a parity change. The fact that Fig. 2 is a straight line indicates the validity of the above assumption, which is consistent with the Mayer[3] theory of nuclear shell structure. Extrapolation of the

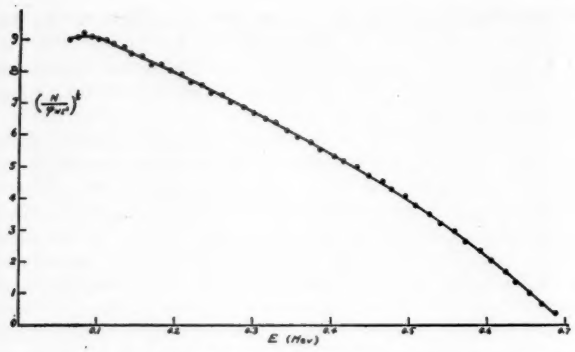

FIG. 1. Allowed Kurie plot of Kr^{85} beta-spectrum.

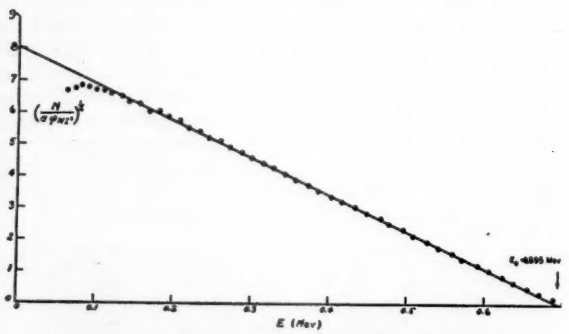

FIG. 2. Kr^{85} beta-spectrum plotted as a first-forbidden transition with $\Delta J = 2$.

straight line yields a maximum energy for the beta-transition of 0.695±0.005 Mev. The value of log (*ft*) is 9 which is in agreement with *ft*-values computed by Nordheim[4] for other first-forbidden transitions with a spin change of two.

Scintillation spectrometer and lead absorption measurements of the gamma-radiation of long-lived fission krypton both indicate that the energy is 0.54±0.02 Mev. Coincidence absorption data show that the gamma-ray is in coincidence with a 0.15±0.02 Mev maximum energy beta-ray. Since extensive purification precludes the presence of another element and since the sum of the energies of the coincident beta- and gamma-rays is the same within experimental error as the energy of the more abundant beta-group of Kr^{85}, these radiations are almost certainly associated with Kr^{85}.

The branching ratio in the decay of Kr^{85} was calculated from the coincidence data and the calibrated detection efficiency of the coincidence gamma-counter. It was found that Kr^{85} decays by emission of a 0.15-Mev beta-ray in coincidence with a 0.54-Mev gamma-ray in 0.65±0.15 percent of the disintegrations.

We would like to thank G. W. Parker for the sample of fission product gases used in this work.

* This document is based on work performed for the Atomic Energy Project at Oak Ridge National Laboratory.

[1] E. J. Hoagland and N. Sugarman, NNES-PPR, Vol. 9B, Paper No. 7.6.1 (January, 1945), unpublished.
[2] H. G. Thode, CR-PRG-37 (November, 1946), unpublished.
[3] M. G. Mayer, Phys. Rev. **78**, 16 (1950).
[4] L. W. Nordheim, Phys. Rev. **78**, 294 (1950).

Argon^{39} Beta-Spectrum

A. R. BROSI, H. ZELDES, AND B. H. KETELLE
*Chemistry Division, Oak Ridge National Laboratory, Oak Ridge, Tennessee**
July 12, 1950

A LONG-LIVED gaseous activity has been removed from several different potassium salts after bombardments in nuclear reactors. Reaction with calcium vapor has shown that the radiations are from a rare gas isotope. This activity is eluted from a charcoal column by helium in the same way as A^{41}. Since the noble gases are readily separated by this procedure the activity is associated with an isotope of argon. This new long-lived argon isotope is presumably A^{39} formed by an (n, p) reaction on K^{39}. An attempt to find the 4-min. activity previously assigned to A^{39} was unsuccessful.

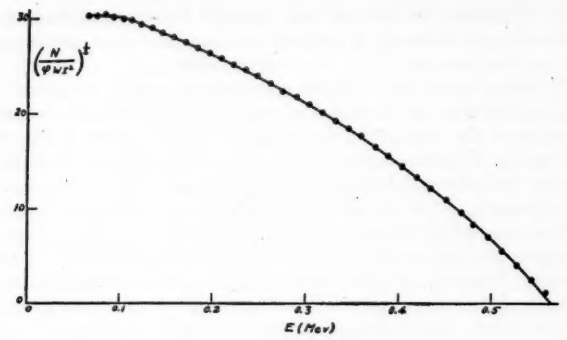

FIG. 1. Allowed Kurie plot of A^{39} beta-spectrum.

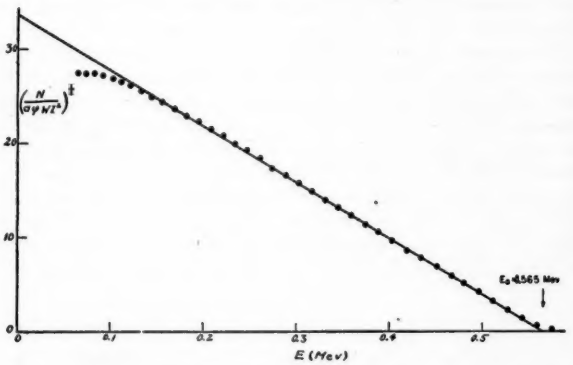

FIG. 2. A^{39} beta-spectrum plotted as a first-forbidden transition with $\Delta J = 2$.

A sample of long-lived argon has been counted in a proportional counter for about one year. Since no definite decrease in activity was observed, it is concluded that the half-life is longer than 15 yr. Further work is being done to establish the mass assignment and the half-life.

When a 0.1-mc source of long-lived argon was counted with enough absorber to remove beta-radiation, no gamma-rays with energies higher than the secondary radiation were detected with a thallium activated NaI scintillation counter. This indicates less than 0.1 percent branching with gamma-radiation more energetic than 300 kev.

The beta-energy distribution of long-lived argon has been measured with a thin lens spectrometer using the same source container that was used in the Kr^{85} measurements.[1] The beta-energy distribution of A^{39} was also found to be that of a forbidden transition. Kurie plots for an allowed and for a first-forbidden transition with a spin change of two are shown in Figs. 1 and 2, respectively. On the assumption of a first-forbidden transition with a spin change of two the maximum energy is 0.565±0.005 Mev. This assumption is consistent with the Mayer[2] shell theory of nuclear structure. Since only a minimum value for the half-life is known, only a minimum value of log(*ft*) can be given. This is 8.7 which is in the region given by Nordheim[3] for transitions of the type assumed.

We would like to thank T. W. DeWitt for his help in this work.

* This document is based on work performed for the Atomic Energy Project at Oak Ridge National Laboratory.

[1] Zeldes, Ketelle, and Brosi, Phys. Rev. **79**, 901 (1950), preceding letter.
[2] M. G. Mayer, Phys. Rev. **78**, 16 (1950).
[3] L. W. Nordheim, Phys. Rev. **78**, 294 (1950).

The Nature of Trapped Hole Color Centers in the Alkali Halides*

E. BURSTEIN AND J. J. OBERLY
Crystal Branch, Metallurgy Division, Naval Research Laboratory, Washington, D. C.
July 11, 1950

THE ultraviolet bands (V-bands) formed in KCl by x-irradiation and in KBr and KI by additive coloration have been attributed by Seitz[1] to centers in which a hole is trapped at a positive ion vacancy. Alexander and Schneider[2] suggest further that bleaching the V-band in KCl, by irradiation in the band, frees the holes which are assumed to have a low mobility. The slow restoration of the band is then attributed to the slow diffusion of the positive ion vacancies to the free but relatively immobile holes which are then retrapped. The recent observation of other ultraviolet bands when KCl and KBr are x-irradiated at low temperatures[3] and the existence of more than one room temperature band indicate, however, that more than one type of trapped hole centers (hereafter called H-centers) are involved. Data obtained at this laboratory on color center formation in KCl, KBr, and KI under various conditions (Fig. 1) have revealed still other bands. It is the purpose of this note to present some suggestions concerning the nature of the centers responsible for the various ultraviolet bands which may account more adequately for the experimental data.

By analogy with the formation of trapped electron centers (hereafter called E-centers) one may in general expect various H-centers to be formed in which one or more holes are trapped at a single positive ion vacancy or at an aggregate of vacancies.[4] Such centers, if they exist, may be expected further to exhibit optical and photo-conductive properties similar to those of the corresponding E-centers.[5] Holes may also be "self-trapped." In addition, two holes may combine to form a halogen molecule (X_2-center) in which a pair of neutral halogen atoms are held together by a covalent bond. In forming an X_2-center the two holes effectively vanish and the optical properties of the center are determined rather by the two electrons which make up the covalent bond. The trapped electron analog of this center, a diatomic alkali molecule, probably also exists under appropriate conditions.

The analogy between E- and H-centers may break down in some cases. For example, the energy of formation of halogen molecules may be sufficiently large, even in the crystal, that the trapping of two holes at a positive ion vacancy will yield an X_2-center having a neighboring positive ion vacancy rather than an F' type of center. It is also possible that an X_2-center having two neighboring positive ion vacancies will be formed when two holes are trapped at a pair of positive ion vacancies. In both cases the vacancies play only an auxiliary role and, depending on the temperature, may or may not remain attached by Coulomb attraction to the X_2-center. X_2-centers which do not have neighboring positive ion vacancies will, at appropriate temperatures, tend to combine with them to form X_2-centers having one or two positive ion vacancies as neighbors.

The numerical distribution of the various H-centers at any given temperature will be considerably different from that of the corresponding E-centers as a result of the very large differences between the rates of thermal diffusion of positive and negative ion vacancies and between those of single holes trapped at single positive ion vacancies (hereafter called G-centers) and single electrons trapped at negative ion vacancies (F-centers). In general only the positive ion vacancies show appreciable thermal diffusion at room temperature. The G-centers, whose activation energy of diffusion will be roughly that of the positive ion vacancy, may also be expected to be mobile at room temperature, whereas F-centers are probably immobile. As a result of the migration of G-centers and positive ion vacancies at room temperature the G-centers will tend to combine with one another and with positive ion vacancies to form such centers as single holes trapped at a pair of positive ion vacancies, X_2-centers, and larger aggregates. The G-centers will also combine with various E-centers which may be present to produce permanent bleaching. This recombination of trapped holes and electrons is largely responsible for the low yields in KBr and still lower yields in KI obtained by room temperature x-irradiation, and also plays an important role in the thermal luminescence of x-irradiated alkali halides. The equilibrium distribution of the various E- and H-centers formed by x-irradiation will depend on a number of factors: the temperature, the number of holes and electrons that are formed, the number of positive and negative ion vacancies, the activation energies for diffusion of the various centers and of the positive

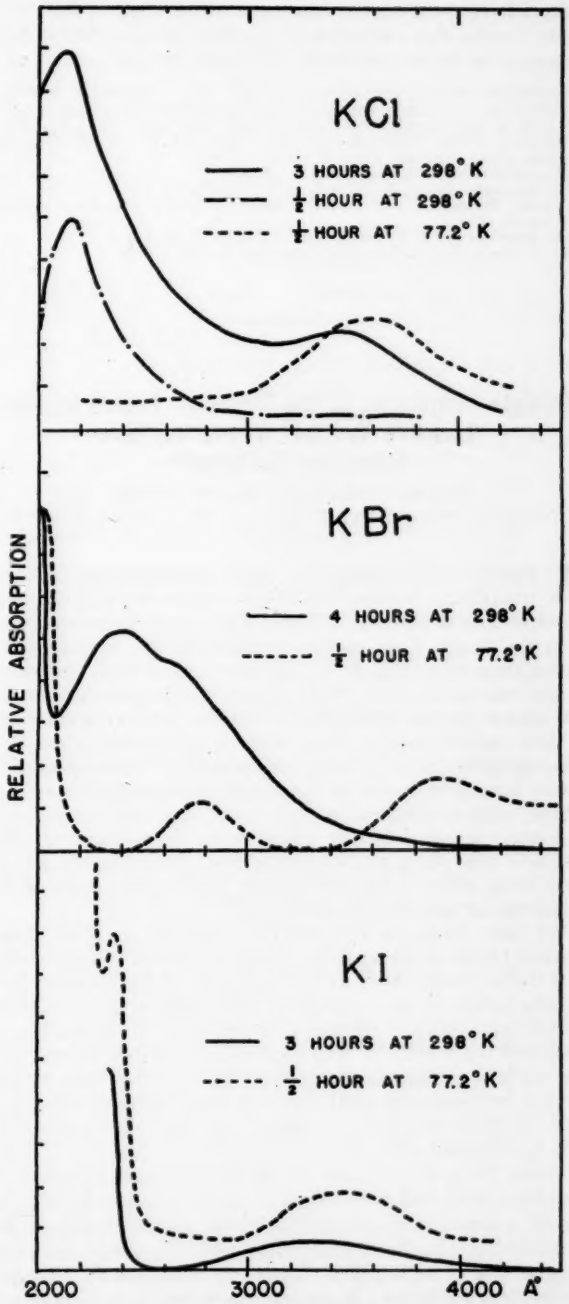

FIG. 1. Absorption bands formed in KCl, KBr, and KI by x-irradiation at room and liquid nitrogen temperatures. The bands at 2000A in KBr and at 2300A in KI have not been previously reported. A corresponding band is probably also formed at the absorption edge in KCl.

and negative ion vacancies, and the energy of formation of the various aggregates.

On the basis of these considerations, it seems probable that the room temperature V-bands reported by Alexander and Schneider[2] for KCl and KBr are due to halogen molecule centers and other aggregates of holes and vacancies rather than to single holes trapped at a single positive ion vacancy. In particular the 2200A band in KCl and the 2300A band in KBr which do not bleach when the F-center is irradiated are probably due to halogen molecule centers with two positive vacancies. Bleaching these centers by irradiation in the band probably involves either the thermal decomposition of the excited center into two G-centers or the splitting away of the positive ion vacancies from the halogen molecule. The slow restoration of the center is then due either to the slow migration of G-centers, or of positive ion vacancies and halogen molecules, and recombination.

* Published with the permission of the U. S. Navy Department without endorsements of statements or opinions of the writers. The authors are on the staff of the Crystal Branch, Metallurgy Division, Naval Research Laboratory, ONR, Washington, D. C. Presented at the Washington Meeting of the American Physical Society, 1950.

[1] F. Seitz, Rev. Mod. Phys. **18**, 384 (1946).
[2] J. Alexander and E. E. Schneider, Nature **164**, 653 (1949).
[3] Casler, Pringsheim- and Yuster, Quarterly Report of Argonne National Laboratory (1949).
[4] E. Burstein and J. J. Oberly, Phys. Rev. **76**, 1254 (1949).
[5] J. J. Oberly and E. Burstein, Phys. Rev. **79**, 217 (1950).

Multiple Scattering of the Particles Producing the "Positive Tracks" Appearing near Beta-Ray Emitters*

GERHART GROETZINGER AND FRED L. RIBE
Institute for Nuclear Studies, University of Chicago, Chicago, Illinois
June 29, 1950

A SERIES of investigators[1-5] have observed cloud-chamber tracks in the neighborhood of beta-ray emitters of curvatures corresponding to positively charged light particles moving away from the source. From energy considerations the particles producing these tracks cannot be positrons resulting from the decay of the beta-ray emitters. While most of the investigators are of the opinion that the cloud-chamber evidence favors the existence of these positive particles (they could not be observed in beta-ray spectrographs), in some recent investigations[6-8] the "positive" tracks have been attributed (1) to electrons emerging from the source, multiply scattered in such a way that their tracks have curvatures opposite to that which would be produced by the magnetic field alone, and (2) to electrons re-entering the source after being either reflected from the walls of the chamber or traversing an (unobserved) full circle.

We have compared the multiple scattering of 20 of these positive tracks emerging from various P^{32} source[9] arrangements with that of about 100 electrons in a mixture of 2 parts argon and 3 parts helium at one atmosphere total pressure in a magnetic field of approximately 340 gauss. The minimum track length was 7 cm and the average in both groups approximately 10 cm. Use was made of a method recently described[10] in which from deflections ω_i between subsequent chords of equal length connecting a series of points of a track an estimate for the momentum and a root-mean-square angle of scattering $[(\omega^2)_{Av}]^{\frac{1}{2}}$ (see Eq. (23) of reference 10) is derived. Due to the shorter minimum length of the tracks which had to be chosen in this investigation in order to include a larger number of positive tracks, a chord length of one centimeter only had to be used for the sake of improved statistics. In a section of such a short length the condition for multiple scattering is not fulfilled in our mixture of helium and argon for the higher momenta considered by us. For the sake of better statistics tracks in the momentum range between 1500 and 2000 gauss-cm were also included, although for such low momenta the

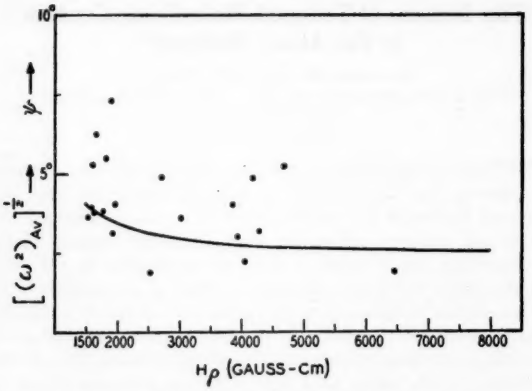

FIG. 1. Dots: root-mean-square scattering angles derived from 20 "positive tracks" as a function of H_ρ. Curve: least-squares curve derived from the root-mean-square scattering angles of 104 electrons.

method is not suitable for the determination of an absolute (experimental) scattering law. Both facts are however of minor importance for a comparison of the scattering of two groups of particles. Figure 1 shows the individual root-mean-square angles of scattering for the 20 positive tracks and a curve ψ_1 obtained by a least-squares fit of the data obtained for 104 electrons. In all individual cases corrections were made for errors in the optics, photography, and the measurements of the deflections, as previously described.[10] The difference between the scattering of the particles responsible for the positive tracks and the electrons, which follows from an inspection of Fig. 1, seems to be significant in view of the fact that all the tracks were obtained under the same conditions and treated in the same manner, and that furthermore it was ascertained in two different ways that the difference in the spectral distributions of the particles producing the "positive tracks" and the electrons from which the 104 cases were selected cannot be responsible for the higher scattering of the positives.

If one wishes to attribute the difference in the scattering to a difference in mass of both groups of particles, he can use the following approach. From the curve ψ_1 one can compute scattering curves corresponding to different masses, m, by the use of the approximate relation $\psi_m \propto 1/(pv)$ and compare the distribution of the individual scattering angles of the electrons about their least-squares curve ψ_1 with the distribution of the individual scattering angles of the positive tracks about the curves ψ_m corresponding to different masses. If a^2 is the ratio between an individual mean square angle $(\omega^2)_{Av}$ and a $\psi_m{}^2$ of the same momentum, then for $k^2 \geqslant 0$ we have plotted in Fig. 2 the number of particles (in percent) for which $a^2 \geqslant k^2$, as a function of k^2. The dashed curve A gives this cumulative distribution for the electrons about ψ_1 and the solid curves B, C, and D the distributions for the positive tracks about ψ_1, $\psi_{1.5}$, ψ_2, and $\psi_{2.5}$ corresponding to 1, 1.5, 2, and 2.5 electron masses. It can be seen that curve D agrees fairly well with curve A from which it follows that the individual root-mean-square scattering angles derived from the positive tracks are distributed about a scattering curve corresponding to mass two in a manner similar to that in which the root-mean-square scattering angles derived from electron tracks are distributed about a scattering curve corresponding to mass one. It should be mentioned in this connection that Smith and Groetzinger[3,11] have derived previously a mass of 1.5 to 2 electron masses for the particles producing the positive tracks from their momentum loss in a foil.

Two further results of some rather extensive investigations to be published later will be mentioned here briefly. It can be shown that it is extremely unlikely that any one of the observed positive tracks of a length exceeding 5 cm and an ionization smaller than five times the minimum ionization is, under the conditions used in our investigations, due to one of the decay electrons of P^{32}

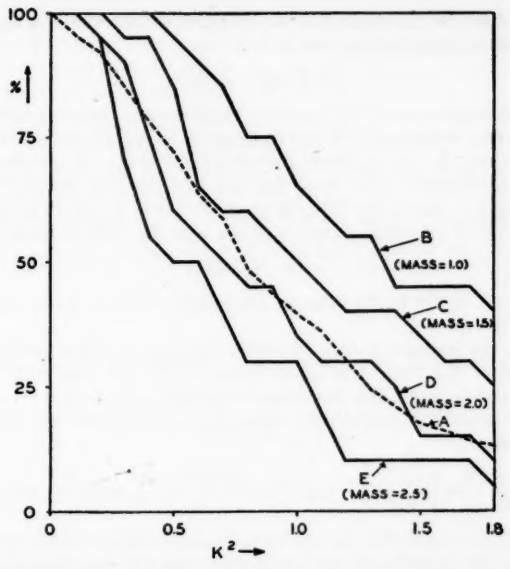

FIG. 2. Cumulative distribution of the mean-square scattering angles of 104 electrons about their least-squares curve (curve *A*), cumulative distributions of the mean-square scattering angles of 20 "positive tracks" about the least-squares scattering curve for the electrons (curve *B*) and about curves corresponding to 1.5, 2, and 2.5 electron masses (curves *C*, *D*, and *E*).

multiply scattered in a direction opposite to that which would occur under the influence of the magnetic field alone. Moreover this improbability already follows from the momentum spectrum of the positive tracks, which was investigated by many observers and which shows that the majority of these tracks have a considerable "positive" curvature, while tracks of a slight curvature are seldom observed. It was found by us on the other hand that, depending on the geometry and the method of investigating these tracks, the number of electrons re-entering the source might be appreciable, but that the number of these spurious positives can be reduced by proper source arrangement and a stereoscopic investigation of the tracks. With these precautions it was found to amount to not more than a few percent in our investigations.

* This research was partly supported by the joint program of the ONR and AEC.

[1] Bradt, Heine, and Scherrer, Helv. Phys. Acta **16**, 491 (1943). (This paper contains an extensive list of the older publications.)
[2] H. G. Heine, Helv. Phys. Acta **17**, 273 (1944).
[3] L. Smith and G. Groetzinger, Phys. Rev. **70**, 96 (1946).
[4] T. H. Pi and C. V. Chao, Phys. Rev. **72**, 639 (1947).
[5] J. S. Barlow and F. T. Rogers, Phys. Rev. **74**, 700 (1948).
[6] C. B. A. McCusker, Nature **161**, 564 (1948).
[7] Erdman, Kokotaila, and Scott, Phys. Rev. **76**, 1262 (1949).
[8] J. H. Spaa and G. J. Sizoo, Physica **15**, 316 (1949).
[9] The radioactive P^{32} was supplied by the Isotope Branch of the AEC, Oak Ridge, Tennessee.
[10] Groetzinger, Berger, and Ribe, Phys. Rev. **77**, 584 (1950).
[11] M. Hessaby, Phys. Rev. **73**, 1128 (1948).

The Absorption of Penetrating Cosmic Rays Underground*

C. A. RANDALL, N. SHERMAN, AND W. E. HAZEN
Randall Laboratory of Physics, University of Michigan, Ann Arbor, Michigan
July 5, 1950

AT a depth of 850 m.w.e. (8.5×10^4 g/cm²) in a salt mine, the absorption of the penetrating component in lead was determined by means of coincidences between two trays of G-M counters separated vertically by 100 cm. Each tray contained 10 cylindrical counters which were one inch in diameter, 30 inches long, and had $\frac{1}{32}$-inch brass walls. A count was recorded when one or more counters in the upper tray fired in coincidence with one or more in the lower tray. The lead absorber was placed between the two trays. The data are shown in Table I. The

TABLE I. Absorption in lead of the penetrating component of cosmic rays.

Lead thickness	Time	Counts	Accidentals	Rate
11.4 cm	589 hr.	1228	116	2.08 ± 0.06 hr^{-1}.
95 cm	144 hr.	297	15	1.95 ± 0.12 hr.$^{-1}$

correction for coincidences due to gamma-rays is negligible,[1] the number of electrons capable of penetrating either thickness of absorber is negligible,[1] and the counter tray separation was the same for both absorber thicknesses. The counting rate was reduced by a factor of 0.94 ± 0.06 when the thick absorber was added.

If the penetrating particles observed in the mine have penetrated the total thickness of earth above the mine (i.e., if the penetrating particles are not produced locally), it is to be expected that the absorption by lead between the counters would be the same as the absorption by an equivalent amount of earth above the counters. The absorption by an equivalent amount of earth can be obtained from the depth-intensity measurements of Wilson.[2] Thus the fractional reduction in intensity is expected to be

$$\frac{\Delta I}{I}=\frac{\gamma\Delta h}{h}=2.7\frac{84\times11.3\times82/207}{8.5\times10^4\times1/2}=0.024,$$

where $\gamma=2.7$ is the slope of Wilson's log depth-log intensity curve at $h=850$ m.w.e. and Δh is the change in thickness of absorber between the counter trays.

Since the attenuation of the penetrating-particle flux is independent of the position of the absorber within the uncertainty of the experiment, it is unlikely that any appreciable fraction of the penetrating particles is produced locally. This result is in marked contrast with the absorption reported by Miyazaki[3] at 3000 m.w.e. and by Barnóthy and Forro[4] at 1000 m.w.e. who report much larger decreases in counting rates with absorbers of about 90 cm of lead, *viz.*, about 70 percent and 30 percent respectively.

* This work was made possible by the cooperation of the International Salt Company and by the financial assistance of the joint program of the ONR and AEC.

[1] C. A. Randall (unpublished).
[2] V. C. Wilson, Phys. Rev. **53**, 377 (1938).
[3] Y. Miyazaki, Phys. Rev. **76**, 1733 (1949).
[4] J. Barnóthy and M. Forro, Phys. Rev. **74**, 1300 (1948).

Internal Conversion Coefficients of Sc^{46}

M. L. MOON, M. A. WAGGONER, AND A. ROBERTS*
Department of Physics, State University of Iowa, Iowa City, Iowa
July 5, 1950

THE gamma-rays following the 0.36-Mev beta-spectrum of Sc^{46} have been investigated as a further test of the theories of internal conversion which have been published recently.[1,2] The upper limit to the abundance of the high energy beta-spectrum[3] (1.49 Mev) was determined to be 0.06 percent rather than 2 percent as previously reported.[3]

The measurements were made with a double-coil thin lens spectrometer using the method described briefly in a recent letter by the authors,[4] and more fully in a paper now in press. The Sc^{46} sources were obtained from a sample of high specific activity material obtained from the Oak Ridge National Laboratory, Union Carbide and Carbon Corporation. The strong sources used in the measurement of internal conversion lines were less than 0.30 mg/cm² average thickness, and the weak sources used to investigate the continuum were less than 0.012 mg/cm². All were mounted on LC-600 films of less than 30 μg/cm², and there was no indication of any line broadening due to source thickness.

The experimentally determined values for the conversion coefficients of *K*, *L*, and *M* shells (unresolved), together with the theoretical[1] conversion coefficients for electric quadrupole radiation and magnetic dipole radiation in the *K* shell, are given in Table I. Assuming that the theoretical *K* value should be increased

TABLE I. Theoretical conversion coefficients in the K shell and experimental values for $K+L+M$ conversion for Sc^{46}.

E_{Mev}	$\alpha_{exp}\times10^4$	Theoretical values E. Q. $\alpha_K\times10^4$	Theoretical values M. D. $\alpha_K\times10^4$
0.88	1.74±0.08	1.51	1.10
1.12	0.98±0.05	0.841	0.686

approximately ten percent to correct for the contribution of L plus M internal conversion and screening, the results classify both gamma-radiations as electric quadrupole. The predicted values for other types of radiations differ by a minimum factor of 1.6 from the experimental values. This result, together with those of recent angular correlation[5] and polarization correlation experiments,[6] fixes the spins and parities of the nuclear levels of $_{22}Ti^{46}$ as 0, 2, 4; same.

Previously reported values[3] of the internal conversion coefficients for Sc^{46} required the radiations to be of a higher multipole order which is in disagreement with the angular correlation results[5,6] and lifetime considerations. The present results appear to remove this inconsistency.

* Now at the University of Rochester.
[1] Rose, Goertzel, Spinrad, Harr, and Strong, Phys. Rev. 76, 184 (1949).
[2] J. R. Reitz, Phys. Rev. 77, 10 (1950).
[3] C. L. Peacock and R. G. Wilkinson, Phys. Rev. 74, 297 (1948).
[4] Waggoner, Moon, and Roberts, Phys. Rev. 78, 295 (1950).
[5] E. L. Brady and M. Deutsch, Phys. Rev. 78, 558 (1950).
[6] F. Metzger and M. Deutsch, Phys. Rev. 78, 551 (1950).

On the Theory of Supersonic Absorption

A. GIERER AND K. WIRTZ
Max Planck Institute for Physics, Göttingen, Germany
June 23, 1950

SUPERSONIC absorption in liquids is larger than the value which follows from the constants of the continuum theory.[1] This indicates that there is a component $\alpha_{rel}=\alpha_{exp}-\alpha_{cont}$ which is due to relaxation in reaching thermodynamic equilibrium, displaced by acoustic waves. In addition to the relaxation of the intramolecular degrees of freedom[2] observed in gases, one can expect a structure dependent relaxation in liquids.[3,4] We can show that, by considering a liquid as a quasicrystalline structure, one gets an absorption which corresponds roughly to the observed value for many liquids. Relaxation absorption is given by the expression

$$\alpha_{rel}=2\pi^2\rho c\nu^2\kappa_i\tau, \quad \nu\ll1/\tau, \tag{1}$$

where c=velocity of sound, ρ=density, ν=frequency. κ_i is the contribution to the total compressibility of the degree of freedom producing the relaxation. The relaxation time τ is a measure of the time required for achieving equilibrium after a sudden displacement from equilibrium, and can be determined from the reaction kinetics of the excitation process. If the concentration N of the excited state is small, τ is proportional to the lifetime of the excited state. If, therefore, the reverse reaction is a second or higher order process, τ is large.

We characterize kinetic effects in liquids such as viscosity, diffusion, and thermal diffusion[5] by the rate, j, with which a molecule displaces its position on the average with respect to its neighbors. These processes presuppose a partial dissociation of the crystal structure, so that the long range order is destroyed by perturbations, i.e., holes. In a regular crystal these can only arise at the expense of a complementary perturbation, and they wander independently through the crystal by a shifting of position of the participating molecules. Creation and destruction of holes cannot follow directly the rapid compressions of sound waves, because a rearrangement within the crystal is necessary which can be described by the fusion of two complementary disturbances. In the usual empirical expression,[5,6]

$$j=j_0\exp(-q/RT); \tag{2}$$

the activation energy for position displacement therefore includes a part q_L, whose activation is determined by second-order reaction equations. It follows from the reaction kinetics of the creation and wandering of the holes that the lifetime and, therefore, the relaxation time of the holes is proportional to $1/j$ and can consequently be expressed in terms of the viscosity. One obtains:

$$\tau=V\eta/2RT, \tag{3}$$

where V is the molar volume. The values of τ are of the order of 10^{-11} sec.

In the isothermal approximation the part κ_i of the compressibility of the holes can be estimated from the hole energy q_L, which determines the concentration of the holes, and the average additional volume v, which follows from the pressure dependence of viscosity:

$$\kappa_i=\frac{v}{V}\frac{dN}{dp}=\frac{v}{V}\frac{v}{RT}\exp(-q_L/RT)=\frac{RT}{V}\left(\frac{d\ln\eta}{dp}\right)^2\exp(-q_L/RT). \tag{4}$$

It can be shown that an additional temperature wave due to the adiabatic character of the sound wave yields at most terms of the same order.

Equations (1) to (3) relate the structure absorption α_{rel} to independently observable quantities and to q_L. There are good reasons for believing that the hole energy q_L is an appreciable fraction of the displacement energy q. The ratio of q_L to q_W, the heat of evaporation, is considered to be roughly equal to the ratio of the hole volume v to the molecular volume V. In Table I,

TABLE I. Data for structural absorption of liquids for high frequencie[8] ($\nu>10^7$ sec.$^{-1}$).

	$\left(\frac{\alpha_{rel}}{\nu^2}\right)_{obs}$	q_L kcal./mole[a]	q kcal./mole[b]	q_L/q_W	v/V[c]
Acetone	24	0.9	1.8	0.12	0.21
Ethyl acetate	30	1.1	2.5	0.12	0.17
Ethyl alcohol	32	1.2	3.9	0.12	0.21
Ethyl bromide	52	0.7	2.1	0.11	0.19
Ethyl iodide	30	1.4	2.2	0.20	0.17
Acetic acid	127	0.7	2.6	0.10	(0.20)
Glycerol	<300	>3	14	>0.15	0.21
Heptane	70	0.7	2.4	0.08	0.14
Propyl alcohol	35	2.0	4.2	0.20	0.23
Oxygen	3	0.47	—	0.29	(0.1)
Argon	2	0.55	—	0.33	(0.1)
Mercury	1	1.6	1.2	0.10	0.04
Benzene	870	—	3.0	—	0.22
Toluene	75	0.8	2.6	0.09	0.16
Xylene	62	1.0	2.6	0.10	0.15

[a] q_L is derived from $(\alpha_{rel})_{obs.}$ by Eqs. (1) to (3).
[b] q from temperature dependence of viscosity.
[c] Interpolated values in brackets.

q_L is calculated on the assumption that α_{rel} is due entirely to structure and its value is compared with the above-mentioned quantities. There is agreement for many monoatomic and molecular liquids.

Other types of liquids with more complicated but symmetrical molecules, e.g., C_6H_6, CCl_4, possess a much larger absorption, which, however, decreases appreciably if some intramolecular substitutions $[C_6H_6\rightarrow C_6H_5CH_3\rightarrow C_6H_4(CH_3)_2]$ are made that hardly affect intermolecular quantities such as viscosity. We assume that in these cases intramolecular relaxation degrees of freedom predominate, whose relaxation time is large in the symmetrical molecules.

Higher order reactions can be considered to be responsible for the much larger relaxation times ($\tau\sim10^{-6}$ sec.) of some liquids. In this way, Lamb and Pinkerton[7] explain the absorption of acetic acid as due to the dissociation of the acetic acid double molecule bound by H-bridges. Using our method, we deduce a binding

energy of the H-bridge equal to 6 to 7 kcal./mole, as one might expect. This is an additional effect which is superposed on structure relaxation that is typical for all liquids. A comprehensive report will be published soon.[8]

[1] G. Stokes, Trans. Camb. Phil. Soc. **8**, 287 (1945).
[2] H. O. Kneser, Ergeb. d. exakt. Naturwiss. **22**, 121 (1949).
[3] P. Debye, Zeits. f. Elektrochemie **45**, 174 (1939).
[4] J. Frankel, *Kinetic Theory of Liquids* (Oxford University Press, London, 1946).
[5] K. Wirtz, Zeits. f. Naturforsch. **3a**, 672 (1948).
[6] Glasstone, Laidler, and Eyring, *The Theory of Rate Processes* (McGraw-Hill Book Company, Inc., New York and London, 1941).
[7] J. Lamb and J. M. M. Pinkerton, Proc. Roy. Soc. **A199**, 114 (1949).
[8] A. Gierer and K. Wirtz, Zeits. f. Naturforsch. **5a**, 270 (1950).

Mobility of Electrons and Holes in Diamond*

E. A. Pearlstein† and R. B. Sutton
Physics Department, Carnegie Institute of Technology, Pittsburgh, Pennsylvania
July 13, 1950

THE mobility of electrons and holes in a diamond crystal counter has been measured using a method somewhat similar to that of McKay.[1] The range of the carriers (either holes or electrons), released by α-particles entering through one electrode, and the rise time of the pulses were measured in an unpolarized sample 2 mm thick. Polarization was eliminated by illuminating the sample with ultraviolet light from a mercury arc, with no field applied, immediately before measurements were taken. During the time measurements were taken no appreciable polarization charge accumulated.

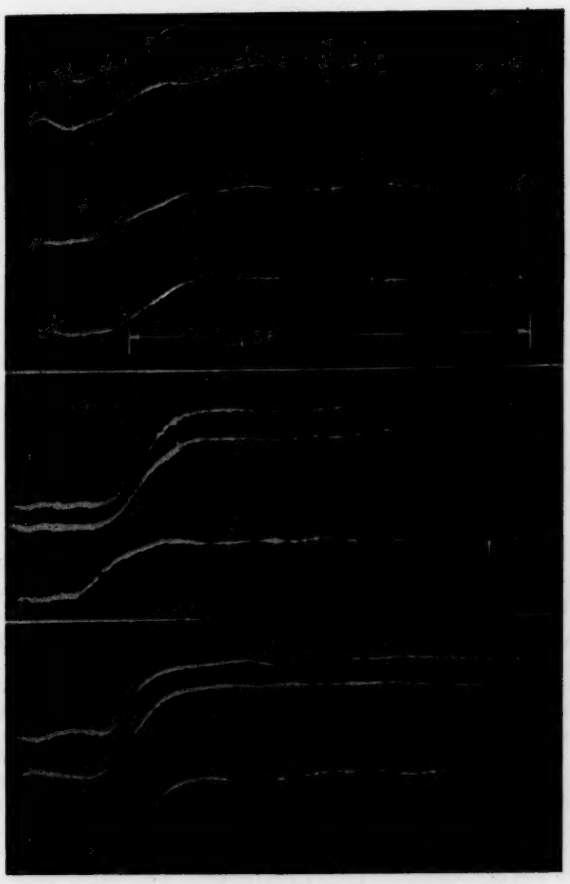

FIG. 1. Electron pulses in diamond. Top: 300 volts across crystal; center: 1200 volts across crystal; bottom: 5000 volts across crystal. Crystal thickness: 2 mm.

The value of range was obtained by measurements of the variation of pulse height with applied voltage. Fields up to 25,000 volt/cm were used. The results give:

$$\text{electrons: } \mu T = 3.5\times10^{-5}\pm10\%\ \text{cm}^2/\text{volt}$$
$$\text{holes: } \mu T = 3.8\times10^{-5}\pm15\%\ \text{cm}^2/\text{volt},$$

where μ = mobility, T = mean free time.

Pulse rise times at various voltages were measured from photographs (Fig. 1) of pulses displayed on a cathode-ray oscilloscope. Delay line amplifiers with an over-all rise time (20 to 80 percent) of 0.009 μsec. were used to amplify the pulses in order to display them on the oscilloscope which had characteristics similar to that described by Kelley.[2] The rise time-voltage dependence for electrons was as expected and gave a value $T = 0.009\pm10$ percent μsec. The dependence for holes deviates from expectation at higher values of voltage. In the low voltage region, where the behavior appeared normal, the value for holes was $T = 0.008\pm15$ percent.

From the values of μT and T the mobility values are:

$$\text{electrons: } \mu = 3900\pm15\%\ \text{cm}^2/\text{sec.-volt},$$
$$\text{holes: } \mu = 4800\pm20\%\ \text{cm}^2/\text{sec.-volt}.$$

Preliminary measurements for electrons have been obtained on a second diamond 1.98 mm thick. For this sample both the range and free time are less than for the first diamond. The value of free time was therefore less accurate since the pulse rise times differed less from the amplifier rise time. Results for electrons are

$$\mu T = 2.1\times10^{-5}\ \text{cm}^2/\text{volt} \quad \text{and} \quad T = 0.0076\ \mu\text{sec}.$$

Thus $\mu = 2760$ cm²/sec.-volt with an estimated error considerably greater than that on the first value.

* This work was supported by the ONR.
† AEC Predoctoral Fellow.
[1] K. G. McKay, Phys. Rev. **74**, 1606 (1948); **77**, 816 (1950).
[2] G. G. Kelley, Rev. Sci. Inst. **21**, 71, 264 (1950).

Upper Limit on the Cross Section for the Scattering of Neutrinos*

J. H. Barrett
Rice Institute, Houston, Texas
July 10, 1950

SEVERAL previous experiments have been performed to attempt to detect the scattering of neutrinos. Crane[1] has given a summary of such results. In an experiment very similar to the author's, Nahmias[2] has set the lowest upper limit of 10^{-30} cm²/atom in air. The present availability of tritium in large quantities seemed to make it possible to set a better value for the upper limit of the cross section.

A Geiger counter was used for detection of the neutrinos. It was assumed that any ionizing event in the counter gas due to neutrinos would give a count. The source of neutrinos was 5 curies of tritium.

The procedure was to count alternately with the tritium placed alongside the counter for several hours and then count with the tritium removed to a considerable distance for several hours. Many trials were made of the background counting rate and of the gross counting rate of background plus neutrinos, always alternating between the two.

In each of the two experiments performed, it was found that the net counting rate was less than the probable error computed by statistical means. It was assumed that any counting rate greater than the probable error could have been detected, and an upper limit on the cross section was computed.

Using a Geiger counter filled with neon at 10 cm Hg pressure, a gross counting rate of (23.45±0.10) counts/min. and a background counting rate of (23.63±0.11) counts/min. were obtained. This gave a net counting rate of (−0.18±0.21) count/min. Assuming that any counting rate greater than 0.21 count/min.

could have been detected, this gives an upper limit of 5×10^{-32} cm²/atom. The number of atoms/cm³ in the counter was calculated to be 6×10^{18}. The number of disintegrations per second in the tritium was 1.8×10^{11}, and it was estimated that one-twentieth of these passed through the counter. The average path length through the counter was 1.2 cm. Supposing the main means of scattering would be by the electrons and assuming eight electrons per atom would be effective in scattering, this gives an upper limit of 6×10^{-33} cm²/electron.

Using another Geiger counter filled with twenty atmospheres of helium, a gross counting rate of (28.95±0.31) counts/min. and a background counting rate of (29.12±0.34) counts/min. were obtained. The net counting rate in this case was (−0.17±0.65) count/min. Using 0.65 count/min. as an upper limit on the counting rate, 7×10^{-34} cm²/atom was the upper limit on the cross section. In calculating this figure, the number of neutrinos and the fraction which passed through the counter were the same as above. The number of atoms/cm³ was 5×10^{20}, and the average path length through the counter was 3.5 cm. Assuming the two electrons in helium to be equally effective for scattering, the upper limit of the cross section is 4×10^{-34} cm²/electron.

* This work was supported by the joint AEC and ONR program.
[1] H. R. Crane, Rev. Mod. Phys. 20, 278 (1948).
[2] M. E. Nahmias, Proc. Camb. Phil. Soc. 31, 99 (1935).

Neutron Binding Energies

J. R. Huizenga, L. B. Magnusson, O. C. Simpson, and G. H. Winslow
Argonne National Laboratory, Chicago, Illinois
July 10, 1950

Up to the present, authors[1] who have calculated neutron binding energies in the heavy isotopes have bridged between the radioactive series by smooth interpolations or by use of the mass formula. There are now sufficient data to give unambiguous energy differences between the $4n$, $4n+3$, and $4n+2$ series, apart from experimental error. Although the possible formation of excited states casts doubt on the result of any single type of experimental neutron binding energy measurement, agreement between the results of two properly chosen methods removes it. In a (d, p) reaction, if (Z, A) is the target nucleus, then $E_n(Z, A+1) = Q_R+Q_d+E_\gamma$, where $E_n(Z, A+1)$ is the neutron binding energy in $(Z, A+1)$, Q_R is the Q-value for the reaction, Q_d is the deuteron binding energy and E_γ is the *total* gamma-energy emitted by the product nucleus, if formed in an excited state. Thus, if the total gamma-energy between the excited and ground states is not included, the calculated binding energy would be equal to or *less* than the true binding energy.

Conversely, for the (d, t) reaction, $E_n(Z, A) = -Q_R+Q_t-Q_d-E_\gamma$. Here the target nucleus is still called (Z, A), and Q_t is the triton binding energy. If an excited state were formed and the total gamma-decay energy not included, the calculated binding energy would be *greater* than the true binding energy. Therefore agreement between the neutron binding energies in a given nucleus as measured by the (d, p) and (d, t) reactions gives this energy unambiguously. Similar considerations show that a (γ, n) reaction gives a result greater than or equal to the true energy, while the result from an (n, γ) reaction is ambiguous unless the gamma-decay scheme is determined. The energies listed in Table I are the results of various investigations for the last neutron in the isotope given. The last column gives conclusions based on the above reasoning. Thus the energy differences between the $4n$, $4n+3$, and $4n+2$ series are known.

Now it seems rather certain that the disintegration energies of Pb^{209}, Pb^{210}, and Bi^{210} are 0.69 Mev, 0.07 Mev, and 1.17 Mev, respectively.[2] The use of these, the disintegration energy[2,3] of Po^{214} and the neutron binding energies in Pb^{208} and Pb^{207}, shows that about 0.4 Mev must be added to the sum of the measured binding energies in Pb^{209} and Bi^{210}. If it is assumed that *only one* of these measurements is in error, the following arguments lead to the choice of 3.87 Mev for the binding energy of Pb^{209}. First, if the 0.4 Mev were added to the experimental binding energy in Pb^{209}, the resultant energy would be greater than that in Bi^{210}. However, it is expected that the addition of an odd proton outside the closed Pb^{208} shell would *increase* the binding energy of an odd neutron outside that shell. Second, the neutron binding energy in Pb^{209} would be only 0.5 Mev less than that of the neutron in Pb^{210}. This difference is expected to be 1.0 Mev or more. Third, if 4.17 Mev were the binding energy of the odd neutron in Bi^{210}, it would be less than that in Bi^{212}, contrary to expectations. The latter (4.36 Mev) is derived from the binding energy in Pb^{208}, the disintegration energies of Th C (2.25 Mev), Ac C'' (1.44 Mev),[4] and known alpha-energies.[2,3]

Table I. Neutron binding energies.

Isotope	Neutron binding energy (Mev) measured by (d, p)[a]	(d, t)[a]	(γ, n)[b]	(n, γ)[c]	Neutron binding energy (Mev)
$_{83}^{210}$	4.14±0.03			4.170±0.015	≥4.17
$_{83}^{209}$		7.44±0.05	7.45±0.2		≤7.44
$_{82}^{209}$	3.87±0.05				≷3.87
$_{82}^{208}$	7.37±0.03	7.37±0.05	7.44±0.10	7.380±0.008	7.38
$_{82}^{207}$	6.71±0.03	6.69±0.05	6.95±0.10	6.719±0.016	6.72
$_{82}^{206}$		8.10±0.05	8.25±0.10		≶8.10

[a] J. A. Harvey, Phys. Rev. 79, 241 (1950).
[b] McElhinney, Hanson, Becker, Duffield, and Diven, Phys. Rev. 75, 542 (1949); H. Palevsky and A. O. Hanson, Phys. Rev. 79, 242 (1950).
[c] Kinsey, Bartholomew, and Walker, Phys. Rev. 78, 77 (1950); Phys. Rev. 78, 481 (1950); private communication.

These experimental energy differences between the four series make it possible to determine other binding energies using energy cycles. Knowledge of these energies may serve as a means of refining the empirical mass formulas. More importantly, they can provide a check on the validity of total decay energies. Arguments like those in the preceding paragraph are also being made for the latter purpose. Work along these lines at present indicates that some of the most critical decay energies are those of Ra B, Ra C, Bi^{213}, $Ms\mathrm{Th}_1$ and $Ms\mathrm{Th}_2$.

[1] A. Berthelot, J. de phys. et rad. (VIII) 3, 17 (1942); K. Way, Phys. Rev. 75, 1448 (1949); M. O. Stern, Rev. Mod. Phys. 21, 316 (1949); A. H. Wapstra, Physica 16, 33 (1950).
[2] See G. T. Seaborg and I. Perlman, Rev. Mod. Phys. 20, 585 (1948) for references.
[3] Perlman, Ghiorso, and Seaborg, Phys. Rev. 77, 26 (1950).
[4] H. D. Evans, Proc. Phys. Soc. London 63, 575 (1950).

The Solar Flare of November 19, 1949 and Cosmic Rays

J. Clay and H. F. Jongen
Amsterdam, Holland
July 10, 1950

Within recent years a great number of physicists, among them Forbush,[1] Ehmert,[2] and Unsöld,[3] have investigated extensively with ion chambers and counters the sudden variations in cosmic-ray intensity coincident with disturbances of the earth's magnetic field, changes in radiofrequency waves from the sun, and ionospheric disturbances and their correlation with solar flares.

As to our contribution to the investigation with the former method, our recording apparatus consists of 3 ion chambers containing Ar at up to 60 atmospheres; one of the chambers is unshielded, one shielded with 12 cm Fe, and one with 110 cm Fe. Normally we have a fourth vessel, likewise under 110 cm Fe, but this one was not in use for the moment. The charge required to compensate the ionization in the vessels is measured every two hours for the unshielded vessel, every hour for the other two, in the form of an excess over a well-known compensation charge.

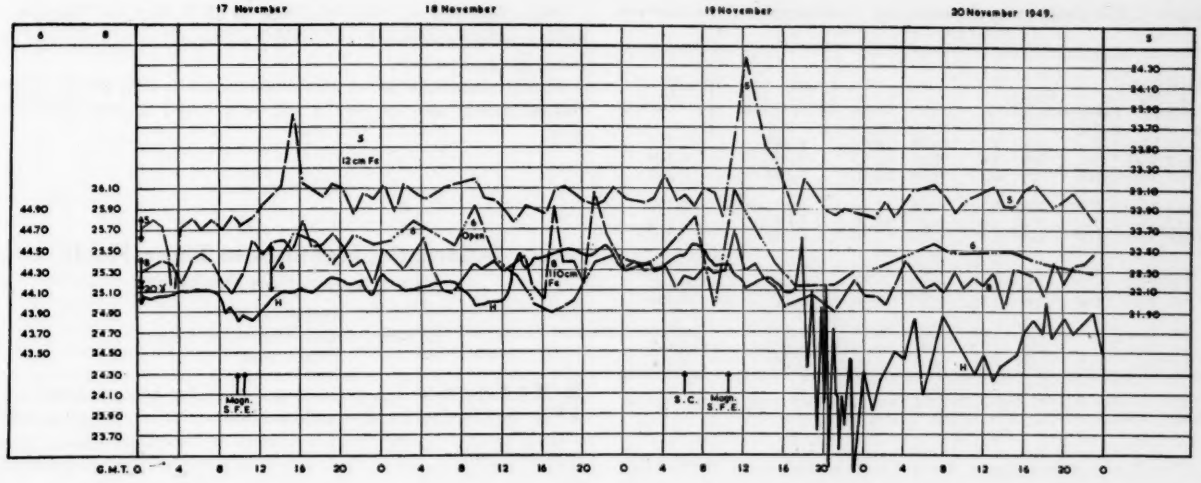

FIG. 1. Observed cosmic-ray intensity and horizontal component of the earth's magnetic field for the period November 17 to 20, 1949.

In this way it is possible to reach an accuracy of 0.1 percent; the last half year however our accuracy has been lowered to 0.2 percent due to frequency changes of the electric network, for which we have corrected as well as possible.

The use of different layers of absorbing material affords us a notion of the energies of the cosmic-ray particles which occur during solar flares. We know at the moment that the observed solar flare effects show great differences in this respect.

The normal case seems to be the following: frequently a small decrease in cosmic-ray intensity and a "sudden commencement" earth magnetically are observed shortly before the flare. But in any case immediately after the flare the earth's magnetic field shows the characteristic solar flare effect, followed within 20 min. to 2 hr. by a steep increment of cosmic-ray intensity, the size of which, however, differs greatly in the cases observed. Then in a decrease generally extending over several hours, the intensity comes down to a level below normal. In most cases considerable magnetic disturbances or a magnetic storm is simultaneously observed. The normal intensity is not regained till one or two days afterward.[4]

Variations of this general behavior of cosmic rays in a case of solar flare have been reported; e.g., by Broxon and Boehmer and by Rose. Broxon and Boehmer[5] found no increment during the flare of May 10, 1949. Our observations on this day give only an excess smaller than one percent in both the unshielded vessel and the one shielded with 12 cm Fe, with a retardation of many hours, but no increment was found under 110 cm Fe. During this flare apparently only particles of low energies were ejected, the greater part of them not being able to penetrate the atmosphere. This is confirmed by Schein's observation on the same day of an increment of 75 percent at very great height.

After the flare of November 19, 1949, Rose[6] did not find a decrease of cosmic-ray intensity, but during the magnetic disturbance setting in about 19.00 found an intensity higher than normal. On November 19 a solar flare of importance 3 was observed by the Wendelstein Solar Observatory (Bavaria), beginning at 10.29 and ending at 11.19 G.M.T. with a maximum at 10.34. Magnetic Station Witteveen of the K.N.M.I., Holland, reports on the same day a sudden commencement of 15γ in H at 6.04 G.M.T., followed by a solar flare effect at 10.30 to 11.00. This solar flare effect is confirmed by a Dellinger fade-out of the Noordwijk radio station (NDRA). After 19.00 on November 19 a magnetic disturbance set in with a maximal range in H of 215γ.

In Fig. 1, which is corrected for changes in barometric pressure, we give the intensities for the various chambers in terms of the compensation voltages, and also the horizontal intensity of the earth's magnetic field. The intensity changes of the cosmic rays here are curious. Before the point marked S.C. there is a small decrease until 6.00 G.M.T., except in the unshielded chamber. Then a minor maximum occurs, followed immediately by a dip, which is negligible, however, in the hard component. The influence of the solar flare of 10.29 G.M.T. is different in our three vessels. The hard component shows an increase of one percent in the period 10.30–11.30, and in the interval 10.00–12.00 the total intensity attains a value somewhat higher than that before the dip. The behavior of the component observed under 12 cm Fe is remarkable. Here we find in the two intervals 10.15–11.15 and 11.15–12.15 a steep increase of nearly seven percent in total. The decrease to normal values lasts in all of the vessels until 17.00 G.M.T. We cannot confirm the observation of Rose, however, that during the magnetic disturbance following the flare the cosmic-ray intensity is higher than before the flare, our mean hour values for the three chambers being somewhat larger on November 18 than on November 20, although we must agree that after such an important flare a larger decrease would be expected.

The Cosmic Relations Bulletin No. 7 (1949) of New Zealand mentions on November 19, 1949 an increment of 15 percent in cosmic-ray intensity followed by a more or less exponential decrease to *normal* values.

Taken all in all, we should conclude that no difference is to be observed between the intensities before and after this flare, which is abnormal.

We are very much indebted to Mr. A. J. Dijker for his help with the classification of the bulky material on this subject for the last four years.

[1] Forbush, Gill, and Vallarta, Rev. Mod. Phys. **21**, 44 (1949).
[2] Ehmert, Zeits. f. Naturforsch. **3a**, 264 (1948).
[3] A. Unsöld, Zeits. f. Astrophys. **26**, 176 (1949).
[4] Clay, Jongen, and Dijker, Proc. Amsterdam **LII**, 897, 923 (1949).
[5] J. W. Broxon and H. W. Boehmer, Phys. Rev. **78**, 411 (1950).
[6] D. C. Rose, Phys. Rev. **78**, 181 (1950).

The Photo-Disintegration of the Deuteron

INGVAR F. E. HANSSON
Åmål, Sweden
July 13, 1950

IN a previous paper[1] L. Hulthén and the present writer have given results of theoretical calculations on the photo-disintegration of the deuteron for the γ-energies 2.62, 2.76, and 6.2 Mev. As experiments are being carried out using γ-rays from radio

TABLE I. Calculated photo-disintegration cross sections of the deuteron (units of 10^{-28} cm²).

Deuteron binding energy	Theory[a]	Meson mass	σ_m	σ_e	σ $(=\sigma_m+\sigma_e)$	$\left[\frac{\sigma(0)}{\sigma(\pi/2)}\right]_{c.m.}$	$\left[\frac{\sigma(0)}{\sigma(\pi/2)}\right]_{lab}$
2.187 Mev	*N*	200	3.47	10.18	13.65	0.185	0.214
2.187 Mev	*O*	200	3.47	9.28	12.75	0.200	0.230
2.187 Mev	*MR*	200	3.47	9.06	12.52	0.203	0.235
2.187 Mev	*N*	300	3.62	7.77	11.40	0.237	0.274
2.187 Mev	*O*	300	3.62	7.57	11.19	0.242	0.279
2.187 Mev	*MR*	300	3.67	7.50	11.17	0.246	0.284
2.237 Mev	*N*	200	3.75	8.07	11.82	0.236	0.276
2.237 Mev	*O*	200	3.75	7.39	11.14	0.253	0.295
2.237 Mev	*MR*	200	3.75	7.22	10.96	0.257	0.300
2.237 Mev	*N*	300	3.92	6.21	10.13	0.296	0.346
2.237 Mev	*O*	300	3.92	6.04	9.96	0.302	0.353
2.237 Mev	*MR*	300	3.97	5.99	9.96	0.307	0.358

[a] *MR* denotes the Møller-Rosenfeld theory, *N* the corresponding neutral theory, and *O* the case of no ^3P-interaction (see reference 1).

gallium[2] the calculations have been extended to 2.52 Mev. Table I gives the calculated values of the photomagnetic and photoelectric cross sections (σ_m and σ_e) in 10^{-28} cm² as a unit and the intensity ratio $\sigma(0)/\sigma(\pi/2)$ in the center-of-mass system (c.m.) as well as in the laboratory system (lab.). The average ratio $[(\sigma(0)+\sigma(\pi))/2\sigma(\pi/2)]_{lab}$ is about one percent higher than $[\sigma(0)/\sigma(\pi/2)]_{c.m.}$.

The present work was carried out during a stay at the Royal Institute of Technology, Stockholm, which was made possible by a grant from the Swedish Atomic Energy Committee.

[1] I. F. E. Hansson and L. Hulthén, Phys. Rev. **76**, 1163 (1949).
[2] Snell, Barker, and Sternberg, Phys. Rev. **75**, 1290 (1949).

An Anomalous Effect Observed in Self-Quenching Counters Containing Neon

A. D. KRUMBEIN
New York University, New York, New York
July 12, 1950

IN the course of some experiments on self-quenching Geiger counters which are to be reported elsewhere, the following phenomenon was observed. Counters filled to 10 cm total pressure with neon-quenching constituent mixtures containing less than 0.1 percent of ethyl acetate or butane exhibited a Geiger plateau region at a higher voltage across the counter than a preceding region of continuous discharge. The counter characteristics from this point on are observed to follow the usual pattern.

As the partial pressure of the quenching constituent is decreased below the point where the above phenomenon sets in, the continuous discharge region preceding the plateau becomes longer while the plateau itself grows shorter, until the latter completely disappears. The starting potential for counters of 0.95 cm cathode radius in this region is between 250 and 300 volts. The effect is most striking with ethyl acetate, and less so with butane. It also occurs to a limited extent with methane, though at a higher partial pressure of this quenching gas.

In counters of smaller cathode radius the effect either does not occur at all or does so only to a limited extent. A counter of 0.14 cm cathode radius does not exhibit this "late plateau" at all, self-quenching action having apparently ceased before a low enough partial pressure of quenching constituent had been reached. A counter of 0.25 cm cathode radius exhibits a region of multiple discharges at a lower voltage across the counter than the plateau region which comes after it but does not have a region of continuous discharge at this lower voltage. Counters having cathode radii of 0.64, 0.95, 1.27, and 1.84 cm all exhibit this "late plateau" effect. In the counter of 0.95 cm cathode radius, however, the phenomenon is more striking than in the counters of both larger and smaller dimensions.

This effect has not been observed at all in counters containing self-quenching gas mixtures in which either argon or helium is the noble gas component.

Further investigation of this phenomenon is now under way in this laboratory and the results will be reported in detail at a later date.

Differential Identities in Three-Field Renormalization Problem

ABDUS SALAM
St. John's College, Cambridge, England
July 5, 1950

MATTHEWS[1] has pointed out that for renormalization to be effective for the combined interaction of charged spinless mesons (scalar interactions), nucleons and electromagnetic field, certain conditions must be satisfied, and has verified these conditions to the lowest order by direct calculation. Here a more general proof is attempted.

Following Dyson[2] we define $\Sigma_P^*(p)$ as the function arising from adding together all integrals corresponding to proper self-energy parts inserted into a proton line of momentum p. Besides the self-energy part consisting of a single point, there are in fact just two irreducible self-energy parts, one arising from the proton's interaction with the electromagnetic field, the other from its interaction with the meson. Define $\Sigma_M^*(p)$ as the corresponding function for meson self-energy graphs. Let $\Lambda_\mu^a(p, p')$ be the function arising from adding together integrals corresponding to proper vertex parts with one external photon and two proton lines, while $\Lambda_\mu^b(p, p')$ stands for vertex parts with one photon and two meson lines. Also let $\Theta_{\mu\nu}(p, p', q)$ be the function arising from adding integrals corresponding to proper C parts (parts with two external meson and two photon lines) defined as capable of replacing the factor $\delta_{\mu\nu}$ from a four-vertex.

From general considerations $\Sigma_M^*(p)$ is at most quadratically, $\Sigma_P^*(p)$ and $\Lambda_\mu^b(p, p')$ are at most linearly, $\Lambda_\mu^a(p, p')$ and $\Theta_{\mu\nu}(p, p', q)$ are at most logarithmically divergent. From invariance considerations their forms are

$$\Sigma_P^*(p)=(A-2\pi i\delta\kappa_0)+B(p\gamma-i\kappa_0)+S_c(p)(p\gamma-i\kappa_0)$$
$$\Sigma_M^*(p)=(A'+\pi i\delta\kappa_0^2)+C(p^2+\kappa^2)+\Pi_c(p)(p^2+\kappa^2)$$
$$\Lambda_\mu^a(p, p')=L^a\gamma_\mu+\Lambda_{\mu c}^a(p, p')$$
$$\Lambda_\mu^b(p, p')=L^b(p_\mu+p_{\mu'})+M^b(p_\mu+p_{\mu'})(p^2+\kappa^2+p'^2+\kappa^2)+\Lambda_{\mu c}^b(p, p')$$
$$\Theta_{\mu\nu}(p, p', q)=R\delta_{\mu\nu}+\Theta_{\mu\nu c}(p, p', q)$$

where $S_c(p)=\Lambda_{\mu c}^a(p, p)=0$ for $i\gamma p+\kappa_0=p^2+\kappa_0^2=0$

$$\Pi_c(p)=0 \text{ for } p^2+\kappa^2=0, \quad \Lambda_{\mu c}^b(p, p')=\frac{\partial\Lambda_{\mu c}}{\partial p_\nu}=\frac{\partial\Lambda_{\mu c}}{\partial p_{\nu'}}=0$$

for $p=p'$ $p^2+\kappa^2=0$ and $\Theta_{\mu\nu c}(p, p', q)=0$ for $p=p'$ $q=0$ and $p^2+u^2=0$.

The possible divergent constants B, C, L etc., are double power series in e and f.

In order to prove our identities, we extend the differential identity $-(1/2\pi)(\partial S_F(p)/\partial p_\mu)=S_F(p)\gamma_\mu S_F(p)$ first given by Ward.[3] For mesons, we have

$$-(1/2\pi i)(\partial\Delta_F(p)/\partial p_\mu)=\Delta_F(p)2p_\mu\Delta_F(p).$$

The insertion of an external photon line (with its energy-momentum set equal to zero) in a charged meson line is described correctly by a single differentiation. The important extension is that a second differentiation of the above with respect to p_ν describes not only the insertion of another photon three-vertex on the same meson line but also the complication of the first three-vertex into a four-vertex. Even while dealing with the three-field problem we can always arrange that the momentum p should follow the charge in any connected graph, so that the internal lines corresponding to neutral particles (neutrons and photons) do not get differentiated. (With certain conditions, closed charged loops

inside neutral lines give no extra divergence. This also leads to the finiteness of all neutron magnetic moment graphs, pointed out by Matthews as essential for renormalization to go through.)

By use of the above technique we easily get the following identities:

$$\Lambda_\mu{}^a(p,p) = -(1/2\pi)\partial\Sigma_F{}^*(p)/\partial p_\mu,$$
$$\Lambda_\mu{}^b(p,p) = -(1/2\pi i)\partial\Sigma_M{}^*(p)/\partial p_\mu,$$
$$\Theta_{\mu\nu}(p,p,0) = \tfrac{1}{2}\partial\Lambda_\mu{}^b(p,p)/\partial p_\mu,$$

so that

$$L^a = -B/2\pi, \quad L^b = R = -C/2\pi i,$$

while M^b is finite. The procedure above covers reducible as well as irreducible graphs.

To have a complete proof of renormalization one still must take account of scattering of mesons by mesons (M parts) and also of considerable overlaps between vertex and C parts. It has been verified, however, that the three-field mixture introduces no great complexities besides those associated with mesons in the electromagnetic field. Work on the complete problem is in progress.

After the above work was completed, the author received a communication from Mr. F. J. Dyson, proving similar identities for interaction of mesons with electromagnetic field, from general arguments of gauge invariance.

Acknowledgments are due Dr. P. T. Matthews, for suggesting the investigation and numerous discussions, and Dr. N. Kemmer for continual help and encouragement.

[1] P. T. Matthews, Phys. Rev. (to be published).
[2] F. J. Dyson, Phys. Rev. **75**, 1736 (1949).
[3] J. C. Ward, Phys. Rev. **77**, 293 (1949); **78**, 182 (1950).

Isotope Effect and Lattice Properties in Superconductivity*

KARL F. HERZFELD
Catholic University of America, Washington, D. C.
AND
EMANUEL MAXWELL, AND RUSSELL B. SCOTT
National Bureau of Standards, Washington, D. C.
July 5, 1950

IN a recent communication,[1] Serin, Reynolds, and Nesbitt have suggested that the isotopic dependence of the superconducting transition temperature in mercury can be expressed by the approximate relation $M^{\frac{1}{2}}T_c$=constant, where M is the average atomic mass and T_c is the transition temperature. From this they have inferred that the ratio of the Debye temperature to the transition temperature is a constant for each of the different isotopes.

It should be pointed out, however, that the data represent a relatively small spread in M and T_c and consequently in trying to fit a relation of the form $M^\alpha T_c$=constant, one finds that the product is approximately constant, to the degree noted by Serin, Reynolds, and Nesbitt, for a comparatively large range of α's. We have examined all of the available data on the isotopes of mercury for the purpose of determining the best value of the exponent. These data are given in Table I and are plotted for mercury in logarithmic form in Fig. 1. A least-squares fit of the best straight line to the points of Fig. 1 yields a slope of 0.378 $\pm$0.021. A line of slope $\frac{1}{2}$ is shown for purposes of comparison.

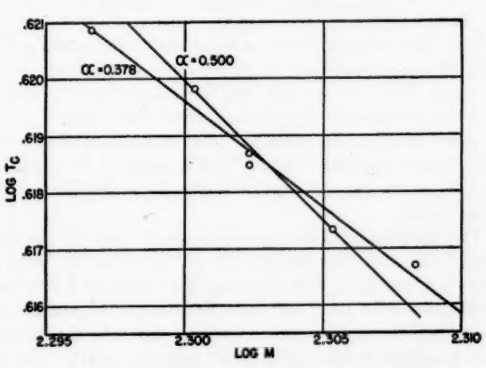

FIG. 1. Plot of logT_c vs. log$M$ for mercury.

TABLE I. Isotope effect on the transition temperature.

Element	M	T_c
Hg^{198}	198.0	4.177[a]
Hg^{199}	199.7	4.167[b]
Nat. Hg	200.6	4.154[b]
Nat. Hg	200.6	4.156[c]
Hg^{202}	202.0	4.147[b]
Hg^{204}	203.4	4.137[b]
Sn^{124}	123.1	3.662[c]
Nat. Sn	118.7	3.715[d]

[a] E. Maxwell, Phys. Rev. **78**, 477 (1950).
[b] Serin, Reynolds, and Nesbitt, Phys. Rev. **78**, 813 (1950).
[c] E. Maxwell, Phys. Rev. **79**, 173 (1950).
[d] E. Laurmann and D. Shoenberg, Proc. Roy. Soc. **A198**, 560 (1949).

TABLE II. Possible theoretical relations of the form $M^\alpha T_c$=constant.

Physical quantity assumed constant	Relation between M and T_c
Thermal energy of the lattice[a]	$M^{3/8}T_c$=const.
Ratio of thermal energy to zero-point energy[a]	$M^{1/2}T_c$=const.
Mean square linear momentum[a]	$M^{3/8}T_c$=const.
Mean square thermal velocity[a]	$M^{1/8}T_c$=const.
Ideal part of normal conductivity just before transition[b]	$M^{2/5}T_c$=const.

[a] From the Debye theory.
[b] A. Sommerfeld and H. Bethe, *Handbuch der Physik* (Springer, Berlin, 1933), Vol. 24, part 2, p. 529, Eq. (37.16).

Recent results[2] on the isotope effect in Sn^{124} tend to reinforce this conclusion. One finds a value of 0.394 for the exponent using the data for tin in Table I.

We may ask whether the equation, $M^{0.378}T_c$=constant, corresponds to the invariance of any significant physical quantity.[3] In Table II we list the relation between M and T_c which would hold if various quantities have critical values (independent of the particular isotope) at the transition temperature. From a purely empirical point of view the total thermal energy of the lattice is indicated as a first choice and the ideal part of the normal conductivity as a second. Evidently more experimental data are needed.

* Supported in part by the ONR.
[1] Serin, Reynolds, and Nesbitt, Phys. Rev. **78**, 813 (1950).
[2] E. Maxwell, Phys. Rev. **79**, 173 (1950).
[3] This constant is not the same for all elements, of course.

Ionization Chamber Bursts at Very High Altitudes

G. W. MCCLURE AND M. A. POMERANTZ
Bartol Research Foundation of the Franklin Institute, Swarthmore, Pennsylvania
July 12, 1950

AN investigation is being conducted to study the atmospheric absorption and the latitude dependence of the radiation which produces high energy nuclear disintegrations in the upper part of the atmosphere. The balloon-borne instruments which are being used throughout the projected series of measurements, contain a cylindrical electron-collection ionization chamber 20 cm long and 6.4 cm in diameter filled with pure argon at a pressure of 5 atmospheres. The ionization pulses are amplified and fed into a radio transmitter keying circuit which is biased to respond to pulses exceeding a preset amplitude. Each chamber contains

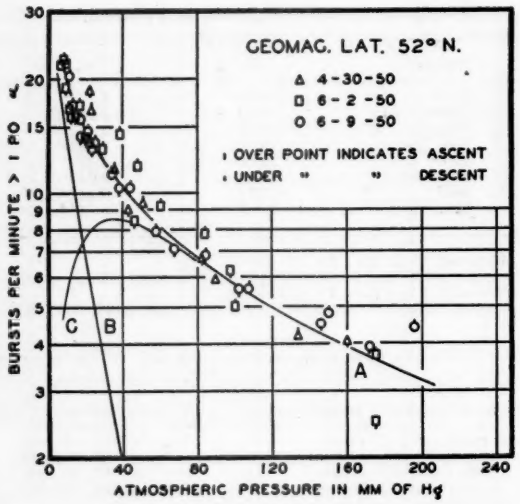

FIG. 1. *A*. Counting rate *vs*. atmospheric pressure for bursts exceeding 1 Po α. *B*. Calculated heavy-nucleus contribution to the total counting rate. *C*. Difference between *A* and *B*. -- bursts produced by protons, neutrons and α-particle.

an electrically controlled Po α-particle source which is used both for calibration and for checking the over-all stability of the instrument during ground tests. The usual radio-sonde methods are employed for relaying temperature and pressure data to the ground station.

In the first experiments a series of instruments biased to respond to pulses ≥ 1.0 Po α have been sent aloft to altitudes up to 103,000 ft. at geomagnetic latitude 52°N. The counting rates recorded in three flights are plotted as a function of atmospheric pressure in Fig. 1. Points obtained during ascent and descent are distinguished by separate symbols. In all the flights the statistical standard deviations in the counting rates vary from 20 percent for points in the neighborhood of 200 mm Hg to 10 percent for the points at the highest altitudes reached. The curve *A* is drawn so that it agrees with most of the points within the standard deviation.

The counts recorded in these measurements result predominantly from two sources: (1) nuclear evaporations occurring in the chamber walls, and (2) heavy nuclei (charge ≥ 8) of the primary radiation.

From photographic emulsion studies Bradt and Peters[1] have determined the mean free paths of heavy nuclei of various charges, and have estimated the intensity of primary nuclei of charge $Z>6$ to be 1.45×10^{-3}/cm²/sec./steradian above the atmosphere. Assuming this value to be correct, the present chamber would be expected to give 41 heavy-nucleus counts/min. at the top of the atmosphere. If it is assumed further that the effective mean free path for collisions in which particles of $Z>8$ are broken down into lighter fragments which cannot be counted by the ionization chamber is 30 g/cm², we obtain curve *B* (Fig. 1) as the heavy nucleus contribution to the ionization chamber counting rate. This calculation takes into account the variation in path length with zenith angle, and is based upon an isotropic angular distribution at the top of the atmosphere.

The difference between the calculated heavy-nucleus counting rate and the total rate measured by the instrument is indicated by Fig. 1, curve *C*. Within the uncertainties involved in the calculation, this curve represents the altitude variation of total flux of protons, neutrons and α-particle, these being presumably the principal source of nuclear disintegrations in the chamber walls. The approximations used in arriving at the heavy-nucleus contribution are of such a nature that values given by curve *B* may be somewhat too high; however, it is doubtful that the over-all error exceeds 50 percent at any point on the calculated curve.

The most interesting feature of curve *C* is the maximum which appears at a depth of approximately 36 mm Hg (49 g/cm²). The occurrence of such a maximum is a characteristic feature of a component of the cosmic radiation which becomes multiplied by a cascade process in penetrating the atmosphere. The fact that the peak occurs at a depth somewhat less than the geometrical mean free path for proton collisions ($\sim$70 g/cm²) is to be expected from the wide zenith-angle distribution of the primary rays.

Similar measurements will be obtained at geomagnetic latitude 69°N during a forthcoming National Geographic Society expedition.

[1] H. L. Bradt and B. Peters, Phys. Rev. **77**, 54 (1950).

On the Origin of the Cosmic Radiation

C. Y. FAN
Department of Physics, The University of Chicago, Chicago, Illinois
May 29, 1950

RECENT measurements[1,2] of the proton component of the cosmic radiation show that the differential energy spectrum, as shown in Fig. 1, appears to indicate that there is a maximum in the low energy end with a gradually increasing slope toward high energies. It is the purpose of this note to show that this fact could be a consequence of the circumstance that the majority of the protons originate from the nucleus of our galaxy.

A description of the mechanism of acceleration of protons in the interstellar spaces is given in Fermi's theory of the origin of the cosmic radiation.[3] According to this theory, low energy protons are accelerated by collisions with the wandering magnetic clouds in the interstellar spaces provided that their initial energies exceed a certain threshold value. Taking into account the average energy loss between collisions, the energy of a proton of initial energy w_0 (including rest energy) after N collisions is given by the formula:

$$w=(w_0-\epsilon/B^2)\exp(B^2N)+\epsilon/B^2 \qquad (1)$$

where ϵ is the average energy loss between collisions and B is the average velocity of the wandering magnetic clouds in units of the velocity of light. Because we are working in such a high energy range it is sufficient, for present purposes, to take ϵ constant. The value of B is taken from Fermi's paper to be 10^{-4}.

Now assume that protons originate from some source at a distance r from the earth, and that some of them reach the earth after many collisions. We can therefore apply the principle of random flight to deduce the energy distribution which reads:

$$P(r,y)dy=\frac{s}{(\pi R^2\ln y)^{\frac{1}{2}}}\cdot\exp\left(-\frac{r^2}{R^2\ln y}\right)\cdot\frac{dy}{y^{1+s}}, \qquad (2)$$

where

$$y=\frac{w-\epsilon/B^2}{w_0-\epsilon/B^2},\quad R^2=\frac{4L^2}{3B^2},\quad s=\frac{\sigma}{M}\left(\frac{D\rho}{B^2}\right).$$

Here L is the average linear displacement between collisions, σ is the proton absorption cross section per nucleon, M is the proton mass, D is the average length of path between collisions, and ρ is the average density of the interstellar matter.

Equation (2) gives the expected spectrum of the proton component if protons originated from a "point source." The adjustment of Eq. (2) to fit the experimental results is facilitated by the following facts.

(a) The experimental energy spectrum around $E\approx10$ Bev has the form $1/E^2$, and that around $E\approx10^4$ Bev has the form $1/E^{2.7}$ (Hilberry's spectrum). This fact suggests that $s=1.5$ in our Eq. (2). Taking $\sigma=2.5\times10^{-25}$ cm² from Fermi's paper, and the energy loss of a high energy proton in passing through the interstellar medium as about 8 Mev/g/cm², we find $(w-\epsilon/B^2)\approx$ the kinetic energy E of the proton.

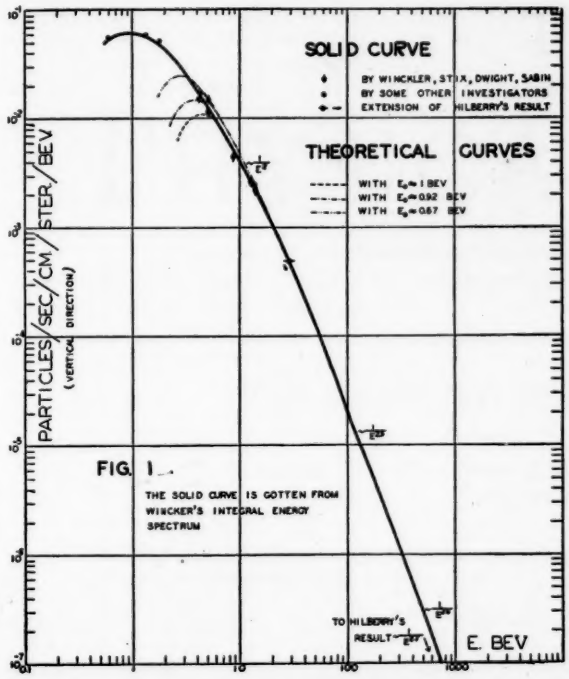

FIG. 1. Comparison of the theoretical formula for the proton energy spectrum with the experimental results.

(b) When we plot Eq. (2) on log-log paper, the shape of the curve is not altered if we assume a different initial energy or multiply by an arbitrary constant.

Taking $(w_0-\epsilon/B^2)$ to be unity and fitting our curve with two arbitrary points of the experimental curve (where we choose $E=7.4$ Bev and $E=20$ Bev), we get:

$$P(r,y)=\frac{115}{(\ln y)^{\frac{1}{2}}}\cdot\exp\left(-\frac{7.4}{\ln y}\right)\cdot\frac{1}{y^{2.5}}. \qquad (2')$$

The comparison with experimental is shown in Fig. 1 where the theoretical curves with different initial energies are obtained by linear translations. (The change of the parameter w_0 causes a horizontal translation, and then a multiplier is introduced to effect a vertical linear translation which will bring the high energy portion of the curve to coincidence except for a small discrepancy which is not indicated.)

It can be seen that if we choose a suitable initial energy spectrum we are able to adjust our curve to fit the experimental results.[4]

If this is not merely due to coincidence, then the assumed source is probably the nucleus of our galaxy because it is the only place, so far as we know, which can supply the necessary energy. Assuming that $D\approx L$ and $\rho\approx 10^{-24}$ g/cc, we find that the distance of our assumed source is just the distance of the center of our galaxy from the earth (3.1×10^{22} cm).

This fact might have two different implications:

(a) If stars, especially early type stars, are able to eject high energy particles (up to one Bev per nucleon) as proposed by different authors,[5] then the conclusion respecting the origin of the cosmic radiation could be that cosmic radiations are particles which were ejected from stars and then accelerated according to Fermi's mechanism in the interstellar spaces. Let us assume that the density of stars is

$$D(a)=(D_0/a)\exp(-a^2/a_0^2), \qquad (3)$$

where "a" is the distance measured from the center of our galaxy and D_0 and a_0 are two constants (which is a simplified form of Oort's description of our galaxy). If we integrate Eq. (2) over the whole space with the weight factor of Eq. (3), we get almost the same results as shown in Fig. 1 except that the maximum of the spectrum shifts toward lower energy. When we choose $(w_0-\epsilon/B^2)=1$ and $a_0^2=r^2/7.4$ for simplicity, the maximum occurs at $E\approx 2$ Bev.

(b) If stars are unable to eject high energy particles, our finding would mean that something like explosions occurred in the nucleus of our galaxy a long time ago over a long period. Our galaxy belongs to the late stage of the normal spiral type. A normal spiral type has its arms fully developed before condensation occurs. This could be understood if our hypothetical mechanism were true because the ejection of a large amount of gas would result in the reduction of the mass of the nucleus, causing arms to be developed by centrifugal force.

At the present moment it is hard to tell which implication is true, but I favor the first because it would give the correct abundance of the heavier nuclear components. A detailed discussion of the heavier nuclear components, the total energy problem, the magnetic property of our galaxy, the age of our galaxy, etc. will be submitted for publication later.

I wish to express my sincere thanks to Professor H. L. Anderson and Professor M. Schein for their helpful criticism and suggestions and to Professor J. R. Winckler for supplying his paper which is as yet unpublished.

[1] Winckler, Stix, Dwight, and Sabin, Phys. Rev. **79**, 656 (1950).
[2] J. A. Van Allen and S. F. Singer, Phys. Rev. **78**, 819 (1950).
[3] E. Fermi, Phys. Rev. **75**, 1169 (1949).
[4] We leave the proper fitting undone here because the position of the maximum is quite uncertain; furthermore, other factors would have important contributions in the low energy region.
[5] K. O. Kiepenheuer and some others mentioned in his paper, Phys. Rev. **78**, 809 (1950).